



HAL
open science

Synthesis of classical and light activated ligands for the glutamatergic transmission

Nunzia Cristiano

► **To cite this version:**

Nunzia Cristiano. Synthesis of classical and light activated ligands for the glutamatergic transmission. Organic chemistry. Université Paris Cité, 2020. English. NNT : 2020UNIP5026 . tel-03881720

HAL Id: tel-03881720

<https://theses.hal.science/tel-03881720>

Submitted on 2 Dec 2022

HAL is a multi-disciplinary open access archive for the deposit and dissemination of scientific research documents, whether they are published or not. The documents may come from teaching and research institutions in France or abroad, or from public or private research centers.

L'archive ouverte pluridisciplinaire **HAL**, est destinée au dépôt et à la diffusion de documents scientifiques de niveau recherche, publiés ou non, émanant des établissements d'enseignement et de recherche français ou étrangers, des laboratoires publics ou privés.

Thèse de doctorat
Préparée à Université de Paris

Ecole doctorale MTCI 563

Laboratoire de Chimie et Biochimie Pharmacologiques et Toxicologiques, UMR8601

Pharmacochimie des Récepteurs et des Transporteurs des α -aminoacides

SYNTHESIS OF CLASSICAL AND LIGHT ACTIVATED LIGANDS FOR THE GLUTAMATERGIC TRANSMISSION

Par Nunzia **CRISTIANO**

Dirigée par Francine ACHER et Isabelle McCORT

En vue de l'obtention du grade de
DOCTEUR DE UNIVERSITÉ DE PARIS

Spécialité Chimie Médicinale/Organique

Présentée et soutenue publiquement à Paris le 01 Décembre 2020

Rapporteur	Pr BOUREL Line	Université de Strasbourg
Rapporteur	Pr CAVELIER Florine	Université de Montpellier
Examineur	Dr PIN Jean-Philippe	Université de Montpellier
Examineur	Pr VIDAL Michel	Université de Paris
Directeur de thèse	Dr McCORT Isabelle	Université de Paris
Co-directeur de thèse	Dr ACHER Francine	Université de Paris



Except where otherwise noted, this work is licensed under
<https://creativecommons.org/licenses/by-nc/3.0/fr/>

Acknowledgements

First of all, thanks to Pr. Line Bourel, Pr. Florine Cavelier, Dr. Jean-Philippe Pin and Pr. Michel Vidal who kindly accepted to be part of my thesis jury and review this work.

Thanks to Dr. Francine Acher and Dr. Isabelle McCort who believed in me since the beginning. They gave me the opportunity to come in Paris to be a PhD student in their group. I appreciated a lot your passion, help and involvement in this work. I am glad for all the things I have learned in these three years collaborating with you.

Thanks to Isabelle Brabet for her collaboration in biological evaluations and to Alexandre Cabayé for molecular modelling studies.

I would like to thank Afaf, Alexandre, Claudia, Cedric, Huan, Louis, Chen-Yu, Yohann, Prisciana, Sebastien, Juliette, Thibault and Riccardo who worked with me during this period. The chemistry with you was funnier, we had such a great time in the lab!

Thanks to all the people of the UMR8601, especially to Alessandra, Giorgina, Amit, Nikola B., Simon, Claire, Huong-Wei, Martin and all the others. You have always been nice to me since the day I arrived and the only french words I knew were “Bonjour” and “Merci”.

Thanks to my parents who gave me the freedom to realize my life choices, even if it was not always easy, you taught me to be strong. Thanks to my brother and my sister for their lifelong support and good advices. Thanks to my grandparents who showed me how to be honest, generous, to appreciate the simple things of the life, to give without expecting anything in return.

Thanks to Marco, Natalia, Johanna, Bastet and Riccardo; I was so lucky to meet good, crazy, funny, mad friends as you in Paris.

Thanks to Clara, Sara and Ilaria. We helped each other a lot during the last years, sometimes a friend can tell you things that you cannot admit to yourself. Thanks to Fiammetta and Carla for the nice time we spent together in Barcelona and your contagious energy.

All my gratitude to the wonderful people I met during these years between the southern and northern Italy, Helsinki, Barcelona and Paris. You taught me the beauty of diversity, the importance of experiencing other cultures and the richness of travelling.

(Paris, October 2020)

Abbreviations

(1R,3R) – ACPD :	(1R,3R)-1-Aminocyclopentane-1,3-dicarboxylic acid
Abs :	Absorbance
AB :	Azobenzene
AC :	Adenyl cyclase
Ac :	Acetyl
ACBC :	1-Aminocyclobutane-1-carboxylic acid
ACEA :	6,7-Dichloro-5-nitro-1,4-dihydro-2,3-quinoxalinedione
AChEi :	Acetylcholinesterase inhibitors
AMN082 :	<i>N,N'</i> -Bis(diphenylmethyl)-1,2-ethanediamine dihydrochloride
AMP :	Adenosine monophosphate
AMPA :	Alpha-amino-3-hydroxy-5-methyl-4-isoxazole propionate
AP-1 :	Activator protein-1
APOE :	Apolipoprotein E
APP :	Amyloid precursor protein
Ar :	Aromatic
ATD :	Amino-terminal domain
ATP :	Adenosine triphosphate
BDNF :	Brain-derived neurotrophic factor
BODIPY :	4,4-Difluoro-4-bora-3a,4a-diaza-s-indacene
c :	Concentration
cAMP :	Cyclic adenosine monophosphate
CaMK :	Ca ²⁺ calmodulin dependent protein kinase
CDI :	1,1'-Carbonyl diimidazole
CNQX :	7-Nitro-2,3-dioxo-1,4-dihydroquinoxaline-6-carbonitrile
CPP :	3-(2-Carboxypiperazin-4-yl)-propyl-1-phosphonic acid
CRD :	Cystein rich Domain
CTD :	C-terminal domain
CYP450 :	Cytochrome P450 enzyme
DAE :	Diarylethene
DASA :	Donor-acceptor Stenhouse adduct
DCM :	Dichloromethane
DEAC :	7-Diethylaminocoumarin
DEDCC :	Diethylcoumarine chromophore
DIEA :	Diisopropylethylamine
DMF :	Dimethylformamide
DMSO :	Dimethyl sulfoxide
DNA :	Deoxyribonucleic acid
DNQX :	6,7-Dinitro-1,4-dihydroquinoxaline-2,3-dione
EAAT :	Excitatory amino acid transporter
EC₅₀ :	Half maximal effective concentration
EGFR :	Epidermal growth factor receptor

eq :	equivalent
ERK :	Extracellular signal-regulated kinase
ESI :	Electrospray ionization
Et :	Ethyl
FDA :	Food and drug administration
g :	gramme
GABA :	Gamma-aminobutyric acid
GPCR :	G-Protein Coupled Receptor
GRK :	G-Protein coupled receptor kinase
GTP :	Guanosine triphosphate
GV196771A :	4,6-Dichloro-3-[[[(3E)-2-oxo-1-phenylpyrrolidin-3-ylidene]methyl]-1H-indole-2-carboxylate
h :	hour
<i>h</i> :	Planck constant
HRMS :	High resolution mass spectroscopy
HTI :	Hemithioindigo
HTS :	High throughput screening
Hz :	Hertz
<i>I</i>₀ :	Incident light intensity
<i>I</i> :	Transmitted light intensity
IC₅₀ :	Half maximal inhibitory concentration
IGF :	Institut de Génomique Fonctionnelle
iGluR :	Ionotropic glutamate receptor
IL :	Intracellular loop
IMAO :	Inhibitor of monoaminoxidase
IP₃ :	Inositol trisphosphate
λ :	Wavelength
L-AP4 :	L-2-Amino-4-phosphonobutyric acid
LBD :	Ligand-binding domain
L-SOP :	L-Serine- <i>O</i> -phosphate
LSP :	Laboratoire des Saints-Pères
LY341495 :	(2S)-2-Amino-2-[(1S,2S)-2-carboxycycloprop-1-yl]-3-(xanth-9-yl)propanoic acid
M :	Molar
MAPK/ERK :	Mitogen activated protein kinase/Extracellular protein kinase
MAP :	Mitogen activated protein
MAP-4 :	2-Amino-2-methyl-4-phosphonobutyric acid
Me :	Methyl
mGluR :	Metabotropic glutamate receptor
mg :	Milligramme

MHz :	MegaHertz
MMPIP :	6-(4-Methoxyphenyl)-5-methyl-3-pyridin-4-ylisoxazolo[4,5-c]pyridin-4(5H)-one
MSG :	Monosodium glutamate
μM :	Micromolar
mL :	Millilitre
mM	Millimolar
min :	Minute
MK-801 :	Dizocilpine
mRNA :	Messenger ribonucleic acid
M-SOP :	(<i>R,S</i>)- α -Methylserine- <i>O</i> -phosphate
mTOR :	Mammalian target of Rapamycin
NAM :	Negative allosteric modulator
<i>N</i>-DCAC :	<i>N</i> -7-(dicarboxymethyl)-aminocoumarin
NDRI :	Dopamine and noradrenaline reuptake inhibitor
NFT :	Neurofibrillary tangle
NIR-TP	Near infrared two photon
NMDA :	<i>N</i> -Methyl-D-aspartate
NMR :	Nuclear magnetic resonance
NPC17742 :	(<i>2R,4R,5S</i>)-2-Amino-4,5-(1,2-cyclohexyl)-7-phosphonoheptanoic acid
NTD :	N terminal domain in the extracellular space
<i>o</i> :	<i>ortho</i>
<i>o</i>-NB :	<i>ortho</i> -nitrobenzyl
<i>o</i>-NPE :	1-(2-Nitrophenyl)ethyl sulfate sodium salt
OP :	One photon
<i>o</i>tBu :	<i>tert</i> -Butyloxy
PAM :	Positive allosteric modulator
PBS :	Phosphate-buffered saline
PC :	Purkinje cell
PCP :	Phencyclidine
PD :	Parkinson's disease
PET :	Positron emission tomography
PHCCC :	<i>N</i> -Phenyl-7-(hydroxylimino)cyclopropa[<i>b</i>]chromen-1a-carboxamide
Φ :	Quantum yield
PKA :	Protein kinase A
pK_a :	Acid dissociation constant
PI3K :	Phosphoinositide 3-kinase
PKC :	Protein kinase C
PLC :	Phospholipase C
PMPA :	4-(Phosphonomethyl)-2-piperazinecarboxylic acid
PBPD :	(<i>2S,3R</i>)-1-(Biphenyl-4-carbonyl)piperazine-2,3-dicarboxylic acid
PPG :	Photoprotecting group
PPDA :	(<i>2S,3R</i>)-1-(Phenanthrene-2-carbonyl)piperazine-2,3-dicarboxylic acid
PS :	Presenilin

PSS:	Photostationary state
PTL :	Photo-switchable tethered ligand
PyCIU :	1-(Chloro-1-pyrrolidinylmethylene)pyrrolidinium hexafluoro-phosphate
Rf :	Retention factor
RNA :	Ribonucleic acid
(R)-PCEP :	(R)-3-Amino-3-carboxypropyl-2'-carboxyethyl phosphinic acid
(R,S)-PPG :	(R,S)-2-Amino-2-(4-phosphonophenyl)acetic acid
RT :	Room temperature
SAM :	Silent allosteric modulator
SAR :	Structure–activity relationship
SEM :	Standard error of the mean
7TM :	Seven transmembrane
(S)-DCPG :	(S)-3,4-Dicarboxyphenylglycine
S_N1 :	Nucleophilic substitution of order 1
S_N2 :	Nucleophilic substitution of order 2
SNARE :	Soluble <i>N</i> -ethylmaleimide-sensitive factor attachment protein receptor
SNRI :	Serotonin–norepinephrine re-uptake inhibitor
(S)-PPG :	(S)-4-Phosphonophenylglycine
SP :	Spiropyran
SSRI :	Selective serotonin re-uptake inhibitor
<i>t</i>- :	<i>tert</i> -
TCA :	Tricyclic antidepressant
TFA :	Trifluoroacetic acid
THF :	Tetrahydrofuran
TLC :	Thin Layer Chromatography
TMD :	Transmembrane domain
TP :	Two photons
TPA :	Two photon absorption
<i>trans</i>-ABCD :	<i>trans</i> -1-Aminocyclobutane-1,3-dicarboxylic acid
UBP141:	(2 <i>R</i> ,3 <i>S</i>)-1-(3-Phenanthrylcarbonyl)-2,3-piperazinedicarboxylic acid
UV :	Ultraviolet
VFT :	Venus flytrap
VGLUT :	Vesicular glutamate transporter
v-HTS :	virtual high throughput screening
XAP044 :	7-Hydroxy-3-(4-iodophenoxy)-4 <i>H</i> -chromen-4-one

Résumé en français

Introduction générale

1- Le Glutamate dans le SNC

Le manuscrit débute par l'historique du glutamate comme neurotransmetteur. Le fonctionnement de la synapse glutamergique est ensuite décrit. Une fois libéré dans la fente synaptique, le glutamate active deux types de récepteurs : des récepteurs ionotropiques (iGluR, **1.3.1**) et metabotropiques (mGluR, **1.3.2**). Les premiers assurent la transmission synaptique rapide. Ce sont des récepteurs canaux dont le canal est formé par 4 sous-unités membranaires. Ils sont de 3 types NMDA (*N*-Methyl-D-Aspartate), AMPA (α -amino-3-hydroxy-5-methyl-4-isoxazole propionate), KA (kainate). Les seconds récepteurs mGlu ont pour rôle de moduler la transmission synaptique. La thèse portant sur le développement d'outils/ligands pour les récepteurs NMDA et mGlu, ils sont présentés plus en détail.

1.3.1.1 Les récepteurs **NMDA** sont activés par le glutamate et un co-agoniste, la glycine ou la D-sérine. La première partie de la thèse portera sur des outils permettant d'étudier le rôle de la D-sérine. C'est pourquoi différents ligands de ce récepteur sont présentés plus en détails. Les récepteurs AMPA et KA sont décrits plus brièvement.

1.3.2 Les récepteurs **mGlu** font partie de la classe C des récepteurs couplés aux protéines G. Ce paragraphe décrit la classification des 8 sous-types en trois groupes I-III, leur distribution sur la synapse glutamatergique, leur structure et mécanisme d'activation, suivi de trois paragraphes consacrés aux récepteurs de chacun des trois groupes. La seconde partie de la thèse portant sur le développement de ligands du sous-type 7 du groupe-III, les ligands de ce groupe sont ensuite détaillés. Deux courts paragraphes mentionnent le fonctionnement des hétéro-dimères et la modulation des mGluR par des nanobodies, deux domaines de prédilection de Jean-Philippe Pin mais aussi des domaines qui représentent un potentiel important pour les développements thérapeutiques.

1.4 Cette dernière section du chapitre d'introduction sur le glutamate, décrit les différentes pathologies du SNC dans lesquelles le glutamate est impliqué. Certaines seront évoquées dans les deux premières parties des résultats.

2- Photopharmacologie

Le second chapitre d'introduction porte sur les deux types d'outils photopharmacologiques préparés au cours de la thèse: les ligands "cagés" et les "photoswitches" (photo-interrupteurs). Ces types d'outils sont extrêmement appréciés par les biologistes.

2.1 Ce paragraphe décrit le principe des **composés "cagés"**, une molécule bioactive liée à une cage pouvant absorber de l'énergie lumineuse (chromophore). La photoactivation permet la rupture de ce lien et la libération du composé d'intérêt en maîtrisant le temps et la localisation de l'évènement. Différents groupements photoactivables décrits dans la littérature sont présentés ainsi que le mécanisme d'excitation à un et deux photons. L'intérêt de l'excitation à deux photons est détaillé.

2.2 Les **photoswitches** sont des molécules qui changent de conformation sous illumination. L'intérêt de tels composés est d'identifier une conformation active et pas l'autre permettant de moduler le fonctionnement d'un système biologique (ou autre) avec la lumière. En général l'une des conformations est plus stable, l'autre est atteinte par absorption à une longueur d'onde définie et le retour se fait soit thermiquement soit par irradiation à une autre longueur d'onde. La difficulté est de trouver de telles molécules présentant à la fois des propriétés biologiques et photophysiques adéquates.

Plusieurs types de photoswitch et leurs propriétés sont décrits. Les azobenzènes et les dérivés d'indigo et hemi-indigo sont présentés plus en détail car certains de ces derniers sont préparés et étudiés dans le chapitre des résultats. La notion d'azologisation est définie, elle permet de comprendre les choix des photoswitches préparés dans la suite du manuscrit.

Résultats et discussion

Ce travail s'inscrit dans les thématiques du laboratoire mais n'est pas dans la continuité de travaux antérieurs.

Ce deuxième chapitre, le plus conséquent décrit les travaux de synthèse qui sont divisés en trois parties distinctes :

3- La première partie concerne **la synthèse de composés cagés du récepteur NMDA**.

Il est d'abord rappelé le contexte biologique de ces synthèses. Les récepteurs NMDA sont activés par la liaison de l'agoniste orthostérique glutamate, en combinaison avec la liaison d'un co-agoniste qui peut être la glycine ou la D-sérine. Cela permet l'ouverture du canal central avec l'entrée des ions Ca^{2+} et la dépolarisation du neurone post-synaptique. La sérine racémase convertit la L-sérine en D-sérine dans les neurones pré-synaptiques. La présence de la D-sérine et de la glycine dans la fente synaptique est régulée par le transporteur alanine-sérine-cystéine (Asc 1) présent dans les astrocytes et les neurones (**Figure 45**). Asc-1 peut donc être considéré comme une cible thérapeutique intéressante en inhibant la recapture mais pas la libération de la D-sérine pour soulager les symptômes de la schizophrénie associés à l'hypofonctionnement des récepteurs NMDA.

La première partie de ce travail a été basée sur la synthèse de deux composés cagés : la *N*-DCAC-D-sérine (**1**) et la *N*-DCAC-glycine (**2**). L'objectif était la synthèse de ces deux composés pour les tester dans des études d'électrophysiologie sur des coupes de cerveau de souris knock-out de la D-sérine racémase. Le but final est d'étudier le rôle de la D-sérine dans l'activation du récepteur NMDA dans des études d'électrophysiologies. Ce projet est réalisé en collaboration avec le Dr Jean-Pierre Mothet de l'Université ENS Paris Saclay.

Le décaageage de la *N*-DCAC-D-sérine et de la *N*-DCAC-glycine sera réalisé par une irradiation à deux photons (**Figure 46**), permettant de libérer les acides aminés afin d'activer les récepteurs NMDA ; la dépolarisation sera enregistrée en électrophysiologie sur des coupes de cerveau de souris knock-out D-sérine. Le choix a été de synthétiser les cages *N*-DCAC-D-sérine (**1**) et *N*-DCAC-glycine (**2**) pour obtenir deux composés solubles dans l'eau, avec de bonnes propriétés photophysiques capables de libérer facilement l'acide aminé souhaité après irradiation. La cage « vide » *N*-DCAC-OH (**3**) a également été synthétisée pour vérifier si elle peut être responsable d'éventuels effets secondaires et être sûr que l'activation est uniquement due à la libération de D-sérine ou de glycine (**Figure 48**).

Concernant la synthèse, la protection sélective de l'amine du 3-aminophénol par le chlorure de 2-méthoxyacétyle en milieu basique conduit au produit **4** avec un rendement de 65%. La formation de la coumarine **5** a été réalisée par condensation de Pechmann à partir du phénol **4** et du β -cétobutanoate d'éthyle. La 7-amino-4-méthylcoumarine **6** a ensuite été obtenue en milieu basique avec un rendement de 57% sur les deux étapes. La dialkylation du groupe amino du composé **6** a été réalisée avec le *tert*-butyl-2-bromoacétate pour conduire au composé **7** après 7 jours à reflux permettant de minimiser la présence du monoalkylé, difficile à séparer du produit désiré. L'oxydation du méthyle en position 4 de la coumarine **7** en alcool correspondant **9** a été réalisée *via* l'oxydation en aldéhyde **8** en présence de dioxyde de sélénium qui a été ensuite directement engagé dans l'étape de réduction en présence de borohydrure de sodium (**Schéma 7**).

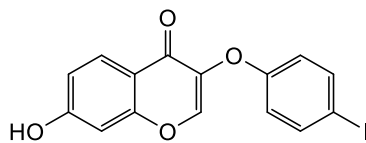
La formation de la liaison carbamate a été particulièrement délicate à partir des acides aminés D-sérine et glycine. Le produit **10** a été obtenu en utilisant le carbonyldiimidazole comme agent de couplage en présence d' Et_3N . Cette réaction a été réalisée dans le DMSO et dans le DMF mais seul le DMSO a conduit au produit attendu (**Schéma 12**). Le produit **11** a été préparé dans les mêmes conditions en remplaçant la D-sérine par de la glycine avec un meilleur rendement (38%).

Les conditions qui ont permis la déprotection des groupements *tert*-butyle du composé **9** ont été dans l'HCl 4 M dans le dioxane conduisant à la cage « vide » **3** avec un rendement de 95% (**Schéma 14**). La déprotection finale de **10** et **11** a été réalisée dans ces conditions pour obtenir les composés **1** et **2** avec des rendements respectifs de 45% et 57% (**Schéma 14**).

Les composés *N*-DCAC-D-Ser **1**, *N*-DCAC-OH **3** et la cage protégée **10** ont été étudiés pour leurs propriétés photo-physicochimiques à l'Institut des Sciences Moléculaires de Bordeaux en collaboration avec l'équipe du Pr Mireille Blanchard-Desce. La cage *N*-DCAC-Gly **2** n'a pas été analysée car elle a été synthétisée plus tard. Ces expériences ont fourni deux spectres d'absorbance photonique et guideront le choix de la meilleure longueur d'onde à utiliser pour le décaageage du composé actif, la D-sérine, avec le pourcentage le plus élevé possible. L'irradiation à deux photons a permis de déterminer la longueur d'onde qui donne la section efficace σ_2 la plus élevée. Le composé **3** dans le DMSO a montré un σ_2 de 13 GM et le composé **1** dans le tampon (pH = 7,2) un σ_2 de 33 GM (**Figure 52**). Avant d'effectuer des expériences physiologiques, il est nécessaire de connaître l'efficacité quantique des cages c'est-à-dire la quantification de la quantité libérée d'acides aminés à différentes concentrations en utilisant une

longueur d'onde donnée. Cette étude sera réalisée à l'Institut des Sciences Moléculaires d'Orsay (ISMO). Les données d'efficacité quantique seront utiles pour les études électrophysiologiques finales réalisées par le groupe du professeur Nigel Emptage de l'Université d'Oxford.

- 4- La deuxième partie, plus conséquente, concerne la **synthèse d'analogues du XAP044** afin de découvrir d'une part, où et comment ce NAM se lie dans le VFTD de mGlu7R et d'autre part, un composé à la fois plus puissant et plus soluble que le XAP044.



XAP044

Il y a plusieurs années, à la demande de Novartis, des études de modélisation moléculaire avaient été réalisées par le Dr Francine Acher et complétées également par Alexandre Cabayé (PhD) pour déterminer le site de liaison du XAP044 au niveau du VFT. Cette étude s'est révélée difficile. Plusieurs hypothèses ont été envisagées. Compte-tenu de la sélectivité du XAP044 vis-à-vis de mGlu7 et des premiers résultats de mutagenèse des Ser 160 et 229, 3 hypothèses de docking ont été proposées (**Figure 60**) :

- 1^{ère}) Orientation du XAP044 le long de la boucle $\beta 10\alpha 7$,
- 2^{ème}) Orientation du XAP044 lié à la S229 et à la S160 le long de l'hélice $\alpha 6$,
- 3^{ème}) Orientation du XAP044 lié à la S229 et à la S160 le long de la boucle $\beta 7\alpha 8$.

Nous avons alors pensé que des données de SAR du ligand pourraient aider à choisir parmi les options de docking. Les principaux aspects considérés pour obtenir ces informations ont été de vérifier si :

- le XAP044 se lie dans une conformation plane ou présentant une torsion
- le cycle chromèn-one du XAP044 est nécessaire
- d'autres substituants peuvent remplacer l'atome d'iode en position *para* du cycle benzénique mais également être introduits dans différentes positions sur les deux cycles aromatiques.
- un photoswitch analogue de XAP044 est actif sous forme *cis* ou *trans*.

Différentes séries ont été synthétisées pour répondre à ces questions :

- **4.1.1** La première approche a concerné la synthèse d'**analogues contraints du XAP044** pour déterminer si le XAP044 se lie dans une conformation plane ou avec une torsion (**Figure 62**).

Les analogues contraints **12a-g** ont été synthétisés en une seule étape à partir de 2-bromo-1-(2-fluorophenyl)ethan-1-one et de salicylate substitués selon des conditions décrites par Miller *et al.* (**Schéma 16**). Les analogues méthoxylés **12b**, **12c** et **12e** ont également été déprotégés pour conduire aux dérivés hydroxylés correspondants **13** (**Schéma 17**). Tous les dérivés méthoxylés et hydroxylés contraints sont inactifs dans des tests où le récepteur mGlu7 est surexprimé dans des cellules HEK (Plateforme ARPEGE, IGF, Montpellier).

- **4.1.2** La deuxième approche a concerné la synthèse d'**analogues ouverts du XAP044** pour déterminer à la fois si le cycle chromèn-one est indispensable et si ces molécules flexibles sont capables de se lier au VFTD avec des orientations et des angles différents par rapport aux précédents dérivés contraints (**Figure 63**).

Les résultats pharmacologiques de l'analogue strict ouvert du XAP044 **16a** (similaire au XAP044) nous ont permis de poursuivre la pharmacomodulation dans cette série.

4.1.2.1 Tout d'abord, la synthèse d'analogues ouverts méthoxylés **14a-e** et **15** a été réalisée à partir du 2-bromo-1-(4-hydroxyphényl)ethan-1-one et de phénols substitués pour étudier à la fois la flexibilité de la molécule et confirmer le rôle du groupement hydroxyle dans la liaison à la Ser 229 du VFTD (**Scheme 19** and **Scheme 20**). Ils se sont tous révélés inactifs, nous nous sommes donc focalisés sur la synthèse d'analogues hydroxylés ouverts, ce qui a représenté la série la plus importante.

4.1.2.2.1 La synthèse la plus efficace pour les analogues ouverts a été réalisée par alkylation du 4-(2-bromoacetyl)phényl acétate **17** par des phénols substitués (**a-x**) en milieu basique (**Table 1**) suivie de la déprotection de l'hydroxyle. Parmi les 24 analogues ouverts hydroxylés, peu d'entre

eux ont montré une activité similaire ou supérieure au XAP044. Lorsque l'iode en position *para* du XAP044 a été remplacé par un atome de brome et qu'un atome de fluor a été ajouté en position *ortho*, le **19u** s'est avéré être le composé le plus actif de la série des analogues ouverts hydroxylés synthétisés (**Table 5**).

4.1.2.2.2 Les substituants du composé **19u** ont donc été conservés pour les synthèses de 3 nouveaux analogues substitués en ajoutant maintenant en position *ortho* du cycle phénolique un deuxième hydroxyle (**23**), un atome de fluor (**27a**) et deux atomes de fluor (**27b**) (**Figure 64**).

En effet, l'hydroxyle en *para* s'est révélé fondamental pour la liaison à la Ser229, la présence d'un deuxième hydroxyle pouvait avoir des effets positifs grâce à des liaisons hydrogène complémentaires. A partir du catéchol, le composé **21** a été synthétisé en utilisant du bromure de bromoacétyle et du trichlorure d'aluminium dans du DCM puis, en utilisant la même méthode que celle vue sur le **Schéma 25** et la **Table 1**, le composé **23** a été obtenu avec un rendement de 23% (**Schéma 28**).

Les analogues ouverts hydroxy-fluorés **27a,b** ont été conçus pour abaisser le pKa du phénol et ainsi favoriser la déprotonation de l'hydroxyle qui pourrait ainsi agir comme un accepteur de liaison hydrogène dans la liaison à la Ser229. Les composés **24a,b** ont été synthétisés à partir du 2-fluorophénol et de 2,6-difluorophénol par acylation de Friedel-Craft en utilisant du bromure de bromoacétyle, du trichlorure d'aluminium et du disulfure de méthyle (**Schéma 30** et **Schéma 31**) suivie de l'alkylation dans des conditions classiques pour obtenir les composés **27a,b** (**Schéma 32**). Le composé **23** mais surtout les **27a,b** se sont révélés les plus actifs parmi tous les analogues de XAP044 synthétisés.

➤ **4.1.3** La troisième grande classe de composés synthétisés de ce projet concerne différentes séries de **photoswitches** afin d'obtenir des informations de liaison pour valider un modèle moléculaire.

Les formes *trans* ou *cis* que peuvent adopter les composés photoswitchables, contrairement aux ligands conventionnels, peuvent agir avec un mécanisme marche-arrêt en répondant aux sources lumineuses sur la cible afin d'activer ou de désactiver le récepteur. De plus, dans le cas du XAP044, savoir qu'un photoswitch est actif sous forme *trans* et inactif sous forme *cis* ou *vice versa*, pouvait donner des informations importantes pour comprendre le mode de liaison du composé.

4.1.3.1 Les **azobenzènes 28a-f** ont été synthétisés par réaction de copolymérisation entre le phénol et différentes anilines (**Schéma 37**). Les composés **28a-f** ont montré un temps de relaxation rapide (**section 4.1.3.1.1**) et aucune activité biologique (**section 4.2**), nous avons donc décidé d'explorer d'autres types de photoswitch.

4.1.3.2 Les analogues de **phénylazoindole** représentent un autre type de photoswitch lié aux azobenzènes où un cycle benzénique est remplacé par un indole. Ces composés sont plans comme les azobenzènes en raison de la liaison diazène centrale et peuvent être isomérisés en isomère *Z* en utilisant une lumière UV tandis que le retour vers l'isomère *E* s'effectue en utilisant une lumière bleue ou verte (**Figure 67**). Le rationnel de leur synthèse provient de la superposition de l'analogue de phénylazoindole sous la forme *Z* avec le XAP044 (**Figure 68**). La synthèse des composés **29a,b** a été réalisée par réaction d'azocopolymérisation et la déméthylation de l'hydroxyle a conduit aux composés **30a,b** (**Schéma 40**). D'après les spectres UV-Vis et la RMN du ¹H, tous les composés n'ont été obtenus qu'en configuration *E* à l'exception du composé **30b**. En effet, ce composé a été obtenu sous forme d'un mélange de 23% d'isomère *E* et 77% d'isomère *Z*. Ceci est probablement dû à l'atome d'iode en position *meta* qui change totalement les propriétés électroniques de la molécule par rapport au composé **30a**. Cela signifie que, alors que les autres composés sont énergétiquement stables sous leur forme solide et en solution dans du DMSO en configuration *E*, le composé **30b** est énergétiquement stable dans le mélange 23% *E* et 77% *Z*, qui correspond à son état photostationnaire (PSS) à 20 °C. Les composés de type phénylazoindole se sont avérés inactifs dans les tests biologiques (**section 4.2**).

4.1.3.3 Les **Aurones** ont ensuite été étudiés car à ce moment, nous nous étions concentrés sur l'orientation 3 pour la liaison du XAP044 au VFTD (**Figure 60**). La superposition d'un analogue de la 6-hydroxyaurone avec le XAP044 avait montré que la configuration *E* correspondrait au XAP044 dans la conformation du modèle de docking (**Figure 71** et **Figure 72**). Les aurones **31a-i** ont été

synthétisées par condensation aldolique (**Schéma 41**). Elles n'ont montré aucune activité biologique confirmant que l'orientation 3 ne peut pas être acceptée comme mode de liaison de XAP044 (**section 4.2** et **section 4.3**). En revanche, elles démontrent des propriétés photo-physiques intéressantes (**section 4.1.3.3.1**) car ces composés possèdent un temps de relaxation long et en particulier pour les composés **31a-d** comme le montre des études cinétiques en irradiant à 365 nm et 440 nm qui ont été réalisées dans quatre solvants différents (**Figure 88** et **Figure 89**). Ces composés peuvent être des outils utiles pour des applications en science des matériaux et en utilisant une irradiation sélective à une longueur d'onde appropriée où le coefficient d'extinction molaire ϵ de l'isomère *E* est différent de l' ϵ de l'isomère *Z* pourrait être un photoswitch également utile en biologie.

4.1.3.4 Enfin une **chalcone 32**, analogue ouvert de l'aurone **31a**, a été synthétisée par condensation de Claisen-Schmidt (**Schéma 43**). Ce composé a une structure plane comme les analogues contraints, les azobenzènes, les phénylazoindoles et les aurones. Elle s'est révélée biologiquement inactive confirmant que le XAP044 se lie dans une conformation non planaire (**section 4.2**).

4.2 Tests pharmacologiques

Les composés analogues du XAP044 décrits dans les paragraphes ci-dessus ont été testés sur la plateforme ARPEGE de l'Institut de Génomique Fonctionnelle (IGF) de Montpellier.

Pour rappel le XAP044 est un modulateur allostérique négatif du récepteur mGlu7. Il est modérément actif, inhibant le L-AP4 avec un IC_{50} de 2.8 μ M dans la publication originale (Gee *et al J Biol Chem* 2014). Dans les tests réalisés à l'IGF, le récepteur mGlu7 est activé par un meilleur agoniste le LSP4-2022. L'inhibition par les nouveaux composés est mesurée par la baisse de l' EC_{50} du LSP4-2022 quand ils sont additionnés à une concentration de 30 ou 100 μ M (**Table 5**). Pour les 3 composés présentant la meilleure inhibition **23**, **27a,b**, les IC_{50} ont été mesurés avec des valeurs de 3.4, 0.96, 0.88 μ M respectivement. Ces valeurs sont à comparer à celle du XAP044 soit 4.3 μ M, dans le même test.

Les données pharmacologiques ont permis de répondre à plusieurs questions :

- Le XAP044 se lie-t-il au VFTD de mGlu7 dans une conformation plane ou présentant une torsion ? Tous les analogues plans sont inactifs, seuls des analogues flexibles présentent une activité. On en déduit que la conformation bioactive du XAP044 n'est pas plane.
- La partie chromone du XAP044 est-elle nécessaire pour l'activité du XAP044 ? L'activité d'analogues ouverts montre que ce cycle n'est pas requis.
- Le groupement hydroxyle du XAP044 est-il essentiel ? La perte d'activité du dérivé méthoxy le confirme.
- L'iode du XAP044 peut-il être remplacé par un autre substituant ? Les groupements nitrile ou nitro sont tolérés mais seul un brome conduit à une activité équivalente au XAP044.
- Quel est l'effet de substituants sur d'autres positions de l'iodophényle ? Seul un atome de fluor sur les positions *ortho* de l'iodophényle est admis, révélant un environnement restreint autour de ce groupe.
- D'autres substituants sont-ils admis en *ortho* du phénol du XAP044 ? Comme indiqué ci-dessus, hydroxyle et fluor augmentent l'effet NAM.

Un résumé de la SAR est présenté sur la **Figure 102**.

4.3 Modélisation moléculaire et validation du mode de liaison

Trois dockings possible pour le XAP044 ont été proposés (**Figure 60**). Des expériences de mutagenèse dirigée et tests fonctionnels ont été réalisés à l'IGF pour valider l'une des trois options.

- L'orientation 1 vers la boucle $\beta_{10\alpha 7}$ a été éliminée car l'inversion de cette boucle avec celle du sous-type 4 (mGlu4) n'affecte pas l'inhibition par le XAP044 alors que 4 résidus sur 7 sont différents.
- Le second docking positionne le XAP044 le long de l'hélice α_6 (**Figure 103**). Il satisfait plusieurs critères : liaison hydrogène avec S160 et S229, contact hydrophobe avec A183, P184, K233, liaison halogène avec S237 et Q240, environnement restreint autour de l'iodophényle et interaction avec deux résidus sélectifs K233 et S237. Ce docking est stable dans une dynamique moléculaire de 3.5 ns.

- Le troisième docking possible positionne le XAP044 le long de la boucle $\beta 7\alpha 8$. Bien que ce docking satisfasse les critères requis, il a été éliminé car totalement instable au cours de dynamiques moléculaires, même avec des contraintes initiales.

Le second docking retenu, les résidus S229, K233 et S237 ont été mutés en alanine pour le valider. Le mutant S229 supprime totalement l'effet du XAP044 alors qu'il n'affecte pas l'activation par un agoniste. Le mutant S237A n'a pas d'effet et K233A réduit l'inhibition. La mutation K233D est en cours pour confirmer l'interaction de K233 avec le XAP044.

Ces données semblent confirmer le mode de liaison du XAP044 qui agirait comme une cale empêchant les deux lobes du VFTD de se refermer et bloquant l'activation du récepteur mGlu7 (**Figure 104 et 107**).

5- Azologization du NAM mGlu7 VU6010608

Une dernière partie, brève, concerne l'« azologisation » du VU6010608, NAM sélectif du récepteur mGlu7 qui se fixe dans le domaine transmembranaire, (**Figure 108**), site classique des modulateurs allostériques, contrairement au XAP044 (**Figure 54**).

Le VU6010608 **35** est composé de deux cycles benzéniques reliés par une liaison amide. La SAR ayant montré que cette liaison amide centrale n'est pas fondamentale, il était envisageable de la remplacer par une liaison diazène pour obtenir l'analogue azobenzène par « azologization » tout en maintenant l'activité biologique (**Figure 110**). Le VU6010608 **35** a tout d'abord été synthétisé (**Schéma 44**) pour pouvoir tester l'activité du composé bioactif de référence et le comparer au dérivé azologue dans le même essai biologique. À partir de l'intermédiaire **34**, le composé mono-hydroxylé **36** a été synthétisé par une réaction d'azo-copulation, suivie de la méthylation de l'hydroxyle pour conduire au produit diméthoxylé **37** (**Schéma 45**).

Une cinétique a été réalisée en RMN du ^1H pour les composés **36** (**Figure 111**) et **37** (**Figure 112**) à la concentration de 8 mM dans le DMSO. Le composé **36** n'a montré aucun changement après 1 h d'irradiation à 365 nm puisque les spectres RMN du ^1H n'ont montré que la présence de l'isomère *E*, ce qui est dû à la relaxation thermique rapide.

En revanche, pour le composé **37**, le groupe méthoxy en position *para* qui a un effet donneur d'électrons permet une relaxation thermique plus lente. En effet, après irradiation à 365 nm pendant 1 h, le composé **37** s'isomérisé à 67% en isomère *Z*. Une irradiation supplémentaire pendant 2 h à 365 nm a montré le même pourcentage, montrant que le PSS à 365 nm correspond à 33% d'isomères *E* et 67% *Z*. Le mélange des deux isomères n'a pas changé pendant neuf jours. Les composés **36** et **37** devaient être testés en tant qu'analogues de photoswitch du composé **35** à l'Institut de Génomique Fonctionnelle de Montpellier. Les produits **36** et **37** étaient impossible à tester car ils précipitent dans un tampon phosphate aux concentrations requises pour les dosages. De manière surprenante, le remplacement de l'amide central de VU6010608 par l'unité diazène conduit à une diminution de la solubilité dans les solvants polaires. Le composé **35** (VU6010608) a été testé à une concentration de 100 μM en présence de LSP4-2022 et n'a pas montré d'effet antagoniste (**Tableau 9**). Le VU6010608 a une CI_{50} de 759 nM lorsqu'il est testé en présence de l'agoniste L-AP4 mais il n'est pas capable d'antagoniser l'agoniste plus puissant, le LSP4-2022, comme le montrent les résultats de cette étude.

Conclusion générale et perspectives

Le travail de thèse a porté sur 3 études :

- La synthèse de *N*-DCAC-D-Ser et *N*-DCAC-Gly pour l'étude de l'activation des récepteurs NMDA
- La synthèse de nouveaux analogues du XAP044 pour aider au docking et découvrir des composés plus puissants
- L'azologisation d'un NAM mGlu7 d'un autre type.

Les études préliminaires pour les expériences *ex-vivo* utilisant les composés cagés sont en cours.

La seconde étude a conduit à 3 composés plus actifs que le XAP044 et aidé à identifier son mode de liaison sur le domaine VFTD du récepteur mGlu7.

Enfin le troisième type de composé issu de l'azologization d'un composé de la littérature n'a pas montré d'activité en raison de son insolubilité aqueuse. Ce dérivé d'azobenzène présente cependant des propriétés photophysiques intéressantes pour d'autres applications en milieu organique.

Table of contents

Acknowledgements

Abbreviations

Résumé en français

Table of contents

General introduction

1. Glutamate in central nervous system	1
1.1. Glutamic acid and umami taste	2
1.2. Glutamic acid as a neurotransmitter	2
1.3. The glutamatergic synapse	4
1.3.1. The ionotropic glutamate receptors (iGluRs).....	5
1.3.1.1. NMDA receptors.....	8
1.3.1.2. AMPA receptors	13
1.3.1.3. Kainate receptors	13
1.3.2. The metabotropic glutamate receptors (mGluRs).....	14
1.3.2.1. Group I of mGluRs	18
1.3.2.2. Group II of mGluRs	20
1.3.2.3. Groupe III of mGluRs	21
1.3.2.3.1. Agonists and antagonists of Group III mGluRs.....	22
1.3.2.3.2. Allosteric modulators of Group III of mGluRs	25
1.3.2.4. mGluRs heterodimers	32
1.3.2.5. mGluRs modulation by nanobodies.....	34
1.4. Therapeutic potential of glutamate receptors.....	35
1.4.1. Schizophrenia	35
1.4.2. Depression.....	37
1.4.3. Anxiety and panic disorder.....	38
1.4.4. Addiction	38
1.4.5. Alzheimer's disease	40
1.4.6. Parkinson's disease	42
1.4.7. Epilepsy	44
2. Photopharmacology	46
2.1. Caged compounds.....	46
2.2. Photoswitches	50
2.2.1. Donor-Acceptor Stenhouse Adducts (DASAs)	51

2.2.2.	Diarylethenes (DAEs)	52
2.2.3.	Retinal	52
2.2.4.	Spiropyrans (SPs)	53
2.2.5.	Azobenzenes (ABs).....	54
2.2.5.1.	Azologization.....	58
2.2.6.	Indigoids and derivatives	59
2.2.6.1.	Indigo and analogs	59
2.2.6.2.	Hemiindigo.....	60
2.2.6.3.	Hemithioindigo (HTIs)	61
2.2.6.4.	Aurones or Hemioxiindigo	63

Results and discussion

3.	Caged compounds of NMDA receptor	68
3.1.	Design and synthesis of caged compounds	68
3.1.1.	Synthesis of the di-tert-butyl- <i>N</i> -DCAC-OH (9)	71
3.1.2.	Synthesis of the protected <i>N</i> -DCAC-D-serine (10) and <i>N</i> -DCAC-glycine (11).....	73
3.1.3.	Synthesis of the <i>N</i> -DCAC-D-serine (1), <i>N</i> -DCAC-glycine (2) and <i>N</i> -DCAC-OH (3).....	75
3.2.	Photophysical properties of caged compounds	77
3.3.	Pharmacological results	81
4.	Synthesis of XAP044 analogs to elucidate the binding mode in the Venus flytrap domain of mgGlu7 receptor.....	82
4.1.	Design and synthesis of XAP044 analogs.....	82
4.1.1.	Synthesis of constrained analogs of XAP044	87
4.1.2.	Synthesis of open analogs of XAP044.....	90
4.1.2.1.	Synthesis of the methoxy open analogs	91
4.1.2.2.	Synthesis of the hydroxyl open analogs	92
4.1.2.2.1.	SAR on the iodobenzene part	92
4.1.2.2.2.	Synthesis of dihydroxyl open analog and fluorine-hydroxyl open analogs	96
4.1.3.	Photoswitch analogs of XAP044	101
4.1.3.1.	Azobenzenes analogs	102
4.1.3.1.1.	Photophysical properties of Azobenzenes	104
4.1.3.2.	Phenylazoindole analogs	107
4.1.3.2.1.	Photophysical properties of Phenylazoindole analogs.....	108
4.1.3.3.	Aurones analogs.....	110
4.1.3.3.1.	Photophysical properties of Aurone analogs	113

4.1.3.4.	Chalcone analog	131
4.1.3.4.1.	Photophysical properties of Chalcone analog	132
4.2.	Pharmacological results	133
4.3.	Molecular modelling and binding mode validation	143
5.	Azologization of the 7TMD NAM VU6010608	149
5.1.	Design and synthesis of VU6010608 azologs	149
5.2.	Photophysical properties of VU6010608 azologs	151
5.3.	Pharmacological results	153
General conclusion and perspectives.....		155
Experimental part		159
General		160
General procedures		161
Chemistry.....		163
Molecular modelling.....		230
Bibliography		232

“We live in a physical world where some laws organize the matter, including living matter, and including our brain. Every synapse is the result of a story, the one of the communication activity between two neurons. And the astrocyte is the architect and director of this wonderful communication.”



Notre cerveau, Hervé Chneiweiss, 2019

Artwork “Neuron”, Alexey Kashpersky

1. GLUTAMATE IN CENTRAL NERVOUS SYSTEM

1.1. Glutamic acid and umami taste

Glutamic acid or glutamate is one of the twenty essential amino acid. It was discovered in 1866 by the German biochemist Karl Heinrich Leopold Ritthausen (**Figure 1**) while he was working on gliadin, a class of proteins present in wheat.¹ Later in 1908 Kikunae Ikeda, professor of the Tokyo Imperial University, found that glutamate was responsible for the particular taste of the broth from *kombu* seaweed. He understood that the taste of *kombu dashi* was distinct from the other four tastes already known (sweet, sour, bitter, and salty), this fifth taste was then named *umami*.²

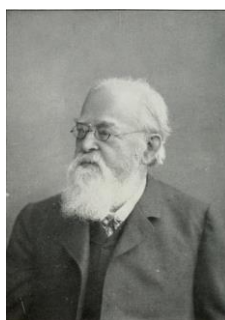
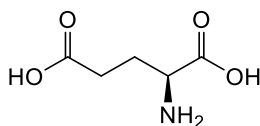


Figure 1. Glutamic acid discovered by Karl Heinrich Leopold Ritthausen.

Monosodium glutamate (MSG), the salt of glutamic acid, is present in different groups of foods as a flavour enhancer and is also used as food additive (E621). The Food and Drug Administration (FDA) declared it is safe to use in limited quantity while an abuse can lead to several potential side effects. Common examples of disorders involve cardiac, circulatory, gastrointestinal, muscular, and neurological problems.³

1.2. Glutamic acid as a neurotransmitter

Outside the community of research scientists, glutamate is probably best known for its taste properties as “monosodium glutamate”. However, the main reason for the ongoing worldwide interest on glutamate is that it is the major excitatory neurotransmitter in the brain.⁴ Before 1921 it was unclear if the synapse was working by bioelectrical or chemical signal but then Otto Loewi's experiments showed the chemical origin of the signal. Basically, in his experiment he dissected out of frogs, two beating hearts: first one with the vagus nerve which controlling heart rate attached, the other heart on its own. A saline solution was containing both hearts. Loewi made the first heart beat slower using an electrical stimulation of the vagus nerve, then he transferred some of the liquid immersing the first heart and put it to the second heart. He saw at this point that also the second heart was beating slower, showing that some soluble chemical released by the vagus

nerve was controlling the heart rate. The unknown chemical was the acetylcholine that was discovered and studied just years later. So Loewi called this substance Vagusstoff corresponding to the German word for substance. The experiment of Loewi was fundamental because it opened the way to understand that the action potential, as an electrical signalling event, causes the chemical release of neurotransmitter from synapses that is ultimately the effector on the tissue.⁵ The transmitter role of glutamate was not realized until the early 1980s for several reasons. First of all, glutamate is a neurotransmitter abundant in brain tissue and then it is involved in multiple metabolic pathways. Depending on the region, there is 5–15 mmol glutamate per kg in brain tissue, a high concentration compared to other amino acid.⁴ The glutamate concentration in plasma is higher than that in cerebrospinal fluid and this is due to the blood–brain barrier that prevent the entry of glutamate into the CNS. For this reason, the glutamate in the brain is mostly synthesized *de novo* by astrocytes. In astrocytes, there is a low concentration of glutamate because the enzyme glutamine synthetase converts glutamate to glutamine allowing the recycling of synaptically released glutamate. Glutamate and glutamine are fundamental in the synthesis of proteins and nucleic acids where also nitrogen is required. Glutamate is produced by the transamination of α -ketoglutarate, an intermediary in the citric-acid cycle, whereas glutamine is synthesized by incorporation of an ammonium ion into glutamate. These reactions are catalysed by glutamate dehydrogenase and glutamine synthetase, two enzymes present in almost all life forms. Starting from glutamate and glutamine different important molecules are biosynthesized as glutathione, polyamine, amino sugars, GABA, γ -aminobutyric acid (**Figure 2**).⁶

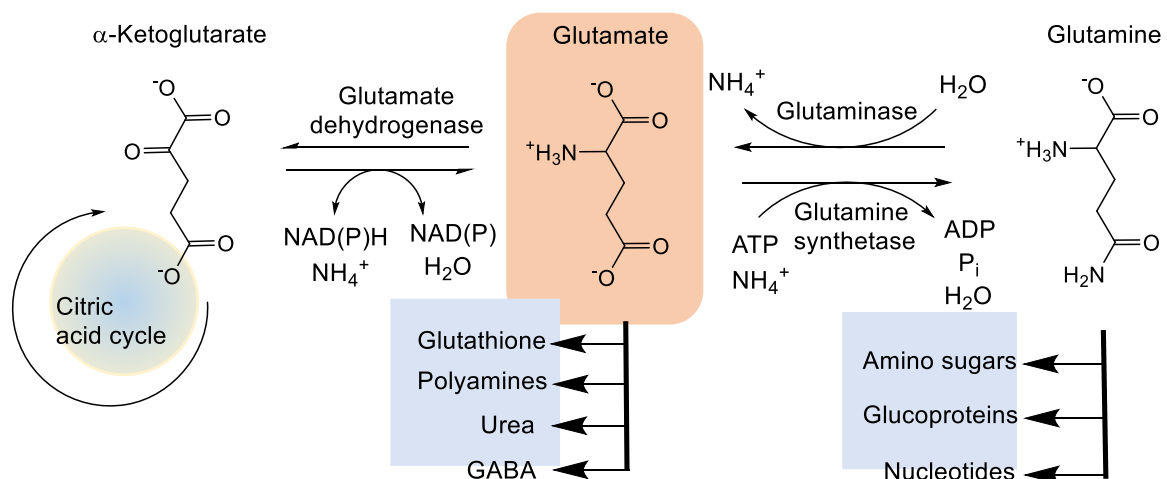


Figure 2. Glutamate as a metabolite.⁶

Glutamate needs to be at the right concentrations in the right places at the right time because it is not just the major mediator of excitatory signals but it is involved also in nervous system

plasticity and cell elimination. Cells are normally sensitive to glutamate and have energy enough to respond to stimulation, and then they remove glutamate with an appropriate rate from the right locations. An excessive release of glutamate due to an excessive activation of glutamate receptors can lead to cells death in a process called “excitotoxicity”. Not just an overactivation but also an underactivation of glutamate receptors is dangerous for cells functions so the right equilibrium is necessary.⁴

1.3. The glutamatergic synapse

Synaptic transmission represents the central process for neuronal communication and it works using neurotransmitters, signalling molecules, released by a presynaptic neuron to activate the receptors of a postsynaptic neuron. The transmission starts with intracellular vesicles loaded with neurotransmitters directed to the presynaptic membrane, then an action potential triggers exocytosis to allow the release of neurotransmitters to the synaptic cleft between the neurons and finally neurotransmitters can bind the receptors on the postsynaptic membrane to activate the signal transduction pathway. The exocytosis of the vesicles is caused by Ca^{2+} -triggered membrane fusion, where at a cellular level two initially separate lipid bilayers merge to form one interconnected structure. A conserved family of proteins called soluble N-ethylmaleimide-sensitive factor attachment protein receptors (SNAREs) are necessary in the process of membrane fusion. Neurotransmitters are released after the depolarization from the axonal terminal to the synaptic cleft in $<1\text{ms}$.⁷ In the case of the glutamatergic synapse (**Figure 3**),⁸ glutamate is stored in vesicles with a medium concentration of 100 mM. These vesicles are able to migrate to the synaptic space under the effect of an electric signal as described above. Then they release the glutamate that can activate two different types of receptors: the ionotropic glutamate receptors (iGluRs) and the metabotropic glutamate receptors (mGluRs). The reuptake of glutamate is also mediated by the excitatory amino acids transporters (EAAT) in the glial cells. Then glutamate is recycled in glutamine by the action of glutamine synthetase. Glutamine enters in the presynaptic neuron *via* the glutamine transporter then it is converted to glutamate by the action of the glutamate synthetase. The neurotransmitter is then stored again in the vesicles *via* the vesicular glutamate transporters (VGLUTs).

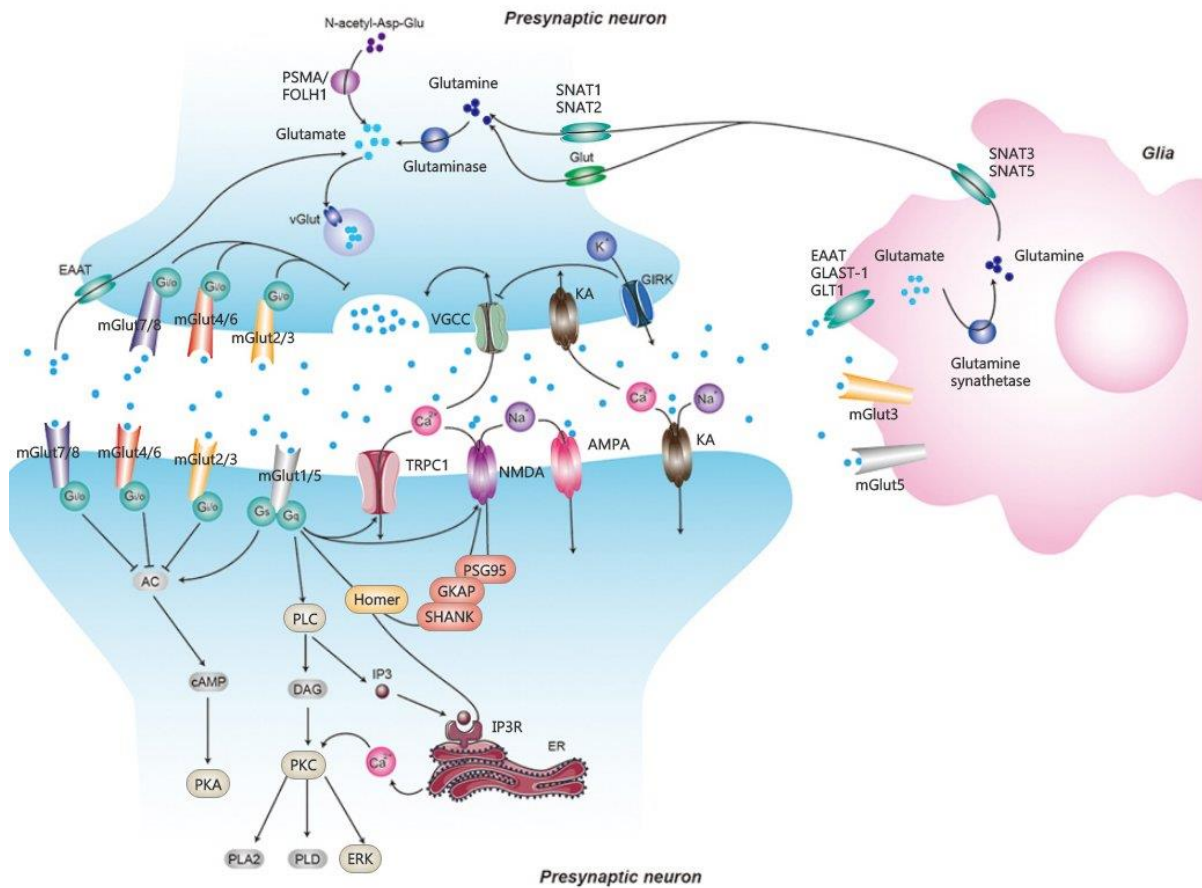


Figure 3. The glutamatergic synapse.⁸

1.3.1. The ionotropic glutamate receptors (iGluRs)

The ionotropic glutamate receptors were named after their selective agonists *i.e.* *N*-methyl-D-aspartate for NMDA receptors, (*S*)- α -amino-3-hydroxy-5-methylisoxazole-4-propionic acid for AMPA and kainate for kainate receptors⁹ (Figure 4). Ionotropic glutamate receptors are ligand gated ion channels formed by a central channel pore surrounded by four subunits. Distinct class of iGluRs have been identified based on these subunits and their pharmacological properties: subtypes GluN1, GluN2A-GluN2D, GluN3A, and GluN3B are present in NMDA receptors, GluA1-GluA4 in AMPA receptors, GluK1-GluK5 in Kainate receptors, GluD1 and GluD2 in δ receptors¹⁰ (Figure 5).

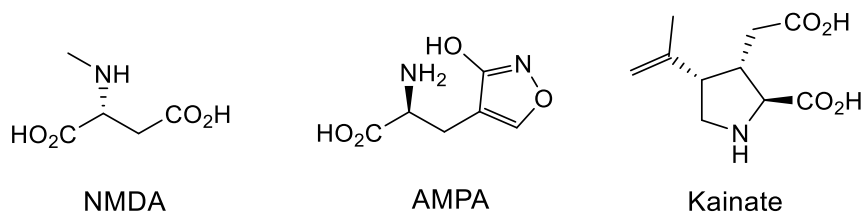


Figure 4. Selective agonists of ionotropic receptors.

The binding of glutamate activates iGluRs, opening the ion channel and giving fast relaying information. Functional receptors are formed only with a subunit composition within the same glutamate receptor class. In synaptic transmission the different classes play different roles to make this complex mechanisms work. All the iGluRs have similar structure in which the subunits are assembled in a "dimer-of-dimers" construction, and each subunit can be divided into four separate domains, an amino-terminal domain (ATD), a ligand-binding domain (LBD), a transmembrane domain (TMD) and C-terminal domain (CTD).¹¹

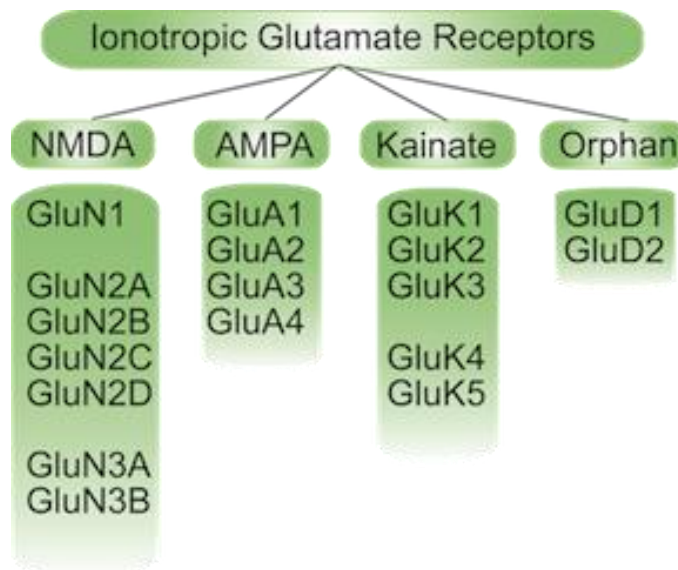


Figure 5. Distinct classes of iGluRs.¹²

Low-resolution (~40-20 Å) technique of electron microscopy was used to show the quaternary glutamate receptor structures.^{13,14} X-ray crystallography was used later to obtain the first high-resolution (3.6 Å) structure of an intact iGluR homotetramer, with a bound rat GluA2 antagonist.¹⁵ The crystal structure showed that iGluRs have a shape like the capital letter 'Y' and are formed of four semi-autonomous domains (>900 residues): the extracellular amino-terminal domain (ATD), the extracellular ligand-binding domain (LBD), the transmembrane domain (TMD), and the intracellular carboxyl-terminal domain (CTD) (**Figure 6**). The TMD is formed by three domains (M1, M3, and M4) and a cytoplasm-facing re-entrant membrane loop (M2), forming the ion channel (**Figure 6a**). In the extracellular region, the ATDs can be found at the 'top' of the receptor, while the LBDs are placed between the ion channel and the ATDs. ATDs and LBDs are ordered as dimers-of-dimers; however, the TMDs exhibit 4-fold symmetry (**Figure 6b**). Overall, the full-length receptor shows a 2-fold symmetry.^{10,12,16}

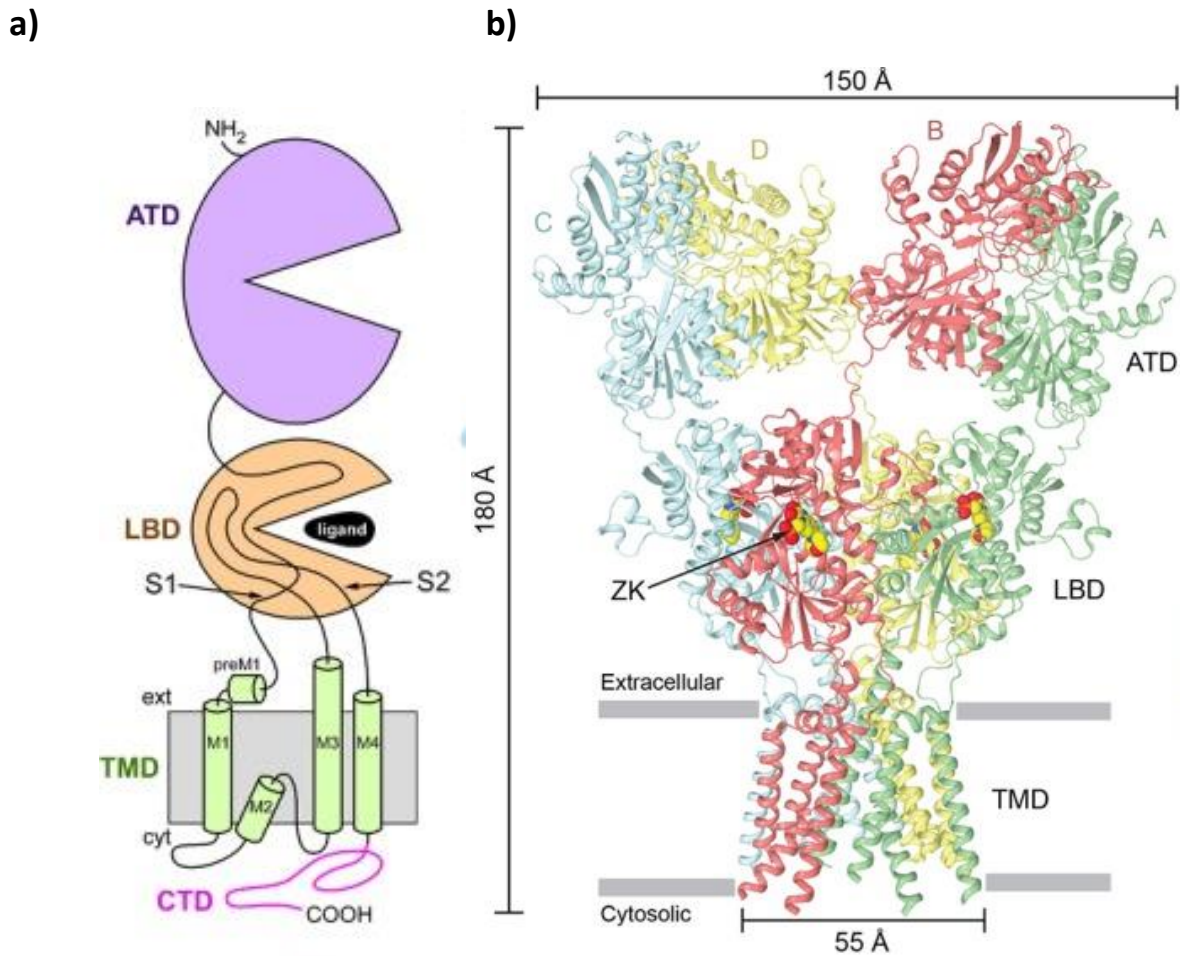


Figure 6. a) Structure of an iGluR subunit. **b)** Crystal structure of a homotetrameric AMPAR composed of GluA2 subunits in the closed, competitive antagonist ZK200775-bound state [Protein Data Bank (PDB) entry 3KG2] viewed parallel to the membrane. Each of the four GluA2 subunits is colored differently: green (A), red (B), blue (C), and yellow (D). ZK200775 molecules are shown as space-filling models.^{10,16}

Ionotropic receptor channel can be opened in response to the binding of ligands (agonists) to the extracellular domain of the channel. This allows the activation of the receptor. Then the agonist either dissociates from the receptor and the receptor can be deactivated returning to its resting state, or one or more additional conformational change of the agonist-bound receptor can occur leading to the decoupled action of agonist binding from receptor activation; so, the receptor is desensitized and cannot be activated by the agonist (**Figure 7**).¹⁷

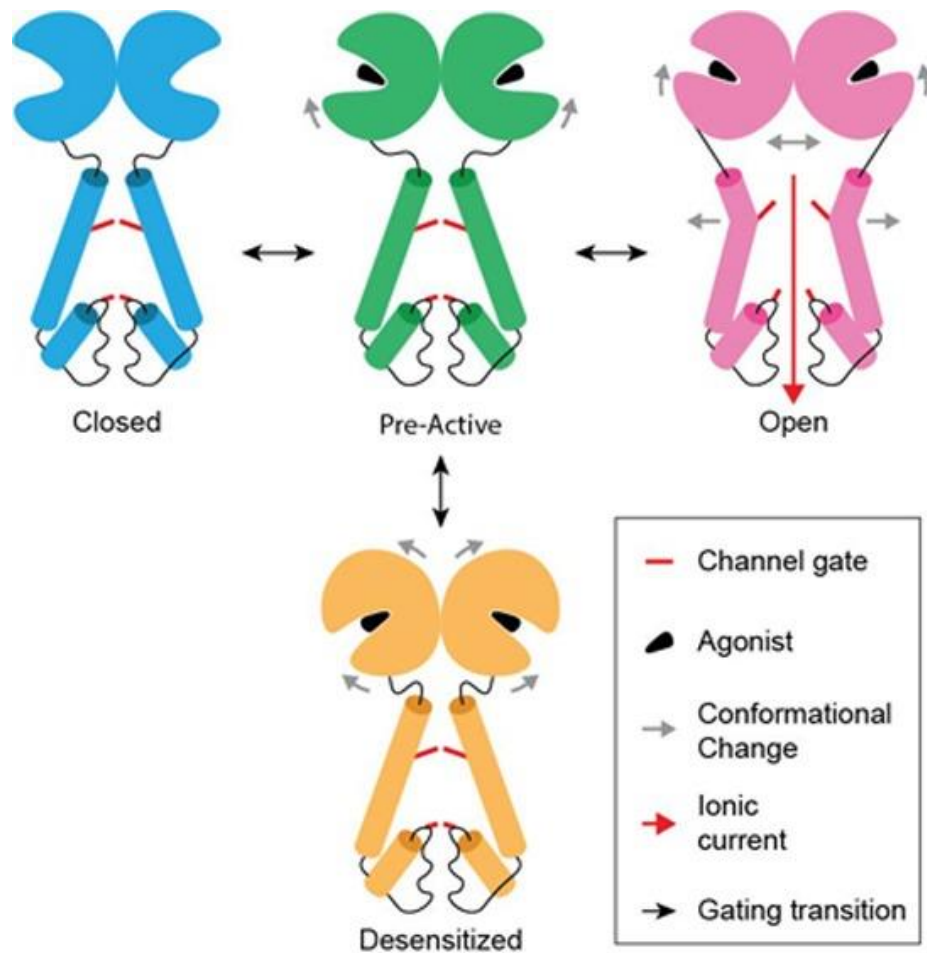


Figure 7. Gating of iGluRs.¹⁰

1.3.1.1. NMDA receptors

NMDARs are one of the three-ionotropic glutamate receptors. They are composed of heterotetramers formed by two NR1 and two NR2 or NR3 subunits. A transmembrane domain, an N terminal domain in the extracellular space (NTD) and an internal C terminal domain form each subunit. The channel pore that can open following the binding of the agonist, is formed by the loops of the four subunits. NMDARs need to be activated by the binding of an agonist like glutamate or NMDA¹⁸ and a co-agonist, like glycine¹⁹ or D-Serine²⁰ (Figure 8).²¹ Agonist are able to bind in the extracellular part of the NR2 subunit while the co-agonist binds the extracellular part of the NR1 or NR3 subunits.²² NMDAR are permeable to different ions as potassium and sodium²³ but especially they show a high permeability for calcium.²⁴ When activated the ion channel of NMDA receptors opens with a combined reversal potential near 0 mV. Ligand binding is responsible for the current flow through the ion channel that is voltage dependent. Extracellular magnesium (Mg^{2+}) and zinc (Zn^{2+}) ions are able to bind to specific sites on the receptor so the

passage of other cations through the open ion channel is blocked. Ca^{2+} flux in NMDARs has a role in synaptic plasticity, involved in learning and memory functions.¹⁸

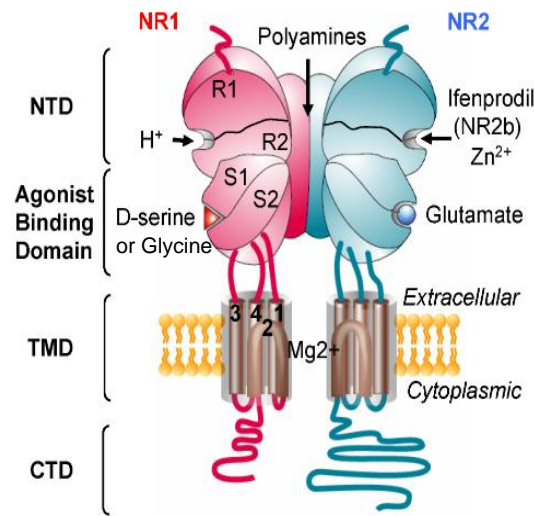


Figure 8. Schematic representation of NMDA receptor.²¹

Pharmacologically several ligands can modulate the activity NMDARs. There are agonists able to interact with the glutamate binding site of NR2 such as NMDA, tetrazolylglycine, (2*S*,1'*R*,2'*S*)-CGG, *trans*-ABCD, (1*R*,3*R*)-ACPD and homoquinolinic acid; but also agonists or partial agonist able to interact with the glycine binding site on NR1 such as D-serine, (*R*)-HA-966, L-687,414, ACPC, ACBC (**Figure 9**). On the other hand, among the antagonists there are D- α -aminoadipate, D-AP5, D-AP7, CPG 37849, CGS 19755, PMPA, CPP, CPP-ene, LY235959, (I), SCZ-EAB-515, NPC 17742, ACPEB, NVP-AAM007, PBPD, PPDA and UBP141 targeted to the glutamate binding site (**Figure 10**); and CNQX, DNQX, ACEA-1021, kynurenic acid, 5,7-dichlorokynurenic acid, L-689,344, L-689,560, [³H] CGP 61594, GV 150526, GV 196771A, L-701,324 and (II) targeted to the glycine binding site (**Figure 11**). Another class of antagonists target the ion permeating channel that represents a binding site for channel blockers as phencyclidine, ketamine, MK-801 and memantine (**Figure 12**).²⁵ This last class of compounds received a major attention due to new application of some of these molecules and the therapeutic potential they can offer. Phencyclidine (PCP), also called as angel dust or zombie drug among other names, is a dissociative anesthetic known as hallucinogen drug used for its mind-altering effects.²⁶ PCP was first synthesized in 1926 and commercialized as an anaesthetic medication in the 1950s-until 1965 when it was retrieved from the market due to the high side effects.^{27,28,29,30}

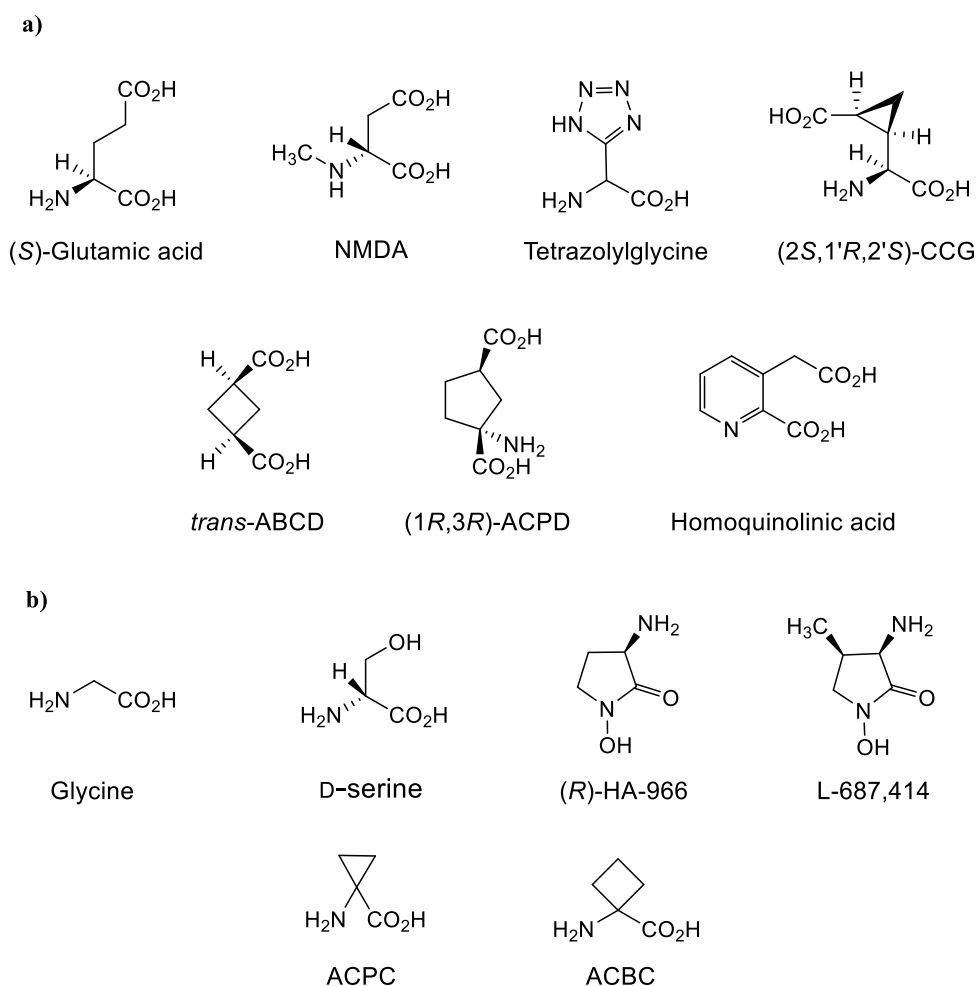


Figure 9. a) Agonists targeted to the glutamate binding site **b)** Agonists targeted to the glycine binding site.

The PCP was replaced by ketamine discovered in 1962 and approved for human use in the United States in 1970.³¹ Ketamine is also a dissociative anaesthetic, which provide an excellent analgesia with a safety profile, so less dangerous compared to PCP. Ketamine is an arylcycloalkylamine existing as *S*(+) and *R*(-) isomers and on the market, it can be found as a racemic mixture of the two. As already said, ketamine shows less side effects compared to PCP but remains a hallucinogen with psychedelic effects that limits it as a popular recreational drug. Especially at lower doses, users can experience mild dissociation with hallucinations and a distortion of time and space. Higher doses induce schizophrenia-like symptoms and body dissociation. Considering its action on CNS modulation, ketamine should be used paying attention to the combination with alcohol, opioids, benzodiazepines and cannabis.^{32,33} Recently an increased interest in ketamine was due to the discovery of its antidepressant effect in major depression that opens new perspectives in drug discovery of NMDA channels blockers for this therapeutic use.

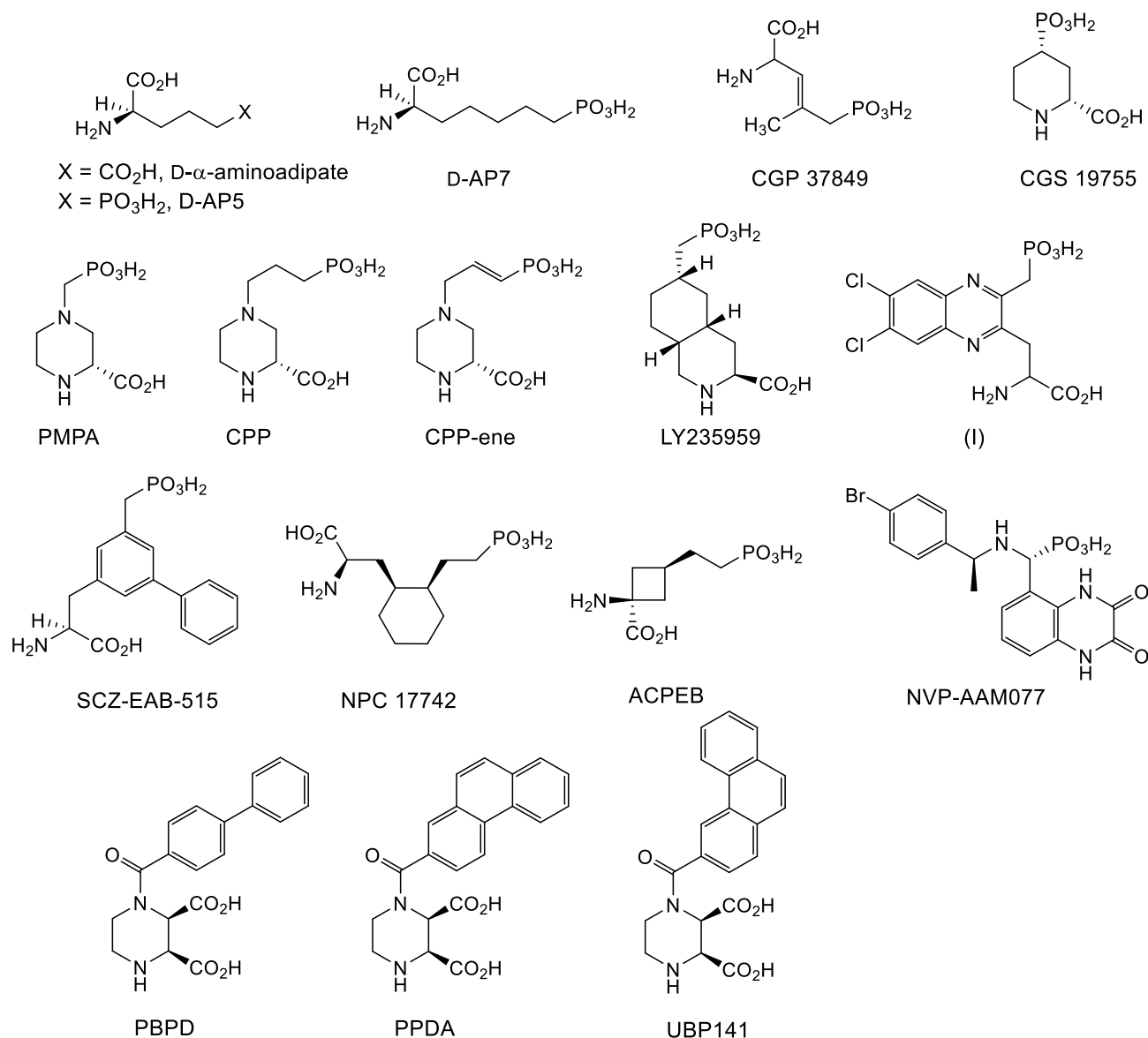


Figure 10. Antagonists targeted to the glutamate binding site.

In fact, most common prescribed drugs for depression are inhibitors of monoaminooxidase (IMAO) and inhibitors of the reuptake of serotonin (SSRI). So this is an opportunity to focus on a drug discovery research on a class of molecules able to reach the same therapeutic effects yet acting with a different pharmacological mechanism.³⁴ MK-801 or dizocilpine is a dissociative anaesthetic with anticonvulsant activity able to induce schizophrenia in animal.^{35,36} Memantine was synthesized in 1968 by Eli Lilly and at the beginning the purpose was to use it as an anti-diabetic agent, but it had no effect in lowering blood sugar, despite its real activity on CNS. Today memantine is an approved drug for Alzheimer's disease treatment even if it less preferred compared to acetylcholinesterase inhibitors (AChEi).³⁷ Allosteric modulation on NMDA receptor is mediated by the action of polyamines able to increase glycine affinity and thus increase NMDAR

responses. Some allosteric modulators are NR2B selective and the compound Ifenprodil is part of this class.²⁵

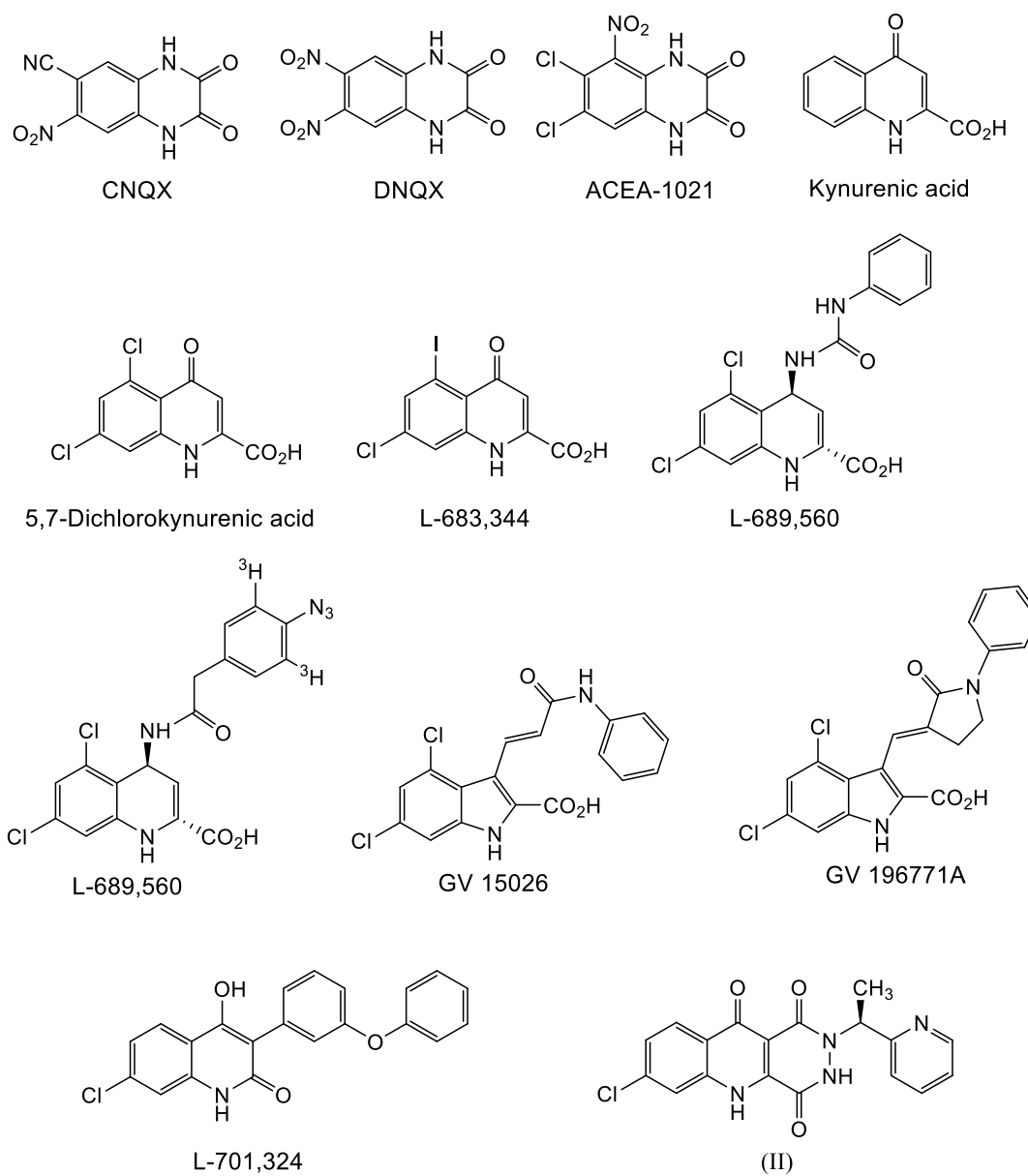


Figure 11. Antagonists targeted to glycine binding site.

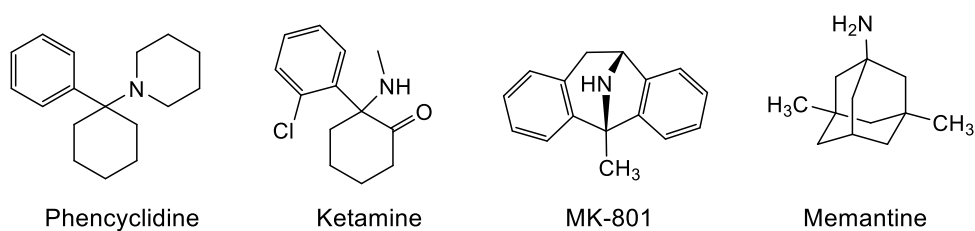


Figure 12. Antagonists acting as channel blockers.

1.3.1.2. AMPA receptors

AMPA receptors have high affinity for the artificial glutamate analogue AMPA, they are homo- or hetero-oligomers composed of the subunits GluA1-GluA4. Their heterotetrameric structure is formed by GluA2 in combination with either GluA1, GluA3 or GluA4. AMPARs, as already seen for NMDARs, play a role in fast excitatory synaptic signalling in the brain and in synaptic plasticity involved in learning and memory.³⁸ AMPAR characteristics are based on its subunit composition and among all the subunits especially GluA2 has a fundamental role on the biophysical properties of the resulting heteromeric complexes.³⁹ In fact in presence of GluA2 within the AMPAR, the Ca^{2+} permeability decreases while in presence of combinations of GluA1, GluA3, and GluA4, the AMPARs are highly permeable to Ca^{2+} as well as K^+ and Na^+ ions.⁴⁰ AMPARs are mostly Ca^{2+} -impermeable as they are mostly formed by hetero-oligomers consisting of GluA1/GluA2 or GluA2/GluA3 subunits.⁴¹

1.3.1.3. Kainate receptors

KARs can be activated selectively by the agonist kainate, they are homo- or hetero-oligomers of the subunits GluK1-GluK5 (GluR5-GluR7, KA1 and KA2). Among these, GluK1-3 are involved in the formation of homomeric or heteromeric receptors, while GluK4 and GluK5 can form only heteromeric receptors with the collaboration of the GluK1-3 subunits.⁴² KARs are present almost everywhere in the brain and as the other ionotropic glutamate receptors, they have a fundamental role in synaptic transmission and neuronal excitability. The understanding of the KARs has been complicated due to the lack of selective agonists or antagonists not common with AMPAR.⁴³ However, the GluK1 subunit has been studied for the development of selective pharmacological agents; that have been synthesized from structurally diverse scaffolds, like synthetic decahydroisoquinolines as well as the natural products willardiine and dysiherbaine.⁴⁴ Furthermore the discovery of 2,3-benzodiazepines, such as GYKI 53655 and GYKI 52466, able to antagonize AMPARs but not KARs,⁴⁵ made possible to better study separately the two receptors. KARs are involved in different neurological conditions, as chronic pain, epilepsy and migraine, so they represent an important target for the development of therapeutics, especially KAR antagonists.⁴⁶

1.3.2. The metabotropic glutamate receptors (mGluRs)

The discovery and the studies related to mGluRs started around mid eighties when it became clear that the glutamate-mediated neurotransmission is more complex and not related just to iGluR as ionotropic channel are not related to phospholipase C (PLC) stimulation.^{47,48} These data led to understand that glutamate activates also second messenger systems through coupling with G-proteins in addition to the activation of ionotropic receptors. G protein coupled receptors (GPCRs) are transmembrane proteins sharing a motif of seven transmembrane α -helices. They are important to transduce the external stimulus to the inside of the cell. There are five different family of GPCRs and mGluRs belong to the C family (**Figure 13**).⁴⁹

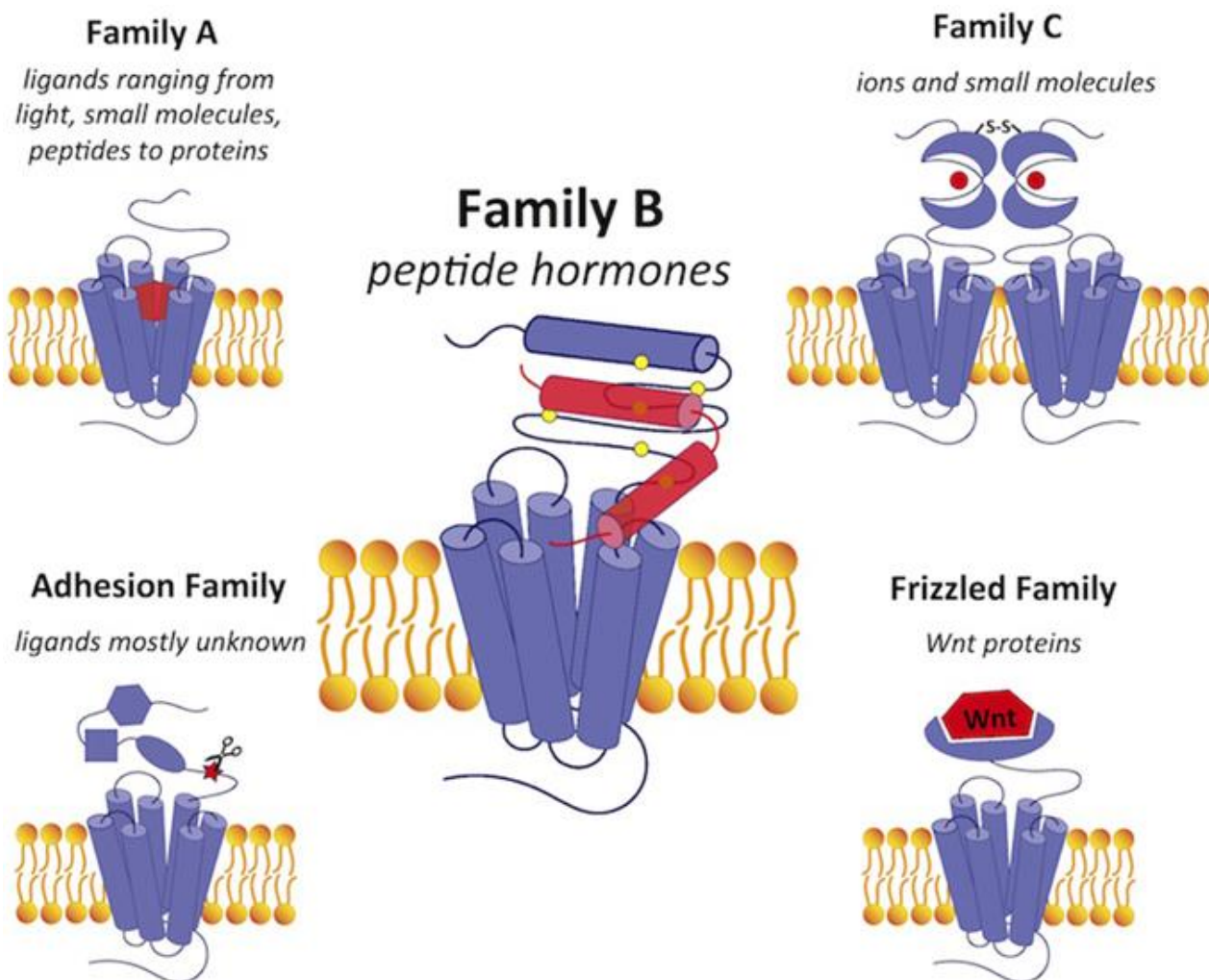


Figure 13. Families of G protein coupled receptors (GPCRs). Metabotropic Glutamate receptors belong to family C of GPCRs.⁴⁹

Metabotropic glutamate receptors have been classified in three groups based on their primary sequence transduction mechanism and pharmacological properties: group I (mGlu1 and 5), group II (mGlu2 and 3) and group III (mGlu4, 6, 7 and 8). The group I receptors activate the

phospholipase C while the group II and III receptors are negatively coupled to adenylyl cyclase, so their activation can inhibit forskolin-stimulated cyclic AMP formation (**Figure 14**).

	Receptor	Transduction mechanism	Prototypic agonists
Group I	mGlu ₁ mGlu ₃	activation of PLC	quisqualate 3,5-DHPG
Group II	mGlu ₂ mGlu ₃	inhibition of adenylate cyclase	DCG-IV 2R,4R-APDC LY354740 LY379268
Group III	mGlu ₄ mGlu ₆ mGlu ₇ mGlu ₈	inhibition of adenylate cyclase	L-AP4 L-AP4 (RS)PPG

Figure 14. Classification of mGlu receptors.

mGluRs have a great potential as pharmacotherapeutic targets due to the characteristics that distinguish them from iGluRs. In fact, unlike the iGlu receptors that mediate fast synaptic neurotransmission, the activation of mGlu receptors acts on the neuronal activity in a similar way as other neurotransmitters such as dopamine and serotonin, which have been highly studied to discover psychoactive molecules for treatment of most psychiatric and neurological disorders.^{50,51} The distribution of these receptors is highly diverse and heterogeneous, so among the eight mGluR subgroups there are different localizations preferred at regional and cellular levels (**Figure 15**).⁵² Furthermore, the different subgroups of mGluRs are found on postsynaptic, presynaptic membranes as well as glial cells. Receptors of group I are mostly localized at the level of the somatodendritic domains postsynaptically, while group II and III receptors are found in axonal terminals and domains at a presynaptic level. All mGluRs are placed far from the release site, especially mGlu2 and mGlu3. mGlu7 receptors represent an exception as they are located close to the release site at the presynaptic terminal. Thus, the main advantage of targeting mGluRs is related to the heterogeneous distribution of the different groups that can lead to selective modification of glutamate neurotransmission based also on the functional and anatomical properties of each subtype despite of targeting iGluRs with a less precise excitation or inhibition of fast synaptic neurotransmission.⁵³

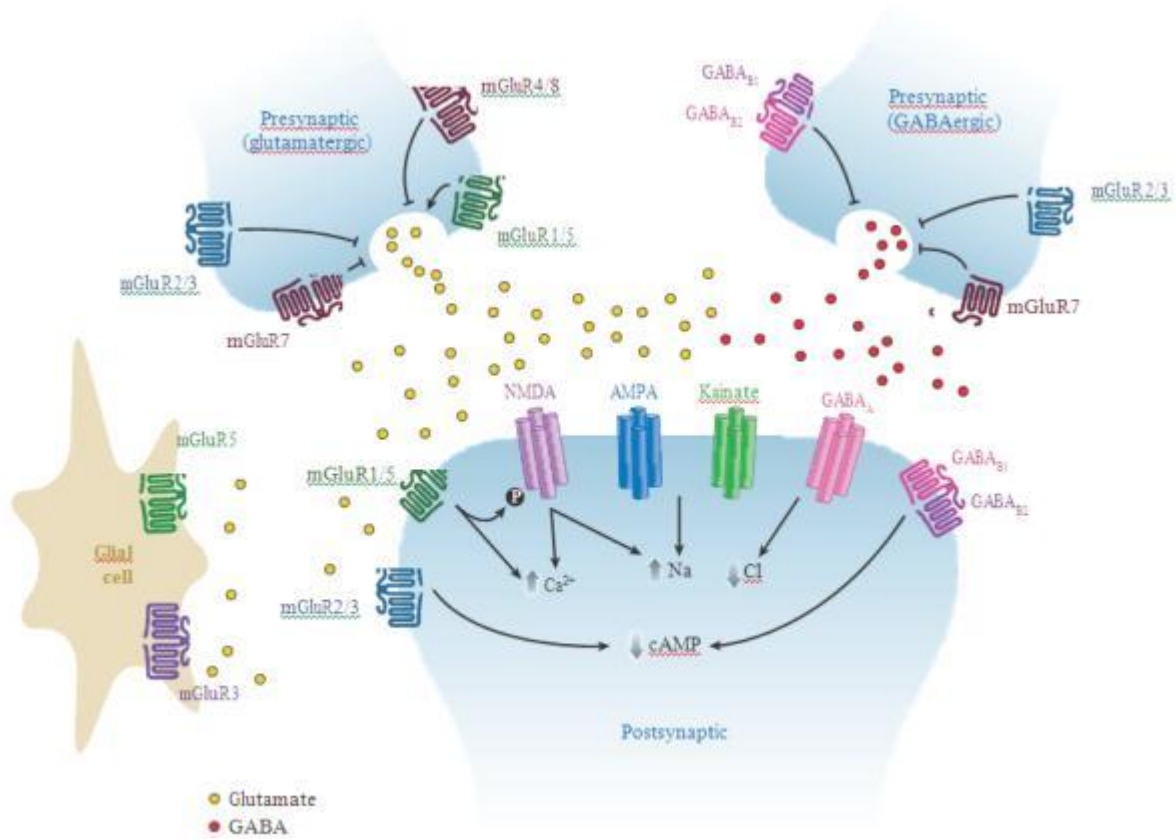


Figure 15. Distribution of different mGluRs subtype at the synapse and on glial cells.⁵²

mGluRs, as mentioned before, are G protein coupled receptors (GPCR) of the C family so they act as a dimer that activates a transduction pathway mediated by G protein activation. GABA_B receptor, the calcium-sensing receptor, and some taste and pheromone receptors belong also to family C of G-protein coupled receptors. The family C GPCR protomer has an extracellular part able to recognize a specific ligand molecule. In the case of mGluRs, the specific ligand molecule is L-glutamate (Glu), the principal excitatory neurotransmitter in the central nerve system. An mGluR protomer is formed by three mainly different parts: the extracellular domain, the 7 transmembrane (TM) domain and the intracellular region. The extracellular domain can be also divided into two parts: the N-terminal ligand binding region, known also as the “Venus flytrap domain” (VFTD) and the cysteine-rich (CR) domain, which connects the ligand-binding domain and the 7TM region.⁵⁴ The VFTD is an additional site present in family C of GPCRs but not in the A family. So in the A family the orthosteric site of ligand binding is located in the 7TM domain where it is possible to find also an allosteric binding site while in the C family the orthosteric site is located in the VFTD and 7TM domain is preferred for allosteric modulation^{55,56} (**Figure 16**).⁵⁷

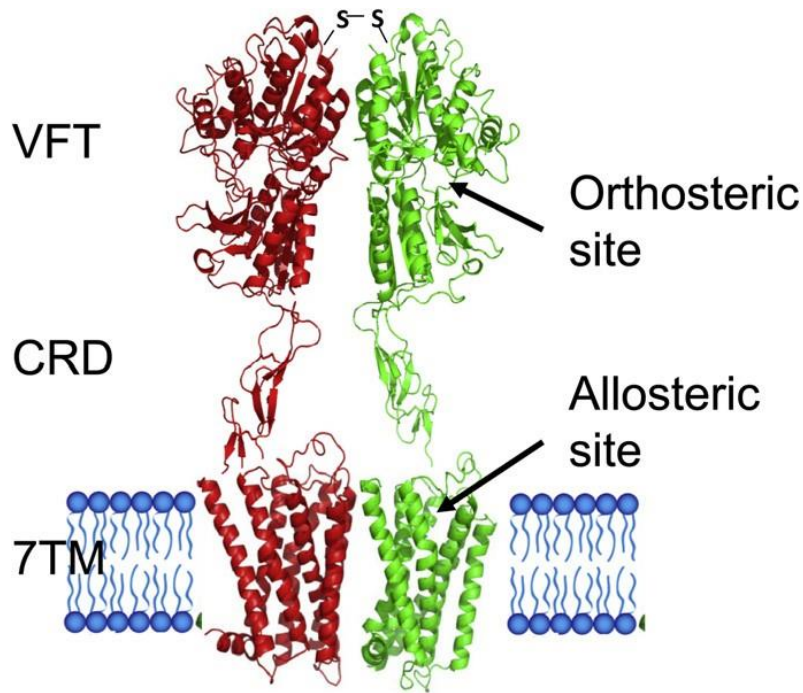


Figure 16. General structure of a dimeric mGlu receptor. Each subunit is composed of a venus flytrap domain (VFTD) linked through a cysteine-rich domain (CRD) to a 7 transmembrane helix domain (7TM). The disulfide bond covalently linking the two subunits is shown on top of the VFTDs (SeS).⁵⁷

For a long time, it was thought that mGluRs can form only homodimers while now it is clear that they can form also heterodimers.⁵⁸ For the activation of family C GPCRs, the closure and stabilisation of the VFTD of the dimer is necessary. In particular the cysteine rich domain has an important role as it connects the VFTD and the 7TMD so it transmit the signal of transduction from the VFTD to the 7TMD having a role in allosteric modulation. The binding of the orthosteric ligands in the VFTD promotes the closure of the two lobes so the signal goes through the cysteine rich domains and it produces conformational changes in the 7TMD that activate the transductional pathways of protein G (**Figure 17**).^{59,60} Since the publication of the full dimer structure and the studies from JP Pin, it was explained how the VFTD and TMD communicate. The rotation of the TMD brings the TM6s in contact but an mGluR without its VFTD or cysteine domain can be still activated by PAMs.^{61,62,63} The activation time window is of almost 50 ms between the binding of the orthosteric ligand and the formation of the active receptor according to site directed mutagenesis data and FRET studies.⁶⁴

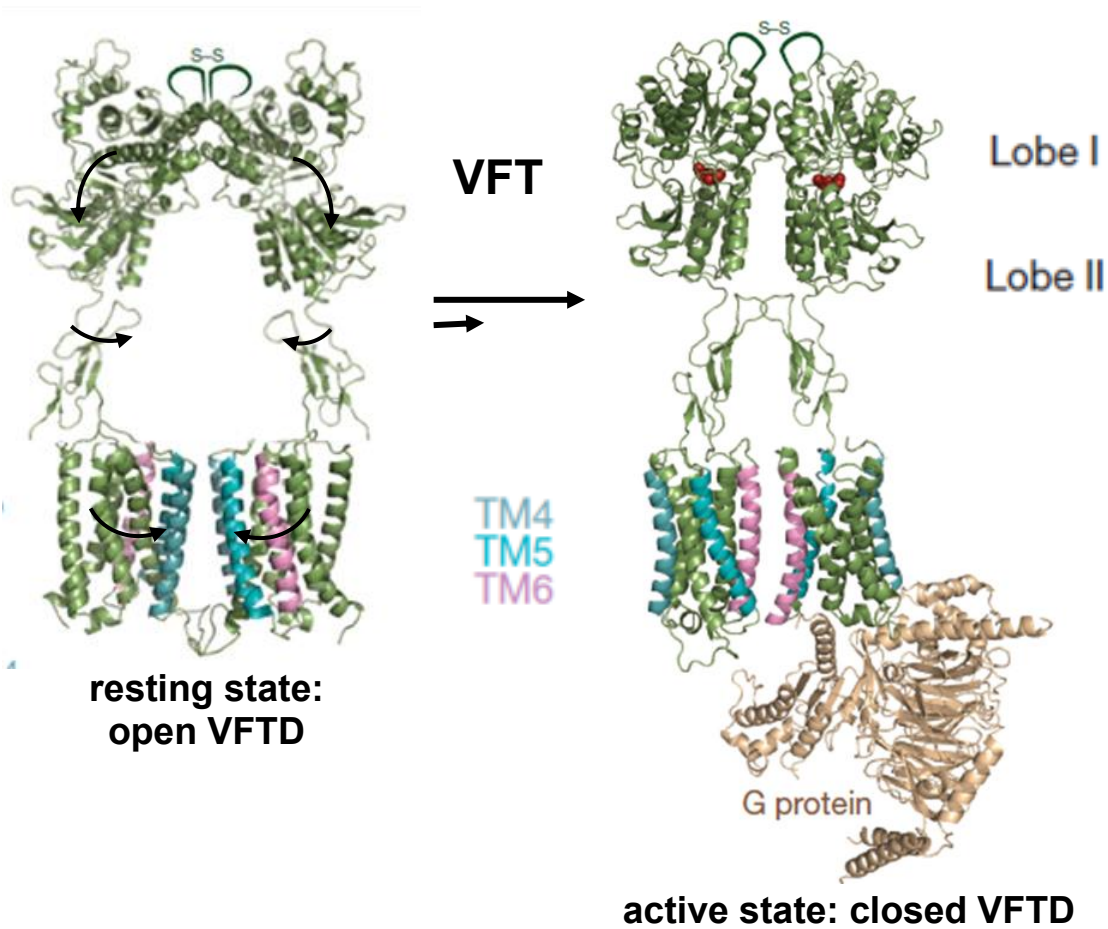


Figure 17. Activation mechanism of mGluR. The dimer activation brings the two TM6 close.⁵⁹

The three groups of mGluRs will be described in the following paragraphs. Group I and group II will be briefly described with no description of the pharmacology while the focus will be on all the aspects of Group III receptors.

1.3.2.1. Group I of mGluRs

Group I mGluRs involves mGlu1 and mGlu5 receptors. Group I mGluRs are able to activate the Gαq/11 proteins leading to a stimulus of PLCβ, resulting in the cleavage of phosphatidylinositol-4,5-bisphosphate with the subsequent formation of the intracellular second messengers, inositol-1,4,5- trisphosphate (IP3), and diacylglycerol. Group I mGluRs can activate also different signaling pathways downstream of Gαq/11 as well as from Gαs and Gαi/o, and other molecules independent of G-protein.⁵² The stimulation of group I mGluRs, depending on the neuronal populations, can activate several protein kinase pathways, including cAMP dependent protein kinase (PKA), Ca²⁺ calmodulin dependent protein kinases (CaMKs), mitogen-activated protein

kinases (MAPKs), phosphoinositide 3-kinase (PI3K), mammalian target of rapamycin (mTOR), p70 S6 kinase, casein kinase 1, and cyclin-dependent protein kinase 5. The stimulation of the receptors allows Ca^{2+} release from intracellular calcium stores by IP3 and Ca^{2+} influx from L-VDCCs during the depolarization of the membrane. Ca^{2+} -calmodulin (CaM) dependent pathways is activated by the postsynaptic increase of Ca^{2+} so, AC1 and CaMKIV are activated. AC1 allows the generation of cAMP that activates PKA. PKA and CaMKIV phosphorylate CREB. ERK1/2 and p38 MAPK are stimulated by G-protein release after mGlu1/5 receptor activation through the mitogen-activated protein kinase kinases MKK/MEK. JNK can be stimulated by transactivation of EGFR by group I mGluRs. PI3K is also initiated by group I mGluR activation. Stimulation of ERK1/2, p38 MAPK, JNK, and PI3K leads to activation of the transcription factors Elk-1, CREB, activator protein-1 (AP-1), c-Jun, and other NF- κ B members such as c-Rel through RSK1 and mitogen and MSK1. The upregulation of the targets such as FMRP, ARC, c-fos, Egr1, and BDNF by these transcriptional factors, could contribute to the modulation of synaptic plasticity in the forms of LTP and LTD (**Figure 18**).⁶⁵ All these pathways are important and fundamental for the modulation of synaptic plasticity by group I mGluRs.^{65,66} mGlu1R are considered involved in neuronal hyperexcitability in the anterior cingulate cortex, considered one of the most important changes connected to the chronification of neuropathic pain.⁶⁷ Two different transmembrane mGlu1R isoforms are present at cerebellar synapses, mGlu1 α R and mGlu1 β R.⁶⁸ mGluR1 is also widely expressed in Purkinje cells (PCs) of the cerebellar cortex where it is indispensable for the formation of eyeblink memory.⁶⁹ The antagonism of mGlu1R reduces the effects of drug abuse especially for cocaine as it inhibits de novo protein synthesis providing a mechanism for the reduction in cocaine-induced conditioned place preference.⁷⁰ mGlu5R is implicated in resilience and stress responses connected to performance in behavioural paradigms that depend on cognitive flexibility. A characterization of cognitive flexibility in mGlu5R knockout (KO) mice conducted with a rodent touchscreen cognitive assessment apparatus showed that the animals knockout of the receptor experience significantly less stress.⁷¹ Concerning drug addiction, it was proven that mGlu5R antagonism inhibits cocaine reinforcement and relapse using the elevation of extracellular glutamate in the nucleus accumbens.⁷² mGlu5R plays a role also in epilepsy as it is consistently observed in resected tissue from patients with epilepsy and is equally prevalent in animal models of epilepsy.⁷³ The group I ligand will be not described in the details but they showed interest as potential therapeutic for addiction⁷⁴ and in parkinsonian muscle rigidity.⁷⁵

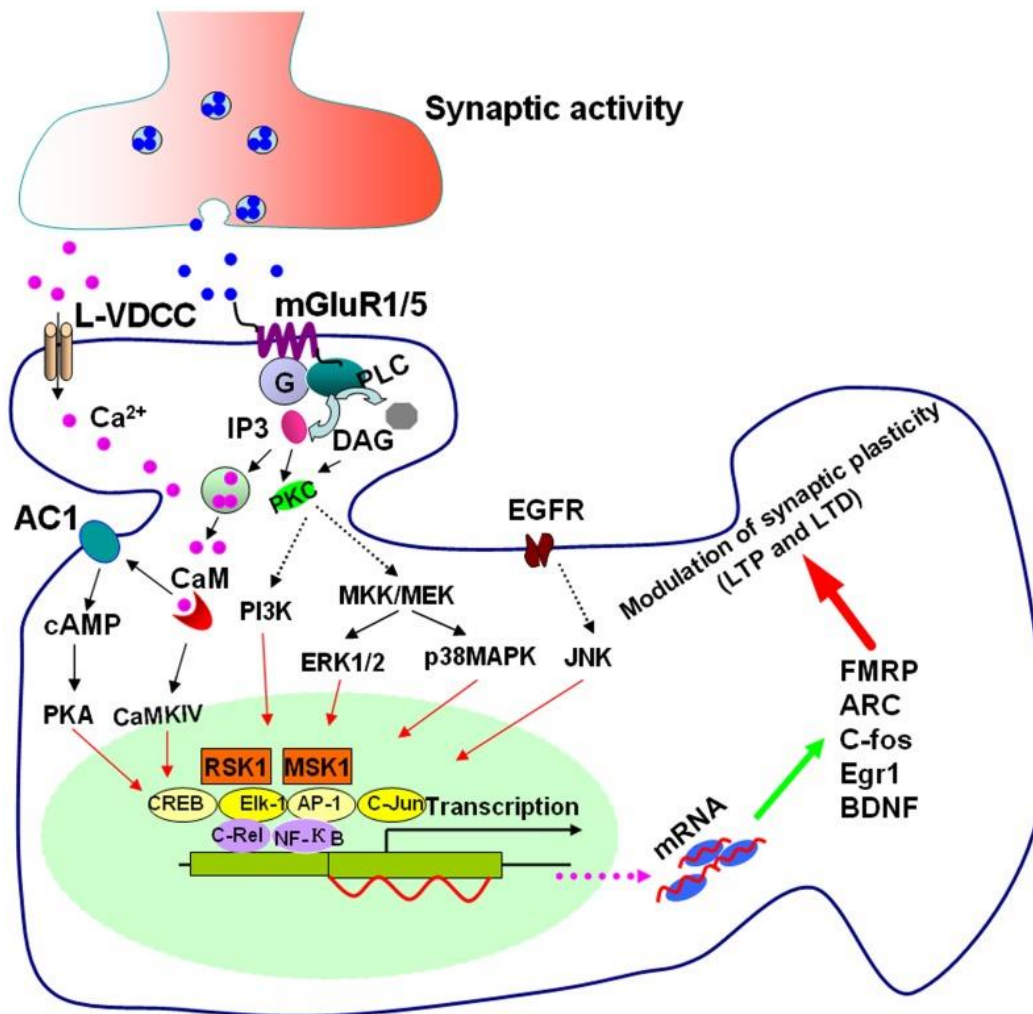


Figure 18. Transductional pathways of Group I mGluRs.⁶⁵

1.3.2.2. Group II of mGluRs

Group II involves mGlu2R and mGlu3R that are Gi/o coupled and lead to the inhibition of adenylyl cyclase and voltage-dependent calcium channels, while promoting the activation of voltage-dependent potassium channels. They act as autoreceptor on the preterminal region away from the active zone of the synapse.⁶⁶ In fact, they are placed on the pre-synaptic membrane far from the synaptic cleft, so they need for their activation a substantial synaptic glutamate release.⁷⁶ Group II mGluRs are found almost everywhere in nervous system, especially in regions and circuits involved in pain perception and nociceptive signaling but also in emotional processing. It seems that mGlu2R and mGlu3R can be found also post-synaptically, mGlu2R is present exclusively on neurons while mGlu3R can be found also on glia cells.⁷⁷ Group II mGluRs can interact with other mGluRs subtype, an example is mGlu2R that can form a heterodimeric complex with mGlu4R that is related to the efficacy of mGlu2R and mGlu4R allosteric modulators.^{61,78} Group II mGluRs are a

target of interest for drug discovery as they are involved in amyotrophic lateral sclerosis, schizophrenia, depression, anxiety, drug addiction, Parkinson's disease,⁵² and pain states.⁷⁹ mGlu2R and mGlu3R, when postsynaptic, are involved in the regulation of NMDAR function. In fact, NMDAR are also implicated in the etiology of schizophrenia so the activation of mGlu2/3 receptors significantly decrease the ratio of AMPA-to-NMDA excitatory postsynaptic currents at Schaffer Collateral-CA1 synapses and enhanced the peak of NMDA-evoked currents in acutely isolated CA1 neurons. Regulation of NMDARs by Gai/o-coupled *via* mGlu2/3 receptors activates Src kinase and potentiates GluN2A-containing NMDAR currents. This is a fundamental mechanism to correct the hypoglutamatergic state found in schizophrenia.⁸⁰ LY341495 (**Figure 19**) is a potent and selective antagonist of the group II of mGluR, mGlu2R and mGlu3R (IC_{50} s = 21 and 14 nM, respectively, for human isoforms). It also blocks less effectively mGlu8R and mGlu7R (IC_{50} s = 173 and 990 nM, respectively) and weakly antagonizes mGlu1R, mGlu5R, and mGlu4R (IC_{50} s = 6.8, 8.2, and 22 μ M, respectively).⁸¹ It was shown to enhance the antidepressant effects of ketamine in the forced swim test in rats⁸² and this mechanism is connected also with dopaminergic transmission.⁸³ The compound, as already said, selectively inhibit mGlu2R over mGlu4R, while the glutamate potency of mGlu2R is about 10-fold higher than mGlu4R when applied alone. In presence of LY341495 the selectivity of glutamate for mGlu2R *versus* mGlu4R is lost.⁸⁴ LY-404,039 (pomaglumetad) is an agonist of mGluRs conceived as a treatment for schizophrenia and psychotic disorders by the modulation of glutamatergic activity.⁸⁵ LY-2140023, a prodrug of LY-404,039, was synthesized due to its poor oral bioavailability⁸⁶ and clinical trials on this compound for schizophrenia were stopped after phase II study as it did not meet its primary endpoint.⁸⁷

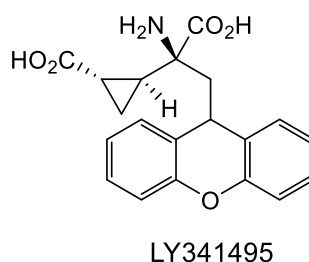


Figure 19. Structure of the selective antagonist LY341495.

1.3.2.3. Groupe III of mGluRs

Group III mGluRs includes mGlu4R, mGlu6R, mGlu7R and mGlu8R subtypes. They function the same way as groupe II mGluRs suppressing neuronal excitability by inhibiting adenylate cyclase and they are mostly expressed presynaptically except mGlu6R. mGlu4 and mGlu7 receptors are

found almost everywhere in the brain,⁸⁸ mGlu6 receptors are found specifically in the retina⁸⁹ and mGlu8 receptors are distributed at low concentrations in the hippocampus, hypothalamus and olfactory bulb.⁸⁸ Group III mGlu receptors can be activated by different orthosteric agonists such as L-(+)-2-amino-4-phosphonobutyric acid (L-AP4) leading to a reduction in glutamate release.⁹⁰ In fact, these receptors play a role when there is an excess of glutamate accumulation in the extracellular space and act as autoreceptor to inhibit the release of additional glutamate at the synapse level.⁹¹ Presynaptic group III mGlu receptors have a major role in physiopathological conditions where there is massive glutamate release, such as epilepsy⁹² or ischemia.⁹³ Group III mGlu receptor agonists showed also anxiolytic- and antidepressant-like effects after central administration in rats⁹⁴ but a study with the mGlu4R agonist LSP1-2111 showed anxiolytic but not antidepressant effect.⁹⁵ The activation of these receptors can inhibit an excessive release of glutamate preventing the activation of postsynaptic receptors and thus avoiding excitotoxicity. mGlu4R is involved in several neurological disorders such as Parkinson's disease, autism and cerebellar ataxia.⁹⁶ mGlu4R plays also a role in pain, mood and anxiety disorders.⁸⁸ Among the group III mGluRs, the mGlu6R subtype has been the less investigated as it is predominantly expressed in the outer part of the inner nuclear layer of rat retina, containing ON-bipolar cells.⁹⁷ This indicates that the development of drugs acting on other subtypes can have important side effects on vision. mGlu6R is involved in night vision and agonist of mGlu6R may be beneficial for some patients with night vision pathologies.⁹⁸ On the opposite, mGlu7R is an interesting target for drug discovery as it is implicated in anxiety,⁹⁹ depression,¹⁰⁰ pain,¹⁰¹ addiction,^{102,103,104} schizophrenia,⁷⁶ epilepsy,¹⁰⁵ Parkinson,¹⁰⁶ and Alzheimer's disease.¹⁰⁷ mGlu8R is related to anxiety as shown in a study on mice deficient for mGlu8 receptor¹⁰⁸ but also in the modulation of chronic pain.¹⁰⁹

1.3.2.3.1. Agonists and antagonists of Group III mGluRs

Several orthosteric agonists and antagonists of group III mGluRs are known (**Figure 20** and **Figure 21**). Most of them are group-III but not subtype selective while a few are selective for a specific subtype. L-2-amino-4-phosphonobutyric acid (or L-AP4) was the first ligand discovered as a selective agonist of the group III mGlu receptors, but it has no selectivity among the subtypes. It is still today one of the most used agonist to study this receptor family.¹¹⁰ L-Serine *O*-phosphate (L-SOP) is a potent agonist selective for subtype 4, 6, 8 and weak for 7 (EC₅₀ = 1-4, 3, 2 and 160-1200 µM for mGlu4, mGlu6, mGlu8 and mGlu7 receptors, respectively). It is used especially in

studies of presynaptic inhibitory modulation of the excitatory glutamatergic transmission at retina and central nervous systems.¹¹¹ (*S*)-PCEP was identified by virtual HTS, this orthosteric ligand is composed of an L-AP4-derived fragment that mimics glutamate and a chain that binds into a neighbouring pocket, offering possibilities to improve affinity and selectivity.¹¹² Starting from this virtual hit other derivatives were synthesized. In particular LSP1-2111, LSP1-3081, LSP4-2022 and LSP2-9166 where the distal chain is replaced by an aromatic or heteroaromatic group.^{113,114} LSP1-2111 is selective for mGlu4R ($EC_{50} = 0.90 \pm 0.13 \mu\text{M}$) with respect to mGlu8R ($EC_{50} = 19.4 \pm 7 \mu\text{M}$).

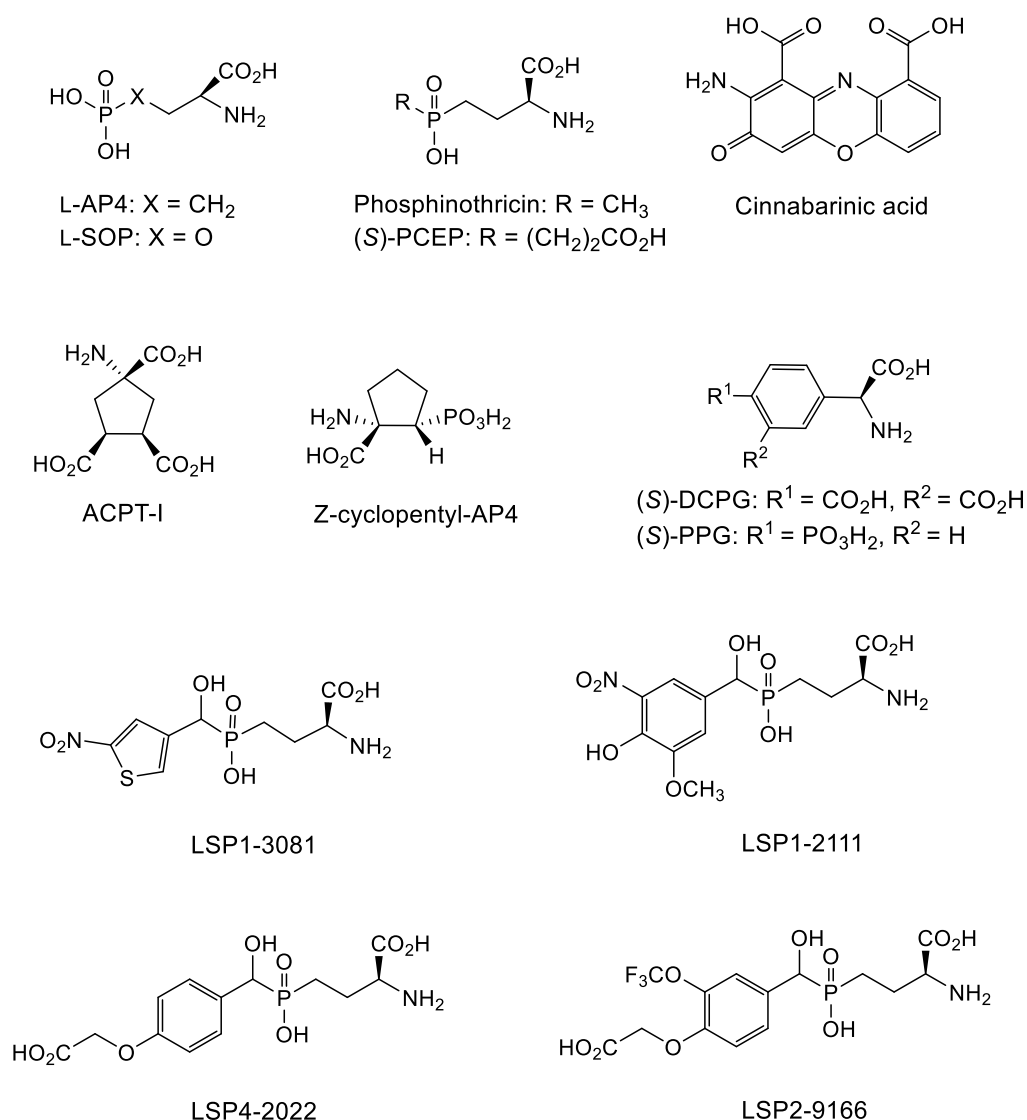
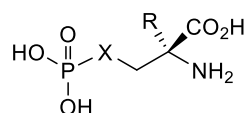
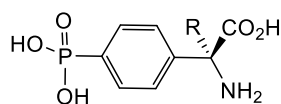


Figure 20. Selective orthosteric agonists of group III of mGluR.

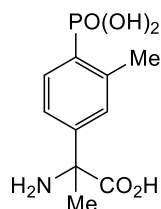
General introduction: Glutamate in central nervous system



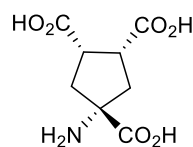
MAP4: X = CH₂, R = Me
MSOP: X = O, R = Me



(S)-MPPG: R = Me
(S)-CPPG: R = cyclopropyl



UBP1112



ACPT-II

Figure 21. Selective orthosteric antagonists of group III of mGluR.

and it has anxiolytic, but not antidepressant-like activity, mediated by serotonergic and GABAergic systems.⁹⁵ Furthermore, it modulates the striatopallidal synapse and alleviates parkinsonian symptoms.¹¹⁵ LSP1-3081 ($EC_{50} = 0.16 \pm 0.03 \mu\text{M}$ for mGlu4R, selectivity mGlu6/mGlu4 = 20.4 and mGlu8/mGlu4 = 3.4) injection improved akinesia measured by the cylinder test demonstrating that mGlu4 receptor selectively modulates striatal glutamate and GABA synaptic transmission, suggesting that it could represent an interesting target for selective pharmacological intervention in movement disorders involving basal ganglia circuitry.¹¹⁶ LSP4-2022 is potent, selective, brain-penetrant mGlu4R agonist with an EC_{50} of 0.11 μM in cell-based assays; displays >100-fold selectivity over mGlu7 and mGlu8 (IC_{50} =11.6 and 29.2 μM), and has no activity at the group I and II mGlu receptors (EC_{50} >100 μM).^{117,118} It has antidepressant effect,¹¹⁹ pain relief¹¹⁴ and in a recent study it was used for the activation of glutamatergic mGlu4R in combination with an agonist of muscarinic M4 receptors to reverse schizophrenia-related changes in rodents.¹²⁰ LSP2-9166, an mGlu4R and mGlu7R agonist, showed a reduction in ethanol consumption and relapse in addiction rat model¹⁰⁴ and a blockage of morphine conditioned place preference (CPP) expression and reinstatement after extinction.¹⁰³ LSP2-9166 showed also anti-epileptic effect on induced epileptic mouse model.¹⁰⁵ ACPT-I is an agonist displaying EC_{50} values of 7.2 μM at mGlu4a receptors and > 1 mM at mGlu1a and mGlu2 receptors.¹²¹ It was shown to be useful as antiparkinsonian strategy.¹²² (S)-3,4-DCPG is a potent and selective mGlu8a receptor agonist ($EC_{50} = 31 \pm 2 \text{ nM}$) that activates metabotropic glutamate receptors on primary afferent terminals in the neonatal rat spinal cord.¹²³ (R,S)-4-phosphonophenylglycine or (S)-PPG is a potent and selective group III metabotropic glutamate receptor agonist with anticonvulsive and neuroprotective

properties in vivo.¹²⁴ Cinnabarinic acid acts as a partial agonist of type 4 metabotropic glutamate receptors while it is inactive on others subtypes. It shows neuroprotective activity.¹²⁵ MAP4 is a weak antagonist or partial agonist at mGlu4R ($IC_{50} > 500 \mu M$).¹²⁶ (S)-MPPG is a moderate antagonist of L-AP4-induced effects in rat spinal cord, thalamic and hippocampal neurons.¹²⁷ Structurally similar is CPPG that is a potent group II/III mGluR antagonist (**Figure 21**). It has 20-fold selectivity for group III over group II. K_i values are 11.5, 17.3 and 4.02 μM for mGlu receptor subtypes mGlu6, mGlu7a and mGlu8a, respectively.¹²⁸ UBP1112 derives from phenylglycine, it is selective for group III mGluR (K_d values are 5.1 and 488 μM for group III and group II mGlu receptors respectively; $IC_{50} > 1$ mM for group I, NMDA, AMPA and kainate receptors).^{129,130} ACPT-II is a general competitive antagonist mGluRs and exhibited a similar affinity for mGlu1aR ($K_B = 115 \pm 2 \mu M$), mGlu2R ($K_B = 88 \pm 21 \mu M$), and mGlu4aR ($K_B = 77 \pm 9 \mu M$), members of group I, II and III mGluRs.¹²¹

1.3.2.3.2. Allosteric modulators of Group III of mGluRs

In the previous paragraph, we have described orthosteric ligands. It is time now to focus on the allosteric modulators. In fact, as previously said, there are two binding sites on mGluRs, one is the competitive site of glutamate where orthosteric ligands can bind and the other one is the allosteric site where modulators can bind. Allosteric modulators are classified in three main groups : the PAMs (positive allosteric modulators), the NAMs (negative allosteric modulators) and the SAMs (silent allosteric modulators).¹³¹ PAMs are able to enhance the affinity or/and the efficacy of the orthosteric ligands, the NAMs, on the contrary, are able to inhibit the action of the orthosteric ligands and the SAMs bind the allosteric site without pharmacological modification. In any case, SAMs have been less explored for drug discovery so we will focus on PAMs and NAMs in this paragraph.^{132,133}

Several positive allosteric modulators of mGlu4R have been reported in literature (**Figure 22**).

General introduction: Glutamate in central nervous system

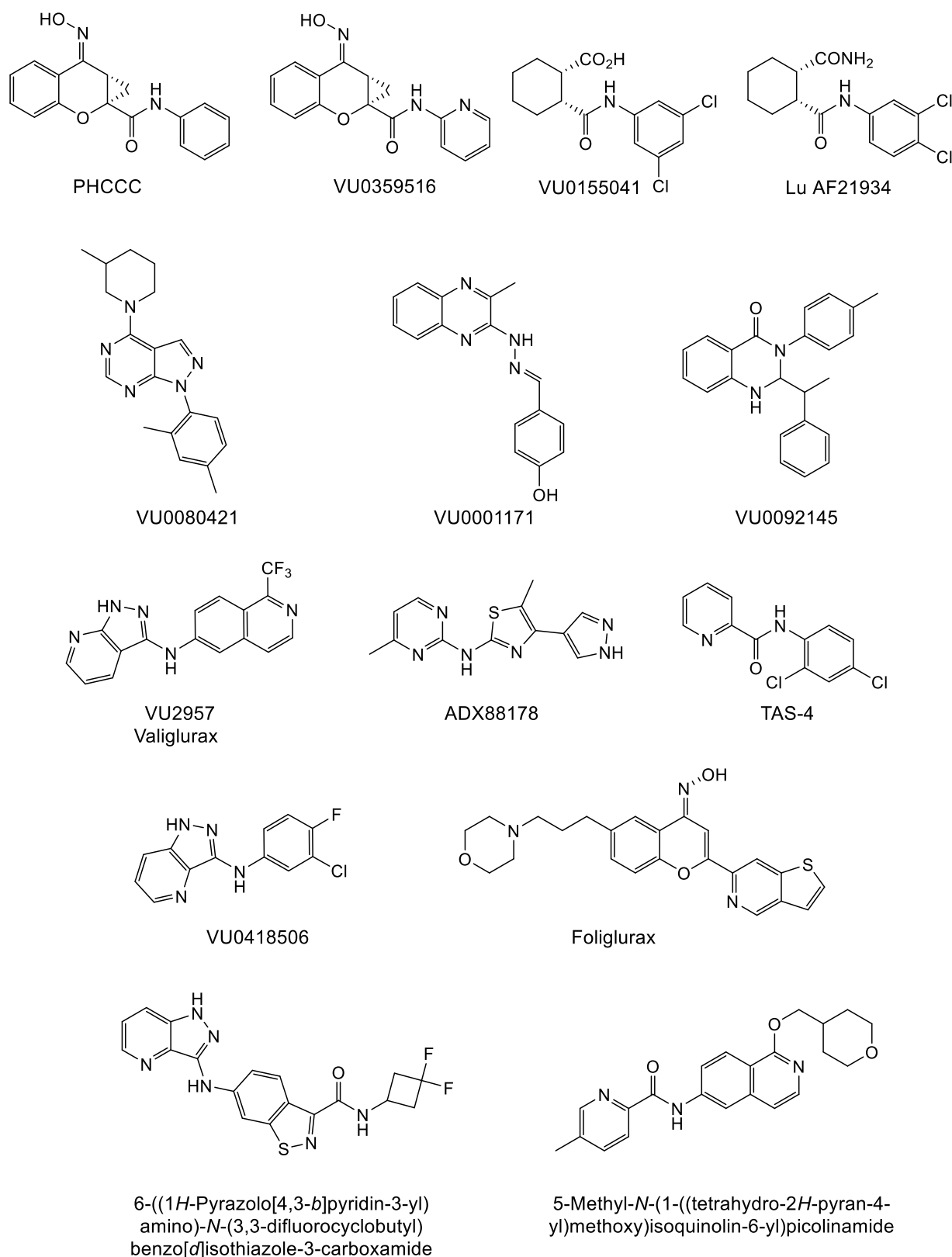


Figure 22. PAMs of mGlu4R.

PHCCC was first discovered as an mGlu1R NAM non selective for subtype 7 and 8¹³⁴ and later Novartis scientists discovered it was the first PAM of mGlu4R.¹³⁵ However, starting from this

compound a numerous new PAMs were discovered by the research group of J. Conn in Vanderbilt University.¹³⁶ Indeed, VU0359516 derives from a SAR study on PHCCC, the new molecule showed an EC₅₀ of 380 nM and a selectivity for mGlu4R.¹³⁶ Using HTS studies, several series of mGlu4R PAMs were discovered. These include VU0155041¹³⁷ and VU0080421,¹³⁸ having an EC₅₀ of 5 μM and 0.75 μM on mGlu4R¹³⁹ and VU001171 (EC₅₀ = 650 nM) and VU0092145 (EC₅₀ = 1.8 μM) which are both selective for mGlu4R.¹³⁹ Lu AF21934 is an mGlu4R PAM that derives from VU0155041. Compound VU0418506 is a more recent mGlu4R PAM but it was shown it induces the CYP1A2.¹⁴⁰ The replacement of the carboxylic function by a primary carboxamide allows LuAF21934 to cross the BBB.¹⁴¹ LuAF21934 with anxiolytic but not antidepressant properties,¹⁴² showed the reduction of harmaline-induced hyperactivity in rats.¹⁴³ Lu AF21934 and VU0155041 are both mGlu4R homodimer and mGlu2/4R heterodimer PAMs¹⁴⁴ whereas other mGlu4R PAMs such as VU0418506 are unable to activate mGlu2/4R heterodimers.¹⁴⁵ Valiglurax (VU2957, EC₅₀ = 64.6 nM) was discovered from the optimization of VU0418506, is mGlu4R selective and was evaluated as a preclinical development candidate for the treatment of Parkinson's disease.^{145,146,147} ADX88178 is a potent positive allosteric modulator for mGlu4R with an EC₅₀ of 4 nM for human mGlu4R. It dose-dependently showed anxiolytic-like effects in the marble burying test and in the elevated plus maze (EPM) test. An antidepressant effect was seen using the forced swim test, indicative of antidepressant-like efficacy.¹⁴⁸ TAS-4 is a potent and selective mGlu4R PAM of the human mGlu4 receptor (EC₅₀ = 287.8 nM), it showed efficacy alone or when administered in combination with L-DOPA in rodent models of movement disorders.¹⁴⁹ Foliglurax (EC₅₀ = 79 nM) resulting from a successful (-)-PHCCC chemical modulation, is a selective mGlu4R PAM developed by Domain Therapeutic and then sold to Prexton Therapeutics for the treatment of Parkinson's disease.¹⁵⁰ Foliglurax has a good pharmacokinetic profile and showed high brain exposure after oral administration so phase II clinical trials were started in July 2017.¹⁵⁰ However, it was recently reported that foliglurax failed in the reduction of the effects associated with long-term use of levodopa, including motor complications, according to data from the phase II trial. For this reason, Lundbeck, the company that currently holds the therapy development and commercial rights, decided to terminate its development program.¹⁵¹ Vanderbilt University published a patent in January 2018 covering benzothiazole and benzisothiazole-substituted compounds as mGlu4R PAMs. 6-((1*H*-pyrazolo[4,3-*b*]pyridin-3-yl)amino)-*N*-(3,3-difluorocyclobutyl)benzo[*d*]isothiazole-3-carboxamide is the most potent one described with an EC₅₀ of 32 nM.¹⁵² A year later, Vanderbilt University published another patent in January 2019 based on pyridine quinolone compounds as

mGlu4R PAMs. 5-methyl-*N*-(1-((tetrahydro-2*H*-pyran-4-yl)methoxy)isoquinolin-6-yl)picolinamide is one of the most potent compounds reported with an EC₅₀ of 34.1 nM.¹⁵³ Concerning the NAMs of mGlu4R (**Figure 23**), VU0448383 has been the first mGlu4R NAM discovered with an IC₅₀ of 8.2 μM. Unfortunately, due to its poor solubility and its moderate potency, it is not actually used as a pharmacological tool.¹⁵⁴ OptoGluNAM4.1 was discovered as a negative modulator of neurotransmission in rodent cerebellar slices at the parallel fiber – Purkinje cell synapse (**Figure 23**). This compound antagonizes in a reversible and photoactivable manner the activation of the receptors. The molecule is active in its *trans* form while the switching to the *cis* form using blue light gives no effect on the receptor.¹⁵⁵

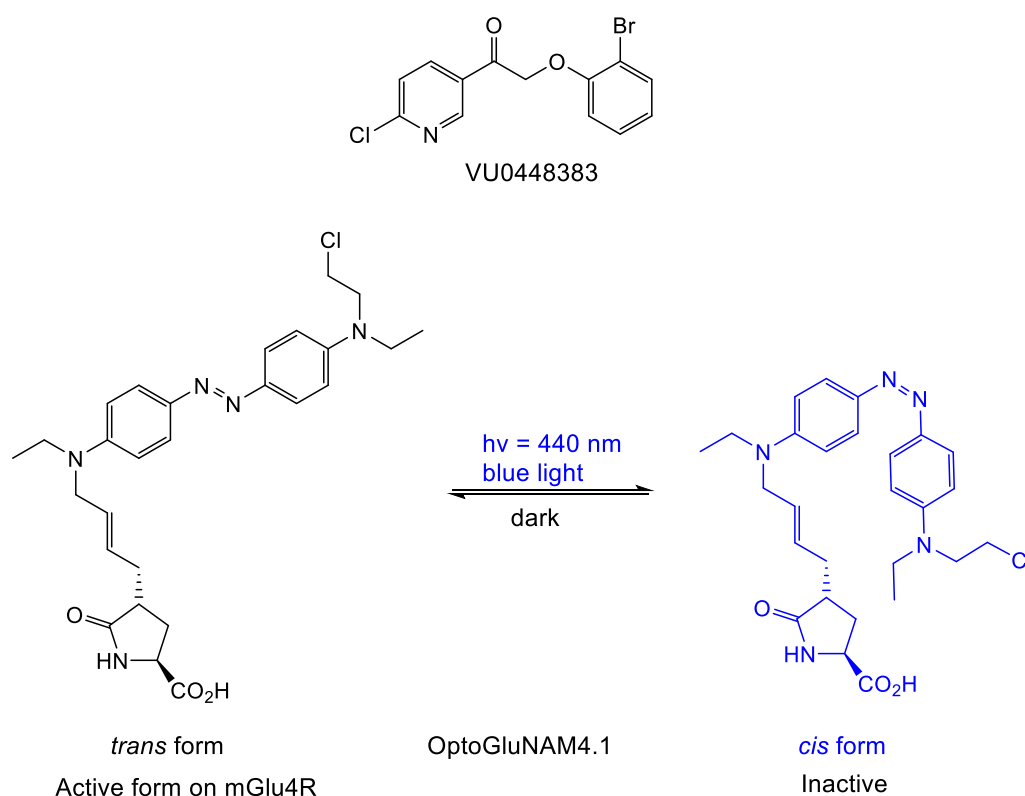


Figure 23. NAMs of mGlu4R.

Concerning mGlu7R there are different PAMs and NAMs reported in literature. Among the PAMs (**Figure 24**), AMN082 was discovered by Novartis in 2005, it is selective for mGlu7R and it seems to bind to the 7TMD as classical allosteric modulators.¹⁵⁶ It showed therapeutic implications in the treatment of cocaine or opioid addiction but also in the treatment of cocaine/opioid polydrug-abusers^{157,158,159} and antidepressant-like effects by modulating glutamatergic signalling.¹⁶⁰ However these results should be taken with caution as AMN082 is rapidly metabolized into a primary metabolite with appreciable affinity for monoamine transporters (SERT, NET, DAT).¹⁶¹

CPD-1 is an mGlu7R PAM discovered by Takeda Pharmaceutical, a patent has been published on May 2018. CPD-1 is selective for human and mouse mGlu7R ($EC_{50} = 6.9 \pm 0.8$ nM and 1.8 ± 3.5 nM, respectively) while it showed no activity on mGlu4R and mGlu8R.¹⁶² In January 2019, Takeda Pharmaceutical published another patent based on indane derivatives as mGlu7R modulators. The compound 2-(cyclopropylmethoxy)-*N*-(*trans*)-(1-methylsulfonyl-2,3-dihydro-1*H*-inden-2-yl)-2-phenylacetamide was purified by chiral chromatography to obtain four different stereoisomers with different activities. Stereoisomer A has the best activity with an EC_{50} of 0.6 nM, stereoisomer B, C and D have an EC_{50} of 4 nM, 39 nM and 16 nM, respectively.¹⁶³ VU6004502 is a brain penetrant PAM displaying an EC_{50} of 3.3 μ M for mGlu7R and higher than 10 μ M for mGlu4R and mGlu8R.¹⁶⁴

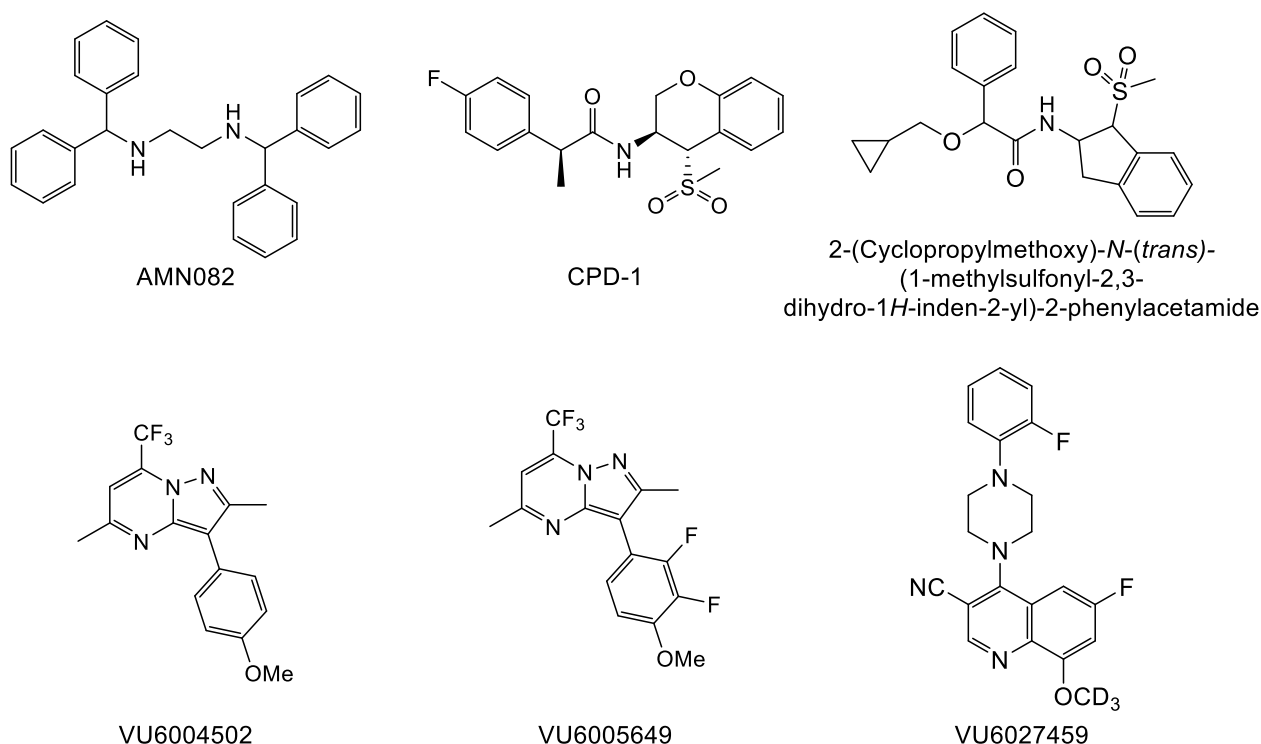


Figure 24. PAMs of mGlu7R.

From a SAR study on this compound, was discovered VU6005649. This compound is definitely more potent on mGlu7R and mGlu8R having an EC_{50} of 649 nM and 2.6 μ M, respectively, while showing always the same value for mGlu4R. Thus, this study led to a new potent PAM highly selective for mGlu7R and mGlu8R.¹⁶⁴ VU6027459 is an mGlu7R PAM discovered from a “molecular switch” starting from a selective mGlu7R NAM. VU6027459 showed CNS penetration in both mice ($K_p = 2.74$) and rats ($k_p = 4.78$), orally bioavailability in rats (%F = 69.59, and the ablation of undesired activity at DAT.¹⁶⁵

Among the NAMS (**Figure 25**), MMPIP was discovered in 2007 by Banyu Pharmaceuticals, it displays an IC_{50} of 26 nM and is selective for mGlu7R having no effect on the other subtypes.¹⁶⁶ This compound showed to be able to reverse the antidepressant-like effects of the PAM AMN082 in rats.¹⁶⁷ In addition, MMPIP is involved in pain as it alleviates and normalizes affective and cognitive behaviour in neuropathic mice.¹⁶⁸ ADX71743 is a selective and brain penetrant NAM of mGlu7R developed by Addex Therapeutics. It has an IC_{50} of 300 nM and shows *in vivo* no impairment of locomotor activity in rats and mice. Furthermore, ADX71743 has an anxiolytic-like profile in the marble burying and elevated plus maze tests.¹⁶⁹ It is also shown that the compound is useful in the treatment of abdominal pain induced by stress in rats.¹⁷⁰ Addex Therapeutics announced in July 2019 that it will lead a consortium for the development of small-molecule NAMS targeting mGlu7R as a potential treatment to reduce fear memory in post-traumatic stress disorder (PTSD). The project, named DiSARM FEAR, has been awarded a €4.85 million Eurostars grant to cover research activities performed by all participants of the consortium.¹⁷¹ A patent published in April 2019 by Pragma Therapeutics shows a series of novel heterocyclic NAMS of mGlu7R. The first example reported is 6-(2,4-dimethylphenyl)-2-(pyridin-2-yl)-5,6,7,8-tetrahydrophthalazin-1(2H)-one and all the others compounds present always the central scaffold of tetrahydrophthalazinone linked to a benzene ring on position 6 and an heterocycle on position 2. All the compounds have been tested *in vitro* and show different IC_{50} values in the order of nM and with the higher value not overpassing 30 nM.¹⁷² VU6010608 was discovered with a SAR study on another analog that had a chlorine atom in place of the trifluoromethoxy group. This substitution lead to a more potent compound with an IC_{50} of 759 nM and efficacy in blocking high frequency stimulated long-term potentiation in electrophysiology studies.^{173,174} VU6012962 represents an amelioration of compounds VU6010608 in fact the replacement of a methoxy group with a cyclopropylmethoxy group lead to an IC_{50} of 347 nM.¹⁷⁴ VU6010608 will be investigated later in the discussion section of this work as it has been studied to obtain an azoster analog using the azologization approach. In fact, starting from a known biologically active compound, it is possible to substitute one group with a diazo- bound to obtain the corresponding photoswitchable compounds.

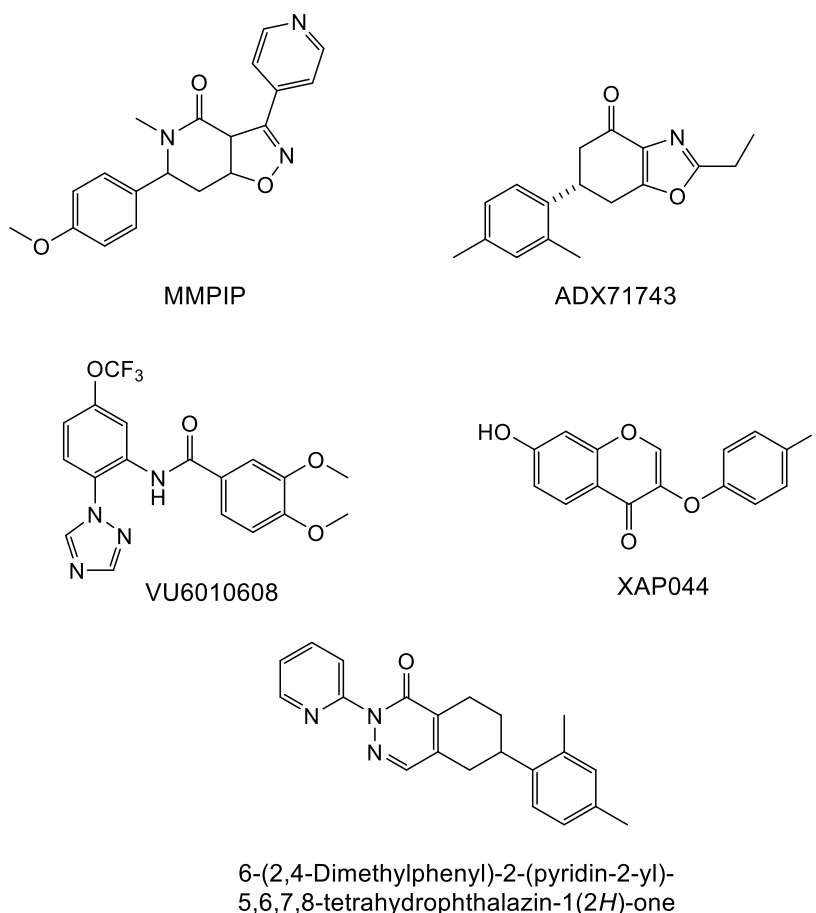


Figure 25. NAMs of mGlu7R.

The azologization approach will be better explained in the next chapter based on photopharmacology. XAP044 is an mGlu7R NAM discovered by Novartis. XAP044 selectively and dose-dependently reduces DL-AP4-induced (4 mM) activation of human mGlu7R ($IC_{50} = 2.8 \mu M$) in a classical $[^{35}S]GTP\gamma S$ binding assay. It is able to inhibit lateral amygdala long term potentiation in brain slices from wild-type mice with an IC_{50} value of 88 nM. This effect is absent in mGlu7R-deficient mice showing that the compound is selective for mGlu7R. It is brain penetrant and it showed anti-stress, antidepressant- and anxiolytic-like efficacy in rodent behavioural tests. Surprisingly, the chimeric receptor studies in recombinant cell line assays showed that XAP044 binds in the VFTD and not in the 7TMD as seen previously for all the others NAMs.¹⁷⁵ The mechanism of binding of the molecule is still unknown and in this thesis, we aimed at providing an answer to this question. The study will be presented and discussed later. A large number of XAP044 analogs has been performed in our lab to gain information for docking studies but also to obtain more potent and more soluble compounds.

Concerning mGlu8R, to our knowledge, there is just one selective PAM known, AZ12216052 (**Figure 26**). It showed reduced measures of anxiety in wild-type mice.^{176,177} VU6005649 (**Figure 24**), is an mGlu7R PAM but also an mGlu8R PAM.¹⁶⁴

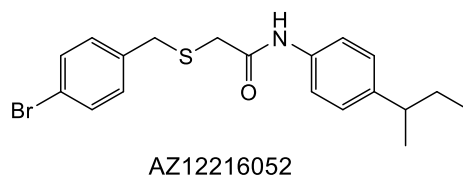


Figure 26. AZ12216052, mGlu8R PAM.

Research on allosteric modulators increased in the last years compared to a decrease in the interest of developing new orthosteric ligands. This is due to the heterogeneity of the 7TMD which allows the discovery of selective molecules among the eight subtypes while the orthosteric site is more conserved in all subtypes. Furthermore, allosteric modulation of mGlu4 and mGlu7 receptors showed interesting therapeutic potential. Indeed in animal models, all mGlu4R PAMs that have been studied, showed positive antiparkinsonian effects and mGlu7R NAMs showed anxiolytic and antidepressant effects. Although no clinical trials with these ligands have yet been successful, there are still hopes for future drugs targeting these receptors.

1.3.2.4. mGluRs heterodimers

mGluRs can form both constitutive homo- and heterodimers. In heterologous cells, group I receptors can assemble as well as group II and III receptors. This leads to 16 possible heterodimers.¹⁷⁸ mGlu2-4 heterodimers activate G-protein by mGlu4 heptahelical domain (HD) exclusively even if both mGlu2R and mGlu4R couple to G proteins. This can be explained by an oriented asymmetry in mGluR heterodimers that can be modulated using allosteric modulators. Furthermore, this gives new information on the communication of two G protein-activating units in a heterodimeric complex. The asymmetric transduction is due to both the dimeric extracellular domain and to the allosteric activation by the partially activated non-functional mGlu2R HD. The mGlu2R subunit has the ability to provide the signal for the activation of G protein by mGlu2R HD that can be achieved if a PAM binds to the mGlu2R HD or if a NAM inhibits mGlu4R HD. The surprising discovery is that both HDs in the mGlu2-4R heterodimer are able to activate G proteins but only that of mGlu4R does it (**Figure 27**).

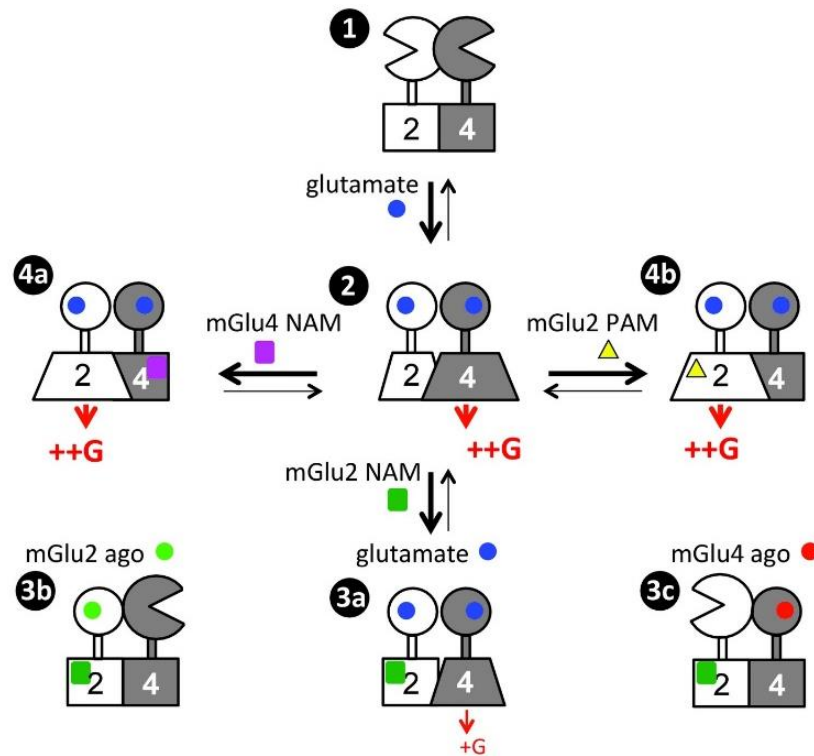


Figure 27. Activation mechanism and allosteric control of mGlu2-4R heterodimer. **1:** The heterodimer is inactive in its basal state. **2:** Glutamate (blue disk) activates both subunits leading to G protein activation by mGlu4R HD with the involvement of a conformational change in the mGlu2R HD. **3:** the addition of an mGlu2R NAM (green square) highly decreases the coupling efficacy of the mGlu2-4R heterodimer activated by glutamate (3a), or avoid detectable coupling if the mGlu2R (3b) or mGlu4R (3c) is specifically activated. **4:** heterodimer mGlu2-4R coupling through the mGlu2R HD thanks to the addition of an mGlu4R NAM (purple square, 4a), or an mGlu2R PAM (yellow triangle, 4b).⁷⁸

This observation is valid also for other heterodimers where there is an mGlu2 and a group III mGlu receptors subunits as the group III HD is always for the coupling and the activation. In the mGlu homodimers we also observe that only one subunit is active at a time but the probability for each subunit to be activated is exactly the same.⁷⁸ The mGlu2/7 heterodimer are widely found in the hippocampus. Normally the mGlu7/7 homodimer has an apparent affinity ~4000-fold lower than other mGluRs for glutamate but in mGlu2/7R heterodimerized there is an high affinity and efficacy for glutamate. In fact, there is a heteromeric cooperativity where the unliganded subunit allows its dimer partner to enhance its glutamate affinity and fully activate the receptor by the single subunit bounds. This cooperation mechanism is related to a different conformational pathways of activation. Usually, in canonical pathways, the LBD closes after the binding of the agonist and then it rotates while in this case LBD rotates even when it is open, leading to a partially activated state even when both members of the dimer are in the Apo state.¹⁷⁹ Heterodimers allow expanding the molecular diversity of mGluRs but the mechanism of heterodimer formation and their expression at cell level is still unknown. A recent study showed, using quantitative fluorescence-based assays,

the relative homo- and heterodimer propensities across group-I, -II, and -III mGluRs.¹⁸⁰ It seems that there is a strong preference for heterodimerization in different cases, for example regarding mGlu2R with mGlu3R, that is widely present in frontal cortex as shown by in situ RNA hybridization and co-immunoprecipitation.¹⁸⁰

The allosteric modulation described until now has been mainly based on homodimer modulation even if some exceptions as VU0155041 and Lu AF21934 have been already cited as mGlu2/4 heterodimer PAMs. Starting from these two compounds Vanderbilt University made an optimization that lead to febuxostat, showing an EC₅₀ of 3.38 mM on mGlu2/4 heterodimer and K_p of 0.03 on rat. The rat mGlu2/4 PAM potency and CNS penetration was increased by replacing the acid of febuxostat with an amide to obtain VU6009638 (mGlu2/4 EC₅₀ = 2.23 mM, K_p = 3.44) (Figure 28).¹⁴⁴

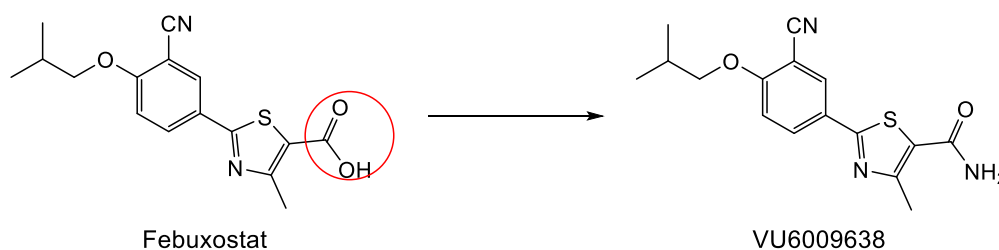


Figure 28. Structure of Febuxostat and VU6009638, mGlu2/4 PAMs.

1.3.2.5. mGluRs modulation by nanobodies

Nanobodies are recombinant, antigen-specific, single-domain, variable fragments of camelid heavy chain-only antibodies. They represent a useful class of biomolecules for research related to their therapeutic application.¹⁸¹

mGluRs can be targeted by nanobodies and three selective mGlu2R antibodies were identified *i.e.* DN1, DN10 and DN13. DN1 binds the receptor in all its conformation while DN10 and DN13 act as PAMs binding the receptor just in its active conformation to potentiate the activity of the agonist. DN10 shows also a partial agonist effect. Despite of classical PAMs, these nanobodies are not binding to 7TM domains but to the VFT domains of the mGlu2R dimer.

The advantage of these nanobodies is that they act as PAMs binding to the VFTD that is a region normally targeted by hydrophilic agonists. This mean that it is possible to develop new PAMs with hydrophilic properties compared to classical PAMs that are hydrophobic, leading to a major diffusion in plasma and cerebrospinal fluid.¹⁸²

1.4. Therapeutic potential of glutamate receptors

Glutamate is the major excitatory neurotransmitter of the CNS as already said and for this reason, its receptors are involved in almost all psychiatric and neurological diseases playing different roles. It is important to remind the complexity of the brain and synapses so that we cannot reduce each disease just to the implication of glutamatergic transmission because many other neurotransmitters like serotonin, acetylcholine, GABA, dopamine and so on, are involved in different manners. In fact, in certain diseases the role of glutamate is predominant compared to other neurotransmitters but in others it plays a secondary role. Anyway, in this part we will discuss in general the aetiology of each disease, focusing on the role of glutamate to understand the interest of our research group in developing novel compounds able to target glutamate receptors.

1.4.1. Schizophrenia

Schizophrenia is a chronic mental disease related to the thoughts, feelings and emotions. People with schizophrenia live in other realities and have lost the contact with the real world. Compared to other mental illness, schizophrenia is less common but its symptoms can be very disabling. There are positive symptoms like maniacal episode, hallucinations (often hearing voices), and disorganized thinking. Negative symptoms include lack of motivation, apathy, social withdrawal like in depression. The first symptoms of the disease are usually gradually seen in young adulthood and can be controlled but not totally resolved. The diagnosis is based on the observation of the symptoms and the study of life experiences of the patient related also to his family. In fact, scientific investigations support the idea that genetic factors play an important role in the development of schizophrenia combined with environmental and social factors, especially childhood trauma, minority ethnicity, residence in an urban area, and social isolation. The symptoms need to be observed at least for six months to make the final diagnosis of schizophrenia. Usually this mental disorder is present with comorbidity of other mental diseases as panic disorder, obsessive-compulsive disorder, depressive disorder, or addiction.^{183,184} The synaptic mechanism underlying schizophrenia is not clear, but studies confirm that different receptors are involved especially dopamine receptors, serotonin receptors and glutamate receptors with the involvement also of oxidative stress.¹⁸⁵ The dopamine hypothesis proposes a hyperactivation of dopamine transmission in the mesolimbic areas and hypoactivation of dopamine transmission in the prefrontal cortex. Furthermore, the amygdala and prefrontal cortex are important for emotional processing and they seem to be involved in the altered dopaminergic transmission¹⁸⁶.

The serotonergic transmission as a cause of schizophrenia was first considered in relation to the LSD drug that shows psychosis similar to those observed in schizophrenia, acting on central serotonergic systems. This idea had no success at the time as all the research efforts were on the understanding of dopamine involvement in the pathophysiology of the disease. Anyway, today the role of serotonin has been demonstrated showing alteration of 5-HT transmission in the brain of patients especially in cerebrospinal fluid studies of 5-HT metabolites and in post-mortem studies of 5-HT receptors. Anomalies in 5HT receptors transmission influence also the dopamine transmission; this is the base of the dopamine-serotonin hypothesis so scientific evidence suggests that both neurotransmitters play a role in schizophrenia pathophysiology.^{187,188,189} Concerning the glutamate receptors role, studies showed the appearance of negative symptoms typical of schizophrenia in normal subjects after the administration of low doses of NMDA receptor antagonists. In fact, ketamine and PCP, NMDA antagonist acting as channel blockers, can induce all the symptoms of schizophrenia in healthy volunteers and can exacerbate the symptoms in patients having already mental diseases.^{33,190,191,192} On the other hand, the administration of placebo-controlled trials with agents that directly or indirectly activate the glycine modulatory site on the NMDA receptor showed a reduction in negative and positive symptoms, and improvement in cognition. Considering all these observations, it seems that hypofunction of the NMDA receptor, can contribute to the pathophysiology of schizophrenia possibly on critical GABAergic interneurons.¹⁹³ Reducing tonic firing of GABAergic interneurons may lead to an increase of glutamate release resulting from disinhibition of glutamate terminals. Considering a circuit of Glu-Gaba-Glu neurons, if the initial Glu neuron or the NMDA receptor on the GABA interneuron are hypoactivated then there is a deficiency in the inhibiting transmission mediated by GABA interneuron with a poor release of GABA neurotransmitter. Consequently, the final Glu neuron will not be inhibited by GABA and it will release an excessive amount of glutamate. Indeed, mGlu 2/3 receptors are presynaptic autoreceptors so when activated by agonists they inhibit synaptic glutamate release, and have been shown to reduce the effects of NMDA receptor antagonists, and amphetamine in both animal and human studies. The reduction of the release of presynaptic glutamate mediated by mGlu2/3 autoreceptors results in the same effect of blocking NMDAR and this is possible as mGlu2/3 autoreceptor are located on the presynaptic neurons and NMDA on the postsynaptic neurons (**Figure 15**).¹⁹⁴ LY-404039 is a group II mGluR agonist that in a sample of patients with chronic schizophrenia, reported significant improvement in positive and negative

symptoms compared with placebo. For all these reasons the development of new agonists of NMDA receptors or group II mGluRs result interesting for the treatment of schizophrenia.¹⁹⁵

1.4.2. Depression

Depression, is a mental disorder characterized by feeling of emptiness, apathy, anhedonia, low energy, low self-esteem, loss of interest and pain without a clear cause. People affected have often false beliefs about reality. It is necessary to observe these symptoms at least for two weeks before to talk about depression and the episode can reappear even after years. Major depressive disorder can interfere seriously with normal life, people with the disturbance avoid work, social interactions and general health care. The major risk of depression is the suicide and almost 2–8% of adults with depression die this way. The cause is a combination of genetic, environmental, and psychological factors. Some factors include the previous family history of the condition, life changes, specific types of medications, chronic health problems and drug addiction. Genetics seems to play an important role as 40% of the risk appears related to genetic factors.^{196,197,198} Depression is correlated with a reduce release of serotonin, noradrenaline and dopamine, so numerous medications act as inhibitors of monoaminooxidase (IMAOs), inhibitors of serotonin reuptake (SSRIs), inhibitors of noradrenaline and serotonin reuptake (SNRIs), inhibitors of dopamine and noradrenaline reuptake (NDRIs). Tricyclic antidepressants (TCA) have also been used to prevent the reabsorption of neurotransmitters serotonin and noradrenaline.^{199,200,201} In the past, a minor attention was given to the role of glutamate receptors in the treatment of the depression but in the last years the situation has changed especially due to the discovery of the antidepressant properties of ketamine, an NMDA receptor antagonist.^{202,203,204} In fact, altered levels of glutamate or GABA, the most important excitatory and inhibitory neurotransmitters in the brain respectively, can lead to changes in brain connectivity observed in depression. The widespread distribution of glutamate and GABA receptors combined with their primary role compared to monoamine system, have led to new pathophysiological theories and new possibility for the treatment of mood disorders.²⁰⁵ NMDA antagonists especially channel blockers and selective GluN2B antagonists are promising for the discovery of new treatments. Furthermore, the binding site of the co-agonist glycine or D-serine, located on GluN2 subunits, has also been proven to be a useful target to treat mood disorder. Concerning the metabotropic glutamate receptors, compounds targeted at mGlu2/3, mGlu5, and mGlu7 receptors have shown therapeutic potential in pre-clinical models of depression.^{206,207,208}

1.4.3. Anxiety and panic disorder

Anxiety is one of all the emotions that belong to human feeling. We can feel a bit anxious during stress periods, before an exam or an important event and so on. This is totally normal and it is not pathological, but when the anxiety starts to be a persistent feeling without control and having an impact on daily life, then in this case it is a real mental disease. Anxiety is characterized by an unknown fear in the future and it gives some physical symptoms as tachycardia, breathing difficulties, dyspnoea, trembling, dizziness and insomnia. There are different types of anxiety, general anxiety is the most common, but there is also anxiety due to post-traumatic stress, social anxiety and phobias. Genetic and environmental factors play a role in the development of anxiety disorders. Sometimes similar symptoms can be produced by hyperthyroidism, heart disease, caffeine, alcohol, drug abuse. The treatment includes psychotherapy, lifestyle changes and medications. Benzodiazepines, able to increase the activity of GABA receptors, are the most prescribed class of medications for anxiety disorders but also antidepressants and beta-blockers can improve the symptoms. Several studies have shown the implication of glutamate receptors in anxiety disorders, especially the group III of mGluRs.^{209,210,211,212} Among all the mGluR subtypes, the mGlu7R seems to be the most related to anxiety and fear. ADX71743, an mGlu7R NAM, showed an anxiolytic-like profile in the marble burying and elevated plus maze tests.¹⁶⁹ Another mGlu7R NAM, XAP044, inhibits lateral amygdala long term potentiation (LTP) in brain slices from wild type mice having an anti-stress and anxiolytic effect.¹⁷⁵ These results led to a growing interest in drug development of new mGlu7R allosteric modulators, especially NAMs, as potential candidates for the treatment of anxiety disorder. Addex Therapeutics is developing an mGlu7R NAM as a novel orally available treatment to reduce fear memory in PTSD.²¹³ NMDA receptors have also shown a role in anxiety as some antagonists like the competitive NMDAR antagonists NVP-AAM077 and Ro25-6981 significantly inhibited anxiety-like and compulsive behaviour in rats. D-Cycloserine at all doses showed significant suppression on anxiety-like and marble-burying behaviour.²¹⁴

1.4.4. Addiction

Addiction represents the compulsory need to repeat an action without the rational control of the person that is not anymore able to stop this habit. This brain disorder leads to an irresistible engagement in rewarding stimuli despite adverse consequences. The term addiction is often related to drug consumption but also to alcohol, nicotine, food, video game, gambling and sex. In

the last years, many efforts have been made to understand how glutamate interacts with other neurotransmitters (in particular, dopamine) in the process of addiction. The interaction of glutamatergic and dopaminergic system seems to play a major role in addiction but there are still some glutamatergic mechanisms that work independently in this process. For example, the control over behaviour by conditioned stimuli appears to depend heavily on glutamatergic transmission.^{215,216} Many studies have focused on addiction to cocaine and glutamate transmission to understand the long-term changes induced by cocaine. A glutamatergic projection from the medial prefrontal cortex to the nucleus accumbens core mediates reinstated drug-seeking. The problem of studying glutamatergic plasticity in addiction is that different drugs, durations of drug administration, and varying withdrawal or abstinence conditions can produce distinct adaptations in glutamate transmission. Thus, the identification of a general role of glutamate for all type of addiction is still a challenge that opens anyway interesting therapeutic applications.²¹⁷ The NMDAR acts as a molecular target for several drugs of abuse. Some modulators as memantine and acamprosate, as well as the partial NMDA agonist D-cycloserine have been tested showing that direct NMDAR modulators are not really efficient in the treatment of drug addiction while the partial agonism of NMDAR may have some efficacy with regards to extinction learning during cue exposure therapy.²¹⁸ Interestingly, studies showed the possibility that cocaine assumption is associated with changes in D-serine signalling, that contribute to synaptic plasticity changes and impairments. In fact, in brain slices from cocaine-treated rats exposed later to saturating levels of exogenous D-serine, the LTP and LTD inducibility were totally restored.²¹⁹ For group III mGluRs, even though limited studies have been attempted at present, emerging evidence ties them to the remodeling of excitatory synapses and persistent drug seeking. Group III mGluRs are distributed predominantly at the presynaptic level of the synapse and thus play their roles *via* a presynaptic mechanism, although a postsynaptic modulation cannot be totally excluded. The research on these receptors in the addiction is growing rapidly using advanced developed pharmacological agents with higher subtype selectivity and conditional knockout mouse line. mGlu7R is highly expressed in the limbic circuit having a role in drug action. In fact, this receptor subtype is involved in addictive effects of psychostimulants, alcohol, and opiates.^{104,103} mGlu7R is not the only subtype with potential in addiction but mGlu4R and mGlu8R are also involved in research on drug action.²²⁰

1.4.5. Alzheimer's disease

Alzheimer's disease (AD) was discovered in 1901 by a clinical psychiatrist and neuroanatomist, Alois Alzheimer, who observed symptoms of paranoia, progressive sleep and memory disturbance, aggression, and confusion in a 50 year-old woman until her death 5 years later. In the 37th Meeting of South-West German Psychiatrists in Tübingen, Alzheimer reported this case describing the plaques and neurofibrillary tangles he noted in the brain histology.²²¹ AD involves a wide range of symptoms, first appears a loss of memory and then problems with language, perception, ability of movement, muscle mass loss and neuropsychiatric disorder. This leads the patient to the impossibility to live a normal life due to the physical and mental disorders. The AD pathogenesis is really complex and involves the connection of several aspects that are not totally understood by now (**Figure 29**).²²² On a genetic basis, two types of AD have been identified: the familiar form of autosomal dominant inheritance, known as early onset familial AD, and the sporadic AD, the commonest form of AD, which affects people older than 65 and doesn't show an autosomal inheritance. In the first case, AD can be attributed to mutations in one of three genes: those encoding for amyloid precursor protein (APP) and presenilins 1 (PS1) and 2 (PS2). These mutations are responsible for an increase in the production of the small protein A β 42 connected to the senile plaques.²²³ In the sporadic AD there is no autosomal-dominant inheritance and the best known genetic risk factor is the inheritance of the ϵ 4 allele of the apolipoprotein E (APOE). The presence of the APOE ϵ 4 allele increases the likelihood to develop AD by three times in heterozygotes.²²⁴ The presence of amyloid plaques or senile plaques is considered a main hallmark of AD. The main components of these plaques are the hydrophobic peptides A β 40 and A β 42, as the derived products of APP, whose aggregation and deposition into insoluble plaques lead to a cascade of various neurotoxic changes that are responsible for the brain and neuronal damage.²²⁵ Another main hallmark of AD is the presence of the neurofibrillary tangles (NFTs), which arise from the hyperphosphorylation of a microtubule-associated protein, *i.e.* tau protein, also as a consequence of A β generation.²²⁶ It seems that the A β accumulation is related with the hyperphosphorylation of tau caused by kinases such as Cdk5 and GSK-3 β , giving first paired helical filaments (PHF) and then the NFTs.²²⁷ APP is present in all humans and it is normally cleaved by the sequential action of the α - and γ -secretase to give non-amyloid products, which display a neuroprotective action. The problem is that in AD, APP is cleaved by the action of β -secretase (BACE-1) and γ -secretase, leading to the over-expression of A β , especially of the most aggregation-prone and neurotoxic A β 42 form, which is involved in the formation of the SPs. For these reasons the inhibition of BACE-1 can be a

good therapeutic strategy to avoid the amyloid cascade and confront AD.²²⁸ The neurodegenerative process and the neuronal death are connected with the oxidative stress of the

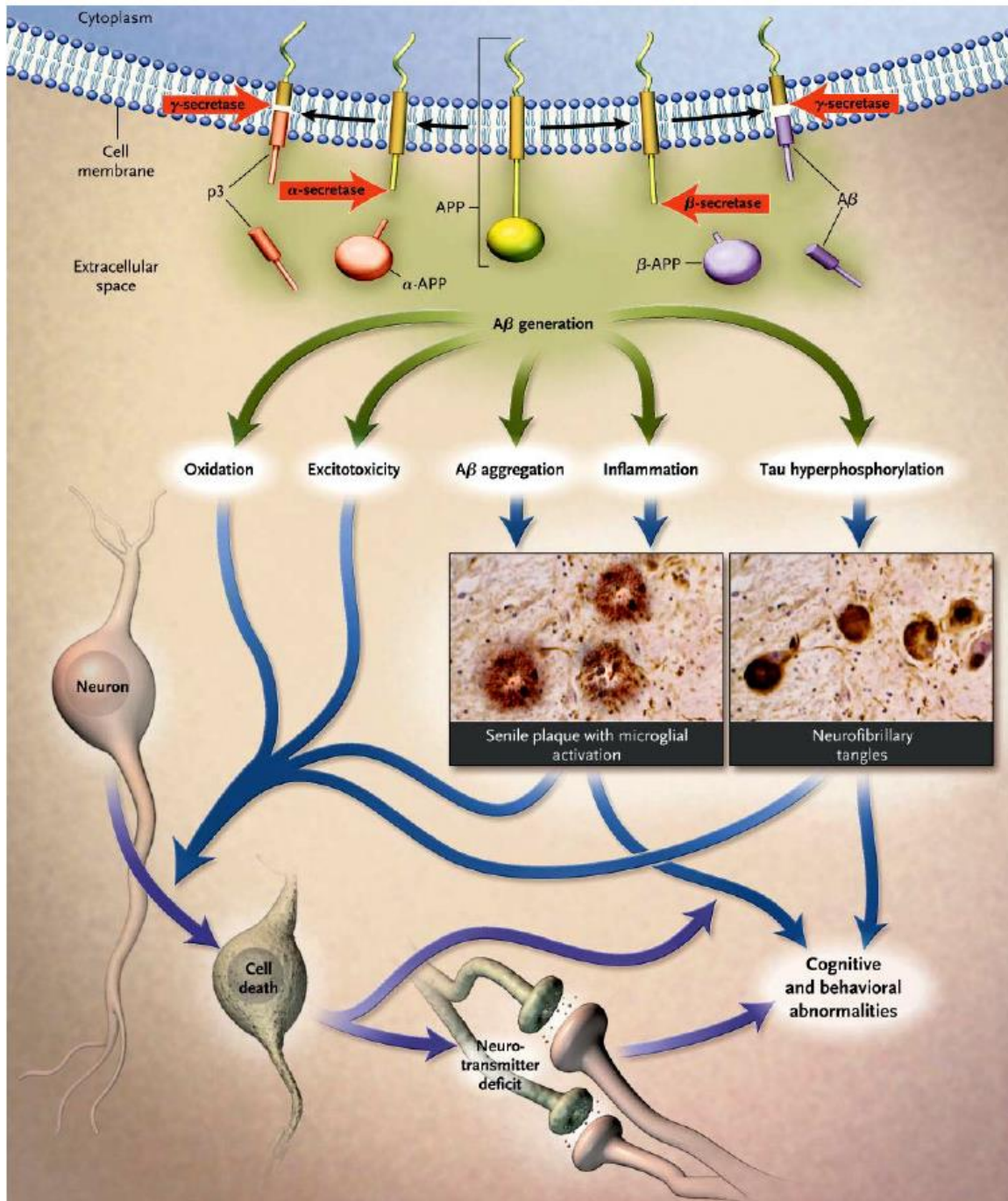


Figure 29. Putative amyloide cascade.²²⁹

neuronal cells and free radicals play a role in these processes. The reactive oxygen species (ROS) are the main actors of the free radical hypothesis of aging, as their accumulation leads to the destruction of important components of cells as nucleus, mitochondrial DNA, membranes, and cytoplasmic proteins.²³⁰ There are different types of ROS as superoxide anion (O_2^-), hydroxyl radical ($HO\cdot$), hydrogen peroxide (H_2O_2), nitric oxide (NO), peroxy (ROO) and reactive aldehyde

(ROCH), with different oxidative power and toxicity. The role of the oxidative stress in AD is related to the A β -induced neurotoxic effects. Indeed, A β treatment showed to increase the levels of hydrogen peroxide and lipid peroxides in *in vitro* experiments using cell models. Furthermore in *in vivo* experiments with AD transgenic mouse models with a mutation of APP and PS1, these animals showed an increase of the hydrogen peroxide and nitric oxide production leading to a lipid and protein oxidative damage related with age-associated A β accumulation, thereby confirming that A β promotes oxidative stress.²³¹ The cause of the ROS formation is an over-activation of the glutamate receptors NMDA and AMPA that leads to a series of events, as the Ca²⁺ increase in the cell, which leads to ROS formation. Targeting NMDA receptors and modulating their activity can be a valuable strategy for antioxidant therapy of AD.²³² The evidence for the involvement of the neurotransmitter acetylcholine (ACh) in AD started in 1976, when different research groups found in autopsies of brain tissue of AD patients a reduced activity of the enzymes related to the production and degradation of ACh. Later on, other groups reported that in living patients with AD there was a deficit of choline acetyltransferase (ChAT), the enzyme responsible for the production of ACh, with this deficit being higher as more advanced was the disease. From these evidences it became clear that an interesting approach to follow was the inhibition of the enzyme involved in the degradation of ACh *i.e.* acetylcholinesterase (AChE). The cholinergic hypothesis of AD gave the stimulus for the synthesis of new drugs able to inhibit AChE and compensate for the deficits in cholinergic neurotransmission.²³³ The rationale for the use of drugs targeting the glutamate NMDA receptor in AD comes from the involvement of the glutamatergic transmission in neuronal excitotoxicity. In fact, an overstimulation of NMDA receptors leads to an increase in the entrance of Ca²⁺ in brain cells, which induces the activation of enzymes like phospholipases, endonucleases, and proteases able to damage cell structures such as the cytoskeleton, membrane, and DNA.²³⁴ There is just one marketed drug that targets NMDA receptors by now *i.e.* memantine, and many studies are focusing their attention on this target. Memantine is a derivative of adamantane, it acts as an NMDA receptor antagonist that blocks the activity of the neurotransmitter glutamate involved in neuroexcitotoxicity, leading to beneficial effects in AD.²³⁵

1.4.6. Parkinson's disease

Parkinson's disease (PD), or simply Parkinson's, is a degenerative disease that progresses slowly and the main symptoms involve the motor system. Usually the progression of PD leads also to non-motor symptoms. The disease is mainly characterized by slowness of movement, shaking,

rigidity and problems in walking. These symptoms have a crucial impact on daily life so, especially in the advanced stage of the disease, patients can suffer of dementia, anxiety and depression. It seems that the development of the disease is due to a combination of genetic and environmental factors. The death of cells in the substantia nigra of the brain, that involves the construction of protein into Lewy's body in the neuron, is the cause of the motor symptoms of PD. The reason of the death of these cells is still not totally clear but it results in a low level of dopamine neurotransmitter. The treatment of PD is based on the restauration of normal level of dopamine using first levodopa (L-DOPA) and then other dopaminergic agonists. As said before PD is a degenerative disease so treatment cannot resolve the disease but it can help to control the motor symptoms. The problem is that the progression of the disease leads to a continuous loss of neurons and dopaminergic treatment starts to be ineffective at a certain point.^{236,237,238} For this reason, research of other medication related to glutamatergic transmission appears particularly promising especially to patients not responding anymore to dopaminergic treatment. In fact, ionotropic and metabotropic glutamate receptors are able to modulate neurotransmission throughout the basal ganglia and it can be useful to target them to contrast the effects of abnormal neurotransmission in PD. The dopaminergic neuron degeneration lead to an imbalance between GABA and glutamate transmission. *In vivo* studies showed that the modulation of glutamate receptors can alleviate primary motor symptoms in PD and can contrast the progressive disappearance of dopamine neurons.²³⁹ The transmission in nigro-striatal pathways in PD involves an imbalance of several neurotransmitters, while dopamine levels are lower, on the opposite there is a glutamatergic hyperactivity. This hyperexcitation due to a high amount of glutamate released leads to excitotoxic events involved in the neurodegenerative process.²⁴⁰ The antagonists of ionotropic receptors have shown to be useful in PD as they reduce the postsynaptic activation. This includes some NMDA competitive antagonists, noncompetitive antagonists and glycine site antagonists. Ifenprodil, an NMDA NAM, showed also positive results in *in vivo* models of PD.²⁴¹ Concerning the group III of mGluRs, the strategy to decrease synaptic glutamate levels is based on the use of agonists and PAMs as group III mGluRs are presynaptic receptors and their activation inhibits glutamate release. In particular, mGlu4R is the most promising subtype to target in PD compared to the others in the same group. The mGlu4R agonist PHCCC showed to reduce the nigrostriatal toxicity due to MPTP in wild type mice but not in mice lacking mGlu4R.^{242,57} The PAM Valiglurax has been evaluated as a preclinical candidate for PD and it was used to create a spray-dried dispersion formulation for clinical application. Preclinical studies are ongoing.¹⁴⁶ Foliglurax

(EC₅₀ = 79 nM) resulting from a successful (-)-PHCCC chemical modulation, is a selective mGlu4R PAM developed by Domain Therapeutic and then sold to Prexton Therapeutics for the treatment of Parkinson's disease.¹⁵⁰ Foliglurax phase II clinical trials started in July 2017.¹⁵⁰ However, it was recently reported that foliglurax failed in the reduction of the effects associated with long-term use of levodopa, including motor complications, according to data from the phase II trial. For this reason, Lundbeck, the company that currently holds the therapy development and commercial rights, decided to terminate its development program.¹⁵¹ Another PAM VU0155041 was shown in models of mice treated with 6-OHDA to induce neurotoxicity, to decrease the level of GFAP (glial fibrillary acidic protein – a predictor of the neuron cell death) and IBA-1 (ionized calcium-binding adaptor molecule 1).²⁴³ Addex Therapeutics is also involved in the drug discovery of new mGlu4R and they are evaluating preclinical studies.²⁴⁴ Targeting mGlu4R with agonists and PAMs in PD is really promising as this receptor subtype has a neuroprotective and anti-inflammatory function thus its modulation can counter PD progression in addition to relieve motor symptoms.⁹⁶

1.4.7. Epilepsy

Epilepsy is characterized by a hyperactivation of the neuronal activity in the SNC. There are several type of epileptic crisis that normally appear with seizures, convulsions and loss of consciousness. During an epileptic attack, the synaptic concentration of glutamate is higher than normal and it is responsible of the hyper excitability of the SNC.^{245,246} In this case, the antagonists of ionotropic glutamate receptors are useful to inhibit the excessive glutamate postsynaptic activation but ionotropic receptors are involved in the rapid transmission of the signal so their modulation can be dangerous and complicated. In fact, in clinical studies all the NMDA antagonists failed to demonstrate safety and efficacy for therapeutic use while just peramppanel, an AMPA antagonist, has been approved to treat some form of epilepsy.^{247,248} On the other hand the group III mGluRs, involved in the modulation of synaptic transmission, represent a good target to control epilepsy. They are presynaptic receptors so their activation using agonists may inhibit the release of glutamate. mGluRs have an epileptogenic potential that was observed in the hippocampus by activation with the agonist (1S,3R)-1-aminocyclopentane-1,3-dicarboxylic acid (ACPD).²⁴⁹ Using the agonists L-AP4 and L-SOP, it was first observed the reduction of epileptic crisis²⁵⁰ but in other studies was observed the opposite effect. The antagonist MCPA showed interestingly antiepileptic effect while antagonists MAP4 and MPPG showed the opposite.²⁵¹ The subtype mGlu4R seems to have an epileptogenic role as the absence of convulsions was observed in mice lacking this receptor subtype.^{252,253} Agonists that activate mGlu5 and mGlu7 receptor function seem to have

positive effects in the treatment of absence epilepsy.²⁵⁴ The mGlu7R subtype is definitely promising in the treatment of epilepsy as observed in a recent study. In fact, the administration of LSP2-9166, an mGlu7/4R agonist, showed an anti-epileptogenic effect in a model of chemically induced epilepsy in preclinical studies.¹⁰⁵ A bidirectional modulation by mGlu4R and mGlu7R was found related to seizure progression and LSP2-9166 was also able to reduce seizure frequency in mouse model injected with kainic acid to develop human mesial temporal lobe epilepsy.¹⁰⁵ All these evidences suggest the important role of mGlu7R in epilepsy and its potential in the drug development of anti-epileptic compounds.²⁵⁴

2. PHOTOPHARMACOLOGY

Photopharmacology is an emerging field related to the biological application of light on molecules that allows the modulation of the pharmacological activity. The main advantages include the selectivity, as light can be delivered with a spatiotemporal precision, and the control of active drug based on the intensity and wavelength of the light. Furthermore, despite of optogenetics, that needs genetic manipulations of proteins, photopharmacology involves just light delivery on molecules targeted to physiological receptors. On the other hand, main drawback concerns the way to deliver photons to the target in tissues and the toxicity of irradiation at UV light.²⁵⁵ Two types of photo-regulated drugs have been developed until now for photopharmacology: photoactivable ligands, also called “caged” compounds and photoswitchables ligands.²⁵⁶

2.1. Caged compounds

Caged compounds are small organic molecules that can be photoactivated by irradiation of light at different wavelengths (**Figure 30**).²⁵⁷ They were invented by biochemists in the late 1970 when nucleotides with photochemically protecting groups were synthesized. The synthesis of *ortho*-nitrobenzyl derivatives of cyclic-AMP and ATP have been described in two articles that appeared in 1977 and 1978.^{258,259} Today caged compounds are widely used to study a great variety of biological processes by physiologists, cell biologists and neuroscientists.

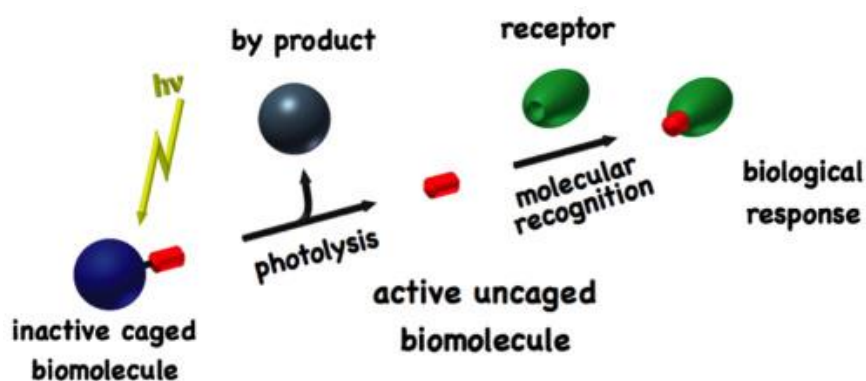
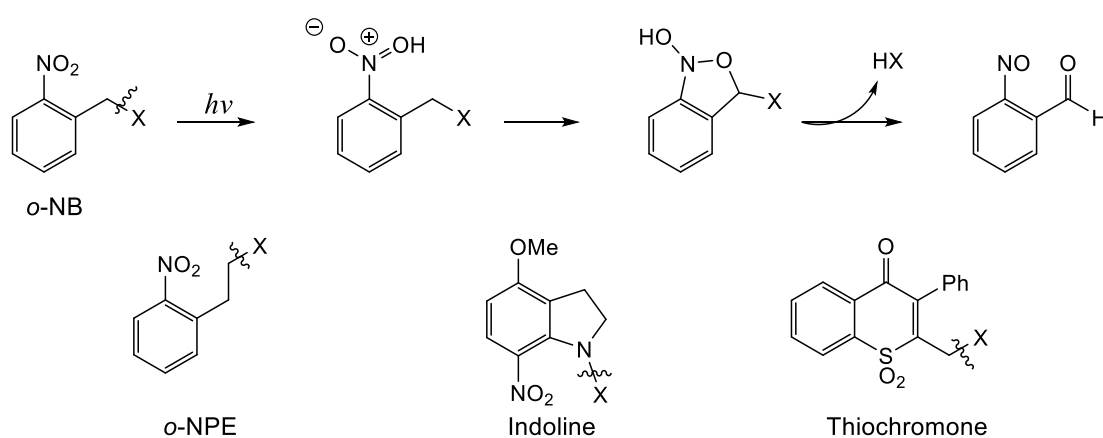


Figure 30. Principle of caged compounds.²⁵⁷

In fact, some examples of caged biomolecules are neurotransmitters, calcium, inositols, nucleotides, peptides, enzymes, mRNA and DNA. All these molecules are caged by covalent modification of one part of their structure with a photoremovable chromophore except in the case Ca^{2+} . The inorganic cation calcium is not able to form covalent bonds to caging groups as the other organic molecules, so a different strategy has been developed. Photolabile derivatives of known

high-affinity calcium chelators (BAPTA, EDTA and EGTA) have been synthesized so upon irradiation these molecules decrease their affinity for calcium leading to uncage some of the bound calcium.²⁶⁰ Several types of photoprotecting groups (PPGs) have been used in physiological studies, they can be divided into two groups based on the photorelease uncaging mechanism: those in which the release is the consequence of an intramolecular rearrangement (nitrophenyl, or cinnamyl-type PPGs), and those that are cleaved directly by S_N1-type solvent-assisted photolysis; the latter offering inherently faster release. The *ortho*-nitrobenzyl-type PPG (*o*-NB) was the first PPG in the 'caging & uncaging' technique in physiological studies (**Figure 31**)²⁶¹

(1) *o*-Nitrophenyl-type



(2) Photo S_N1-type

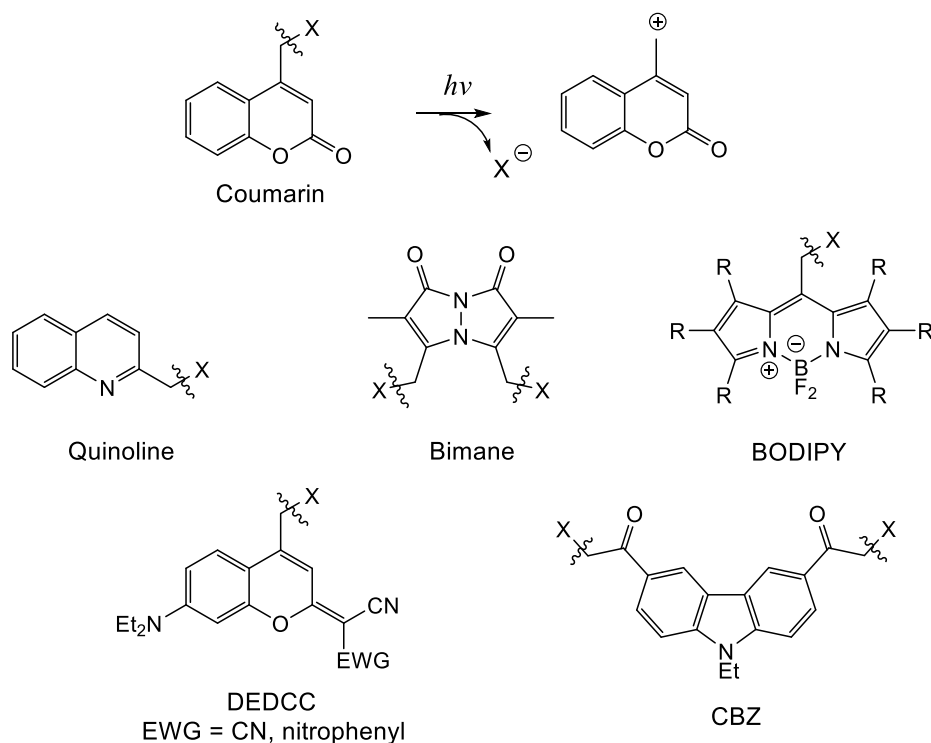


Figure 31. Photoprotecting groups (PPGs).²⁶¹

Caged compounds need to have certain properties to be useful in biological study, specially water solubility, water stability, high decaging rate (chemical efficiency) and photochemical efficiency. All caged compounds are used with living cells and neurons are the most sensitive cells among them, so water solubility is fundamental, as even small amounts of organic solvents can be toxic. Biologists can allow the use of 0.1% of DMSO in buffer in extreme cases, but ideally, no organic solvent should be present in the buffer solution. Organic synthesis is generally carried out in nonaqueous solvents, but the final step of the synthesis usually makes the caged compound water-soluble. Aqueous stability is another important property of caged compounds and it depends on the chemical bonds used for caged compounds. Esters and to a lesser extent amides are sensitive to aqueous hydrolysis, while ethers, amines and carbamates are not or less. Poor aqueous stability results in the spontaneous hydrolytic release of the caged compound, leading to impossible application in biology.²⁶⁰ For example, neurotransmitter GABA caged by an ester bond to coumarin chromophores is photoreleased quickly but is unstable in (frozen) solution. On the other hand, when caged *via* a carbamate, its release is slower, but the compounds have water stability. When phenols (*e.g.*, serotonin or capsaicin) are caged *via* a carbonate, they are effectively stable and released quickly. The stability of all these caged compounds depends on the pH of the aqueous solution but usually they are less stable above pH 8. Other caged compounds, as all ethers and amines caged with nitrobenzyl groups are completely stable and impossible to hydrolyze.

Chemical efficiency refers to the chemical yield of active product released compared to the amount of caged compound photolyzed. Most uncaging reactions are quite efficient chemically, but quite difficult to obtain 100% of release.²⁶²

The photochemical efficiency is $\epsilon \cdot \phi$. The molar extinction coefficient, ϵ , refers to the ability of a molecule (chromophore) to absorb light or photons. Considering the Beer-Lambert's law:

$\epsilon = \log(I_0 / I_t) \times c \times l$, where I_0 is the initial light intensity, I_t is the transmitted light intensity and $\log(I_0 / I_t)$ is the optical density and l is the optical path length. The quantum yield of photolysis ϕ measures how many excited molecules give a product, with the normal maximum being 1.²⁶⁰

Photochemical efficiency is important for near infrared two photon (NIR-TP) irradiation, necessary for *in vivo* studies. Two photon absorbance (TPA) was theorized by Maria Göppert-Mayer (1931) who realized that Paul Dirac's dispersion theory could apply to two-photon (2P) excitation as well as light transmission. She developed the idea that the absorption of light from the ground state

(S_0) to excited state (S_1) goes *via* a “virtual intermediate electronic excited state” K in the case of two-photon excitation ($h\nu_2$) while it goes directly in one-photon absorption ($h\nu_1$) (**Figure 32**).²⁶³

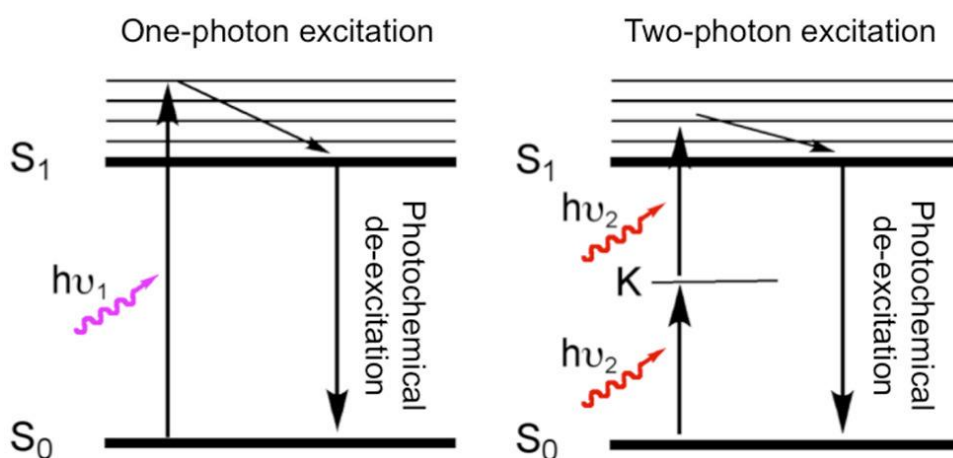


Figure 32. Jablonski diagram illustrating the absorption of light from the ground state (S_0) to excited state (S_1) in one-photon (OP) and two-photon (TP) excitation.²⁶³

In the TP excitation process, much lower energy photons can be used to bring molecules to the electronically excited state (S_1). In fact, $h\nu_2 = 1/2 \times h\nu_1$ represents the half of the energy of the corresponding OP excitation ($E = h\nu$). TP cross-section (σ_2) is the index of the efficiency of the TP absorption process and is expressed using the Göppert-Mayer (GM) unit. Using the equation $\delta_u = \sigma_2 \times \phi_u$, where ϕ_u is the quantum yield of the uncaging reaction, it is possible to obtain the uncaging efficiency (δ_u) of the TP excitation process. The use of NIR-TP excitation process despite of one photon excitation allows less photo-damage to living tissue, higher three-dimensional (3D) spatial resolution, deeper penetration in turbid tissues and lower light scattering (**Figure 33**).²⁶¹

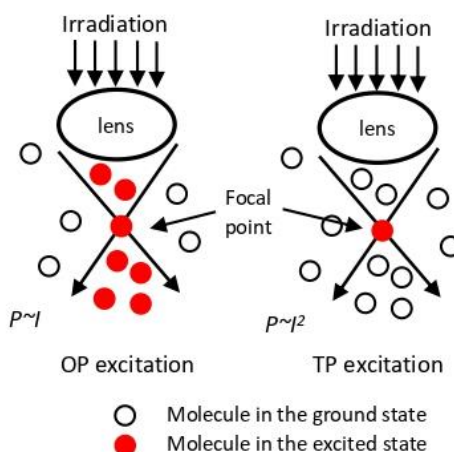


Figure 33. Spatial resolution of OP and TP excitation. TP excitation process allows only molecules located at the focal point to be excited, since the probability (P) of excitation is proportional to the light intensity (I) squared.²⁶¹

Several strategies have been developed to design chromophores with a strong TP absorption: π -conjugation, and dipolar, quadrupolar and octupolar systems. Examples of π -conjugation are benzene, naphthalene and stilbene with a higher σ_2 constant of 12 GM at 514 nm for stilbene.

In dipolar systems, the introduction of an electron-donating substituent (D) and an electron-withdrawing substituent (A), at both ends of the stilbene, leads to a molecule with a dipolar character (D- π -A) and an increase of σ_2 up to 100 GM at 830 nm.

Quadrupolar system (D- π -A- π -D or A- π -D- π -A) is obtained starting from stilbene structure by introducing designs of push-push or pull-pull substituents at each end of the central skeletal structure. For example, the introduction of a fluorenyl ring between two stilbenes moieties increases the π -conjugation so that σ_2 reaches a significant red-shift, leading for example to 1300 GM at 740 nm.

Finally, in octupolar system triangular structures such as 1,3,5-trisubstituted-benzene [D(- π -A)₃ or A(- π -D)₃] show an octupolar character *via* the introduction of push (D) or pull (A) substituents with excellent increase of TP absorption. The insertion of multiple π -conjugation increases TP absorption cross-section values of molecules, but also their hydrophobicity. Caged compounds need to be soluble in water, as explained before, so it is necessary to have a good compromise between the TP absorption and solubility properties.²⁶¹

2.2. Photoswitches

Photoswitches are moieties able to change their structure upon irradiation with different wavelengths of light and for this property; they have been studied for various applications as light-triggered materials and photochromic systems applicable in a biological context. There are several examples of switchable nano-particles (NPs), liquid crystals, metal-organic framework (MOF) systems, elastomers, light-triggered sol-gel systems, photo-switchable catalysts and molecular motors.²⁶⁴ Photochromism, defined as a reversible phototransformation of a chemical species between two forms having different absorption spectra, is an aspect present in different molecular scaffolds. During this process, not only the absorption spectra but also various physicochemical properties change, such as the dielectric constant, refractive index, oxidation/reduction potential and geometrical structure.²⁶⁵

2.2.1. Donor-Acceptor Stenhouse Adducts (DASAs)

Donor-acceptor Stenhouse adducts (DASAs) represent a new class of photoswitch that have recently been reported by Read de Alaniz and coworkers.²⁶⁶ The work on this class of photoswitches comes from Stenhouse in 1870 who observed some colored cyanine dyes when ring-opening a 2-furaldehyde in the presence of two equivalents of amine and one equivalent of protic acid.²⁶⁷ The interest on these photoswitches derives from their unusual properties. In fact, they belong to a group of photochromic switches, the thermally stable form is colored while the photoinduced isomerised form is colourless. The core structure of the DASA class of photoresponsive molecules is made up of a donor amine and an acceptor dicarbonyl ring motif. The colored DASA becomes colourless upon irradiation with visible light (**Figure 34**) and this process initiates with a light-controlled alkene isomerization followed by a thermal 4π electrocyclicization to the colourless state. Synthetic modifications are possible on the donor and acceptor portions of the molecule allowing the tunability of the optical and chemical behaviour of the photoisomer.²⁶⁸

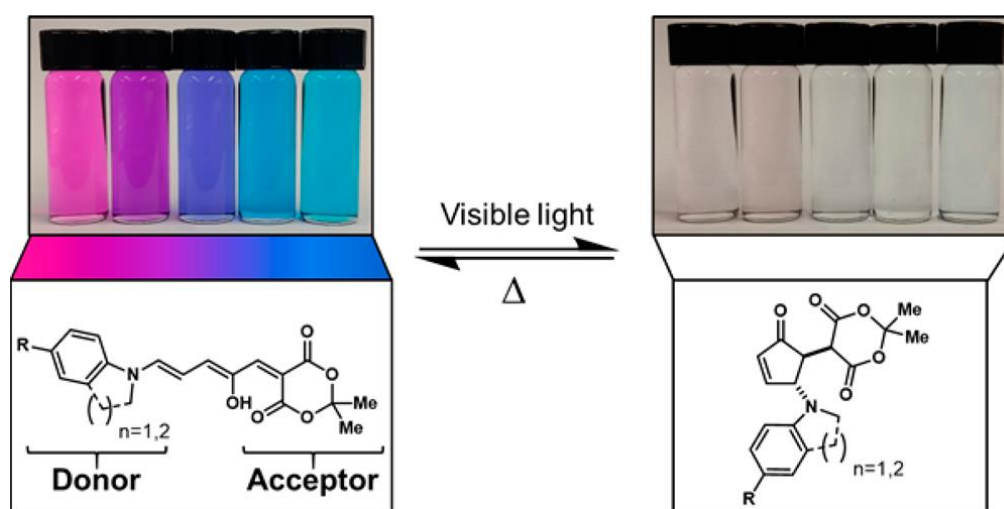


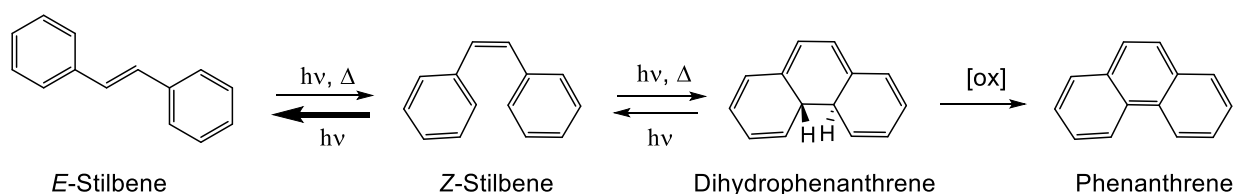
Figure 34. DASAs are generally characterized by an aniline based donors part and a Meldrum's acid acceptor scaffold. The open colored isomer (left) is converted in the colorless closed isomer (right) using visible light irradiation.²⁶⁸

DASAs show T-type photochromism between the spatially extended π -conjugated colored form and the compact colourless zwitterionic form. Furthermore, they also play on the hydrophobicity because the open form of the DASA molecule is hydrophobic, while the closed form is hydrophilic.²⁶⁹ In aqueous medium, the open form is not stable and converts to the cyclic zwitterionic form irreversibly but it has recently been reported that a new self-assembled Pd₈ molecular vessel (MV) can stabilize and store the open form of DASA even in aqueous

medium.²⁷⁰ The photoisomerization kinetics of DASA change is based on different concentrations, it switches efficiently at micromolar concentrations in both liquid solution and in polymers, but when the photochrome concentration is increased there is a dramatic inhibition of the photoisomerization.²⁷¹

2.2.2. Diarylethenes (DAEs)

Diarylethenes are 1,2-aryldisubstituted ethene derivatives, basic examples being stilbene and 1,2-diphenylethene. The thermally stable *E*-form of stilbene can be photoswitched to the instable *Z*-form, that upon further photonic excitation can undergo to a 6π -electrocyclic ring-closing reaction in air with subsequent oxidation to yield the stable product phenanthrene *via* hydrogen elimination (**Scheme 1**). This last reaction can be avoided methylating the *ortho* positions of the phenyl rings to obtain a longer thermal lifetime of this switch that normally is only 1.5 minutes at room temperature. On the other hand, in anhydrous conditions the isomerization is reversible.^{267,272}



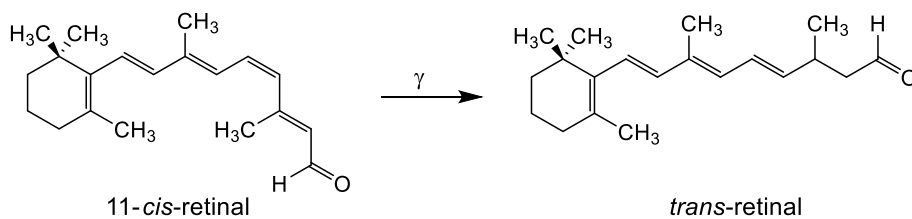
Scheme 1. Photothermal reactions of stilbene, leading to the irreversible formation of phenanthrene.

The introduction of heteroatoms in the aromatic ring systems increases the thermal stability of the closed form giving a bistable photoswitch while it lowers the aromatic stabilization energy of the open form.²⁷³ DAE cyclization process must be induced by UV light but the extension in the π -conjugation with electron donating groups leads to derivative able to photocyclize under 405-nm light with a good photochromic efficiency. Thus, absorption and moderate fluorescence can be switched effectively in both directions by visible lights (405 and 520 nm, respectively) using this strategy.²⁷⁴

2.2.3. Retinal

Retinal is a conjugated chromophore present in the human eye and represents one of the forms of vitamin A. 11-*cis*-Retinal isomer capture a photon of the correct wavelength photoswitching into an all-*trans*-retinal isomer (**Scheme 2**). This configuration changed isomer binds to an opsin

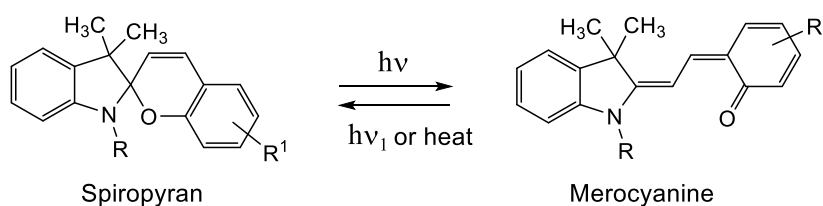
protein in the retina that leads to chemical signalling cascade that can result in perception of light or images by the human brain.



Scheme 2. 11-*cis*-retinal isomerization into *trans*-retinal.

2.2.4. Spiropyrans (SPs)

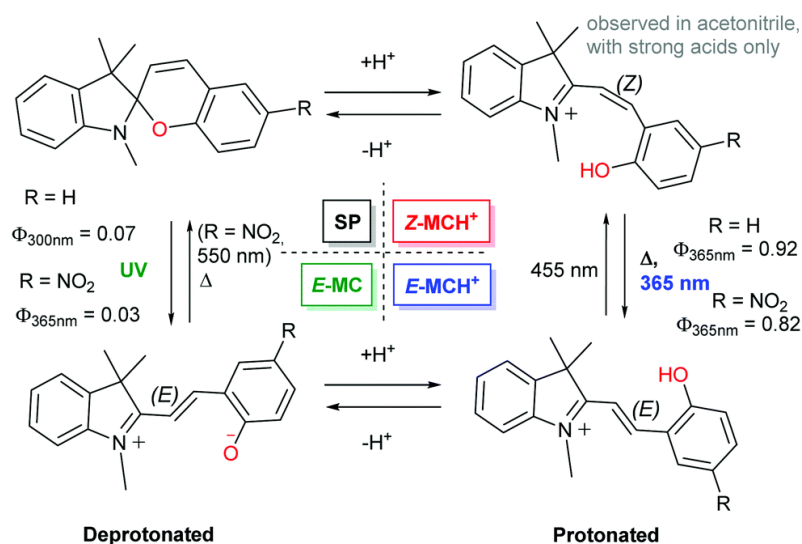
The interest for spiropyrans started at the beginning of the 20th century with the research of Decker and Fellenberg and barely 50 years later their photochromism was discovered by Fischer and Hirshberg.²⁷⁵ The spiropyran photoswitch consists of a ring-closed spiro-form (SP) derived from a chromene connected to an indoline moiety *via* a spiro-carbon. The spiropyran molecule is uncolored but then by photochromic reaction it switches to the colored merocyanine (MC) form (**Scheme 3**).



Scheme 3. Photo- and thermoconversion between spiropyran and merocyanine.²⁷⁶

Spiropyrans can be activated not only by light but by different other stimuli such as acids and bases, solvents, and metal ions, so there is a growing interest for this kind of compounds.²⁷⁷ Furthermore, due to their thermochromism, the change in visible colouration made this new class of colour-changing compounds attractive, as they could be studied without the use of optical equipment. A reversible colour change upon heating was not observed in the original dibenzospiropyran but thermochromism was observed commonly in its naphto- and indolino-derivatives. The solvent has an effect on the progressive colouring of spiropyrans as the increase of solvent polarity is linked to the decrease in the energy of the polar merocyanine forms. This is related to differences in solvation energy and possible H-bonding interactions.²⁷⁸ The mechanism of photoisomerization of spiropyrans starts with an initial photo-induced cleavage of the C1-O bond followed by a *cis/trans* isomerization (over the C2-C3 bond) in the course of SP → MC conversion. In this way, the molecule is transformed from the bulky SP to the planar MC which

electronic conjugation gives an intense visible absorption.²⁷⁹ SPs have acidochromic properties capable of changing color due to charge-induced change in ionization. In particular, in the presence of protons, the polar merocyanine form can be stabilized relative to the apolar spiropyran form. Furthermore, the use of stronger acids enable the bistable *Z/E* photoswitching of the ring-opened merocyanin (**Scheme 4**).²⁷⁸

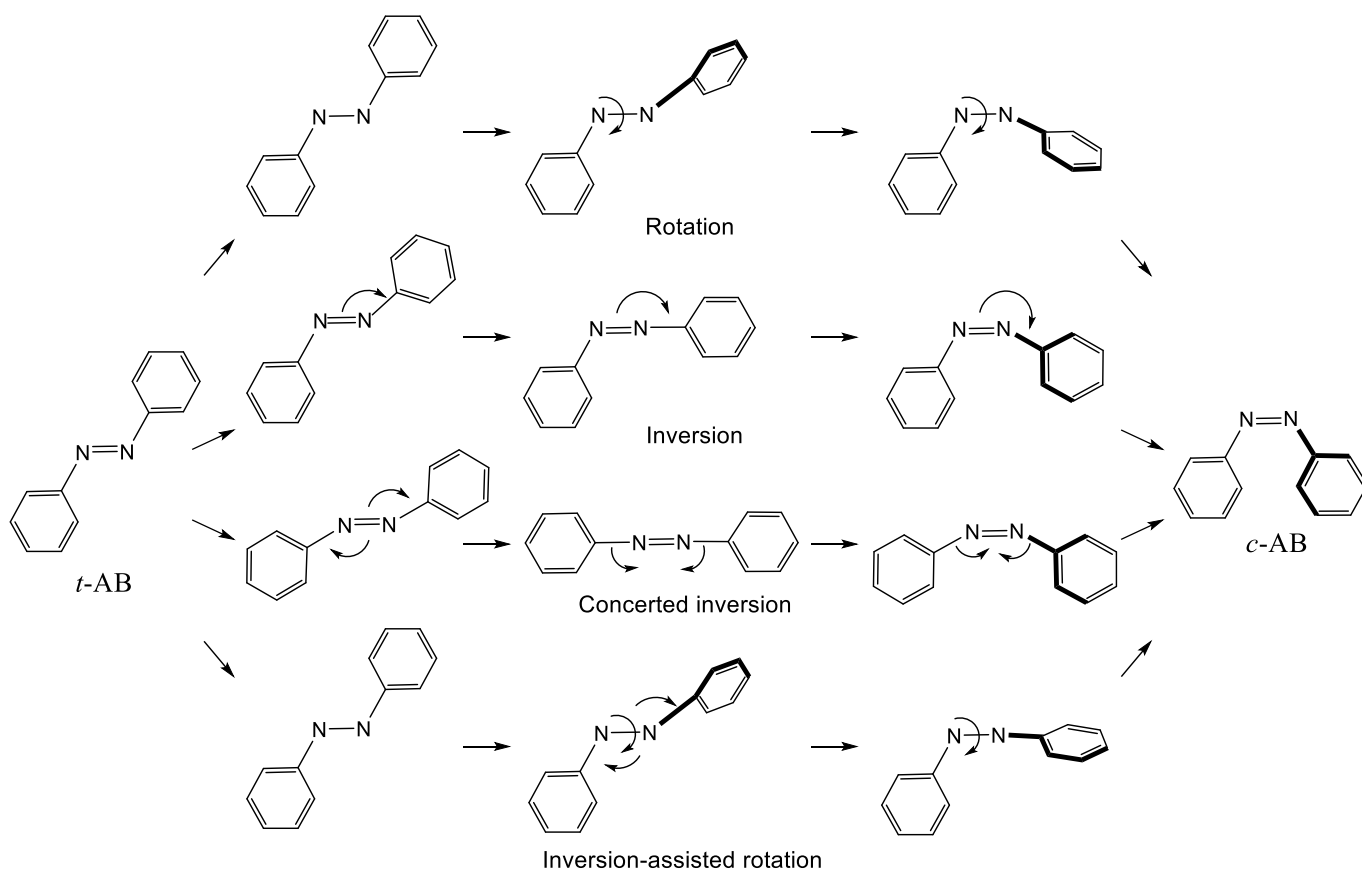


Scheme 4. Four different states of pH-gated photochromism in acetonitrile are obtained using strong acids. The use of weak acids limits the acidochromism observation.²⁷⁸

2.2.5. Azobenzenes (ABs)

Azobenzenes form one of the largest class of photoswitchable molecules and their success is due to the easy synthesis, the fatigue resistant photoswitching and the application in biology. Classic azobenzene consists of two azo-bridged benzene rings, which exists in two isomeric forms: the thermally-favored *E*-form and the *Z*-form, which is unstable and thermally reverts to the *E*-form, but this reaction can also be triggered with light. The main limiting characteristic of azobenzenes is the thermal instability toward isomerization associated with the *Z*-form that is due to the proposed dipolar transition state. Therefore, in general the rate of thermal *Z* → *E* isomerization increases with solvent polarity.²⁸⁰ The *trans*-AB absorption spectrum shows two bands in the UV visible region, the strongest UV band around λ_{max} 320 nm that arises from the symmetry allowed $\pi \rightarrow \pi^*$ transition and the weaker band in the visible region around λ_{max} 450 nm that remains unresolved even at low temperatures and corresponds to the symmetry forbidden $n \rightarrow \pi^*$ transition. On the other hand, $\pi \rightarrow \pi^*$ transitions of *cis*-AB around 250 nm are weaker, but the $n \rightarrow \pi^*$ transition around 450 nm absorbs more strongly than *trans*-AB. The *trans* → *cis* isomerization of *trans*-AB follows both $S_1 \rightarrow S_0$ and $S_2 \rightarrow S_0$ excitation and *cis*-AB into *trans*-AB

exciting to the S_1 or S_2 state.²⁸¹ According to X-ray and computational studies *trans*-AB have a planar structure with C_2 symmetry, while *cis*-AB has a non-planar conformation with C_2 symmetry.²⁸² AB photoisomerization is due to four different proposed mechanisms: rotation, inversion, concerted inversion, inversion-assisted rotation.²⁸¹ In the rotation mechanism there is the break of the N=N π -bond that leads to the free rotation about the N–N bond. Rotation changes the C–N–N–C dihedral angle while the N–N–C angle remains fixed at almost 120° . On the contrary, in the inversion mechanism, there is a transition state with one sp hybridized azo-nitrogen atom, this means that one N=N–C angle increases to 180° while the C–N=N–C dihedral angle remains fixed at 0° . In isomerization by concerted inversion there is a linear transition state so both N=N–C bond angles increase to 180° , while in inversion-assisted rotation there are at the same time large changes in the C–N=N–C dihedral angle and smaller but significant changes in the N=N–C angles (Scheme 5).²⁸¹



Scheme 5. Different proposed mechanism of photoisomerization.²⁸¹

The isomerisation mechanism of azobenzene is influenced by the addition of electron donating and/or electron withdrawing substituents.²⁸¹ Furthermore, the addition of substituents to azobenzene can have a large effect on the properties of the photoswitch, as the thermal isomerisation rate or the wavelength and intensity of absorption maxima. Four different classes

have been identified based on the substituents: azobenzenes, aminoazobenzenes, push-pull azobenzenes and protonated azobenzenes (**Figure 35**). The azobenzene class includes substituted azobenzenes whose properties are similar to those of azobenzene itself, so the $\pi \rightarrow \pi^*$ transition occurs in the UV region and it is well separated from the $n \rightarrow \pi^*$ transition. In aminoazobenzenes there are electron donating substituents leading the $\pi \rightarrow \pi^*$ transition to shift to higher wavelengths giving the overlap between the two transitions. The thermal isomerisation rates are faster than for azobenzene itself, and half-lives range from several hours to milliseconds. Finally, in protonated and push-pull azobenzenes the $\pi \rightarrow \pi^*$ and $n \rightarrow \pi^*$ are nearly degenerated in energy.²⁸¹

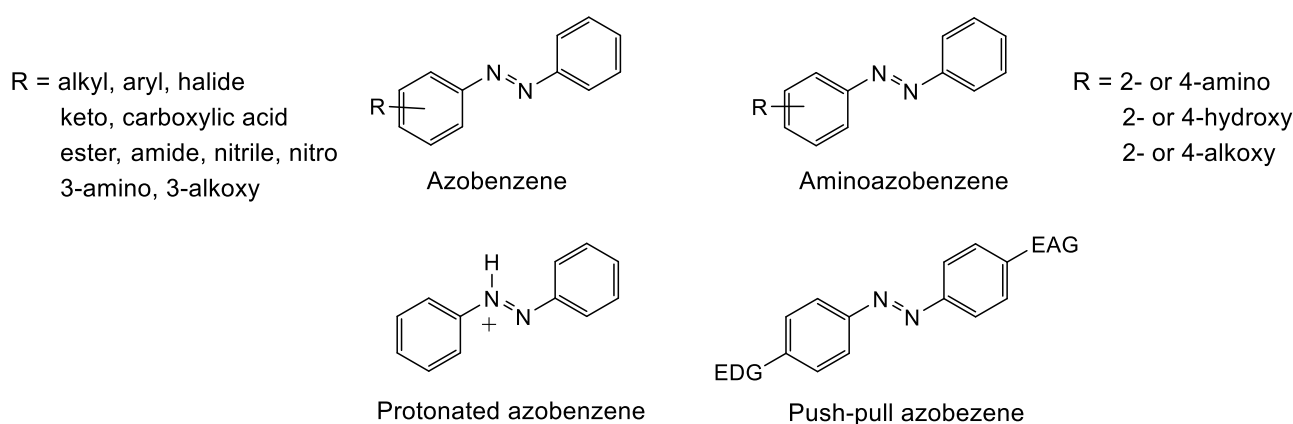


Figure 35. Different classes of azobenzenes.

The donor–acceptor substitution system of the push-pull gives a strong charge transfer into the $\pi\text{-}\pi^*$ electronic that leads to a large red-shift of the $\pi\text{-}\pi^*$ absorption band from the near-UV into the visible region in contrast with the normally much weaker $n\text{-}\pi^*$ transition of conventional azobenzenes. Consequently, the energy barrier of the S_0 electronic ground state is lowered between the two isomers and the thermal $Z \rightarrow E$ back-isomerisation at room temperature is faster than usual compared to classic azobenzenes as it happens in times of just seconds to milliseconds, depending on the solvent.²⁸³ Push-pull substituents at the *para* positions delocalizes the azobenzene chromophore leading to higher wavelength absorption like in infrared region allowing the penetration in human tissues. Unfortunately, this lowers the thermal barrier for the interconversion of the isomer, this is a problem especially in biological application when it is necessary to have a certain stability of the *cis* isomer. This problem can be overcome in different ways by using C2-bridged azobenzene or an antenna to enhance two photon absorption or even the most common method, *ortho* substitution. Electron-donating groups in *ortho* enhance the delocalization affecting the electronic barrier for isomerization and giving slow down thermal

relaxation. The amino groups in position *ortho* to the azo group give higher wavelength photoswitching maintaining slow thermal relaxation in water, but this approach gave photobleaching so other groups are preferred. Methoxy groups are less electron donors than amino groups, but a tetra-*ortho*-methoxy substitution results in sufficiently separated $n\rightarrow\pi^*$ transitions of *cis* and *trans* isomers with blue light and *trans* to *cis* isomerization with green light avoiding the use of UV. In addition, thermal relaxation is really slow in aqueous solution without observing photobleaching.²⁸⁴ The tetra-*ortho*-fluoro substitution gives the same effect of the tetra-*ortho*-methoxy substitution and adding *para*-substituents as electron-withdrawing ester groups allows for further tuning of the absorption spectra, giving rise to a 50 nm separation of the $n\rightarrow\pi^*$ transitions.²⁸⁵ It is possible also to combine *ortho*-fluorination to control the *cis*-lifetimes with longer relaxation time, and *ortho*-amination to enhance the visible-light absorption.²⁸⁶ Azobenzene substituted in *para* by imidazolium salts were used to prepare the respective (NHC)AuCl complexes showing $E\rightarrow Z$ photo-isomerization by irradiation with UV light and slower thermal relaxation compared to other azobenzene compounds.²⁸⁷ Azobenzene based photoswitches can be used to target neuronal receptors allowing optical control of neuronal excitability. These tools can be used to control complex biological systems as the rodent brain and the visual system. New probes are constantly being developed to manipulate a wide variety of signalling pathways (Figure 36).²⁸⁸

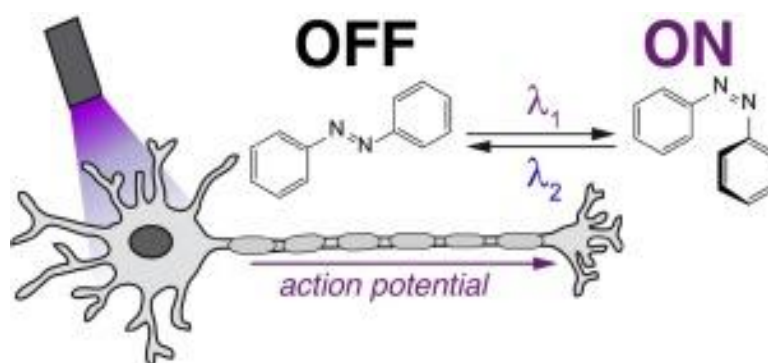


Figure 36. On-off mechanism of a photoswitch azobenzene on neuronal receptors.²⁸⁸

Recently, the synthesis of azobenzene photoswitches with both high two-photon absorption cross section and slow thermal back-isomerization has been reported.²⁸⁹ These compounds show optimized two-photon neuronal stimulation both in light scattering brain tissue and in *Caenorhabditis elegans* nematodes, resulting in photoresponse activities comparable to those obtained under one-photon excitation. In conclusion, pharmacologically selective azobenzene photoswitches are useful tools to study intact neuronal circuits in three dimensions.²⁸⁹ Despite of

the pharmacological interest of this work, azobenzenes have also many applications in material and polymer chemistry.^{290,291}

2.2.5.1. Azologization

New photoswitches can be created by the approach of azologization, *i.e.* the insertion of a diazene unit to replace other functional group. Indeed, many bioactive molecules have similar units to azobenzene, comprising two benzene on either side of different linkers such as stilbenes, *N*-aryl benzamides, benzyl phenyl ethers, benzyl anilines and so on.²⁹² All these functional groups can be replaced by the diazene unit leading to novel photoswitchable analogs called “azosters”.

A recent study by Trauner *et al.*²⁹² showed that searching in database as PDB ligand, Drug Bank and ChEMBL, more than 40000 bioactive molecules are amenable to azologization. Best group to be replaced are *N*-aryl benzamides, 1,2-diarylethanes and benzyl phenyl ethers rather than benzylanilines and sulfonamides. Based on shape similarity scoring functions (3DAPfp) and analyses of dihedral angles the majority of azosters are expected to be active in their *trans* form. The importance of this approach is demonstrated with new photoswitches capable of targeting nuclear hormone receptor (RAR) and lipid processing enzyme (LTA₄ hydrolase).²⁹² On the other hand, azologization of the serotonin 5-hydroxytryptamine 3 receptor (5-HT₃R) antagonist led to nine different azosters, which showed loss of inhibition in patch-clamp studies for all compounds except one.²⁹³ This can be explained by the partial restriction of the thioether *via* incorporation of an azo bridge, which results in an increase of steric demand with loss of activity. In fact, azologization of the less potent compounds resulted in a complete loss of inhibitory activity, while only the originally most potent derivative kept recordable antagonist activity.²⁹³ Azologization of escitalopram, a human serotonin transporter (hSERT) inhibitor, led to a photoswitch that is less active in the *trans* form and highly active in the *cis* form. Using UV light, it is possible to switch the *trans* form to the *cis* which can be converted back to *trans* by 460 nm wavelength irradiation. The *cis* configuration exhibited nanomolar potency and is 43-fold more potent as an inhibitor than the *trans* configuration.²⁹⁴

Recently, the azologization approach was used for the synthesis of β 2-adrenoceptors (β 2-AR) antagonists. Normally, these compounds are constituted of an aromatic ring connected to an ethanolamine backbone through an oxymethylene bridge. The hydrophobic moiety represents the only part of these molecules that is not necessary for the binding to the receptor allowing certain variations to create new azologs. Finally, its replacement with a *p*-acetamido azobenzene led to the synthesis of Photoazolol-1 and -2, two potent β 2-AR antagonists. Surprisingly, the two new

azolones are structural isomers but they exhibit opposite light-regulated pharmacological properties as Photoazolone-1 is most active in the *trans* form while for Photoazolone-2 the best antagonism is observed under the *cis* form. Anyway, both molecules showed the ability to control receptor activation by light irradiation.²⁹⁵

2.2.6. Indigoids and derivatives

Indigoid photoswitches belong to a class of chromophores derived from the parent indigo dye. Unlike other photoswitches, these compounds are able to absorb in the visible region of the spectrum in both *cis/trans* form without adding substituents and avoiding the use of UV light. In recent years, the favorable properties of particular photochromism, efficient photoreactions, and high thermal bistability have led to increased interest in this class of photoswitches. Actually, some applications include the field of supramolecular and biological chemistry, the field of molecular machines and also smart molecules.²⁹⁶

2.2.6.1. Indigo and analogs

Indigo is one of the most known dyes and derives from the plant *Indigofera tinctoria* common in India, Java and China. The plant contains indican so that fermentation followed by air oxidation of the indoxyl moiety leads to the final indigo compound. Plant-based blue indigo production was useful more than one century ago before the development of an industrial synthesis of the first Indigo by BASF that was brought to the market in July 1897. Among the various alternative synthesis routes discovered, the Heumann-Pfleger process is the more efficient and it is still the standard method of industrial indigo manufacture. In this process, phenylglycine, produced from aniline, formaldehyde and hydrogen cyanide, is fused with sodium amide under anhydrous, alkaline conditions.²⁹⁷ The cross-conjugated arrangement of two electron donors and two electron acceptors at a C=C bond is responsible for the color of indigoid dyes. Basically each donor (X) and acceptor (C=O) pair is bonded to benzene, the electron donor can be different atoms, as shown in **Figure 37**.²⁹⁸

X and X' = NH, NR (Indigo)
 O (Oxindigo)
 S (Thioindigo)
 Se (Selenoindigo)
 Te (Telluroindigo)

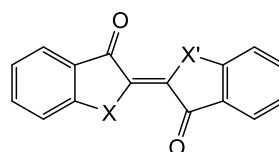


Figure 37. Structure of indigo and analogs.

Electron donor atom X can be also different giving unsymmetrical indigo derivatives. Anyway, today the interest is mainly focused on indigo and thioindigo.²⁹⁸ Indigo shows high photostability due to an efficient excited state proton transfer, which prevents destructive side reactions and gives the original ground state after light absorption. For these reasons, indigo cannot photoisomerize but the substitution of the NH protons with carbon-based alkyl or acetyl substituents gives indigo analogs able to photoisomerize.²⁹⁶

2.2.6.2. Hemi-indigo

Hemi-indigo, which is constituted of one half indigo and one half stilbene sharing central double bond (**Figure 38**), was first described by Adolf von Baeyer in 1883 and was named “Indogenide” after its synthesis by condensation of indoxyllic acid and aldehydes. Although it has been known as a chromophore for over 100 years and exhibits established spectroscopic properties, the photochemistry of hemi-indigo has long been unexplored, particularly with regard to photoswitch applications.²⁹⁹

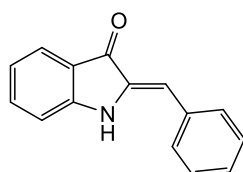


Figure 38. Structure of hemi-indigo.

Donor substituents on hemi-indigo lead to formidable photoswitches with nearly perfect reversible switching behaviour in the red part of the visible spectrum. In particular, the amine substituents at the stilbene moiety can give a strong push (electron-donating stilbene)–pull (electron-accepting carbonyl group) character through the central double bond, which leads to a significant red shift of the absorption. The same effect can be also obtained using different substituents at the nitrogen atom of the indigo fragment. This leads to a precise photocontrol of their geometry at wavelengths up to 565 nm in the *Z* to *E* switching direction and up to 680 nm in the *E* to *Z* direction and high thermal stability of the individual isomeric *Z* and *E* states.²⁹⁹ Recently, a series of water soluble hemi-indigo derivatives was synthesized to study their properties in aqueous medium. The dimethoxy hemi-indigo derivative shows great photochromic performance in water resulting in usefulness for the development of photoswitchable binders for biomolecules. The introduction of an alkylamino group to the dimethoxy hemi-indigo core allowed to obtain an

HIV1 RNA-binding hemi-indigo derivative with photoswitchable fluorescent properties (**Figure 39**).³⁰⁰

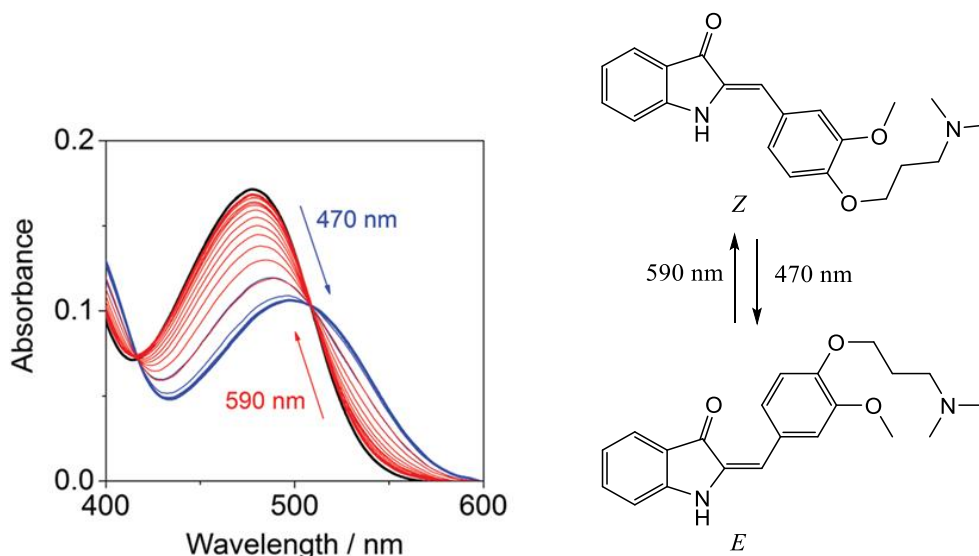


Figure 39. Hemi-indigo *Z*–*E* isomerization shown by absorption spectra ($c = 15 \text{ mM}$).³⁰⁰

2.2.6.3. Hemithioindigo (HTIs)

HTIs, are hemi-indigo in which the amine is replaced by a sulfur atom (**Figure 40**). Photoisomerization of the central double bond give the *Z* and *E* configurations, with the *Z* configuration being the thermodynamically stable form and *E* being the metastable one. HTIs are highly bistable switching system because the barrier for the thermal *E/Z* isomerization of HTIs (typically $>27 \text{ kcal/mol}$) is significantly higher than the corresponding barrier for the thermal *cis/trans* isomerization of the most commonly used azobenzenes (*ca.* 625 kcal/mol).

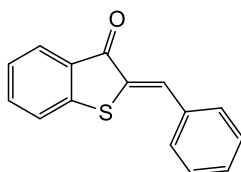


Figure 40. Structure of hemithioindigo.

Furthermore, these compounds show highly fatigue resistant isomerization so the isomerization process can be repeated thousand times before the deterioration of the dye. The introduction of electron-donor substituents enhances the donor capacity of the stilbene part, increasing the donor-acceptor character of the central double bond. In these conditions, a red-shifted absorption is possible but the thermal back isomerization is accelerated.³⁰¹ The group of Newhouse synthesized in 2017 pyrrole hemithioindigo photoswitches designed to possess a key intramolecular hydrogen-bond interaction in only one isomeric state, leading to quantitative

isomerization using blue, green and red light.³⁰² The recent addition of conjugated π -systems on both 3' and 5' positions of the pyrrole ring gave longer-wavelength photoswitches with quantitative isomerization and improved tunability properties (**Figure 41**).³⁰³

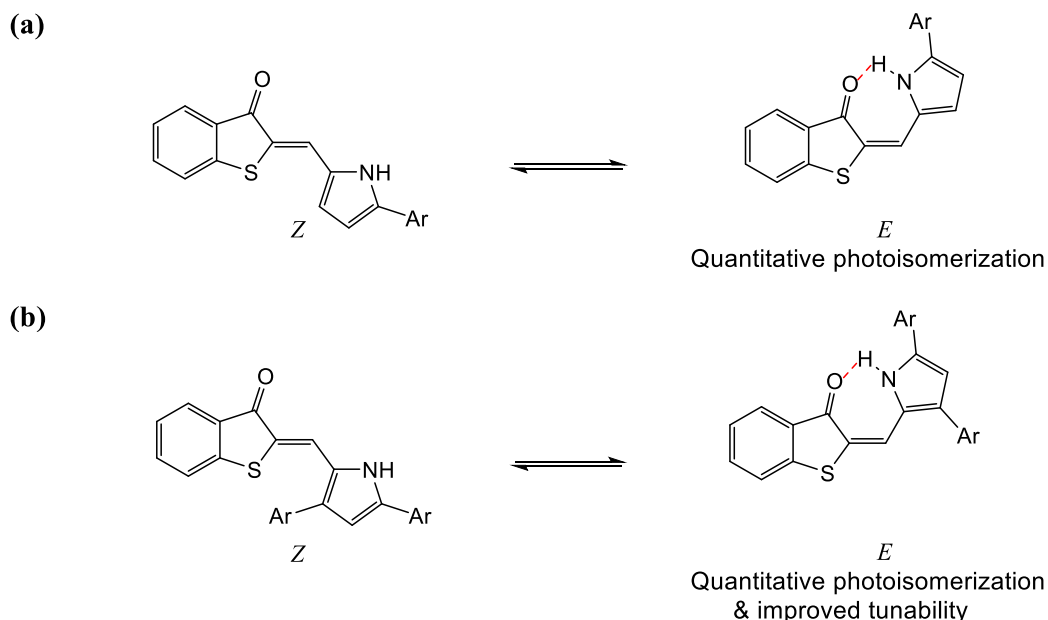


Figure 41. (a) Structure of pyrrole hemithioindigo (b) Derivatives of pyrrole hemithioindigo with π -extension.

HTIs have been used in biological applications to create light-switchable peptides³⁰⁴ and to optically control microtubule depolymerisation and cell death in unmodified mammalian cells.³⁰⁵ Recently, iminothioindoxyl, structurally similar to thioindigo has been synthesized showing excellent photochemical properties. The structure of iminothioindoxyl is a hybrid of thioindigo and azobenzene (**Figure 42**). The stable *Z*-isomer shows an absorption band in the 400-500 nm region in spite of the thermally unstable *E* isomer that absorb at 500-600 nm. The two isomers show a 100 nm band separation in the visible range in all solvents even in aqueous solution with a half-life of milliseconds. Thus, this class of compounds can have useful applications in photoresponsive materials and photopharmacology due to the defined separation of the two isomers and the fast thermal relaxation.³⁰⁶

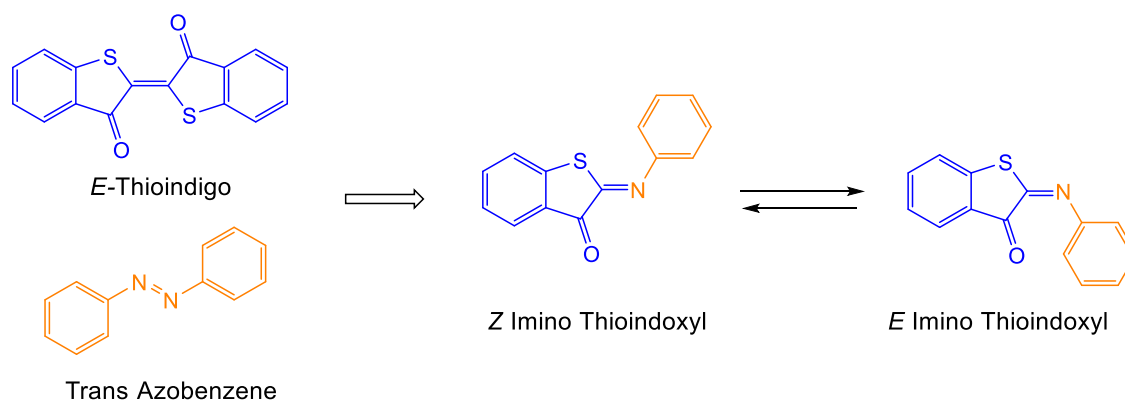


Figure 42. Design of Imino Thioindoxyl.

2.2.6.4. Aurones or Hemioxiindigo

Aurones belong to the flavonoid class of compounds, which includes the flavones, flavonols, isoflavones, flavanones, chalcones. All these compounds are yellow natural dyes suitable for dyeing purposes (**Figure 43**).³⁰⁷ Aurones, structurally isomers of flavones, consist of a benzofuranone ring linked through a carbon-carbon double bond to a phenyl moiety. Among the large family of flavonoids, aurones are distributed in numerous families and species, including plants such as *Ceanothus americanus* (New Jersey tea), *Glycyrrhiza glabra* (licorice) or *Vaccinium oxycoccus* (European cranberry).³⁰⁸ In addition to the flowering plants, aurones are also found in gymnosperms bryophytes and brown algae (4'-chloroaurone).³⁰⁹

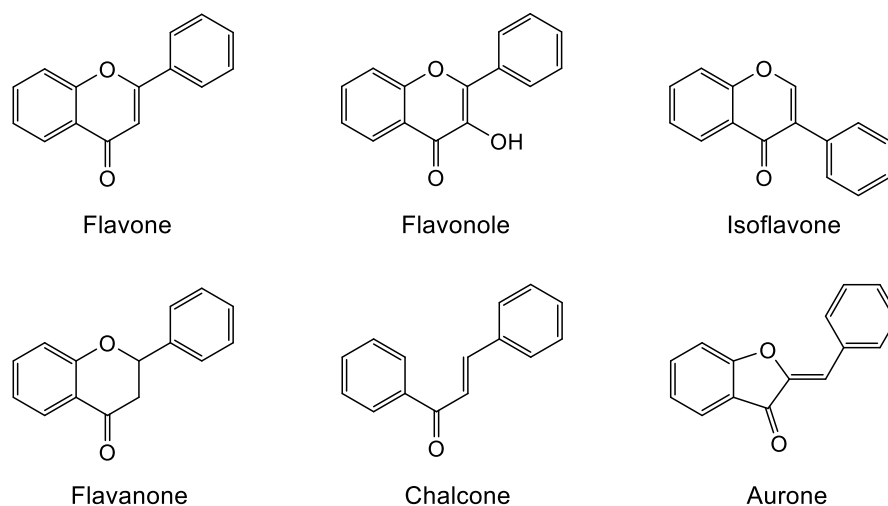
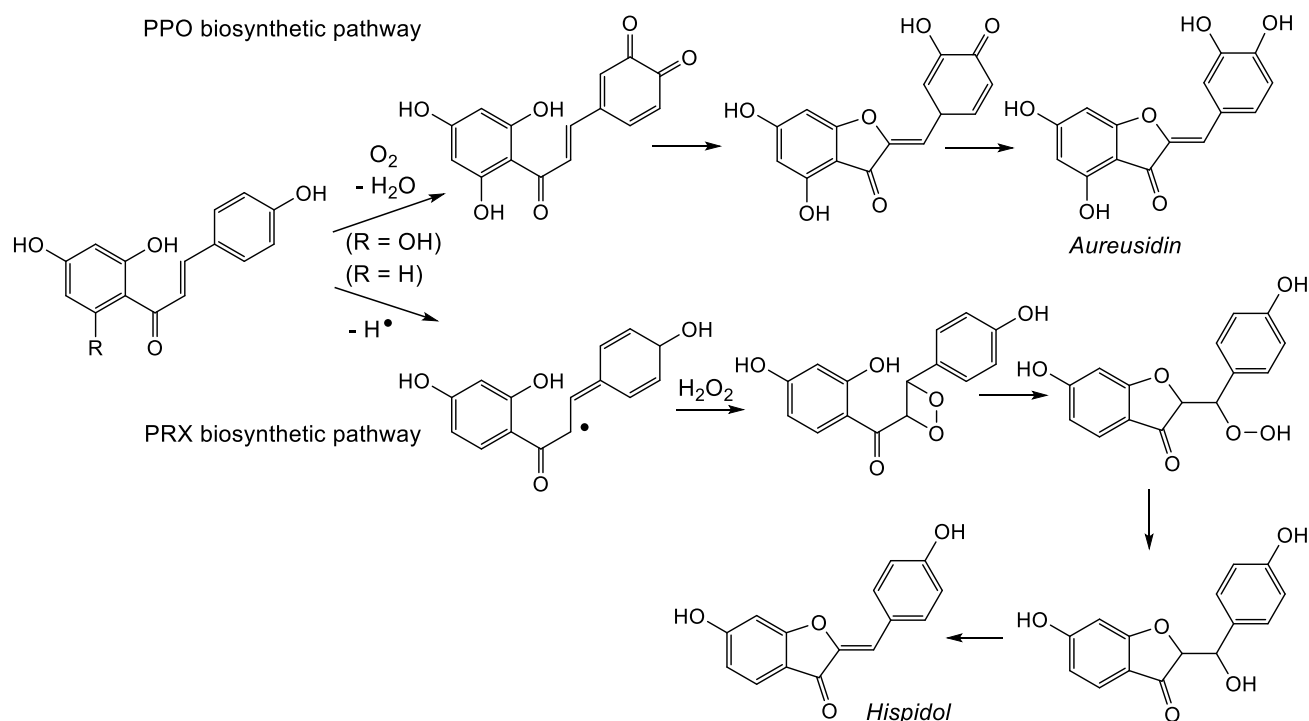


Figure 43. Compounds of the flavonoid class.

In general, there is a remarkably low amount of aurones in plants, compared with other flavonoids, so that a clear correlation has not been established between their traditional therapeutic use and isolated bioactive derivatives. Aurones are biosynthesized starting from coumaryl-CoA through hydroxylation and oxidative cyclization mediated by the metalloenzyme Aureusidin synthase. This

biosynthetic pathway leads to the formation of 3',4'-dihydroxy and 3',4',5'-trihydroxyaurones but other aurones, such as hispidol or 4,6,4'-trihydroxyaurone, are synthesized through different pathways. Unlike the aureusidin pathway, the synthesis of hispidol is catalyzed by a peroxidase, with the involvement of a hydrogen peroxide molecule (**Scheme 6**).³⁰⁸ A common method to prepare aurones is based on the aldol-like condensation of benzofuran-3(2H)-ones with benzaldehydes in basic or acid conditions. The synthetic approach gives the geometric (*Z*)-isomer, that is generally more stable thermodynamically than the (*E*)-isomer. An alternative method is the Steglich esterification followed by a Suzuki coupling.³¹⁰ Inspired by biosynthetic pathway, aurones can be prepared starting from chalcones by oxidative cyclization performed in various conditions, using mercury(II) acetate, thallium(II) nitrate, tetrabutylammonium tribromide or copper(II) bromide.³⁰⁸ The benzofuranone part of the aurone structure is linked to the UV-vis spectral and cytotoxicity properties of aurones. The position of the substituent on benzofuranone turns out to be more important than the exact substituent, aurones with halogen or hydroxy at the 4-position are red-shifted by roughly 10 nm compared to the unsubstituted compound. A halogen or methyl at the 5-position likewise displays a similar shift while hydroxylation at the 6-position displays a significant blue shift by roughly 40 nm.



Scheme 6. Biosynthetic pathways for aurones: the “PPO” pathway involves a plant polyphenol oxidase; the “PRX” involves a peroxidase.³⁰⁸

Concerning the toxicity, halogens in 6- or 7- positions display the lowest cytotoxicity while hydroxylation or substitution at the 4-position lead to higher cytotoxicity, though often no worse than the unsubstituted benzofuranone system.³¹¹ The position of a methoxy group in the 4-position of benzofuranone moiety and the presence of a bromine atom in *para* position of the benzene ring had a strong influence on the fluorescence behaviour of the aurones. The aurone scaffold bearing methoxy and bromine substituents is interesting for developing further fluorescence applications such as visible-range optical sensors.³¹²

Both *E*- and *Z*-isomers of aurones can be found in nature, although the latter is much more abundant. TD-DFT calculations showed *Z*-isomers are more stable than *E*-isomers with energy difference of 3.07 kcalmol⁻¹ for unsubstituted aurone.³¹³ The thermodynamic stability of both isomers is similar, which can be one of the reasons for their simultaneous rise in nature. DFT calculations gave also information about the geometry of aurones that resulted to be planar for both *Z*- and *E*-isomers of aurones.³¹³

In medicinal chemistry aurones have been described for their antitumor and antioxidant activities, cancer chemoprevention, anti-tyrosinase activities, antimicrobial and antiviral activities, anti-inflammatory activities, acetylcholinesterase inhibition and anti-diabetic and anti-obesity activities.³⁰⁸ Recently, a novel multiphotochromic system based on a first generation donor–acceptor Stenhouse adduct (DASA) and an aurone has been described. This system shows the physicochemical properties of the two photoswitches and the four isomers are selectively reachable with three different wavelengths of light (**Figure 44**). Multi-addressable behavior of the system could be beneficial for potential applications such as logic devices and photo-printing.³¹⁴

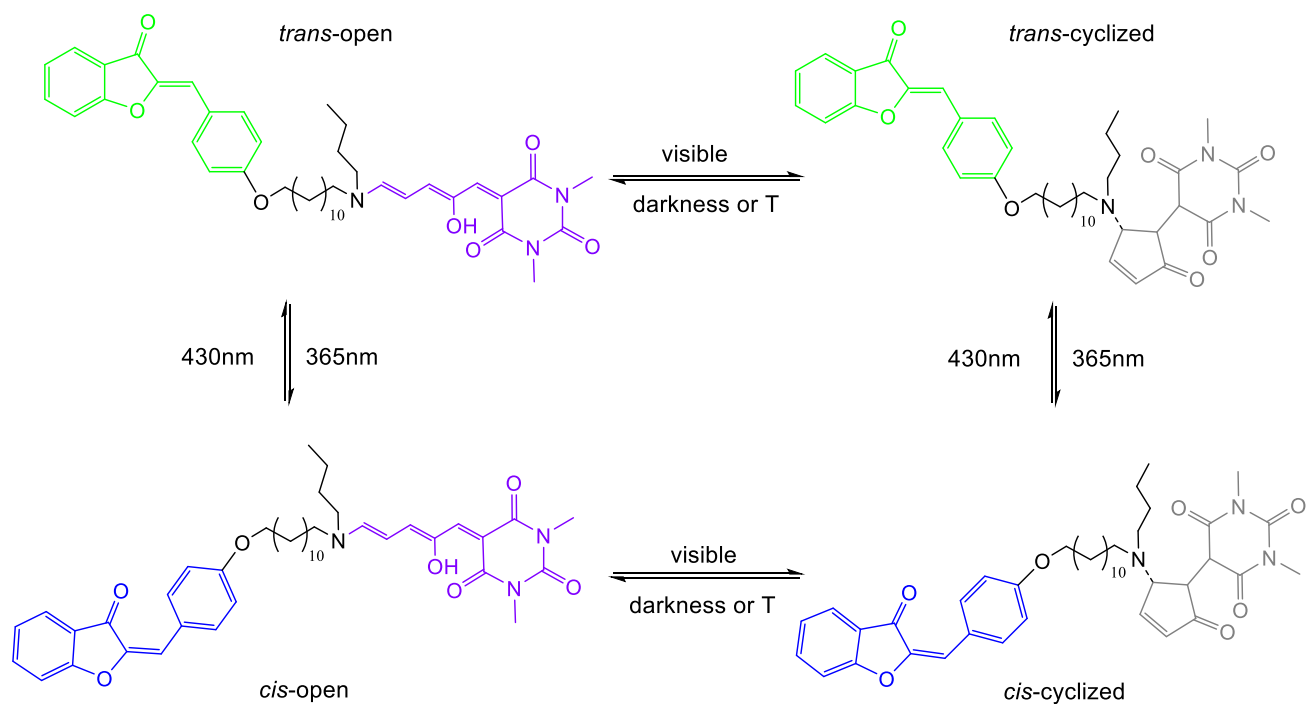


Figure 44. A bis-photochromic molecule switching in toluene at 298 K. Four states are shown using different wavelengths and a thermal relaxation.³¹⁴

Results and discussion

3. CAGED COMPOUNDS OF NMDA RECEPTOR

3.1. Design and synthesis of caged compounds

The first part of this work has been based on the synthesis of two caged compounds: the *N*-DCAC caged D-Serine (**1**) and the *N*-DCAC caged Glycine (**2**). Our aim was the synthesis of these two compounds to test them in electrophysiology studies on brain slices of D-serine racemase knockout mice. The final goal is to investigate the role of D-serine in NMDA activation. In fact, in electrophysiological studies, the potential action of the postsynaptic neuron depolarization will be recorded, proving the hyperactivation of NMDA receptors due to the release of the co-agonist D-serine or glycine from cages **1** and **2**. The project is carried out in collaboration with Dr Jean-Pierre Mothet from ENS Paris Saclay University.

NMDA receptors, as already described in chapter 1.3.1.1., are activated by the binding of the orthosteric agonist glutamate, in combination with the binding of a coagonist that can be either glycine or D-serine. This allows the opening of the central channel with the entrance of Ca²⁺ ions and the depolarization of the postsynaptic neuron.^{21,20} Although the amino acids of the L configuration are most prevalent in mammals, there are racemases, pyridoxal phosphate-dependent enzyme (PLP), for aspartate³¹⁵ and serine in the brain. The serine racemase converts the L-serine in D-serine in presynaptic neurons.³¹⁶ The synaptic availability of D-serine and glycine is regulated by the alanine-serine-cysteine transporter (Asc 1) present in astrocytes and neurons. Asc-1 is able to regulate the efflux and the uptake of D-serine and glycine by exchange with other neutral amino acids leading to the regulation of NMDA neurotransmission. On this basis, Asc-1 can be considered as a valid therapeutic target by inhibiting uptake but not the release of D-serine to relieve symptoms of schizophrenia associated with hypofunction of NMDA receptors (**Figure 45**).^{193,317,318}

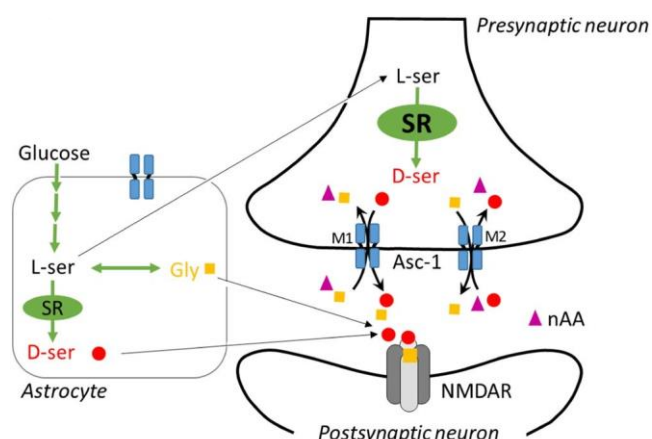


Figure 45. Asc-1 transporter is shown in blue, it controls the release of D-serine (red) in exchange of glycine (yellow) and other natural amino acids (violet). NMDA receptors (grey) are activated by the binding of glutamate with a co-agonist glycine or D-serine. M1 represents the mechanism of efflux of D-serine through Asc-1 and M2 the uptake of D-serine to the presynaptic neuron.³¹⁸

The choice of N-DCAC cages and the synthesis of *N*-DCAC-D-serine (**1**) and *N*-DCAC-glycine (**2**) are presented below. The uncaging of *N*-DCAC-D-serine and *N*-DCAC-glycine will be achieved with two photon irradiation (**Figure 46**), to release a major amount of amino acid in order to activate NMDA receptors; the depolarization will be recorded in electrophysiology on brain slices of D-serine knock-out mice. Preliminary photophysical studies of the caged compounds have been carried out at the Institute of Molecular Science of Bordeaux in collaboration with Prof Mireille Blanchard Desce. The electrophysiological studies will be performed by the group of Nigel Emptage at the Department of Pharmacology of the University of Oxford.

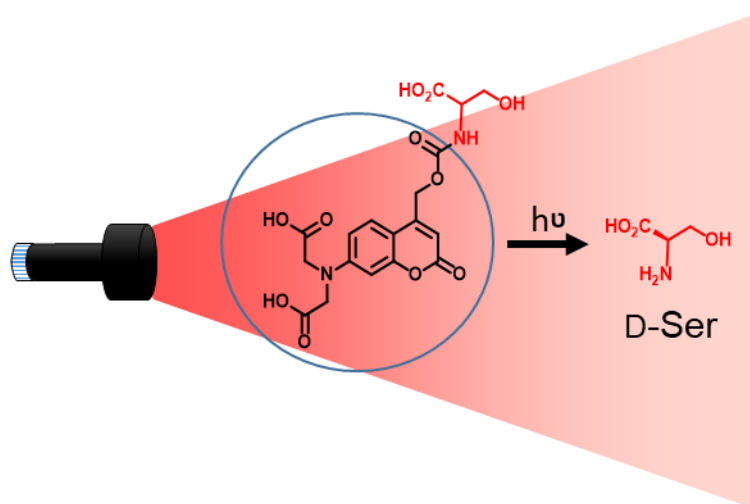


Figure 46. Uncaging D-serine using two photon irradiation.

The caged compounds of our study, were inspired from the *N*-DCAC-GABA³¹⁹ [(7-diacetic acid)-aminocoumarin], the DEAC-OH (7-diethylaminocoumarin)³²⁰ and DEAC450³²¹³¹⁹ cages described by the group of Prof Ellis-Davies from the Icahn School of Medicine at Mount Sinai

in New York (**Figure 47**). In particular, they synthesized a DEAC450 caged glutamate (DEAC450-Glu) and a DEAC450 caged GABA (DEAC450-GABA) starting from DEAC-OH cage and the release of the neurotransmitter was achieved at 900 nm irradiation. In fact, DEAC450-Glu and DEAC450-GABA have an extended π -electron moiety at the 3-position that shifts the absorption spectrum maximum of DEAC from 375 nm to 450 nm. In the case of *N*-DCAC-GABA, the uncaging was achieved at 830 nm to release the highest percentage of GABA.^{322,320,319} A BBCMACMoc-Ser-OH (7-di-*tert*-butoxycarbonylmethyl)amino]coumarin caged compound attached to L-serine by a carbamate bond was synthesized by Tanighughi *et al.* for the solid phase synthesis of a click peptide.³²³ In our study we synthesized the same compound bearing the D-serine and the glycine to obtain after the deprotection step, the corresponding *N*-DCAC caged compounds.

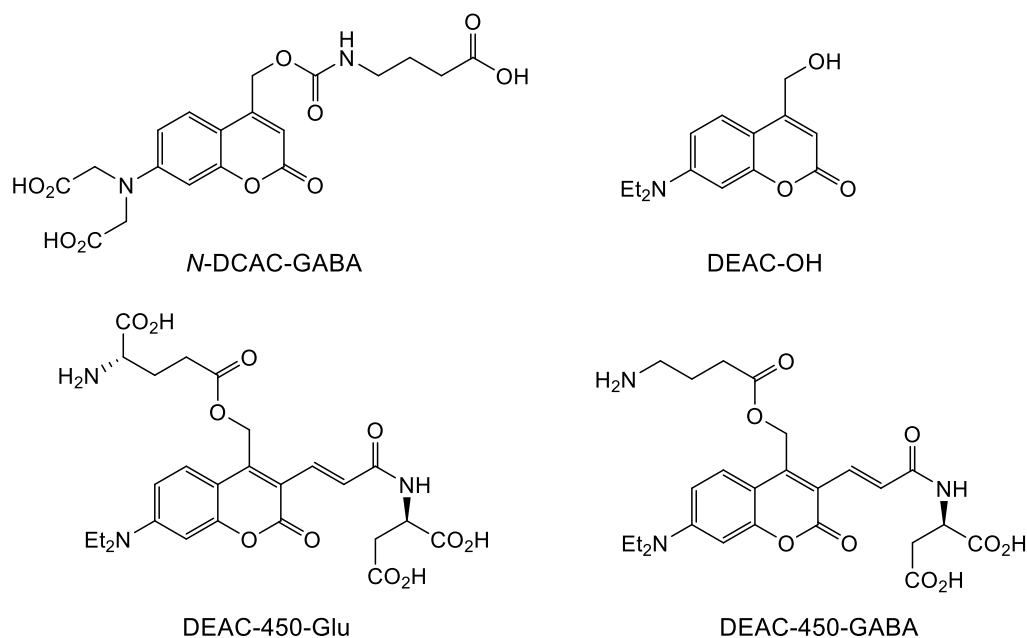


Figure 47. Structure of *N*-DCAC-GABA, DEAC-OH, DEAC-450-Glu and DEAC-450-GABA.

The choice was to synthesize the cages *N*-DCAC-D-serine (**1**) and *N*-DCAC-glycine (**2**) to obtain two compounds soluble in water, with good photophysical properties and that require less synthetic steps compared to DEAC450-caged ligands. Furthermore, the carbamate bond is more stable than the ester bond and this avoid an unwanted spontaneous uncaging during either the synthesis or electrophysiological recordings. Yet these caged compounds remain sensitive to irradiation to release the biological active product. The *N*-DCAC-OH (**3**) was also synthesized to check whether the free cage may be responsible of any side effects and be sure that the activation is only due to the release of D-serine or glycine (**Figure 48**).

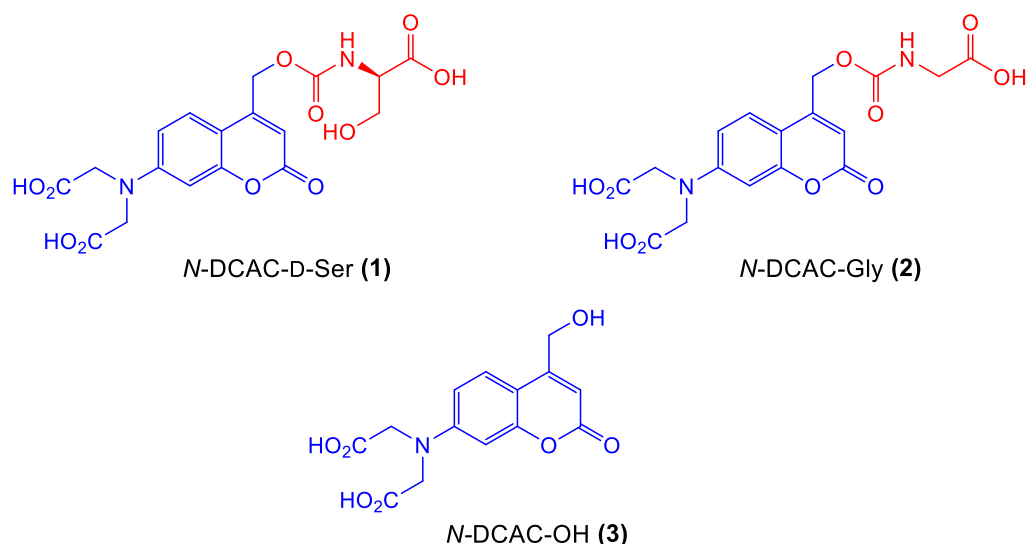
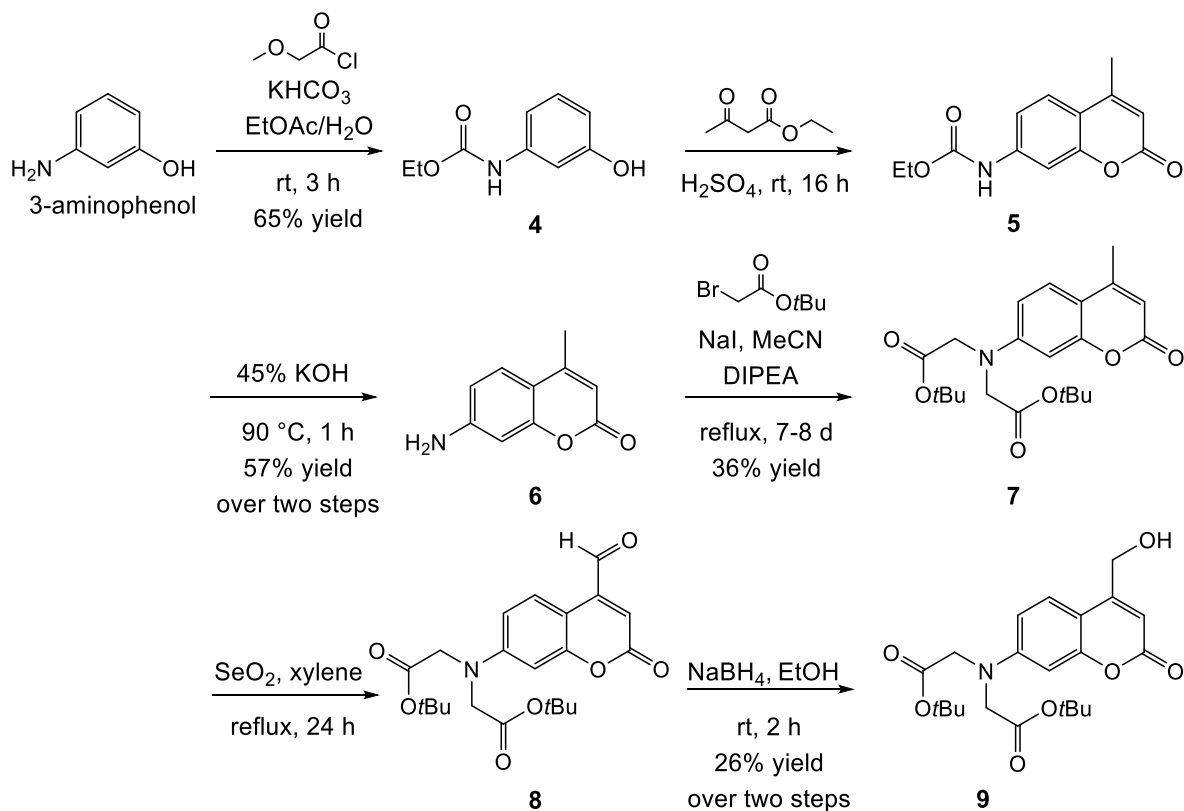


Figure 48. Structure of synthesized *N*-DCAC-D-Ser (**1**), *N*-DCAC-Gly (**2**) and *N*-DCAC-OH (**3**).

3.1.1. Synthesis of the di-*tert*-butyl-*N*-DCAC-OH (**9**)

The diprotected *N*-DCAC-OH (**9**) was synthesized using a synthetic way reported by Noguchi *et al.*, where the synthesis of a photo-triggered and water-soluble protecting group was described from the expensive commercially available 7-amino-4-methylcoumarin **6**³²⁴ in 3 steps (**Scheme 7**).

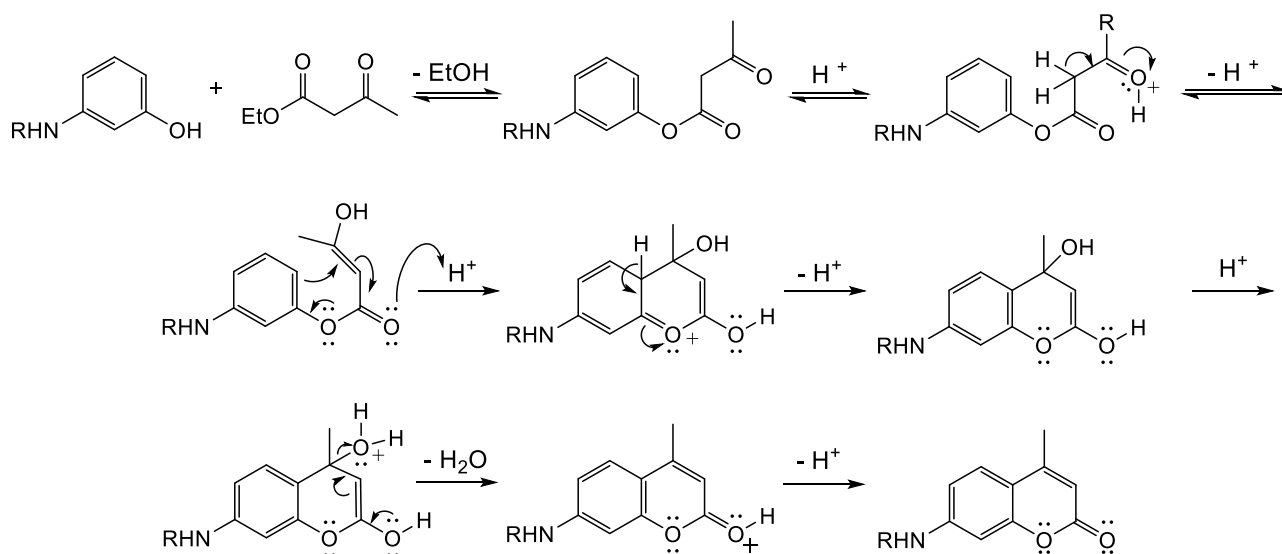
We synthesized the empty *N*-diprotected cage **9** from 3-aminophenol in 6 steps.



Scheme 7. Synthesis of the di-*tert*-butyl-*N*-DCAC-OH (**9**).

The selective protection of the amine of 3-aminophenol using 2-methoxyacetyl chloride in basic medium led to the product **4** in 65% yield. The formation of coumarin **5** was achieved by Pechmann condensation from phenol **4** with ethyl β -keto butanoate.³²⁵

The Pechmann reaction is conducted with a strong Brønstedt acid such as sulphuric acid, methanesulfonic acid or a Lewis acid such as AlCl_3 .³²⁶ The acid successively catalyzes the transesterification, the keto-enolic tautomerization, the Michael addition that leads to the formation of the coumarin skeleton and finally, the dehydration allows the rearomatization as (Scheme 8).



Scheme 8. Mechanism Pechmann reaction.

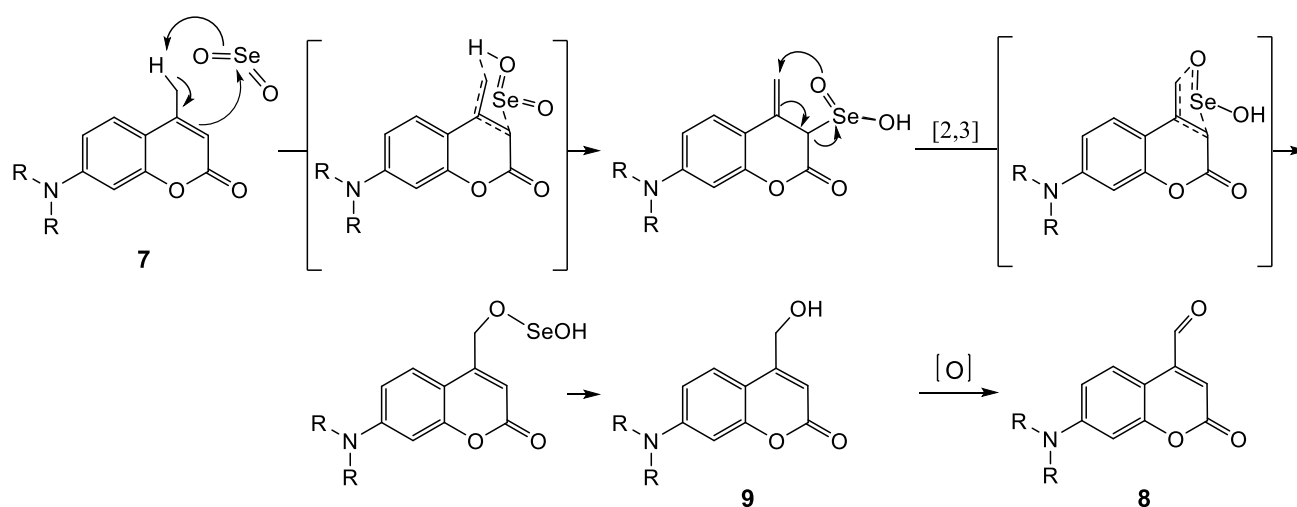
The 7-protected aminocoumarin **5** was then deprotected in basic medium to afford the 7-amino-4-methylcoumarin **6** in 57% yield over the two steps.

Subsequently, the dialkylation of the amino group of compound **6** was carried out with *tert*-butyl-2-bromoacetate to yield compound **7**. Indeed, protection of the carboxylic groups was necessary to avoid the formation of an amide bond with D-serine and the *tert*-butyl group was chosen to be compatible with the deprotection of the final product.

Surprisingly, this reaction did not occur correctly under the reported conditions, where **7** was obtained in 68% yield.³²⁴ Indeed, after heating 4 days, the NMR of the crude mixture showed that the monoalkylated product was still present in a large proportion (62%) with respect to the dialkylated product (38%). These two compounds could not be separated by column chromatography. In contrast, when the reaction has been carried out for 7 days, the percentage of monoalkylated product was really lower (16%) compared to the percentage of dialkylated product (84%) and the purification was easier to recover the pure product **7**. The reaction in the

same conditions was run for 8 days and the same percentage of monoalkylated and dialkylated products were obtained. A crystallization in cyclohexane and diethyl ether gave the pure compound **7** in 36% yield.

The oxidation of methyl in position 4 of coumarin **7** to the corresponding alcohol **9** was carried out by selenium dioxide,³²⁷ which is an effective reagent for the incorporation of oxygen in the benzylic position. The most nucleophilic carbon of the compound attacks this reagent, which after a sigmatropic rearrangement leads to alcohol, which in turn can be oxidized to aldehyde (**Scheme 9**). The crude mixture was taken directly to the reduction step using sodium borohydride to give product **9**.



Scheme 9. Mechanism of oxidation with selenium dioxide.

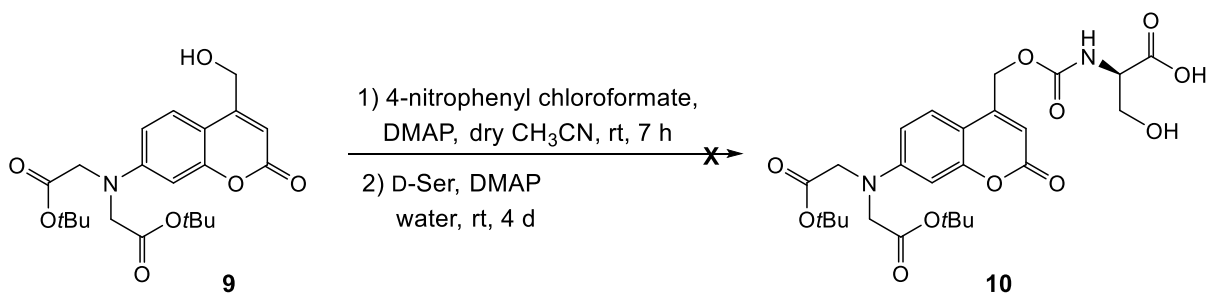
3.1.2. Synthesis of the protected *N*-DCAC-*D*-serine (**10**) and *N*-DCAC-glycine (**11**)

Carbamates can be prepared in several ways, traditionally starting from an amine with the use of coupling agents as chloroformate and CDI.³²⁸

The coupling with *D*-serine and glycine to obtain products **10** and **11** required different essays before finding the best conditions.

The formation of the carbamate bond of the *N*-DCAC-GABA synthesized by Kantevari *et al.* was achieved in presence of 4-nitrophenyl chloroformate (2 eq), DMAP (3 eq) in THF with 4-aminobutyric acid *tert*-butylester (1 eq) to get the product in 56% yield.³¹⁹ Taniguchi *et al.* used the same reagents with the same equivalents but L-serine replaced the 4-aminobutyric acid *tert*-butyl ester and acetonitrile and water were used as solvent. These reaction conditions gave a 60% yield.³²³

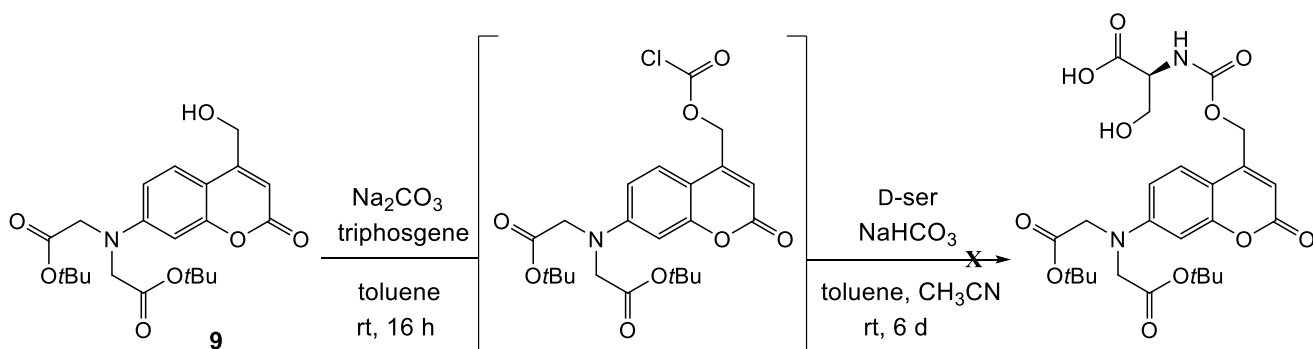
Product **6** was stirred in the same conditions of Taniguchi *et al.* using D-serine but the starting material was recovered along with by-products (**Scheme 10**).



Scheme 10. Attempt to the coupling of D-serine.

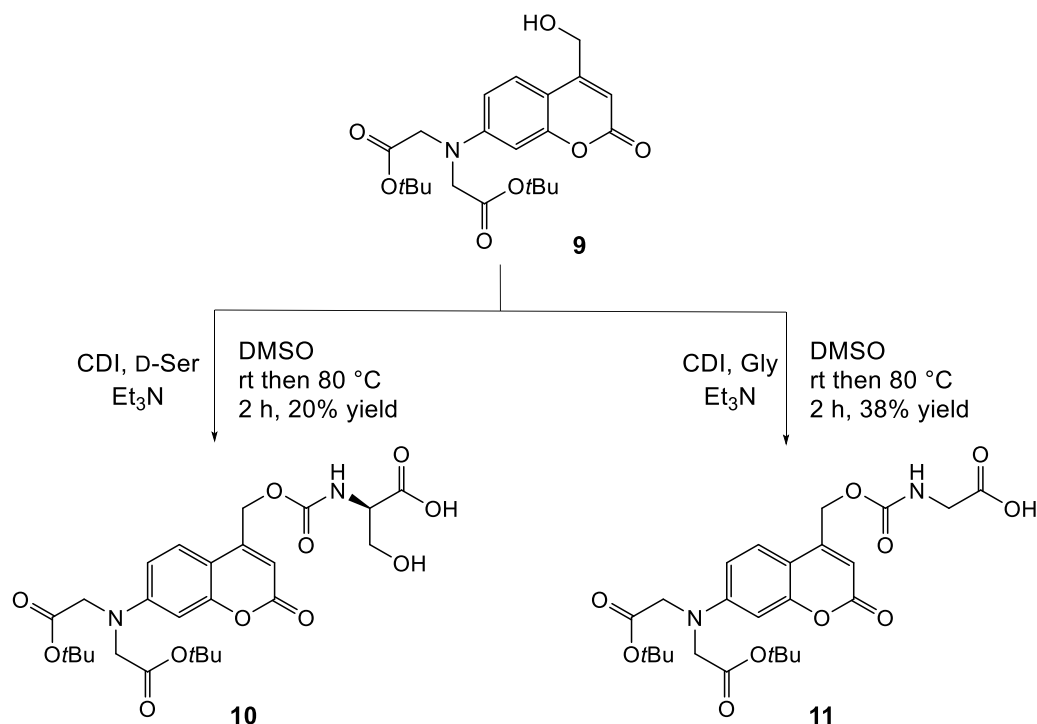
The reaction performed in the same conditions without water also led to a failure.

A further approach was the activation of **9** with an acyl chloride to allow the coupling with D-ser but only the starting material was recovered (**Scheme 11**).



Scheme 11. Attempt to the coupling of D-serine.

Finally, the product **10** was obtained using carbonyldiimidazole as coupling agent in presence of Et₃N.³²⁹ This reaction was performed in DMSO and in DMF but the product was only obtained in DMSO (**Scheme 12**). Product **11** was prepared the same way replacing D-serine with glycine with a better yield (38%) as in this case, in the glycine there is not the other hydroxy present in D-serine thus avoiding other side products (**Scheme 12**).

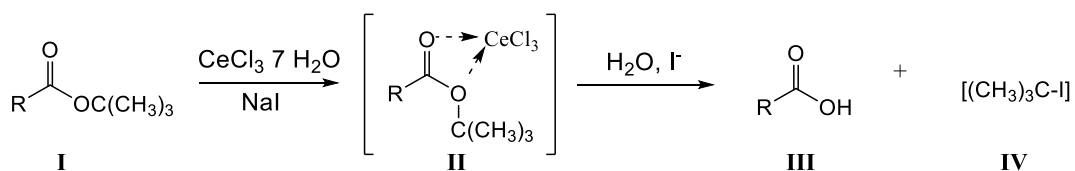


Scheme 12. Coupling with D-serine and glycine.

3.1.3. Synthesis of the *N*-DCAC-D-serine (**1**), *N*-DCAC-glycine (**2**) and *N*-DCAC-OH (**3**)

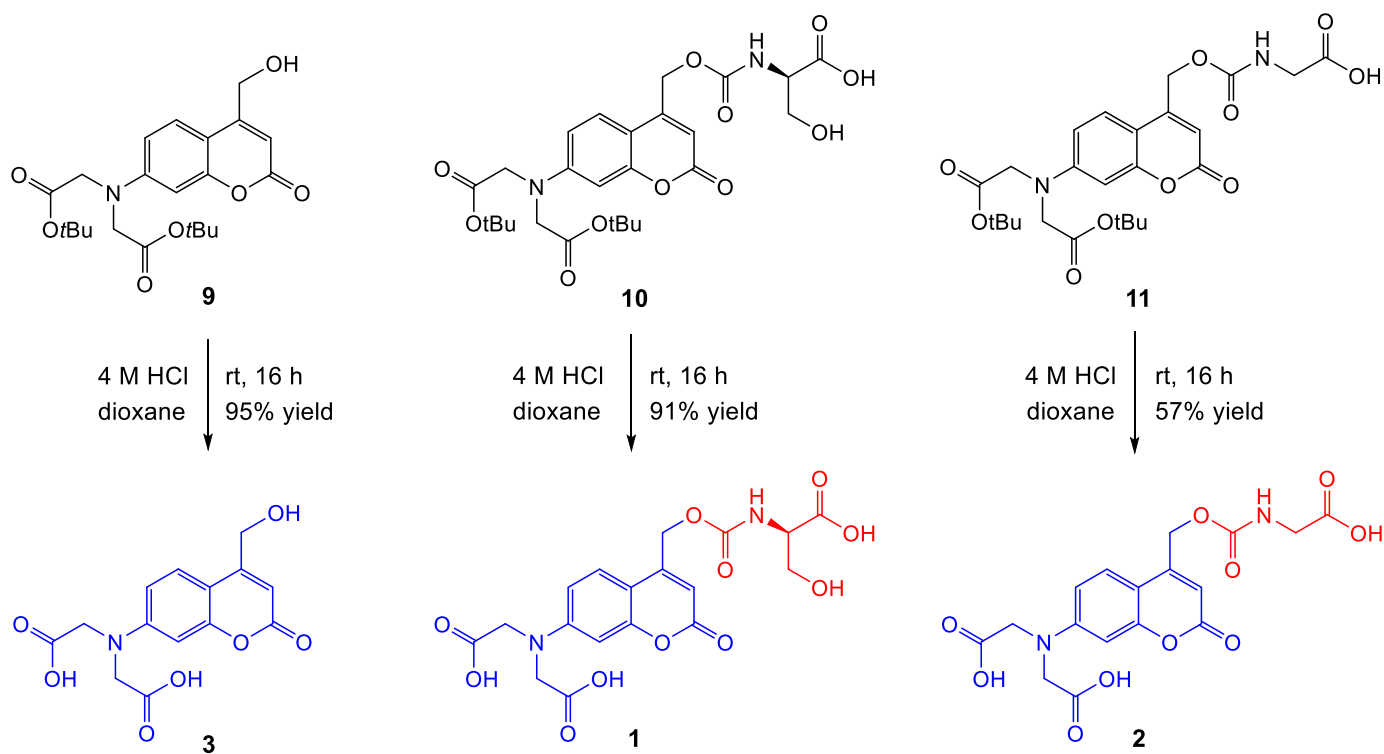
Deprotection of the di-*tert*-butyl ester of compound **9** in classical TFA/DCM 1:1 conditions led after three days at room temperature to the monoprotected product (80%) and some starting material left (20%). The use of 3 M aqueous HCl with THF and acetonitrile led after 4 days to the same result.

Cerium(III) chloride heptahydrate and sodium iodide were used to achieve a total deprotection as they promote the *tert*butyl ester cleavage through the selective coordination of cerium with *tert*-butyl ester oxygen atoms to form a complex (II) which then undergoes water hydrolysis to carboxylic acid (III), liberating the *tert*-butyl carbocation. The latter is trapped by nucleophilic attack of iodide ion to afford *tert*butyl iodide IV (**Scheme 13**).^{330,331}

Scheme 13. Deprotection mechanism using CeCl₃·7 H₂O.

Unfortunately, this method needs a long work-up to take off completely the *tert*-butyl iodide. Finally, compound **9** was deprotected with 4 M HCl in dioxane leading to product **3** in 95% yield (**Scheme 14**).

The final deprotection of **10** and **11** was achieved in these latter conditions to get compounds **1** and **2** in 45% yield and 57% yield, respectively (**Scheme 14**).



Scheme 14. Synthesis of *N*-DCAC-D-Ser (**1**) and *N*-DCAC-Gly (**2**) *N*-DCAC-OH (**3**).

3.2. Photophysical properties of caged compounds

Once the final deprotection was achieved, compounds **1**, **3** and **10** were studied for their photophysical-chemical properties at the Institute of Molecular Science of Bordeaux. These experiments provided two photon absorbance spectra and will guide the choice of the best wavelength to use for the uncaging of the active compound D-serine in the highest possible percentage. The *N*-DCAC-Gly (**2**) was not analyzed as it was synthesized later and at the beginning of the project, we focused only on the synthesis and study of the *N*-DCAC-D-Ser (**1**).

At the beginning, the absorption and emission properties were investigated; so first UV spectroscopy and then fluorescence spectroscopy were used to characterize the compounds.

Ultraviolet–visible spectroscopy refers to absorption in the ultraviolet-visible spectral region. This means it uses light in the visible and adjacent ranges. The absorption or reflectance in the visible range directly affects the perceived colour of the chemicals involved. In this region of the electromagnetic spectrum, atoms and molecules undergo electronic transitions. Absorption spectroscopy is complementary to fluorescence spectroscopy, in that fluorescence deals with transitions from the excited state to the ground state, while absorption measures transitions from the ground state to the excited state. The base of the absorbance or optical density in the UV-spectroscopy is explained by Beer-Lambert law. As shown in **Figure 49** I_0 is the intensity of light that enters in the cuvette while I is the intensity of light going out, so the difference between I and I_0 represents the intensity that has been absorbed by the sample in the cuvette. The ratio between I and I_0 is called transmittance (T) and absorbance is the logarithm of the T^{-1} .

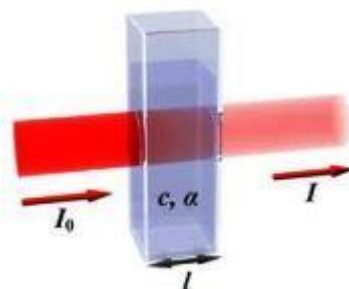


Figure 49. Cuvette used to record absorption spectra.

$$T = I/I_0 \quad A = \log I_0/I = \log T^{-1} \quad A = \epsilon \times l \times C$$

The absorbance is directly proportional to the concentration of the solution C , to the length of the cuvette l and to the molar absorptivity ϵ . The absorbance is adimensional.

The compounds **3** and **10** were dissolved in DMSO while compound **1** first in water then in phosphate buffer (pH = 7.2) and the concentration modulated just to obtain a maximum of absorbance close to 1.0 (**Figure 50**). The finding of the wavelength at the maximum absorbance is necessary to calculate the quantic yield ϕ of the emission.

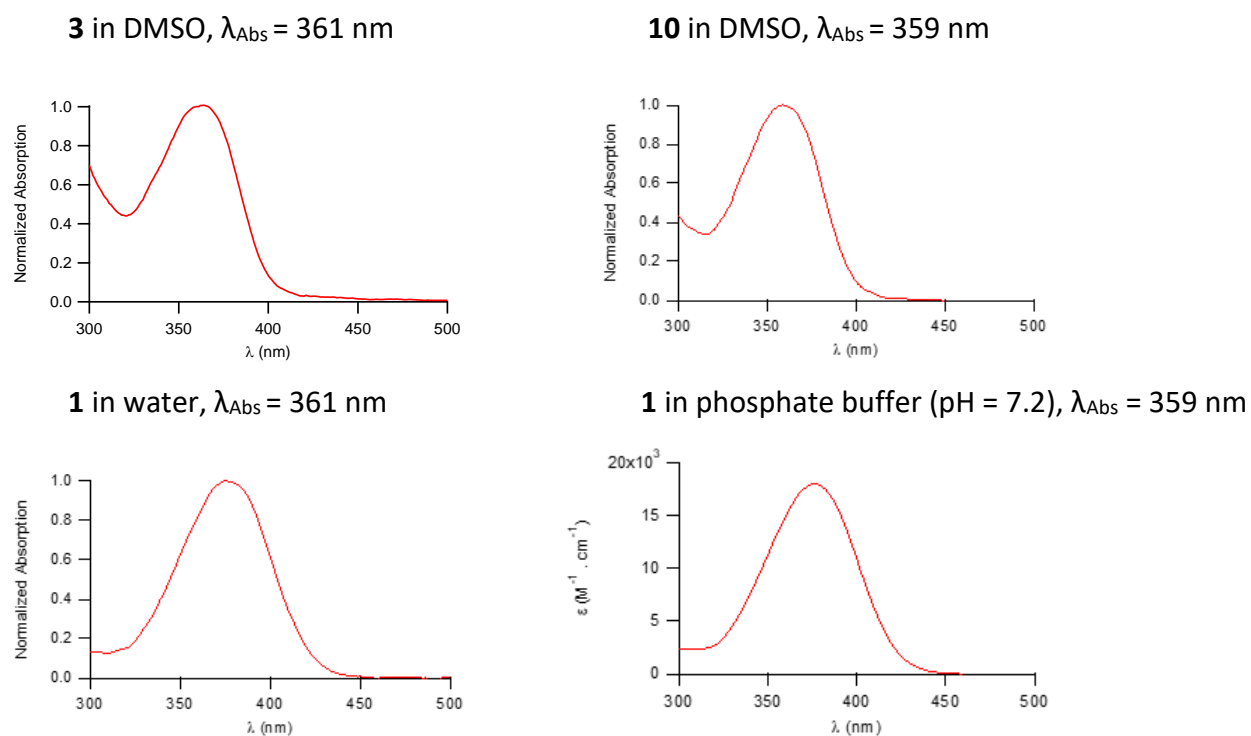


Figure 50. Absorption spectra of products **1**, **3** and **10**.

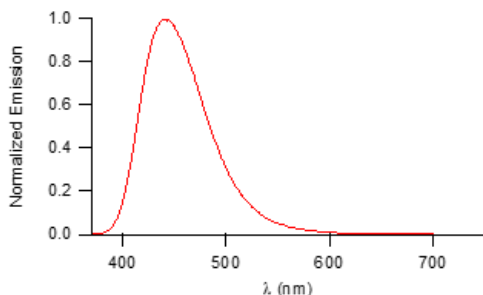
The emission is studied with the fluorescence spectroscopy. Absorbing a photon, the species is first excited, from its ground electronic state to one of the various vibrational states in the excited electronic state. Collisions with other molecules cause the excited molecule to lose vibrational energy until it reaches the lowest vibrational state of the excited electronic state.

The molecule then drops down to one of the various vibrational levels of the ground electronic state again, emitting a photon in the process. As molecules may drop down into any of several vibrational levels in the ground state, the emitted photons will have different energies, and thus frequencies. Therefore, by analysing the different frequencies of light emitted in fluorescent spectroscopy, along with their relative intensities, the structure of the different vibrational levels can be determined.

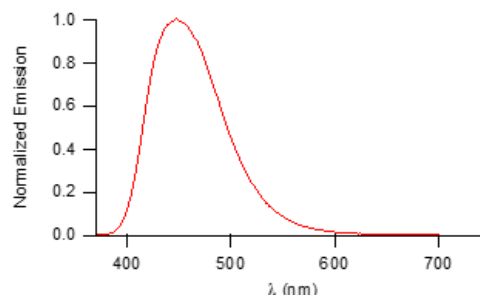
An emission map is measured by recording the emission spectra resulting from a range of excitation wavelengths and combining them all together.

The data collected from absorption and emission spectra are used to calculate the quantum yield ϕ (Figure 51).

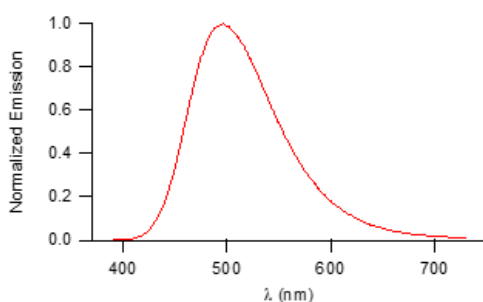
3 in DMSO, $\lambda_{em} = 442$ nm, $\phi = 0.49$



10 in DMSO, $\lambda_{em} = 446$ nm, $\phi = 0.93$



1 in water, $\lambda_{em} = 496$ nm, $\phi = 0.22$



1 in buffer (pH = 7.2), $\lambda_{em} = 497$ nm, $\phi = 0.22$

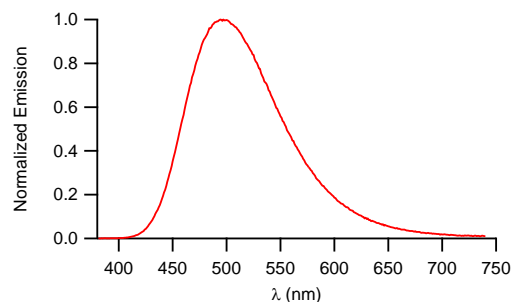


Figure 51. Fluorescence spectra of products **1**, **3** and **10**.

The fluorescence quantum yield is defined as the ratio of the number of photons emitted to the number of photons absorbed. Experimentally, relative fluorescence quantum yields can be determined by measuring fluorescence of a fluorophore of known quantum yield with the same experimental parameters as the substance in question. In the experiments, the reference used for all the compounds was the fluorescein in NaOH (0.1M) ($\phi = 0.9$). The quantum yield is then calculated by:

$$\phi (\%) = \phi_{ref} \times (i_{r_{prod}}/i_{r_{ref}})^2 \times (J_{em_{prod}}^{em}/J_{em_{ref}}^{em}) \times (1 - e^{-\ln 10 \times D_{oref}} / 1 - e^{-\ln 10 \times D_{oprod}})$$

The optical density **DO** was calculated before in the absorption spectra, the parameters of the reference fluorescein are already described in literature and the **ir** represents the refraction index of the solvent used.

Finally, the integral represents the area under the emission curve. Using a specific software, it is easy to calculate automatically all these values and find the quantum yields of the products.

At this point, it was possible to conduct the two-photon experiment to find the wavelength that gives the highest cross section σ_2 . The molecular two-photon cross-section is usually quoted in

units of Goepfert-Mayer (GM) (after the Nobel laureate Maria Goepfert-Mayer discovery), where 1 GM corresponds to $10^{-50} \text{ cm}^4 \text{ s photon}^{-1}$. Even in this case, a reference of fluorescein was used and the σ_2 calculated in a range of wavelength between 600 nm and 1030 nm for compounds **3** in DMSO and **1** in phosphate buffer (**Figure 52**).

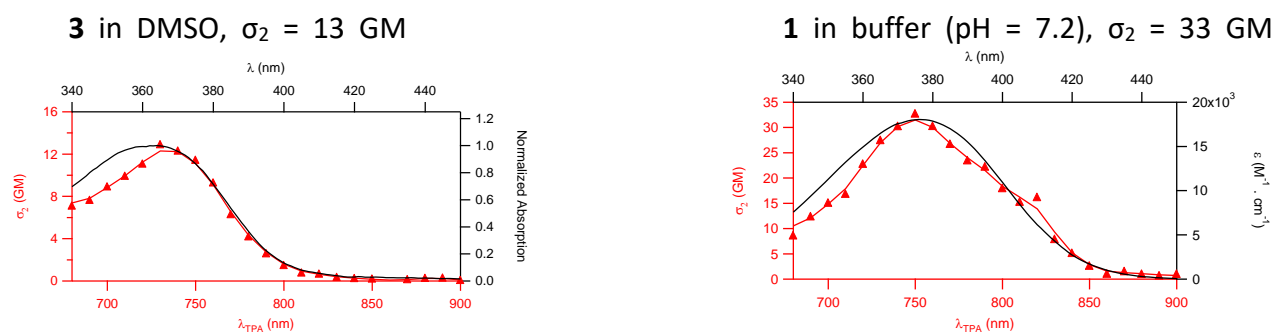


Figure 52. TPA spectra of products **1** and **3**.

It is interesting to note the difference of σ_2 between the two compounds, this is probably due to the solvent and to the carboxylate charges on the nitrogen atom that change polarization giving a bathochromic shift. The highest σ_2 is at a wavelength of 750 nm so the best irradiation for uncaging should be at a wavelength between 720-750 nm to obtain the major release of D-serine.

Concerning compound **2**, the absorption spectra in 0.1 M phosphate buffer (pH = 7.2) showed a λ_{max} at 376 nm (**Figure 53**). Unfortunately, TPA experiment was not run on this product.

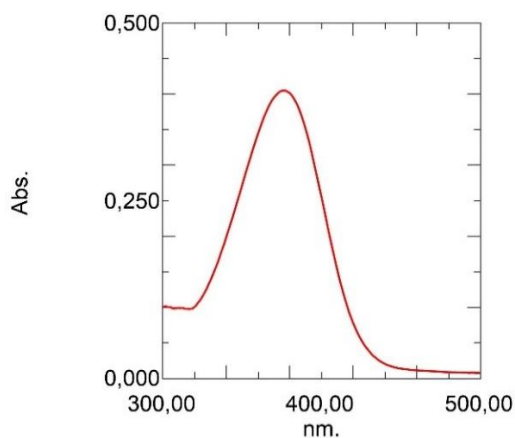


Figure 53. Absorption spectra of product **2**.

The DEAC-450 and the DEAC-OH cages^{320,322} (**Figure 47**) reported in literature show a TPA maximum at 900 nm irradiation, a higher wavelength compared to the 750 nm of our caged compound. This is due to the extended π -electron moiety at the 3-position that is missing in compounds **1** and **2**. In the case of *N*-DCAC-GABA³¹⁹ (**Figure 47**), the TPA maximum absorbance is at 830 nm, a closer value to the TPA maximum absorbance of 750 nm of product **1**. In fact,

N-DCAC-GABA shows the same chromophore of the *N*-DCAC-D-Ser while the amino acid part is different.

3.3. Pharmacological results

As described in chapter 3.1, we have developed new probes for the photo-uncaging of amino acids (D-serine and glycine) by one and two photon irradiation. The cage is a 7-(dicarboxymethyl)-amino coumarin (*N*-DCAC) to which we have attached the glycine, or D-serine, two neurotransmitters we are interested in to validate Asc-1 as a therapeutic target in schizophrenia. A major release of D-serine or glycine by Asc-1 should give a hyperactivation of NMDA receptors that have been shown to be hypoactivated in schizophrenia.

This diethylamino coumarines cages have been widely used for the last 20 years to photo-uncage different neurotransmitters such as glutamate or GABA. This technique allows to control spatially and temporally the release of neurotransmitter and to study the consequences of this on the activity of neurons. Before running physiological experiments, it is necessary to know the quantum efficiency of our cages *i.e.* the quantification of the released amount of amino acid at different concentration using a given wavelength. This study will be performed at the Institute of Molecular Science of Orsay (ISMO) where the samples will be subjected to different durations (1 to 20 msec) and intensities (2 to 20 mW) of light irradiation at 375 nm (1 photon) and 750 nm (2 photons). Then, by analytical techniques it will be possible to measure the quantity of the free amino acid and the amount of empty cage on small sample quantities (10-20 μ l). In practice, this would involve introducing a few microliters (ideally 5-10 μ l at different concentrations 1-20 mM) of the cage containing the neurotransmitter in a quartz microcuvette (5-10 μ l) of a spectrofluorimeter coupled to a source irradiation at 375 nm and 750 nm. Each sample thus analysed would then be sent to the Institute Galien in collaboration with Myriam Taverna's team for the analysis by capillary electrophoresis-mass spectroscopy (CE-MS) to quantify the empty cage and the released of amino acids. The data of quantum efficiency will be useful for the final electrophysiological studies performed by the group of Prof Nigel Emptage of the University of Oxford. They will test each compound on some D-serine knock-out mice brain slices, the two photon irradiation will allow the spatial and temporal control of the release. At the same time, they will record the action potential of the neurons to prove the effective activation of NMDA receptors with the elicited depolarization of the postsynaptic neuron.

4. SYNTHESIS OF XAP044 ANALOGS TO ELUCIDATE THE BINDING MODE IN THE VENUS FLYTRAP DOMAIN OF MGLU7 RECEPTOR

4.1. Design and synthesis of XAP044 analogs

XAP044 is a negative allosteric modulator (NAM) of mGlu7R discovered by Novartis.¹⁷⁵ Usually, as already described in the introduction chapter, allosteric modulators bind in the 7TMD of mGluRs but XAP044 binds in the VFTD, known to be the target of orthosteric ligands (**Figure 54**).¹⁷⁵

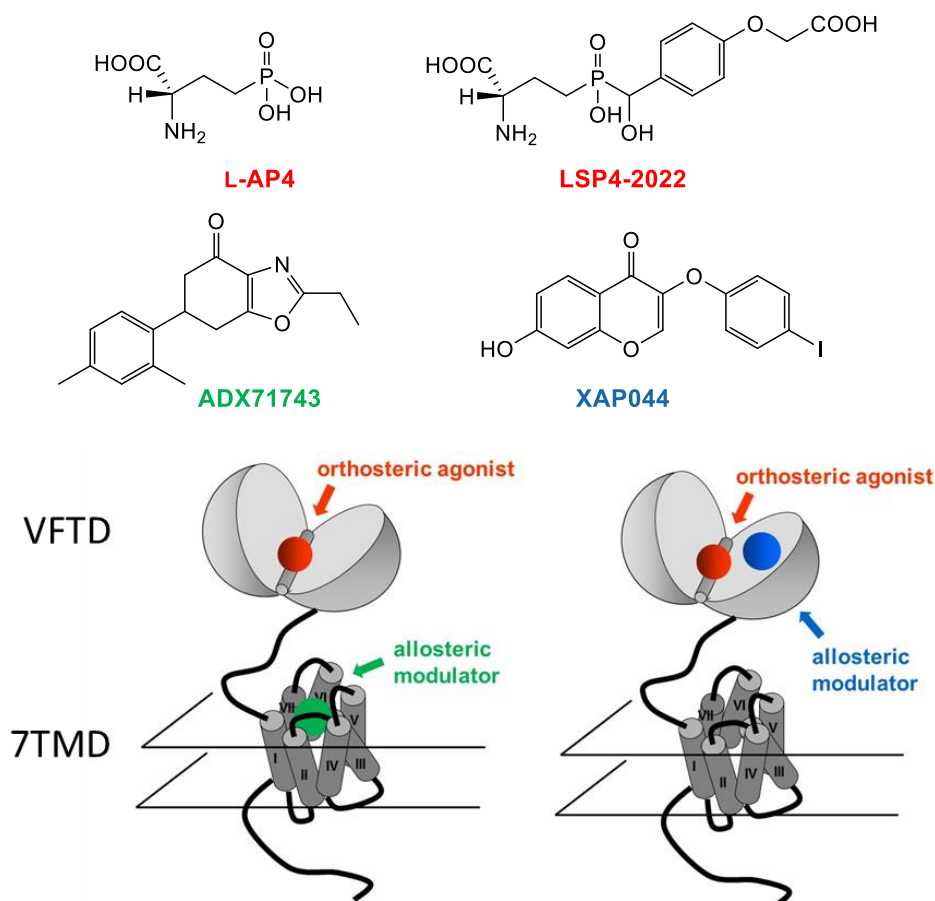


Figure 54. Orthosteric agonists L-AP4 and LSP4-2022^{113,117} are shown in red at their binding site into the VFTD. The NAM ADX71743 (green), selective for mGlu7R, binds to the 7TMD as usual allosteric modulators. XAP044 (blue) is an mGlu7 NAM that binds to the VFTD.^{175,169,110,117}

Indeed, Novartis scientists showed that XAP044 is selective for mGlu7R binding into the VFTD and not in the 7TMD as normally expected.¹⁷⁵ They tried to understand the exact site of binding of the molecule in the VFTD but they were not able to carry out further investigations. Consequently, they asked to the group of Dr. Francine Acher to propose a valid binding model for XAP044 using molecular modelling. For that study, they gave us limited information about the SAR of XAP044 analogs they had synthesized.

This project is highly multidisciplinary as it involves medicinal chemistry, pharmacology and molecular modelling. Dr. Francine Acher and Alexandre Cabayé, another PhD student of our group, have been involved in the docking studies, molecular dynamics and their analysis. All the pharmacological studies were performed at the Institute of Functional Genomic of Montpellier in collaboration with Dr. Jean-Philippe Pin and Isabelle Brabet. My contribution to this work, is related to all chemical aspects and the synthesis of all XAP044 analogs, under the supervision of Dr. Isabelle McCort. This collaboration was fundamental to answer two main questions: first “Where and how is XAP044 binding in the VFTD of mGlu7R?” and “Can we discover a more potent and soluble analog of XAP044?”

Three different hypotheses of XAP044 binding were proposed by Dr. Francine Acher and Alexandre Cabayé. To validate one of these hypotheses, it was necessary to perform mutagenesis studies on selective residues of the VFTD of mGlu7R and synthesize different XAP044 analogs to check if the SAR is in agreement with the proposed docking. In fact, the mutagenesis of a key residue revealed by the 3D-model binding of the molecule is expected to cause a loss of activity and thus support the binding mode hypothesis. Furthermore, the synthesis of novel XAP044 analogs allows investigating the different positions of the ligand giving information to confirm or reject a binding hypothesis (**Figure 55**).

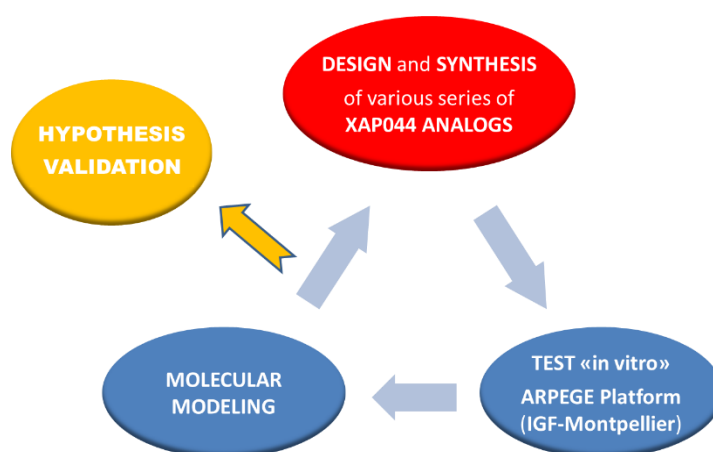


Figure 55. Rational to validate a binding hypothesis.

The synthesis of novel analogs of XAP044 was also aiming at the discovery of a more potent compound with good solubility properties. Indeed, XAP044 is not a useful tool in biology due to its poor aqueous solubility related to the presence of the chromone scaffold. A new potent and more soluble analog of XAP044 would be a much greater tool for research in biology and neuroscience related to psychiatric disease especially anxiety.

We first asked through what mechanism is XAP044 blocking mGlu7R activation. Is it by preventing the closure of the VFT protomers or by blocking the dimer transition from the resting state to the active state (**Figure 17** and **Figure 56**).

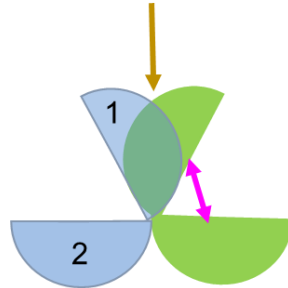


Figure 56. XAP044 can act by preventing the closure of VFTD protomers (violet arrow) or by blocking the dimer transition to the active state (gold arrow).

First, a 3D-model of the mGlu7 closed VFTD was built. It was noticed that the rigid body movement of the lobes brings closer the bottom part of helix α 3 and the top part of helix α 6. Keeping these structural elements apart will have a similar effect as blocking the flexibility of the three linkers at the hinge and results in preventing the VFTD closure. The two facing residues are S160 and S229, upon VFTD closing **S160** (lobe1) and **S229** (lobe2) get the closest (**Figure 57**).

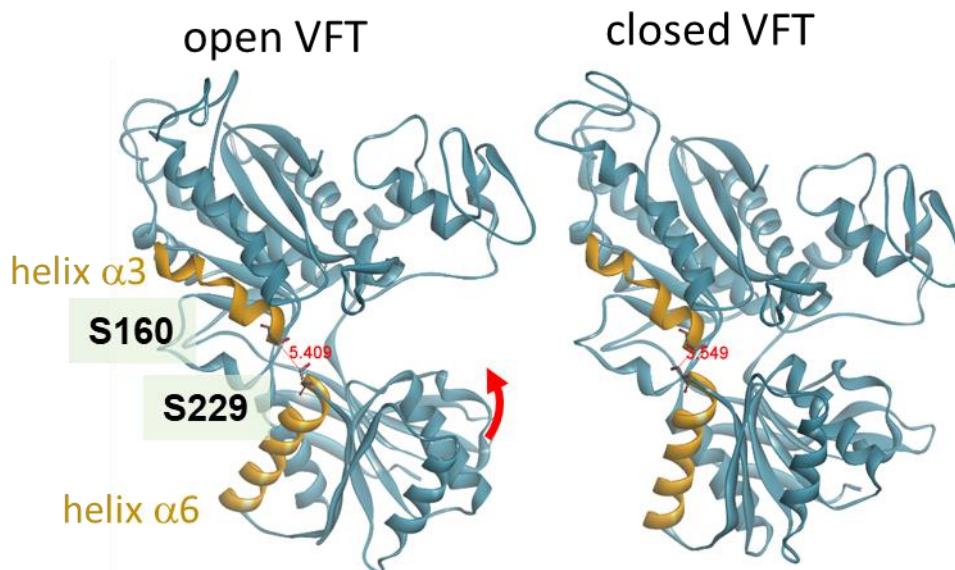


Figure 57. On the left, the open VFTD with S160 and S229 at a distance of 5.41 Å (distance between C α). On the right, the closed VFTD with S160 and S229 that get closer at a distance of 3.55 Å. For the generation of 3D-models see experimental part.

Mutagenesis studies performed at the IGF in Montpellier revealed that the S229A mutation abolishes the inhibition effect of XAP044 and the S160A mutation reduces drastically the LSP4 2022 activation of mGlu7R. Furthermore, our colleagues at IGF showed that XAP044 is a

selective antagonist of mGlu7R but also a weak agonist of mGlu2R. This helped us to conclude that XAP044 may be binding to S229 and possibly to S160, it may behave as a wedge in the closing movement of the VFTD (**Figure 58**).

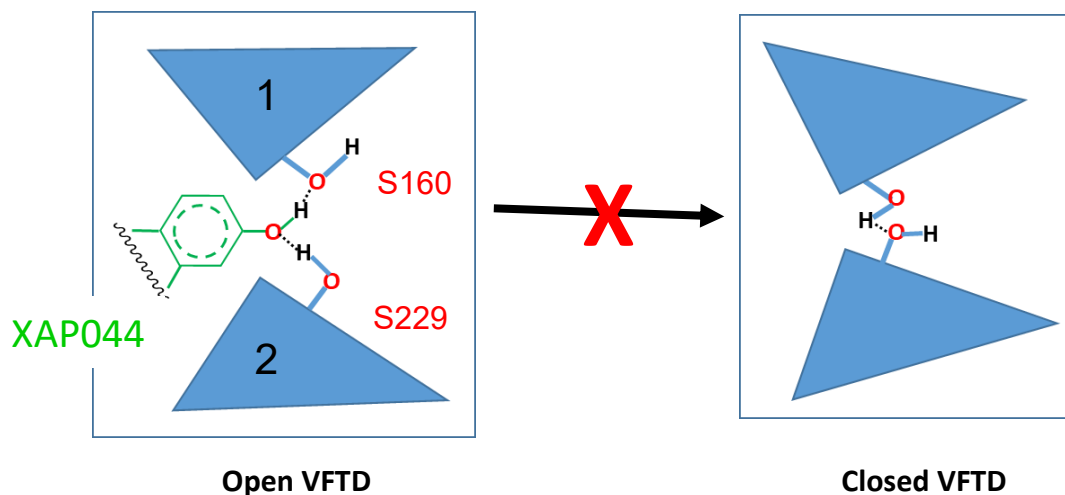


Figure 58. Supposed blocking of the movement of the VFTD by XAP044.

Starting from this assumption, Dr Francine Acher and Alexandre Cabayé investigated the residues at 15 Å around S229 (**Figure 59**).

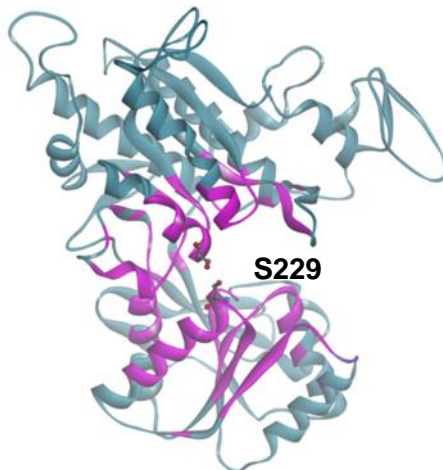


Figure 59. Residues investigated around Ser229 to propose a binding hypothesis.

Taking into account the selectivity of XAP044 for the mGlu7 receptor over other subtypes of mGluRs, three possible orientations around S229 have been proposed for the docking:

- The first hypothesis considers the orientation of XAP044 along loop $\beta_{10\alpha 7}$
- The second hypothesis shows the orientation of XAP044 bound to S229 and S160 along helix α_6 .
- Finally, the third hypothesis considers the orientation of XAP044 bound to S229 and S160 along loop $\beta_{7\alpha 8}$ (**Figure 60**).

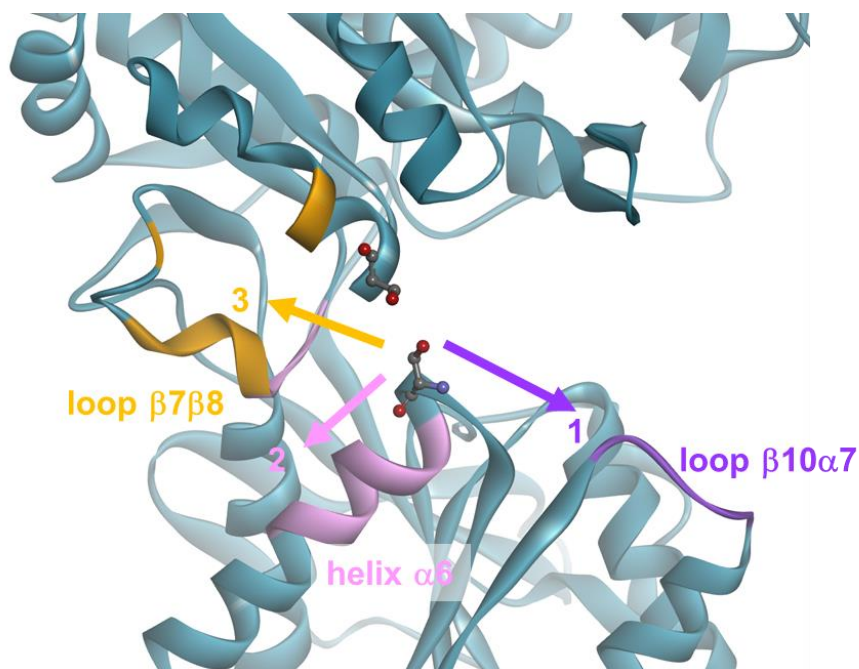


Figure 60. Three hypothesis for XAP044 binding to selective residues in the VFTD.

The details about the dockings and the molecular dynamics are described in the results 4.3 section. The agreement with the SAR and the confirmation by mutagenesis studies are critical for the validation of a final binding mode hypothesis.

Concerning the medicinal chemistry, the design and synthesis of novel analogs were planned in consideration of some points to investigate for the validation of a binding mode. The main aspects considered were whether:

- XAP044 binds in a planar or twisted conformation
- the replacement of the hydroxy group leads to the loss of inhibition as it probably binds to Ser229
- the chromone scaffold of XAP044 is necessary for the binding or it can be replaced
- other substituents can replace the iodine atom in *para* position of the benzene ring
- other substituents are accepted in different positions of the two aromatic rings
- it is possible to discover a photoswitch analog of XAP044 active in *cis* or *trans* form to obtain details about the binding mode

The phenoxy moiety at position 3 of the chromen-4-one of the XAP044 allows some flexibility to the molecule, which can twist with different angles of rotation. This means that the molecule can bind the VFTD in a planar or a twisted conformation. Our approach consisted in synthesizing different rigid planar analogs of XAP044 to evaluate their activity in order to support or not a planar bioactive conformation. The constrained derivatives were generated by linking the

chromen-4-one moiety and the phenyl ring (**Figure 61**). The importance of the chromone scaffold of XAP044 was investigated by “cutting” part of the original molecule to obtain novel open and more flexible derivatives. Accordingly, a series of (4-phenoxy)ethanone was synthesized (**Figure 61**).

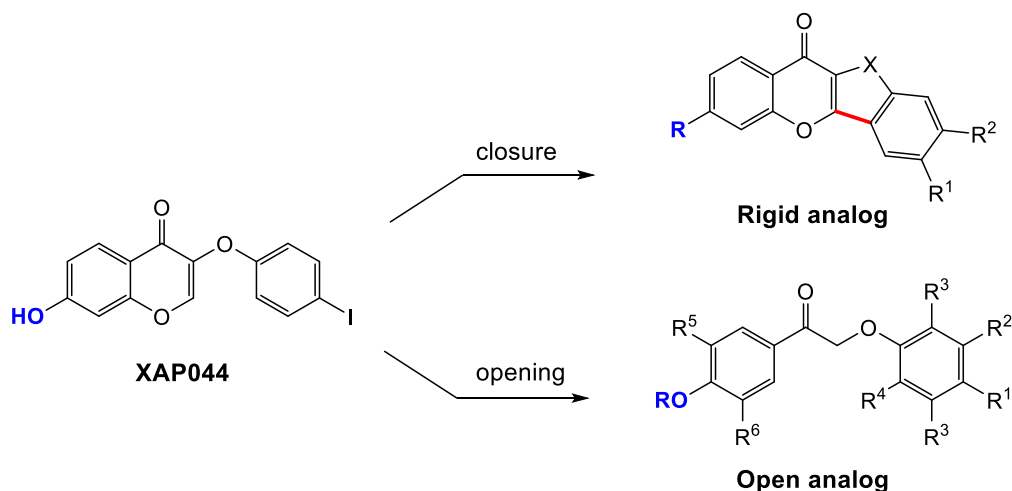


Figure 61. Strategy of closure and opening of XAP044 analogs.

The hydroxy group of the XAP044 was replaced with a methoxy group in different rigid and open analogs to confirm the importance of this group for the binding to the Ser229 as suggested in our hypothesis in **Figure 60**.

Several substituents have been studied, especially in open analogs, at all positions of the ring bearing the iodine atom. The *meta* position of the *para* hydroxy benzene ring was also investigated.

Photoswitch molecules were also synthesized with the aim to obtain an active photoswitch analog of XAP044 and understanding its binding mode. In particular, three different classes of photoswitch compounds were considered: azobenzenes analogs, phenylazaindole analogs and aurone analogs.

The design of the new analogs has been adjusted according to the biological results. Yet they were synthesized by series often before the previous series results would be available.

4.1.1. Synthesis of constrained analogs of XAP044

The first approach to get information on the binding mode of XAP044 was the synthesis of constrained analogs by restricting the flexibility of the central part of the molecule (**Figure 61**).

In fact, the phenoxy moiety at position 3 of the chromen-4-one allows the molecule to be flexible with the possibility of different ways to bind to the VFTD, especially in the cleft and at the dimer interface of the two lobes (**Figure 56**). On the contrary, a rigid structure allows a simpler modelling as it is planar, giving less binding possibility in the VFTD. Superimposition of XAP044 and the constrained analogs (**Figure 62**) shows the spatial disposition of the iodo substituent.

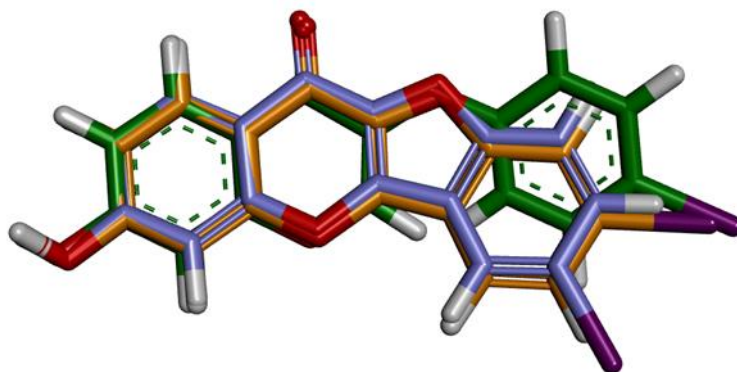
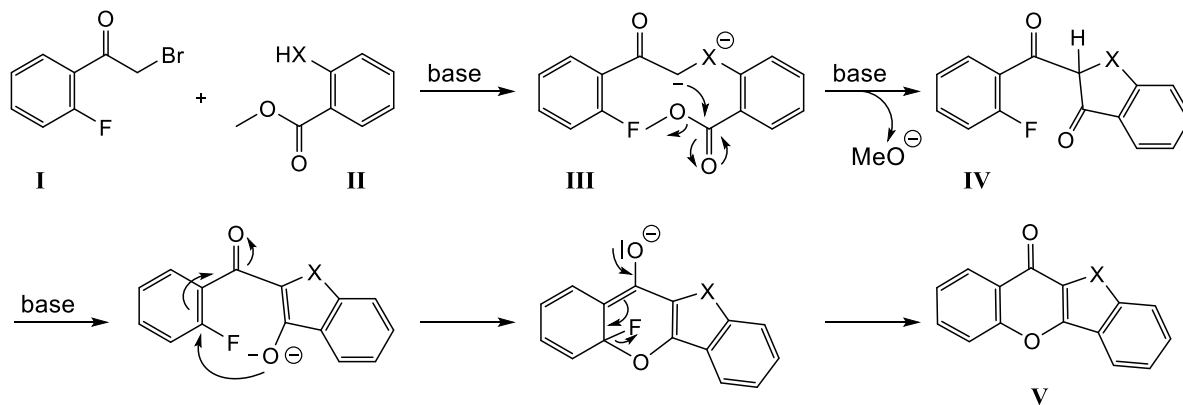


Figure 62. Superimposition of the chromen-4-one moieties of **13e** (mauve C) and **13g** (orange C) and XAP044 in a planar conformation (green C).

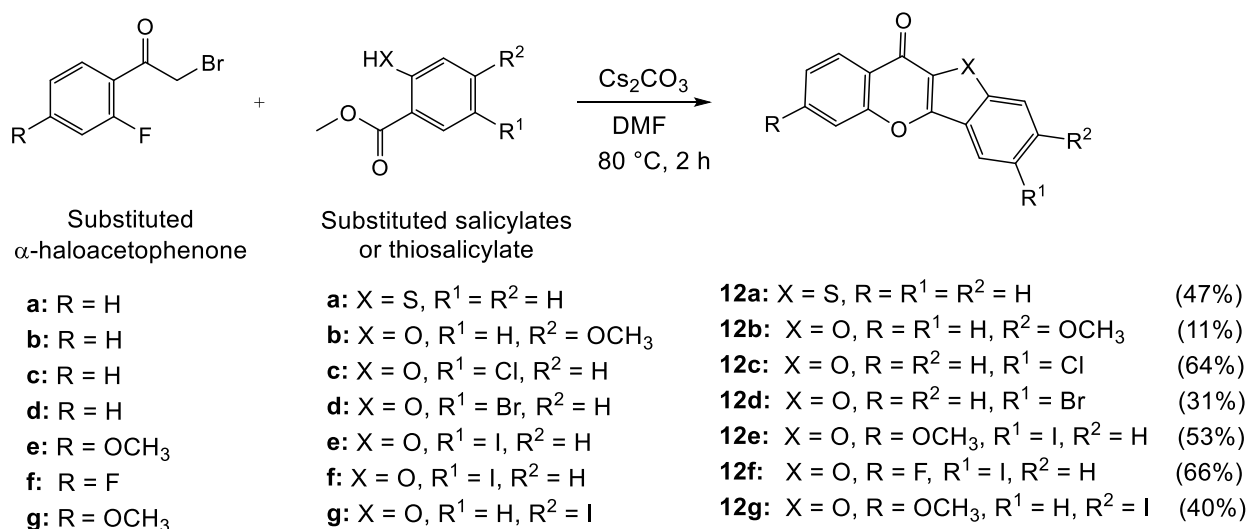
The constrained analogs were quickly synthesized starting from a reaction described by Miller *et al.* (**Scheme 15**).³³²



Scheme 15. Mechanism of reaction for the synthesis of constrained analogs.

In the first step a salicylate or thiosalicylate **II** is deprotonated with a base and the resulting anion reacts with α -haloacetophenone **I** to form the substituted adduct **III**. Subsequent deprotonation of ketone **III** allows for the intramolecular acylation of the α -carbanion enolate to give the benzofuran-3-one or benzothiophene-3-one **IV** that is deprotonated, setting up the final ring closure step, an intramolecular *ipso*-fluoro substitution *via* the enolate oxygen to give **V**.

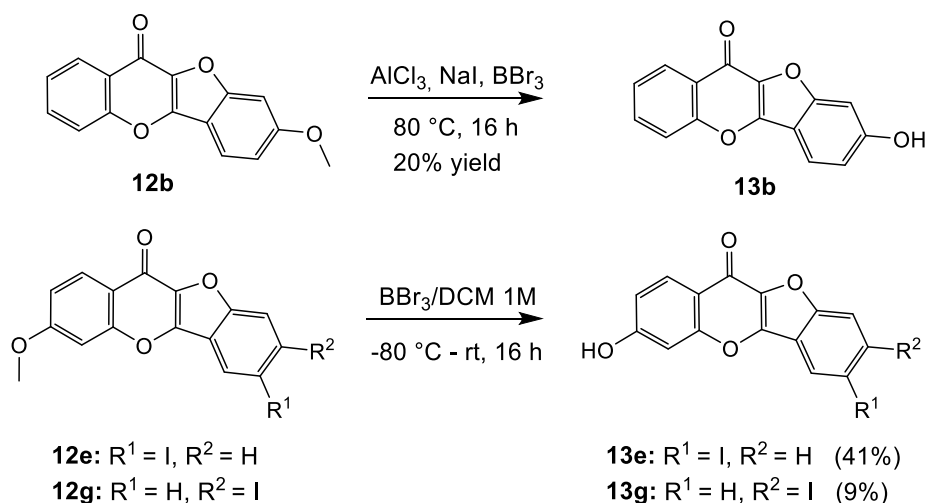
Starting from this general reaction mechanism constrained analogs **12a-12g** were easily synthesized in one-step (**Scheme 16**).



Scheme 16. Synthesis of constrained analogs **12a-g**.

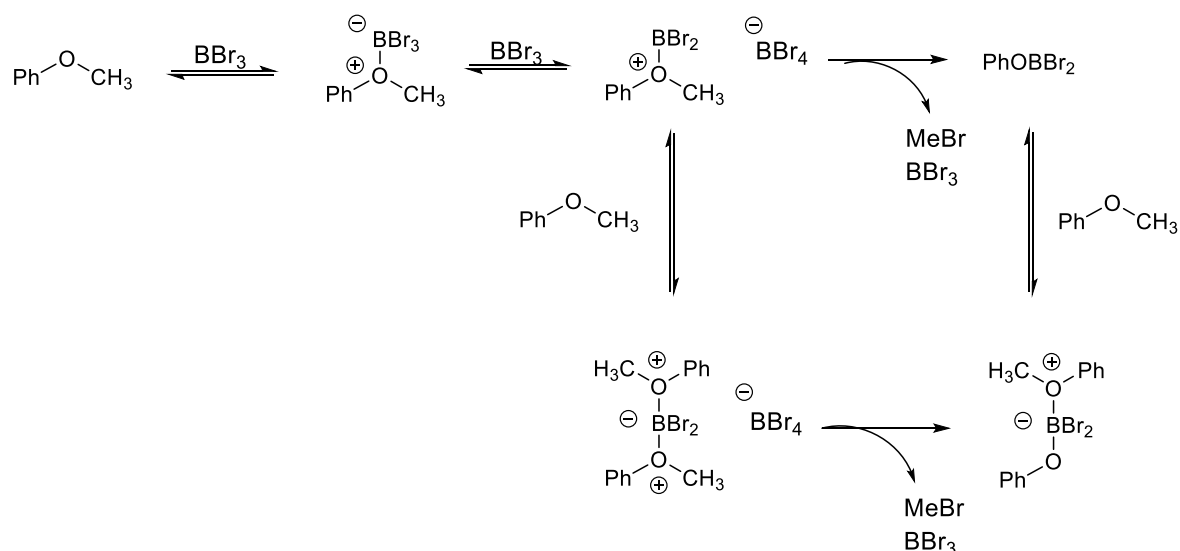
Deprotection of **12b** to give **13a** was obtained by a demethylation of the methoxy group in position 3 using AlCl₃, NaI and BBr₃ in small amount while for the product **13b** and **13c** the demethylation was achieved starting from **12e** and **12g** respectively using just BBr₃ in 1M DCM without AlCl₃ and NaI (**Scheme 17**).

The deprotection of **12b** was achieved by a green chemistry reaction where no solvent was used. This method worked to obtain **13b** but anyway it had a yield of just 20% so the deprotection of **12e** and **12g** was performed in different conditions. An assay was made on **12e** with AlBr₃ and NaI in DCM stirring the reaction at 80 °C³³³ but no deprotection was observed during six hours so that the starting material was recovered. Another assay was performed using BBr₃ in 1 M DCM at -80 °C for 30 minutes then at room temperature overnight.³³⁴ This last method worked better to afford product **13e** in 41% yield and **13g** in 9% yield only, due to problems during the purification.



Scheme 17. Demethylation to afford product **13b,e,g**.

BBr_3 is a Lewis acid commonly used for the demethylation of arylmethyl ethers. By coordinating with oxygen, it promotes the C-O bond cleavage into an alkyl bromide and an alkoxyborane, which is hydrolyzed to the corresponding alcohol during workup. The cleavage of aryl methyl ethers proceeds through a bimolecular mechanism and has been described for demethylation (**Scheme 18**).³³⁵



Scheme 18. Proposed mechanisms for demethylation with BBr_3 .

4.1.2. Synthesis of open analogs of XAP044

The rationale of the synthesis of open analogs is related to the research of flexible molecules able to bind the VFTD with different orientation and angles compared to the previous constrained derivatives. Furthermore, the aim was also to discover more potent analogs with a higher solubility in aqueous solvents compared to XAP044. To check if the chromen-4-one could be chopped, we synthesized the (4-hydroxyphenylethanone) derivatives.

According to our blocking hypothesis shown in **Figure 58** and to previous data from Novartis model as well as mutagenesis studies at IGF (see **Table 7** section 4.3), the hydroxy group of XAP044 appears to be fundamental for the binding to serine 229. Considering this data, the first approach was to synthesize open analogs bearing a methoxy group to replace the hydroxy group of XAP044 analogs (**Figure 63**).

If the (4-hydroxyphenyl)ethanone analog would be still active as XAP044, the expectation was to obtain inactive analogs to confirm the importance of the hydroxy for the binding and confirm the involvement of Serine 229. In addition, some open hydroxy analogs were synthesized to gain

precious information concerning the SAR, to find active analogs of XAP044 and to help in the validation of the modelling hypothesis (**Figure 63**).

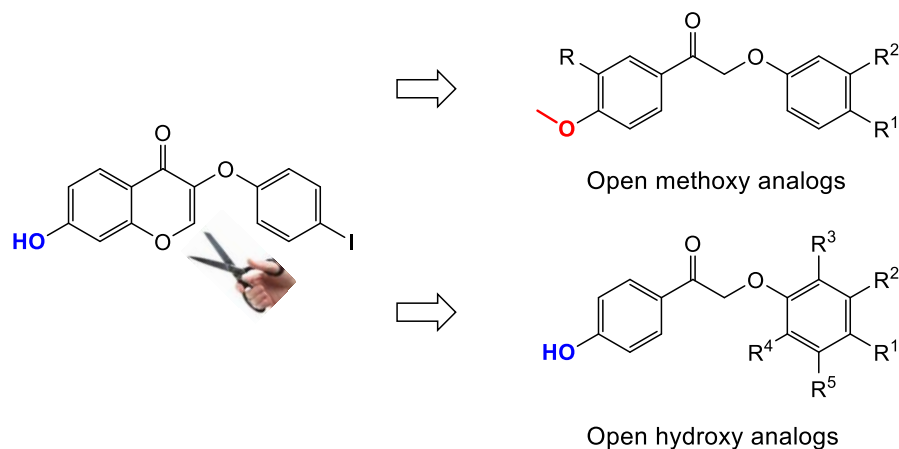
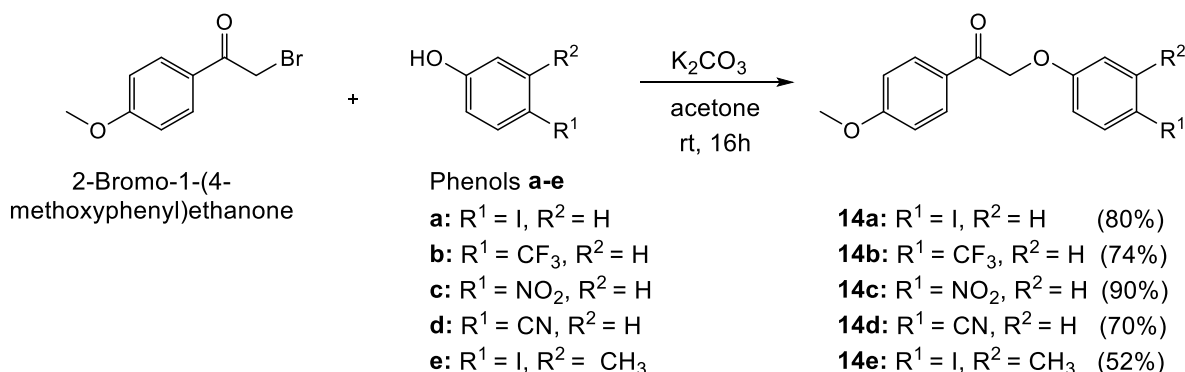


Figure 63. Open analogs of XAP044.

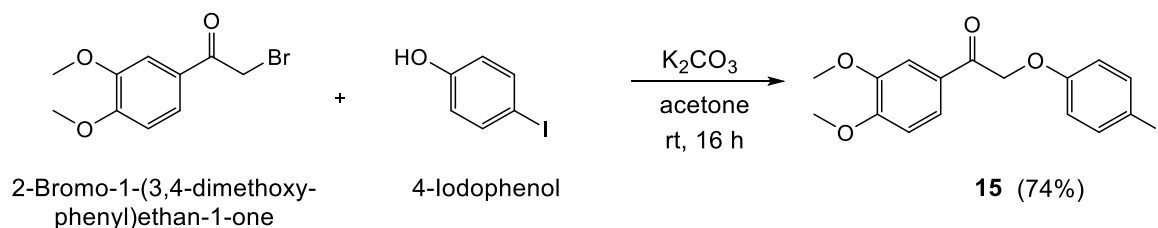
4.1.2.1. Synthesis of the methoxy open analogs

The synthesis of several open methoxy analogs was easily achieved by a nucleophilic substitution of 2-bromo-1-(4-methoxyphenyl)ethanone by various phenols (**Scheme 19**).



Scheme 19. Synthesis of open methoxy analogs **14a-e**.

The synthesis of the open methoxy analog **14a** bearing another methoxy group in *meta* position was also carried out to allow the exploration of this position (**Scheme 20**).



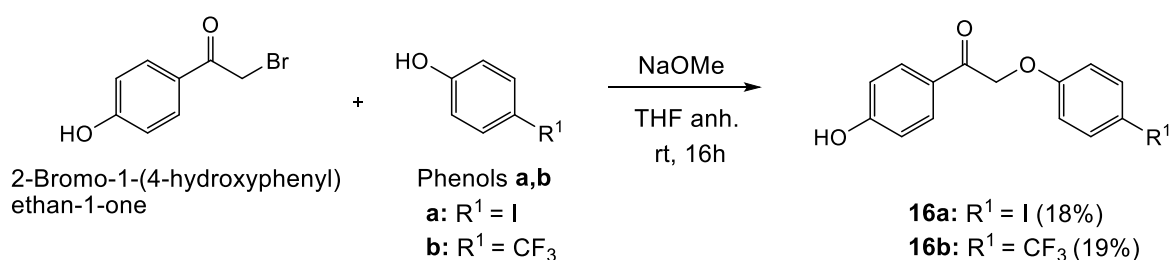
Scheme 20. Synthesis of open dimethoxy analog **15**.

4.1.2.2. Synthesis of the hydroxy open analogs of XAP044

4.1.2.2.1. SAR on the iodobenzene part

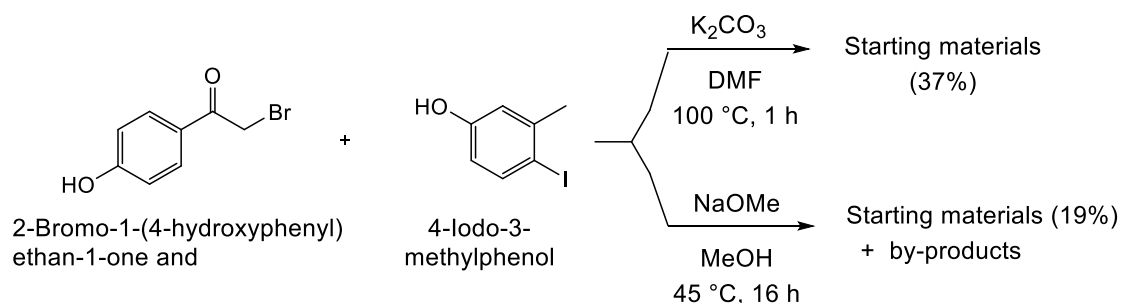
The synthesis of the various hydroxy open analogs of XAP044 was achieved using different methods.

The demethylation of the methoxy open analogs using BBr_3 in 1 M DCM was investigated on product **14a**. Unfortunately, BBr_3 coordinates to the oxygen of the phenoxy moiety of the molecule leading to degradation. Consequently, next approach involved the synthesis of compounds **16a-b** using sodium methylate in THF starting from 2-bromo-1-(4-hydroxyphenyl)ethan-1-one and phenols (**Scheme 21**). This method did not give the desired products because, even if the reaction worked correctly, the crude contained many impurities. The total purification of the final desired compounds turned out to be complicated with low yields. For these reasons, other methods were investigated to obtain an easier purification of the final compounds and higher yields.



Scheme 21. Synthesis of compounds **16a-b**.

Starting from 2-bromo-1-(4-hydroxyphenyl)ethan-1-one and the desired phenol, two different reactions were performed using in the first case potassium carbonate in DMF and in the second sodium methylate in methanol. Starting materials were recovered for the first reaction and starting materials and by-products for the second (**Scheme 22**).

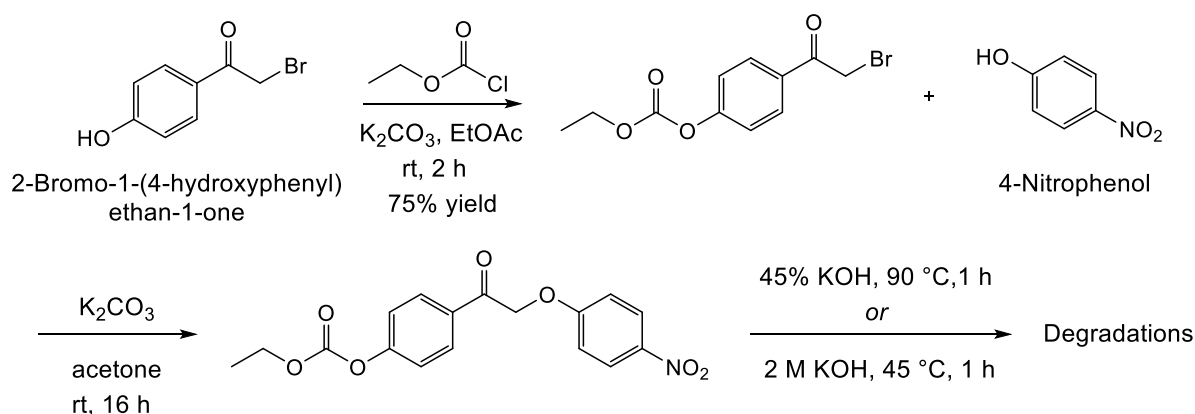


Scheme 22. Attempt to the synthesis of hydroxy open analogs.

In the previous conditions shown in **Scheme 21**, both reagents bear a hydroxy group highly reactive after deprotonation with the base. This leads to by-products together with the desired

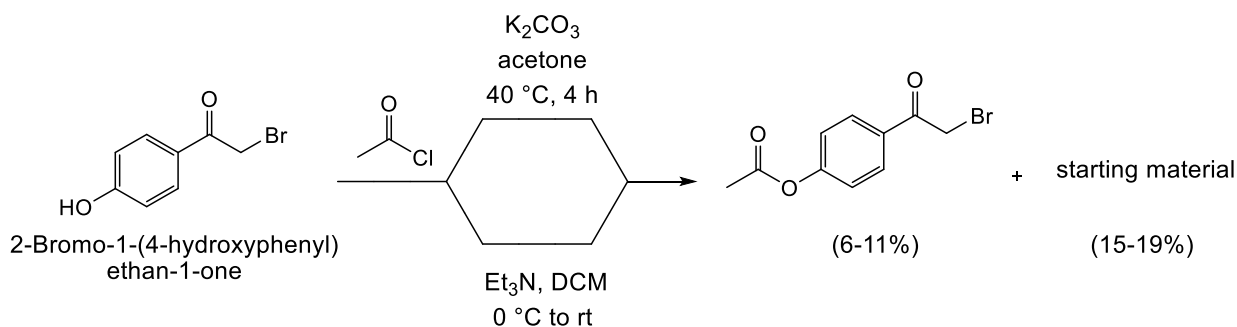
compound and some remaining starting material. In this perspective, the new strategy of synthesis involved first the protection of 2-bromo-1-(4-hydroxyphenyl)ethan-1-one, then its coupling to the desired phenol and finally the deprotection to obtain the hydroxy open analog.

The first protecting group we investigated was ethyl formate that was attached to the hydroxy group using ethyl chloroformate with potassium carbonate in ethyl acetate. The reaction worked properly then the other phenol was coupled using potassium carbonate and acetone as seen in **Scheme 19** and **Scheme 20**. The final deprotection using basic conditions led to unidentified products (**Scheme 23**).



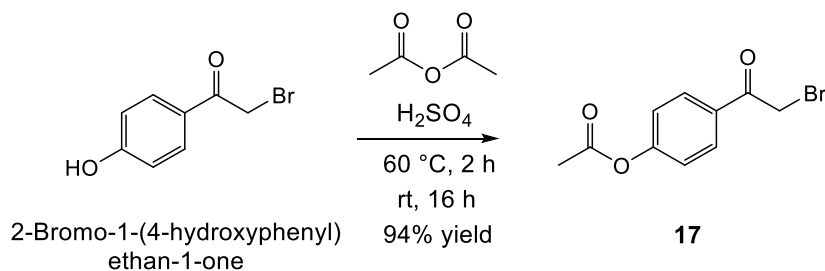
Scheme 23. Attempt to the synthesis of open hydroxy analogs.

Considering the previous problem in the deprotection of the protective group of 2-bromo-1-(4-hydroxyphenyl)ethan-1-one, our search was focused on one of the easiest cleavable protective group in mild conditions *i.e.* acetyl group. The first two attempts were performed using first acetyl chloride with potassium carbonate in acetone and then acetyl chloride with triethylamine in DCM. These methods gave the recovery of the starting material with few milligrams of the desired products (**Scheme 24**).



Scheme 24. Attempts for the acetylation of 2-bromo-1-(4-hydroxyphenyl)ethan-1-one.

Finally, the acetylation of 2-bromo-1-(4-hydroxyphenyl)ethan-1-one was achieved in 94% yield using acetic anhydride and sulphuric acid (**Scheme 25**).



Scheme 25. Acetylation of 2-bromo-1-(4-hydroxyphenyl)ethan-1-one.

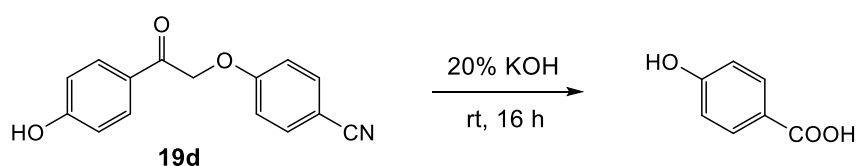
The alkylation of different phenols **a–x** (**Table 1**) was performed in the conditions already described in **Scheme 19** and **Scheme 20** and the resulting compounds **18a–x** were subsequently deacetylated using sodium acetate in ethanol. This approach allowed to synthesize the 24 hydroxy open analogs listed in **Table 1**.

	R¹	R²	R³	R⁴	R⁵	19a-x
a	I	CH ₃	H	H	H	71%
b	I	H	CH ₃	H	H	34%
c	NO ₂	H	H	H	H	48%
d	CN	H	H	H	H	66%
e	Cl	H	Cl	H	H	62%
f	CH ₃	H	H	H	H	57%
g	OCH ₃	H	H	H	H	58%
h	OCH ₃	OCH ₃	H	H	H	37%
i	Br	H	H	H	H	45%
j	Cl	H	H	H	H	61%
k	Br	H	Br	H	H	74%
l	Br	H	Cl	H	H	89%
m	CHO	F	H	H	H	31%
n	NO ₂	NO ₂	H	H	H	34%
o	CN	F	H	H	F	87%
p	Br	H	F	F	H	46%
q	H	I	H	H	H	50%
r	F	H	F	H	H	72%
s	SONH ₂	H	H	H	H	33%
t	Br	H	Cl	Cl	H	50%
u	Br	H	F	H	H	35%
v	H	OH	H	H	H	25%
w	OH	H	H	H	H	7%
x	CO ₂ H	H	H	H	H	9%

Table 1. Phenols **a-x** used for the synthesis of **18a-x** and **19a-x**.

The yields of compounds **19a-x** are variable as the different substituents of phenols **a-x** can be inert or in other cases reactive leading to by-products. The low yields of products **19w,x** are due to the presence in *para* position of the phenols **w,x** of a hydroxy group and a carboxylic group, respectively. Compounds **18a-n** and **18s,t** were purified before the final deprotection, **18o-r** and **18u-x** were used directly in the next step as a crude material.

The hydrolysis of the nitrile in compound **19d** to get **19x**, using a 20% solution of potassium hydroxide led to a degradation as the hydroxy group from KOH attacks the activated carbon between the carbonyl and the phenoxy. 4-Hydroxybenzoic acid was recovered (**Scheme 26**).



Scheme 26. Attempt to the synthesis of **19x** by hydrolysis of compounds **19d**.

Alternately, compound **19x** was obtained, as described in **Table 1**, from **17** and 4-hydroxy benzoic acid.

4.1.2.2.2. Synthesis of dihydroxy open analog and fluorine-hydroxy open analog

The last investigation focused on the benzene ring bearing the hydroxy group in the XAP044 open analogs. A second hydroxy group in a first analog and then one and two fluorine atoms in *meta* positions have been introduced. Indeed, as the *para*-hydroxy group showed to be fundamental for the binding to Ser229, another hydroxy group and/or a fluorine atom in *meta* position may have positive effects on the hydrogen bond with the Ser229. A second hydroxy in *meta* position could form a second hydrogen bond while two fluorine atoms in *meta* position lower the pK_a of the phenol and thus, allow further deprotonation. This phenolate may be a strong hydrogen bond acceptor.

When iodine in *para* position of XAP044 was replaced with a bromine atom and a fluorine atom was added in *ortho* position, **19u** was found to be the most active compound in the series of the hydroxy open analogs series synthesized (see section 4.2, **Table 5**). So these substituents were chosen for the syntheses of the three new analogs (**Figure 64**).

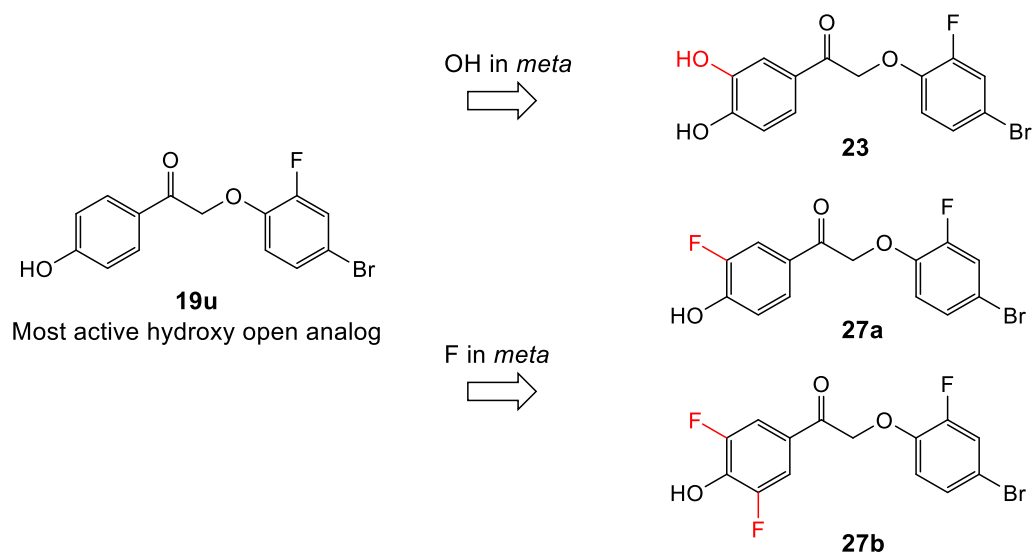
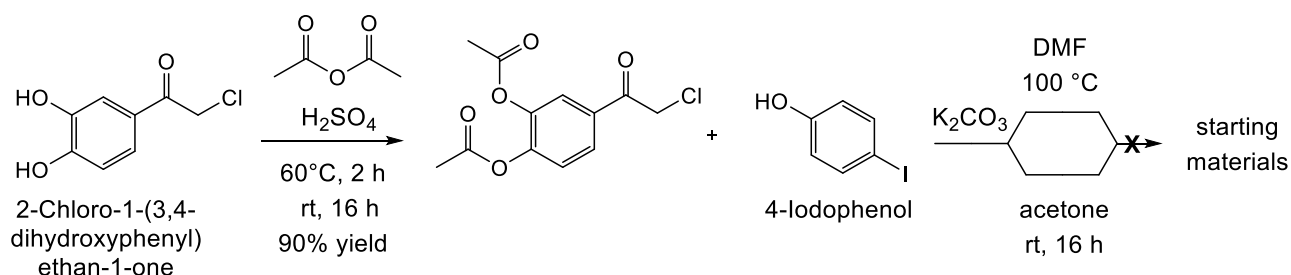


Figure 64. Rational design from **19u** of dihydroxy analog **23** and hydroxy-fluorine analogs **27a,b**.

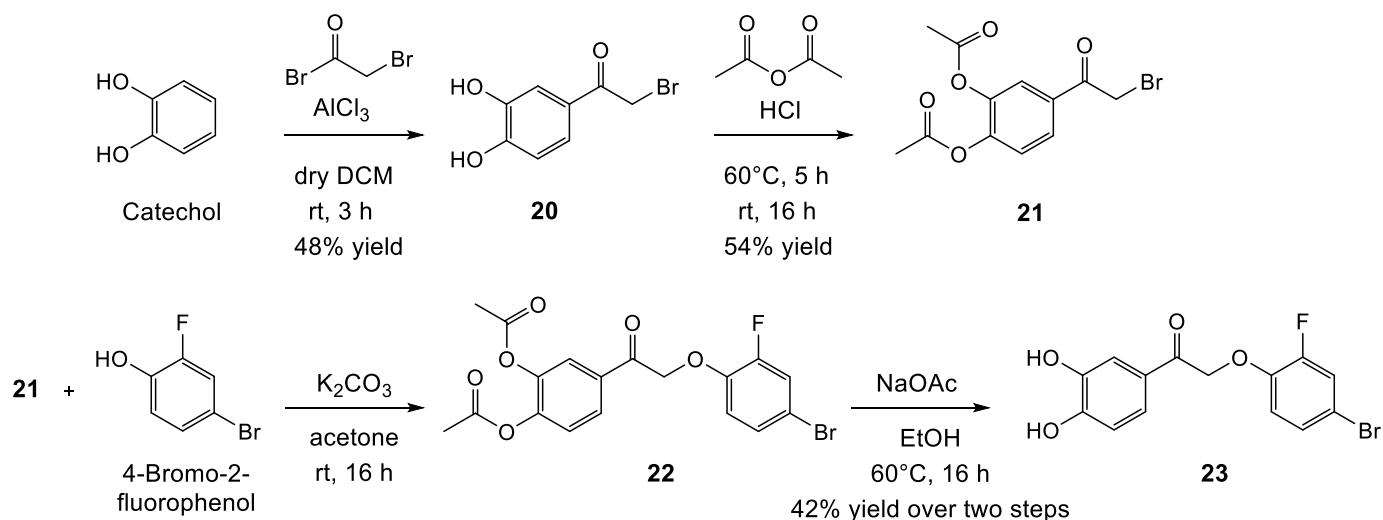
a) Synthesis of **23**

A first attempt to the synthesis of the dihydroxy open analog started from the commercially available 2-chloro-1-(3,4-dihydroxyphenyl)ethan-1-one, protecting the two hydroxys with two acetyl groups. Then the coupling with the 4-iodophenol was tried using first potassium carbonate in acetone and then potassium carbonate in DMF. In both cases, no alkylation occurred and the starting materials were recovered (**Scheme 27**).



Scheme 27. Attempts to the synthesis of dihydroxy open analogs.

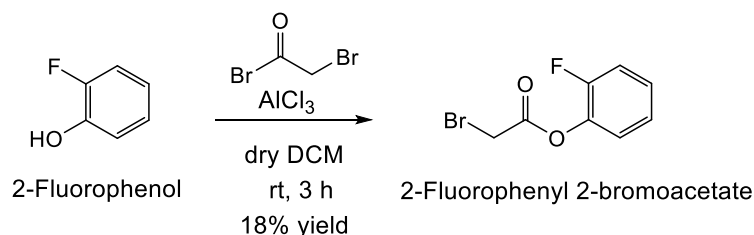
Finally, compound **20** was obtained starting from catechol and bromoacetyl bromide by a Friedel-Crafts acylation using aluminium trichloride in dry DCM in 48% yield and then the same procedure reported in **Table 1** was followed to afford compound **23** in 42% yield (**Scheme 28**).



Scheme 28. Synthesis of the dihydroxy open analog **23**.

b) Synthesis of **27a** and **27b**

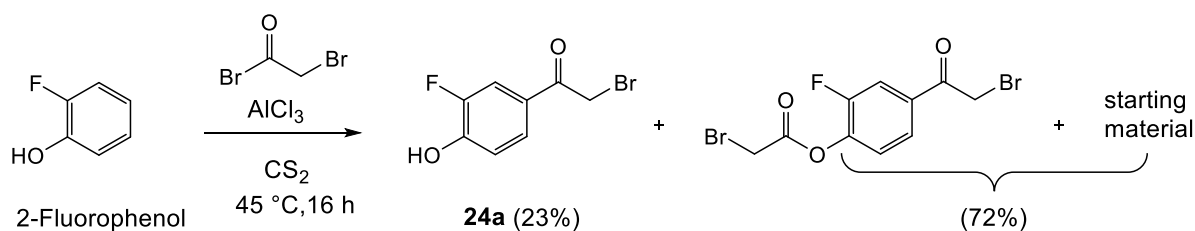
We first began the synthesis of the alpha fluorophenol analog **27a** in the conditions described in **Scheme 28** but from 2-fluorophenol. Unfortunately, the desired acylated product was not obtained but instead the ester was recovered in 18% yield (**Scheme 29**).



Scheme 29. Attempt to the synthesis of 2-bromo-1-(3-fluoro-4-hydroxyphenyl)ethan-1-one.

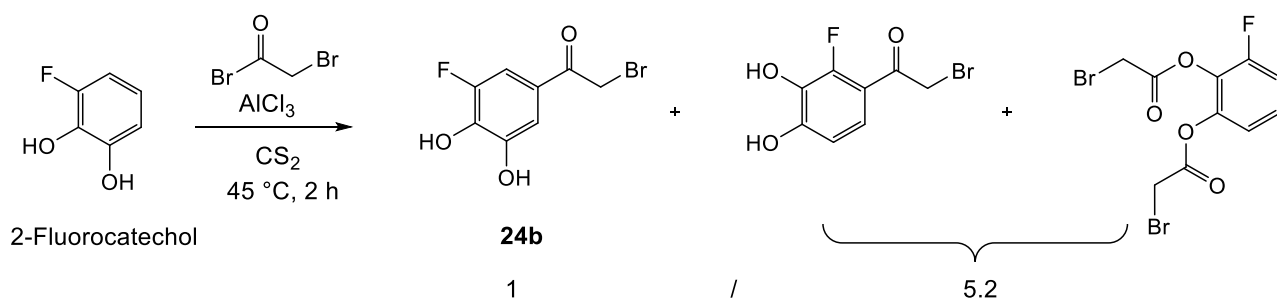
The presence of the fluorine totally change the reactivity compared to the catechol due to the decreased pK_a values. In fact the pK_a 's of the hydroxy groups of the catechol are 7.0 and 11.9, while in the case of 2-fluorophenol and 2,6-difluorophenol the pK_a of the hydroxy groups are more acidic with values of 6.8 and 6.0 respectively (predicted pK_a 's at Chemicalize website).

According to literature, the best conditions to use in this case are an excess of AlCl_3 (6 eq compared to the 2 eq used in **Scheme 28** for catechol), the replacement of DCM by carbon disulfide as solvent and heating at reflux.³³⁶ The product was obtained in 23% yield along with starting material and 4-(2-bromoacetyl)-2-fluorophenyl 2-bromoacetate that were also recovered (**Scheme 30**).



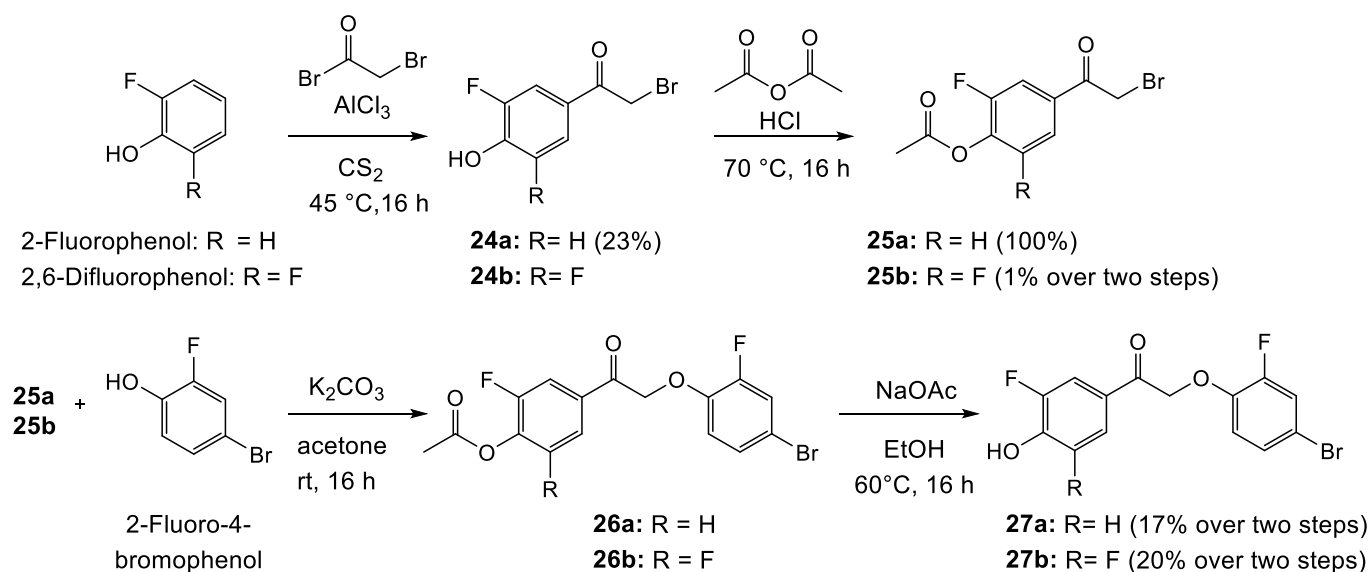
Scheme 30. Synthesis of **24a**.

These Friedel-Craft conditions have been tried using 2,6-difluorophenol to get product **24b** but the yield was very low. Indeed, the desired product was obtained along with aluminum complexes (56% yield), a mixture of the isomers and the di-acylated compounds in a ratio of 1/5.2 (**Scheme 31**). Compound **24b** and its isomer were not separated as they showed the same R_f in different eluents. A protection of the hydroxy groups with acetyl was attempted but ^1H NMR spectra showed that the desired product was not present and neither the starting material.



Scheme 31. Synthesis of product **24b**.

The final synthesis of the hydroxy-fluoro open analogs **27a,b** is summarized in **Scheme 32**, following the same reactions depicted in **Scheme 28** for the dihydroxy open analog.

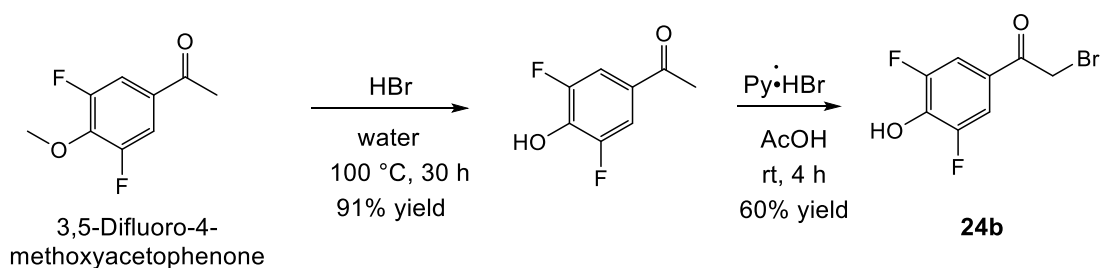


Scheme 32. Synthesis of the hydroxy-fluoro open analogs **27a,b**.

The alkylation of **25a,b** occurred with 2-fluoro-4-bromo-phenol to give products **26a,b** that were taken as crude for the deprotection to get the final hydroxy-fluoro analogs **27a,b**.

The presence of a second fluorine atom in *meta* position drastically changed the reactivity of 2,6-difluorophenol in the Friedel-Craft reaction. Thus, product **24b** must be synthesized using a different method to obtain a higher yield, but for reasons of time, this was not carried out.

Starting from the commercially available 3,5-difluoro-4-methoxyacetophenone, it is possible to deprotect the hydroxy group using HBr in water at reflux temperature to get the 1-(3,5-difluoro-4-hydroxyphenyl)ethan-1-one. The α -bromination using pyridine hydrobromide in acetic acid at room temperature should lead to the desired product with higher yield according to literature (**Scheme 33**).^{337,338}



Scheme 33. Alternative synthesis of product **24b** to obtain higher yields according to literature.^{337,338}

Another analog (**Figure 65**) related to the dihydroxy open analog **23** was attempted starting from 2-fluoro-catechol for the synthesis. The reaction was performed using the same conditions seen for catechol in **Scheme 28** *i.e.* AlCl_3 in DCM but, either the desired product nor by-products were identified.

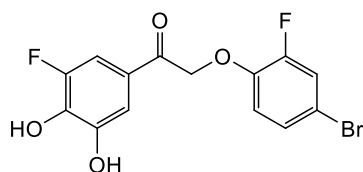


Figure 65. Planned dihydroxy-fluoro open analog.

Concerning the XAP044 project, constrained and open analogs have been developed in this section. These compounds can be defined as “classic” ones in comparison to those that possess photoswitchable properties and are described in the following sections of this thesis.

The biological activity of all these “classic” analogs of XAP044 will be discussed in the pharmacological results sections 4.2. In the following part of the results and discussion chapter, we will describe some photoswitch analogs of XAP044.

4.1.3. Photoswitch analogs

The interest in photoswitch compounds was driven first by the desire to gain binding information to validate a molecular model and to discover a new active photoswitch analog of XAP044. In fact, photoswitch compounds can have two structural isomers, as they can adopt *trans* or *cis* forms. The advantage of these molecules is that, unlike conventional ligands, they may act with an on-off mechanism on the target in order to activate or deactivate the receptor responding to light sources. Furthermore, in the case of XAP044, knowing that a photoswitch is active in the *trans* form and inactive in the *cis* form or vice versa, would give important information to understand the mode of binding of the compound. Ideally, for the activation of a biological target, a good photoswitch should be active in its less energetic stable form to be easily switched to the most energetic stable one to turn off the biological activity.

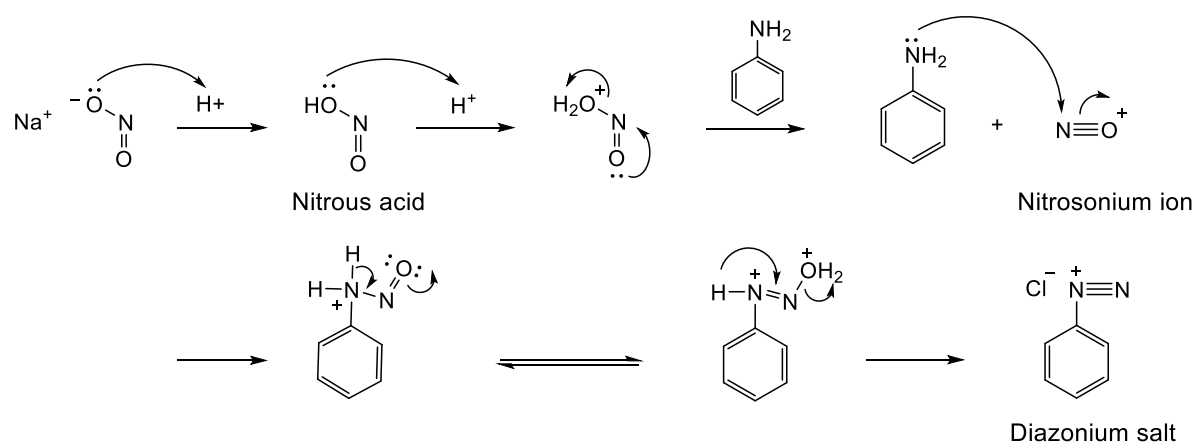
Three different types of photoswitches were synthesized: azobenzene derivatives, phenylazindole derivatives and aurone derivatives. These compounds have different photophysical properties as photoswitches. UV-Vis and ¹HNMR spectra were used in combination with an irradiation lamp source to investigate their properties.

4.1.3.1 Azobenzenes

Azobenzenes have been already described in chapter 2.2.5. They represent a first approach of synthesis of photoswitch analogs as they are the most studied and well known molecules among this class.

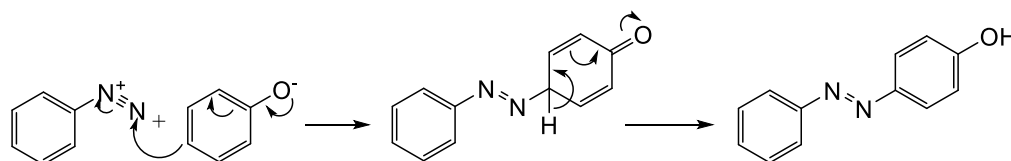
Azobenzenes can be synthesized in many different ways as reported in literature.^{339,340} One of the most popular methods is the azo coupling reaction based on the initial diazotization of an aromatic primary amine under acidic conditions using sodium nitrite at low temperature, followed by the reaction with an electron rich aromatic nucleophile in basic conditions.

The reaction sequence of diazotation process is given below (**Scheme 34**):



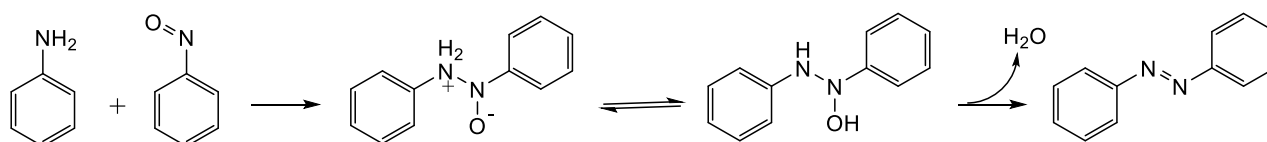
Scheme 34. Mechanism of diazotation.

The nucleophile, which can be a phenol or an aniline, mainly orients the substitution in the *para* position of this electron donor group on the activated aromatic ring (**Scheme 35**). When this position is not available, the substitution occurs in the *ortho* position.³³⁹



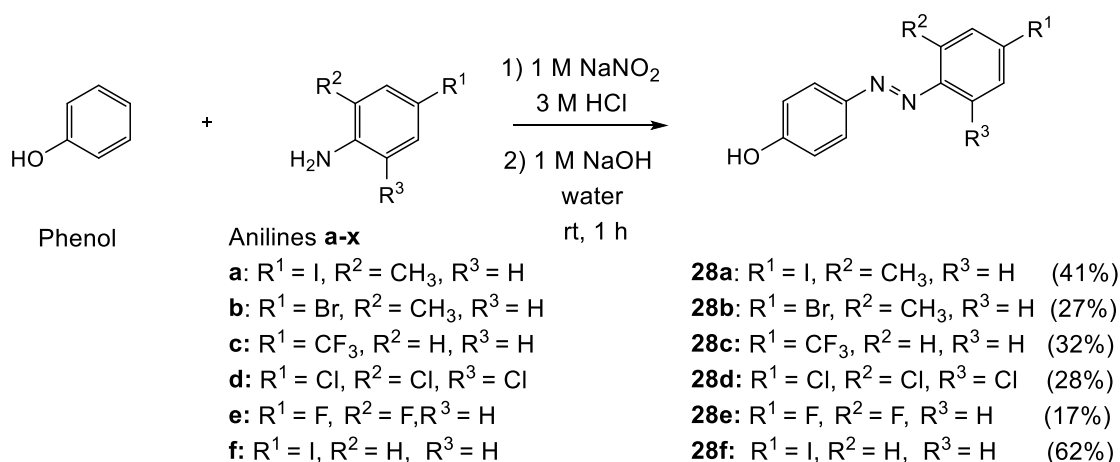
Scheme 35. Mechanism of diazocoupling reaction.

Mills reaction gives the corresponding azo benzene starting from aromatic nitroso derivatives and anilines in glacial acetic acid at room temperature and in good yields. The mechanism involves the attack of aniline on the nitroso derivatives in acid media leading to azobenzene after dehydration of the intermediate (**Scheme 36**).³⁴⁰



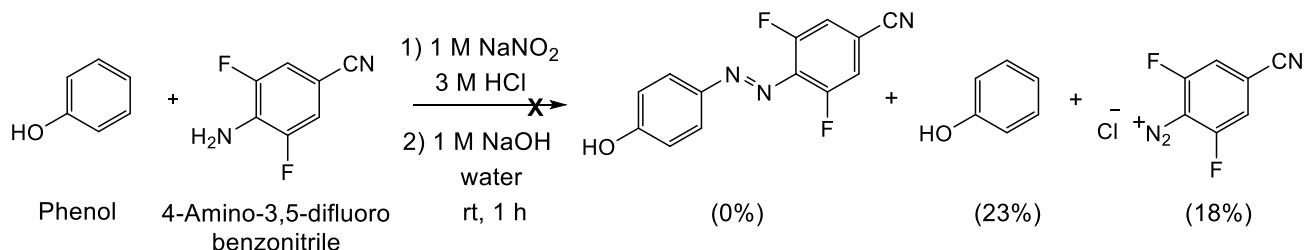
Scheme 36. Mechanism of Mills reaction.

Six different azobenzenes analogs were synthesized using the azo-coupling reaction starting from phenol and different substituted anilines (**Scheme 37**).



Scheme 37. Synthesis of azobenzene analogs **28a-f**.

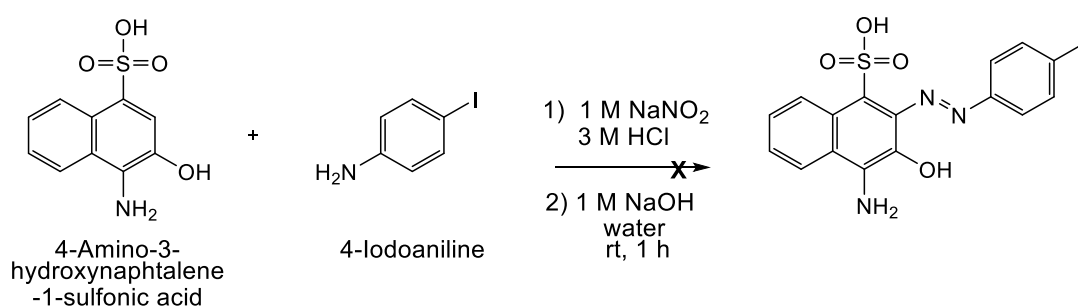
Overall, the reaction yields was low to medium, between 17% and 62% except from 4-amino-3,5-difluorobenzonitrile, where the desired product was not recovered (**Scheme 38**).



Scheme 38. Attempt to the synthesis of an azobenzene.

The azocoupling is a quick reaction, so one hour normally is even enough to allow the starting materials to react giving the final product. The presence of the fluorine in *ortho* position of the aniline can have an electronic-withdrawing effect that impedes the first step of the reaction (**Scheme 34**), so other reaction conditions should be explored in this case. Franck-Cyril Favre-Besse, a former PhD student of our group, showed in his thesis that the presence of atoms with an attractive inductive effect, like fluorine in *ortho* position of the aniline, decreases the kinetic of the reaction.³⁴¹ This observation is in agreement with what we observed in **Scheme 38**.

Another type of azobenzene was attempted starting from 4-iodoaniline and 4-amino-3-hydroxy-1-naphthalene sulfonic acid in the classic conditions previously used. In this case, one benzene ring was replaced with the naphthalene scaffold (**Scheme 39**). Normally in the azobenzene reaction, an activated azene compound is coupled to a phenol or an aniline (**Scheme 35**). The diazene attaches to the *para* position of the phenol but if this position is occupied then the preferred one is the *ortho* position. In the case of 4-amino-3-hydroxy-1-naphthalene sulfonic acid, the only available position to attach the azene is in *ortho* of the hydroxyl group. Anyway, this reaction did not lead to the desired product probably because the sulfonic acid group and the amine group of the starting material interferes with the normal mechanism of the reaction.



Scheme 39. Attempt to the synthesis of a naphthalene-azobenzene.

4.1.3.1.1. Photophysical properties of Azobenzenes

The compounds **28a-f** were obtained in the *trans* form according to UV-Vis spectra recorded in a mixture of DMSO and water (**Figure 66**). The aqueous solution was chosen to comply with biological assays.

Azobenzenes are normally more stable in their *trans* form as they require a higher energy to be stable in their *cis* form. The substitution with fluorine atoms in the four *ortho* positions on the two benzene rings can promote the stability of the *cis* form.^{280,284} The compounds **28a** and **28f** were dissolved in DMSO at a concentration of 3 mM. Their UV spectra displayed an absorption maximum at 358 nm and 314 nm. They were thus irradiated in an NMR tube with UV light at 365nm during one hour. The ¹HNMR spectra of compounds **28a** and **28f** in their *trans* form were already recorded, so the aim was to follow the isomerization to the *cis* isomer by ¹HNMR recording. Unfortunately, this was not possible as the thermal relaxation of this type of azobenzenes is too fast as reported in literature in the order of milliseconds or nanoseconds.²⁸⁵ Therefore, it was impossible to record the ¹HNMR spectra of the isomerization because after five minutes from the end of the irradiation only the *trans* isomer was visible in the ¹HNMR spectrum.

In the case of compounds with a fast thermal relaxation, the ^1H NMR spectra should be recorded directly during the irradiation using a special optical fiber-based illumination setup. In the NMR platform of our laboratory, there is no such type of LED-illumination device to allow the recording of these types of spectra. It was anyway possible to follow the *E-Z* isomerization of another type of photoswitch compounds that present a longer relaxation time as will be shown below in section 4.1.3.2.1.

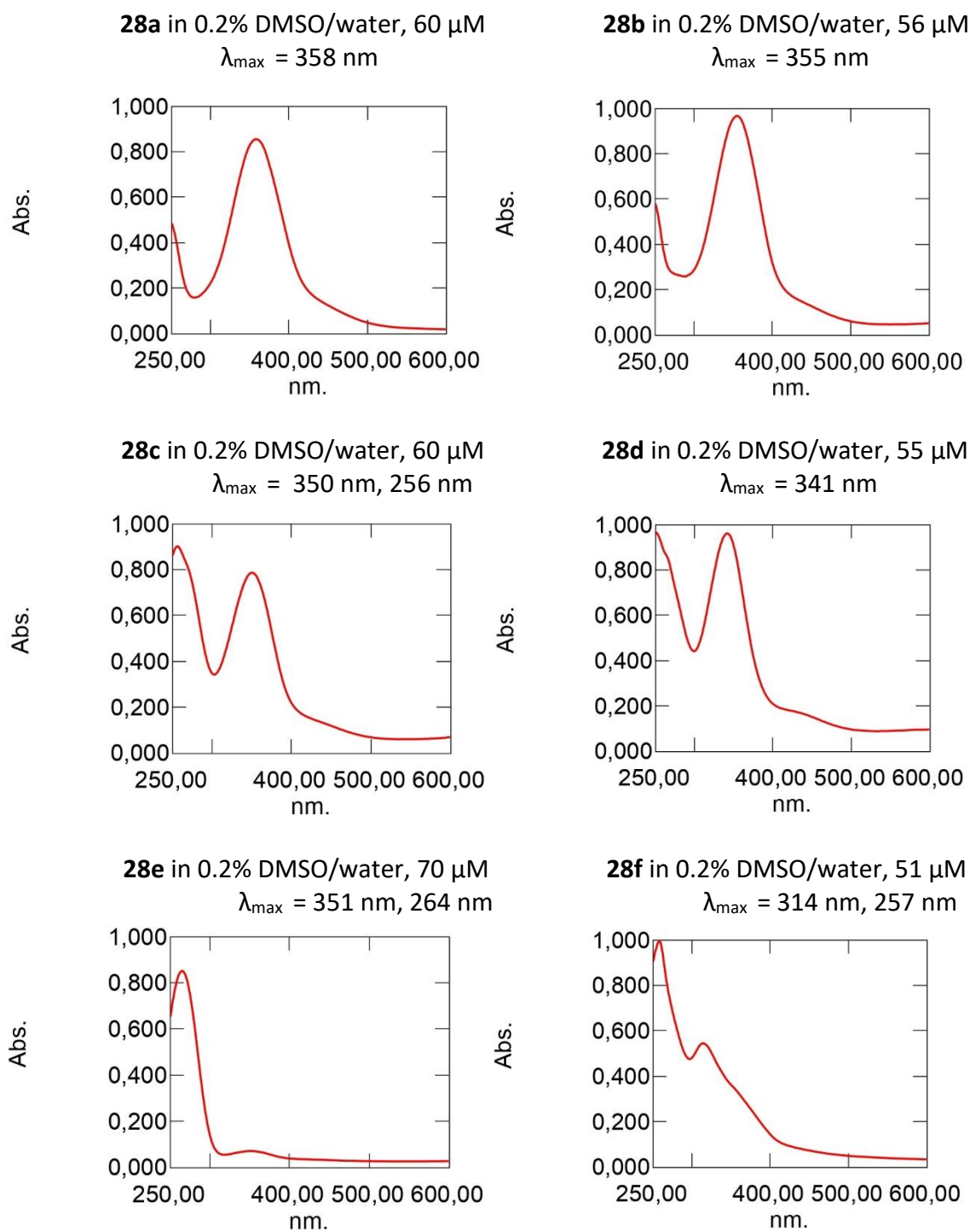


Figure 66. UV-Vis spectra of compounds **28a-f**.

4.1.3.2. Phenylazoindole analogs

Phenylazoindole analogs represent another type of photoswitch related to azobenzenes where a benzene ring is replaced by an indole. These compounds are planar like the azobenzenes due to the central diazene bond and can be switched to their *Z* isomer using UV light while switched to their *E* isomer using blue or green light (**Figure 67**). The rationale of their synthesis is due to a superimposition of the phenylazoindole analog with the XAP044 where the *Z* form of the hydroxyl-phenylazoindole matches with XAP044 (**Figure 68**). Furthermore, the replacement of the chromone with an indole can improve solubility properties as it is known that chromone scaffold, even if it has been used in medicinal chemistry, displays poor solubility properties.^{342,343,344}

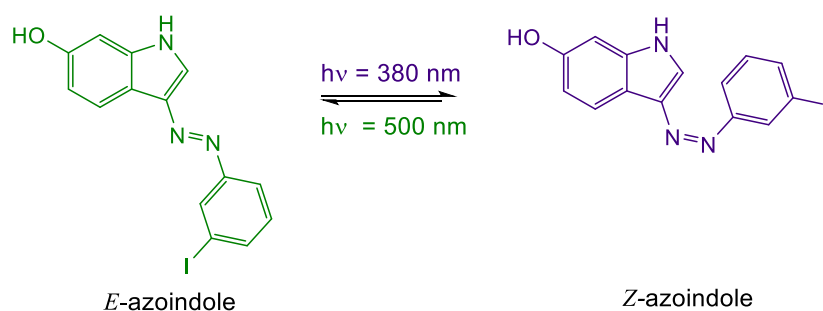


Figure 67. Phenylazoindole in *E* and *Z* form switched using UV and visible light.

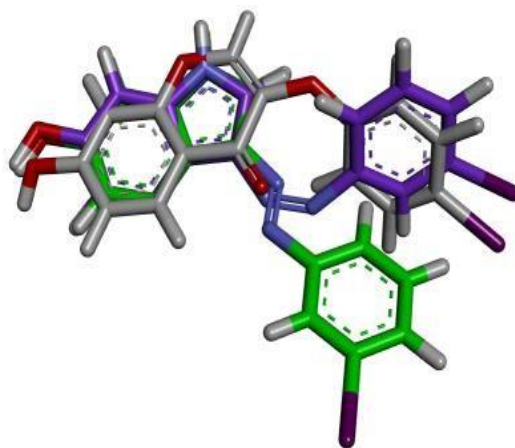
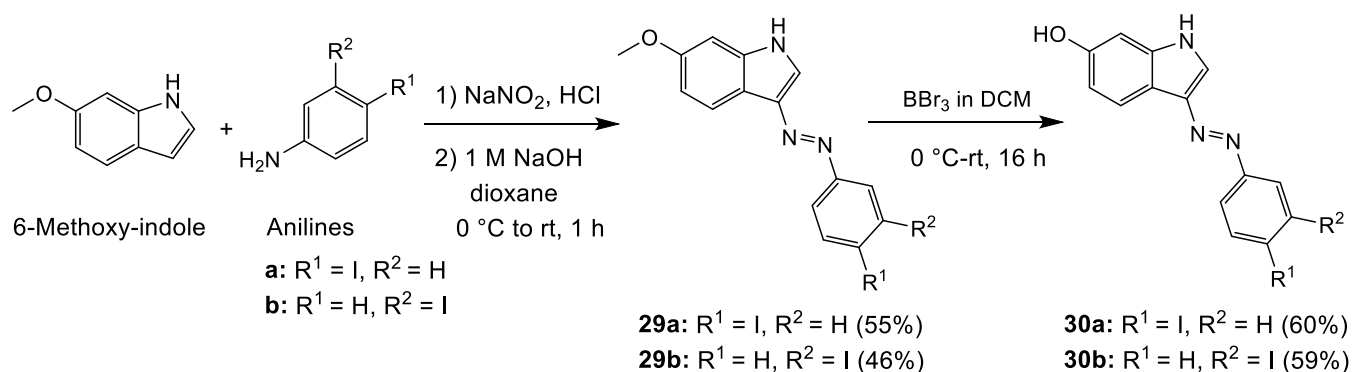


Figure 68. Superimposition of XAP044 (grey) in a planar conformation with the *trans* phenylazoindole (green) and the *cis* phenylazoindole (violet). The *cis* isomer seems to match with XAP044.

The synthesis of phenylazoindole compounds was achieved by azocoupling reaction as already seen for azobenzene in **Scheme 37** but the water was replaced with dioxane in order to (better) solubilize 6-methoxyindole.^{345,346} Two different analogs **29a,b** were synthesized bearing an iodine in *para* and *meta* positions of the benzene ring, respectively. The two compounds were then demethylated using BBr_3 in 1 M DCM to get the final products **30a,b** (**Scheme 40**).



Scheme 40. Synthesis of phenylazoindole compounds **29a,b** and **30a,b**.

4.1.3.2.1. Photophysical properties of Phenylazoindole analogs

According to UV-Vis and ^1H NMR spectra, all compounds were only obtained in *E* configuration except for compound **30b**. Indeed, this compound was obtained as a mixture of 23% of *E* isomer and 77% of *Z* isomer. This is probably due to the iodine atom in *meta* position that changes totally the electronic properties of the molecule compared to compound **30a**. This means that, while the other compounds are energetically stable in their solid form and dissolved in DMSO in *E* configuration, compound **30b** is energetically stable in the mixture 23% *E* and 77% *Z* its photostationary state (PSS) at 20°C. This hypothesis was confirmed by allowing compound **30b** to stand in DMSO in an NMR tube during 13 days protected from light, and observing that the percentage of the two isomers remained the same (**Figure 69**).

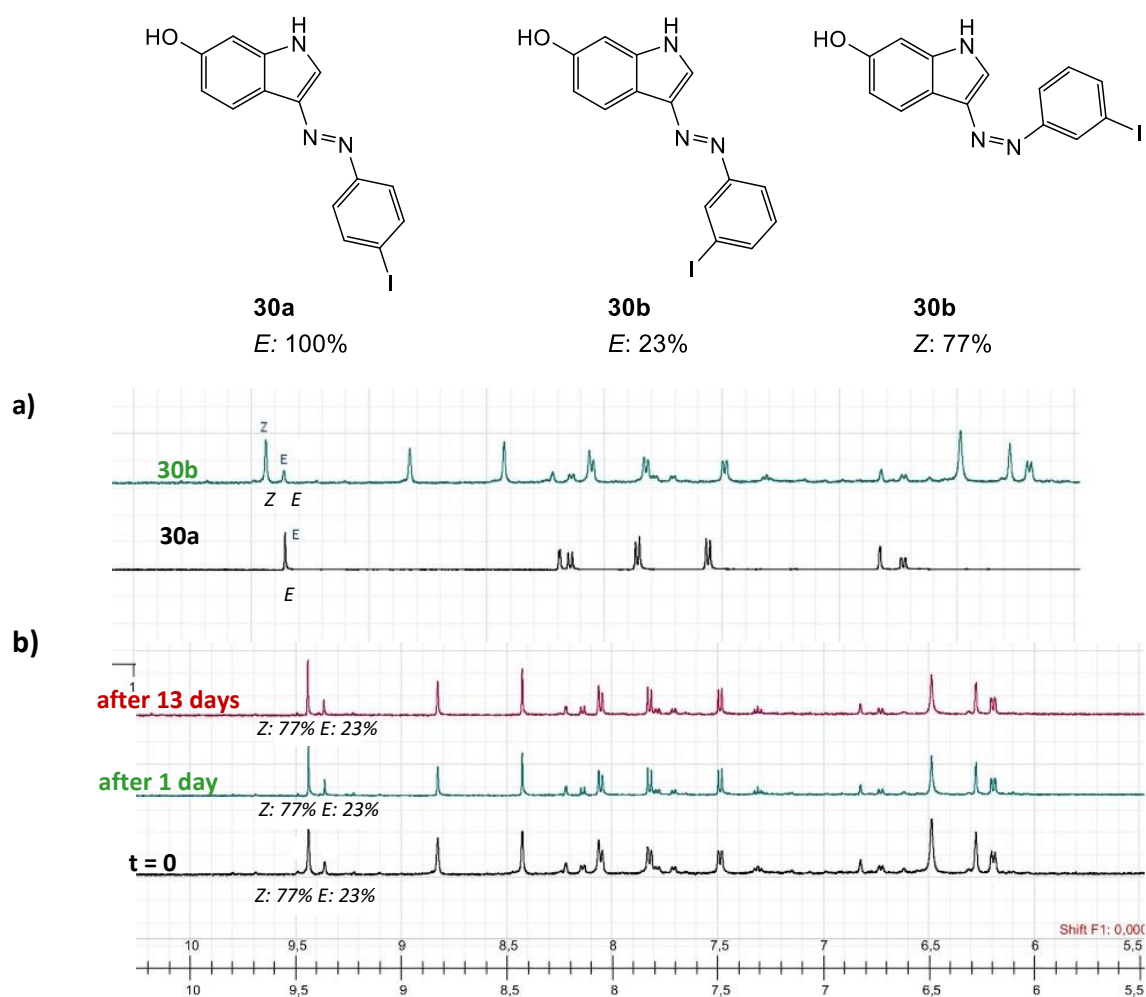


Figure 69. Comparison between product **30a** and **30b**. **a)** Superimposition of the ^1H NMR spectra in DMSO of products **30a** at 2 mM (black) and **30b** (green). **b)** ^1H NMR spectra of product **30b** in DMSO at time 0 (black), after one day (green) and after 13 days (red). Proportions of *E* and *Z* isomer were stable during 13 days in the same DMSO solution.

UV-Vis spectra in DMSO and water of compounds **29a,b** and **30a** confirmed the *E* isomer. In the case of product **30b** the *E* isomer is only present in 23% while clearly the other *Z* isomer is predominantly present (**Figure 69** and **Figure 70**).

The UV spectra of **30a** and **30b** show clearly that the two compounds are different isomers. The spectra of product **30a** is well defined with a maximum wavelength at 386 nm that characterize the *E* isomer. It is impossible to find a maximum of absorbance in the spectra of product **30b** as it is a mixture of the two *Z* and *E* isomers.

The pharmacological properties of phenylazoindoles will be presented in section 4.2.

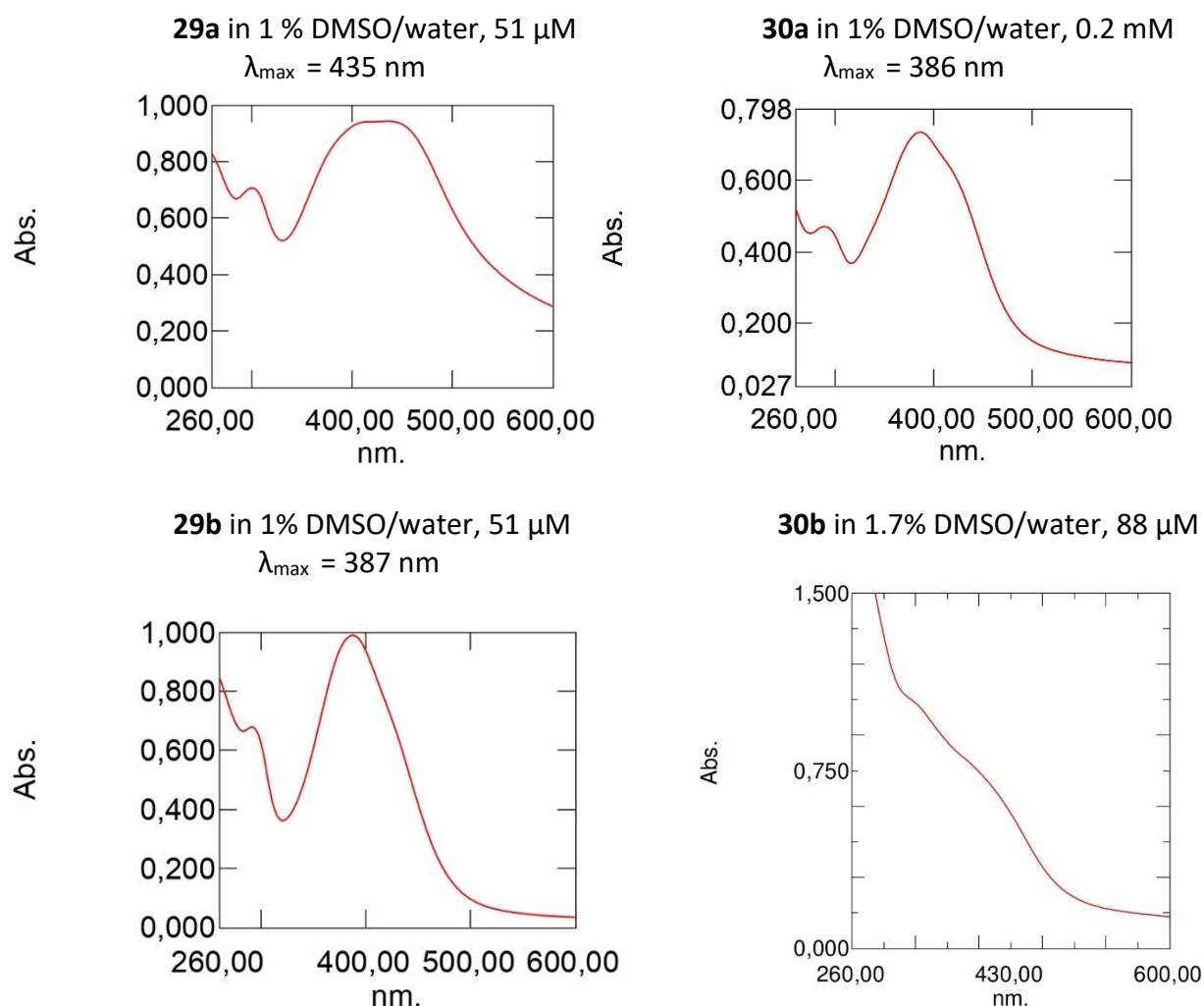


Figure 70. UV-Vis spectra of compounds **29a,b** and **30a,b**.

4.1.3.3. Aurones analogs

Aurones are natural compounds that belong to the flavonoid class. They are yellow dyes consisting in a benzofuranone ring linked through a carbon-carbon double bond to a phenyl moiety.³⁰⁹ The interest in synthesizing this compound was related to their structural similarity with the XAP044 and the aim was to replace the chromone ring with a benzofuranone ring to obtain a photoswitch analog and improve the solubility. Indeed, as already seen with azobenzene and the phenylazindole analogs, they have the ability to be switched between *Z* and *E* isomers using different wavelength irradiation. They have also a planar structure and an improved solubility compared to XAP044. While, in the azobenzene and the phenylazindole analogs the switch is due to the central diazene bond, for the aurones it is due to the central carbon-carbon double bond. Furthermore, their photophysical properties are different compared to previous synthesized switches. In fact, in the case of azobenzene and phenylazindole analogs the energetically stable isomer is usually the *E* while for the aurones it is the *Z* configuration. They also show a longer

relaxation time that allows to perform ^1H NMR kinetics, thus the properties of different synthesized compounds of this class were studied using both NMR and UV-Vis spectroscopy.

The initial study with aurones was based on the choice of orientation 3 for the docking of XAP044 (**Figure 60**). At that time, we thought that orientation 2 was not validated. The superimposition of a 6-hydroxyaurone analog with XAP044 showed that the *E* configuration would perfectly fit with XAP044 in the conformation of the docking model (**Figure 71**).

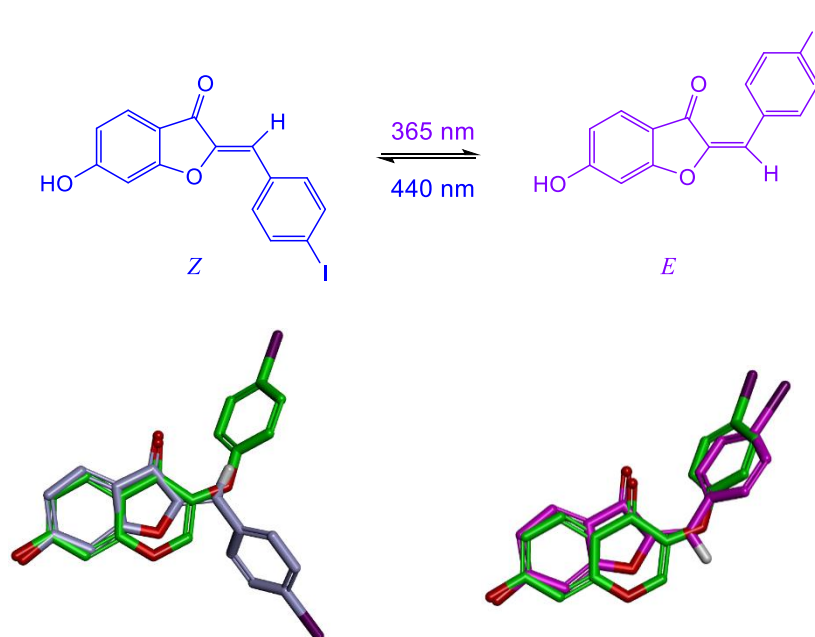


Figure 71. Superimposition of XAP044 in the docking conformation of orientation 3 with a 6-hydroxyaurone analog. On the left, XAP044 (green) is superimposed with the *Z* isomer of the 6-hydroxyaurone (mauve). On the right, XAP044 (green) is superimposed with the *E* isomer of the 6-hydroxyaurone (magenta). The *E* configuration of the 6-hydroxyaurone fits with the hypothesized binding conformation of XAP044 when oriented to loop $\beta 7\beta 8$ in the mGlu7 VFTD (see **Figure 60** and section 4.3).

However, at a late stage of the thesis, we invalidated the orientation 3 of XAP044 binding to mGlu7R and chose orientation 2 along helix $\alpha 6$ (**Figure 60** and Section 4.3). In that case, none of the aurone isomers fitted with the bioactive conformation of XAP044 (**Figure 72**).

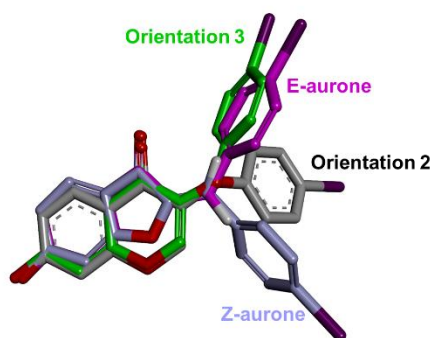
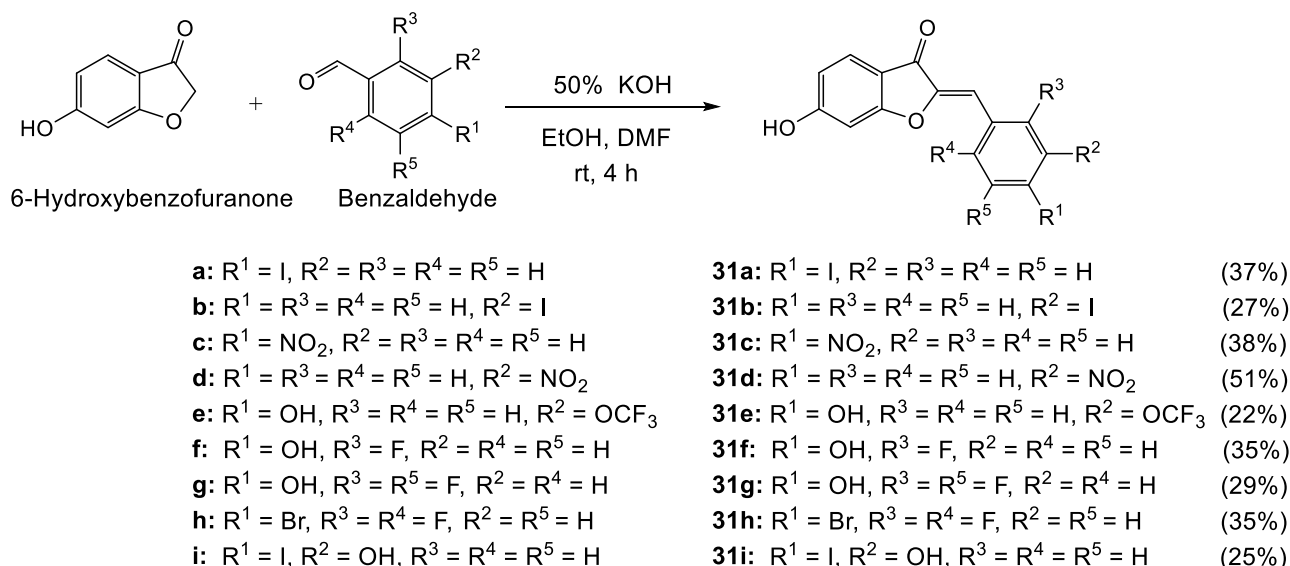


Figure 72. Superimposition of XAP044 conformations in the two orientations of mGlu7R docking with the 6-hydroxyaurone analog *E* and *Z* isomers. The aurone isomers do not fit with XAP044 in orientation 2 conformation.

Based on the initial hypothesis, nine different aurones were synthesized by aldolic condensation (**Scheme 41**). The first four analogs **31a-d** bear an iodine atom or a nitro group in *para* or *meta* positions of the phenyl ring. The iodine atom was chosen to mimic exactly the structure of XAP044 and the nitro group because **19c** (**Table 1**) revealed a NAM activity at mGlu7R (section 4.2). The other five aurones **31e-i** bear a fluorine atom in the ortho position of the phenyl ring because the activity of compound **19i** (*para* bromo) was increased with such a substituent (**19k**). The hydroxyl groups were introduced to obtain more soluble aurones.



Scheme 41. Synthesis of aurone analogs **31a-i**.

Aldolic condensation can be catalysed by a base *via* enolate formation or by an acid *via* enol formation. In the first part of the mechanism, there is an aldol reaction and then a dehydration reaction. The aldol addition product can be dehydrated *via* a strong base in an enolate mechanism

or *via* acid-catalysed enol mechanism.^{347,348} In the synthesis of aurones **31a-i** a strong base as potassium hydroxide is used *via* enolate mechanism.

4.1.3.3.1. Photophysical properties of Aurone analogs

All the aurones were obtained in *Z* configuration as reported in literature.³¹⁰ In fact, the most energetic stable configuration is the *Z* for this type of dyes. In contrast with azobenzene, the UV spectra of the aurone alone does not allow the assignment of the configuration of the compound because usually the maximum wavelengths of absorbance of the *Z* and *E* isomers are close in value. Azobenzenes have a maximum absorbance wavelength around 365 nm for the *trans* isomer and 440 nm for the *cis* isomer while for the aurones these values are closer and also depend on the solvent. Nevertheless, the difference in molar extinction coefficient still allows to switch configurations. ¹HNMR spectra of aurones also confirmed the *Z* configuration and ¹HNMR kinetic studies of photoisomerization were performed using an irradiation lamp.

If a pure *Z* or *E* aurone isomer is available and not the other one, a mixture may still be evaluated and its biological activity compared to that of the pure isomer. Mixtures of *Z/E* isomers were prepared for the first four aurones **31a-d** to allow the biological tests of **31a-d Z** and of the **31a-d E/Z** mixtures. Compounds **31a-d E/Z**, were prepared by irradiation at 365 nm of compounds **31a-d Z** dissolved in EtOAc as described in **Table 2**.

Compound	Mg	Volume EtOAc (mL)	Time (h) _{hy=365nm}	<i>E</i> (%)	<i>Z</i> (%)
31a Z	30	30	10	77	23
31b Z	50	50	14	77	23
31c Z	30	30	10	77	23
31d Z	30	30	10	53	47

Table 2. Preparation of compounds **31a-d E/Z**

The *E* isomer and the *Z* isomer of the mixture were not separated by chromatography because the *E* configuration isomerized to the *Z* on silica gel.

The aurones **31e-i** were only tested in their *Z* configuration because we observed by ¹HNMR kinetics in DMSO that they spontaneously evolved towards the *E* configuration over time.

Apparently, UV light irradiation of such compounds in a polar protic solvent such as MeOH can lead to degradation or undesirable photochemical reaction. On the contrary, aurones **31a-d** showed stability in DMSO, a longer relaxation time and as a result are stable in their *Z/E* percentage after irradiation. Furthermore, biological assays are usually performed in a maximum of 0.1% DMSO in water and when the polarity of the solvent increases the thermal relaxation is faster.^{311,312} Aurones **31a-d Z/E** were found to be stable at least one hour after dissolution in 0.1% DMSO in 0.1 M PBS at pH 7.2, which allows their *Z/E* mixture to be tested in biological assays.

Concerning the compounds **31a-d** (Figure 73), ¹HNMR spectra kinetic in DMSO showed that compounds **31a,c Z** can be switched faster to the *E* configurations than return to the *Z* configuration by irradiation at 365 nm and 440 nm, respectively. The wavelength of 365 nm was chosen for irradiation because of λ_{\max} values close to this value for compounds **31a-d Z** (Figure 78). UV-Vis spectra of products **31a-d Z** in 0.2% DMSO/PBS showed these compounds could absorb at 365 nm the necessary energy to switch to the *E* form. It is necessary also to precise that the lamp used can irradiate just at three different wavelengths (365 nm, 440 nm and 490 nm) and this represented a limitation for our study. A higher percentage of interconversion was observed for **31a,c Z** and this is due probably to the presence of withdrawing groups *i.e.* iodine atom and nitro group in the *para* position. On the other hand, for products **31b,d Z** the interconversion yield was lower due to the presence of the iodine atom and the nitro group in the *meta* position.

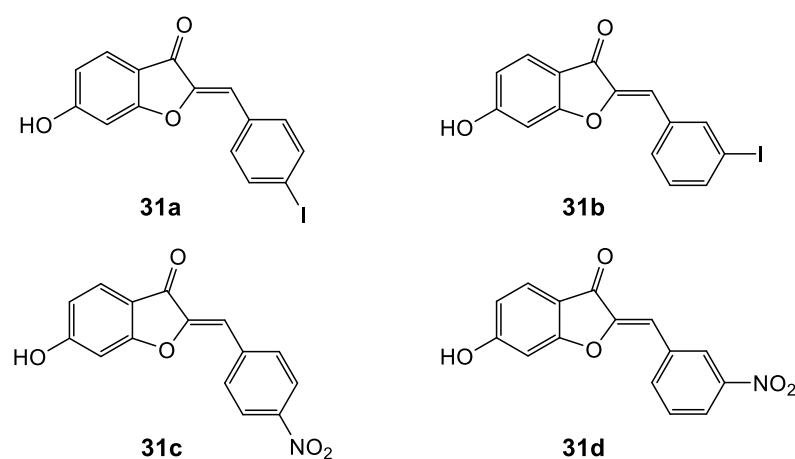


Figure 73. Compounds **31a-d**.

Product **31a Z** was dissolved in DMSO at concentration of 9 mM in an NMR tube. The *Z* isomer was converted to 77% of *E* isomer after 10 h of irradiation at 365 nm (photo stationary state PSS at 395 nm) then after 1 h of irradiation at 440 nm only 9% of *E* isomer remained (PSS at 440 nm) (Figure 74).

The same experiment was performed for product **31b Z** dissolved in DMSO with a concentration of 9 mM in an NMR tube. The *Z* isomer was converted to 72% of *E* isomer after 10 h irradiation at 365 nm (PSS at 365nm) and after 6 h of irradiation at 440 nm only 16% of *E* isomer remained (PSS at 440 nm) (**Figure 75**).

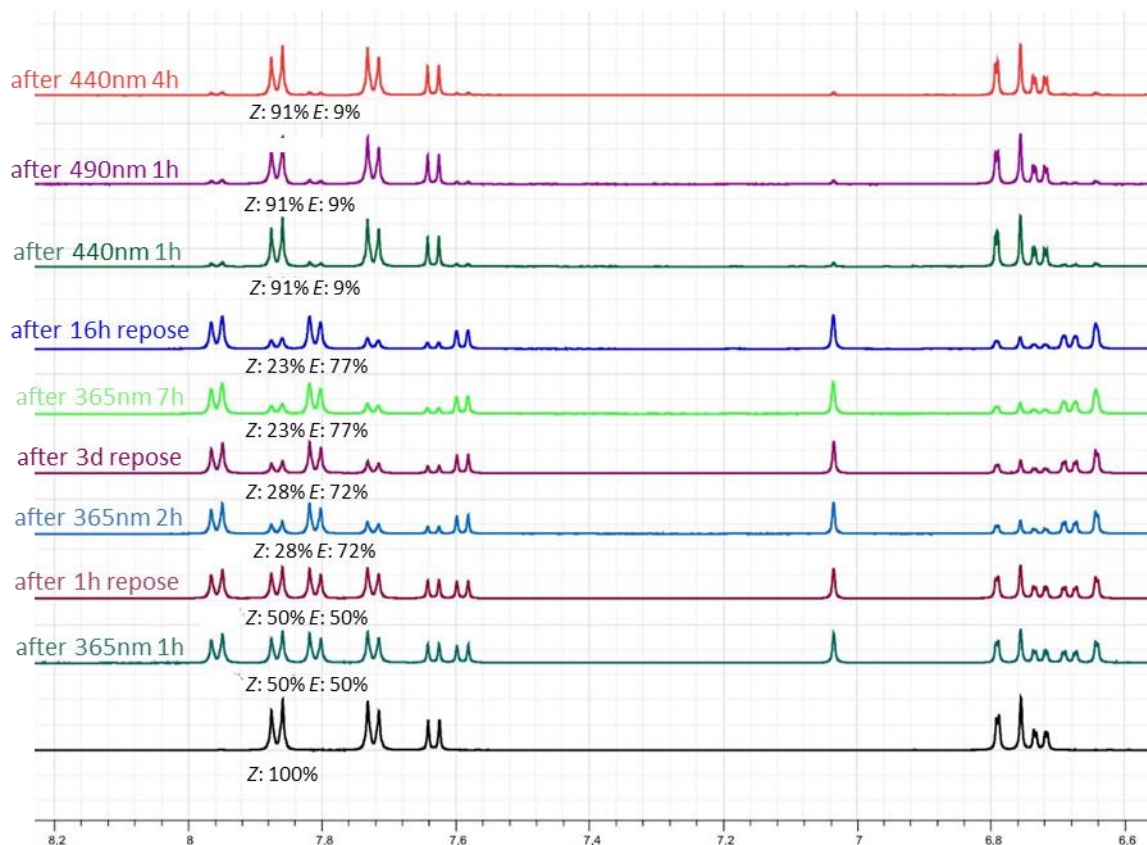


Figure 74. Irradiation of compound **31a Z** at 365 nm and 440 nm in DMSO.

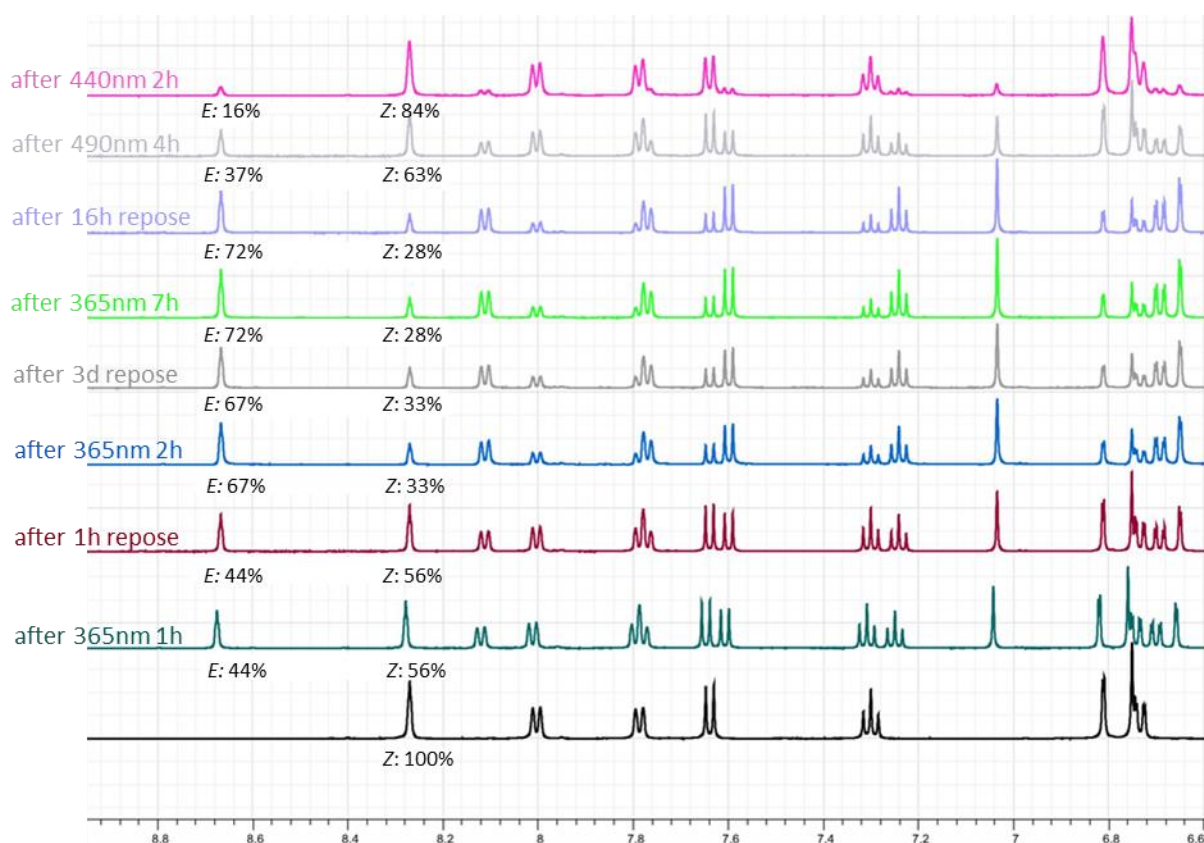


Figure 75. Irradiation of compound **31b Z** at 365 nm and 440 nm in DMSO.

Products **31c Z** and **31d Z** were also dissolved in DMSO at a concentration of 9 mM in an NMR tube. Compound **31c Z** was converted to 53% *E* and 47% *Z* isomers after 13 h irradiation at 365 nm (PSS at 365 nm) and these percentages remain stable after five days (**Figure 76**). **31d Z** was converted to 44% *E* and 56% *Z* isomers after 13 h irradiation at 365 nm (PSS at 365 nm) and the percentage remained stable after five days (**Figure 77**).

UV-Vis spectra of compounds **31a-d** were recorded in four different solvents: DMSO, EtOAc, MeOH and a mixture 0.2% DMSO/PBS. In **Figure 78** are reported the UV-Vis spectra in 0.2% DMSO/PBS. Compounds **31c,d Z** bearing nitro group in *para* and *meta* position show a maximum wavelength absorbance around 400 nm compared to **31a,b Z** that have a maximum wavelength absorbance closer to 365 nm.

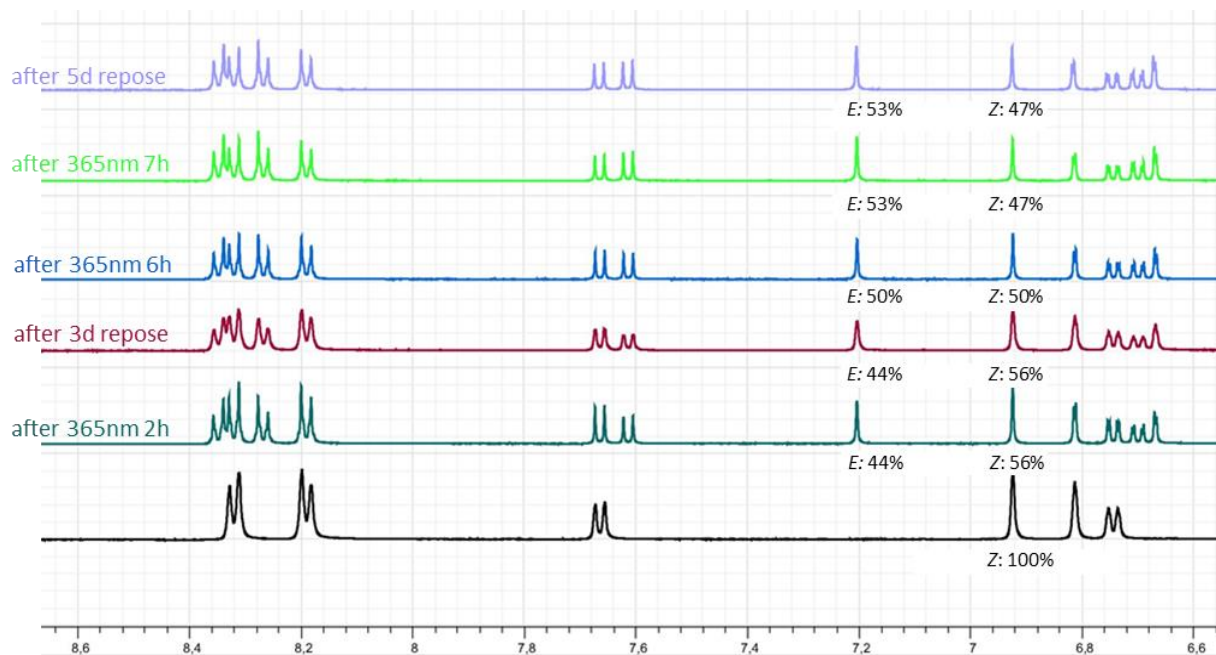


Figure 76. Irradiation of compound 31c Z at 365 nm in DMSO.

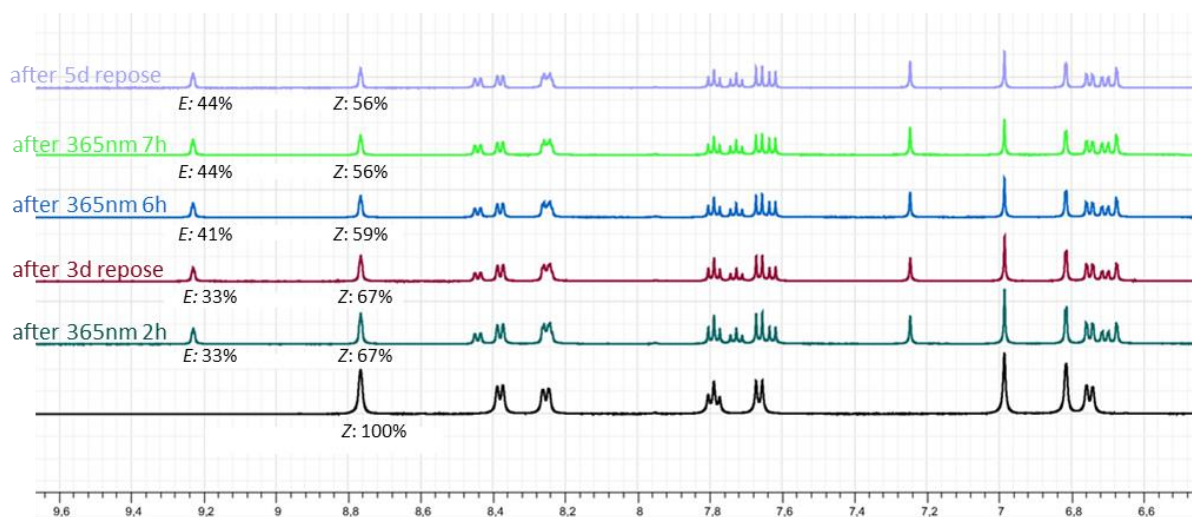


Figure 77. Irradiation of compound 31d Z at 365 nm in DMSO.

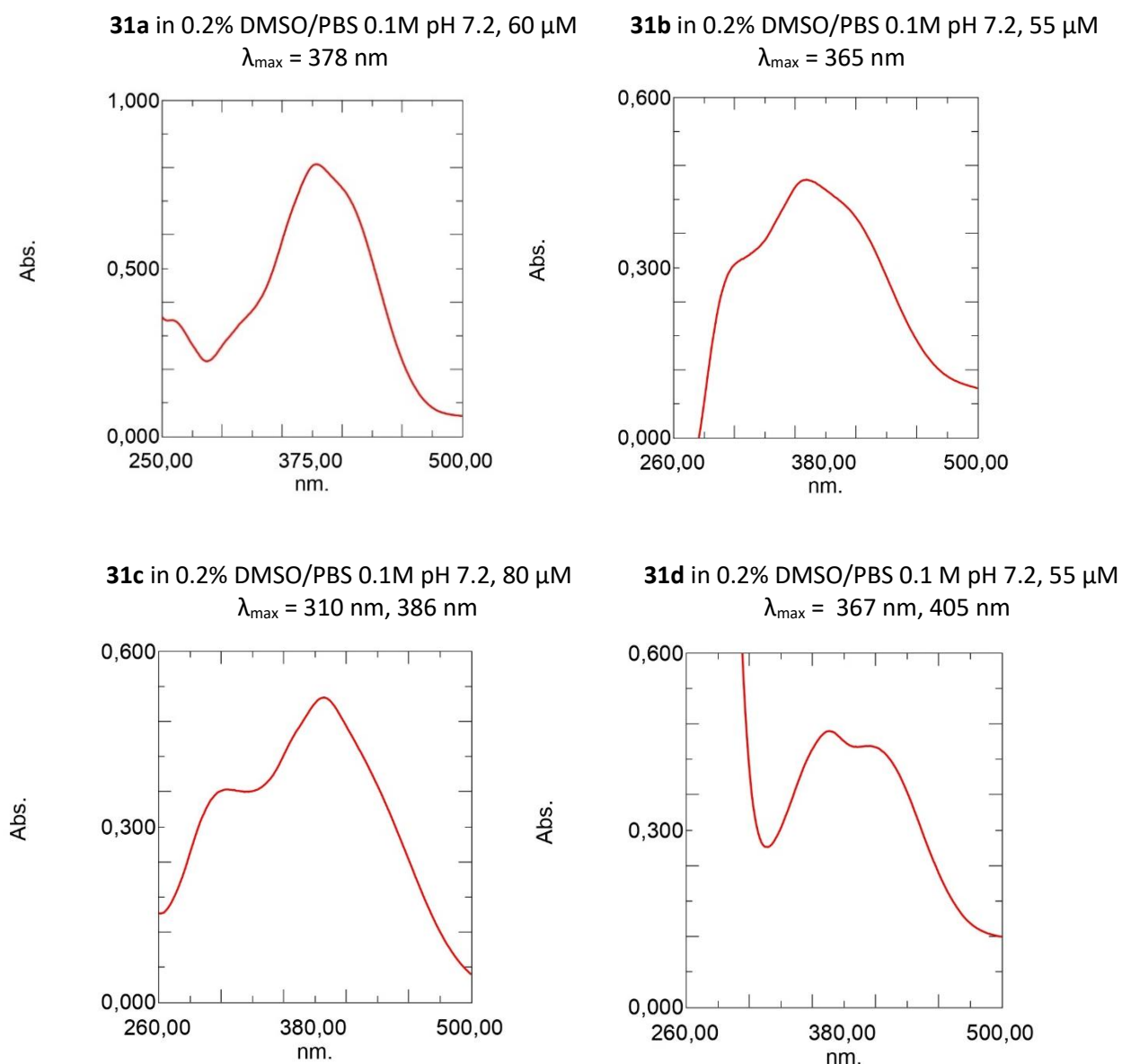


Figure 78. UV-Vis spectra of products **31a-d Z** in 0.2% DMSO/PBS.

The compounds **31e-i** (**Figure 79**) showed less stability in DMSO solution compared to aurones **31a-d**. Compound **31e Z** in DMSO at a concentration of 9 mM spontaneously convert to 16% of *E* isomer in 24 h without irradiation according to ^1H NMR spectra (**Figure 80**). In fact, the *E/Z* spectra showed the double of the peaks of *Z* isomer spectra and the integration between each *E/Z* peak resulted proportional to the percentage of *E* and *Z* isomers.

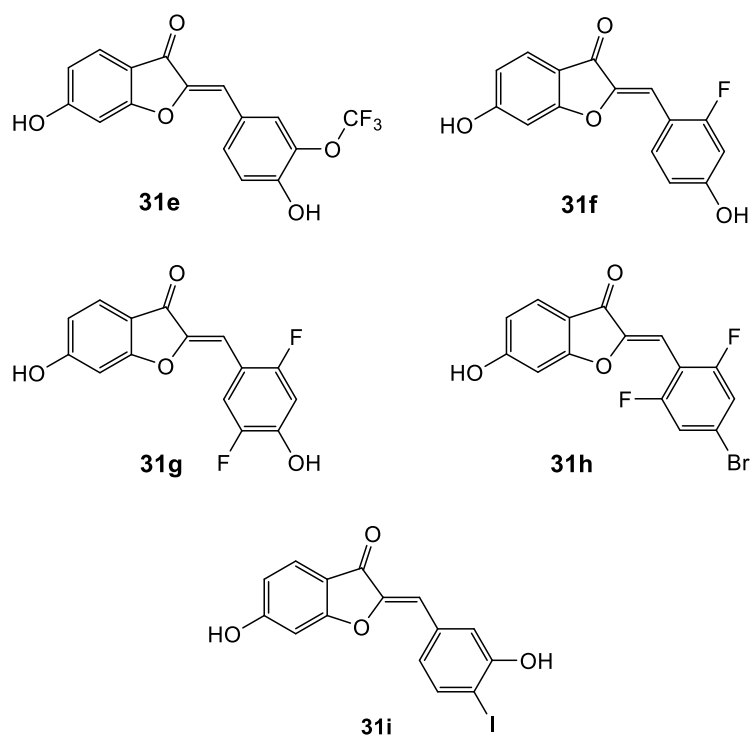


Figure 79. Compounds **31e-i**.

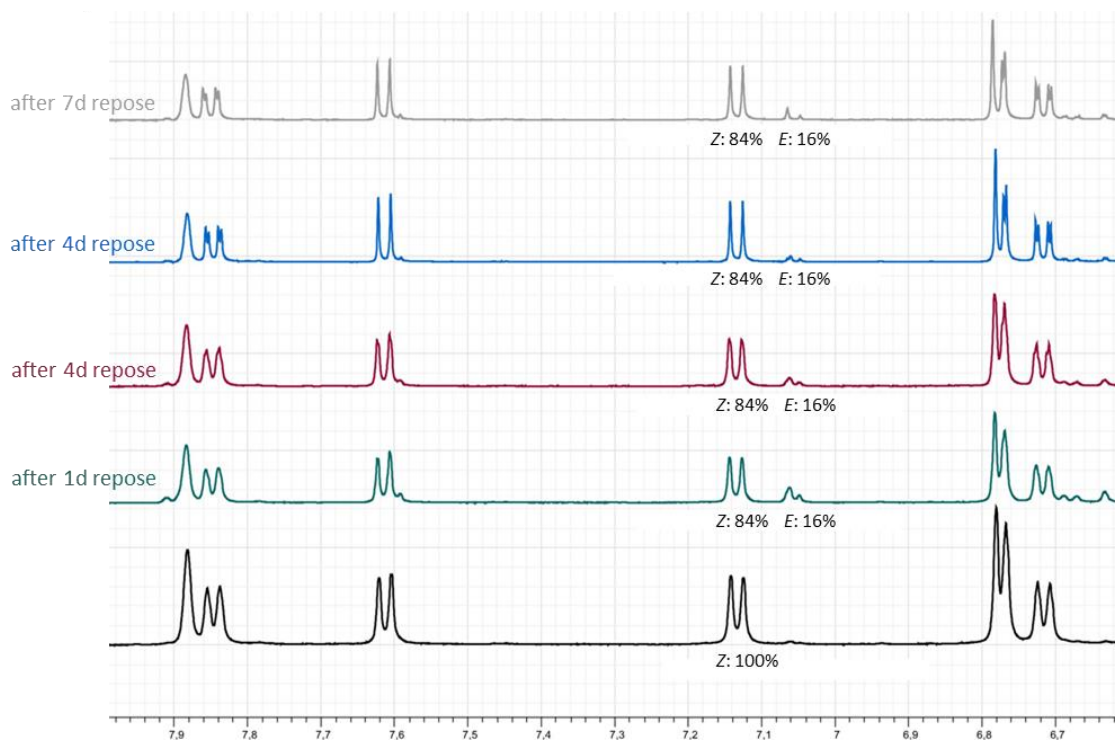


Figure 80. Isomerization of compound **31e Z** in DMSO.

Compound **31f Z** in the same conditions showed a spontaneous isomerization into *E* isomer of 9% in four days, (**Figure 81**) while for compound **31g Z** the same rate of conversion was observed after five days (**Figure 82**).

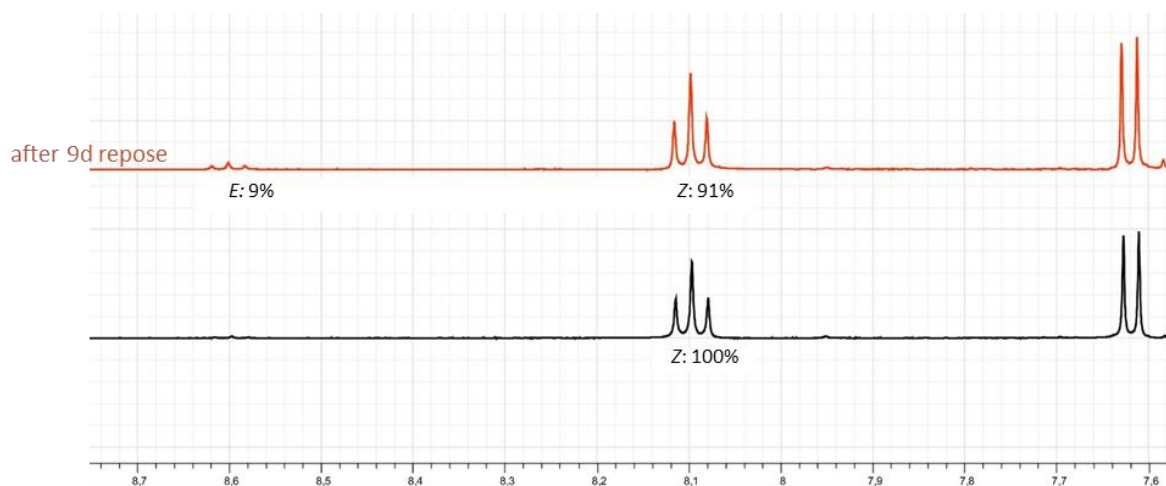


Figure 81. Isomerization of compound **31f Z** in DMSO.

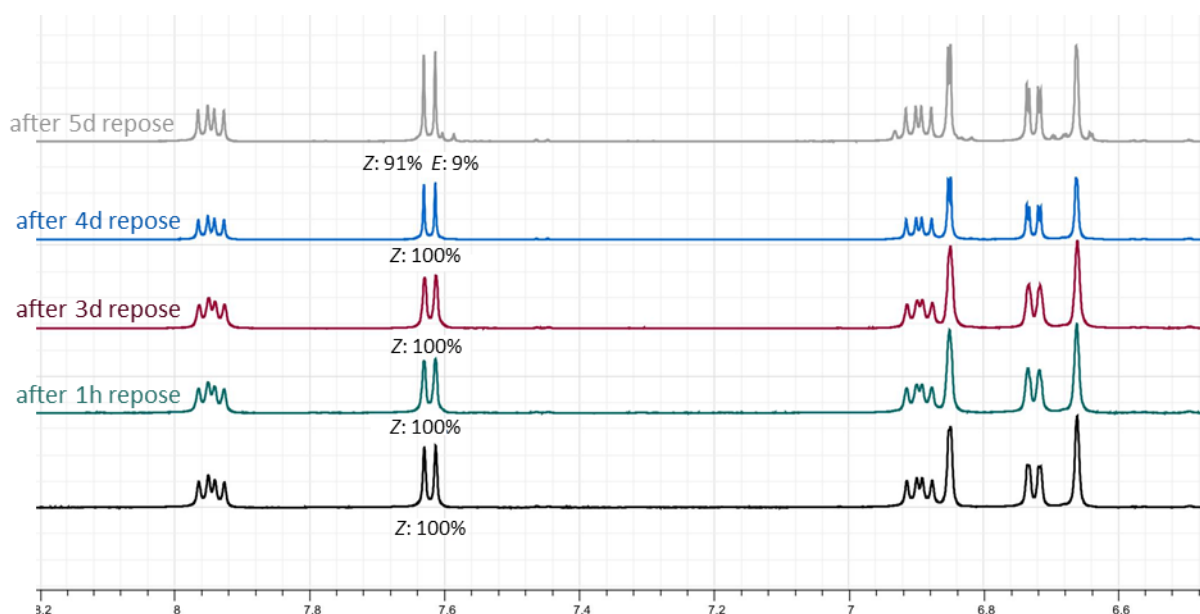


Figure 82. Isomerization of compound **31g Z** in DMSO.

Product **31h Z** spontaneously convert to 44% of *E* isomer in two days (**Figure 83**). Compound **31h Z** was irradiated to try to get the maximum percentage of *E* isomer and separate it by chromatography. The compound (100 mg) was dissolved in 25 mL acetone and irradiated at 365 nm during 4 h then 1 mL was evaporated and dissolved in DMSO at a concentration of 9 mM in an NMR tube to obtain 21% of the *E* isomer and 79% *Z* isomer. A further irradiation for a total of 6 h at 365 nm gave 31% of the *E* isomer and 69% *Z* isomer. After one night in repose in the dark, the proportion of the two isomers did not change. MeOH (10 mL) was added to the solution and let repose two nights in the dark and the same proportion of the two isomers was found but apparently the product started to degrade or a photochemical reaction took place. Surprisingly, after another irradiation at 365 nm for 6 h it was clear that the compound in the acetone/MeOH

solution spontaneously degraded or maybe the irradiation when adding MeOH, catalysed a photochemical reaction to the formation of another product (**Figure 84**). In compound **31h** the presence of withdrawing substituents in *ortho* and *para* positions may favourite a Michael addition on the double bond with degradation of the molecule in polar solvents as MeOH.

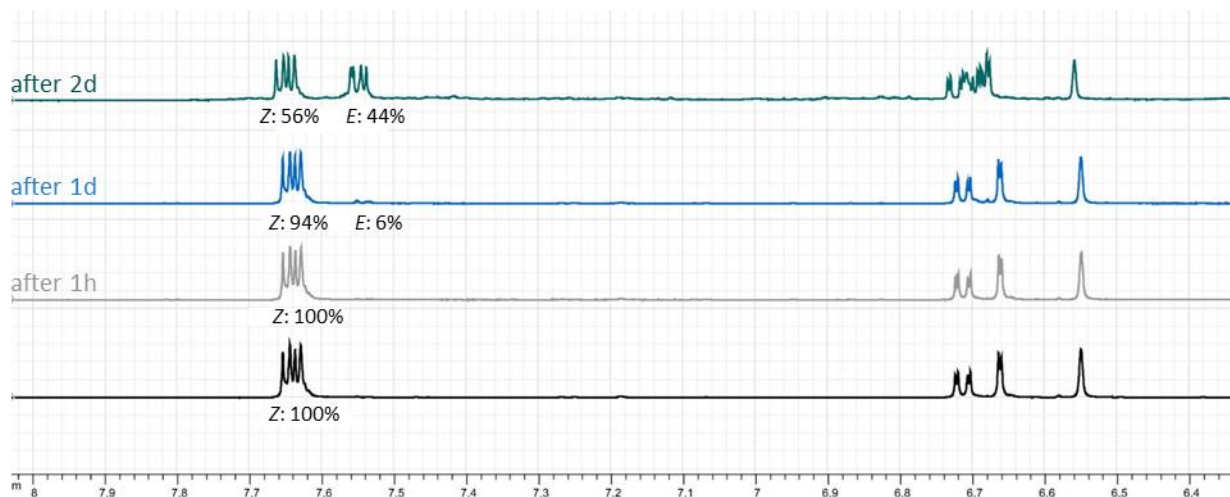


Figure 83. Isomerization of compound **31h-Z** in DMSO.

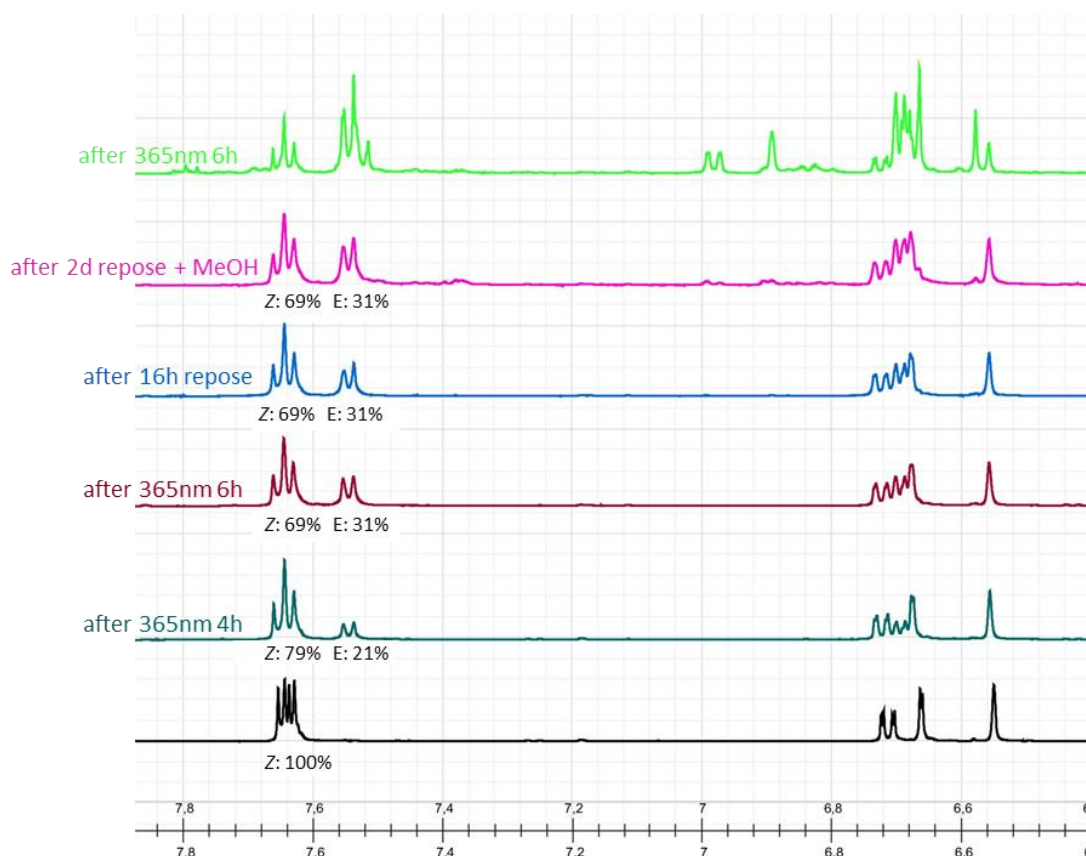


Figure 84. Irradiation of compound **31h-Z** at 365 nm in DMSO.

Due to all these observations, it is obvious that these compounds **31e-i** are not enough stable compared to the previously synthesized compounds **31a-d**. This is probably due to the presence

of fluorine atoms and an additional hydroxyl group that catalyse spontaneously the conversion of the isomers and can lead to degradation or undesirable photochemical reaction when irradiated with UV light. UV-Vis spectra of the products **31e-i** were recorded in 0.05-0.06% DMSO/PBS 0.1M pH 7.2 (Figure 85).

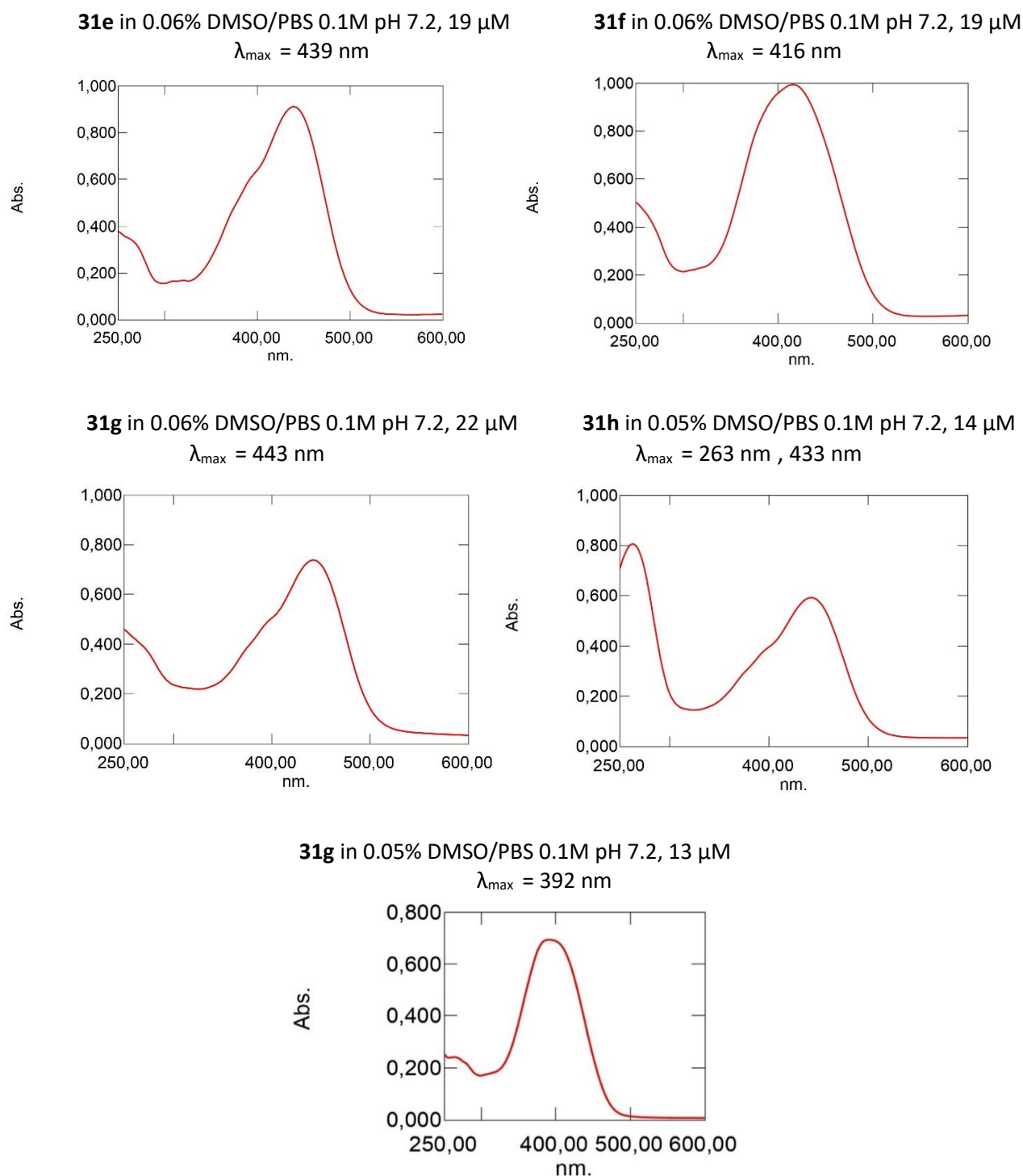
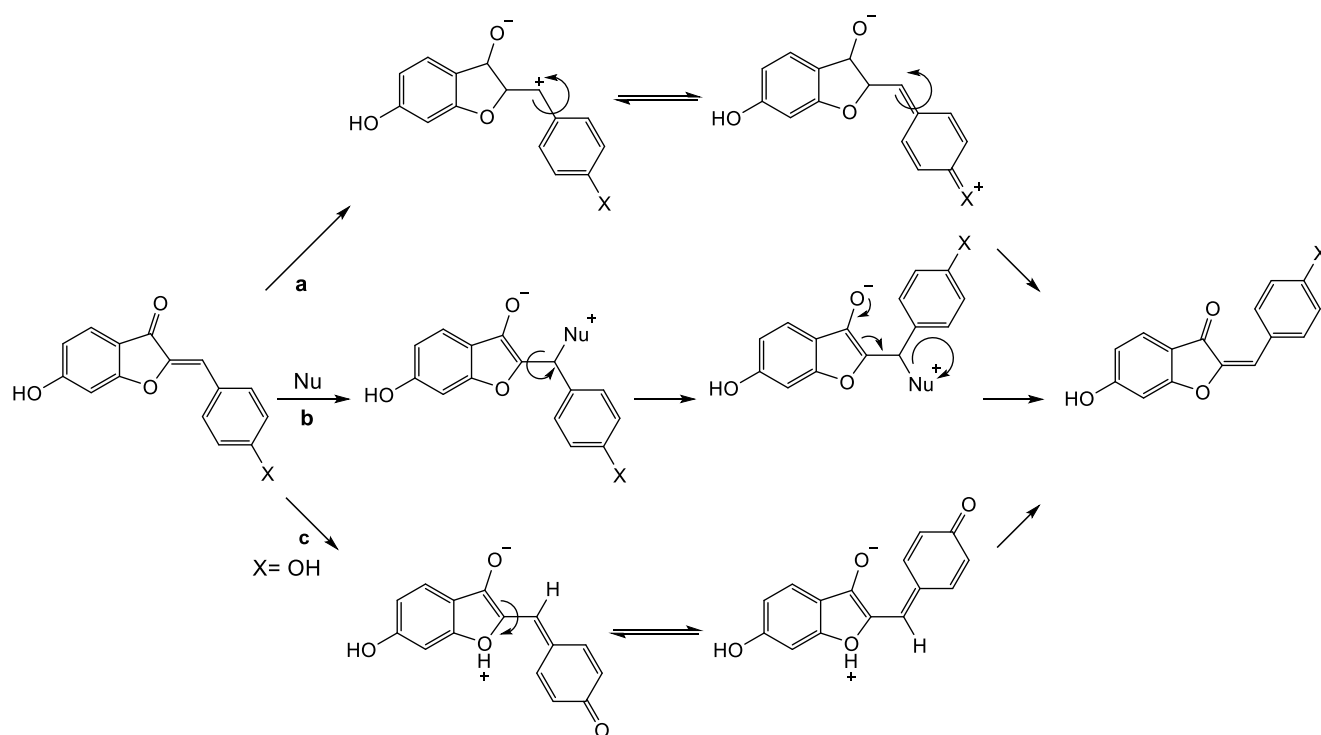


Figure 85. UV-Vis spectra of compounds **31e-i** Z.

Compounds **31e-h Z** showed higher maximum wavelength absorbance compared to compounds **31a-d Z**. As described by Shanker et al.³⁴⁹ the substitution in *para* position by an atom or a group with donating or withdrawing effect results in opposite properties. The hydroxyl group in *para* position of compounds **31e-g** has a donor effect compared to compound **31a-d** leading to a bathochromic shift. Compound **31h** presents a halogen, withdrawing substituent, in *para* position but the fluorine in *ortho* positions may have a positive effect on the red-shift. Compound **31i** shows the addition of a hydroxy group in *meta* position compared to **31a** and the λ_{\max} observed are similar. This confirm that donor substituent like hydroxy group in *para* position, as observed for **31e-g** favour red-shift while donor substituent in *meta* position, as in **31i**, does not show this effect.

In the case of the azobenzenes the isomerization of the two isomers is due to a mechanism of rotation or isomerization (see **Scheme 5** in section 2.2.5) and the same can be observed for phenylazindole compounds.³⁴⁶ Furthermore in azobenzene a push-pull system based on an electron donor group in *para* of a benzene and an electron withdrawing group in *para* of the other benzene slows the thermal isomerization as well the *tetra* substitution with fluorine in *ortho* positions.^{284,285} Phenylazindole thermal relaxation can be slowed from ms to days by the substitution of the nitrogen of the indole with a electron donor group as a methyl.³⁴⁵ Aurones show longer thermal isomerization time when substituted in *para* or *meta* positions of the benzene ring with electron withdrawing groups as observed for compound **31a-d**. The substitution with electron donor group in *para* of the benzene, as in **31e-g** gives a faster thermal isomerization time. Compound **31g** shows also a faster thermal isomerization due to the substitutuion in *ortho* positions with fluorine. The mechanism of isomerization cannot involve the rotation as they lack the diazene bond present in azobenzenes and phenylazindoles. Similarly to isomerization pathways described in literature for green florescent protein chromophores,³⁵⁰ isomerization of aurones can be due to a direct inversion mechanism, to the addition and elimination of a nucleophile and to a tautomerization mechanism (**Scheme 42**). The addition and elimination of a nucleophile mechanism explains the faster thermal isomerization observed in polar solvents as methanol or water. The tautomerism mechanism is observed for compounds bearing a hydroxy group in *para* position of the benzene ring as in the case of compounds **31e-g**.



Scheme 42. Isomerization mechanism for aurones: **a)** direct, **b)** addition/elimination and **c)** tautomerism.

Compounds **31a-d** were studied by kinetics of irradiation at 365 nm and 440 nm using UV-Vis spectroscopy. Each compound was studied in four different solvents *i.e.* DMSO, EtOAc, MeOH and 0.2% DMSO/PBS at a concentration between 45 and 80 μM in order to study the isomerization properties of these four compounds depending on the polarity of the solvent. Starting from *Z* isomer each compound was irradiated at 365 nm for a maximum of 60 seconds directly in the UV cuvette. This led to the formation of the *E* isomer that was then irradiated at 440 nm to go back to the *Z* isomer (**Figure 86**).

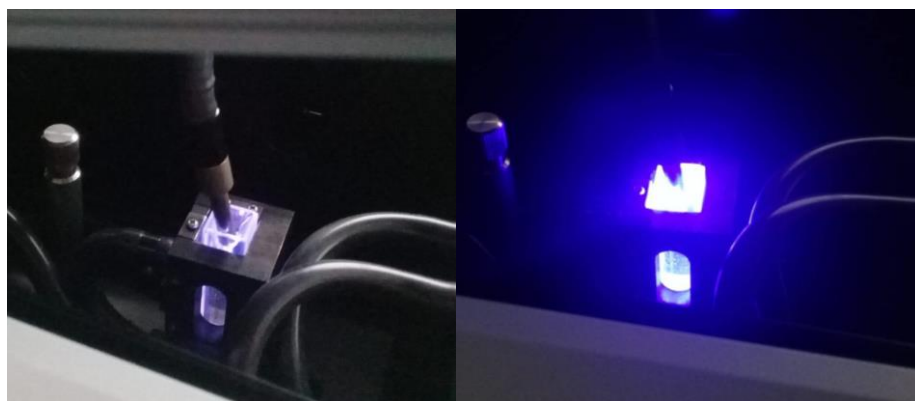


Figure 86. On the left irradiation with UV light at 365 nm. On the right irradiation with blue light at 440 nm.

The protocol of the kinetic starts with a registration of UV-Vis spectrum at the time 0. Then other UV-Vis spectra are registered using 365 nm irradiation after 5, 10, 20, 30, 50 and 60 seconds. Another UV-Vis spectrum is recorded after 60 seconds without irradiation. Then the irradiation is switched to 440 nm and UV-Vis spectra recorded after 5, 10, 20, 30, 50 and 60 seconds. After 60 seconds without irradiation last spectrum is recorded. In **Figure 87** are shown the kinetics of compound **31a** in DMSO, EtOAc, MeOH and 0.2% DMSO/PBS, following the protocol described above. To simplify the reading of the kinetics and better understanding the property of the compound in the different solvents, in **Figure 88** are shown only the curves relative to the time 0, the irradiation at 365 nm after 60 seconds and the irradiation at 440 nm after 60 seconds.

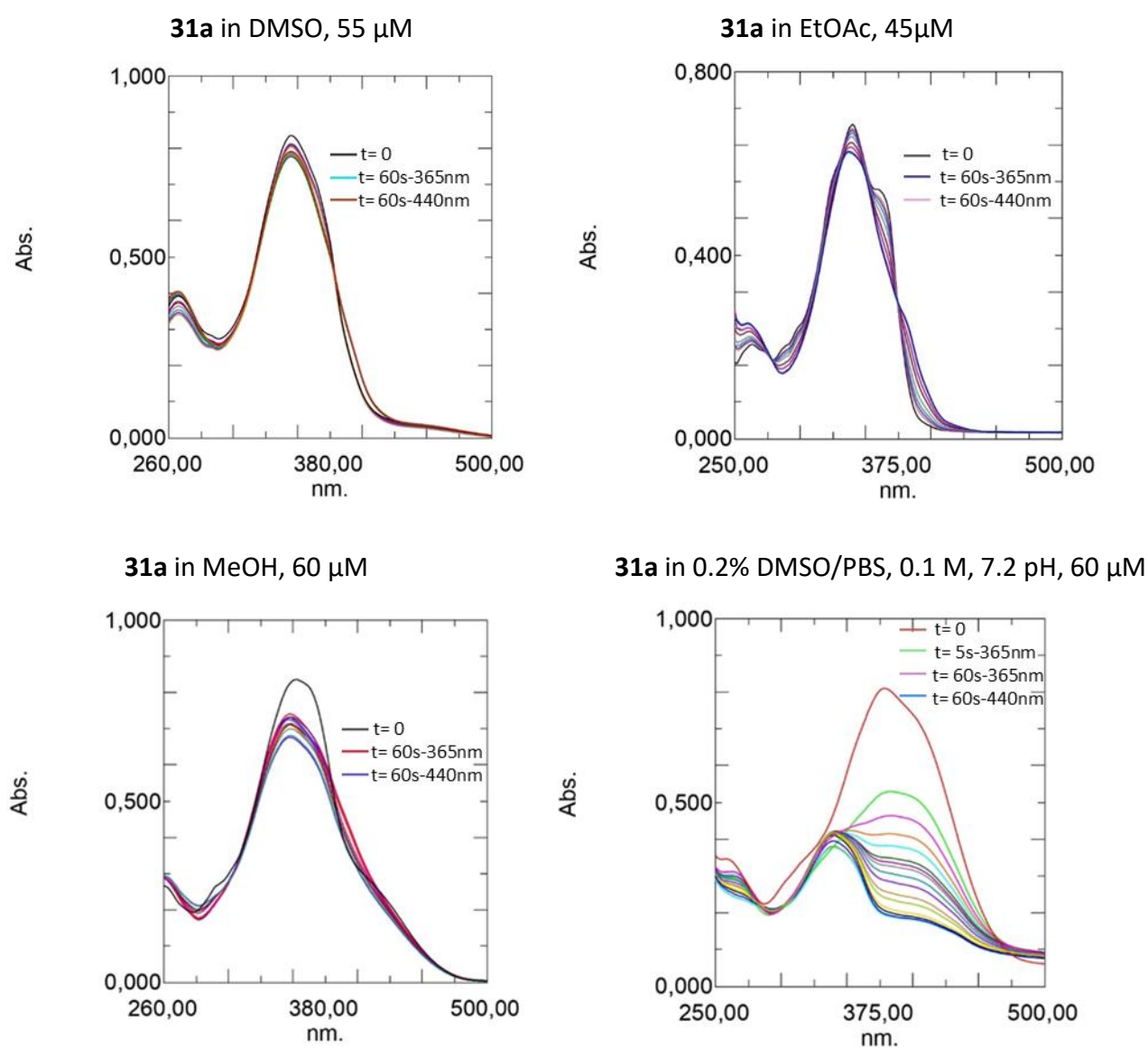


Figure 87. Compound **31a** kinetics by UV-Vis spectra in DMSO, EtOAc, MeOH and 0.2% DMSO/PBS. Spectra were recorded at the $t=0$ s, then after 5, 10, 20, 30, 50, 60 s irradiation at 365 nm. After 60 s without irradiation another spectra was recorded. After irradiation at 440 nm, spectra were recorded at time 5, 10, 20, 30, 50, 60 s. Another spectra was recorded after 60 s without irradiation.

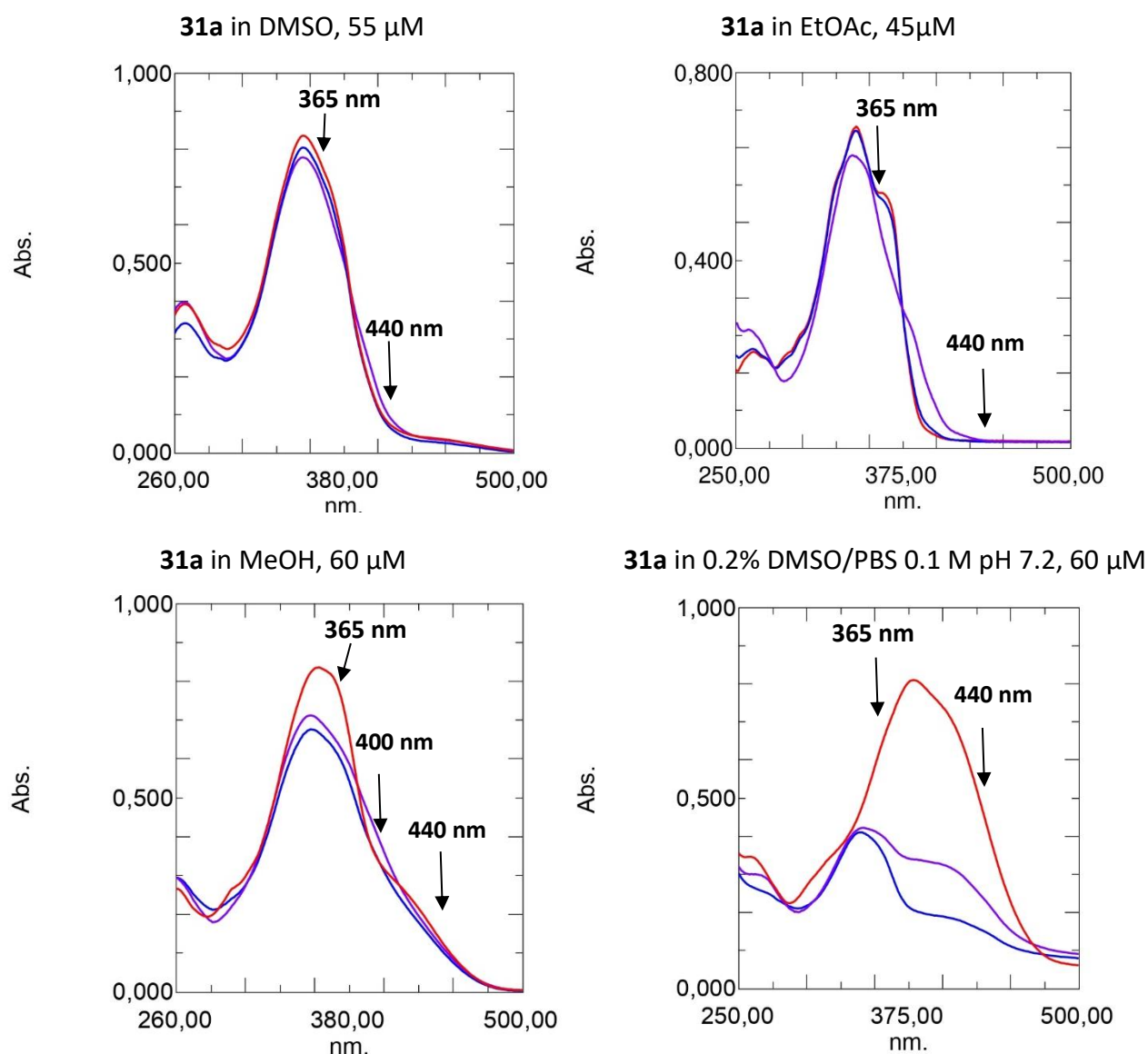


Figure 88. Compound **31a** kinetics are shown in DMSO, EtOAc, MeOH and 0.2% DMSO/PBS. Spectra at time 0 (red), after 60s irradiation at 365 nm (violet) and after 60s irradiation at 440 nm (blue) were selected.

The two configurations *Z* and *E* of the aurones have usually maximum wavelengths absorbance that are similar in contrast of other photoswitches as azobenzenes. The solvent have a major influence on the difference between the *Z* and *E* configuration proportion and absorbance. Anyway, in the case of the aurones, the recognition of the *Z* and *E* isomer should be more focused on the profile of the curve compared to the wavelength. The kinetic in DMSO shows that the compound **31a** *Z* ($t = 0$, red curve) is switched in its *E* isomer ($t = 60s$ $h\nu$ 365 nm, violet curve) and then using 60s of irradiation at 440 nm re-switched to *Z* isomer (blue curve). The two isomers have the same λ_{max} but at 440 nm the red curve (*Z* isomer) is below the violet curve (*E* isomer) so at 440 nm the *E* isomer absorbs more compared to the *Z* isomer. The difference of absorbance of the two isomers at the same wavelength is due to the different molar extinction coefficient ξ . For this

reason, the irradiation at 440 nm allows to go back to the *Z* isomer obtaining the blue curve. In the case of the kinetics in EtOAc, the curves of the two isomers have different profiles and it is easier to see the difference. Anyway, the rationale is the same; the *E* isomer (violet curve) absorbs more energy at 440 nm so it is completely switched back to the *Z* isomer (blue curve totally superimposable to red curve). In the case of MeOH and 0.2% DMSO/PBS the *Z* isomer was switched to the *E* isomer (violet curve) with 60 s of UV light irradiation but it was impossible to re-switch them back to the *Z* isomer. In fact, in this case at 365 nm and at 440 nm the *Z* isomer (red curve) absorbs always more energy compared to the *E* isomer (violet curve). Therefore, the irradiation at 440 nm (blue curve) confirmed we have still the *E* isomer (same as violet curve). In the case of the kinetic in 0.2% DMSO/PBS the violet and blue curves are not totally the same, probably because the violet curve represents a partial isomerization towards the *E* isomer that was not completed at the 100% while irradiation for 60s at 440 nm allowed total isomerization to *E* configuration (blue curve). These kinetics demonstrate that in protic polar solvents as MeOH and PBS, the compound **31a** can be used as a photoswitch just using wavelength of irradiation corresponding to the part of the spectra where *Z* isomer curve is below the *E* isomer curve. This corresponds to a wavelength close to 400 nm in the case of MeOH and around 500 nm for PBS. As in our group there is not a lamp with the possibility to choose all the desired wavelengths, it was impossible to attempt the switch to the *Z* configuration. Furthermore, as the absorbance difference at these wavelengths is not too different for the two isomers, the energy required for the isomerization of *E* to *Z* configuration is probably too high and may require a longer irradiation that can damage the compound.

These kinetics were performed also on compounds **31b-d** to verify if the difference between an iodine and a nitro group or a *para* and *meta* position of substitution, can have an impact on the photophysical properties of the compounds in different solvents, compared to what was observed for **31a**.

31b showed conversion to *E* isomer but no return to *Z* at 440 nm in DMSO, the same was obtained in EtOAc, MeOH and PBS. In DMSO, the only wavelengths where *E* isomer absorbs more than *Z* is around 330-340 nm, the same in PBS.

31c showed conversion to *E* isomers and return to *Z* in DMSO, EtOAc and MeOH. In PBS at 440 nm it is not possible but using a wavelength above 500 nm may be tempting, especially because the use of visible-red shifted wavelength would be a benefit for biological application limiting the risk of degradation by UV irradiation (**Figure 89**).

Compound **31d** showed conversion to *E* and return to *Z* in DMSO and EtOAc but no return to *Z* was observed in MeOH and PBS at 440 nm. In the case of MeOH, *E* isomer absorb more around 400 nm but the difference of absorption of the *Z* and *E* curves are very close so the isomerization of *E* to *Z* seems difficult to attempt. Finally in PBS, *E* should be converted to *Z* using a wavelength around 330-340 nm but at such wavelengths other reactions than photoswitch may occur. The comparison of compounds **31a-d** shows that it is easier to switch from *Z* to *E* configuration and *vice versa* for the compounds **31a-c** bearing an iodine or a nitro group in the *para* position of the phenyl ring. Compound **31c** can be switched at 440 nm from *E* to *Z* isomer in MeOH while in the case of **31a** it was not possible as the best wavelength of irradiation is around 400 nm (**Figure 89**).

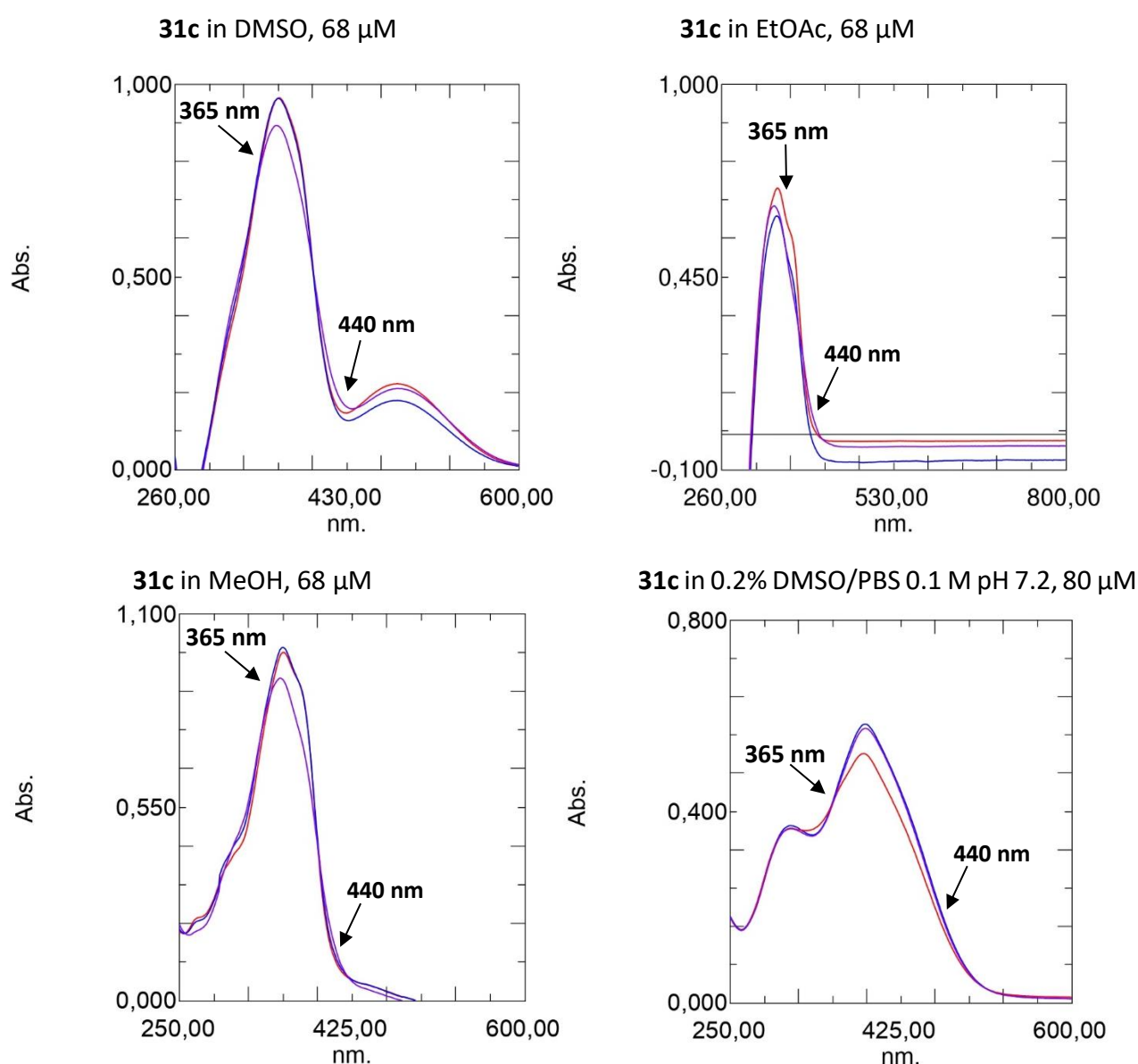


Figure 89. Compound **31c** kinetics are shown in DMSO, EtOAc, MeOH and DMSO/PBS. Spectra at time 0 (red), after 60 s irradiation at 365 nm (violet) and after 60 s irradiation at 440 nm (blue) were selected.

The respect of Beer-Lambert's law (Section 3.2) was confirmed by recording UV-Vis spectra of compound **31a** in EtOAc at different concentrations at the λ_{max} of 340 nm. The relation between the concentration and the absorbance is proportional as shown **Figure 90**.

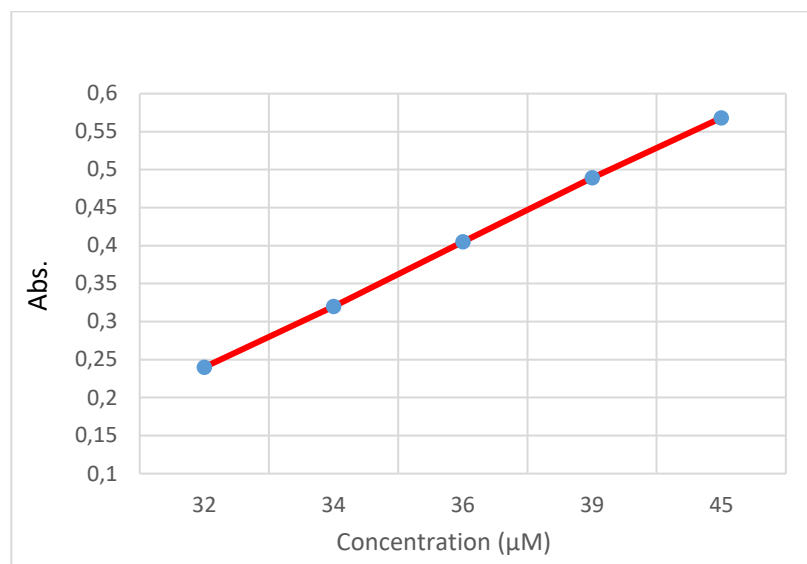


Figure 90. The absorbance of compound **31a Z** in EtOAc at different concentrations between 32-45 μM at 340 nm. The absorbance and the concentration are proportional according to the Beer-Lambert's law ($\text{Abs} = \xi \times l \times C$ as reported in section 3.2 and **Figure 49**).

Compound **31a** was irradiated from *Z* to *E* isomers at 365 nm and vice versa at 440 nm for 10 cycles in DMSO. This proves the fatigue-resistant property of the compound to a series of sequential isomerization (**Figure 91**).

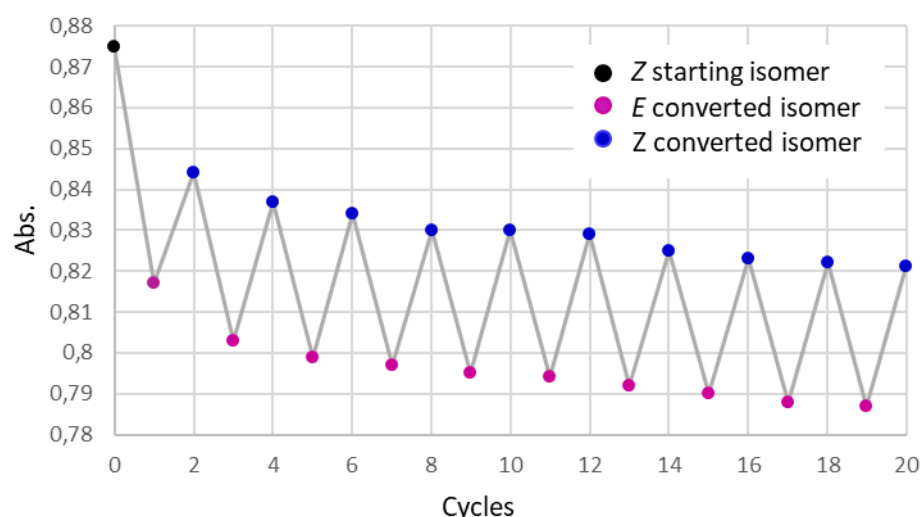


Figure 91. Isomerization of compound **31a** for 10 complete cycles of conversion of *Z* isomer (blue) to *E* isomer (purple) and vice versa in DMSO using irradiation wavelengths at 365 nm and 440 nm.

In **Table 3** are reported the maximum absorbance wavelenghts λ_{\max} (nm) and the molecular extinction coefficient ϵ ($\text{L}\cdot\text{mol}^{-1}\cdot\text{cm}^{-1}$) calculated by Beer-Lambert's law for compounds **31a-d Z** in DMSO, EtOAc, MeOH and 0.2% DMSO/PBS.

Compound	Phenyl Substituent	λ_{\max}	ϵ	λ_{\max}	ϵ	λ_{\max}	ϵ	λ_{\max}	ϵ
		DMSO	DMSO	EtOAc	EtOAc	MeOH	MeOH	PBS	PBS
31a	4-I	351	15200	340	13955	359	15218	378	13500
31b	3-I	336	12600	328	11036	342	7654	365	8272
31c	4-NO ₂	363	14191	348	10352	355	14573	386	6512
31d	3-NO ₂	339	13647	329	10132	338	14617	367	5837

Table 3. λ_{\max} (nm) and the ϵ ($\text{L}\cdot\text{mol}^{-1}\cdot\text{cm}^{-1}$) of compounds **31a-d** in DMSO, EtOAc, MeOH and 0.2% DMSO/PBS.

According to literature³⁴⁹ compounds **31a,c** bearing withdrawing groups in *para* position are more red-shifted in all the four solvents compared to compounds **31b,d** where the withdrawing substituents are in *meta* position.

In summary, in this section, the physico-chemical properties of aurones **31a-i** have been reported. These compounds were first synthesized to investigate the binding mode of XAP044 with the challenge to find a novel photoswitch analog able to bind the VFT domain of mGlu7R. Despite of the pharmacological results described in section 4.2, compounds **31a-i** showed interesting properties for application in material science. In particular, the kinetic studies on compounds **31a-d** showed their fatigue resistant property and the opportunity to easily isomerize in different organic solvents as DMSO, EtOAc and MeOH if irradiated at a proper wavelength. The opportunity to use these compounds in biology remains a challenge as in our study it was impossible in 0.2% DMSO/PBS to re-switch **31 a-d E** to the original **31a-d Z** isomers. Our limitation was mainly due to the availability for the irradiation of only three wavelengths (365 nm, 440 nm and 490 nm) but a selective irradiation at a proper wavelength where the molar extinction coefficient ϵ of the *E* isomer is even slightly higher than the ϵ of the *Z* isomer could show a valuable photoswitch useful in biology.

4.1.3.4. Chalcone analog

After the synthesis of aurones, another type of photoswitch from the chalcone family was synthesized. Chalcone is the precursor of aurone in the biological synthetic pathway, it is structurally similar to the aurone except for the benzofuranone ring which is opened to have just two benzene rings and a central propenone (**Figure 92**).

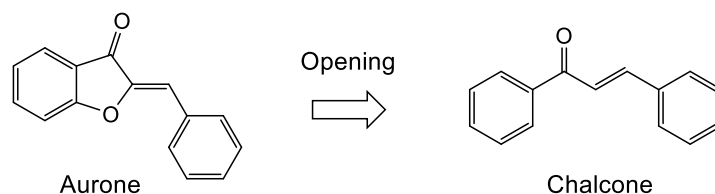


Figure 92. Structure of aurone and chalcone.

In the investigation to understand the binding mode of XAP044 and to find new active compounds, our approach has been to modify its structure. At the beginning, rigid analogs were synthesized, and then the chromone ring was cut leading to the open analogs and aurone photoswitches synthesized to replace the chromone by a benzofuranone to obtain photoswitch analogs. Chalcone **32** represented the last investigation as the open form of aurone **31a** and a planar analog of **16a** (**Figure 93**).

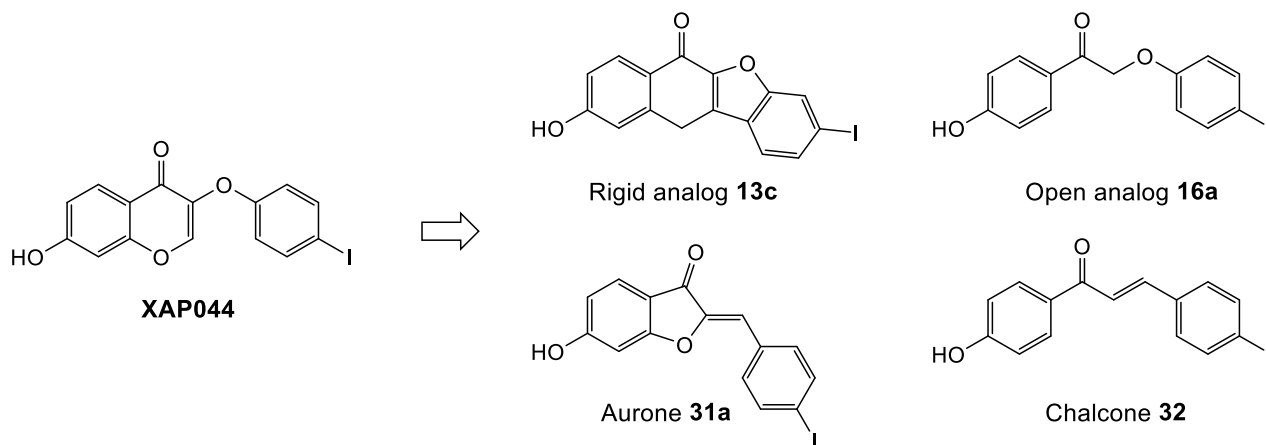
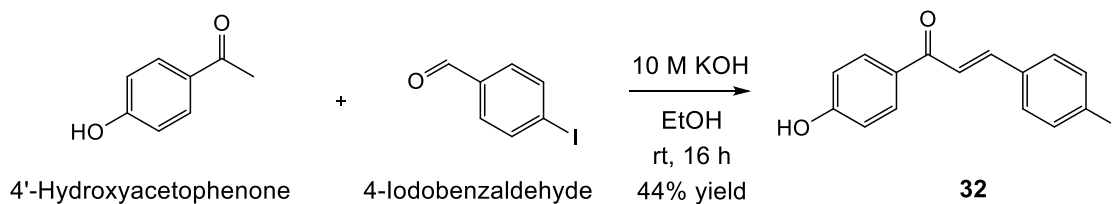


Figure 93. Structural comparison of XAP044 analogs.

Chalcone have a planar structure like the aurones and are always present in the *trans* conformation.³⁵¹ In contrast to the other photoswitch molecules described before, chalcones are not really used as photoswitch because they require a high-energy absorbance to switch to their *cis* form. Furthermore, their thermal relaxation is very fast in the order of ns.³⁵² However, chalcone **32** is a planar analog of **16a**, a flexible derivative of XAP044. This molecule was thus synthesized and assayed to probe the bioactive conformation of **16a**.

Chalcone **32** was synthesized by Claisen-Schmidt condensation starting from 4'-hydroxyacetophenone and 4-iodobenzaldehyde in a 10 M potassium hydroxide solution in EtOH (**Scheme 43**).



Scheme 43. Synthesis of compound **32**.

4.1.3.4.1. Photophysical properties of Chalcone analog

Absorbance UV-Vis spectra of **32** was recorded in 0.2% DMSO/PBS (**Figure 94**).

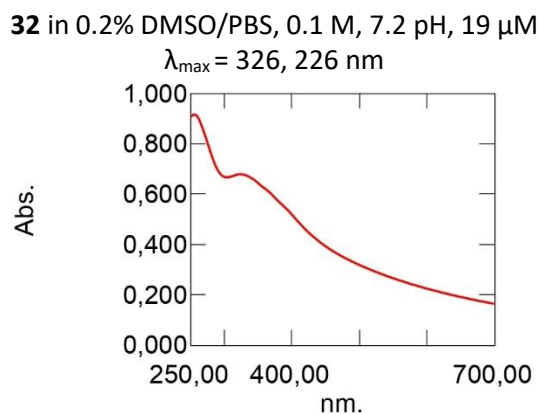


Figure 94. UV-Vis spectra of compound **32**.

Compound **32** was not irradiated and not spectroscopically studied because the aim was just to test its *trans* conformation, that is the one superimposable with planar XAP044, and compared it to aurone derivatives. In fact, as the aurone, the chalcone has a planar structure but explores a different space (**Figure 95**). The biological data of all compounds will be discussed in the pharmacological section 4.2, focusing on the similar and different properties of all analogs to better understand the SAR.

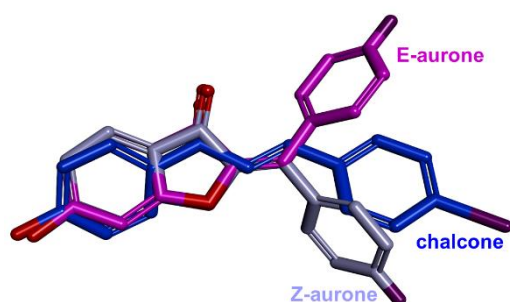


Figure 95. Superimposition of chalcone **32** (*trans* configuration) and aurone **31a** (*Z* and *E* configurations).

In this last part of the discussion, different photoswitch analogs of XAP044 have been described: azobenzenes, phenylazindole, aurone and chalcone analogs. These molecules have interesting photophysical properties due to their ability to switch between two different configurations under light irradiation. Their biological activity at mGlu7R will be discussed later in the next section. Anyway, the study of their photophysical properties confirms that these compounds, especially the aurones, are interesting versatile chemical tools that can be used, not just with a photo pharmacological purpose, but also in several other applications related for example to material science.

4.2. Pharmacological results

As explained at the beginning of chapter 4.1 and shown in **Figure 60**, three different hypotheses were formulated for the binding of XAP044 to the VFTD.

The first hypothesis considers the orientation of XAP044 along the loop $\beta_{10}\alpha_7$, the second shows the orientation of XAP044 bonded to S229 and S160 along the helix α_6 and the third one considers the orientation of XAP044 bounded to S229 and S160 along the loop $\beta_7\alpha_8$. The synthesis of different XAP044 analogs and the mutagenesis of selective residues were fundamental to validate and confirm one these hypotheses about the binding mode.

All compounds were tested measuring first the EC_{50} of the agonist LSP4-2022 on mGlu7 receptor^{113,117} and then the reduction of the activity on mGlu7R of LSP4-2022 in combination with XAP044 at the concentration of 100 μ M or 30 μ M. The EC_{50} of LSP4-2022 on mGlu7R increases with the addition of XAP044 due to its inhibition of LSP4-2022 activation. The value of EC_{50} of LSP4-2022 in presence of XAP044 was the reference for the comparison with all the XAP044 analogs tested in combination of LSP4-2022. Basically, if the value of the EC_{50} of LSP4-2022 with the XAP044 analog is similar to the value of EC_{50} of LSP4-2022 tested alone then it is possible to conclude that the analog has no inhibiting effect. If the value of the EC_{50} of LSP4-2022 with the XAP044 analog is similar to the value of EC_{50} of LSP4-2022 tested in combination with XAP044 then it is possible to conclude that the analog has an inhibitory activity comparable with that of XAP044. Finally, if the value of the EC_{50} of LSP4-2022 in combination with the XAP044 analog is higher compared to the value of EC_{50} of LSP4-2022 tested in combination with XAP044 then it is possible to conclude that the analog has an inhibitory activity superior to that of XAP044. Starting from these data, it was possible to have the necessary informations to adjust the design for the planning

of novel active derivatives of XAP044. In **Table 5** are reported as examples the EC₅₀ values of LSP4-2022 in combination of some hydroxy open analogs of XAP044.

The compounds that showed in these assays a major inhibition compared to XAP044, were then tested at different concentrations in combination with LSP4-2022 to obtain different dose-response curves (DR). The DRs of the active compounds in combination with LSP4-2022 at its EC₈₀ concentration allowed the determination of the final IC₅₀.

All these data were useful to obtain a complete SAR and to answer to several questions regarding the binding mode of XAP044.

Is XAP044 binding to the VFTD in a planar or twisted conformation?

Among all the different derivatives synthesized, just few open analogs showed an inhibition activity higher or comparable to XAP044. The constrained analogs and all the photoswitch analogs showed no inhibition. This result confirmed that XAP044 is interacting with the VFTD in a twisted conformation with an "angle" for binding. In fact, the constrained and the photoswitch analogs synthesized have in common the planar conformation while the open analogs have a flexible carbon-oxygen bond (C₃-O, **Figure 96**) that allows different angles of rotation.

Is the chromone scaffold of XAP044 necessary for the binding or it can be replaced?

The chromone scaffold is not necessary for the activity, in fact the open analog **16a** showed the same inhibition activity as XAP044 even though the chromone was not present (**Figure 96**).

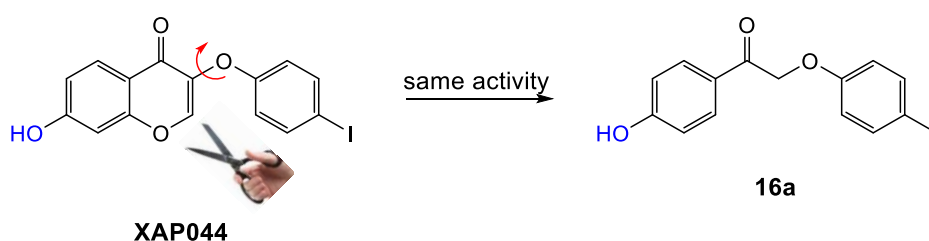


Figure 96. The open analog **16a** shows the same activity as XAP044. The flexible C₃-O bond of XAP044 is indicated by a red arrow.

The replacement of the hydroxyl group leads to the loss of inhibition as it probably binds to Ser229/S160.

Among the open analogs, just few compounds bearing the hydroxyl group in *para* position of the phenylethanone ring, as in XAP044, resulted in active antagonists while the methoxy open analogs were inactive. This confirmed the important role of the hydroxyl group for the binding to the VFTD.

S229/S160 hydrogen bonds may be disrupted and steric hindrance may also prevent the binding (**Figure 97**).

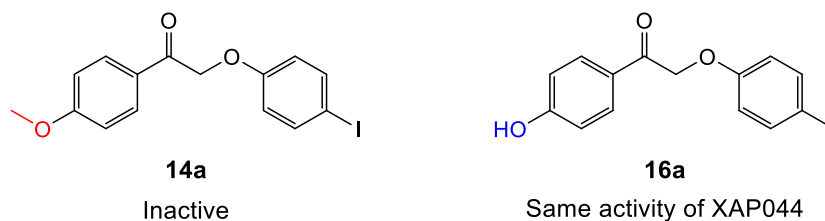


Figure 97. Product **14a** shows a loss of activity seen for product **16a** because the wedge interaction with the VFTD may be disrupted (see **Figure 58**).

Can the iodine atom in *para* position of the benzene ring be replaced by other substituents?

The iodine atom was replaced with many different substituents but just a few of them were able to maintain the same activity as XAP044. The replacement with a nitrile or a nitro group in compounds **19c** and **19d** leads to a decrease in the activity compared to XAP044/**16a** while other halogens such as chlorine or bromine (**19i**, **19j**) are well accepted. Especially the replacement with bromine shows the same activity as XAP044/**16a** (**Table 5**). Electron donor and hydrophobic groups as a methyl or a methoxy (**19f**, **19g**) give a total loss of the activity. The same results with hydrophilic groups as a hydroxyl, a carboxyl and a sulfamide (**19s**, **19u**, **19x**). This may indicate that the iodine atom of XAP044/**16a** binds to the VFTD by a halogen bond.³⁵³

Are there other substituents accepted in *ortho* and/or *meta* positions of the iodobenzene ring?

All the open analogs bearing a substituent in *ortho* and/or *meta* position of the *para* iodine or *para* bromine phenyl ring resulted inactive besides fluorine substituents. Indeed, compounds **19p** and **19u** (**Figure 98**) showed an activity as they hold a fluorine in one *ortho* position (**19p**) or both *ortho* positions (**19u**). Compounds **19p** showed a small increase of activity compared to XAP044/**16a** and **19u** resulted in an even more active compound than **19p** (**Table 5**). In fact, fluorine is the smallest among the halogens so it does not give steric hindrance. All other substituents including other halogens in *ortho* and/or *meta* positions gave inactive derivatives. This confirms that the iodobenzene ring of XAP044/**16a** binds in an environment where a halogen bond is possible with the *para* substituent but in other positions, atoms larger than hydrogen or fluorine are not accepted due to steric hindrance.

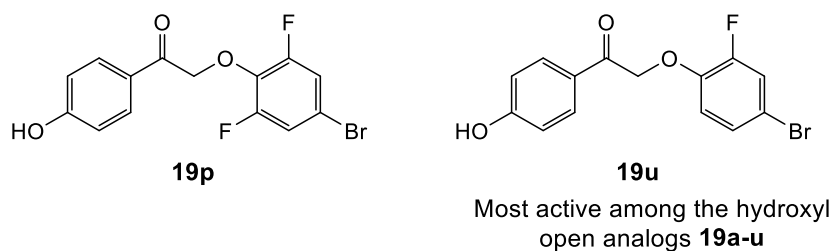


Figure 98. Structure of compounds **19p** and **19u**.

Are there other substituents accepted in *ortho* positions of the phenol ring of XAP044 able to increase the inhibition activity?

The dihydroxyl open derivate **23** and especially the fluorine-hydroxyl open analogs **27 a,b** (Figure 99) showed a major increase of activity compared to XAP044/**16a** (Figure 100, Figure 101 and Table 6). In the case of product **23**, this is due to the additional hydroxyl in *ortho* position of the phenol ring that can participate in hydrogen bonds with S229 and/or S160 and also S159. In the case of product **27a,b**, the fluorine substitution resulted in the most potent analogs found. The fluorine in one or both *ortho* positions can lower the pKa (Table 4) Thus, the proportion of compounds in the deprotonated form at pH 7.2 are increased. Consequently, the increase of the activity found for **27a,b** shows that the hydroxyl group of the XAP044 may act as an acceptor of hydrogen bonds more than as a donor, as shown in Figure 58.

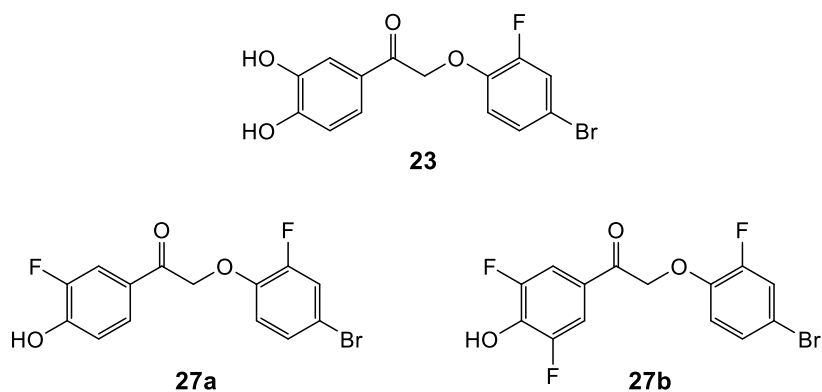
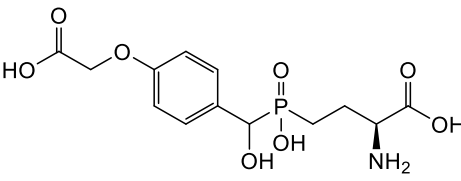
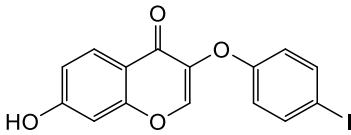
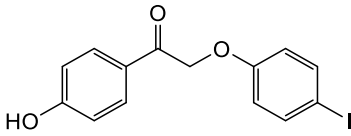
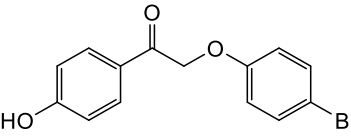
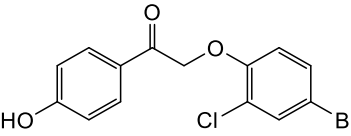
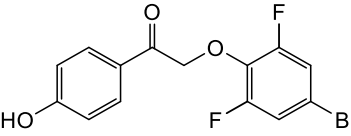


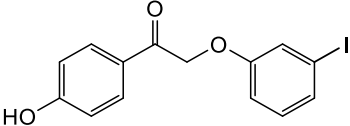
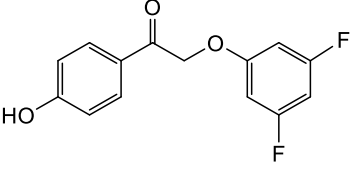
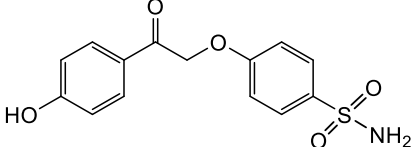
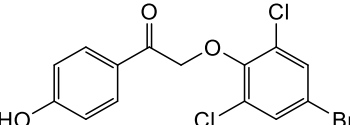
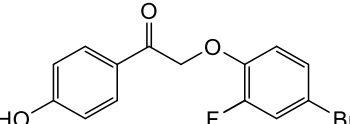
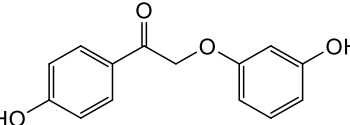
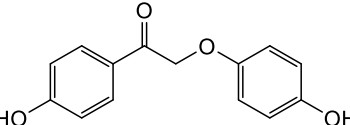
Figure 99. Structures of the most active compounds **23** and **27a,b**.

Compounds	16a	23	27a	27b
pKa	7.7	7.8 and 11.8	6.7	5.9

Table 4. Predicted pKa's calculated at the Chemicalize website (<https://chemicalize.com/welcome#/calculation>). Note, the pKa of **16a** is decreased compared to classical phenols (pKa 10.2) because of the conjugated carbonyl group.

In **Table 5** are reported the EC₅₀ values of LSP4-2022 tested with some hydroxy open analogs of XAP044. XAP044 was tested in combination with LSP4-2022 as a reference.

N°	COMPOUNDS	DR of the agonist (LSP4-2022) with compound (100 μM) Mean value	Sem+/-	n
LSP4-2022		-logEC ₅₀ /-logEC ₅₀ 2022 : 1.00	0.00	30
		-logEC ₅₀ : 4.56	0.04	30
		EC ₅₀ : 3.33 X 10 ⁻⁵	5.05 X 10 ⁻⁶	30
LSP4-2022 + XAP044		-logEC ₅₀ /-logEC ₅₀ 2022 : 0.83	0.01	26
		-logEC ₅₀ : 3.76	0.04	26
		EC ₅₀ : 1.91 X 10 ⁻⁴	1.63 X 10 ⁻⁵	26
LSP4-2022 + 16a		-logEC ₅₀ /-logEC ₅₀ 2022 : 0.83	0.01	10
		-logEC ₅₀ : 3.88	0.04	10
		EC ₅₀ : 1.38 X 10 ⁻⁴	1.30 X 10 ⁻⁵	10
LSP4-2022 + 19i		-logEC ₅₀ /-logEC ₅₀ 2022 : 0.82	0.01	3
		-logEC ₅₀ : 3.96	0.03	3
		EC ₅₀ : 1.10 X 10 ⁻⁴	1.10 X 10 ⁻⁴	3
LSP4-2022 + 19l		-logEC ₅₀ /-logEC ₅₀ 2022 : 0.89	0.04	3
		-logEC ₅₀ : 4.31	0.19	3
		EC ₅₀ : 5.90 X 10 ⁻⁵	2.71 X 10 ⁻⁵	3
LSP4-2022 + 19p		-logEC ₅₀ /-logEC ₅₀ 2022 : 0.85	0.03	8
		-logEC ₅₀ : 3.76	0.05	8
		EC ₅₀ : 2.40 X 10 ⁻⁵	2.59 X 10 ⁻⁵	8

LSP4-2022 + 19q		$-\log EC_{50}/-\log EC_{502022} : 1.02$	0.03	4
		$-\log EC_{50} : 4.35$	0.09	4
		$EC_{50} : 4.58 \times 10^{-5}$	1.11×10^{-5}	4
LSP4-2022 + 19r		$-\log EC_{50}/-\log EC_{502022} : 1.04$	0.03	4
		$-\log EC_{50} : 4.44$	0.06	4
		$EC_{50} : 3.74 \times 10^{-5}$	4.59×10^{-6}	4
LSP4-2022 + 19s		$-\log EC_{50}/-\log EC_{502022} : 1.06$	0.03	4
		$-\log EC_{50} : 4.53$	0.03	4
		$EC_{50} : 2.94 \times 10^{-5}$	2.09×10^{-6}	4
LSP4-2022 + 19t		$-\log EC_{50}/-\log EC_{502022} : 1.01$	0.01	3
		$-\log EC_{50} : 4.92$	0.05	3
		$EC_{50} : 1.21 \times 10^{-5}$	1.26×10^{-5}	3
LSP4-2022 + 19u		$-\log EC_{50}/-\log EC_{502022} : 0.76$	0.01	10
		$-\log EC_{50} : 3.54$	0.05	10
		$EC_{50} : 3.12 \times 10^{-4}$	3.97×10^{-5}	10
LSP4-2022 + 19v		$-\log EC_{50}/-\log EC_{502022} : 1.03$	0.01	3
		$-\log EC_{50} : 4.83$	0.05	3
		$EC_{50} : 1.51 \times 10^{-5}$	1.72×10^{-6}	3
LSP4-2022 + 19w		$-\log EC_{50}/-\log EC_{502022} : 1.06$	0.01	3
		$-\log EC_{50} : 4.95$	0.05	3
		$EC_{50} : 1.13 \times 10^{-5}$	1.30×10^{-6}	3

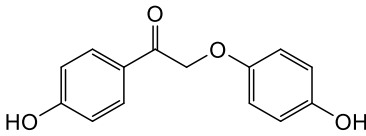
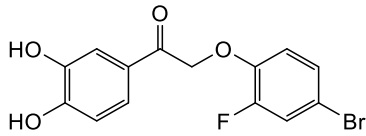
LSP4-2022 + 19x		$-\log EC_{50} / -\log EC_{50}^{2022} : 1.07$	0.01	3
		$-\log EC_{50} : 5.00$	0.08	3
		$EC_{50} : 1.03 \times 10^{-5}$	1.91×10^{-6}	3
LSP4-2022 + 23		$-\log EC_{50} / -\log EC_{50}^{2022} : 0.76$	0.01	6
		$-\log EC_{50} : 3.47$	0.05	6
		>300		11

Table 5. EC_{50} values of LSP4-2022 in combination with some hydroxy open analogs. XAP044 was also tested with LSP4-2022 and used as reference.

The DR of LSP4-2022 was measured in presence of various concentrations of each of the most active compounds *i.e.* **19u**, **23** and **27a,b**. IC₅₀'s were calculated from the DR of each compound in the presence of the EC₈₀ concentration of LSP4-2022 (**Figure 100** and **Figure 101**).

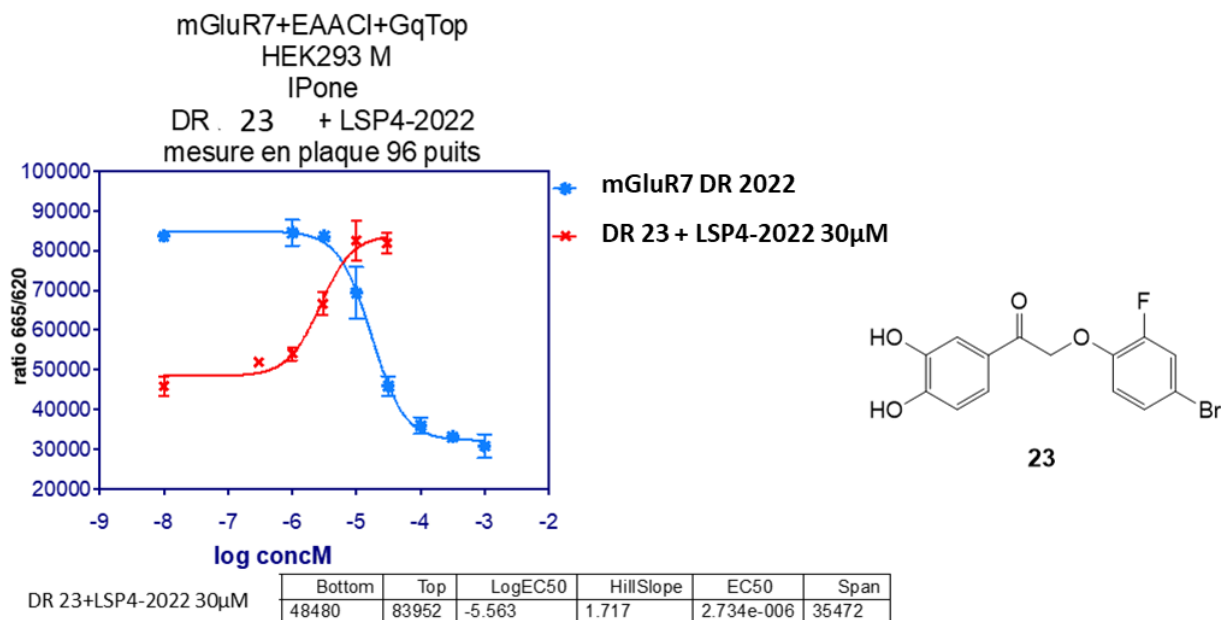


Figure 100. DR of product **23**.

In **Table 6** are reported the IC₅₀ values. XAP044 has an IC₅₀ of 4.3±1.2 µM when tested with LSP4-2022 while Novartis scientists found an IC₅₀ of 2.8 µM¹⁷⁵ using the agonist L-AP4 and a different functional assay. Compound **23** showed an IC₅₀ of 3.4±0.6 µM, a value slightly better than the IC₅₀ of XAP044. Surprisingly compounds **27a** and **27b** have an IC₅₀ of 0.96±0.25 µM and 0.88±0.12 µM, showing a significant increase in the inhibition activity.

Products **27a,b** confirmed the importance of the hydrogen bond with S229 supporting its key role in the blocking of the VFTD closure by XAP044 and analogs. The fluorine in *ortho* position of the phenol can lower its pK_a in **27a,b** so that it will be predominantly deprotonated and thus act as hydrogen bond acceptor. In the case of XAP044/**16a** and other hydroxyl open analogs, the compounds are partly deprotonated so this may explain a weaker binding to the receptor. Consequently, these products showed a lower inhibition activity. Regarding compound **23**, it is similarly deprotonated as **16a**. Yet its increased potency may be due to additional H-bond between the *meta* hydroxyl and backbone and/or S159 of the VFTD.

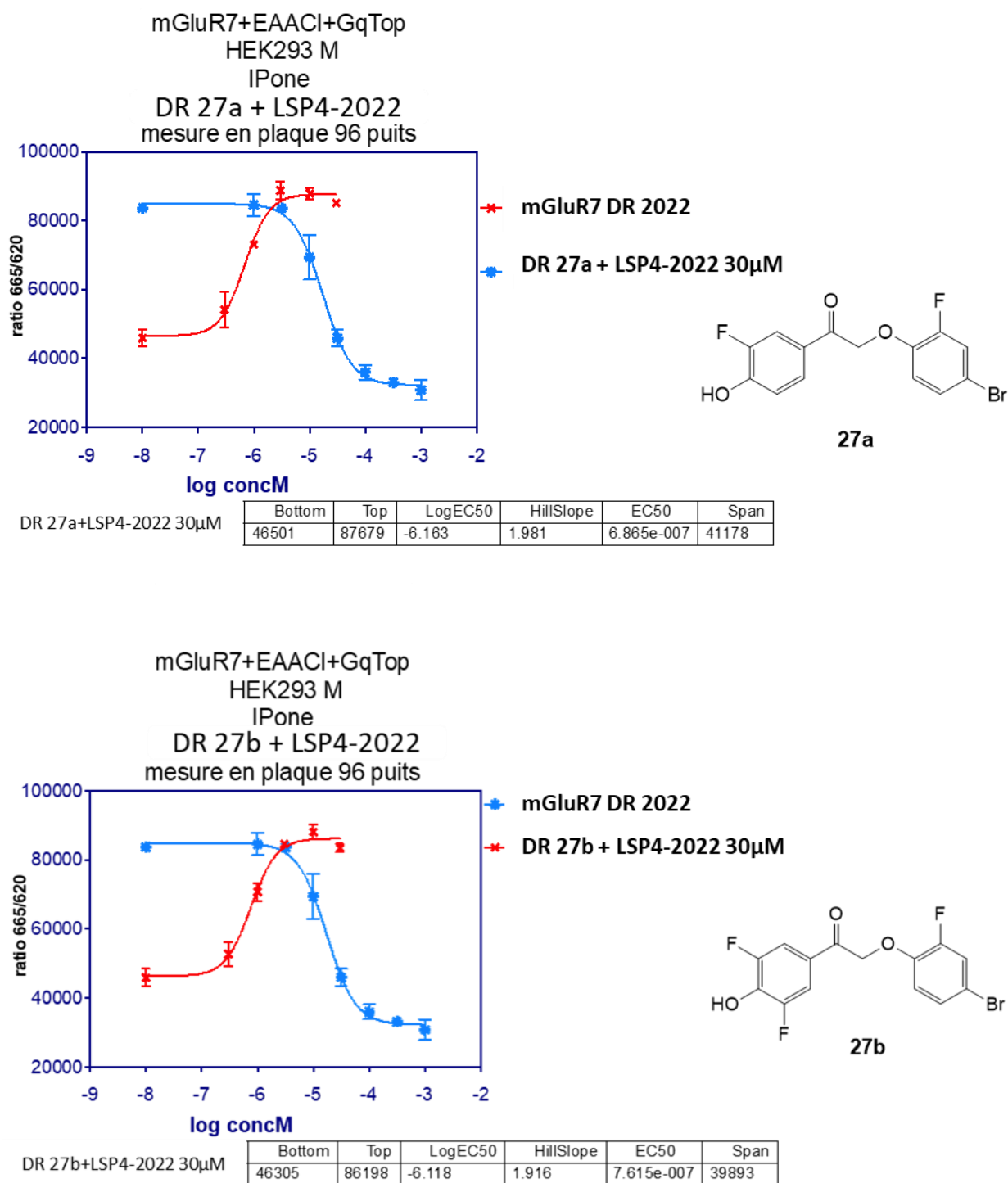


Figure 101. DR of products 27a and 27b.

		mean value	sem+/-	n
LSP4-2022	$-\log EC_{50}$	4.76	0.06	7
	EC_{50}	1.85E-05	2.60E-06	7
DR XAP044 + 30 μ M LSP4-2022	$-\log IC_{50}$	5.40	0.12	3
	IC_{50}	4.33E-06	1.16E-06	3
DR 23 + 30 μ M LSP4-2022	$-\log IC_{50}$	5.48	0.07	3
	IC_{50}	3.44E-06	6.22E-07	3
DR 27a + 30 μ M LSP4-2022	$-\log IC_{50}$	6.07	0.13	4
	IC_{50}	9.57E-07	2.49E-07	4
DR 27b + 30 μ M LSP4-2022	$-\log IC_{50}$	6.06	0.06	2
	IC_{50}	8.81E-07	1.20E-07	2

Table 6. IC_{50} values for XAP044, 23, 27a and 27b.

Product **27a** and **27b** have a similar value of IC_{50} so a fluorine in *ortho* is sufficient to lower enough the pK_a but a second fluorine in *ortho* is well accepted maintaining the inhibition activity.

All the different analogs of XAP044/**16a** synthesized were useful to obtain a complete SAR and to validate a hypothesis of a binding mode to mGlu7 VFTD. Among all these compounds, products **27a** and **27b** showed a significant increase of the inhibition activity compared to XAP044. Furthermore, **27a** and **27b** have better solubility properties as they do not hold the chromone scaffold present in XAP044. Products **27a** and **27b** represent a great discovery as they are among the most potent and selective mGlu7R NAMs discovered by now and in contrast with other NAMs they bind to the VFTD of mGlu7R. Compounds **27a,b** will be useful for further *in vivo* studies in the future related especially to anxiety. All observations of this section are summarized in the SAR shown in **Figure 102**.

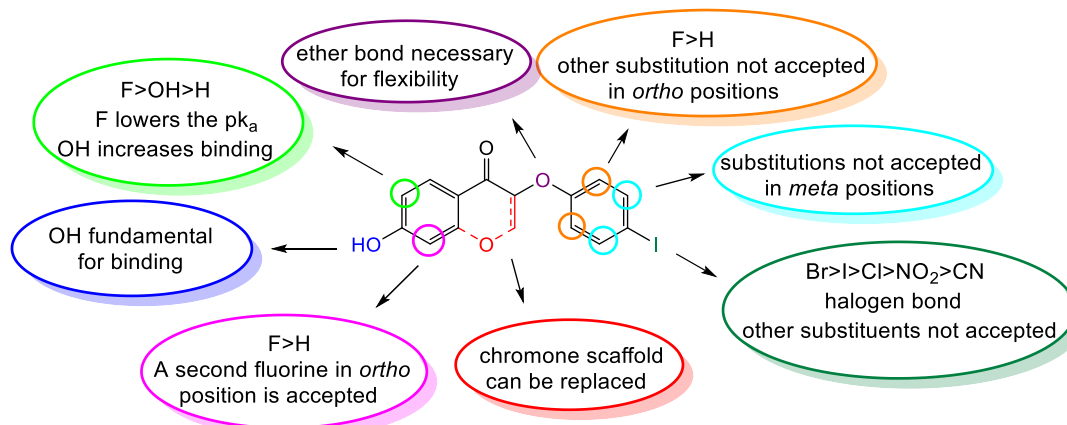


Figure 102. SAR of 16a.

4.3. Molecular modelling and binding mode validation

The molecular modeling experiments were carried out by Alexandre Cabayé from our group. Three different hypothesis of binding were formulated at the beginning of this project (**Figure 60**). The first one considers XAP044 binding along loop $\beta 10\alpha 7$ but this option was ruled out, as loop $\beta 10\alpha 7$ swapped with that of mGlu4R did not affect XAP044 inhibition. Several residues (4 out of 7) of that loop differ between mGlu4 and mGlu7 receptors, it is thus expected that if XAP044 would be binding to that loop, binding and activity of XAP044 would be affected by the inversion by loosing selective interactions.

The second orientation is the docking of XAP044 bound to S160 and S229 along helix $\alpha 6$ (**Figure 103**), where K233 and S237 are selective residues of mGlu7R. This docking shows:

- hydrogen bond with S160 and S229
- hydrophobic contacts with A183, P184, K233
- halogen bond with S237, Q240
- Restricted environment around the iodophenyl group in agreement with SAR
- mGlu7 selectivity because of K233 and S237 interactions

Furthermore, this docking was stable in 3.5 ns molecular dynamics.

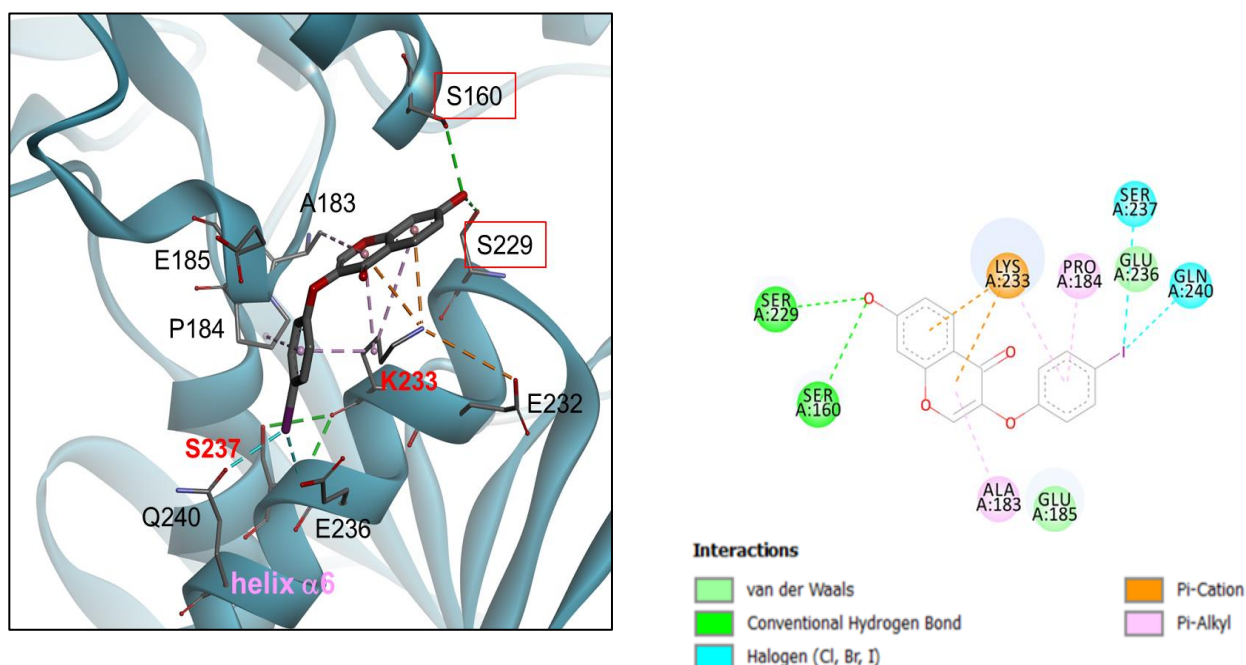


Figure 103. Dockings of XAP044 along helix $\alpha 6$ bound to S160 and S229.

Figure 104 shows how XAP044 in the second orientation along helix α_6 , may block the closing movement of the VFTD and behaves as a wedge. Preventing the VFTD closure will inhibit the receptor activation (**Figure 58**).

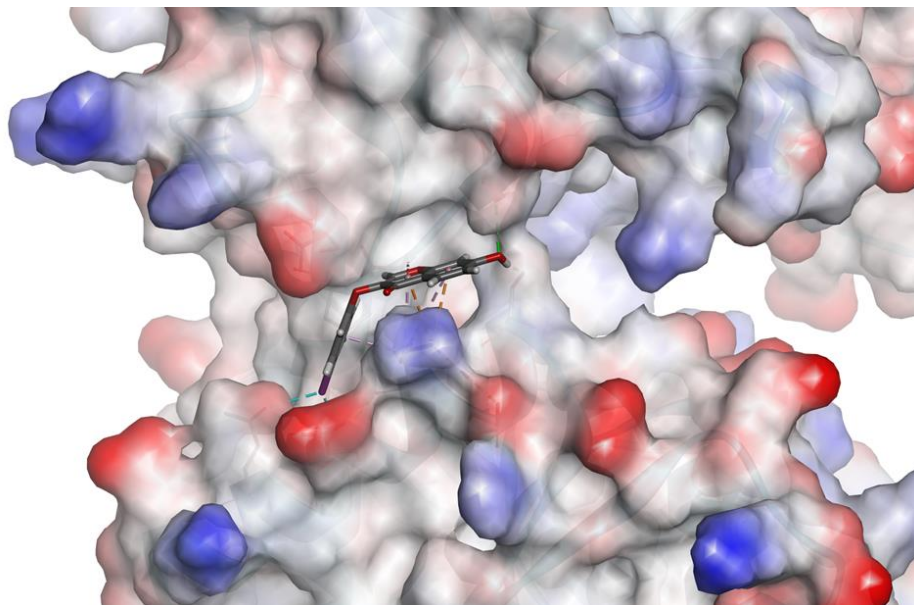


Figure 104. XAP044 bound to S160/ S229 and along helix α_6 , blocks the hinge movement of mGlu7 VFTD which will result in preventing receptor activation. The surface of the VFTD is displayed as solvent interpolated charge surface.

In the third orientation, XAP044 is bound to S160 and S229 and oriented to loop $\beta_7\alpha_8$ (**Figure 105**).

This docking shows:

- hydrogen bond with S160 and S229
- hydrophobic contacts with I163, R191, Y192
- halogen bond with D188
- restricted environment around the iodophenyl group in agreement with SAR
- mGlu7 selectivity because of E185-K233 specific interaction.

Although this docking seemed satisfactory, it was ruled out because it was unstable in molecular dynamics in contrast to what was observed for the second orientation.

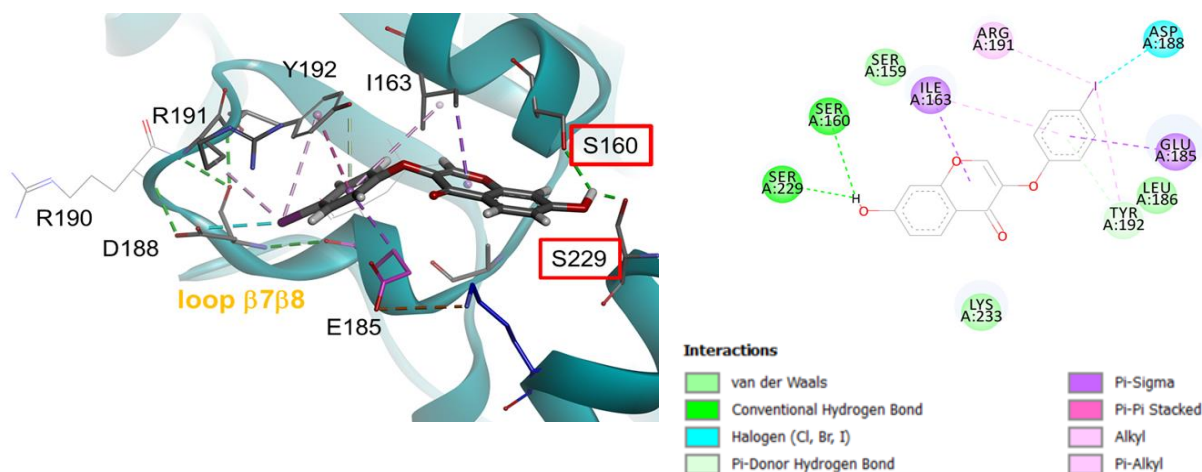


Figure 105. Docking of XAP044 oriented to loop $\beta7\alpha8$ and bound to S160 and S229.

Figure 106 shows how in this other orientation to loop $\beta7\alpha8$, XAP044 may also bind to the hinge of the VFTD and block the closure of the two lobes.

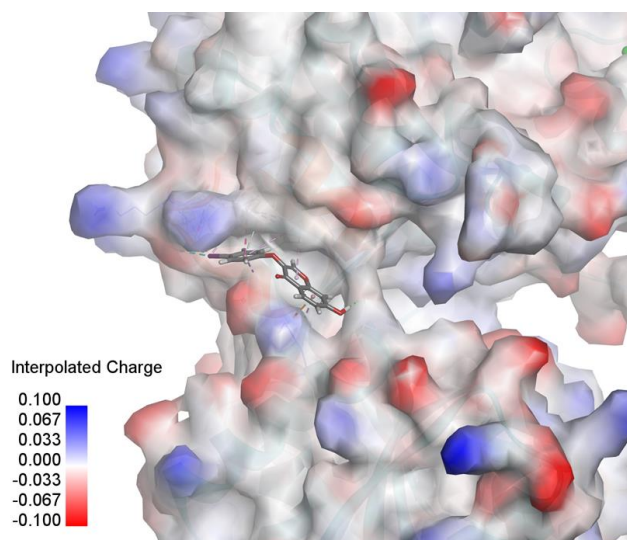


Figure 106. XAP044 bound to S160/S229 and oriented to loop $\beta7\alpha8$ of the mGlu7 VFTD. This binding may also block the hinge movement and prevent activation. The surface of the VFTD is displayed as solvent interpolated charge surface.

Considering the molecular dynamics, the docking with orientation along the helix $\alpha6$ was selected. Next, we proceeded to the validation of this model by mutagenesis experiments and functional assays. The experiments were run by Isabelle Brabet in the group of Jean-Philippe Pin at the Institut de Génomique Fonctionnelle in Montpellier on the ARPEGE platform. The results are presented in **Table 7**.

	pEC50			
	mGlu7	S229A	K233A	S237A
LSP4-2022	4.51	4.80	4.1	4.74
LSP4-2022 + 100μM XAP044	3.60	4.58	3.54	3.7
ratio	0.8	0.95	0.86	0.78
No XAP044 inhibition	1			
Full XAP044 inhibition	0.8			
Effect on XAP044 inhibition		abolished	reduced	no effect

Table 7. Effect of mGlu7R mutations on XAP044 inhibition of LSP4-2022 activation. mGlu7R was expressed in HEK cells. iPone readout from Cisbio was used for the functional assays.

The mutation of S229 to S229A totally abolishes the inhibition activity of XAP044 confirming its fundamental role in the binding of XAP044 to the VFTD of mGlu7R. The mutation of K233, an mGlu7R selective residue, to K233A reduces the inhibition activity of XAP044 so probably K233 takes part to the binding of XAP044 to the VFTD. The mutation of S237 in S237A had no effect on the binding showing that this residue is either not implicated in the binding or makes weak interactions.

When virtually checking the effect of mutating K233 to all 20 amino acids, on the stability of the complex with XAP044, we found that alanine is the least destabilizing mutation (**Table 8**). Indeed alanine may still make some hydrophobic contacts with the ligand. Consequently, a further validation was necessary for the interaction with that residue K233. According to **Table 8**, we selected the K233D mutation with a high electrostatic term. The generation of the mutant and functional assays are on going. We expect an increased destabilization that would further validate our XAP044 binding model.

	Mutation	Mutation Energy	Effect of Mutation	VDW Term	Electrostatic Term	Entropy Term	Non-polar Term
1	A:LYS233>LYS	-0.19	NEUTRAL	-0.01	-0.18	0	0
2	A:LYS233>ARG	0.1	NEUTRAL	0.61	-0.29	0.11	0
3	A:LYS233>PRO	0.16	NEUTRAL	2.7	-0.34	-1.06	0
4	A:LYS233>MET	0.17	NEUTRAL	0.8	0.03	-0.33	0
5	A:LYS233>ASN	0.21	NEUTRAL	1.56	0.1	-0.84	0
6	A:LYS233>PHE	0.25	NEUTRAL	1.18	0.23	-0.71	0
7	A:LYS233>CYS	0.28	NEUTRAL	2.84	-0.24	-1.13	0
8	A:LYS233>HIS	0.28	NEUTRAL	1.67	-0.06	-0.62	0
9	A:LYS233>LEU	0.32	NEUTRAL	1.67	0.08	-0.74	0
10	A:LYS233>TRP	0.41	NEUTRAL	1.6	0.24	-0.79	0
11	A:LYS233>ALA	0.54	DESTABILIZING	3.33	-0.19	-1.17	0
12	A:LYS233>SER	0.62	DESTABILIZING	2.64	-0.07	-0.79	0
13	A:LYS233>TYR	0.64	DESTABILIZING	1.35	0.24	-0.34	0
14	A:LYS233>GLU	0.83	DESTABILIZING	-0.16	1.24	-0.41	0
15	A:LYS233>GLY	0.92	DESTABILIZING	4.27	-0.29	-1.16	0
16	A:LYS233>GLN	1.07	DESTABILIZING	1.92	0.47	-0.45	0
17	A:LYS233>ASP	1.38	DESTABILIZING	2.33	0.97	-0.94	0
18	A:LYS233>THR	1.42	DESTABILIZING	3.97	0.03	-0.75	0
19	A:LYS233>ILE	1.51	DESTABILIZING	3.8	0.1	-0.61	0
20	A:LYS233>VAL	1.72	DESTABILIZING	4.88	-0.1	-0.77	0

Table 8. Virtual mutation of K233 by the 20AA in the model of XAP044 docked along helix6 and followed by 3.5 ns molecular dynamics. Ala is the least destabilizing mutation. Asp seems the best mutation to disrupt the hydrophobic interactions.

The docking of XAP044 bound to S229 and S160 along helix α_6 of mGlu7 VFTD, has been disclosed by 3D-models, dockings and molecular dynamics. The agreement with the SAR and the mutagenesis data was fundamental to validate this binding model.

To summarize our modeling findings, XAP044 behaves as a wedge preventing the VFTD closure and the receptor activation by the binding of S229 and S160 along the helix 6 (**Figure 107**).

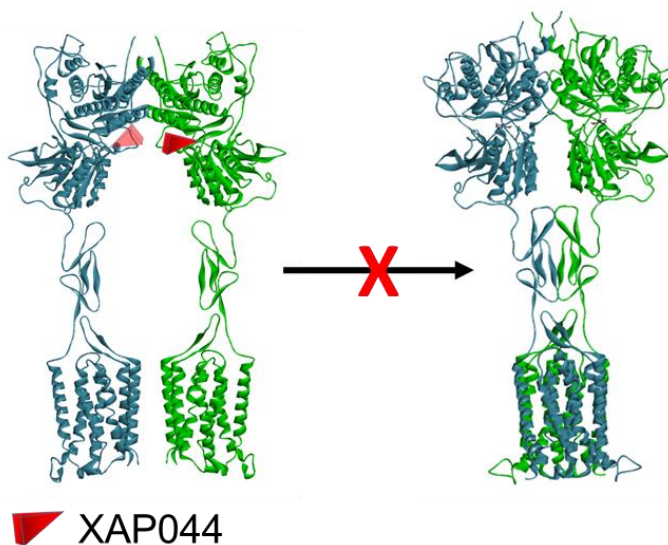


Figure 107. XAP044 acts as a wedge inhibiting the VFTD closure and the dimer activation.

5. AZOLOGIZATION OF THE 7TMD NAM VU6010608

5.1. Design and synthesis of VU6010608 azologs

VU6010608 (**Figure 108**) is an mGlu7R NAM that bind to the 7TMD.¹⁷³ It was discovered with an SAR study on an analog that had a chlorine atom in place of the trifluoromethoxy group. This substitution led to a more potent compound with an IC₅₀ of 759 nM and efficacy in blocking high frequency stimulated long-term potentiation in electrophysiology studies. VU6010608 binds to the 7TMD, the classic site of allosteric modulators, in contrast to what was seen before for XAP044 (**Figure 54**).^{173,175}

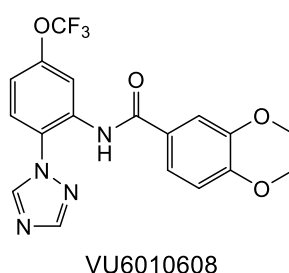


Figure 108. Structure of VU6010608.

VU6010608 is composed of two benzene rings connected by a central amide bond. One benzene bears a trifluoromethoxy group in *meta* position and a triazole in *ortho* position. The other benzene ring bears two methoxy groups in *meta* and *para* positions. The central amide can be easily replaced with a diazene bond to obtain the classical scaffold of an azobenzene. The replacement of a chemical function with another group to obtain a photoswitch molecule starting from non photoactivable ligands is called azologization.^{292,293} Many bioactive molecules have motifs that are isostere of azobenzene, these are two benzene rings linked by different linkers as stilbenes, *N*-aryl benzamides, benzyl phenyl ethers, benzyl anilines and so on. All these functional groups can be replaced by the diazene unit leading to novel photoswitchable analogs called “azosters”.²⁹²

There is an important criterion which must be taken into account each time a linker is replaced with a diazene unit to create a photoswitch starting from a bioactive molecule, that is to say, the role that the group to replace has in the binding to the receptor and in the SAR. Indeed, if a specific group, according to SAR, has not a primary function in the binding then it can be replaced by a diazene unit without problems. On the contrary, if the group is demonstrated to be necessary for the binding to the target, then its replacement leads to the loss of the biological activity.

In the case of compound VU6010608, the SAR showed the role of each chemical function, highlighting what is fundamental and what is not (**Figure 109**).

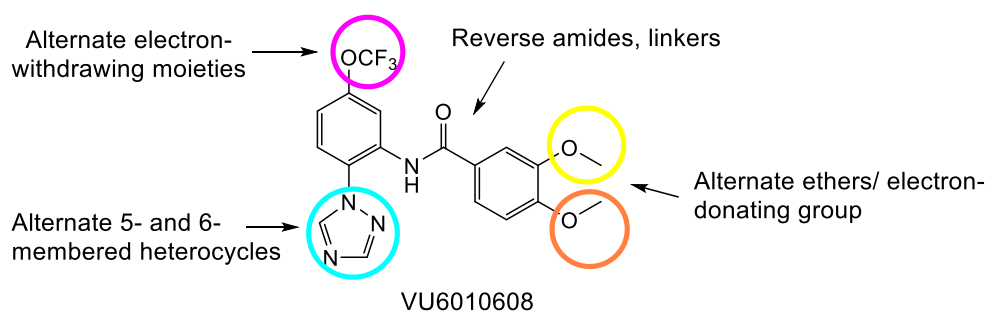


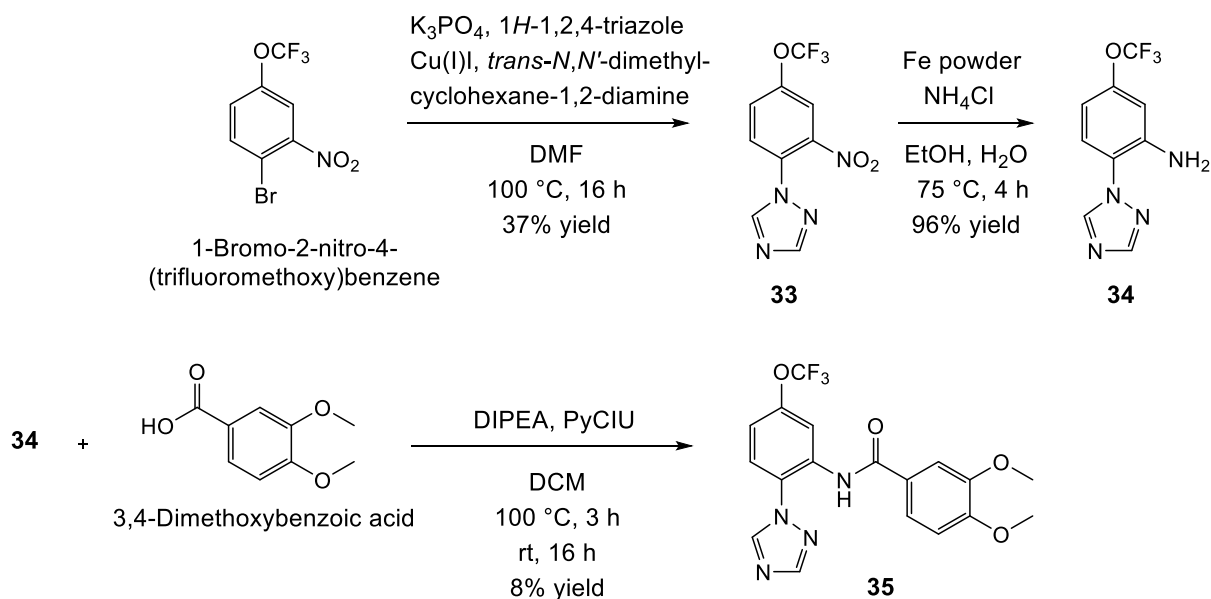
Figure 109. SAR of VU6010608.

According to SAR the amide is not fundamental so the central linker can be replaced maintaining the biological activity (**Figure 110**).



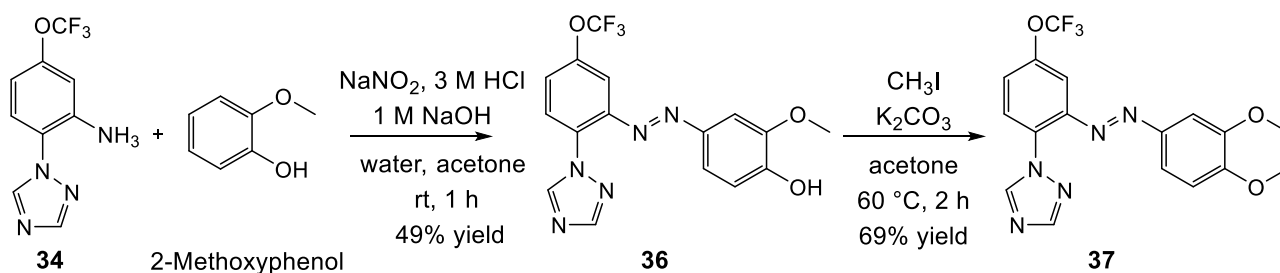
Figure 110. Azologization approach used.

First, compound VU6010608 **35** was synthesized to test the activity of the reference bioactive compound for comparison with the azolog derivative in the same biological assay. The original synthesis¹⁷³ was followed starting from 1-bromo-2-nitro-4-(trifluoromethoxy)benzene that was attached to triazole *via* copper catalysed C-N reaction to get compound **33**. The nitro group was reduced with iron powder and ammonium chloride to obtain the amine **34** that gave by peptidic coupling with 3,4-dimethoxy benzoic acid, the final product **35**. For the coupling *N,N*-diisopropylethylamine was used as base and 1-(chloro-1-pyrrolidinylmethylene)pyrrolidinium hexafluorophosphate (PyCIU) as reagent for peptide synthesis (**Scheme 44**).



Scheme 44. Synthesis of compound 35.

Starting from compound **34**, compound **36** was synthesized using azo-coupling reaction. Protection of the hydroxyl group with methyl iodide gave product **37** (Scheme 45).



Scheme 45. Synthesis of compound 36 and 37.

5.2. Photophysical properties of VU6010608 azologs

Compound **36** and **37** were both planned to be tested as photoswitch analog of compound **35** in biological assay. ^1H NMR kinetic in DMSO at a concentration 8 mM was performed for compound **36** (Figure 111) and compound **37** (Figure 112). Compound **36** showed no changes after irradiation at 365 nm for 1 h, ^1H NMR spectra showed only the *E* configuration. This is due to the fast thermal relaxation already seen in the case of azobenzenes. On the contrary, in compound **37** the methoxy group in *para* position has an electron donor effect that allows a slower thermal relaxation.²⁸⁴ Compound **37** isomerizes to the 67% of *Z* isomer after irradiation at 365 nm during 1h. A further irradiation for 2h at 365 nm showed the same percentage, showing that the PSS at 365 nm corresponds to 33% *E* and 67% *Z* isomers. The mixture of the two isomers thermally return at room temperature to 63% *E* and 37% *Z* (PSS in DMSO) and did not change during nine days.

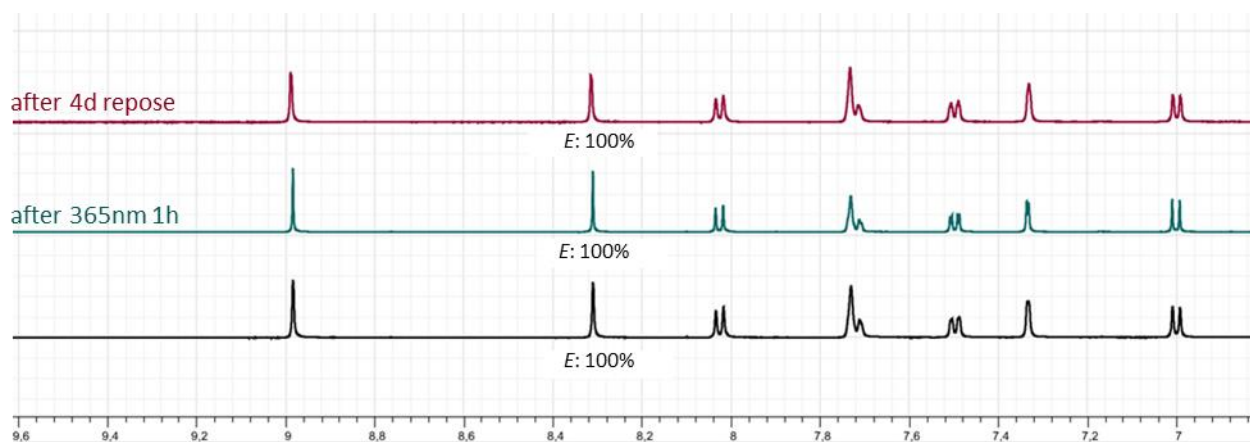


Figure 111. Irradiation of compound **36** at 365 nm in DMSO.

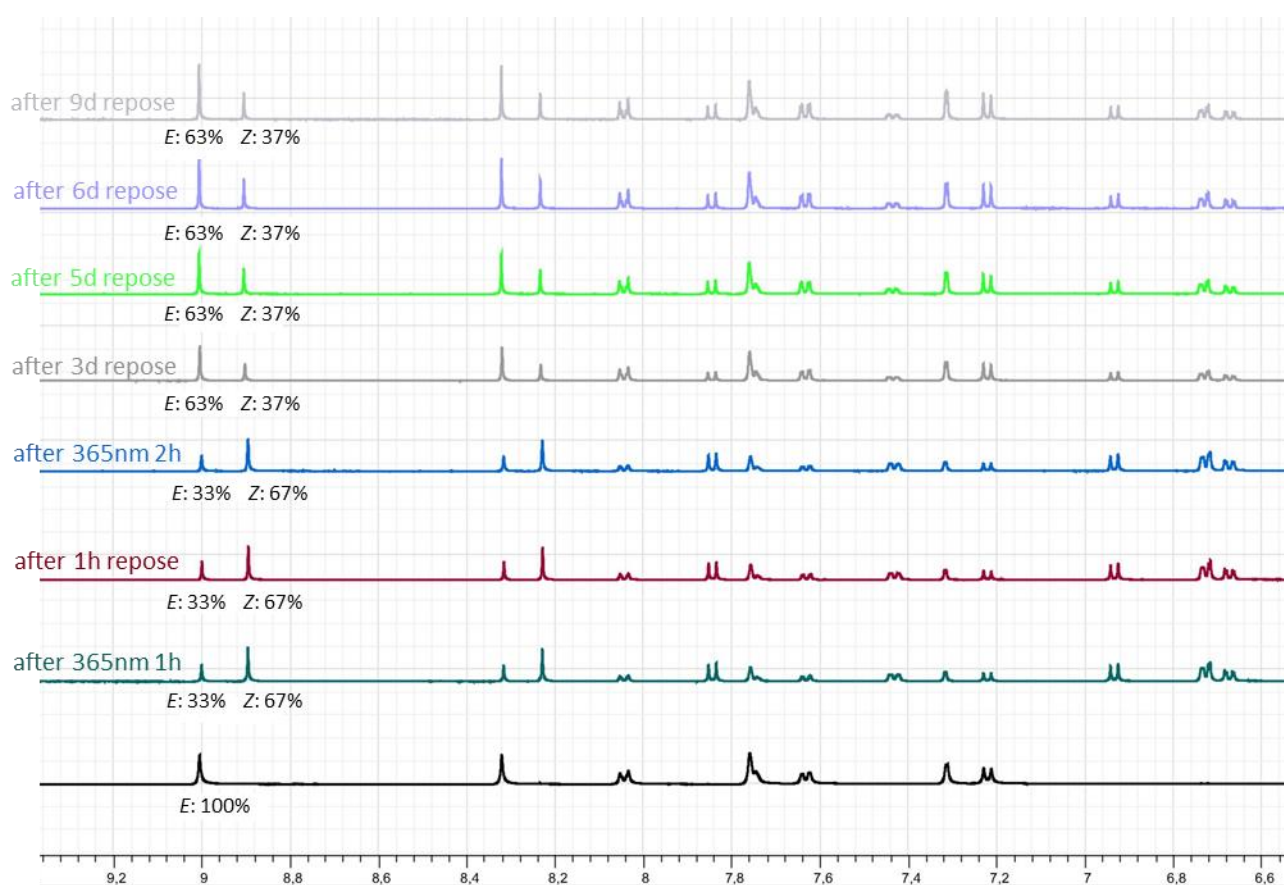


Figure 112. Irradiation of compound **37** in DMSO.

UV-Vis spectra in 0.5 %DMSO/ water were recorded for compounds **36** and **37** (Figure 113).

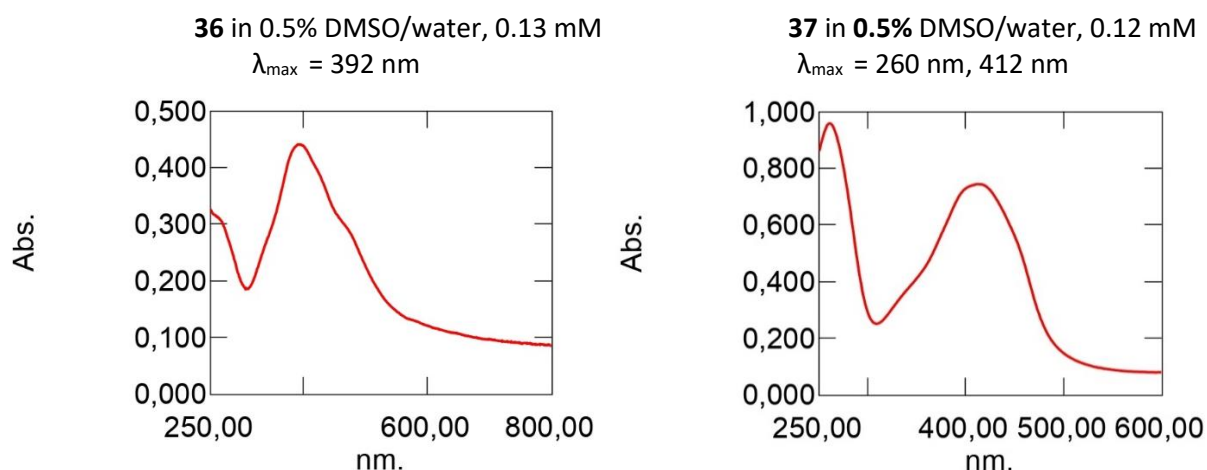


Figure 113. UV-Vis absorption spectra of compounds **36** and **37**.

5.3. Pharmacological results

The assays were performed at IGF as indicated above. Products **36** and **37** were impossible to test as they precipitate in phosphate buffer at concentrations required for the assays. Surprisingly, the replacement of the central amide of VU6010608 with the diazene unit leads to a decrease of the solubility in polar solvents. Unfortunately, these compounds represent a good example of azologization approach without application in biology.

Compounds **35** (VU6010608) was synthesized as reference to compare its activity with compounds **36** and **37** as described above (Scheme 44). First the EC₅₀ of the agonist LSP4-2022 on mGlu7R was measured then the reduction in the activity on mGlu7R of LSP4-2022 in combination with compound **35** was evaluated (Table 9).

		Mean value	Sem+/-	n
LSP4-2022	$-\log EC_{50}/-\log EC_{50}2022$	1.00	0.00	30
	$-\log EC_{50}$	4.56	0.04	30
	EC ₅₀	3.33E-05	5.02E-06	30
LSP42022 + 35 (VU6010608) 100 μM	$-\log EC_{50}/-\log EC_{50}2022$	0.93	0.01	3
	$-\log EC_{50}$	4.53	0.04	3
	EC ₅₀	2.98E-05	2.63E-06	3

Table 9. DR LSP4-2022 in combination with compound **35** (VU6010608) 100 μM.

Compound **35** was tested at a concentration of 100 μM in the presence of LSP4-2022 and incredibly, the value of EC_{50} of LSP4-2022 does not increase showing that the reference product VU6010608 cannot antagonize the agonist LSP4-2022. In fact, VU6010608 has an IC_{50} of 759 nM when tested with the agonist L-AP4¹⁷³ but it is not able to antagonize the stronger agonist LSP4-2022 as showed by the results of this study.

GENERAL CONCLUSION AND PERSPECTIVES

This work has been focused on three main projects:

- the synthesis of the *N*-DCAC-D-serine and *N*-DCAC-glycine for NMDA receptors
- the synthesis of several analogs of XAP044 to elucidate its binding mode in the VFTD and to discover novel potent mGlu7R NAMs
- the azologization of the mGlu7 NAM VU6010608 to synthesize the corresponding photoswitch analog

In the first part of the manuscript, the *N*-DCAC-D-serine **1** and *N*-DCAC-glycine **2** (**Figure 114**) were synthesized (Chapter 3.1). These compounds will be tested in electrophysiological studies on brain slices of knock-out D-serine racemase mice to uncage by photolysis the amino acid and measure the potential action of the NMDA receptor. These studies aim at studying the role of D-serine/glycine at NMDA receptor at a cellular level. On the other hand, increased synaptic concentration of D-serine/glycine may result from stimulation of Asc-1 transporter efflux. This transporter may be a promising target for diseases where a hypofunction of NMDA receptors has been observed such as schizophrenia.

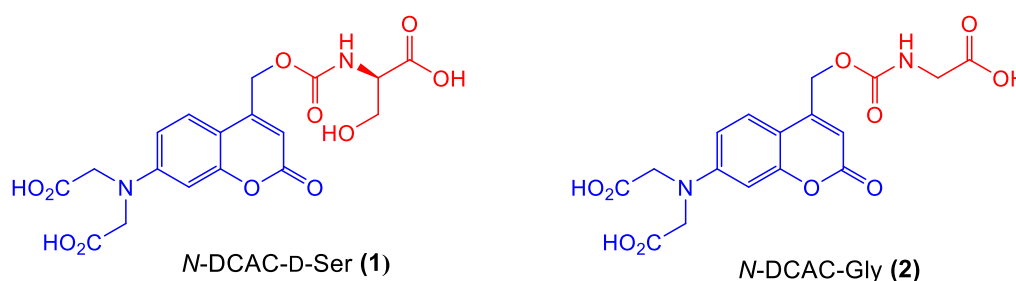


Figure 114. Structure of the *N*-DCAC-D-serine **1** and *N*-DCAC-glycine **2**.

In the second part of the manuscript, the mGlu7R NAM XAP044, discovered by Novartis, was investigated. XAP044 is the first mGlu7R NAM able to bind to the VFTD in contrast to previously described allosteric modulators. Anyway, the exact mechanism of binding to the VFTD has not been previously elucidated. Three hypothesis of binding were proposed (**Figure 60**) and the synthesis of different XAP044 analogs (Chapter 4.1) was achieved allowing to support the final binding mode. Our hypothesis of docking of XAP044 bound to S160 and S229 along the helix α_6 (

Figure 115) was validated by SAR agreement and mutagenesis data.

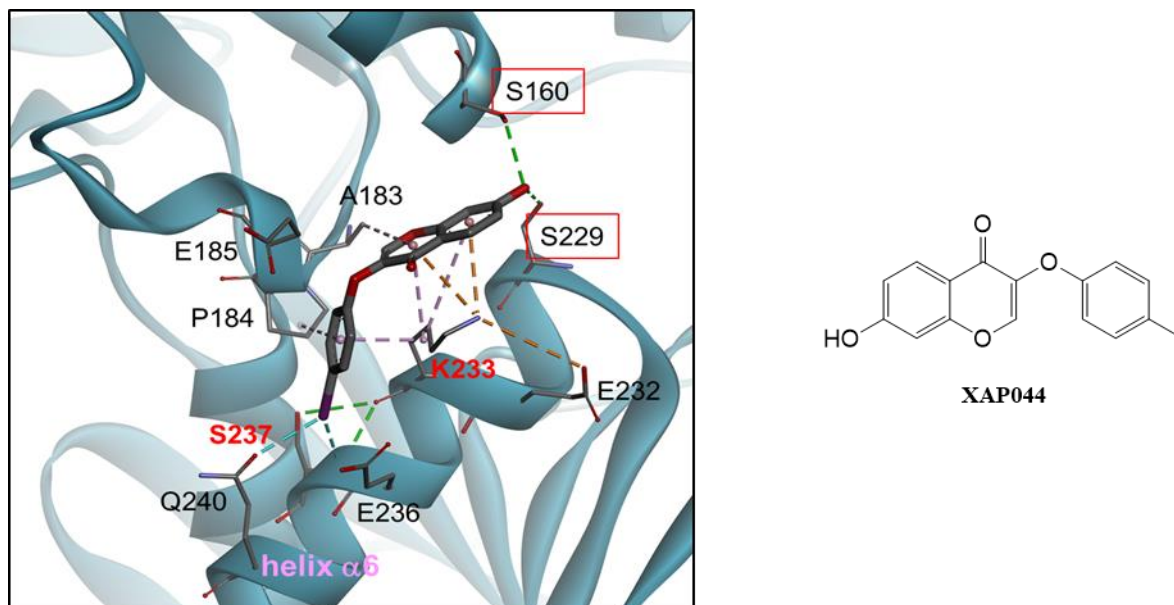


Figure 115. Docking of XAP044 bound to S160 and S229 along the helix $\alpha 6$.

The XAP044 analogs were tested with the agonist LSP4-2022 to measure their inhibitory activity compared to the XAP044. Among all the XAP044 analogs synthesized, compounds **27a** ($IC_{50} = 0.957 \mu M$) and **27b** ($IC_{50} = 0.881 \mu M$) (**Figure 116**) showed the best inhibitory activity, 5 times more potent than XAP044 ($IC_{50} = 4.33 \mu M$). Furthermore, these compounds showed better solubility properties compared to XAP044 as they lack the chromone scaffold. For all these reasons, **27a** and **27b** represent a useful tool for future biological and pharmacological studies related to the involvement of mGlu7R in psychiatric disorders especially anxiety. Currently, they are among the most potent mGlu7R NAMs discovered by now.

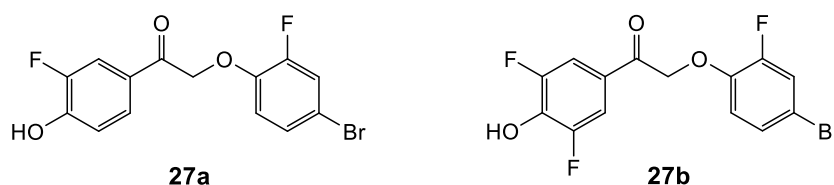


Figure 116. Compounds **27a** and **27b**.

In the last part of this work the azologization of the mGlu7R NAM VU6010608 reported by Reed *et al.* was achieved with the synthesis of the corresponding azolog **37** (Chapter 5.1). Our initial aim was to synthesize a photoswitch NAM azolog of VU6010608 active in the *trans* conformation and inactive in the *cis* conformation (**Figure 117**). Unfortunately, the replacement of the central amide bond of VU6010608 by a diazene in compound **37** highly decreased the solubility properties and it was not possible to dissolve **37** in phosphate buffer in *in vitro* studies. Compound **37** represents a good example of azologization approach but with no application in biology due to bad solubility properties. Interestingly, compound **35** (VU6010608), synthesized as reference for *in vitro* studies, showed no inhibitory activity on LSP4-2022. This proves that VU6010608 is an mGlu7R NAM able to inhibit a weak agonist such as L-AP4 according to Reed *et al.* but not with the most potent LSP4-2022.

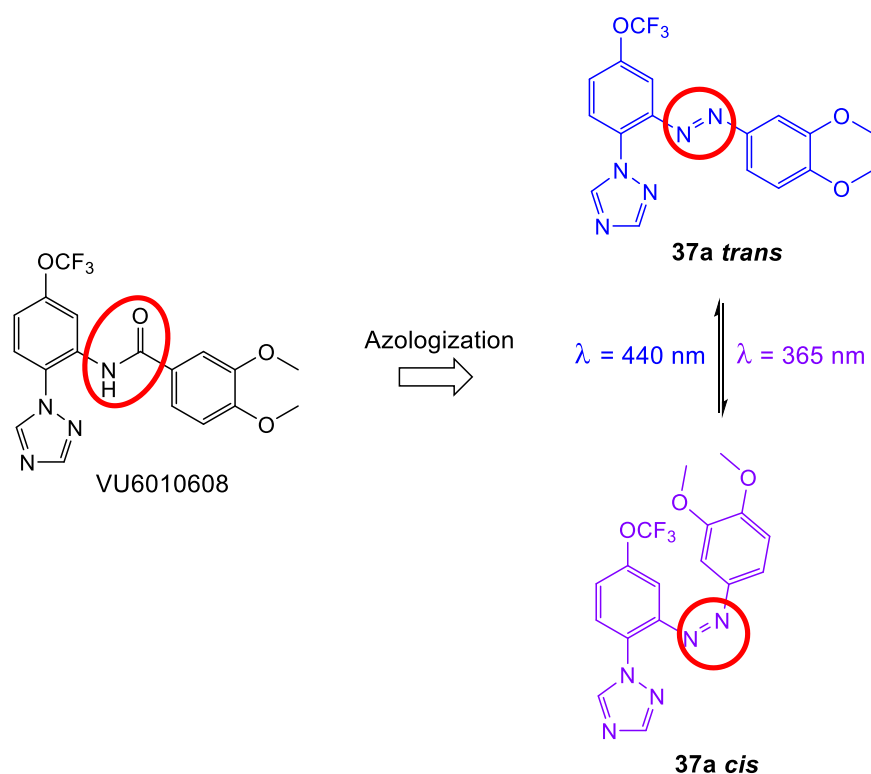


Figure 117. Azologization of VU6010608. The azolog **37** is shown in the *trans* (blue) and *cis* (violet) form.

Experimental section

EXPERIMENTAL SECTION**General**

All chemicals and solvents were purchased from commercial suppliers (Sigma, Alpha Aesar, Acros, FluoroChem....) and used as received. Anhydrous solvents were purchased from Sigma. Dry tetrahydrofuran (THF) and dichloromethane (CH_2Cl_2) were obtained by distillation.

All reactions were carried out under argon atmosphere with anhydrous solvent, and were monitored by thinlayer chromatography (TLC) with silica gel Merck 60 F254, on aluminium sheets. Manual flash column chromatography was performed with VWR silica gel 60 (40–63 μm). Automated flash chromatography was performed with an Isolera One Biotage apparatus with detectors at 254 nm and 280 nm, using Büchi FlashPure silica. Solvent systems were given according to (s/s: v/v).

^1H (500.16 MHz), ^{13}C (125.78 MHz), and ^{19}F (470.57 MHz) NMR spectra were recorded on an Avance II 500 Bruker spectrometer. Chemical shifts (δ , ppm) are given with reference to deuterated solvents for ^1H and ^{13}C NMR respectively, CD_3OD : 3.31, 49.15; D_2O : 4.78; CDCl_3 : 7.24, 77.23; $\text{DMSO-}d_6$: 2.50, 39.51. Signal multiplicity is described as follows: s (singlet), d (doublet), t (triplet), q (quartet), m (multiplet). Broad signals are described as br. Coupling constants (J) are given in Hz. In the experimental part, the numbering of the molecules is only related to the attribution of the atoms.

IR spectra were obtained with a Perkin-Elmer Spectrum One FT-IR spectrometer equipped with a MIRacle™ single reflection horizontal ATR unit (zirconium-selenium crystal).

Mass spectra (MS) were recorded with a LCQadvantage (ThermoFinnigan) mass spectrometer with positive (ESI^+) or negative (ESI^-) electrospray ionization (ionization tension 4.5 kV, injection temperature 240 °C). HPLC-MS analyses were performed on a Thermo Finnigan LCQ Advantage Instrument as described above, equipped for HPLC with a Phenomenex RP Polar column (50 mm x 2.1 mm, 2.6 μm). Products were eluted with the following gradient using solvent A ($\text{H}_2\text{O}/\text{HCO}_2\text{H}$: 100/0.1), solvent B ($\text{MeCN}/\text{HCO}_2\text{H}$: 100/0.1): 100% A linear increase from 0 to 100% B for 20 min, 100% B from 20 to 30 min, 100% B linear increase from 0 to 100% A from 30 to 40 min.

UV spectra were obtained with a UV-2700i UV-Vis Spectrophotometer from Shimadzu, resolution 0.1 nm, light Source deuterium, wavenumber range from 185 to 900 nm.

CoolLed *pE* excitation system, with three irradiation wavelengths (365 nm, 440 nm and 490 nm), was kindly provided by Laetitia Mony from Institut de Biologie, Ecole Normale Supérieure, ENS, UMR 8197 CNRS.

General procedures

General procedure A:

A 4 M HCl solution in dioxane (0.040–0.066 M) was added to the di-*tert*-butyl diacetate at 0 °C. The reaction mixture was stirred at room temperature overnight then concentrated under *vacuo*. The crude residue was purified by column chromatography on silica gel.

General procedure B:

NC1-118 (1 eq) and CDI (1.1 eq) were dissolved in dry DMSO (0.3 M) and stirred at room temperature overnight. Et₃N (1.2 eq) and the desired amino acid (1.1 eq) were added to the solution that was stirred at 80 °C for 2 h and let at room temperature overnight. After cooling to 0 °C, water was added and the mixture was acidified to pH 3-4 with 1 M aqueous HCl solution. The precipitate was extracted with EtOAc (3x). The organic layer was washed with water (2x), dried with Na₂SO₄, filtered and the solvent evaporated to give the crude product. The crude residue was purified by column chromatography on silica gel (50% EtOAc, 50% CH₂Cl₂/MeOH/H₂O/AcOH, 7:3:0.6:0.3) to yield the desired product.

General procedure C:

Salicylate or thiosalicylate (1 eq), α -haloacetophenone (1 eq) and Cs₂CO₃ (1.7 eq) in DMF (0.05 M) were heated at 90 °C for 1.5 h. The reaction mixture was poured into water and extracted with CH₂Cl₂ (3x), washed with brine (2x), dried over MgSO₄, filtered and evaporated *in vacuo* to obtain the crude product that was triturated with MeOH to yield the desired product.

General procedure D:

Iodomethoxybenzofuro[3,2-*b*]chromen-11-one or indole derivatives (1 eq) and 1 M BBr₃ in CH₂Cl₂ (0.06 M) was stirred at –80 °C then at room temperature overnight. The reaction mixture was evaporated under *vacuo* and the resulted solid washed with saturated NaHCO₃ solution (2x). The crude residue was purified by trituration or by column chromatography on silica gel to yield the desired product.

General procedure E:

The phenol derivative (1 eq) and K₂CO₃ (1.1 eq) were stirred at room temperature in acetone (0.16 M) for 1 h. Then 2-bromo-1-(4-methoxyphenyl)ethan-1-one (1 eq) was added to the mixture and stirred overnight. The suspension was then filtered and evaporated *in vacuo*. The solid was dissolved in EtOAc, washed with 5% aqueous NaOH (2x) then water (2x). The organic phase was dried over Na₂SO₄, filtered and evaporated *in vacuo*. The crude product was purified to yield the desired products.

General procedure F:

To a solution of sodium methylate (1.46 eq) in anhydrous THF (0.18 M) was added the phenol derivative (1 eq) and the mixture was stirred at room temperature 6 h. 2-Bromo-1-(4-hydroxyphenyl)ethan-1-one was then added to the mixture and stirred overnight. The crude

residue was purified by column chromatography on silica gel (Cyclohexane/EtOAc, 7:3) to yield the desired product.

General procedure G:

Bromohydroxyphenylethanone (1 eq), acetic anhydride (0.84 M) and concentrated HCl were stirred at 60 °C for 2 h then at room temperature overnight. The resulting mixture was extracted with EtOAc (3x). The organic phases were washed with water and brine (2x), dried over MgSO₄ and concentrated *in vacuo*. The crude residue was purified to yield the desired product.

General procedure H:

The phenoxyacetylphenyl acetate derivative (1 eq) in EtOH (0.06 M) and NaOAc (10 eq) in water (3.8 M) was stirred at reflux overnight. The resulting mixture was extracted with EtOAc (3x). The organic phase was washed with water and brine (2x), dried over MgSO₄ and concentrated *in vacuo*. The crude residue was purified by column chromatography on silica gel to yield the desired product.

General procedure I:

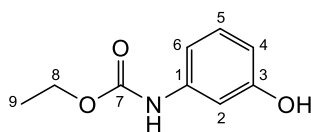
To a solution of fluorophenol (1 eq) in CS₂ (0.45 M) was added portionwise AlCl₃ (6 eq) and the reaction was stirred at room temperature for 10 min. Then 2-bromoacetyl bromide (1.3 eq) was added and the reaction mixture heated at reflux overnight. The reaction mixture was filtered and extracted with EtOAc (3x), washed with 1 M aqueous HCl and brine (2x). Then dried with Na₂SO₄, filtered and evaporated *in vacuo*. The crude residue was purified to obtain the desired product.

General procedure J:

Aniline derivative (1.0 eq) in 3 M aqueous HCl (1.25 M), water (1 M) and 1 M aqueous solution NaNO₂ (1 M) was stirred at 0 °C for 15 min. Then the mixture was slowly added to a stirred solution of phenol derivative or 6-methoxyindole (1.0 eq) in 1 M aqueous NaOH (0.5 M) and stirring was continued at room temperature for 1 h. The resulting mixture was extracted with EtOAc (3x). The organic phase was washed with water (2x), brine (2x), dried over MgSO₄ and concentrated *in vacuo*. The crude residue was purified by column chromatography on silica gel to yield the desired product.

General procedure K:

To a stirred solution of 6-hydroxybenzofuranone (1.0 eq) in a solution of ethanol-DMF (0.44 M, 1/1) were added 4-nitrobenzaldehyde (1.0 eq) and 50% aqueous solution of KOH (2.6 M). The mixture was stirred 4 h at room temperature. The reaction mixture was poured into hot water with vigorous stirring then concentrated aqueous HCl was added until pH 1–2. After cooling, the precipitate was filtered, washed with water (2x) and recrystallized from mixture DMF-MeOH to yield the desired products.

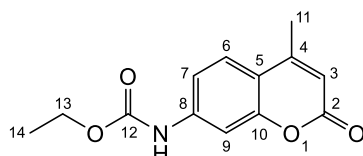
Ethyl (3-hydroxyphenyl)carbamate: 4

$C_9H_{11}NO_3$
MW = 181.19 g/mol

Ethyl chloroformate (35.5 mL, 0.372 mol, 1.16 eq) was added dropwise during 30 min under stirring at 0 °C to a suspension of 3-aminophenol (35.0 g, 0.321 mol, 1 eq) and $KHCO_3$ (33.4 g, 0.398 mol, 1.24 mol) in EtOAc (270 mL) and water (20 mL). The mixture was stirred for 1 h then water (60 mL) was added and stirring was maintained for 2 h. The aqueous phase was then separated and the organic phase was washed with water (50 mL), 1 M aqueous H_2SO_4 (50 mL), water (50 mL), brine (50 mL) then dried with $MgSO_4$ and evaporated *in vacuo* to give the crude product as a liquid brown oil. Crystallization in toluene led to compound **5** as white solid (38.0 g, 0.210 mol) in 65% yield.

Rf = 0.45 (Cyclohexane/EtOAc, 6:4)

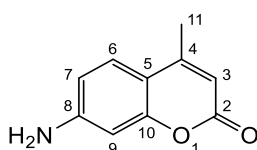
1H NMR (500 MHz, CD_3OD) δ : 7.06 (t, $J_{H-5,H-4} = J_{H-5,H-6} = 8.0$ Hz, 1H, H-5), 7.02 (s, 1H, H-2), 6.81 (d, $J_{H-6,H-5} = 8.0$ Hz, 1H, H-6), 6.45 (dd, $J_{H-4,H-5} = 8.0$ Hz, $J_{H-4,H-2} = 2.5$ Hz, 1H, H-4), 4.16 (q, $J_{H-8,H-9} = 7.0$ Hz, 2H, H-8), 1.29 (t, $J_{H-9,H-8} = 7.0$ Hz, 3H, H-9).

Ethyl (4-methyl-2-oxo-2H-chromen-7-yl)carbamate: 5

$C_{13}H_{13}NO_4$
MW = 247.25 g/mol

To a mixture of **4** (38.0 g, 0.210 mol, 1 eq) and ethyl acetoacetate (38 mL, 0.294 mol, 1.4 eq) was added dropwise concentrated H_2SO_4 (92 mL, 1.722 mol, 8.2 eq). The mixture was stirred at room temperature overnight then quenched with a mixture of water and ice (100 mL). The precipitate was separated by filtration and washed with water, methanol and diethyl ether to give the crude product **5** as a yellow solid in quantitative yield.

1H NMR (500 MHz, $CDCl_3$) δ : 7.48 (d, $J_{H-6,H-7} = 9.0$ Hz, 1H, H-6), 7.46 (d, $J_{H-9,H-7} = 2.0$ Hz, 1H, H-9), 7.39 (brd, $J_{H-7,H-6} = 8.5$ Hz, 1H, H-7), 7.31 (brs, 1H, NH), 6.45 (s, 1H, H-3), 4.23 (q, $J_{H-13,H-14} = 7.5$ Hz, 2H, H-13), 2.37 (s, 3H, H-11), 1.29 (t, $J_{H-14,H-13} = 7.5$ Hz, 3H, H-14).

7-Amino-4-methyl-2H-chromen-2-one: 6

$C_{10}H_9NO_2$
MW = 175.19 g/mol

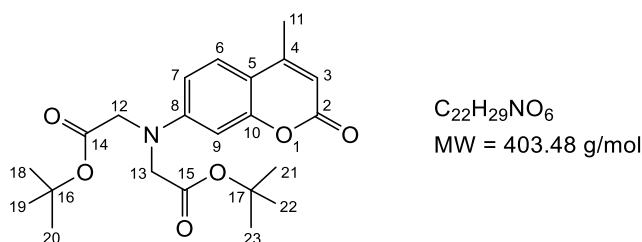
The crude coumarine **5** in a 45% aqueous solution of KOH (300 mL) was stirred at 90 °C for 1 h. After cooling to 0 °C, the reaction mixture was then diluted with water (100 mL) and acidified

with concentrated aqueous HCl until pH 5-6. Finally, 1 M aqueous NaOH was added to pH 8 to obtain a precipitate, which was separated by filtration and washed with water, methanol and diethyl ether to get compound **6** as a yellow solid (20.82 g, 0.12 mol) in 25% yield over the two steps.

R_f = 0.71 (CH₂Cl₂/MeOH, 9:1)

¹H NMR (500 MHz, CDCl₃) δ: 8.04 (d, J_{H-6,H-7} = 8.0 Hz, 1H, H-6), 7.94 (s, 1H, H-9), 7.26 (d, J_{H-7,H-6} = 8.0 Hz, 1H, H-7), 6.70 (s, 1H, H-3), 2.24 (s, 3H, H-11).

Di-*tert*-butyl 2,2'-((4-methyl-2-oxo-2H-chromen-7-yl)azanediyl)diacetate: **7**



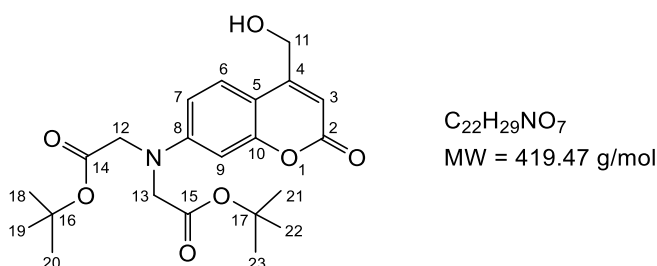
Compound **6** (5.93 g, 33.9 mmol, 1 eq), NaI (5.08 g, 33.9 mmol, 1 eq), diisopropylethylamine (29 mL, 0.169 mol, 5 eq) and bromoacetic acid *tert*-butylester (50 mL, 0.339 mol, 10 eq) in acetonitrile (110 mL) were refluxed for 8 days. The reaction mixture was cooled to room temperature, filtered and the solvent was removed under reduced pressure. The residue was dissolved in EtOAc (100 mL), washed with water (3x50 mL) and brine (3x 50 mL), dried over MgSO₄ and concentrated *in vacuo* to give the crude product as a dark brown oil. Crystallization in cyclohexane and diethyl ether led to compound **7** as a yellow solid (5.18 g, 12.8 mmol) in 38% yield.

R_f = 0.5 (Cyclohexane/EtOAc, 7:3)

¹H NMR (500 MHz, CDCl₃) δ: 7.40 (d, J_{H-6,H-7} = 9.0 Hz, 1H, H-6), 6.51 (dd, J_{H-7,H-6} = 9.0 Hz, J_{H-7,H-9} = 2.0 Hz, 1H, H-7), 6.43 (d, J_{H-9,H-7} = 2.0 Hz, 1H, H-9), 6.01 (s, 1H, H-3), 4.03 (s, 4H, H-12, H-13), 2.32 (s, 3H, H-11), 1.46 (s, 18H, H-18, H-19, H-20, H-21, H-22, H-23).

¹³C NMR (126 MHz, CDCl₃) δ: 169.2 (C-14, C-15), 162.0 (C-2), 155.7 (C-10), 152.8 (C-4), 151.3 (C-8), 125.8 (C-6), 111.4 (C-3), 110.6 (C-5), 109.1 (C-7), 99.3 (C-9), 82.6 (C-15, C-17), 54.6 (C-12, C-13), 28.3 (C-18, C-19, C-20, C-21, C-22, C-23), 18.6 (C-11).

Di-*tert*-butyl 2,2'-((4-(hydroxymethyl)-2-oxo-2H-chromen-7-yl)azanediyl)diacetate: **9**

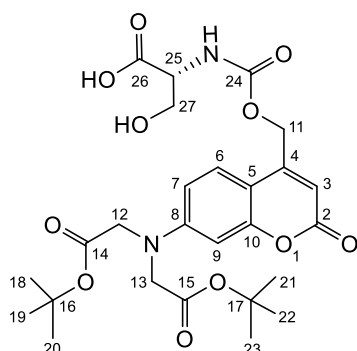


Selenium dioxide (1.62 g, 14.6 mmol, 1.49 eq) and 4-methyl coumarin **7** (3.95 g, 10.0 mmol, 1 eq) in *p*-xylene (96 mL) were refluxed with vigorous stirring for 24 h. The mixture was filtered and concentrated under reduced pressure. The dark brown oil was dissolved in EtOH (115 mL) then sodium borohydride (0.186 g, 4.9 mmol, 0.5 eq) was added and the solution was stirred for 2 h at room temperature. Thereafter, the suspension was carefully hydrolyzed with 1 M aqueous HCl (10 mL), diluted with H₂O and partially concentrated under reduced pressure to remove EtOH. The resulting mixture was extracted with EtOAc (3x30 mL). The organic phases were washed with water and brine, dried over MgSO₄ and concentrated *in vacuo* to give the crude product as an orange solid. The residue was purified by column chromatography on silica gel (Cyclohexane/EtOAc, 7:3) to get **9** as a yellow solid (1.62 g, 3.862 mmol) in 26% yield.

R_f = 0.44 (Cyclohexane/EtOAc, 7:3)

¹H NMR (500 MHz, CDCl₃) δ: 7.27 (d, *J*_{H-6,H-7} = 8.5 Hz, 1H, H-6), 6.46 (dd, *J*_{H-7,H-6} = 8.5 Hz, *J*_{H-7,H-9} = 2.0 Hz, 1H, H-7), 6.43 (d, *J*_{H-9,H-7} = 2.0 Hz, 1H, H-9), 6.30 (s, 1H, H-3), 4.76 (d, *J*_{H-11,OH} = 4.5 Hz, 2H, H-11), 4.03 (s, 4H, H-12, H-13), 1.46 (s, 18H, H-18, H-19, H-20, H-21, H-22, H-23).

(((7-(Bis(2-(*tert*-butoxy)-2-oxoethyl)amino)-2-oxo-2H-chromen-4-yl)methoxy)carbonyl)-D-serine: 10



C₂₆H₃₄N₂O₁₁
MW = 550.56 g/mol

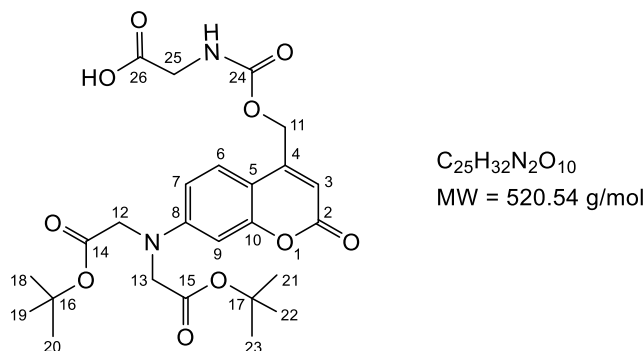
The *general procedure B* was followed using **9** (0.400 g, 0.954 mmol, 1 eq) and CDI (0.170 g, 1.049 mmol, 1.1 eq) were dissolved in DMSO (3 mL). Et₃N (0.16 mL, 1.145 mmol, 1.2 eq) and D-serine (0.120 g, 1.145 mmol, 1.1 eq) in DMSO (0.5 mL) were added to the solution. Compound **10** was obtained as a light yellow powder (0.103 g, 0.187 mmol) in 20% yield.

R_f = 0.62 (50% EtOAc, 50% CH₂Cl₂/MeOH/H₂O/AcOH 7:3:0.6:0.3)

¹H NMR (500 MHz, DMSO-*d*₆) δ: 7.51 (d, *J*_{H-6,H-7} = *J*_{NH,H-25} = 9.0 Hz, 2H, NH, H-6), 6.57 (dd, *J*_{H-7,H-6} = 9.0 Hz, *J*_{H-7,H-9} = 2.5 Hz, 1H, H-7), 6.46 (d, *J*_{H-9,H-7} = 2.5 Hz, 1H, H-9), 6.14 (s, 1H, H-3), 5.26 (s, 2H, H-11), 4.19 (s, 4H, H-12, H-13), 4.01 (m, 1H, H-25), 3.65 (m, 2H, H-27), 1.42 (s, 18H, H-18, H-19, H-20, H-21, H-22, H-23).

¹³C NMR (126 MHz, DMSO-*d*₆) δ: 172.0 (C-26), 168.8 (C-14, C-15), 160.4 (C-2), 155.3 (C-24), 154.9 (C-10), 151.6 (C-8), 151.3 (C-4), 125.2 (C-6), 109.1 (C-3), 107.0 (C-5), 106.0 (C-7), 98.2 (C-9), 81.1 (C-16, C-17), 61.4 (C-27), 61.0 (C-12, C-13), 56.6 (C-11), 53.5 (C-25), 27.7 (C-18, C-19, C-20, C-21, C-22, C-23).

((7-(Bis(2-(*tert*-butoxy)-2-oxoethyl)amino)-2-oxo-2*H*-chromen-4-yl)methoxy)carbonyl) glycine: **11**



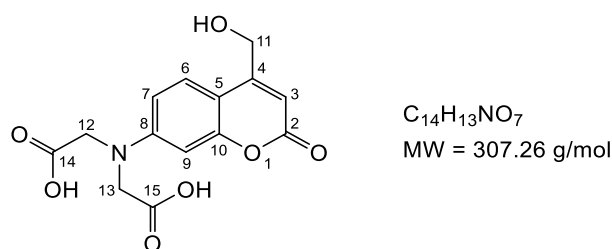
The *general procedure B* was followed using **9** (0.400 g, 0.954 mmol, 1 eq) and CDI (0.174 g, 1.049 mmol, 1.1 eq) were dissolved in dry DMSO (3 mL). Et₃N (0.16 mL, 1.145 mmol, 1.2 eq) and glycine (0.086 g, 1.145 mmol, 1.1 eq) were added to the solution. Compound **11** was obtained as a light yellow powder (0.191 g, 0.366 mmol) in 38% yield.

R_f = 0.70 (50% EtOAc, 50% CH₂Cl₂/MeOH/H₂O/AcOH, 7:3:0.6:0.3)

¹H NMR (500 MHz, DMSO-*d*₆) δ: 12.56 (s, 1H, OH), 7.80 (t, *J*_{NH,H-25} = 6.0 Hz, 1H, NH), 7.51 (d, *J*_{H-6,H-7} = 8.5 Hz, 1H, H-6), 6.58 (dd, *J*_{H-7,H-6} = 9.0 Hz, *J*_{H-7,H-9} = 2.5 Hz, 1H, H-7), 6.46 (d, *J*_{H-9,H-7} = 2.5 Hz, 1H, H-9), 6.08 (s, 1H, H-3), 5.27 (s, 2H, H-11), 4.18 (s, 4H, H-12, H-13), 3.71 (d, *J*_{H-25,NH} = 6.0 Hz, 2H, H-25), 1.42 (s, 18H, H-18, H-19, H-20, H-21, H-22, H-23).

¹³C NMR (126 MHz, DMSO-*d*₆) δ: 171.3 (C-26), 168.7 (C-14, C-15), 160.4 (C-2), 155.8 (C-24), 154.9 (C-10), 151.7 (C-8), 151.3 (C-4), 125.1 (C-6), 109.1 (C-3), 107.0 (C-5), 106.0 (C-7), 98.1 (C-9), 81.1 (C-16, C-17), 61.1 (C-12, C-14), 53.5 (C-11), 42.2 (C-25), 27.7 (C-18, C-19, C-20, C-21, C-22, C-23).

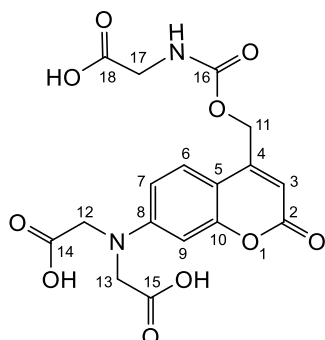
2,2'-((4-(Hydroxymethyl)-2-oxo-2*H*-chromen-7-yl)azanediyl)diacetic acid (*N*-DCAC-OH): **3**



The *general procedure A* was followed using **9** (0.050 g, 0.135 mmol) and 4 M HCl in dioxane (6 mL). The crude residue was purified by column chromatography on silica gel (50% EtOAc, 50% CH₂Cl₂/MeOH/H₂O/AcOH 7:3:0.6/0.3) then crystallized with cyclohexane and Et₂O and recrystallized with MeOH and cyclohexane to yield *N*-DCAC-OH **3** as a beige solid (0.039 g, 0.126 mmol) in 95% yield.

R_f = 0.11 (CH₃CN/TFA, 100:0.1)

2,2'-((4-(((carboxymethyl)carbamoyl)oxy)methyl)-2-oxo-2H-chromen-yl)azanediyldiacetic acid (N-DCAC-glycine): 2



$C_{17}H_{16}N_2O_{10}$
MW = 408.32 g/mol

The *general procedure A* was followed using compound **11** (0.150 g, 0.288 mmol) and 4 M HCl in dioxane (15 mL). The crude residue was purified by reverse phase column chromatography (CH₃CN/TFA, 100:0.1) to get *N*-DCAC-glycine **2** as yellow powder (0.067 g, 0.164 mmol) in 57 % yield.

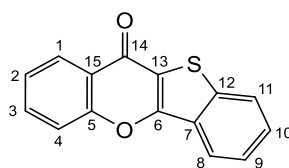
R_f = 0.67 (CH₂Cl₂/MeOH/H₂O/AcOH, 7:3:0.6:0.3)

¹H NMR (500 MHz, D₂O) δ: 7.61 (d, *J*_{H-6,H-7} = 9.0 Hz, 1H, H-6), 6.69 (d, *J*_{H-7,H-6} = 9.0 Hz, 1H, H-7), 6.57 (s, 1H, H-9), 6.26 (s, 1H, H-3), 5.37 (s, 2H, H-11), 4.32 (s, 4H, H-12, H-13), 3.93 (s, 2H, H-17).

¹³C NMR (126 MHz, D₂O) δ: 177.3 (C-18), 164.8 (C-14, C-15), 157.8 (C-2), 155.1 (C-16), 152.9 (C-10), 150.7 (C-8, C-4), 125.5 (C-6), 109.5 (C-3), 107.9 (C-5), 106.0 (C-7), 98.2 (C-9), 62.4 (C-12, C-13), 55.4 (C-11), 43.07 (C-17).

MS (ESI⁻) *m/z*: 407.07 [M – H]⁻.

UV/Vis (0.1 M PBS pH 7.2, 0.12 mM): λ_{max} (ε) = 376 (3375), 247 (3016), 208 (6725) nm (L.mol⁻¹.cm⁻¹).

11H-Benzo[4,5]thieno[3,2-b]chromen-11-one: 12a

C₁₅H₈O₂S
MW = 252.29 g/mol

The *general procedure C* was followed using methyl thiosalicylate (0.24 mL, 1.72 mmol), 2-bromo-2'-fluoroacetophenone (0.24 mL, 1.72 mmol) and Cs₂CO₃ (0.955 g, 2.92 mmol) in DMF (30 mL) to get **12a** as a pink solid (0.205 g, 0.812 mmol) in 47% yield.

R_f = 0.80 (Cyclohexane/EtOAc : 7/3)

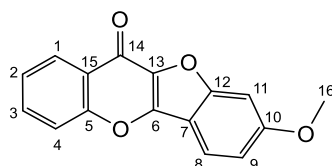
¹H NMR (500 MHz, CDCl₃) δ: 8.32 (d, *J*_{H-8,H-9} = 8.0 Hz, 1H, H-8), 8.08 (d, *J*_{H-11,H-10} = 8.0 Hz, 1H, H-11), 7.83 (d, *J*_{H-1,H-2} = 7.5 Hz, 1H, H-1), 7.69 (t, *J*_{H-3,H-2} = *J*_{H-3,H-4} = 7.5 Hz, 1H, H-3), 7.59 (d, *J*_{H-10,H-11} = 8.0 Hz, 1H, H-10), 7.51 (t, *J*_{H-4,H-3} = 7.5 Hz, 1H, H-4), 7.45 (t, *J*_{H-9,H-8} = *J*_{H-9,H-10} = 8.0 Hz, 1H, H-9), 7.41 (t, *J*_{H-2,H-1} = *J*_{H-2,H-3} = 7.5 Hz, 1H, H-2).

¹³C NMR (126 MHz, CDCl₃) δ: 173.2 (C-14), 156.0 (C-6), 153.7 (C-5), 140.0 (C-12), 133.7 (C-3), 129.3 (C-2), 129.2 (C-4), 126.0 (C-8), 125.1 (C-9), 125.0 (C-2), 123.8 (C-1), 122.7 (C-11), 122.4 (C-15), 120.8 (C-13), 118.0 (C-10).

MS (ESI⁻) *m/z*: 251.03 [M - H]⁻.

IR *v*_{max}/cm⁻¹: 1638, 1618, 1606, 1560, 1526, 1481, 1459, 1415, 1334, 1311, 1246, 1217, 1178, 1135, 1098, 1064, 1018, 937, 876, 788, 745, 731, 688, 642.

HPLC-MS (ESI) *m/z*; (λ = 235 nm): Rt = 13.39 min; 253.0312 [M + H]⁺.

8-Methoxy-11H-benzofuro[3,2-b]chromen-11-one: 12b

C₁₆H₁₀O₄
MW = 266.25 g/mol

The *general procedure C* was followed using methyl 2-hydroxy-4-methoxybenzoate (0.313 g, 1.72 mmol), 2-bromo-2'-fluoroacetophenone (0.24 mL, 1.72 mmol) and Cs₂CO₃ (0.955 g, 2.92 mmol) in DMF (30 mL) to get **12b** as a white solid (0.050 g, 0.187 mmol) in 11% yield.

R_f = 0.65 (Cyclohexane/EtOAc, 7:3)

¹H NMR (500 MHz, CDCl₃) δ: 8.42 (dd, *J*_{H-1,H-2} = 8.0 Hz, *J*_{H-1,H-3} = 1.5 Hz, 1H, H-1), 7.78 (d, *J*_{H-8,H-9} = 9.0 Hz, 1H, H-8), 7.68 (dt, *J*_{H-3,H-2} = *J*_{H-3,H-4} = 8.5 Hz, *J*_{H-3,H-1} = 1.5 Hz, 1H, H-3), 7.62 (d, *J*_{H-4,H-3} = 8.5 Hz, 1H, H-4), 7.44 (t, *J*_{H-2,H-1} = *J*_{H-2,H-3} = 7.5 Hz, 1H, H-2), 7.06 (d, *J*_{H-11,H-9} = 2.0 Hz, 1H, H-11), 7.01 (dd, *J*_{H-9,H-8} = 8.5 Hz, *J*_{H-9,H-11} = 2.0 Hz, 1H, H-9), 3.89 (s, 3H, H-16).

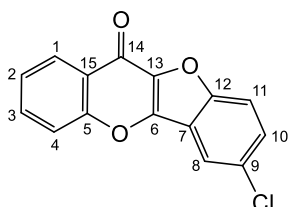
¹³C NMR (126 MHz, CDCl₃) δ: 166.5 (C-14), 162.9 (C-10), 157.2 (C-12), 155.8 (C-5), 149.7 (C-q), 137.0 (C-q), 133.2 (C-3), 126.7 (C-1), 125.3 (C-q), 124.9 (C-2), 121.2 (C-8), 118.3 (C-4), 114.8 (C-9), 111.2 (C-7), 96.6 (C-11), 56.1 (C-16).

MS (ESI⁺) m/z: 267.06 [M + H]⁺.

IR $\nu_{\text{max}}/\text{cm}^{-1}$: 1663, 1620, 1471, 1449, 1433, 1417, 1337, 1278, 1233, 1193, 1165, 1148, 1106, 1016, 982, 946, 900, 833, 813, 787, 759, 696, 668, 654, 636.

HPLC-MS (ESI) m/z; ($\lambda = 235 \text{ nm}$): Rt = 12.55 min; 267.0647 [M + H]⁺.

7-Chloro-11H-benzofuro[3,2-b]chromen-11-one: 12c



$\text{C}_{15}\text{H}_7\text{ClO}_3$
MW = 270.67 g/mol

The *general procedure C* was followed using methyl-5-chloro-2-hydroxybenzoate (0.321 g, 1.72 mmol), 2-bromo-2'-fluoroacetophenone (0.24 mL, 1.72 mmol) and Cs_2CO_3 (0.955 g, 2.93 mmol) in DMF (30 mL) to get **12c** as an orange solid (0.297 g, 1.097 mmol) in 64% yield.

Rf = 0.86 (Cyclohexane/EtOAc, 7:3)

¹H NMR (500 MHz, CDCl_3) δ : 8.45 (d, $J_{\text{H-1,H-2}} = 8.0 \text{ Hz}$, 1H, H-1), 7.96 (s, 1H, H-8), 7.75 (t, $J_{\text{H-3,H-2}} = J_{\text{H-3,H-4}} = 8.0 \text{ Hz}$, 1H, H-3), 7.67 (d, $J_{\text{H-4,H-3}} = 8.0 \text{ Hz}$, 1H, H-4), 7.62 (d, $J_{\text{H-11,H-10}} = 8.5 \text{ Hz}$, 1H, H-11), 7.56 (d, $J_{\text{H-10,H-11}} = 8.5 \text{ Hz}$, 1H, H-10), 7.49 (t, $J_{\text{H-2,H-1}} = 7.5 \text{ Hz}$, 1H, H-2).

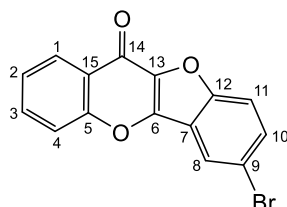
¹³C NMR (126 MHz, CDCl_3) δ : 167.5 (C-14), 156.0 (C-5), 153.5 (C-12), 148.1 (C-q), 138.5 (C-13), 134.0 (C-3), 131.0 (C-10), 130.3 (C-9), 126.8 (C-1), 125.3 (C-2), 120.3 (C-8), 119.5 (C-q), 118.6 (C-4), 114.9 (C-11).

MS (ESI⁺) m/z: 271.01 [M + H]⁺.

IR $\nu_{\text{max}}/\text{cm}^{-1}$: 1671, 1609, 1489, 1466, 1420, 1318, 1279, 1197, 1117, 1057, 996, 930, 857, 813, 754, 714, 698, 671, 639, 629, 617.

HPLC-MS (ESI) m/z; ($\lambda = 235 \text{ nm}$): Rt = 13.54 min; 271.0162 [M + H]⁺.

7-Bromo-11H-benzofuro[3,2-b]chromen-11-one: 12d



$\text{C}_{15}\text{H}_7\text{BrO}_3$
MW = 315.12 g/mol

The *general procedure C* was followed using methyl-5-bromo-2-hydroxybenzoate (0.397 g, 1.72 mmol), 2-bromo-2'-fluoroacetophenone (0.24 mL, 1.72 mmol) and Cs_2CO_3 (0.955 g, 2.93 mmol) in DMF (30 mL) to get **12d** as a light orange solid (0.170 g, 0.539 mmol) in 31% yield.

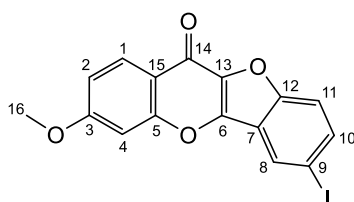
Rf = 0.58 (Cyclohexane/EtOAc, 7:3)

¹H NMR (500 MHz, CDCl₃) δ : 8.45 (d, $J_{H-1,H-2}$ = 8.0 Hz, 1H, H-1), 8.12 (d, $J_{H-8,H-10}$ = 1.5 Hz 1H, H-8), 7.75 (t, $J_{H-3,H-2}$ = $J_{H-3,H-4}$ = 7.5 Hz, 1H, H-3), 7.70 (dd, $J_{H-10,H-11}$ = 9.0 Hz, $J_{H-10,H-8}$ = 1.5 Hz, 1H, H-10), 7.67 (d, $J_{H-4,H-3}$ = 8.0 Hz, 1H, H-4), 7.56 (d, $J_{H-11,H-10}$ = 9.0 Hz, 1H, H-11), 7.49 (t, $J_{H-2,H-1}$ = 7.5 Hz, 1H, H-2).

¹³C NMR (126 MHz, CDCl₃) δ : 167.5 (C-14), 156.1 (C-5), 153.9 (C-12), 147.9 (C-q), 138.3 (C-13), 134.0 (C-3), 133.6 (C-10), 126.8 (C-1), 125.3 (C-2), 123.4 (C-8), 120.1 (C-9), 118.6 (C-4), 117.5 (C-7), 115.3 (C-11).

IR $\nu_{\max}/\text{cm}^{-1}$: 1674, 1605, 1485, 1458, 1318, 1274, 1193, 1119, 991, 926, 860, 827, 759, 694, 666, 637.

7-Iodo-3-methoxy-11H-benzofuro[3,2-b]chromen-11-one: 12e



C₁₆H₉IO₄
MW = 392.15 g/mol

The *general procedure C* was followed using methyl-5-iodosalicylate (0.478 g, 1.72 mmol), 2-fluoro-4-methoxyphenacylbromide (0.425 g, 1.72 mmol) and Cs₂CO₃ (0.955 g, 2.93 mmol) in DMF (25 mL) to get **12e** as a yellow solid (0.355 g, 0.905 mmol) in 53% yield.

¹H NMR (500 MHz, CDCl₃) δ : 8.33 (d, $J_{H-1,H-2}$ = 8.0 Hz, 1H, H-1), 8.28 (d, $J_{H-8,H-10}$ = 2.0 Hz, 1H, H-8), 7.85 (dd, $J_{H-10,H-11}$ = 8.5 Hz, $J_{H-10,H-8}$ = 2.0 Hz, 1H, H-10), 7.44 (d, $J_{H-11,H-10}$ = 8.5 Hz, 1H, H-11), 7.05 (brs, 1H, H-4), 7.04 (dd, $J_{H-2,H-1}$ = 8.0 Hz, $J_{H-2,H-4}$ = 2.5 Hz, 1H, H-2), 3.50 (s, 3H, H-16).

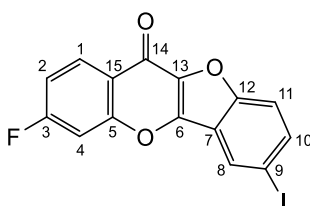
¹³C NMR (126 MHz, CDCl₃) δ : 167.2 (C-14), 164.4 (C-3), 157.9 (C-q), 154.3 (C-q), 147.1 (C-q), 138.7 (C-10), 138.1 (C-q), 129.3 (C-8), 128.1 (C-1), 120.8 (C-q), 119.1 (C-q), 115.6 (C-11), 114.3 (C-2), 101.2 (C-4), 87.4 (C-9), 56.2 (C-16).

Rf = 0.90 (Cyclohexane/EtOAc, 7:3)

IR $\nu_{\max}/\text{cm}^{-1}$: 1640, 1625, 1607, 1477, 1432, 1311, 1262, 1246, 1199, 1173, 1120, 1105, 1032, 991, 955, 919, 857, 839, 825, 766, 749, 693, 659, 651, 637, 630.

HPLC-MS (ESI) m/z; (λ = 235 nm): Rt = 14.54 min; 392.9609 [M + H]⁺.

Fluoro-7-iodo-11H-benzofuro[3,2-b]chromen-11-one: 12f



C₁₅H₆FIO₃
MW = 380.11 g/mol

The *general procedure C* was followed using methyl-5-iodosalicylate (0.478 g, 1.72 mmol), 2-chloro-2',4'-difluoroacetophenone (0.328 g, 1.72 mmol, 0.25 mL) and Cs₂CO₃ (0.955 g, 2.93 mmol) in DMF (25 mL) to get **12f** as an orange solid (0.221 g, 0.581 mmol) in 66% yield.

R_f = 0.91 (Cyclohexane/EtOAc, 7:3)

¹H NMR (500 MHz, CDCl₃) δ: 8.46 (dd, J_{H-1,H-2} = 8.5 Hz, J_{H-1,F} = 6.0 Hz, 1H, H-1), 8.31 (d, J_{H-8,H-10} = 2.0 Hz, 1H, H-8), 7.88 (dd, J_{H-10,H-11} = 8.5 Hz, J_{H-10,H-8} = 2.0 Hz, 1H, H-10), 7.45 (d, J_{H-11,H-10} = 8.5 Hz, 1H, H-11), 7.35 (dd, J_{H-4,F} = 8.5 Hz, J_{H-4,H-2} = 2.5 Hz, 1H, H-4), 7.22 (ddd, J_{H-2,F} = 10.0 Hz, J_{H-2,H-1} = 8.5 Hz, J_{H-2,H-4} = 2.5 Hz, 1H, H-2).

¹³C NMR (126 MHz, CDCl₃) δ: 166.6 (C-14), 165.8 (d, J_{C-3,F} = 256.4 Hz, C-3), 157.0 (d, J_{C-5,F} = 13.6 Hz, C-5), 154.5 (C-12), 147.8 (C-q), 139.3 (C-10), 137.9 (C-13), 129.5 (C-8), 129.2 (d, J = 11.0 Hz, C-1), 122.2 (C-q), 120.5 (C-q), 115.6 (C-11), 114.2 (d, J_{C-2,F} = 21.8 Hz, C-2), 105.4 (d, J_{C-4,F} = 26.3 Hz, C-4), 87.7 (C-9).

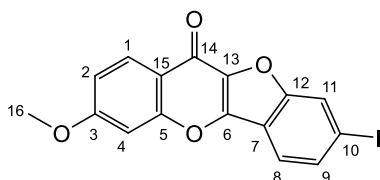
¹⁹F NMR (470 MHz, DMSO-*d*₆) δ: -103.3 (dd, J = 15.5 Hz, J = 8.5 Hz)

¹⁹F_{cpd} NMR (470 MHz, DMSO-*d*₆) δ: -103.3

IR ν_{max}/cm⁻¹: 1681, 1615, 1601, 1472, 1437, 1311, 1240, 1208, 1192, 1170, 1139, 1100, 991, 964, 852, 827, 763, 698, 658, 635, 618.

HPLC-MS (ESI) m/z; (λ = 235 nm): Rt = 14.86 min; 380.9414 [M + H]⁺.

8-Iodo-3-methoxy-5a,10a-dihydro-11H-benzofuro[3,2-b]chromen-11-one: **12g**



C₁₆H₉IO₄
MW = 392.15 g/mol

The *general procedure C* was followed using methyl-2-hydroxy-4-iodobenzoate (0.400 g, 1.44 mmol), 2-bromo-2'-fluoro-4'-methoxyacetophenone (0.355 g, 1.44 mmol) and Cs₂CO₃ (0.769 g, 2.44 mmol) in DMF (30 mL) to get **12g** as a pink solid (0.226 g, 0.576 mmol) in 40% yield.

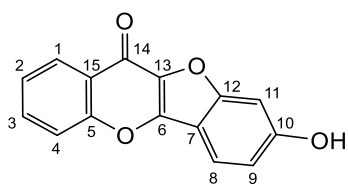
¹H NMR (500 MHz, CDCl₃) δ: 8.34 (d, J_{H-1,H-2} = 8.5 Hz, 1H, H-1), 8.05 (brd, J_{H-11,H-9} = 1.5 Hz, 1H, H-11), 7.75 (dd, J_{H-9,H-8} = 8.5 Hz, J_{H-9,H-11} = 1.5 Hz, 1H, H-9), 7.66 (d, J_{H-8,H-9} = 8.5 Hz, 1H, H-8), 7.06 (d, J_{H-4,H-2} = 2.0 Hz, 1H, H-4), 7.04 (dd, J_{H-2,H-1} = 8.5 Hz, J_{H-2,H-4} = 2.0 Hz, 1H, H-2), 3.94 (s, 3H, H-16).

¹³C NMR (126 MHz, CDCl₃) δ: 167.1 (C-14), 164.4 (C-q), 157.9 (C-q), 155.0 (C-q), 148.3 (C-q), 137.6 (C-13), 133.7 (C-9), 128.0 (C-1), 123.0 (C-11), 121.5 (C-8), 119.1 (C-q), 118.0 (C-q), 114.2 (C-2), 101.2 (C-4), 95.0 (C-10), 56.2 (C-16).

R_f = 0.54 (Cyclohexane/EtOAc, 7:3)

HRMS (ESI⁺) m/z: 392.96 [M + H]⁺.

IR ν_{max}/cm⁻¹: 1654, 1612, 1480, 1452, 1390, 1349, 1302, 1247, 1211, 1192, 1174, 1119, 1104, 980, 953, 916, 870, 847, 806, 765, 744.

8-Hydroxy-11H-benzofuro[3,2-b]chromen-11-one: 13b

$C_{15}H_8O_4$
MW = 252.23 g/mol

8-Methoxy-11H-benzofuro[3,2-b]chromen-11-one **12b** (0.300 g, 1.13 mmol, 1 eq), $AlCl_3$ (0.602 g, 4.52 mmol, 4 eq) and NaI (0.677 g, 4.52 mmol, 4 eq) were heated at 80 °C for 4 h. Then 1 M BBr_3 in CH_2Cl_2 (0.26 mL, 2.26 mmol, 2 eq) was added to a temperature of 30 °C for 1 h and left at room temperature overnight. The reaction mixture was diluted with 5% aqueous solution of $Na_2S_2O_3$ (50 mL) and extracted with CH_2Cl_2 (3×30 mL). Then dried over $MgSO_4$, filtered and evaporated *in vacuo* to obtain the crude product (0.152 g). The crude residue was purified by column chromatography on silica gel ($CH_2Cl_2/MeOH$, 9:1) to recover **13b** as a white solid (0.057 g, 0.225 mmol) in 20% yield.

Rf = 0.25 (Cyclohexane/EtOAc, 7:3)

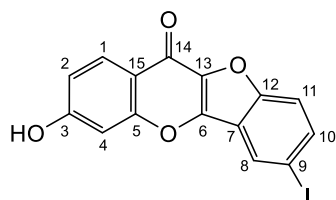
1H NMR (500 MHz, $DMSO-d_6$) δ : 10.69 (s, 1H, OH), 8.27 (d, $J_{H-1,H-2} = 8.0$ Hz, 1H, H-1), 7.90 (d, $J_{H-8,H-9} = 8.0$ Hz, 1H, H-8), 7.87–7.84 (m, 2H, H-3, H-4), 7.57 (m, 1H, H-2), 7.13 (s, 1H, H-11), 7.03 (d, $J_{H-9,H-8} = 8.0$ Hz, 1H, H-9).

^{13}C NMR (126 MHz, $DMSO-d_6$) δ : 164.8 (C-14), 161.3 (C-q), 156.6 (C-q), 155.0 (C-q), 149.4 (C-q), 135.7 (C-q), 133.5 (C-3), 125.5 (C-1), 125.1 (C-2), 124.6 (C-q), 121.4 (C-8), 118.4 (C-4), 115.0 (C-9), 109.1 (C-q), 98.6 (C-11).

MS (ESI⁻) m/z: Calculated for $C_{15}H_7O_4$ [M - H]⁻: 251.042. Found 251.034.

IR ν_{max}/cm^{-1} : 3200, 1642, 1611, 1577, 1557, 1519, 1473, 1434, 1354, 1332, 1279, 1242, 1221, 1192, 1168, 1156, 1108, 992, 955, 907, 864, 838, 809, 786, 749, 698, 684, 668, 648, 626, 607.

HPLC-MS (ESI) m/z; ($\lambda = 235$ nm): Rt = 7.41 min; 251.0343 [M - H]⁻.

3-Hydroxy-7-iodo-11H-benzofuro[3,2-b]chromen-11-one: 13e

$C_{15}H_7IO_4$
MW = 378.12 g/mol

The *general procedure D* was followed using 7-iodo-3-methoxy-11H-benzofuro[3,2-b]chromen-11-one **12e** (0.390 g, 0.995 mmol, 1 eq) and 1 M BBr_3 in CH_2Cl_2 (16 mL, 91.8 mmol, 94 eq). Finally, acetone was used to solubilize some impurities to give **13e** as a white solid (0.160 g, 0.449 mmol) in 41% yield.

Rf = 0.45 (Cyclohexane/EtOAc 7:3)

^1H NMR (500 MHz, DMSO- d_6) δ : 11.02 (s, 1H, OH), 8.41 (d, $J_{\text{H-8,H-10}} = 1.5$ Hz, 1H, H-8), 8.09 (d, $J_{\text{H-1,H-2}} = 9.0$ Hz, 1H, H-1), 7.97 (dd, $J_{\text{H-10,H-11}} = 9.0$ Hz, $J_{\text{H-10,H-8}} = 1.5$ Hz 1H, H-10), 7.69 (d, $J_{\text{H-10,H-11}} = 7.5$ Hz, 1H, H-11), 7.05 (d, $J_{\text{H-4,H-2}} = 2.0$ Hz 1H, H-4), 7.00 (dd, $J_{\text{H-2,H-1}} = 9.0$ Hz, $J_{\text{H-2,H-4}} = 2.0$ Hz 1H, H-2).

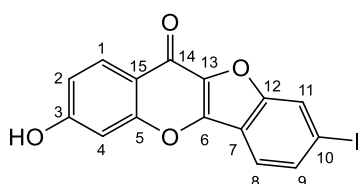
^{13}C NMR (126 MHz, DMSO- d_6) δ : 165.7 (C-14), 162.9 (C-3), 157.2 (C-5), 153.2 (C-q), 146.3 (C-q), 138.4 (C-10), 137.0 (C-q), 128.7 (C-8), 127.2 (C-1), 120.1 (C-q), 117.0 (C-q), 115.6 (C-11), 114.9 (C-2), 102.8 (C-4), 88.4 (C-9).

MS (ESI $^-$) m/z: Calculated for $\text{C}_{15}\text{H}_6\text{IO}_4$ $[\text{M} - \text{H}]^-$: 376.939. Found 376.931.

IR $\nu_{\text{max}}/\text{cm}^{-1}$: 3092, 1638, 1626, 1574, 1560, 1508, 1479, 1453, 1420, 1382, 1329, 1314, 1283, 1263, 1210, 1200, 1170, 1117, 1103, 997, 964, 925, 863, 836, 805, 764, 753, 700, 694, 652, 641, 623.

HPLC-MS (ESI) m/z; ($\lambda = 235$ nm): $R_t = 9.52$ min; 376.9304 $[\text{M} - \text{H}]^-$.

3-Hydroxy-8-iodo-5a,10a-dihydro-11H-benzofuro[3,2-b]chromen-11-one: **13g**



$\text{C}_{15}\text{H}_7\text{IO}_4$
MW = 378.12 g/mol

The *general procedure D* was followed using 7-iodo-3-methoxy-11H-benzofuro[3,2-b]chromen-11-one **12g** (0.100 g, 0.255 mmol, 1 eq) and 1 M BBr_3 in CH_2Cl_2 (10 mL). The crude was purified by flash column chromatography (Cyhex/EtOAc, 8:2) to get **13g** as a pink solid (0.009 g, 0.024 mmol) in 9% yield.

Rf = 0.45 (Cyclohexane/EtOAc 7:3)

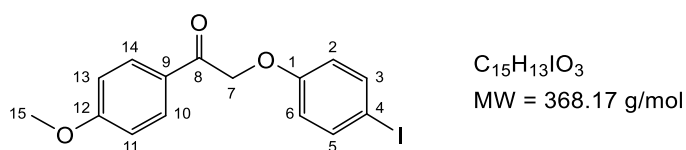
^1H NMR (500 MHz, DMSO- d_6) δ : 10.97 (s, 1H, OH), 8.37 (s, 1H, H-11), 8.12 (d, $J_{\text{H-1,H-2}} = 8.5$ Hz, 1H, H-1), 7.91–7.83 (m, 2H, H-8, H-9), 7.09 (brs, 1H, H-4), 7.02 (d, $J_{\text{H-2,H-1}} = 8.5$ Hz, 1H, H-2).

^{13}C NMR (126 MHz, DMSO- d_6) δ : 165.8 (C-14), 162.8 (C-q), 157.2 (C-q), 154.1 (C-q), 147.5 (C-q), 136.5 (C-q), 133.3 (C-9), 127.2 (C-1), 122.1 (C-11), 122.0 (C-8), 117.2 (C-q), 117.1 (C-q), 114.8 (C-2), 102.8 (C-4), 96.0 (C-10).

HRMS (ESI $^-$) m/z: Calculated for $\text{C}_{15}\text{H}_6\text{IO}_4$ $[\text{M} - \text{H}]^-$: 376.9389. Found 376.9304.

IR $\nu_{\text{max}}/\text{cm}^{-1}$: 3017, 2922, 2851, 1738, 1651, 1621, 1605, 1589, 1480, 1446, 1365, 1353, 1253, 1246, 1229, 1217, 1206, 1175, 1115, 1103, 991, 968, 919, 858, 848, 799, 768, 719.

HPLC-MS (ESI) m/z; ($\lambda = 235$ nm): $R_t = 16.84$ min; 376.9301 $[\text{M} - \text{H}]^-$.

2-(4-Iodophenoxy)-1-(4-methoxyphenyl)ethan-1-one: 14a

The *general procedure E* was followed using 4-iodophenol (0.288 g, 1.31 mmol) and K₂CO₃ (0.200 g, 1.44 mmol) in acetone (8 mL) and 2-bromo-1-(4-methoxyphenyl)ethan-1-one (0.300 g, 1.309 mmol). The crude product was triturated in ethanol to yield **14a** as a white solid (0.385 g, 1.045 mmol) in 80 % yield.

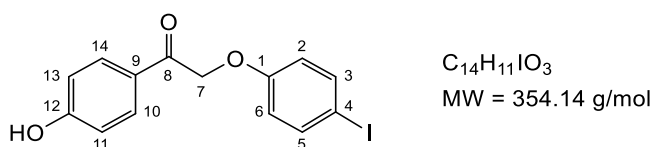
R_f = 0.67 (Cyclohexane/EtOAc, 7:3)

¹H NMR (500 MHz, DMSO-*d*₆) δ: 7.99 (d, $J_{\text{H-10,H-11}} = J_{\text{H-14,H-13}} = 9.0$ Hz, 2H, H-10, H-14), 7.58 (d, $J_{\text{H-3,H-2}} = J_{\text{H-5,H-6}} = 9.0$ Hz, 2H, H-3, H-5), 7.08 (d, $J_{\text{H-11,H-10}} = J_{\text{H-13,H-14}} = 9.0$ Hz, 2H, H-11, H-13), 6.80 (d, $J_{\text{H-2,H-3}} = J_{\text{H-6,H-5}} = 9.0$ Hz, 2H, H-2, H-6), 5.50 (s, 2H, H-7), 3.86 (s, 3H, H-15).

¹³C NMR (126 MHz, DMSO-*d*₆) δ: 192.5 (C-8), 163.6 (C-1), 158.0 (C-12), 137.8 (C-3, C-5), 130.2 (C-9), 127.2 (C-10, C-14), 117.4 (C-2, C-6), 114.0 (C-11, C-13), 83.3 (C-4), 69.9 (C-7), 55.6 (C-15).

IR $\nu_{\text{max}}/\text{cm}^{-1}$: 2932, 2841, 1685, 1605, 1586, 1575, 1511, 1485, 1436, 1419, 1399, 1290, 1257, 1174, 1115, 1092, 1061, 1027, 1009, 999, 985, 869, 844, 824, 817, 760.

HPLC-MS (ESI) m/z; ($\lambda = 235$ nm): Rt = 14.30 min; 366.9829 [M – H][–].

2-(4-Iodophenoxy)-1-(4-methoxyphenyl)ethan-1-one: 16a

The *general procedure F* was followed using sodium methylate (0.075 g, 1.359 mmol) in anhydrous THF (8 mL) and 4-iodophenol (0.205 g, 0.93 mmol). Then 2-bromo-1-(4-hydroxyphenyl)ethan-1-one was added to the mixture. Compound **16a** was obtained as a white solid (0.059 g, 0.166 mmol) in 18% yield.

R_f = 0.19 (Cyclohexane/EtOAc, 8:2)

¹H NMR (500 MHz, DMSO-*d*₆) δ: 10.4 (s, 1H, OH), 7.88 (d, $J_{\text{H-10,H-11}} = J_{\text{H-14,H-13}} = 8.5$ Hz, 2H, H-10, H-14), 7.57 (d, $J_{\text{H-3,H-2}} = J_{\text{H-5,H-6}} = 9.0$ Hz, 2H, H-3, H-5), 6.88 (d, $J_{\text{H-11,H-10}} = J_{\text{H-13,H-14}} = 8.5$ Hz, 2H, H-11, H-13), 6.79 (d, $J_{\text{H-2,H-3}} = J_{\text{H-6,H-5}} = 9.0$ Hz, 2H, H-2, H-6), 5.45 (s, 2H, H-7).

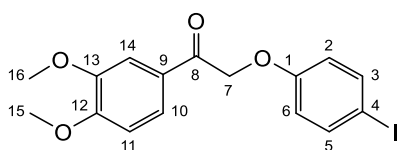
¹³C NMR (126 MHz, DMSO-*d*₆) δ: 192.2 (C-8), 162.6 (C-12), 158.0 (C-1), 137.7 (C-10, C-14), 130.4 (C-3, C-5), 125.8 (C-9), 117.4 (C-2, C-6), 115.4 (C-11, C-13), 83.3 (C-4), 69.7 (C-7).

HRMS (ESI[–]) m/z: Calculated for C₁₄H₁₂IO₃ [M – H][–]: 352.9753. Found 352.9684.

IR $\nu_{\text{max}}/\text{cm}^{-1}$: 3674, 3134, 2970, 2920, 1664, 1605, 1572, 1515, 1484, 1438, 1401, 1377, 1362, 1343, 1293, 1261, 1240, 1218, 1166, 1110, 1078, 1057, 1003, 988, 865, 838, 820, 797, 781, 721.

HPLC-MS (ESI) m/z; ($\lambda = 235$ nm): $R_t = 12.65$ min; 352.9668 [M – H][–].

2-(4-Iodophenoxy)-1-(4-methoxyphenyl)ethan-1-one: 15



$C_{16}H_{15}IO_4$
MW = 398.20 g/mol

The *general procedure E* was followed using 4-iodophenol (0.288 g, 1.31 mmol) and K_2CO_3 (0.200 g, 1.44 mmol) in acetone (8 mL) and 2-bromo-1-(3,4-dimethoxyphenyl)ethan-1-one (0.339 g, 1.309 mmol). The crude product was triturated in ethanol to yield **15** as a brown solid (0.386 g, 0.991 mmol) in 74 % yield.

Rf = 0.49 (Cyclohexane/EtOAc, 7:3)

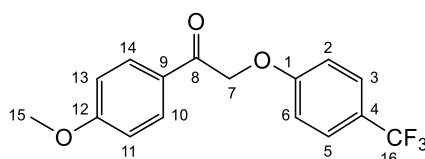
¹H NMR (500 MHz, DMSO-*d*₆) δ : 7.70 (dd, $J_{H-10,H-11} = 8.5$ Hz, $J_{H-10,H-14} = 2.0$ Hz, 1H, H-10), 7.58 (d, $J_{H-3,H-2} = J_{H-5,H-6} = 9.0$ Hz, 2H, H-3, H-5), 7.47 (d, $J_{H-14,H-10} = 2.0$ Hz, 1H, H-14), 7.11 (d, $J_{H-11,H-10} = 8.5$ Hz, 1H, H-11), 6.81 (d, $J_{H-2,H-3} = J_{H-6,H-5} = 9.0$ Hz, 2H, H-2, H-6), 5.52 (s, 2H, H-7), 3.86 (s, 3H, H-16), 3.83 (s, 3H, H-15).

¹³C NMR (126 MHz, DMSO-*d*₆) δ : 192.6 (C-8), 158.0 (C-1), 153.6 (C-12), 148.7 (C-13), 137.8 (C-3, C-5), 127.1 (C-9), 122.5 (C-10), 117.4 (C-2, C-6), 111.0 (C-11), 110.1 (C-14), 83.3 (C-4), 69.8 (C-7), 55.8 (C-16), 55.6 (C-15).

IR ν_{max}/cm^{-1} : 2923, 1682, 1585, 1510, 1485, 1468, 1419, 1350, 1267, 1228, 1205, 1167, 1152, 1080, 1061, 1018, 1008, 891, 865, 825, 801, 766.

HPLC-MS (ESI) m/z; ($\lambda = 235$ nm): $R_t = 13.56$ min; 396.9977 [M – H][–].

2-(4-Iodophenoxy)-1-(4-methoxyphenyl)ethan-1-one: 14b



$C_{16}H_{13}F_3O_3$
MW = 310.27 g/mol

The *general procedure E* was followed using 4-(trifluoromethyl)phenol (0.212 g, 1.31 mmol) and K_2CO_3 (0.200 g, 1.44 mmol) in acetone (8 mL) and 2-bromo-1-(4-methoxyphenyl)ethan-1-one (0.300 g, 1.309 mmol). The crude product was triturated in ethanol to yield **14b** as a yellow solid (0.386 g, 1.244 mmol) in 74 % yield.

Rf = 0.58 (Cyclohexane/EtOAc, 7:3)

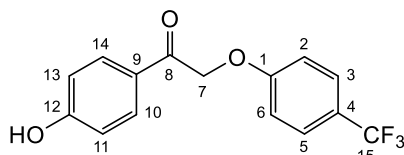
¹H NMR (500 MHz, DMSO-*d*₆) δ : 8.01 (d, $J_{H-10,H-11} = J_{H-14,H-13} = 9.0$ Hz, 2H, H-10, H-14), 7.65 (d, $J_{H-3,H-2} = J_{H-5,H-6} = 9.0$ Hz, 2H, H-3, H-5), 7.14 (d, $J_{H-11,H-10} = J_{H-13,H-14} = 9.0$ Hz, 2H, H-11, H-13), 7.10 (d, $J_{H-2,H-3} = J_{H-6,H-5} = 9.0$ Hz, 2H, H-2, H-6), 5.62 (d, 2H, H-7), 3.87 (s, 3H, H-15).

^{13}C NMR (126 MHz, DMSO- d_6) δ : 192.2 (C-8), 163.6 (C-1), 160.9 (C-12), 130.2 (C-10, C-14), 127.1 (C-3), 126.8 (C-5), 126.7 (C-9), 124.5 (q, $J_{\text{C-16,F}} = 271.5$ Hz, C-16), 121.4 (C-4), 115.2 (C-11, C-13), 114.1 (C-2, C-6), 70.0 (C-7), 55.6 (C-15).

^{19}F _{cpd} NMR (470 MHz, DMSO- d_6) δ : -59.8.

IR $\nu_{\text{max}}/\text{cm}^{-1}$: 1697, 1689, 1614, 1598, 1511, 1466, 1421, 1329, 1309, 1269, 1237, 1161, 1113, 1065, 1030, 1008, 983, 874, 833, 824, 740.

1-(4-Hydroxyphenyl)-2-(4-(trifluoromethyl)phenoxy)ethan-1-one: **16b**



$\text{C}_{15}\text{H}_{11}\text{F}_3\text{O}_3$
MW = 296.25 g/mol

The *general procedure F* was followed sodium methylate (0.075 g, 1.359 mmol) in THF (8 mL) and 4-(trifluoromethyl)phenol (0.150 g, 0.93 mmol). 2-Bromo-1-(4-hydroxyphenyl)ethan-1-one (0.200 g, 0.93 mmol) was added to the mixture. Product **16b** as a white solid (0.054 g, 0.182 mmol) in 19% yield.

Rf = 0.33 (Cyclohexane/EtOAc, 7:3)

^1H NMR (500 MHz, DMSO- d_6) δ : 10.48 (s, 1H, OH), 7.90 (d, $J_{\text{H-10,H-11}} = J_{\text{H-14,H-13}} = 8.5$ Hz, 2H, H-10, H-14), 7.63 (d, $J_{\text{H-3,H-2}} = J_{\text{H-5,H-6}} = 8.5$ Hz, 2H, H-3, H-5), 7.12 (d, $J_{\text{H-11,H-10}} = J_{\text{H-13,H-14}} = 8.5$ Hz, 2H, H-11, H-13), 6.89 (d, $J_{\text{H-2,H-3}} = J_{\text{H-6,H-5}} = 8.5$ Hz, 2H, H-2, H-6), 5.59 (s, 2H, H-7).

^{13}C NMR (126 MHz, DMSO- d_6) δ : 191.8 (C-8), 162.6 (C-1), 161.0 (C-12), 130.5 (C-10, C-14), 126.8 (C-3, C-5), 125.7 (C-9), 123.4 (q, $J_{\text{C-15,F}} = 271.1$ Hz, C-15), 121.1 (C-4), 115.4 (C-2, C-6), 115.1 (C-11, C-13), 69.8 (C-7).

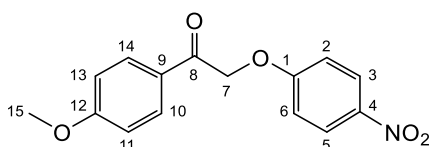
^{19}F _{cpd} NMR (470 MHz, DMSO- d_6) δ : -59.8.

HRMS (ESI⁻) m/z : Calculated for $\text{C}_{12}\text{H}_7\text{Cl}_3\text{N}_2\text{O}$ $[\text{M} - \text{H}]^-$: 295.0660. Found 295.0589.

IR $\nu_{\text{max}}/\text{cm}^{-1}$: 3147, 2931, 1670, 1607, 1573, 1518, 1439, 1423, 1378, 1331, 1310, 1293, 1217, 1168, 1107, 1063, 1011, 988, 836, 809, 774, 720.

HPLC-MS (ESI) m/z ; ($\lambda = 235$ nm): $R_t = 12.66$ min; 295.0573 $[\text{M} - \text{H}]^-$.

1-(4-Methoxyphenyl)-2-(4-nitrophenoxy)ethan-1-one: **14c**



$\text{C}_{15}\text{H}_{13}\text{NO}_5$
MW = 287.27 g/mol

The *general procedure E* was followed using 4-nitrophenol (0.182 g, 1.31 mmol) and K_2CO_3 (0.200 g, 1.44 mmol) in acetone (8 mL) and 2-bromo-1-(4-methoxyphenyl)ethan-1-one (0.300 g, 1.309 mmol). The crude product was triturated in ethanol to yield **14c** as a white solid (0.303 g, 1.054 mmol) in 90% yield.

Rf = 0.55 (Cyclohexane/EtOAc, 7:3)

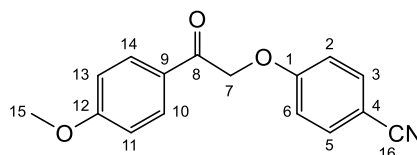
¹H NMR (500 MHz, DMSO-*d*₆) δ: 8.19 (d, $J_{\text{H-10,H-11}} = J_{\text{H-14,H-13}} = 9.5$ Hz, 2H, H-10, H-14), 8.00 (d, $J_{\text{H-3,H-2}} = J_{\text{H-5,H-6}} = 9.0$ Hz, 2H, H-3, H-5), 7.17 (d, $J_{\text{H-11,H-10}} = J_{\text{H-13,H-14}} = 9.5$ Hz, 2H, H-11, H-13), $J_{\text{H-2,H-3}} = J_{\text{H-6,H-5}} = 9.0$ Hz, 2H, H-2, H-6), 5.74 (s, 2H, H-2, H-6), 3.87 (s, 3H, H-15).

¹³C NMR (126 MHz, DMSO-*d*₆) δ: 191.8 (C-8), 163.7 (C-1), 163.4 (C-12), 141.0 (C-3, C-5), 130.3 (C-9), 127.0 (C-10, C-14), 125.7 (C-2, C-6), 115.3 (C-11, C-13), 114.1 (C-4), 70.4 (C-7), 55.6 (C-15).

IR $\nu_{\text{max}}/\text{cm}^{-1}$: 1689, 1594, 1505, 1434, 1390, 1333, 1300, 1269, 1241, 1170, 1109, 1075, 1024, 1010, 981, 878, 853, 834, 807, 751.

HPLC-MS (ESI) m/z; ($\lambda = 235$ nm): Rt = 12.61 min; 286.0711 [M - H]⁻.

4-(2-(4-Methoxyphenyl)-2-oxoethoxy)benzonitrile: 14d



C₁₆H₁₃NO₃
MW = 267.28 g/mol

The *general procedure E* was followed using 4-cyanophenol (0.156 g, 1.31 mmol) and K₂CO₃ (0.200 g, 1.44 mmol) in acetone (8 mL) and 2-bromo-1-(4-methoxyphenyl)ethan-1-one (0.300 g, 1.309 mmol). The crude product was triturated in ethanol to yield **14d** as a white solid (0.243 g, 0.845 mmol) in 70 % yield.

Rf = 0.45 (Cyclohexane/EtOAc, 7:3)

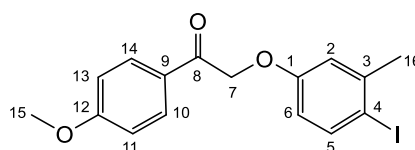
¹H NMR (500 MHz, DMSO-*d*₆) δ: 8.00 (d, $J_{\text{H-10,H-11}} = J_{\text{H-14,H-13}} = 9.0$ Hz, 2H, H-10, H-14), 7.77 (d, $J_{\text{H-3,H-2}} = J_{\text{H-5,H-6}} = 9.0$ Hz, 2H, H-3, H-5), 7.14 (d, $J_{\text{H-11,H-10}} = J_{\text{H-13,H-14}} = 9.0$ Hz, 2H, H-11, H-13), 7.10 (d, $J_{\text{H-2,H-3}} = J_{\text{H-6,H-5}} = 9.0$ Hz, 2H, H-2, H-6), 5.68 (s, 2H, H-7), 3.87 (s, 3H, H-15).

¹³C NMR (126 MHz, DMSO-*d*₆) δ: 192.0 (C-8), 163.7 (C-12), 161.6 (C-1), 134.0 (C-3, C-5), 130.2 (C-10, C-14), 127.0 (C-9), 119.1 (C-16), 115.8 (C-11, C-13), 114.1 (C-2, C-6), 103.0 (C-4), 70.0 (C-7), 55.6 (C-15).

IR $\nu_{\text{max}}/\text{cm}^{-1}$: 2225, 1676, 1600, 1510, 1443, 1418, 1374, 1319, 1307, 1267, 1256, 1236, 1187, 1171, 1119, 1075, 1030, 1013, 973, 843, 826, 816, 774.

HPLC-MS (ESI) m/z; ($\lambda = 235$ nm): Rt = 12.02 min; 266.0812 [M - H]⁻.

2-(4-Iodo-3-methylphenoxy)-1-(4-methoxyphenyl)ethan-1-one: 14e



C₁₆H₁₅IO₃
MW = 382.20 g/mol

The *general procedure E* was followed using 4-iodo-3-methylphenol (0.306 g, 1.31 mmol) and K₂CO₃ (0.200 g, 1.44 mmol) in acetone (8 mL) and 2-bromo-1-(4-methoxyphenyl) ethanone

(0.300 g, 1.309 mmol). The crude product was triturated in ethanol to yield **14e** as a white solid (0.243 g, 0.635 mmol) in 52 % yield.

R_f = 0.67 (Cyclohexane/EtOAc, 7:3)

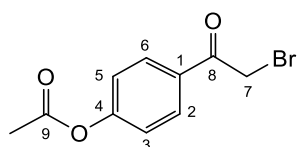
¹H NMR (500 MHz, DMSO-*d*₆) δ: 8.00 (d, *J*_{H-10,H-11} = *J*_{H-14,H-13} = 9.0 Hz, 2H, H-10, H-14), 7.66 (d, *J*_{H-5,H-6} = 8.5 Hz, 1H, H-5), 7.09 (d, *J*_{H-11,H-10} = *J*_{H-13,H-14} = 9.0 Hz, 2H, H-11, H-13), 7.02 (d, *J*_{H-2,H-6} = 3.0 Hz, 1H, H-2), 6.60 (dd, *J*_{H-6,H-5} = 8.5 Hz, *J*_{H-6,H-2} = 3.0 Hz, 1H, H-6), 5.49 (s, 2H, H-7), 3.87 (s, 3H, H-15), 2.32 (s, 3H, H-16).

¹³C NMR (126 MHz, DMSO-*d*₆) δ: 192.6 (C-8), 163.6 (C-12), 158.4 (C-1), 141.7 (C-4), 138.9 (C-2), 130.2 (C-10, C-14), 127.2 (C-9), 116.7 (C-5), 114.5 (C-11, C-13), 114.0 (C-6), 90.0 (C-4), 69.8 (C-7), 55.6 (C-15), 27.5 (C-16).

IR ν_{max}/cm⁻¹: 1686, 1600, 1565, 1514, 1473, 1458, 1431, 1324, 1290, 1271, 1238, 1176, 1152, 1118, 1098, 1031, 1011, 985, 933, 861, 825, 816, 792.

HPLC-MS (ESI) m/z; (λ = 235 nm): Rt = 15.01 min; 380.9977 [M - H]⁻.

4-(2-Bromoacetyl)phenyl acetate: 17



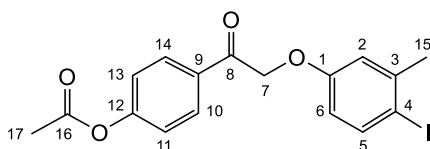
C₁₀H₉BrO₃
MW = 257.08 g/mol

The *general procedure G* was followed using 2-bromo-1-(4-hydroxyphenyl)ethan-1-one (5.00 g, 23.57 mmol), acetic anhydride (28 mL) and concentrated HCl (13 drops). Crystallization in pentane and recrystallization in water afford the product **17** as a white solid (5.68 g, 0.221 mol) in 94% yield.

R_f = 0.56 (Cyclohexane/EtOAc, 7:3)

¹H NMR (500 MHz, DMSO-*d*₆) δ: 8.06 (d, *J*_{H-2,H-3} = *J*_{H-6,H-5} = 8.5 Hz, 2H, H-2, H-6), 7.33 (d, *J*_{H-3,H-2} = *J*_{H-5,H-6} = 8.5 Hz, 2H, H-3, H-5), 5.91 (s, 2H, H-7), 2.31 (s, 3H, H-10).

4-(2-(4-Iodo-3-methylphenoxy)acetyl)phenyl acetate: 18a



C₁₇H₁₅I O₄
MW = 410.21 g/mol

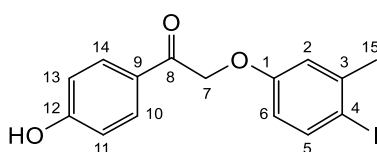
The *general procedure E* was followed using 4-iodo-3-methylphenol (0.315 g, 1.35 mmol) and K₂CO₃ (0.205 g, 1.48 mmol) in acetone (8 mL) and the acetate **17** (0.345 g, 1.35 mmol). The crude residue was purified by column chromatography on silica gel (Cyclohexane/EtOAc, 7:3) to obtain **18a** as a white solid (0.157 g, 0.382 mmol) in 28 % yield.

R_f = 0.54 (Cyclohexane/EtOAc, 7:3)

¹H NMR (500 MHz, DMSO-*d*₆) δ : 8.07 (d, $J_{\text{H-10,H-11}} = J_{\text{H-14,H-13}} = 8.5$ Hz, 2H, H-10, H-14), 7.66 (d, $J_{\text{H-5,H-6}} = 8.5$ Hz, 1H, H-5), 7.33 (d, $J_{\text{H-11,H-10}} = J_{\text{H-13,H-14}} = 8.5$ Hz, 2H, H-11, H-13), 7.04 (d, $J_{\text{H-2,H-6}} = 3.0$ Hz, 1H, H-2), 6.62 (dd, $J_{\text{H-6,H-5}} = 8.5$ Hz, $J_{\text{H-6,H-2}} = 3.0$ Hz, 1H, H-6), 5.56 (s, 2H, H-7), 2.32 (s, 3H, H-17), 2.31 (s, 3H, H-15).

¹³C NMR (126 MHz, DMSO-*d*₆) δ : 193.4 (C-8), 169.0 (C-16), 158.3 (C-1), 154.6 (C-12), 141.9 (C-3), 139.0 (C-5), 132.0 (C-9), 129.7 (C-10, C-14), 122.4 (C-11, C-13), 116.7 (C-2), 114.6 (C-6), 90.2 (C-4), 70.1 (C-7), 27.6 (C-17), 21.0 (C-15).

4-(2-(4-Iodo-3-methylphenoxy)acetyl)phenyl acetate: **19a**



$\text{C}_{15}\text{H}_{13}\text{IO}_3$
MW = 368.17 g/mol

The *general procedure H* was followed using **18a** (0.157 g, 0.38 mmol) in EtOH (6 mL) and NaOAc (0.314 g, 3.83 mmol) in water (1 mL). The crude residue was purified by column chromatography (Cyclohexane/EtOAc, 9:1) on silica gel to yield **19a** as a white solid (0.100 g, 0.271 mmol) in 71% yield.

Rf = 0.33 (Cyclohexane/EtOAc, 7:3)

¹H NMR (500 MHz, DMSO-*d*₆) δ : 10.45 (s, 1H, OH), 7.88 (d, $J_{\text{H-10,H-11}} = J_{\text{H-14,H-13}} = 7.5$ Hz, 2H, H-10, H-14), 7.64 (d, $J_{\text{H-5,H-6}} = 9.0$ Hz, 1H, H-5), 6.99 (s, 1H, H-2), 6.88 (d, $J_{\text{H-11,H-10}} = J_{\text{H-13,H-14}} = 7.5$ Hz, 2H, H-11, H-13), 6.58 (dd, $J_{\text{H-6,H-5}} = 9.0$ Hz, $J = 3.0$ Hz, 1H, H-6), 5.43 (s, 2H, H-7), 2.31 (s, 3H, H-15).

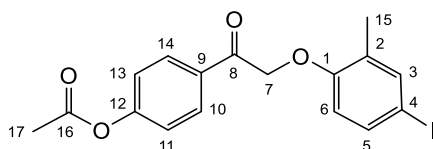
¹³C NMR (126 MHz, DMSO-*d*₆) δ : 192.2 (C-8), 162.5 (C-12), 158.4 (C-1), 141.7 (C-3), 138.9 (C-5), 130.4 (C-10, C-14), 125.9 (C-9), 116.7 (C-2), 115.5 (C-11, C-13), 114.5 (C-6), 90.0 (C-4), 70.0 (C-7), 27.5 (C-15).

HRMS (ESI⁻) m/z : Calculated for $\text{C}_{15}\text{H}_{12}\text{IO}_3$ $[\text{M} - \text{H}]^-$: 366.9909. Found 366.9836.

IR $\nu_{\text{max}}/\text{cm}^{-1}$: 3160, 1664, 1604, 1571, 1515, 1471, 1437, 1405, 1376, 1291, 1241, 1221, 1165, 1140, 1091, 1013, 988, 933, 878, 836, 818, 787.

HPLC-MS (ESI) m/z ; ($\lambda = 235$ nm): $R_t = 13.26$ min; 366.9804 $[\text{M} - \text{H}]^-$.

4-(2-(4-Iodo-2-methylphenoxy)acetyl)phenyl acetate: **18b**



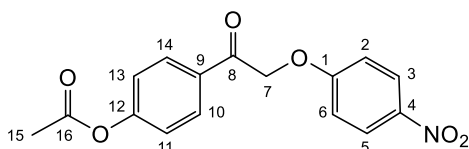
$\text{C}_{17}\text{H}_{15}\text{IO}_4$
MW = 410.21 g/mol

The *general procedure E* was followed using 4-iodo-2-methylphenol (0.315 g, 1.35 mmol) and K_2CO_3 (0.205 g, 1.48 mmol) in acetone (8 mL) then the acetate **17** (0.345 g, 1.35 mmol). The crude residue was purified by column chromatography on silica gel (Cyclohexane/EtOAc, 7:3) to obtain **18b** as a white solid (0.259 g, 0.631 mmol) in 47% yield.

Rf = 0.60 (Cyclohexane/EtOAc, 7:3)

¹H NMR (500 MHz, DMSO-*d*₆) δ: 8.07 (d, $J_{\text{H-10,H-11}} = J_{\text{H-14,H-13}} = 8.5$ Hz, 2H, H-10, H-14), 7.51 (dd, $J_{\text{H-3,H-5}} = 2.0$ Hz, $J = 0.5$ Hz, 1H, H-3), 7.42 (dd, $J_{\text{H-5,H-6}} = 8.5$ Hz, $J_{\text{H-5,H-3}} = 2.0$ Hz, 1H, H-5), 7.34 (d, $J_{\text{H-11,H-10}} = J_{\text{H-13,H-14}} = 8.5$ Hz, 2H, H-11, H-13), 6.75 (d, $J_{\text{H-6,H-5}} = 8.5$ Hz, 1H, H-6), 5.60 (s, 2H, H-7), 2.32 (s, 3H, H-17), 2.20 (s, 3H, H-15).

4-(2-(4-Nitrophenoxy)acetyl)phenyl acetate: 18c



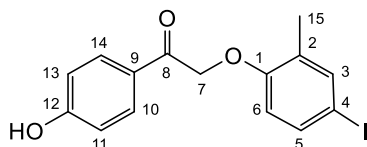
C₁₆H₁₃NO₆
MW = 315.28 g/mol

The *general procedure E* was followed using 4-nitrophenol (0.187 g, 1.35 mmol) and K₂CO₃ (0.205 g, 1.48 mmol) in acetone (8 mL) then the acetate **17** (0.345 g, 1.35 mmol). The crude residue was purified by column chromatography on silica gel (Cyclohexane/EtOAc, 8:2) to obtain **18c** as a yellow-white solid (0.211 g, 0.669 mmol) in 50% yield.

Rf = 0.28 (Cyclohexane/EtOAc, 7:3)

¹H NMR (500 MHz, DMSO-*d*₆) δ: 8.20 (d, $J_{\text{H-3,H-2}} = J_{\text{H-5,H-6}} = 9.0$ Hz, 2H, H-3, H-5), 8.09 (d, $J_{\text{H-10,H-11}} = J_{\text{H-14,H-13}} = 8.5$ Hz, 2H, H-10, H-14), 7.36 (d, $J_{\text{H-11,H-10}} = J_{\text{H-13,H-14}} = 8.5$ Hz, 2H, H-11, H-13), 7.20 (d, $J_{\text{H-2,H-3}} = J_{\text{H-6,H-5}} = 9.0$ Hz, 2H, H-2, H-6), 5.82 (s, 2H, H-7), 2.32 (s, 3H, H-15).

4-(2-(4-Iodo-2-methylphenoxy)acetyl)phenyl acetate: 19b



C₁₅H₁₃I₃O₃
MW = 368.17 g/mol

The *general procedure H* was followed using **18b** (0.259 g, 0.631 mmol) in EtOH (8 mL) and NaOAc (0.517 g, 6.31 mmol) in water (1 mL). The crude residue was purified by column chromatography on silica gel (Cyclohexane/EtOAc, 7:3) to yield **19b** as a white solid (0.078 g, 0.211 mmol) in 34% yield.

Rf = 0.54 (Cyclohexane/EtOAc, 6:4)

¹H NMR (500 MHz, DMSO-*d*₆) δ: 10.45 (s, 1H, OH), 7.88 (d, $J_{\text{H-10,H-11}} = J_{\text{H-14,H-13}} = 8.5$ Hz, 2H, H-10, H-14), 7.49 (d, $J = 1.5$ Hz, 1H, H-3), 7.40 (dd, $J_{\text{H-5,H-6}} = 8.5$ Hz, $J_{\text{H-5,H-3}} = 1.5$ Hz, 1H, H-5), 6.88 (d, $J_{\text{H-11,H-10}} = J_{\text{H-13,H-14}} = 8.5$ Hz, 2H, H-11, H-13), 6.67 (d, $J_{\text{H-6,H-5}} = 8.5$ Hz, 1H, H-6), 5.46 (s, 2H, H-7), 2.18 (s, 3H, H-15).

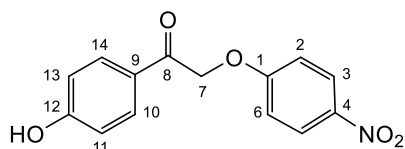
¹³C NMR (126 MHz, DMSO-*d*₆) δ: 192.4 (C-8), 162.6 (C-12), 156.2 (C-1), 138.5 (C-5), 135.1 (C-3), 130.4 (C-10, C-14), 129.1 (C-9), 125.9 (C-2), 115.3 (C-11, C-13), 114.2 (C-6), 83.2 (C-4), 70.0 (C-7), 16.0 (C-15).

HRMS (ESI⁻) m/z: Calculated for C₁₅H₁₂O₃ [M - H]⁻: 366.9909. Found 366.9837.

IR $\nu_{\max}/\text{cm}^{-1}$: 3202, 1665, 1602, 1574, 1518, 1488, 1438, 1369, 1305, 1286, 1248, 1222, 1191, 1172, 1152, 1137, 979, 877, 842, 816, 802, 742, 718.

HPLC-MS (ESI) m/z; ($\lambda = 235$ nm): Rt = 13.62 min; 366.9804 [M - H]⁻.

1-(4-Hydroxyphenyl)-2-(4-nitrophenoxy)ethan-1-one: 19c



C₁₄H₁₁NO₅
MW = 273.24 g/mol

The *general procedure H* was followed using **18c** (0.211 g, 0.669 mmol) in EtOH (7 mL) and NaOAc (0.549 g, 6.69 mmol) in water (1 mL). The crude residue was purified by column chromatography on silica gel (Cyclohexane/EtOAc, 7:3) to yield **19c** as a white solid (0.088 g, 0.322 mmol) in 48% yield.

Rf = 0.30 (Cyclohexane/EtOAc, 6:4)

¹H NMR (500 MHz, DMSO-*d*₆) δ : 10.50 (s, 1H, OH), 8.19 (d, $J_{\text{H-3,H-2}} = J_{\text{H-5,H-6}} = 9.0$ Hz, 2H, H-3, H-5), 7.90 (d, $J_{\text{H-10,H-11}} = J_{\text{H-14,H-13}} = 9.0$ Hz, 2H, H-10, H-14), 7.15 (d, $J_{\text{H-2,H-3}} = J_{\text{H-6,H-5}} = 9.0$ Hz, 2H, H-2, H-6), 6.90 (d, $J_{\text{H-11,H-10}} = J_{\text{H-13,H-14}} = 9.0$ Hz, 2H, H-11, H-13), 5.70 (s, 2H, H-7).

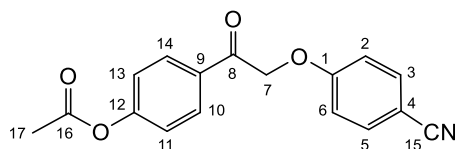
¹³C NMR (126 MHz, DMSO-*d*₆) δ : 191.4 (C-8), 163.5 (C-12), 162.7 (C-1), 140.9 (C-4), 130.5 (C-10, C-14), 125.7 (C-3, C-5), 125.6 (C-9), 115.4 (C-11, C-13), 115.2 (C-2, C-6), 70.3 (C-7).

HRMS (ESI⁻) m/z: Calculated for C₁₄H₁₀NO₅ [M - H]⁻: 272.0637. Found 272.0561.

IR $\nu_{\max}/\text{cm}^{-1}$: 3371, 1675, 1596, 1507, 1446, 1428, 1380, 1331, 1299, 1275, 1250, 1237, 1175, 1108, 1072, 986, 879, 843, 752.

HPLC-MS (ESI) m/z; ($\lambda = 235$ nm): Rt = 10.88 min; 272.0554 [M - H]⁻.

4-(2-(4-Cyanophenoxy)acetyl)phenyl acetate: 18d

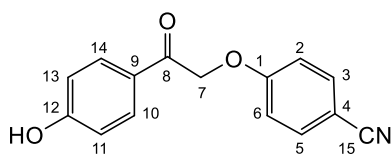


C₁₇H₁₃NO₄
MW = 295.29 g/mol

The *general procedure E* was followed using 4-cyanophenol (0.160 g, 1.35 mmol) and K₂CO₃ (0.205 g, 1.48 mmol) in acetone (8 mL) then the acetate **17** (0.345 g, 1.35 mmol). The crude residue was purified by column chromatography on silica gel (Cyclohexane/EtOAc, 7:3) to get **18d** as a white solid (0.226 g, 0.765 mmol) in 57% yield.

Rf = 0.50 (Cyclohexane/EtOAc, 6:4)

¹H NMR (500 MHz, DMSO-*d*₆) δ : 8.08 (d, $J_{\text{H-10,H-11}} = J_{\text{H-14,H-13}} = 8.5$ Hz, 2H, H-10, H-14), 7.76 (d, $J_{\text{H-3,H-2}} = J_{\text{H-5,H-6}} = 8.5$ Hz, 2H, H-3, H-5), 7.35 (d, $J_{\text{H-11,H-10}} = J_{\text{H-13,H-14}} = 8.5$ Hz, 2H, H-11, H-13), 7.16 (d, $J_{\text{H-2,H-3}} = J_{\text{H-6,H-5}} = 8.5$ Hz, 1H, H-2, H-6), 5.74 (s, 1H, H-7), 2.31 (s, 3H, H-17).

4-(2-(4-Hydroxyphenyl)-2-oxoethoxy)benzonitrile: 19d

$C_{15}H_{11}NO_3$
MW = 253.26 g/mol

The *general procedure H* was followed using **18d** (0.224 g, 0.758 mmol) in EtOH (8 mL) and NaOAc (0.622 g, 7.58 mmol) in water (1 mL). The crude residue was purified by column chromatography on silica gel (Cyclohexane/EtOAc, 7:3) to yield **19d** as a white solid (0.126 g, 0.497 mmol) in 66% yield.

Rf = 0.32 (Cyclohexane/EtOAc, 6:4)

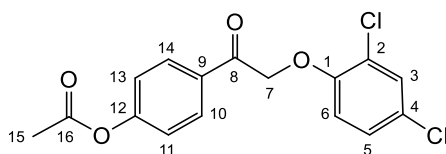
1H NMR (500 MHz, DMSO- d_6) δ : 10.48 (s, 1H, OH), 7.89 (d, $J_{H-3,H-2} = J_{H-5,H-6} = 9.0$ Hz, 2H, H-3, H-5), 7.75 (d, $J_{H-10,H-11} = J_{H-14,H-13} = 9.0$ Hz, 2H, H-10, H-14), 7.11 (d, $J_{H-2,H-3} = J_{H-6,H-5} = 9.0$ Hz, 2H, H-2, H-6), 6.89 (d, $J_{H-11,H-10} = J_{H-13,H-14} = 9.0$ Hz, 2H, H-11, H-13), 5.62 (s, 2H, H-7).

^{13}C NMR (126 MHz, DMSO- d_6) δ : 191.6 (C-8), 162.7 (C-12), 161.6 (C-1), 134.0 (C-10, C-14), 130.5 (C-3, C-5), 125.7 (C-9), 119.1 (C-16), 115.7 (C-11, C-13), 115.4 (C-2, C-6), 103.0 (C-4), 70.0 (C-7).

HRMS (ESI $^-$) m/z: Calculated for $C_{15}H_{10}NO_3$ [M - H] $^-$: 252.0739. Found 252.0664.

IR ν_{max}/cm^{-1} : 3275, 2923, 2230, 1692, 1604, 1584, 1507, 1439, 1420, 1386, 1366, 1304, 1288, 1269, 1223, 1169, 1116, 1082, 983, 873, 852, 823, 810.

HPLC-MS (ESI) m/z; ($\lambda = 235$ nm): Rt = 10.15 min; 252.0739 [M - H] $^-$.

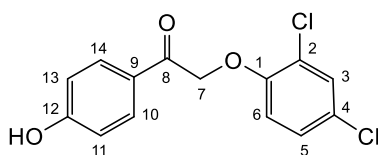
4-(2-(2,4-Dichlorophenoxy)acetyl)phenyl acetate: 18e

$C_{16}H_{12}Cl_2O_4$
MW = 339.17 g/mol

The *general procedure E* was followed using 2,4-dichlorophenol (0.219 g, 1.35 mmol) and K_2CO_3 (0.205 g, 1.48 mmol) in acetone (8 mL) and the acetate **17** (0.345 g, 1.35 mmol). The crude residue was recrystallized in water to get the product **18e** as a white solid (0.236 g, 0.696 mmol) in 52% yield.

Rf = 0.50 (Cyclohexane/EtOAc, 6:4)

1H NMR (500 MHz, DMSO- d_6) δ : 8.07 (d, $J_{H-10,H-11} = J_{H-14,H-13} = 8.5$ Hz, 2H, H-10, H-14), 7.59 (d, $J_{H-3,H-5} = 2.5$ Hz, 1H, H-3), 7.35 (d, $J_{H-11,H-10} = J_{H-13,H-14} = 9.0$ Hz, 2H, H-11, H-13), 7.31 (dd, $J_{H-5,H-6} = 9.0$ Hz, $J_{H-5,H-3} = 2.5$ Hz, 1H, H-5), 7.12 (d, $J_{H-6,H-5} = 9.0$ Hz, 1H, H-6) 5.75 (s, 2H, H-7), 2.31 (s, 3H, H-15).

2-(2,4-Dichlorophenoxy)-1-(4-hydroxyphenyl)ethan-1-one: 19e

$C_{14}H_{10}Cl_2O_3$
MW = 297.13 g/mol

The *general procedure H* was followed using the acetate **18e** (0.236 g, 0.696 mmol) in EtOH (8 mL) and NaOAc (0.570 g, 6.958 mmol) in water (1 mL). The crude residue was purified by column chromatography on silica gel (Cyclohexane/EtOAc, 7:3) to yield **19e** as a white solid (0.127 g, 0.427 mmol) in 62% yield.

R_f = 0.24 (Cyclohexane/EtOAc, 7:3)

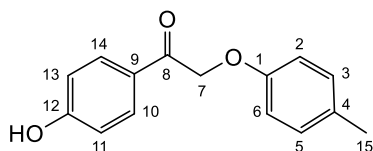
¹H NMR (500 MHz, DMSO-*d*₆) δ: 10.48 (s, 1H, OH), 7.88 (d, $J_{H-10,H-11} = J_{H-14,H-13} = 8.5$ Hz, 2H, H-10, H-14), 7.58 (d, $J_{H-3,H-5} = 2.5$ Hz, 1H, H-3), 7.30 (dd, $J_{H-5,H-6} = 9.0$ Hz, $J_{H-5,H-3} = 2.5$ Hz, 1H, H-5), 7.03 (d, $J_{H-6,H-5} = 9.0$ Hz, 1H, H-6), 6.89 (d, $J_{H-11,H-10} = J_{H-13,H-14} = 8.5$ Hz, 2H, H-11, H-13), 5.63 (s, 2H, H-7).

¹³C NMR (126 MHz, DMSO-*d*₆) δ: 191.6 (C-8), 162.7 (C-12), 152.6 (C-1), 130.4 (C-10, C-14), 129.2 (C-3), 127.8 (C-5), 125.6 (C-9), 124.5 (C-2), 122.1 (C-4), 115.3 (C-11, C-13), 115.2 (C-6), 70.5 (C-7).

HRMS (ESI⁻) m/z: Calculated for C₁₄H₉Cl₂O₃ [M - H]⁻: 295.0007. Found 294.9934.

IR ν_{max}/cm⁻¹: 3265, 2920, 1675, 1602, 1576, 1516, 1484, 1436, 1391, 1365, 1287, 1248, 1217, 1174, 1103, 1087, 1056, 989, 857, 833, 808, 793, 741, 721.

HPLC-MS (ESI) m/z; (λ = 235 nm): Rt = 13.02 min; 294.9921 [M - H]⁻.

1-(4-Hydroxyphenyl)-2-(*p*-tolylloxy)ethan-1-one: 19f

$C_{15}H_{14}O_3$
MW = 242.27 g/mol

The *general procedure E* was followed using *p*-cresol (0.085 g, 1.35 mmol) and K₂CO₃ (0.205 g, 1.48 mmol) in acetone (8 mL) and the acetate **17** (0.200 g, 0.781 mmol). The crude residue was purified by column chromatography on silica gel (Cyclohexane/EtOAc, 7:3) to yield **19f** as a white solid (0.226 g, 0.933 mmol) in 57% yield.

R_f = 0.25 (Cyclohexane/EtOAc, 7:3)

¹H NMR (500 MHz, DMSO-*d*₆) δ: 10.43 (s, 1H, OH), 7.89 (d, $J_{H-10,H-11} = J_{H-14,H-13} = 9.0$ Hz, 2H, H-10, H-14), 7.06 (d, $J_{H-3,H-2} = J_{H-5,H-6} = 9.0$ Hz, 2H, H-3, H-5), 6.88 (d, $J_{H-11,H-10} = J_{H-13,H-14} = 9.0$ Hz, 2H, H-11, H-13), 6.81 (d, $J_{H-2,H-3} = J_{H-6,H-5} = 9.0$ Hz, 2H, H-2, H-6), 5.36 (s, 2H, H-7), 2.22 (s, 3H, H-16).

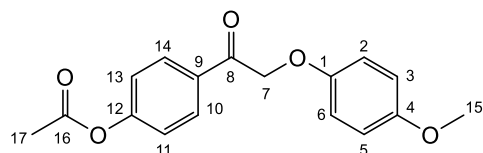
¹³C NMR (126 MHz, DMSO-*d*₆) δ: 192.7 (C-8), 162.4 (C-12), 155.9 (C-1), 130.4 (C-10, C-14), 129.6 (C-3, C-5), 129.3 (C-9), 126.0 (C-4), 115.3 (C-11, C-13), 114.3 (C-2, C-6), 70.0 (C-7), 20.0 (C-15).

HRMS (ESI⁻) m/z: Calculated for C₁₅H₁₃O₃ [M - H]⁻: 241.0943. Found 241.0687.

IR $\nu_{\max}/\text{cm}^{-1}$: 3287, 2922, 1705, 1673, 1605, 1578, 1512, 1434, 1378, 1296, 1229, 1169, 1109, 1089, 989, 877, 839, 824, 814, 801.

HPLC-MS (ESI) m/z ; ($\lambda = 235 \text{ nm}$): $R_t = 11.45 \text{ min}$; 241.0850 $[M - H]^-$.

4-(2-(4-Methoxyphenoxy)acetyl)phenyl acetate: **18g**



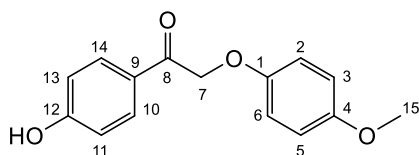
$\text{C}_{17}\text{H}_{16}\text{O}_5$
MW = 300.31 g/mol

The *general procedure E* was followed using 4-methoxyphenol (0.145 g, 1.17 mmol) and K_2CO_3 (0.178 g, 1.29 mmol) in acetone (7 mL) and the acetate **17** (0.300 g, 1.17 mmol). The crude residue was recrystallized in water to obtain the product **18g** as a white solid (0.095 g, 0.316 mmol) in 27% yield.

$R_f = 0.36$ (Cyclohexane/EtOAc, 7:3)

$^1\text{H NMR}$ (500 MHz, $\text{DMSO-}d_6$) δ : 8.07 (d, $J_{\text{H-10,H-11}} = J_{\text{H-14,H-13}} = 8.5 \text{ Hz}$, 2H, H-10, H-14), 7.33 (d, $J_{\text{H-11,H-10}} = J_{\text{H-13,H-14}} = 8.5 \text{ Hz}$, 2H, H-11, H-13), 6.91 (d, $J_{\text{H-3,H-2}} = J_{\text{H-5,H-6}} = 9.5 \text{ Hz}$, 2H, H-3, H-5), 6.84 (d, $J_{\text{H-2,H-3}} = J_{\text{H-6,H-5}} = 9.0 \text{ Hz}$, 2H, H-2, H-6), 5.47 (s, 2H, H-7), 3.69 (s, 3H, H-15), 2.31 (s, 3H, H-17).

1-(4-Hydroxyphenyl)-2-(4-methoxyphenoxy)ethan-1-one: **19g**



$\text{C}_{15}\text{H}_{14}\text{O}_4$
MW = 258.27 g/mol

The *general procedure H* was followed using acetate **18g** (0.095 g, 0.316 mmol) in EtOH (5 mL) and NaOAc (0.259 g, 3.16 mmol) in water (1 mL). The crude residue was purified by column chromatography on silica gel (Cyclohexane/EtOAc, 7:3) to yield **19g** as a white solid (0.047 g, 0.181 mmol) in 58% yield.

$R_f = 0.22$ (Cyclohexane/EtOAc, 7:3)

$^1\text{H NMR}$ (500 MHz, $\text{DMSO-}d_6$) δ : 10.43 (s, 1H, OH), 7.89 (d, $J_{\text{H-10,H-11}} = J_{\text{H-14,H-13}} = 9.0 \text{ Hz}$, 2H, H-10, H-14), 6.88-6.82 (m, 6H, H-11, H-13, H-2, H-6, H-3, H-5), 5.33 (s, 2H, H-7), 3.69 (s, 3H, H-15).

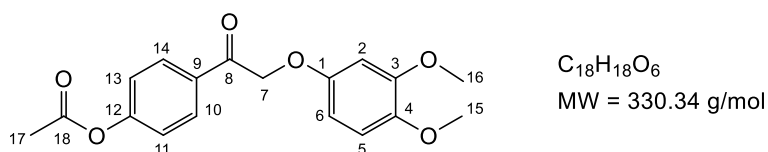
$^{13}\text{C NMR}$ (126 MHz, $\text{DMSO-}d_6$) δ : 192.8 (C-8), 162.4 (C-12), 153.5 (C-1), 152.0 (C-4), 130.4 (C-10, C-14), 126.0 (C-9), 115.4 (C-11, C-13), 115.3 (C-3, C-5), 114.5 (C-2, C-6), 70.3 (C-7), 55.3 (C-16).

HRMS (ESI $^-$) m/z : Calculated for $\text{C}_{15}\text{H}_{13}\text{O}_4$ $[M - H]^-$: 257.0892. Found 257.0818.

IR $\nu_{\max}/\text{cm}^{-1}$: 3172, 1672, 1604, 1577, 1508, 1466, 1445, 1383, 1362, 1288, 1250, 1226, 1171, 1109, 1087, 1039, 1007, 990, 872, 842, 812, 773, 722.

HPLC-MS (ESI) m/z; ($\lambda = 235$ nm): $R_t = 10.46$ min; 257.0805 [M - H]⁻.

4-(2-(4-Methoxyphenoxy)acetyl)phenyl acetate: 18h



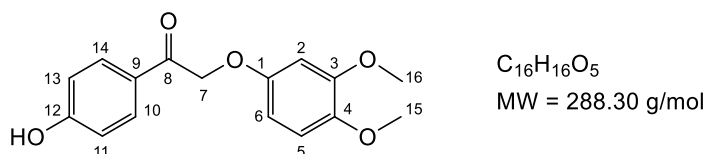
The *general procedure E* was followed using 3,4-dimethoxyphenol (0.300 g, 1.17 mmol) and K_2CO_3 (0.178 g, 1.29 mmol) in acetone (7 mL) and the acetate **17** (0.300 g, 1.17 mmol). The crude residue was purified by column chromatography on silica gel (Cyclohexane/EtOAc, 7:3) to get **18h** as a white solid (0.153 g, 0.463 mmol) in 43% yield.

$R_f = 0.27$ (Cyclohexane/EtOAc, 7:3)

1H NMR (500 MHz, DMSO- d_6) δ : 8.08 (d, $J_{H-10,H-11} = J_{H-14,H-13} = 8.5$ Hz, 2H, H-10, H-14), 7.33 (d, $J_{H-11,H-10} = J_{H-13,H-14} = 8.5$ Hz, 2H, H-11, H-13), 6.83 (d, $J_{H-5,H-6} = 8.5$ Hz, 1H, H-5), 6.66 (d, $J_{H-2,H-6} = 2.5$ Hz, 1H, H-2), 6.45 (dd, $J_{H-6,H-5} = 8.5$ Hz, $J_{H-6,H-2} = 2.5$ Hz, 1H, H-6), 5.46 (s, 2H, H-7), 3.74 (s, 3H, H-16), 3.68 (s, 3H, H-15), 2.31 (s, 3H, H-17).

^{13}C NMR (126 MHz, DMSO- d_6) δ : 193.8 (C-8), 168.8 (C-18), 154.4 (C-12), 152.4 (C-1), 149.6 (C-3), 143.4 (C-4), 132.1 (C-9), 129.6 (C-10, C-14), 122.2 (C-11, C-13), 112.7 (C-5), 104.5 (C-6), 101.1 (C-2), 70.6 (C-7), 56.1 (C-15), 55.5 (C-16), 20.8 (C-17).

4-(2-(4-Hydroxyphenyl)-2-oxoethoxy)benzonitrile: 19h



The *general procedure H* was followed using the acetate **18h** (0.253 g, 0.877 mmol) in EtOH (7 mL) and NaOAc (0.719 g, 8.77 mmol) in water (1 mL). The crude residue was purified by column chromatography on silica gel (Cyclohexane/EtOAc, 7:3) to yield **19h** as a white solid (0.103 g, 0.357 mmol) in 37% yield.

$R_f = 0.5$ (Cyclohexane/EtOAc, 6:4)

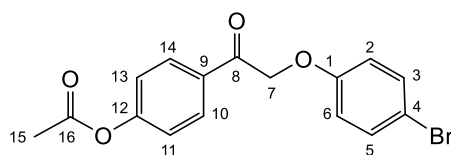
1H NMR (500 MHz, DMSO- d_6) δ : 10.43 (s, 1H, OH), 7.90 (d, $J_{H-10,H-11} = J_{H-14,H-13} = 8.0$ Hz, 2H, H-10, H-14), 6.88 (d, $J_{H-11,H-10} = J_{H-13,H-14} = 7.5$ Hz, 2H, H-11, H-13), 6.82 (d, $J_{H-5,H-6} = 9.0$ Hz, 1H, H-5), 6.63 (d, $J_{H-2,H-6} = 1.5$ Hz, 1H, H-2), 6.41 (dd, $J_{H-6,H-5} = 9.0$ Hz, $J_{H-6,H-2} = 1.5$ Hz, 1H, H-6), 5.33 (s, 2H, H-7), 3.73 (s, 3H, H-16), 3.68 (s, 3H, H-15).

^{13}C NMR (126 MHz, DMSO- d_6) δ : 192.7 (C-8), 162.4 (C-12), 152.6 (C-1), 149.6 (C-9), 143.3 (C-4), 130.4 (C-10, C-14), 126.1 (C-3), 115.3 (C-11, C-13), 112.7 (C-5), 104.4 (C-2), 101.1 (C-6), 70.2 (C-7), 56.1 (C-16), 55.5 (C-15).

MS (ESI⁻) m/z: Calculated for $C_{16}H_{15}O_5$ [M - H]⁻: 287.0998. Found 287.0927.

IR $\nu_{\text{max}}/\text{cm}^{-1}$: 3219, 1671, 1600, 1512, 1448, 1285, 1265, 1229, 1204, 1145, 1095, 1026, 994, 834, 788, 754.

HPLC-MS (ESI) m/z ; ($\lambda = 235 \text{ nm}$): $R_t = 9.87 \text{ min}$; 287.0905 [M - H]⁻.

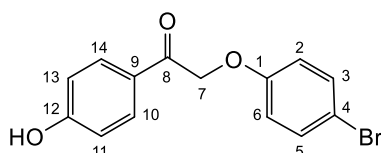
4-(2-(4-Bromophenoxy)acetyl)phenyl acetate: 18i

$C_{16}H_{13}BrO_4$
MW = 349.18 g/mol

The *general procedure E* was followed using 4-bromophenol (0.202 g, 1.17 mmol) and K_2CO_3 (0.178 g, 1.29 mmol) in acetone (7 mL) and the acetate **17** (0.300 g, 1.17 mmol). The crude residue was purified by column chromatography on silica gel (Cyclohexane/EtOAc, 7:3) to obtain **18i** as a white solid (0.118 g, 0.337 mmol) in 29% yield.

R_f = 0.63 (Cyclohexane/EtOAc, 6:4)

¹H NMR (500 MHz, DMSO-*d*₆) δ: 8.07 (d, $J_{H-10,H-11} = J_{H-14,H-13} = 8.5$ Hz, 2H, H-10, H-14), 7.44 (d, $J_{H-11,H-10} = J_{H-13,H-14} = 8.5$ Hz, 2H, H-11, H-13), 7.34 (d, $J_{H-3,H-2} = J_{H-5,H-6} = 8.5$ Hz, 2H, H-3, H-5), 6.96 (d, $J_{H-2,H-3} = J_{H-6,H-5} = 8.5$ Hz, 2H, H-2, H-6), 5.59 (s, 2H, H-7), 2.31 (s, 3H, H-15).

2-(4-Bromophenoxy)-1-(4-hydroxyphenyl)ethan-1-one: 19i

$C_{14}H_{11}BrO_3$
MW = 307.14 g/mol

The *general procedure H* was followed using the acetate **18i** (0.118 g, 0.384 mmol) in EtOH (5 mL) and NaOAc (0.315 g, 3.84 mmol) in water (0.5 mL). The crude residue was purified by column chromatography on silica gel (Cyclohexane/EtOAc, 7:3) to yield **19i** as a white solid (0.053 g, 0.172 mmol) in 45% yield.

R_f = 0.46 (Cyclohexane/EtOAc, 7:3)

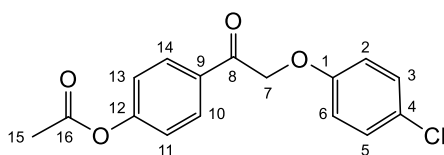
¹H NMR (500 MHz, DMSO-*d*₆) δ: 10.46 (s, 1H, OH), 7.89 (d, $J_{H-10,H-11} = J_{H-14,H-13} = 9.0$ Hz, 2H, H-10, H-14), 7.43 (d, $J_{H-11,H-10} = J_{H-13,H-14} = 9.0$ Hz, 2H, H-11, H-13), 6.91 (d, $J_{H-3,H-2} = J_{H-5,H-6} = 9.0$ Hz, 2H, H-3, H-5), 6.88 (d, $J_{H-2,H-3} = J_{H-6,H-5} = 9.0$ Hz, 2H, H-2, H-6), 5.46 (s, 2H, H-7).

¹³C NMR (126 MHz, DMSO-*d*₆) δ: 192.1 (C-8), 162.5 (C-12), 157.4 (C-1), 131.9 (C-11, C-13), 130.4 (C-10, C-14), 125.8 (C-9), 116.9 (C-3, C-5), 115.3 (C-2, C-6), 112.0 (C-4), 69.8 (C-7).

HRMS (ESI⁻) m/z: Calculated for $C_{14}H_{10}BrO_3$ [M - H]⁻: 304.9892. Found 304.9819.

IR ν_{max}/cm^{-1} : 3136, 2972, 1665, 1606, 1573, 1515, 1488, 1438, 1379, 1293, 1261, 1241, 1220, 1166, 1069, 1005, 990, 867, 837, 795.

HPLC-MS (ESI) m/z; ($\lambda = 235$ nm): Rt = 12.17 min; 304.9807 [M - H]⁻.

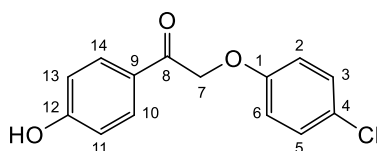
4-(2-(4-Chlorophenoxy)acetyl)phenyl acetate: 18j

$C_{16}H_{13}ClO_4$
MW = 304.73 g/mol

The *general procedure E* was followed using 4-chlorophenol (0.151 g, 1.17 mmol) and K_2CO_3 (0.178 g, 1.29 mmol) in acetone (7 mL) and **17** (0.300 g, 1.17 mmol). The crude residue was purified by column chromatography on silica gel (Cyclohexane/EtOAc, 7:3) to get **18j** as a white solid (0.057 g, 0.187 mmol) in 17% yield.

Rf = 0.66 (Cyclohexane/EtOAc, 7:3)

1H NMR (500 MHz, DMSO- d_6) δ : 8.07 (d, $J_{H-10,H-11} = J_{H-14,H-13} = 9.0$ Hz, 2H, H-10, H-14), 7.34 (d, $J_{H-11,H-10} = J_{H-13,H-14} = 9.0$ Hz, 2H, H-11, H-13), 7.32 (d, $J_{H-3,H-2} = J_{H-5,H-6} = 9.0$ Hz, 2H, H-3, H-5), 7.01 (d, $J_{H-2,H-3} = J_{H-6,H-5} = 9.0$ Hz, 2H, H-2, H-6), 5.59 (s, 1H, H-7), 2.31 (s, 3H, H-15).

2-(4-Chlorophenoxy)-1-(4-hydroxyphenyl)ethan-1-one: 19j

$C_{14}H_{11}ClO_3$
MW = 262.69 g/mol

The *general procedure H* was followed using **18j** (0.057 g, 0.187 mmol) in EtOH (5 mL) and NaOAc (0.153 g, 1.87 mmol) in water (0.5 mL). The crude residue was purified by column chromatography on silica gel (Cyclohexane/EtOAc, 8:2) to yield **19j** as a white solid (0.030 g, 0.114 mmol) in 61% yield.

1H NMR (500 MHz, DMSO- d_6) δ : 10.46 (s, 1H, OH), 7.89 (d, $J_{H-10,H-11} = J_{H-14,H-13} = 8.5$ Hz, 2H, H-10, H-14), 7.31 (d, $J_{H-3,H-2} = J_{H-5,H-6} = 9.0$ Hz, 2H, H-3, H-5), 6.96 (d, $J_{H-2,H-3} = J_{H-6,H-5} = 9.0$ Hz, 2H, H-2, H-6), 6.88 (d, $J_{H-13,H-14} = J_{H-10,H-11} = 8.5$ Hz, 2H, H-11, H-13), 5.46 (s, 2H, H-7).

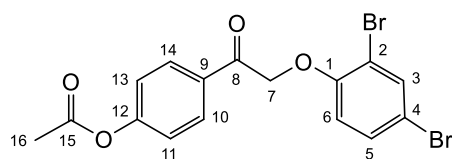
^{13}C NMR (126 MHz, DMSO- d_6) δ : 192.2 (C-8), 162.5 (C-12), 156.9 (C-1), 130.4 (C-10, C-14), 129.0 (C-3, C-5), 125.8 (C-9), 124.4 (C-4), 116.3 (C-2, C-6), 115.3 (C-11, C-13), 69.9 (C-7).

Rf = 0.42 (Cyclohexane/EtOAc, 7:3)

HRMS (ESI $^-$) m/z: Calculated for $C_{14}H_{10}O_3Cl$ [M - H] $^-$: 261.0397. Found 261.0319.

IR ν_{max}/cm^{-1} : 3119, 1667, 1601, 1574, 1515, 1492, 1438, 1378, 1362, 1292, 1240, 1220, 1165, 1093, 1076, 1009, 990, 836, 819, 792, 720.

HPLC-MS (ESI) m/z; ($\lambda = 235$ nm): Rt = 11.45 min; 261.0305 [M - H] $^-$.

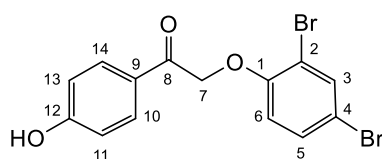
4-(2-(2,4-Dibromophenoxy)acetyl)phenyl acetate: 18k

$C_{16}H_{12}Br_2O_4$
MW = 428.08 g/mol

The *general procedure E* was followed using 2,4-dibromophenol (0.295 g, 1.17 mmol) and K_2CO_3 (0.178 g, 1.29 mmol) in acetone (8 mL) and **17** (0.300 g, 1.17 mmol). The crude residue was purified by column chromatography on silica gel (Cyclohexane/EtOAc, 8:2) to obtain **18k** as a white solid (0.217 g, 0.506 mmol) in 43% yield.

Rf = 0.42 (Cyclohexane/EtOAc, 7:3)

1H NMR (500 MHz, $DMSO-d_6$) δ : 8.06 (d, $J_{H-10,H-11} = J_{H-14,H-13} = 8.5$ Hz, 2H, H-10, H-14), 7.81 (d, $J_{H-3,H-5} = 2.5$ Hz, 1H, H-3), 7.46 (dd, $J_{H-5,H-6} = 8.5$ Hz, $J_{H-5,H-3} = 2.5$ Hz, 1H, H-5), 7.34 (d, $J_{H-11,H-10} = J_{H-13,H-14} = 8.5$ Hz, 2H, H-11, H-13), 7.03 (d, $J_{H-6,H-5} = 8.5$ Hz, 1H, H-6), 5.74 (s, 2H, H-7), 2.31 (s, 3H, H-16).

2-(2-(2,4-Dibromophenoxy)-1-(4-hydroxyphenyl)ethan-1-one: 19k

$C_{14}H_{10}Br_2O_3$
MW = 386.04 g/mol

The *general procedure H* was followed using **18k** (0.217 g, 0.507 mmol) in EtOH (7 mL) and NaOAc (0.416 g, 5.07 mmol) in water (1 mL). The crude residue was purified by column chromatography on silica gel (Cyclohexane/EtOAc, 8:2) to get **19k** as a white solid (0.144 g, 0.373 mmol) in 74% yield.

Rf = 0.44 (Cyclohexane/EtOAc, 7:3)

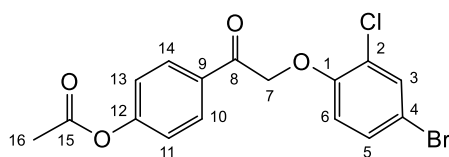
1H NMR (500 MHz, $DMSO-d_6$) δ : 10.47 (s, 1H, OH), 7.88 (d, $J_{H-10,H-11} = J_{H-14,H-13} = 8.5$ Hz, 2H, H-10, H-14), 7.79 (d, $J_{H-3,H-5} = 2.5$ Hz, 1H, H-3), 7.45 (dd, $J_{H-5,H-6} = 8.5$ Hz, $J_{H-5,H-3} = 2.5$ Hz, 1H, H-5), 6.94 (d, $J_{H-6,H-5} = 8.5$ Hz, 1H, H-6), 6.88 (d, $J_{H-11,H-10} = J_{H-13,H-14} = 8.5$ Hz, 2H, H-11, H-13), 5.62 (s, 2H, H-7).

^{13}C NMR (126 MHz, $DMSO-d_6$) δ : 191.6 (C-8), 162.6 (C-12), 154.0 (C-1), 134.6 (C-5), 131.3 (C-3), 130.4 (C-10, C-14), 125.7 (C-9), 115.5 (C-2), 115.3 (C-11, C-13), 112.2 (C-4), 111.8 (C-6), 70.6 (C-7).

HRMS (ESI⁻) m/z: Calculated for $C_{14}H_9Br_2O_3$ $[M - H]^-$: 382.8997. Found 382.8918.

IR ν_{max}/cm^{-1} : 3363, 2924, 1674, 1603, 1576, 1515, 1473, 1430, 1360, 1300, 1245, 1215, 1171, 1110, 1082, 1038, 969, 872, 837, 816, 795, 730.

HPLC-MS (ESI) m/z; ($\lambda = 235$ nm): $R_t = 13.43$ min; 384.8876 $[M + H]^+$.

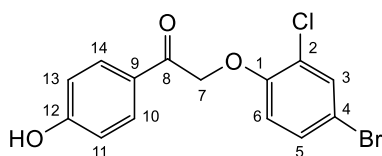
4-(2-(4-Bromo-2-chlorophenoxy)acetyl)phenyl acetate: 18I

$C_{16}H_{12}BrClO_4$
MW = 383.62 g/mol

The *general procedure E* was followed using 4-bromo-2-chlorophenol (0.243 g, 1.17 mmol) and K_2CO_3 (0.178 g, 1.29 mmol) in acetone (8 mL) and **17** (0.300 g, 1.17 mmol). The crude residue was used in the next step without purification. **18I** as a white solid (0.401 g, 1.045 mmol) in 89% yield.

Rf = 0.46 (Cyclohexane/EtOAc, 7:3)

1H NMR (500 MHz, DMSO- d_6) δ : 8.06 (d, $J_{H-10,H-11} = J_{H-14,H-13} = 8.5$ Hz, 2H, H-10, H-14), 7.69 (d, $J_{H-3,H-5} = 2.0$ Hz, 1H, H-3), 7.42 (dq, $J_{H-5,H-6} = 9.0$ Hz, $J_{H-5,H-3} = 2.0$ Hz, 1H, H-5), 7.35 (d, $J_{H-11,H-10} = J_{H-13,H-14} = 8.5$ Hz, 2H, H-11, H-13), 7.07 (d, $J_{H-6,H-5} = 9.0$ Hz, 1H, H-6), 5.75 (s, 2H, H-7), 2.31 (s, 3H, H-16).

2-(4-Bromo-2-chlorophenoxy)-1-(4-hydroxyphenyl)ethan-1-one: 19I

$C_{14}H_{10}BrClO_3$
MW = 341.59 g/mol

The *general procedure H* was followed using **18I** (0.401 g, 1.045 mmol) in EtOH (8 mL) and NaOAc (0.857 g, 10.45 mmol) in water (1 mL). The crude residue was purified by column chromatography on silica gel (Cyclohexane/EtOAc, 8:2) to furnish **19I** as a white solid (0.158 g, 0.462 mmol) in 44% yield.

Rf = 0.50 (Cyclohexane/EtOAc, 7:3)

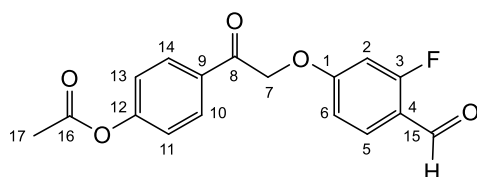
1H NMR (500 MHz, DMSO- d_6) δ : 10.48 (s, 1H, OH), 7.88 (d, $J_{H-10,H-11} = J_{H-14,H-13} = 8.5$ Hz, 2H, H-10, H-14), 7.68 (d, $J_{H-3,H-5} = 2.0$ Hz, 1H, H-3), 7.42 (d, $J_{H-5,H-6} = 8.5$ Hz, $J_{H-5,H-3} = 2.0$ Hz, 1H, H-5), 6.98 (d, $J_{H-6,H-5} = 8.5$ Hz, 1H, H-6), 6.89 (d, $J_{H-11,H-10} = J_{H-13,H-14} = 8.5$ Hz, 2H, H-11, H-13), 5.63 (s, 2H, H-7).

^{13}C NMR (126 MHz, DMSO- d_6) δ : 191.6 (C-8), 162.7 (C-12), 153.1 (C-1), 131.9 (C-5), 130.7 (C-3), 130.5 (C-10, C-14), 125.7 (C-9), 122.5 (C-4), 115.7 (C-2), 115.4 (C-11, C-13), 111.8 (C-6), 70.5 (C-7).

HRMS (ESI $^-$) m/z: Calculated for $C_{14}H_{11}BrClO_3$ [M - H] $^+$: 340.9502. Found 340.9578.

IR ν_{max}/cm^{-1} : 3268, 1675, 1602, 1576, 1517, 1485, 1436, 1288, 1256, 1244, 1215, 1175, 1090, 989, 858, 834, 793, 744, 712.

HPLC-MS (ESI) m/z; ($\lambda = 235$ nm): Rt = 13.22 min; 340.9390 [M - H] $^-$.

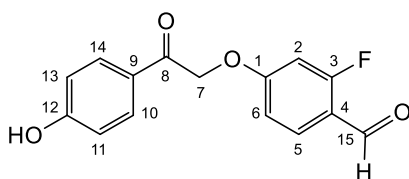
4-(2-(3-Fluoro-4-formylphenoxy)acetyl)phenyl acetate: 18mC₁₇H₁₃FO₅

MW = 316.28 g/mol

The *general procedure E* was followed using 2-fluoro-4-hydroxybenzaldehyde (0.164 g, 1.17 mmol) and K₂CO₃ (0.178 g, 1.29 mmol) in acetone (7 mL) and **17** (0.300 g, 1.17 mmol). The crude residue was purified by column chromatography on silica gel (Cyclohexane/EtOAc, 8:2) to get **18m** as a white solid (0.115 g, 0.363 mmol) in 31% yield.

R_f = 0.49 (Cyclohexane/EtOAc, 6:4)

¹H NMR (500 MHz, DMSO-*d*₆) δ: 10.08 (s, 1H, CHO), 8.08 (d, *J*_{H-10,H-11} = *J*_{H-14,H-13} = 8.5 Hz, 2H, H-10, H-14), 7.78 (t, *J*_{H-5,H-6} = *J*_{H-5,F} = 8.5 Hz, 1H, H-5), 7.36 (d, *J*_{H-11,H-10} = *J*_{H-13,H-14} = 8.5 Hz, 2H, H-11, H-13), 7.12 (dd, *J*_{H-2,F} = 13.0 Hz, *J*_{H-2,H-6} = 2.5 Hz, 1H, H-2), 7.02 (dd, *J*_{H-6,H-5} = 8.5 Hz, *J*_{H-6,H-2} = 2.5 Hz, 1H, H-6), 5.78 (s, 2H, H-7), 2.31 (s, 3H, H-17).

2-(2,4-Dibromophenoxy)-1-(4-hydroxyphenyl)ethan-1-one: 19mC₁₅H₁₁FO₄

MW = 274.25 g/mol

The *general procedure H* was followed using 2-fluoro-4-(2-(4-hydroxyphenyl)-2-oxoethoxy)benzaldehyde **18m** (0.115 g, 0.363 mmol) in EtOH (6 mL) and NaOAc (0.298 g, 3.63 mmol) in water (1 mL). The crude residue was purified by column chromatography on silica gel (Cyclohexane/EtOAc, 7:3) to yield **19m** as a white solid (0.087 g, 0.317 mmol) in 87% yield.

R_f = 0.36 (Cyclohexane/EtOAc, 6:4)

¹H NMR (500 MHz, DMSO-*d*₆) δ: 10.49 (s, 1H, OH), 10.06 (s, 1H, CHO), 7.90 (d, *J*_{H-10,H-11} = *J*_{H-14,H-13} = 9.0 Hz, 2H, H-10, H-14), 7.77 (t, *J*_{H-5,H-6} = *J*_{H-5,F} = 8.5 Hz, 1H, H-5), 7.05 (dd, *J*_{H-2,F} = 13.0 Hz, *J*_{H-2,H-6} = 2.0 Hz, 1H, H-2), 6.97 (dd, *J*_{H-6,H-5} = 8.5 Hz, *J*_{H-6,H-2} = 2.0 Hz, 1H, H-6), 6.90 (d, *J*_{H-11,H-10} = *J*_{H-13,H-14} = 9.0 Hz, 2H, H-11, H-13), 5.67 (s, 2H, H-7).

¹³C NMR (126 MHz, DMSO-*d*₆) δ: 191.2 (C-8), 186.1 (d, *J*_{C-15,F} = 4.5 Hz, C-15), 180.3 (d, *J*_{C-3,F} = 257.0 Hz, C-3), 170.9 (C-1), 162.7 (C-12), 130.6 (C-5), 130.5 (C-10, C-14), 125.6 (C-9), 115.3 (C-11, C-13), 112.2 (C-6), 102.5 (d, *J*_{C-2,F} = 24.2 Hz, C-2), 70.3 (C-7).

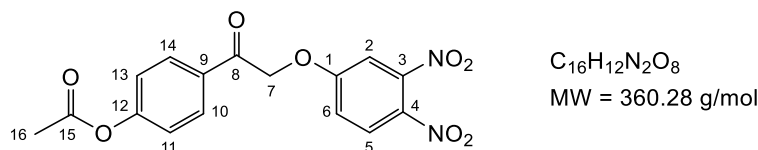
¹⁹F_{cpd} NMR (470 MHz, DMSO-*d*₆) δ: -118.4.

MS (ESI⁻) m/z: Calculated for C₁₅H₁₀FO₄ [M - H]⁻: 273.1. Found 273.1.

IR ν_{max}/cm⁻¹: 3160, 2964, 2921, 1692, 1666, 1615, 1575, 1501, 1434, 1379, 1344, 1291, 1249, 1223, 1162, 1101, 1067, 994, 839, 809.

HPLC-MS (ESI) m/z; ($\lambda = 235 \text{ nm}$): $R_t = 10.15 \text{ min}$; 273.0564 $[M - H]^-$.

4-(2-(3,4-Dinitrophenoxy)acetyl)phenyl acetate: 18n

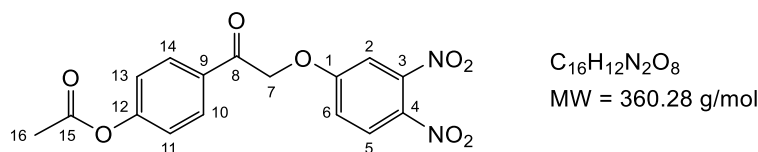


The *general procedure E* was followed using 3,4-dinitrophenol (0.215 g, 1.17 mmol) and K_2CO_3 (0.178 g, 1.29 mmol) in acetone (7 mL) and **17** (0.300 g, 1.17 mmol). The crude residue **18n** was used in the next step without further purification (0.373 g, 1.035 mmol) in 88% yield.

Rf = 0.60 (Cyclohexane/EtOAc, 6:4)

1H NMR (500 MHz, DMSO- d_6) δ : 8.25 (d, $J_{H-5,H-6} = 9.0 \text{ Hz}$, 1H, H-5), 8.07 (d, $J_{H-10,H-11} = J_{H-14,H-13} = 8.5 \text{ Hz}$, 2H, H-10, H-14), 7.92 (d, $J_{H-2,H-6} = 3.0 \text{ Hz}$, 1H, H-2), 7.48 (dd, $J_{H-6,H-5} = 9.0 \text{ Hz}$, $J_{H-6,H-2} = 3.0 \text{ Hz}$, 1H, H-6), 7.36 (d, $J_{H-11,H-10} = J_{H-13,H-14} = 8.5 \text{ Hz}$, 2H, H-11, H-13), 5.91 (s, 2H, H-7), 2.31 (s, 3H, H-16).

2-(3,4-Dinitrophenoxy)-1-(4-hydroxyphenyl)ethan-1-one: 19n



The *general procedure H* was followed using acetate **18n** (0.370 g, 1.027 mmol) in EtOH (8 mL) and NaOAc (0.842 g, 10.27 mmol) in water (1 mL). The crude residue was purified by column chromatography on silica gel (Cyclohexane/EtOAc, 7:3) to yield **19n** as a yellow solid (0.124 g, 0.389 mmol) in 34% yield.

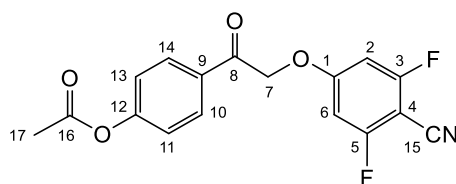
Rf = 0.36 (Cyclohexane/EtOAc, 6:4)

1H NMR (500 MHz, DMSO- d_6) δ : 10.52 (s, 1H, OH), 8.24 (d, $J_{H-5,H-6} = 9.0 \text{ Hz}$, 1H, H-5), 7.88 (d, $J_{H-10,H-11} = J_{H-14,H-13} = 9.0 \text{ Hz}$, 2H, H-10, H-14), 7.86 (d, $J_{H-2,H-6} = 3.0 \text{ Hz}$, 1H, H-2), 7.43 (dd, $J_{H-6,H-5} = 9.0 \text{ Hz}$, $J_{H-6,H-2} = 3.0 \text{ Hz}$, 1H, H-6), 6.90 (d, $J_{H-11,H-10} = J_{H-13,H-14} = 9.0 \text{ Hz}$, 2H, H-11, H-13), 5.80 (s, 2H, H-7).

^{13}C NMR (126 MHz, DMSO- d_6) δ : 190.7 (C-8), 163.0 (C-12), 162.8 (C-1), 145.0 (C-5), 133.2 (C-10, C-14), 130.5 (C-9), 127.9 (C-3), 125.4 (C-4), 118.3 (C-6), 115.4 (C-11, C-13), 111.1 (C-2), 71.0 (C-7).

MS (ESI $^-$) m/z: Calculated for $C_{14}H_{09}N_2O_4$ $[M - H]^-$: 317.2. Found 317.1.

IR ν_{max}/cm^{-1} : 3171, 2923, 2853, 1729, 1663, 1603, 1573, 1551, 1539, 1514, 1491, 1465, 1439, 1365, 1348, 1322, 1290, 1252, 1240, 1215, 1171, 1084, 992, 931, 903, 838, 823, 775, 748, 723.

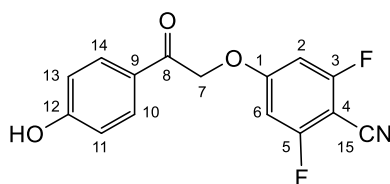
4-(2-(4-Cyano-3,5-difluorophenoxy)acetyl)phenyl acetate: 18o

$C_{17}H_{11}F_2N_2O_4$
MW = 331.27 g/mol

The *general procedure E* was followed using 2,6-difluoro-4-hydroxybenzonitrile (0.181 g, 1.17 mmol) and K_2CO_3 (0.178 g, 1.29 mmol) in acetone (7 mL) and **17** (0.300 g, 1.17 mmol). The crude residue **18o** (0.369 g, 1.113 mmol) obtained in 95% yield was used in the next step without further purification.

Rf = 0.28 (Cyclohexane/EtOAc, 7:3)

1H NMR (500 MHz, DMSO- d_6) δ : 8.06 (d, $J_{H-10,H-11} = J_{H-14,H-13} = 7.5$ Hz, 2H, H-10, H-14), 7.35 (d, $J_{H-11,H-10} = J_{H-13,H-14} = 7.5$ Hz, 2H, H-11, H-13), 7.23 (d, $J_{H-2,F-3} = J_{H-6,F-5} = 9.0$ Hz, 2H, H-2, H-6), 5.91 (s, 2H, H-7), 2.31 (s, 3H, H-17).

2,6-Difluoro-4-(2-(4-hydroxyphenyl)-2-oxoethoxy)benzonitrile: 19o

$C_{15}H_9F_2NO_3$
MW = 289.24 g/mol

The *general procedure H* was followed using acetate **18o** (0.365 g, 1.102 mmol) in EtOH (8 mL) and NaOAc (0.904 g, 11.02 mmol) in water (1 mL). The crude residue was recrystallized from methanol to obtain **19o** as a white pink solid (0.278 g, 0.961 mmol) in 87% yield.

Rf = 0.30 (Cyclohexane/EtOAc, 6:4)

1H NMR (500 MHz, DMSO- d_6) δ : 10.50 (s, 1H, OH), 7.88 (d, $J_{H-10,H-11} = J_{H-14,H-13} = 9.0$ Hz, 2H, H-10, H-14), 7.17 (d, $J_{H-2,F} = J_{H-6,F} = 10.5$ Hz, 2H, H-2, H-6), 6.90 (d, $J_{H-11,H-10} = J_{H-13,H-14} = 9.0$ Hz, 2H, H-11, H-13), 5.80 (s, 2H, H-7).

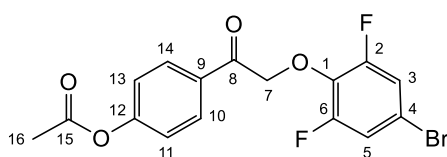
^{13}C NMR (126 MHz, DMSO- d_6) δ : 190.6 (C-8), 164.7 (t, $J_{C-1,F} = 14.1$ Hz, C-1), 163.4 (dd, $J_{C-3,F-3} = J_{C-5,F-5} = 254.3$ Hz, $J_{C-3,F-5} = J_{C-5,F-3} = 8.1$ Hz, C-3, C-5), 162.7 (C-12), 130.5 (C-10, C-14), 125.4 (C-9), 115.3 (C-11, C-13), 109.9 (C-15), 100.3 (d, $J_{C-2,F-3} = J_{C-6,F-5} = 23.7$ Hz, C-2, C-6), 83.0 (C-4), 71.0 (C-7).

$^{19}F_{cpd}$ NMR (470 MHz, DMSO- d_6) δ : -105.6.

HRMS (ESI $^-$) m/z: Calculated for $C_{15}H_8F_2NO_3$ [M - H] $^-$: 288.0472. Found 288.0479.

IR ν_{max}/cm^{-1} : 3113, 2239, 1668, 1635, 1604, 1577, 1513, 1495, 1456, 1437, 1392, 1374, 1360, 1284, 1256, 1228, 1200, 1194, 1179, 1064, 1043, 1010, 968, 867, 851, 823, 805, 719.

HPLC-MS (ESI) m/z; ($\lambda = 235$ nm): Rt = 11.59 min; 288.0470 [M - H] $^-$.

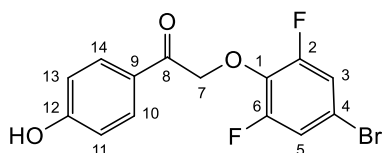
4-(2-(4-Bromo-2,6-difluorophenoxy)acetyl)phenyl acetate: 18p

$C_{16}H_{11}BrF_2O_4$
MW = 385.16 g/mol

The *general procedure E* was followed using 4-bromo-2,6-difluorophenol (0.122 g, 0.586 mmol) and K_2CO_3 (0.089 g, 0.645 mmol) in acetone (4 mL) and **17** (0.150 g, 0.586 mmol). The crude residue **18p** was used in the next step without further purification (0.268 g).

Rf = 0.34 (Cyclohexane/EtOAc, 6:4).

1H NMR (500 MHz, DMSO- d_6) δ : 8.00 (d, $J_{H-10,H-11} = J_{H-14,H-13} = 9.0$ Hz, 2H, H-10, H-14), 7.50 (d, $J_{H-11,H-10} = J_{H-13,H-14} = 9.0$ Hz, 2H, H-11, H-14), 7.32 (d, $J_{H-3,F-2} = J_{H-5,F-6} = 9.0$ Hz, 2H, H-3, H-5), 5.69 (s, 2H, H-7), 2.30 (s, 3H, H-16).

2-(4-Bromo-2,6-difluorophenoxy)-1-(4-hydroxyphenyl)ethan-1-one: 19p

$C_{14}H_9BrF_2O_3$
MW = 343.12 g/mol

The *general procedure H* was followed using **18p** (0.260 g, 0.675 mmol) in EtOH (8 mL) and NaOAc (0.553 g, 6.750 mmol) in water (1 mL). The crude residue was crystallized in cyclohexane to obtain **19p** as a white solid (0.106 g, 0.309 mmol) in 46% yield.

Rf = 0.30 (Cyclohexane/EtOAc, 6:4)

1H NMR (500 MHz, DMSO- d_6) δ : 10.47 (s, 1H, OH), 7.82 (d, $J_{H-10,H-11} = J_{H-14,H-13} = 8.5$ Hz, 2H, H-10, H-14), 7.48 (d, $J_{H-3,F-2} = J_{H-5,F-6} = 8.5$ Hz, 2H, H-3, H-5), 6.86 (d, $J_{H-11,H-10} = J_{H-13,H-14} = 8.5$ Hz, 2H, H-11, H-13), 5.58 (s, 2H, H-7).

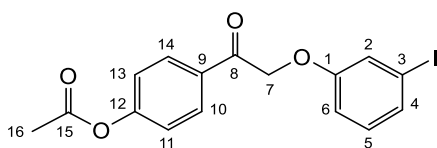
^{13}C NMR (126 MHz, DMSO- d_6) δ : 191.7 (C-8), 162.6 (C-12), 154.3 (dd, $J_{C-2,F-2} = J_{C-6,F-6} = 250.1$ Hz, $J_{C-2,F-6} = J_{C-6,F-2} = 7.0$ Hz, C-2, C-6), 134.4 (C-1), 130.3 (C-10, C-14), 125.3 (C-9), 116.2 (dd, $J_{C-3,F-2} = J_{C-5,F-6} = 26.8$ Hz, $J_{C-3,F-6} = J_{C-5,F-2} = 12.2$ Hz, C-3, C-5), 115.4 (C-11, C-13), 112.6 (d, $J_{C-4,F} = 12.2$ Hz, C-4), 74.1 (C-7).

$^{19}F_{cpd}$ NMR (470 MHz, DMSO- d_6) δ : -127.3.

HRMS (ESI $^-$) m/z : Calculated for $C_{14}H_8BrF_2O_3$ $[M - H]^-$: 340.9703. Found 340.9611.

IR ν_{max}/cm^{-1} : 3228, 2925, 1666, 1602, 1575, 1516, 1496, 1423, 1372, 1320, 1283, 1255, 1217, 1173, 1090, 1068, 1037, 1003, 977, 877, 861, 853, 813, 726.

HPLC-MS (ESI) m/z ; ($\lambda = 235$ nm): $R_t = 12.69$ min; 340.9622 $[M - H]^-$.

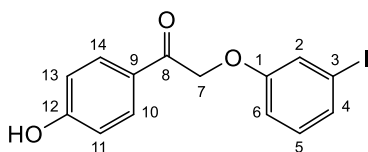
4-(2-(3-Iodophenoxy)acetyl)phenyl acetate: 18q

$C_{16}H_{13}IO_4$
MW = 396.18 g/mol

The *general procedure E* was followed using 3-iodophenol (0.203 g, 1.172 mmol) and K_2CO_3 (0.178 g, 1.289 mmol) in acetone (8 mL) and 4-(2-bromoacetyl)phenyl acetate **17** (0.300 g, 1.172 mmol). The crude residue **18q** was used in the next step without further purification (0.146 g, 29% yield).

Rf = 0.27 (Cyclohexane/EtOAc, 7:3)

1H NMR (500 MHz, $DMSO-d_6$) δ : 8.08 (d, $J_{H-10,H-11} = J_{H-14,H-13} = 8.5$ Hz, 2H, H-10, H-14), 7.39 (s, 1H, H-2), 7.34 (d, $J_{H-11,H-10} = J_{H-13,H-14} = 8.5$ Hz, 2H, H-11, H-13), 7.31 (d, $J_{H-4,H-5} = 8.0$ Hz, 1H, H-4), 7.07 (t, $J_{H-5,H-4} = J_{H-5,H-6} = 8.0$ Hz, 1H, H-5), 7.00 (td, $J_{H-6,H-5} = 8.0$ Hz, 1H, H-6), 5.61 (s, 2H, H-7), 2.31 (s, 3H, H-16).

1-(4-Hydroxyphenyl)-2-(3-iodophenoxy)ethan-1-one: 19q

$C_{14}H_{11}IO_3$
MW = 354.14 g/mol

The *general procedure H* was followed using the acetate **18q** (0.140 g, 0.353 mmol) in EtOH (5 mL) and NaOAc (0.290 g, 3.530 mmol) in water (1 mL). The crude residue was crystallized in cyclohexane to obtain **19q** as a white solid (0.063 g, 0.177 mmol) in 50% yield.

Rf = 0.24 (Cyclohexane/EtOAc, 7:3)

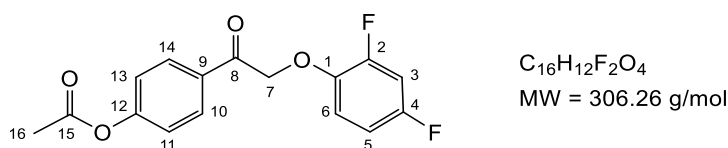
1H NMR (500 MHz, $DMSO-d_6$) δ : 10.46 (s, 1H, OH), 7.89 (d, $J_{H-10,H-11} = J_{H-14,H-13} = 9.0$ Hz, 2H, H-10, H-14), 7.33 (t, $J_{H-2,H-4} = J_{H-2,H-6} = 2.0$ Hz, 1H, H-2), 7.30 (d, $J_{H-4,H-5} = 8.0$ Hz, 1H, H-4), 7.06 (t, $J_{H-5,H-4} = J_{H-5,H-6} = 8.5$ Hz, 1H, H-5), 6.96 (dd, $J_{H-6,H-5} = 8.5$ Hz, $J_{H-6,H-2} = 2.0$ Hz, 1H, H-6), 6.88 (d, $J_{H-11,H-10} = J_{H-13,H-14} = 9.0$ Hz, 2H, H-11, H-13), 5.48 (s, 2H, H-7).

^{13}C NMR (126 MHz, $DMSO-d_6$) δ : 192.0 (C-8), 162.5 (C-12), 158.8 (C-1), 131.1 (C-5), 130.4 (C-10, C-14), 129.6 (C-4), 125.8 (C-9), 123.0 (C-2), 115.3 (C-11, C-13), 114.6 (C-6), 94.8 (C-3), 69.7 (C-7).

HRMS (ESI⁻) m/z: Calculated for $C_{14}H_{10}IO_3$ [M - H]⁻: 352.9753. Found 352.9660.

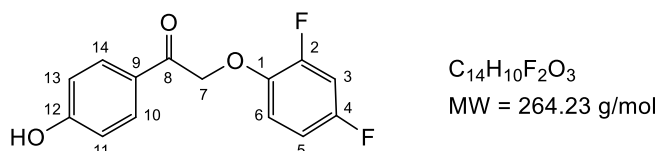
IR ν_{max}/cm^{-1} : 3673, 3203, 2988, 2901, 1667, 1603, 1574, 1517, 1478, 1437, 1421, 1380, 1287, 1271, 1241, 1217, 1173, 1080, 1066, 988, 886, 833, 812, 772, 721.

HPLC-MS (ESI) m/z; ($\lambda = 235$ nm): Rt = 12.57 min; 352.9663 [M - H]⁻.

4-(2-(2,4-Difluorophenoxy)acetyl)phenyl acetate: 18r

The *general procedure E* was followed using 3,5-difluorophenol (0.076 g, 0.586 mmol) and K_2CO_3 (0.089 g, 0.645 mmol) in acetone (4 mL) and 4-(2-bromoacetyl)phenyl acetate **17** (0.150 g, 0.586 mmol). The crude residue **18r** was used without further purification (0.143 g, 72% yield).

Rf = 0.28 (Cyclohexane/EtOAc 7:3)

2-(2,4-difluorophenoxy)-1-(4-hydroxyphenyl)ethan-1-one: 19r

The *general procedure H* was followed using the acetate **18r** (0.143 g, 0.492 mmol) in EtOH (5 mL) and NaOAc (0.404 g, 4.920 mmol) in water (1 mL). The crude residue was crystallized in cyclohexane to obtain **19r** as a white solid (0.060 g, 0.227 mmol) in 46% yield.

Rf = 0.23 (Cyclohexane/EtOAc, 7:3)

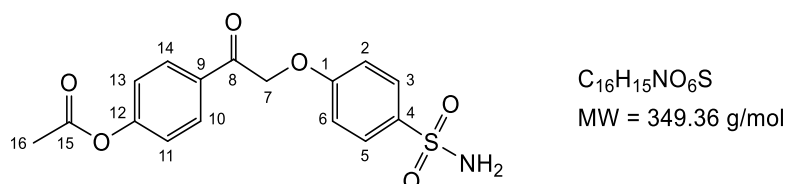
1H NMR (500 MHz, DMSO- d_6) δ : 10.48 (s, 1H, OH), 7.89 (d, $J_{H-10,H-11} = J_{H-14,H-13} = 8.5$ Hz, 2H, H-10, H-14), 6.89 (d, $J_{H-14,H-13} = J_{H-10,H-11} = 8.5$ Hz, 2H, H-11, H-13), 6.81–.73 (m, 3H, H-3, H-5, H-6), 5.60 (s, 2H, H-7).

^{13}C NMR (126 MHz, DMSO- d_6) δ : 191.5 (C-8), 162.6 (C-12), 160.4 (d, $J_{C-1,F-2} = 14.6$ Hz, C-1), 130.4 (C-10, C-14), 125.7 (C-9), 115.3 (C-11, C-13), 98.9 (2d, $J_{C-5,F-4} = 28.7$ Hz, $J_{C-6,F-2} = J_{C-6,F-4} = 14.0$ Hz, C-5, C-6), 96.2 (t, $J_{C-3,F-2} = J_{C-3,F-4} = 26.5$ Hz, C-3), 70.2 (C-7).

HRMS (ESI $^-$) m/z: Calculated for $C_{14}H_9F_2O_3$ [M – H] $^-$: 263.0598. Found 263.0511.

IR ν_{max}/cm^{-1} : 3241, 1669, 1627, 1600, 1578, 1519, 1479, 1436, 1388, 1365, 1349, 1312, 1295, 1258, 1250, 1213, 1160, 1111, 1083, 1018, 1000, 992, 965, 859, 840, 823, 807, 734, 715.

HPLC-MS (ESI) m/z; ($\lambda = 235$ nm): Rt = 11.71 min; 263.0516 [M – H] $^-$.

4-(2-(4-Sulfamoylphenoxy)acetyl)phenyl acetate: 18s

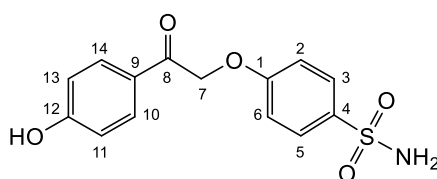
The *general procedure E* was followed using 4-hydroxybenzosulfonamide (0.202 g, 1.172 mmol) and K_2CO_3 (0.178 g, 1.289 mmol) in acetone (8 mL) and 4-(2-bromoacetyl)phenyl acetate **17**

(0.300 g, 1.172 mmol). The crude residue was purified by column chromatography on silica gel (CH₂Cl₂/MeOH 10:0.1) to get **18s** as a white solid (0.068 g, 0.194 mmol) in 17% yield.

R_f = 0.13 (CH₂Cl₂/MeOH 99:1)

¹H NMR (500 MHz, DMSO-*d*₆) δ: 8.09 (d, *J*_{H-10,H-11} = *J*_{H-14,H-13} = 8.5 Hz, 2H, H-10, H-14), 7.74 (d, *J*_{H-3,H-2} = *J*_{H-5,H-6} = 9.0 Hz, 2H, H-3, H-5), 7.36 (d, *J*_{H-11,H-10} = *J*_{H-13,H-14} = 8.5 Hz, 2H, H-11, H-13), 7.20 (s, 2H, NH₂), 7.14 (d, *J*_{H-2,H-3} = *J*_{H-6,H-5} = 9.0 Hz, 2H, H-2, H-6), 5.71 (s, 2H, H-7), 2.32 (s, 3H, H-16).

4-(2-(4-Hydroxyphenyl)-2-oxoethoxy)benzenesulfonamide: **19s**



C₁₄H₁₃NO₅S
MW = 307.32 g/mol

The *general procedure H* was followed using 4-(2-(4-hydroxyphenyl)-2-oxoethoxy)benzenesulfonamide **18s** (0.068 g, 0.221 mmol) in EtOH (4 mL) and NaOAc (0.181 g, 2.221 mmol) in water (0.5 mL). The crude residue was purified by column chromatography on silica gel (DCM/MeOH, 9.9:0.1) to yield **19s** as a white solid (0.022 g, 0.071 mmol) in 33% yield.

R_f = 0.10 (CH₂Cl₂/MeOH, 99:1)

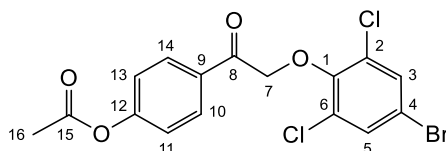
¹H NMR (500 MHz, DMSO-*d*₆) δ: 10.47 (s, 1H, OH), 7.90 (d, *J*_{H-10,H-11} = *J*_{H-14,H-13} = 9.0 Hz, 2H, H-10, H-14), 7.72 (d, *J*_{H-3,H-2} = *J*_{H-5,H-6} = 7.0 Hz, 2H, H-3, H-5), 7.18 (s, 2H, NH₂), 7.08 (d, *J*_{H-11,H-10} = *J*_{H-13,H-14} = 9.0 Hz, 2H, H-11, H-13), 6.89 (d, *J*_{H-2,H-3} = *J*_{H-6,H-5} = 7.0 Hz, 2H, H-2, H-6), 5.58 (s, 2H, H-7).

¹³C NMR (126 MHz, DMSO-*d*₆) δ: 191.8 (C-8), 162.6 (C-12), 160.4 (C-1), 136.3 (C-4), 130.4 (C-10, C-14), 127.5 (C-3, C-5), 125.7 (C-9), 115.3 (C-2, C-6), 114.6 (C-11, C-13), 69.8 (C-7).

HRMS (ESI⁻) *m/z*: Calculated for C₁₄H₁₂NO₅S [M - H]⁻: 306.0514. Found 306.0427.

IR ν_{max}/cm⁻¹: 3380, 3269, 3109, 2924, 1672, 1598, 1578, 1519, 1503, 1426, 1412, 1396, 1372, 1333, 1306, 1250, 1232, 1180, 1158, 1097, 1076, 994, 900, 824, 780.

4-(2-(4-Bromo-2,6-dichlorophenoxy)acetyl)phenyl acetate: **18t**



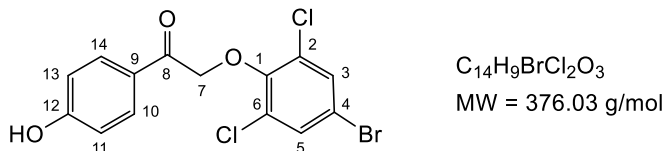
C₁₆H₁₁BrCl₂O₄
MW = 418.06 g/mol

The *general procedure E* was followed using 4-bromo-2,6-dichlorophenol (0.289 g, 1.172 mmol) and K₂CO₃ (0.178 g, 1.289 mmol) in acetone (8 mL) and **17** (0.300 g, 1.172 mmol). The crude residue was crystallized in cyclohexane to obtain **18t** a white solid (0.147 g, 71% yield).

R_f = 0.87 (Cyclohexane/EtOAc, 7:3)

¹H NMR (500 MHz, DMSO-*d*₆) δ : 8.04 (d, $J_{\text{H-10,H-11}} = J_{\text{H-14,H-13}} = 9.0$ Hz, 2H, H-10, H-14), 7.83 (s, 2H, H-3, H-5), 7.32 (d, $J_{\text{H-11,H-10}} = J_{\text{H-13,H-14}} = 9.0$ Hz, 2H, H-11, H-13), 5.46 (s, 2H, H-7), 2.30 (s, 3H, H-16).

2-(4-Bromo-2,6-dichlorophenoxy)-1-(4-hydroxyphenyl)ethan-1-one: **19t**



The *general procedure H* was followed using the acetate **18t** (0.147 g, 0.351 mmol) in EtOH (6 mL) and NaOAc (0.287 g, 3.510 mmol) in water (1 mL). The crude residue was purified by column chromatography on silica gel (Cyclohexane/EtOAc, 7:3) to yield **19t** as a white solid (0.066 g, 0.175 mmol) in 50% yield.

R_f = 0.45 (Cyclohexane/EtOAc, 7:3)

¹H NMR (500 MHz, DMSO-*d*₆) δ : 10.47 (s, 1H, OH), 7.86 (d, $J_{\text{H-10,H-11}} = J_{\text{H-14,H-13}} = 8.5$ Hz, 2H, H-10, H-14), 7.82 (s, 2H, H-3, H-5), 6.86 (d, $J_{\text{H-11,H-10}} = J_{\text{H-13,H-14}} = 8.5$ Hz, 2H, H-11, H-13), 5.33 (s, 2H, H-7).

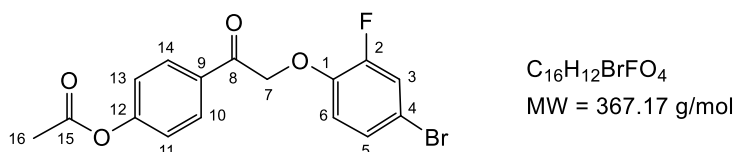
¹³C NMR (126 MHz, DMSO-*d*₆) δ : 190.7 (C-8), 162.6 (C-12), 150.1 (C-1), 131.6 (C-3, C-5), 130.5 (C-10, C-14), 129.4 (C-2, C-6), 125.5 (C-9), 116.5 (C-4), 115.4 (C-11, C-13), 74.3 (C-7).

MS (ESI⁺) *m/z*: 374.90 [M + H]⁺.

IR ν_{max} /cm⁻¹: 3169, 2971, 2901, 1667, 1601, 1573, 1556, 1518, 1455, 1429, 1416, 1394, 1381, 1294, 1248, 1219, 1172, 1065, 982, 879, 852, 840, 821, 800, 743.

HPLC-MS (ESI) *m/z*; ($\lambda = 235$ nm): *R_t* = 13.54 min; 374.8999 [M + H]⁺.

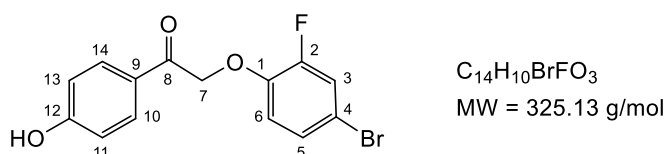
4-(2-(4-Bromo-2-fluorophenoxy)acetyl)phenyl acetate: **18u**



The *general procedure E* was followed using 4-bromo-2-fluorophenol (0.223 g, 1.17 mmol) and K₂CO₃ (0.178 g, 1.29 mmol) in acetone (8 mL) and 4-(2-bromoacetyl)phenyl acetate **17** (0.300 g, 1.17 mmol). The crude residue was used in the next step without further purification **18u** as a white solid (0.225 g, 52% yield).

R_f = 0.57 (Cyclohexane/EtOAc, 7:3)

¹H NMR (500 MHz, DMSO-*d*₆) δ : 8.06 (d, $J_{\text{H-10,H-11}} = J_{\text{H-14,H-13}} = 9.0$ Hz, 2H, H-10, H-14), 7.56 (dd, $J_{\text{H-3,F}} = 12.0$ Hz, $J_{\text{H-3,H-5}} = 2.5$ Hz, 1H, H-3), 7.34 (d, $J_{\text{H-11,H-10}} = J_{\text{H-13,H-14}} = 9.0$ Hz, 1H, H-11, H-13), 7.28 (dd, $J_{\text{H-5,H-6}} = 9.0$ Hz, $J_{\text{H-5,H-3}} = 2.5$ Hz, 1H, H-5), 7.13 (t, $J_{\text{H-6,H-5}} = J_{\text{H-6,F}} = 9.0$ Hz, 1H, H-6), 5.75 (s, 2H, H-7), 2.31 (s, 3H, H-16).

2-(4-Bromo-2-fluorophenoxy)-1-(4-hydroxyphenyl)ethan-1-one: 19u

The *general procedure H* was followed using 4-(2-(4-bromo-2-chlorophenoxy)acetyl)phenyl acetate **18u** (0.401 g, 1.045 mmol) in EtOH (8 mL) and NaOAc (0.857 g, 10.45 mmol) in water (1 mL). The crude residue was purified by column chromatography on silica gel (Cyclohexane/EtOAc, 7:3) to yield **19u** as a white solid (0.067 g, 0.206 mmol) in 35% yield.

R_f = 0.31 (Cyclohexane/EtOAc, 7:3)

¹H NMR (500 MHz, DMSO-*d*₆) δ: 10.48 (s, 1H, OH), 7.88 (d, *J*_{H-10,H-11} = *J*_{H-14,H-13} = 9.0 Hz, 2H, H-10, H-14), 7.54 (dd, *J*_{H-3,F} = 11.0 Hz, *J*_{H-3,H-5} = 1.0 Hz, 1H, H-3), 7.27 (d, *J*_{H-5,H-6} = 9.0 Hz, 1H, H-5), 7.05 (t, *J*_{H-6,H-5} = *J*_{H-6,F} = 9.0 Hz, 1H, H-6), 6.89 (d, *J*_{H-11,H-10} = *J*_{H-13,H-14} = 9.0 Hz, 2H, H-11, H-13), 5.59 (s, 2H, H-7).

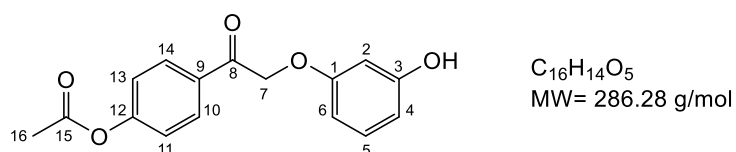
¹³C NMR (126 MHz, DMSO-*d*₆) δ: 191.7 (C-8), 162.6 (C-12), 151.4 (d, *J*_{C-2,F} = 248.9 Hz, C-2), 145.6 (d, *J*_{C-1,F} = 10.1 Hz, C-1), 130.4 (C-10, C-14), 127.3 (d, *J*_{C-5,F} = 3.1 Hz C-5), 125.7 (C-9), 119.2 (d, *J*_{C-3,F} = 21.4 Hz, C-3), 116.7 (C-6), 115.3 (C-11, C-13), 111.1 (d, *J*_{C-4,F} = 8.6 Hz, C-4), 70.4 (C-7).

¹⁹F_{cpd} NMR (470 MHz, DMSO-*d*₆) δ: -131.2.

HRMS (ESI⁻) *m/z*: Calculated for C₁₄H₉BrFO₃ [M - H]⁻: 322.9797. Found 322.9728.

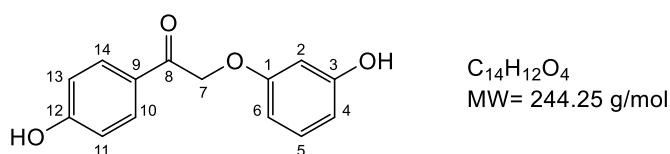
IR *v*_{max}/cm⁻¹: 3304, 2988, 2971, 2922, 1681, 1603, 1579, 1506, 1438, 1409, 1391, 1307, 1278, 1268, 1253, 1246, 1222, 1203, 1182, 1136, 1110, 1084, 1066, 1056, 989, 879, 851, 834, 811, 804, 791, 708.

HPLC-MS (ESI) *m/z*; (λ = 235 nm): Rt = 12.54 min; 322.9718 [M - H]⁻.

4-(2-(3-Hydroxyphenoxy)acetyl)phenyl acetate: 18v

The *general procedure E* was followed using resorcinol monoacetate (0.269 g, 1.172 mmol) and K₂CO₃ (0.178 g, 1.289 mmol) in acetone (8 mL) and 4-(2-bromoacetyl)phenyl acetate **17** (0.300 g, 1.172 mmol). The crude residue **18v** was used in the next step without further purification (0.469 g).

R_f = 0.45 (Cyclohexane/EtOAc, 6:4)

2-(3-Hydroxyphenoxy)-1-(4-hydroxyphenyl)ethan-1-one: 19v

The *general procedure H* was followed using **18v** (0.469 g) in EtOH (7 mL) and NaOAc (0.600 g, 7.31 mmol) in water (1 mL). The crude residue was purified by column chromatography on silica gel (Cyclohexane/EtOAc, 6:4) to yield **19v** as a white solid (0.068 g, 0.278 mmol) in 25% yield.

1H NMR (500 MHz, DMSO- d_6) δ : 10.44 (s, 1H, OH), 9.34 (s, 1H, OH), 7.80 (d, $J_{H-10,H-11} = J_{H-14,H-13} = 9.0$ Hz, 2H, H-10, H-14), 7.02 (t, $J_{H-5,H-4} = J_{H-5,H-6} = 8.0$ Hz, 1H, H-5), 6.88 (d, $J_{H-11,H-10} = J_{H-13,H-14} = 9.0$ Hz, 2H, H-11, H-13), 6.35 (dd, $J_{H-6,H-5} = 8.0$ Hz, $J_{H-6,H-2} = 2.5$ Hz, 1H, H-6), 6.34 (dd, $J_{H-4,H-5} = 8.0$ Hz, $J_{H-4,H-2} = 2.5$ Hz, 1H, H-4), 6.30 (t, $J_{H-2,H-4} = J_{H-2,H-6} = 2.5$ Hz, 1H, H-2), 5.34 (s, 2H, H-7).

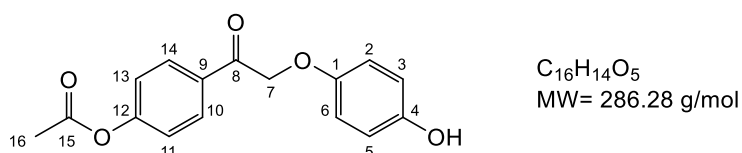
^{13}C NMR (126 MHz, DMSO- d_6) δ : 192.6 (C-8), 162.5 (C-12), 159.2 (C-1), 158.4 (C-3), 130.4 (C-10, C-14), 129.7 (C-5), 125.9 (C-9), 115.3 (C-11, C-13), 108.0 (C-4), 105.3 (C-6), 101.9 (C-2), 69.6 (C-7).

R_f = 0.25 (Cyclohexane/EtOAc, 6:4)

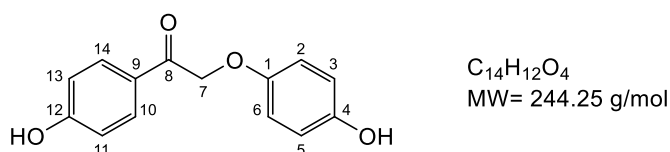
HRMS (ESI⁻) m/z: Calculated for $C_{14}H_{11}O_4$ [M - H]⁻: 243.0736. Found 243.0657.

IR ν_{max}/cm^{-1} : 3660, 3324, 2988, 2901, 1682, 1601, 1593, 1510, 1493, 1450, 1434, 1383, 1332, 1284, 1241, 1183, 1159, 1100, 1109, 1078, 1066, 1057, 1002, 993, 876, 827, 762.

HPLC-MS (ESI) m/z; ($\lambda = 235$ nm): R_t = 8.16 min; 243.0648 [M - H]⁻.

4-(2-(4-Hydroxyphenoxy)acetyl)phenyl acetate: 18w

The *general procedure E* was followed using hydroquinone (0.129 g, 1.172 mmol) and K_2CO_3 (0.178 g, 1.289 mmol) in acetone (8 mL) and 4-(2-bromoacetyl)phenyl acetate **17** (0.300 g, 1.172 mmol). The crude residue **18w** was used in the next step without further purification (0.251 g).

2-(3-Hydroxyphenoxy)-1-(4-hydroxyphenyl)ethan-1-one: 19w

The *general procedure H* was followed using **18w** (0.251 g) in EtOH (5 mL) and NaOAc (0.400 g, 4.87 mmol) in water (1 mL). The crude residue was purified by column chromatography on silica gel (Cyclohexane/EtOAc, 6:4) to yield **19w** as a white solid (0.021 g, 0.08 mmol) in 7% yield.

¹H NMR (500 MHz, DMSO-*d*₆) δ : 10.50 (s, 1H, OH), 8.96 (s, 1H, OH), 7.88 (d, $J_{\text{H-10,H-11}} = J_{\text{H-14,H-13}} = 8.5$ Hz, 2H, H-10, H-14), 6.87 (d, $J_{\text{H-2,H-3}} = J_{\text{H-6,H-5}} = 8.5$ Hz, 2H, H-3, H-5), 6.74 (d, $J_{\text{H-3,H-2}} = J_{\text{H-5,H-6}} = 8.5$ Hz, 2H, H-2, H-6), 6.64 (d, $J_{\text{H-10,H-11}} = J_{\text{H-14,H-13}} = 8.5$ Hz, 2H, H-11, H-13), 5.26 (s, 2H, H-7).

¹³C NMR (126 MHz, DMSO-*d*₆) δ : 193.1 (C-8), 162.4 (C-12), 151.4 (C-1), 150.8 (C-4), 130.4 (C-10, C-14), 126.1 (C-9), 115.6 (C-11, C-13), 115.5 (C-2, C-6), 115.3 (C-3, C-5), 70.4 (C-7).

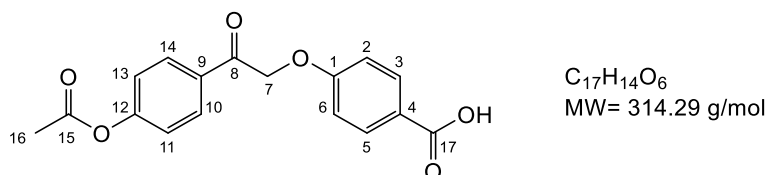
R_f = 0.125 (Cyclohexane/EtOAc, 7:3)

HRMS (ESI⁻) *m/z*: Calculated for C₁₄H₁₁O₄ [M – H]⁻: 243.0736. Found 243.0658.

IR ν_{max} /cm⁻¹: 3430, 2918, 2850, 1654, 1600, 1589, 1514, 1506, 1446, 1433, 1360, 1291, 1263, 1236, 1212, 1169, 1121, 1108, 1085, 998, 987, 879, 835, 741.

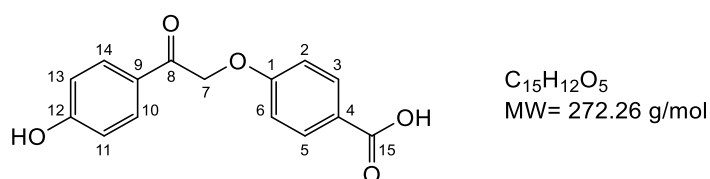
HPLC-MS (ESI) *m/z*; ($\lambda = 235$ nm): *R_t* = 7.46 min; 243.0656 [M – H]⁻.

4-(2-(4-Acetoxyphenyl)-2-oxoethoxy)benzoic acid: **18x**



The *general procedure E* was followed using 4-hydroxybenzoic acid (0.162 g, 1.172 mmol) and K₂CO₃ (0.178 g, 1.289 mmol) in acetone (8 mL) and 4-(2-bromoacetyl)phenyl acetate **17** (0.300 g, 1.172 mmol). The crude residue **18x** was used in the next step without further purification (0.305 g).

4-(2-(4-Hydroxyphenyl)-2-oxoethoxy)benzoic acid: **19x**



The *general procedure H* was followed using **18x** (0.305 g) in EtOH (5 mL) and NaOAc (0.500 g, 6.09 mmol) in water (1 mL). The crude residue was purified by column chromatography on silica gel (Cyclohexane/EtOAc/CH₃COOH, 6:4:0.1) to yield **19x** as a white solid (0.029 g, 0.11 mmol) in 9% yield.

¹H NMR (500 MHz, DMSO-*d*₆) δ : 10.47, 10.37 (2s, 2H, OH), 7.87 (d, $J_{\text{H-3,H-2}} = J_{\text{H-5,H-6}} = J_{\text{H-10,H-11}} = J_{\text{H-14,H-13}} = 9.0$ Hz, 4H, H-3, H-5, H-10, H-14), 6.89, 6.88 (2d, $J_{\text{H-2,H-3}} = J_{\text{H-6,H-5}} = J_{\text{H-11,H-10}} = J_{\text{H-13,H-14}} = 9.0$ Hz, 4H, H-2, H-6, H-11, H-13), 5.55 (s, 2H, H-7).

¹³C NMR (126 MHz, DMSO-*d*₆) δ : 190.9 (C-8), 165.0 (C-1), 162.6, 162.2 (C-12, C-15), 131.6 (C-3, C-5), 130.3 (C-10, C-14), 125.5 (C-9), 119.9 (C-4), 115.4, 115.3 (C-2, C-6, C-11, C-13), 66.2 (C-7).

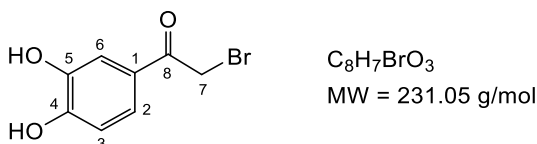
R_f = 0.16 (Cyclohexane/EtOAc, 6:4)

HRMS (ESI⁻) m/z: Calculated for C₁₅H₁₁O₅ [M – H]⁻: 271.0685. Found 271.0610.

IR ν_{max} /cm⁻¹: 3027, 2970, 2926, 1738, 1728, 1673, 1598, 1508, 1442, 1424, 1366, 1284, 1229, 1217, 1168, 1135, 1116, 973, 843, 764.

HPLC-MS (ESI) m/z; (λ = 235 nm): Rt = 9.31 min; 271.0606 [M – H]⁻.

2-Bromo-1-(3,4-dihydroxyphenyl)ethan-1-one: **20**



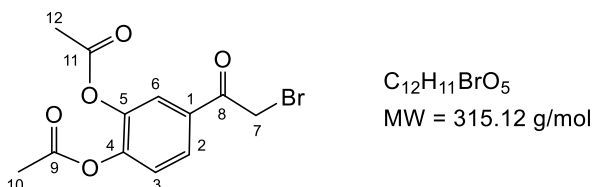
A solution of catechol (1.0 g, 9.082 mmol) in dry CH₂Cl₂ (12 mL) was added slowly into a stirred suspension of AlCl₃ (2.421 g, 18.164 mmol) in dry CH₂Cl₂ (5 mL). After 15 min, bromoacetyl bromide (0.58 mL, 4.768 mmol) was added dropwise. The mixture was left stirred for 3 h at room temperature and then poured onto crushed ice (200 mL). Concentrated aqueous HCl was then added (5 mL) and the mixture extracted with diethyl ether (3x30 mL). The combined organic extracts were washed with brine (30 mL), dried with MgSO₄ and evaporated under reduced pressure. The crude residue was purified by column chromatography on silica gel (Cyclohexane/EtOAc, 8:2) to get **20** as a white solid (0.433 g, 1.874 mmol) in 48% yield.

Rf = 0.5 (Cyclohexane/EtOAc, 6:4)

¹H NMR (500 MHz, DMSO-*d*₆) δ : 10.03 (s, 1H, OH-4), 9.41 (s, 1H, OH-5), 7.41 (dd, $J_{\text{H-2,H-3}}$ = 8.5 Hz, $J_{\text{H-2,H-6}}$ = 2.0 Hz 1H, H-2), 7.36 (d, $J_{\text{H-6,H-2}}$ = 2.0 Hz 1H, H-6), 6.83 (d, $J_{\text{H-3,H-2}}$ = 8.5 Hz, 1H, H-3), 4.72 (s, 2H, H-7).

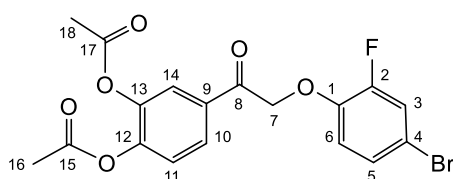
¹³C NMR (126 MHz, DMSO-*d*₆) δ : 194.5 (C-8), 150.9 (C-4), 144.9 (C-5), 125.4 (C-1), 122.8 (C-6), 116.4 (C-2), 115.0 (C-3), 88.3 (C-7).

4-(2-Bromoacetyl)-1,2-phenylene diacetate: **21**



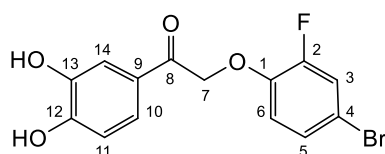
The *general procedure G* was followed using **20** (0.433 g, 1.374 mmol), acetic anhydride (15 mL) and HCl conc. (5 drops). Crystallization in pentane and recrystallization in water afforded the product **21** as a white solid (0.232 g, 0.736 mmol) in 54% yield.

¹H NMR (500 MHz, DMSO-*d*₆) δ : 7.97 (dd, $J_{\text{H-2,H-3}}$ = 8.5 Hz, $J_{\text{H-2,H-6}}$ = 2.0 Hz, 1H, H-2), 7.90 (d, $J_{\text{H-6,H-2}}$ = 2.0 Hz, 1H, H-6), 7.48 (d, $J_{\text{H-3,H-2}}$ = 8.5 Hz, 1H, H-3), 4.93 (s, 2H, H-7), 2.31 (s, 6H, H-10, H-12).

4-(2-(4-Bromo-2-fluorophenoxy)acetyl)-1,2-phenylene diacetate: 22

$C_{18}H_{14}BrFO_6$
MW = 425.21 g/mol

The *general procedure E* was followed using 2-fluoro-4-bromophenol (0.08 mL, 0.729 mmol) and K_2CO_3 (0.110 g, 0.802 mmol) in acetone (5 mL) and the diacetate **21** (0.230 g, 0.729 mmol). The crude residue **22** (0.221 g, 0.519 mmol) obtained as a white solid in quantitative yield and used in the next step without further purification.

2-(4-Bromo-2-fluorophenoxy)-1-(3,4-dihydroxyphenyl)ethan-1-one: 23

$C_{14}H_{10}BrFO_4$
MW = 341.13 g/mol

The *general procedure H* was followed using compound **22** (0.221 g, 0.519 mmol) in EtOH (7 mL) and NaOAc (0.426 g, 82.03 mmol) in water (1 mL). The crude residue was purified by column chromatography on silica gel (Cyclohexane/EtOAc, 6:4) to yield **23** as a white solid (0.075 g, 0.219 mmol) in 42% yield.

R_f = 0.08 (Cyclohexane/EtOAc, 7:3)

¹H NMR (500 MHz, DMSO-*d*₆) δ : 9.69 (s, 2H, OH), 7.54 (dd, $J_{H-3,F} = 11$ Hz, $J_{H-3,H-5} = 2.0$ Hz, 1H, H-3), 7.41 (d, $J_{H-10,H-11} = 8.0$ Hz, $J_{H-10,H-14} = 2.0$ Hz, 1H, H-10), 7.35 (d, $J_{H-14,H-10} = 2.0$ Hz, 1H, H-14), 7.26 (dt, $J_{H-5,H-6} = 9.0$ Hz, $J_{H-5,H-3} = J_{H-5,F} = 1.5$ Hz, 1H, H-5), 7.02 (t, $J_{H-6,H-5} = J_{H-6,F} = 9.0$ Hz, 1H, H-6), 6.84 (d, $J_{H-11,H-10} = 8.0$ Hz, 1H, H-11), 5.56 (s, 2H, H-7).

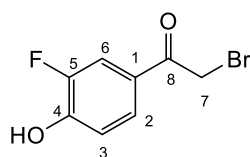
¹³C NMR (126 MHz, DMSO-*d*₆) δ : 191.7 (C-8), 151.4 (d, $J_{C-2,F} = 249.3$ Hz, C-2), 151.3 (C-q), 145.7 (d, $J_{C-1,F} = 10.0$ Hz, C-1), 145.4 (C-q), 127.3 (C-5), 125.9 (C-9), 121.2 (C-10), 119.2 (d, $J_{C-3,F} = 21.4$ Hz, C-3), 116.7 (C-6), 115.1 (C-11), 114.6 (C-14), 111.1 (d, $J_{C-4,F} = 8.7$ Hz, C-4), 70.3 (C-7).

¹⁹F_{cpd} NMR (470 MHz, DMSO-*d*₆) δ : -131.3.

HRMS (ESI⁻) m/z: Calculated for $C_{14}H_9BrFO_4$ [M - H]⁻: 338.9746. Found 338.9668.

IR ν_{max}/cm^{-1} : 3479, 3277, 1692, 1602, 1521, 1506, 1474, 1437, 1387, 1337, 1287, 1276, 1265, 1211, 1188, 1129, 1082, 1015, 948, 909, 882, 846, 819, 794.

HPLC-MS (ESI) m/z; ($\lambda = 235$ nm): Rt = 11.69 min; 340.9645 [M + H]⁺.

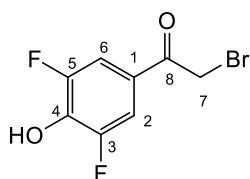
2-Bromo-1-(3-fluoro-4-hydroxyphenyl)ethan-1-one: 24a

$C_8H_6BrFO_2$
MW = 233.06 g/mol

The *general procedure I* was followed using 2-fluorophenol (0.8 mL, 8.92 mmol) in CS_2 (20 mL) and $AlCl_3$ (7.135 g, 53.52 mmol). Then 2-bromoacetyl bromide (1.40 mL, 11.59 mmol) was added to the reaction mixture. The crude product was purified by flash column chromatography (CyHex/EtOAc, 9:1) to obtain **24a** as a white solid (0.480 g, 2.059 mmol) in 23% yield.

Rf = 0.18 (Cyclohexane/EtOAc 8:2)

1H NMR (500 MHz, $DMSO-d_6$) δ : 11.04 (s, 1H, OH), 7.78 (dd, $J_{H-6,F} = 12.0$ Hz, $J_{H-6,H-2} = 1.0$ Hz, 1H, H-6), 7.72 (dd, $J_{H-2,H-3} = 8.5$ Hz, $J_{H-2,H-6} = 1.0$ Hz, 1H, H-2), 7.06 (t, $J_{H-3,H-2} = J_{H-3,F} = 8.5$ Hz, 1H, H-3), 4.81 (s, 2H, H-7).

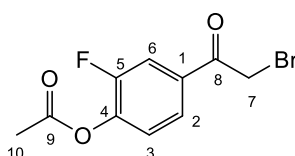
2-Bromo-1-(3,5-difluoro-4-hydroxyphenyl)ethan-1-one: 24b

$C_8H_5BrF_2O_2$
MW = 251.02 g/mol

The *general procedure I* was followed using 2,6-difluorophenol (2 g, 15.37 mmol) in CS_2 (40 mL) and $AlCl_3$ (12.31 g, 92.24 mmol). Then 2-Bromoacetyl bromide (2.42 mL, 19.98 mmol) was added to the reaction mixture. The crude product was purified by flash column chromatography (CyHex/EtOAc, 9:1) to obtain **24b** as a white-silver solid (0.790 g) in quantitative yield.

Rf = 0.35 (Cyclohexane/EtOAc 8:2)

1H NMR (500 MHz, $DMSO-d_6$) δ : 11.47 (s, 1H, OH), 7.71 (d, $J_{H-2,F-3} = J_{H-6,F-5} = 7.5$ Hz, 2H, H-2, H-6), 4.85 (s, 2H, H-7).

4-(2-Bromoacetyl)-2-fluorophenyl acetate: 25a

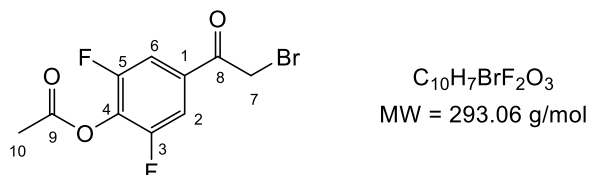
$C_8H_6BrFO_2$
MW = 233.06 g/mol

The *general procedure G* was followed using **24a** (0.250 g, 1.072 mmol), acetic anhydride (20 mL) and HCl conc. (10 drops). The crude product was purified by recrystallization in EtOH to obtain **25a** as a white solid (0.249 g, 1.098 mmol) in 100% yield.

Rf = 0.66 (Cyclohexane/EtOAc 8:2)

¹H NMR (500 MHz, DMSO-*d*₆) δ : 7.99 (dd, $J_{\text{H-6,F}} = 11.0$ Hz, $J_{\text{H-6,H-2}} = 1.5$ Hz, 1H, H-6), 7.90 (dd, $J_{\text{H-2,H-3}} = 8.5$ Hz, $J_{\text{H-2,H-6}} = 1.0$ Hz, 1H, H-2), 7.51 (t, $J = 8.0$ Hz, 1H, H-3), 4.96 (s, 2H, H-7), 2.37 (s, 3H, H-10).

4-(2-Bromoacetyl)-2,6-difluorophenyl acetate: 25b

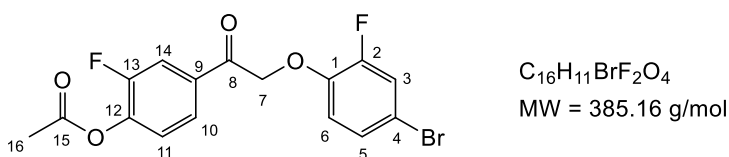


The *general procedure G* was followed using **24b** (0.790 g), acetic anhydride (30 mL) and HCl conc. (10 drops). The crude product was recrystallized from EtOH to obtain **25b** as a white solid (0.053 g, 0.180 mmol) in 1% yield over two step.

Rf = 0.65 (Cyclohexane/EtOAc 8:2)

¹H NMR (500 MHz, DMSO-*d*₆) δ : 7.92 (d, $J_{\text{H-2,F-3}} = J_{\text{H-6,F-5}} = 8.0$ Hz, 2H, H-2, H-6), 5.21 (s, 2H, H-7), 2.44 (s, 3H, H-10).

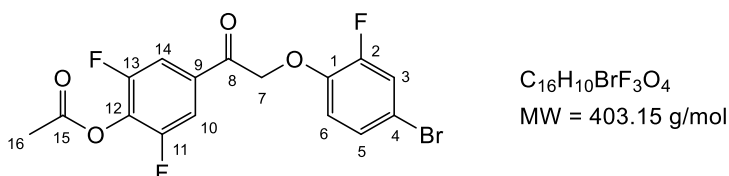
4-(2-(4-Bromo-2-fluorophenoxy)acetyl)-2-fluorophenyl acetate: 26a



The *general procedure E* was followed using 2-fluoro-4-bromophenol (0.1 mL, 0.90 mmol) and K_2CO_3 (0.127 g, 0.90 mmol) in acetone (10 mL) and **25a** (0.053 g, 0.180 mmol). The crude residue **26a**, as a brown oil (0.236 g), was used in the next step without further purification.

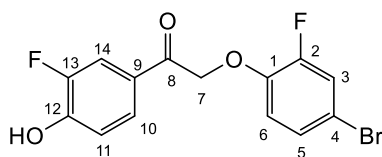
Rf = 0.50 (Cyclohexane/EtOAc, 7:3)

4-(2-(4-Bromo-2-fluorophenoxy)acetyl)-2,6-difluorophenyl acetate: 26b



The *general procedure E* was followed using 2-fluoro-4-bromophenol (0.019 mL, 0.180 mmol) and K_2CO_3 (0.027 g, 0.198 mmol) in acetone (4 mL) and **25b** (0.249 g, 0.90 mmol). The crude residue **26b** (0.236 g) was used in the next step without further purification.

Rf = 0.25 (Cyclohexane/EtOAc, 7:3)

2-(4-Bromo-2-fluorophenoxy)-1-(3-fluoro-4-hydroxyphenyl)ethan-1-one: 27a

$C_{14}H_9BrF_2O_3$
MW = 343.12 g/mol

The *general procedure H* was followed using **26a** (0.381 g, 0.0989 mmol) in EtOH (6 mL) and NaOAc (0.811 g, 9.89 mmol) in water (1 mL). The crude residue was purified by column chromatography on silica gel (Cyclohexane/EtOAc, 8:2) to yield **27a** as a white solid (0.059 g, 0.171 mmol) in 17% yield over two steps.

Rf = 0.28 (Cyclohexane/EtOAc, 7:3)

1H NMR (500 MHz, DMSO- d_6) δ : 11.01 (s, 1H, OH), 7.79 (dd, $J_{H-14,F-13} = 12.0$ Hz, $J_{H-14,H-10} = 1.5$ Hz, 1H, H-14), 7.71 (dd, $J_{H-10,H-11} = 8.5$ Hz, $J_{H-10,H-14} = 1.5$ Hz, 1H, H-10), 7.55 (dd, $J_{H-3,F-2} = 11.0$ Hz, $J_{H-3,H-5} = 2.0$ Hz, 1H, H-3), 7.28 (dd, $J_{H-5,H-6} = 9.0$ Hz, $J_{H-5,H-3} = 1.5$ Hz, 1H, H-5), 7.08 (t, $J_{H-6,H-5} = J_{H-11,10} = 9.0$ Hz, 2H, H-6, H-11), 5.61 (s, 2H, H-7).

^{13}C NMR (126 MHz, DMSO- d_6) δ : 191.3 (C-8), 151.4 (d, $J_{C-2,F} = 249.3$ Hz, C-2), 150.5 (d, $J_{C-13,F} = 242.9$ Hz, C-13), 150.5 (C-12), 145.5 (d, $J_{C-1,F-1} = 10.0$ Hz, C-1), 127.3 (d, $J = 3.1$ Hz, C-5), 127.2 (C-9), 125.8 (d, $J_{C-9,F} = 4.0$ Hz, C-9), 125.6 (C-10), 119.2 (d, $J_{C-3,F} = 21.0$ Hz, C-3), 117.5 (C-6), 116.7 (C-11), 115.9 (d, $J_{C-14,F} = 19.0$ Hz, C-14), 111.3 (d, $J_{C-4,F} = 8.1$ Hz, C-4), 70.5 (C-7).

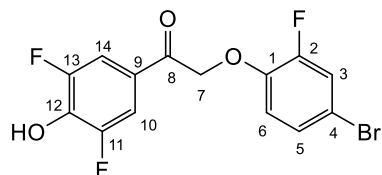
^{19}F NMR (470 MHz, DMSO- d_6) δ : -131.3 (t, $J = 9.4$ Hz), -135.8 (dd, $J = 11.3$ Hz, $J = 9.4$ Hz).

$^{19}F_{cpd}$ NMR (470 MHz, DMSO- d_6) δ : -131.3, -135.8.

HRMS (ESI $^-$) m/z: Calculated for $C_{14}H_8BrF_2O_3$ [M - H] $^-$: 340.9703. Found 340.9618.

IR ν_{max}/cm^{-1} : 3026, 2970, 2946, 1728, 1669, 1587, 1527, 1491, 1455, 1448, 1434, 1366, 1314, 1277, 1260, 1229, 1217, 1205, 1177, 1135, 1063, 1013, 891, 828, 818, 785.

HPLC-MS (ESI) m/z; ($\lambda = 235$ nm): Rt = 12.87 min; 340.9621 [M - H] $^-$.

2-(4-Bromo-2-fluorophenoxy)-1-(3-fluoro-4-hydroxyphenyl)ethan-1-one: 27b

$C_{14}H_8BrF_3O_3$
MW = 361.11 g/mol

The *general procedure H* was followed using **26b** (0.236 g) in EtOH (5 mL) and NaOAc (0.480 g, 5.85 mmol) in water (0.5 mL). The crude residue was purified by column chromatography on silica gel (Cyclohexane/EtOAc, 8:2) and triturated in pentane to yield **27b** (0.013 g, 0.036 mmol) in 20% yield over two steps.

Rf = 0.25 (Cyclohexane/EtOAc, 7:3)

¹H NMR (500 MHz, DMSO-*d*₆) δ : 11.45 (s, 1H, OH), 7.72 (d, $J_{\text{H-10, F-11}} = J_{\text{H-14, F}} = 7.5$ Hz, 2H, H-10, H-14), 7.55 (dd, $J_{\text{H-3, F}} = 10.5$ Hz, $J_{\text{H-3, H-5}} = 1.5$ Hz, 1H, H-3), 7.29 (brd, $J_{\text{H-5, H-6}} = 8.5$ Hz, 1H, H-5), 7.11 (t, $J_{\text{H-6, H-5}} = J_{\text{H-6, F}} = 8.5$ Hz, 1H, H-6), 5.62 (s, 2H, H-7).

¹³C NMR (126 MHz, DMSO-*d*₆) δ : 191.9 (C-8), 151.8 (dd, $J_{\text{C-11, F-11}} = J_{\text{C-13, F-13}} = 244.3$ Hz, $J_{\text{C-11, F-13}} = J_{\text{C-13, F-11}} = 6.8$ Hz, C-11, C-13), 151.4 (d, $J_{\text{C-2, F}} = 249.4$ Hz, C-2), 145.4 (d, $J_{\text{C-1, F}} = 10.1$ Hz, C-1), 139.5 (C-12), 127.3 (d, $J = 3.1$ Hz, C-5), 124.1 (t, $J_{\text{C-9, F}} = 6.4$ Hz, C-9) 119.3 (d, $J_{\text{C-3, F}} = 21.4$ Hz, C-3), 116.8 (C-6), 112.0 (dd, $J = 16.4$ Hz, $J = 6.0$ Hz, C-10, C-14), 111.4 (d, $J_{\text{C-4, F}} = 8.7$ Hz, C-4), 70.5 (C-7).

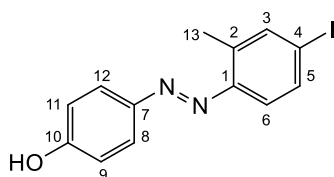
¹⁹F NMR (470 MHz, DMSO-*d*₆) δ : -131.2 (t, $J = 9.4$ Hz), -131.4 (s)

¹⁹F_{cpd} NMR (470 MHz, DMSO-*d*₆) δ : -131.2, -131.4.

HRMS (ESI⁻) m/z : Calculated for C₁₄H₇BrF₃O₃ [M - H]⁻: 358.9609. Found 358.9523.

IR $\nu_{\text{max}}/\text{cm}^{-1}$: 3178, 2921, 1685, 1619, 1591, 1530, 1493, 1440, 1409, 1388, 1334, 1276, 1254, 1199, 1174, 1120, 1072, 1063, 1030, 1012, 914, 891, 858, 836, 813, 785, 747, 719.

HPLC-MS (ESI) m/z ; ($\lambda = 235$ nm): $R_t = 13.32$ min; 358.9537 [M - H]⁻.

(E)-4-((4-Iodo-2-methylphenyl)diazenyl)phenol: 28a

$C_{13}H_{11}IN_2O$
MW = 338.15 g/mol

The *general procedure J* was followed using 4-iodo-2-methylaniline (0.291 g, 1.25 mmol) in 3 M aqueous HCl (1 mL), water (1.25 ml) and 1 M aqueous solution $NaNO_2$ (1.25 mL). Then the mixture was slowly added to a stirred solution of phenol (0.118 g, 1.25 mmol) in 1 M aqueous NaOH. The crude residue was purified by column chromatography (Cyclohexane/EtOAc, 7:3) on silica gel to yield the desired product **28a** as an orange solid (0.173 g, 0.511 mmol) in 41% yield.

Rf = 0.67 (Cyclohexane/EtOAc, 7:3)

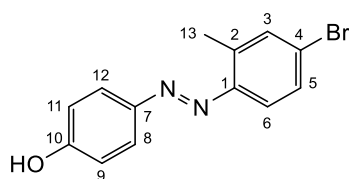
1H NMR (500 MHz, DMSO- d_6) δ : 10.30 (s, 1H, OH), 7.81 (s, 2H, H-5, H-6), 7.79 (s, 1H, H-3), 7.66 (dd, $J_{H-8,H-9}$ = 8.5 Hz, $J_{H-8,H-12}$ = 1.0 Hz, 1H, H-8), 7.29 (br?d, $J_{H-12,H-11}$ = 8.5 Hz, 1H, H-12), 6.95 (d, $J_{H-9,H-8}$ = $J_{H-11,H-12}$ = 8.5 Hz, 2H, H-9, H-11), 2.60 (s, 3H, H-13).

^{13}C NMR (126 MHz, DMSO- d_6) δ : 161.1 (C-10), 149.4 (C-1), 145.6 (C-7), 139.6 (C-3), 139.1 (C-5), 135.4 (C-2), 125.0 (C-8, C-12), 116.9 (C-6), 116.0 (C-9, C-11), 97.3 (C-4), 16.4 (C-13).

HRMS (ESI $^-$) m/z: Calculated for $C_{13}H_{10}IN_2O$ [M - H] $^-$: 336.9916. Found 336.9847.

IR ν_{max}/cm^{-1} : 3153, 1597, 1579, 1504, 1469, 1426, 1382, 1274, 1229, 1176, 1143, 1114, 1071, 940, 860, 838, 768.

UV/Vis (0.2% DMSO/water, 0.06 mM): λ_{max} (ϵ) = 358 (14266) nm ($L \cdot mol^{-1} \cdot cm^{-1}$).

(E)-4-((4-Bromo-2-methylphenyl)diazenyl)phenol: 28b

$C_{13}H_{11}BrN_2O$
MW = 291.15 g/mol

The *general procedure J* was followed using 4-bromo-2-methylaniline (0.232 g, 1.25 mmol) in 3 M HCl (1 mL), water (1.25 ml) and 1 M aqueous solution $NaNO_2$ (1.25 mL). Then the mixture was slowly added to a stirred solution of phenol (0.118 g, 1.25 mmol) in 1 M NaOH. The crude residue was purified by column chromatography (Cyclohexane/EtOAc, 7:3) on silica gel to yield **28b** obtained as a yellow solid (0.097 g, 0.333 mmol) in 27 % yield.

Rf = 0.69 (Cyclohexane/EtOAc, 7:3)

1H NMR (500 MHz, DMSO- d_6) δ : 10.31 (s, 1H, OH), 7.80 (d, $J_{H-5,H-6}$ = 8.5 Hz, 2H, H-5, H-6), 7.64 (s, 1H, H-3), 7.49 (dd, $J_{H-12,H-11}$ = 8.5 Hz, $J_{H-12,H-8}$ = 2.0 Hz, 1H, H-12), 7.45 (dd, $J_{H-8,H-9}$ = 9.0 Hz, $J_{H-8,H-12}$ = 2.0 Hz, 1H, H-8), 6.94 (d, $J_{H-9,H-8}$ = $J_{H-11,H-12}$ = 9.0 Hz, 2H, H-9, H-11), 2.63 (s, 3H, H-13).

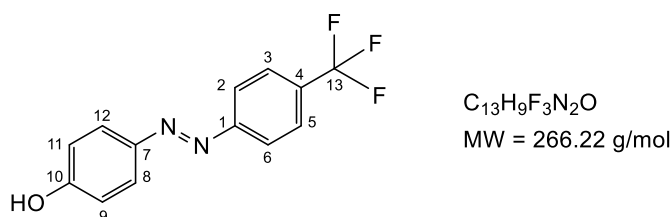
¹³C NMR (126 MHz, DMSO-*d*₆) δ : 161.1 (C-10), 149.0 (C-1), 145.6 (C-7), 139.2 (C-3), 133.7 (C-5), 129.5 (C-2), 125.0 (C-8, C-12), 123.5 (C-6), 117.0 (C-9, C-11), 116.0 (C-4), 16.7 (C-13).

HRMS (ESI⁻) *m/z*: Calculated for C₁₃H₁₀BrN₂O [M – H]⁻: 289.0055. Found 288.9987.

IR ν_{max} /cm⁻¹: 3302, 2921, 2852, 1714, 1597, 1589, 1570, 1503, 1473, 1435, 1374, 1351, 1294, 1257, 1226, 1175, 1142, 1113, 1097, 1076, 939, 865, 840, 768, 725.

UV/Vis (0.2% DMSO/water, 0.056 mM): λ_{max} (ϵ) = 355 (17285) nm (L.mol⁻¹.cm⁻¹).

(*E*)-4-((4-(Trifluoromethyl)phenyl)diazenyl)phenol: 28c



The *general procedure J* was followed using 4-aminobenzotrifluoride (0.16 mL, 1.25 mmol) in 3 M HCl (1 mL), water (1.25 mL) and 1 M aqueous solution NaNO₂ (1.25 mL). Then the mixture was slowly added to a stirred solution of phenol (0.118 g, 1.25 mmol) in 1M NaOH. The crude residue was purified by column chromatography (Cyclohexane/EtOAc, 7:3) on silica gel to yield **28c** as an orange solid (0.102 g, 0.383 mmol) in 32 % yield.

R_f = 0.85 (Cyclohexane/EtOAc, 7:3)

¹H NMR (500 MHz, DMSO-*d*₆) δ : 10.47 (s, 1H, OH), 7.99 (d, $J_{\text{H-2,H-3}} = J_{\text{H-6,H-5}} = 8.5$ Hz, 2H, H-2, H-6), 7.93 (d, $J_{\text{H-3,H-2}} = J_{\text{H-5,H-6}} = 8.5$ Hz, 2H, H-3, H-5), 7.87 (d, $J_{\text{H-8,H-9}} = J_{\text{H-12,H-11}} = 9.0$ Hz, 2H, H-8, H-12), 6.98 (d, $J_{\text{H-9,H-8}} = J_{\text{H-11,H-12}} = 9.0$ Hz, 2H, H-9, H-11).

¹³C NMR (126 MHz, DMSO-*d*₆) δ : 161.8 (C-10), 154.3 (C-1), 145.2 (C-7), 129.8 (q, $J_{\text{C-4,F}} = 31.7$ Hz, C-4), 126.5 (d, $J_{\text{C-3,F}} = J_{\text{C-5,F}} = 3.5$ Hz, C-3, C-5), 125.4 (C-8, C-12), 125.1 (q, $J_{\text{C-13,F}} = 271.9$ Hz, C-13), 122.6 (C-2, C-6), 116.1 (C-9, C-11).

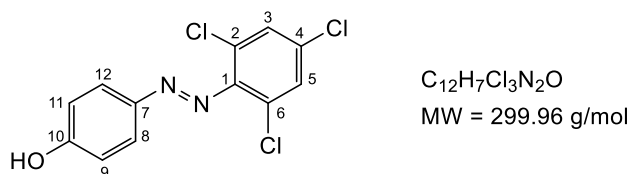
¹⁹F_{cpd} NMR (470 MHz, DMSO-*d*₆) δ : –60.9.

HRMS (ESI⁻) *m/z*: Calculated for C₁₃H₈F₃N₂O [M – H]⁻: 265.0667. Found 265.0596.

IR ν_{max} /cm⁻¹: 3674, 2987, 2901, 1588, 1406, 1393, 1382, 1324, 1250, 1229, 1168, 1100, 1066, 1057, 1027, 892, 850.

UV/Vis (0.2% DMSO/water, 0.06 mM): λ_{max} (ϵ) = 350 (13116), 256 (15033) nm (L.mol⁻¹.cm⁻¹).

(*E*)-4-((2,4,6-trichlorophenyl)diazenyl)phenol: 28d



The *general procedure J* was followed using 2,4,6-trichloroaniline (0.245 g, 1.25 mmol) in 3 M HCl (1 mL), water (1.25 mL) and 1 M aqueous solution NaNO₂ (1.25 mL). Then the mixture was slowly added to a stirred solution of phenol (0.118 g, 1.25 mmol) in 1 M NaOH (2.5 mL). The crude residue was purified by column chromatography (Cyclohexane/EtOAc, 7:3) on silica gel to yield **28d** as an orange solid (0.106 g, 0.353 mmol) in 28 % yield.

¹H NMR (500 MHz, DMSO-*d*₆) δ : 10.6 (s, 1H, OH), 7.84 (s, 1H, H-3), 7.83 (d, $J_{\text{H-9,H-8}} = J_{\text{H-11,H-12}} = 8.5$ Hz, 2H, H-9, H-11), 7.82 (s, 1H, H-5), 6.98 (d, $J_{\text{H-8,H-9}} = J_{\text{H-12,H-11}} = 8.5$ Hz, 2H, H-8, H-12).

¹³C NMR (126 MHz, DMSO-*d*₆) δ : 162.6 (C-10), 146.8 (C-1), 145.0 (C-7), 132.1 (C-4), 129.0 (C-9, C-11), 126.6 (C-2, C-6), 125.4 (C-3, C-5), 116.1 (C-8, C-12).

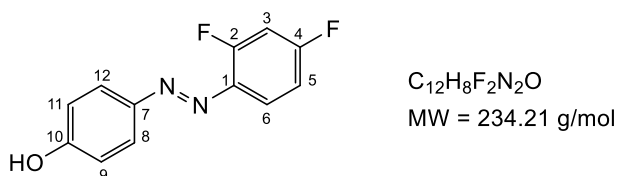
R_f = 0.58 (Cyclohexane/EtOAc, 7:3)

HRMS (ESI⁻) *m/z*: Calculated for C₁₂H₆Cl₃N₂O [M – H]⁻: 299.9624. Found 298.9554.

IR ν_{max} /cm⁻¹: 3082, 1603, 1549, 1504, 1434, 1382, 1284, 1223, 1186, 1145, 1102, 896, 854, 838, 825, 801, 745, 716.

UV/Vis (0.2% DMSO/water, , 0.055 mM): λ_{max} (ϵ) = 341 (17509) nm (L.mol⁻¹.cm⁻¹).

(*E*)-4-((2,4-difluorophenyl)diazenyl)phenol: 28e



The *general procedure J* was followed using 2,4-difluoroaniline (0.161 g, 1.25 mmol) in 3 M HCl (1 mL), water (1.25 mL) and 1 M aqueous solution NaNO₂ (1.25 mL). Then the mixture was slowly added to a stirred solution of phenol (0.118 g, 1.25 mmol) in 1 M NaOH. The crude residue was purified by column chromatography (Cyclohexane/EtOAc, 8:2) on silica gel to yield **28e** as an orange solid (0.050 g, 0.213 mmol) in 17 % yield.

R_f = 0.36 (Cyclohexane/EtOAc, 8:2)

¹H NMR (500 MHz, DMSO-*d*₆) δ : 10.52 (s, 1H, OH), 7.79 (d, $J_{\text{H-8,H-9}} = J_{\text{H-12,H-11}} = 9.0$ Hz, 2H, H-8, H-12), 7.74 (dt, 1H, $J_{\text{H-6,H-5}} = J_{\text{H-6,F}} = 9.0$ Hz, $J_{\text{H-6,F}} = 6.5$ Hz, H-6), 7.47 (ddd, $J_{\text{H-3,F}} = 10$ Hz, $J_{\text{H-3,F}} = 9.0$ Hz, $J_{\text{H-3,H-5}} = 2.0$ Hz, 1H, H-3), 7.19 (m, 1H, H-5), 6.94 (d, $J_{\text{H-9,H-8}} = J_{\text{H-11,H-12}} = 9.0$ Hz, 2H, H-9, H-11).

¹³C NMR (126 MHz, DMSO-*d*₆) δ : 163.5 (dd, $J_{\text{C-4,F-4}} = 252.0$ Hz, $J_{\text{C-4,F-2}} = 12.6$ Hz, C-4), 161.6 (C-10), 159.3 (dd, $J_{\text{C-2,F-2}} = 257.0$ Hz, $J_{\text{C-2,F-4}} = 12.6$ Hz, C-2), 145.6 (C-7), 137.3 (dd, $J = 7.6$ Hz, $J = 3.8$ Hz, C-1), 125.4 (C-8, C-12), 119.2 (d, $J_{\text{C-6,F-2}} = 11.0$ Hz, C-6), 116.3 (C-9, C-11), 112.5 (dd, $J_{\text{C-5,F-4}} = 25.2$ Hz, $J_{\text{C-5,F-2}} = 3.1$ Hz, C-5), 105.5 (t, $J_{\text{C-3,F}} = 25.2$ Hz, C-3).

¹⁹F NMR (470 MHz, DMSO-*d*₆) δ : -106.7 (d, $J = 7.5$ Hz), -120.8 (d, $J = 9.4$ Hz).

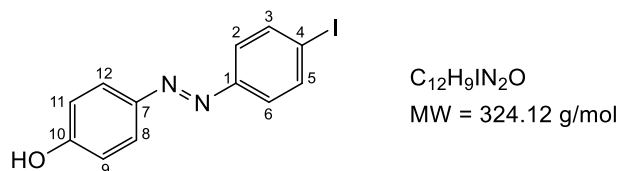
¹⁹F_{cpd} NMR (470 MHz, DMSO-*d*₆) δ : -106.7, -120.8.

HRMS (ESI⁻) m/z: Calculated for C₁₂H₇F₂N₂O [M – H]⁻: 233.0605. Found 233.0530.

IR ν_{max} /cm⁻¹: 3228, 2919, 2850, 1609, 1598, 1588, 1493, 1475, 1455, 1390, 1307, 1278, 1224, 1143, 1106, 964, 859, 844, 829, 775, 731.

UV/Vis (0.2% DMSO/water, 0.07 mM): λ_{max} (ϵ) = 351 (1000), 264 (12171) nm (L.mol⁻¹.cm⁻¹).

(E)-4-((4-Iodophenyl)diazenyl)phenol: 28f



The *general procedure J* was followed using 4-iodoaniline (0.273 g, 1.25 mmol) in 3 M aqueous HCl (1 mL), water (1.25 mL) and 1 M aqueous solution NaNO₂ (1.25 mL). Then the mixture was slowly added to a stirred solution of phenol (0.118 g, 1.25 mmol) in 1 M NaOH (2.5 mL). The crude residue was purified by column chromatography (Cyclohexane/EtOAc, 8:2) on silica gel to yield the product **28f** as a red solid (0.252 g, 0.777 mmol) in 62% yield.

R_f = 0.53 (Cyclohexane/EtOAc, 7:3)

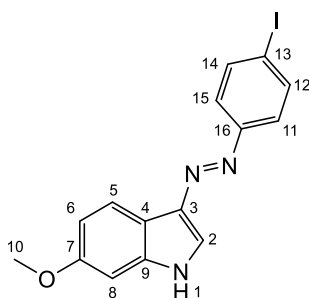
¹H NMR (500 MHz, DMSO-*d*₆) δ : 10.35 (s, 1H, OH), 7.93 (d, $J_{\text{H-3,H-2}} = J_{\text{H-5,H-6}} = 8.0$ Hz, 2H, H-3, H-5), 7.80 (d, $J_{\text{H-2,H-3}} = J_{\text{H-6,H-5}} = 9.0$ Hz, 2H, H-2, H-6), 7.59 (d, $J_{\text{H-8,H-9}} = J_{\text{H-12,H-11}} = 8.5$ Hz, 2H, H-8, H-12), 6.94 (d, $J_{\text{H-9,H-8}} = J_{\text{H-11,H-12}} = 8.5$ Hz, 2H, H-9, H-11).

¹³C NMR (126 MHz, DMSO-*d*₆) δ : 161.3 (C-10), 151.4 (C-1), 145.1 (C-7), 138.2 (C-3, C-5), 125.0 (C-2, C-6), 124.0 (C-8, C-12), 116.0 (C-9, C-11), 97.4 (C-4).

HRMS (ESI⁻) m/z: Calculated for C₁₂H₈I₂N₂O [M – H]⁻: 322.9760. Found 322.9694.

IR ν_{max} /cm⁻¹: 3288, 1599, 1504, 1475, 1443, 1392, 1248, 1142, 1102, 1053, 1004, 842, 725.

UV/Vis (0.2% DMSO/water, 0.051 mM): λ_{max} (ϵ) = 314 (10686), 257 (19509) nm (L.mol⁻¹.cm⁻¹).

(E)-3-((4-Iodophenyl)diazenyl)-6-methoxy-1H-indole: 29aC₁₅H₁₂IN₃O

MW = 377.19 g/mol

The *general procedure J* was followed using 4-iodoaniline (0.273 g, 1.25 mmol) in 3 M aqueous HCl (1 mL), water (1.25 mL) and 1 M aqueous solution NaNO₂ (1.25 mL). Then the mixture was slowly added to a stirred solution of 6-methoxyindole (0.183 g, 1.25 mmol) in 1 M NaOH (2.5 mL) and dioxane (2 mL). The crude residue was purified by column chromatography (Cyclohexane/EtOAc, 8:2) on silica gel to yield **29a** as a dark red solid (0.261 g, 0.699 mmol) in 55% yield.

Rf = 0.10 (Cyclohexane/EtOAc, 8:2)

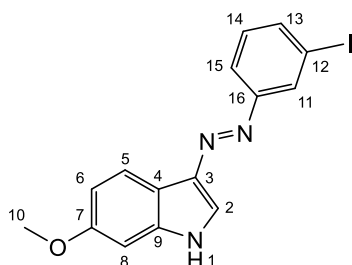
¹H NMR (500 MHz, DMSO-*d*₆) δ : 11.96 (s, 1H, NH), 8.26 (s, 1H, H-2), 8.23 (d, $J_{\text{H-5,H-6}} = 8.5$ Hz, 1H, H-5), 7.87 (d, $J_{\text{H-12,H-11}} = J_{\text{H-14,H-15}} = 8.5$ Hz, 2H, H-12, H-14), 7.57 (d, $J_{\text{H-11,H-12}} = J_{\text{H-15,H-14}} = 8.5$ Hz, 2H, H-11, H-15), 6.97 (s, 1H, H-8), 6.86 (d, $J_{\text{H-6,H-5}} = 8.5$ Hz, 1H, H-6), 3.81 (s, 3H, H-10).

¹³C NMR (126 MHz, DMSO-*d*₆) δ : 157.0 (C-7), 152.7 (C-9), 137.9 (C-12, C-14), 137.8 (C-16), 135.8 (C-4), 133.7 (C-2), 123.2 (C-11, C-15), 123.0 (C-5), 112.2 (C-3), 112.0 (C-6), 95.4 (C-8), 94.6 (C-13), 55.2 (C-10).

MS (ESI⁻) *m/z*: Calculated for C₁₅H₁₁IN₃O [M – H]⁻: 376.0. Found 376.0.

IR ν_{max} /cm⁻¹: 3173, 1629, 1578, 1567, 1525, 1511, 1475, 1451, 1431, 1409, 1377, 1334, 1303, 1266, 1242, 1189, 1164, 1147, 1113, 1097, 1087, 1056, 1023, 1003, 927, 841, 826, 809, 753, 728.

UV/Vis (1% DMSO/water, 51 μ M): λ_{max} (ϵ) = 435 (18509), 300 (13843) nm (L.mol⁻¹.cm⁻¹).

(E)-3-((3-Iodophenyl)diazenyl)-6-methoxy-1H-indole: 29bC₁₅H₁₂IN₃O

MW = 377.19 g/mol

The *general procedure J* was followed using 3-iodoaniline (0.273 g, 1.25 mmol) in 3 M HCl (1 mL), water (1.25 mL) and 1 M aqueous solution NaNO₂ (1.25 mL). Then the mixture was slowly added to a stirred solution of 6-methoxyindole (0.183 g, 1.25 mmol) in 1 M NaOH (2.5 mL) and dioxane

(2 mL). The crude residue was purified by column chromatography (Cyclohexane/EtOAc, 8:2) on silica gel to yield **29b** as an orange-red solid (0.215 g, 0.570 mmol) in 46% yield.

R_f = 0.10 (Cyclohexane/EtOAc, 8:2)

¹H NMR (500 MHz, DMSO-*d*₆) δ : 12.00 (brs, 1H, NH), 8.30 (d, $J_{\text{H-2,NH}} = 2.5$ Hz, 1H, H-2), 8.23 (d, $J_{\text{H-5,H-6}} = 8.5$ Hz, 1H, H-5), 8.09 (s, 1H, H-11), 7.81 (d, $J_{\text{H-15,H-14}} = 8.0$ Hz, 1H, H-15), 7.73 (d, $J_{\text{H-13,H-14}} = 8.0$ Hz, 1H, H-13), 7.32 (t, $J_{\text{H-14,H-13}} = J_{\text{H-14,H-15}} = 8.0$ Hz, 1H, H-14), 6.98 (d, $J_{\text{H-8,H-6}} = 2.0$ Hz, 1H, H-8), 6.87 (dd, $J_{\text{H-6,H-5}} = 8.5$ Hz, $J_{\text{H-6,H-8}} = 2.0$ Hz, 1H, H-6), 3.81 (s, 1H, H-10).

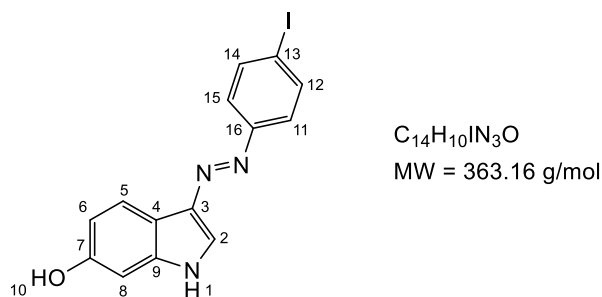
¹³C NMR (126 MHz, DMSO-*d*₆) δ : 157.1 (C-7), 154.3 (C-16), 137.8 (C-q), 136.8 (C-13), 135.8 (C-q), 134.2 (C-2), 131.2 (C-14), 128.3 (C-11), 123.1 (C-5), 122.0 (C-15), 112.1 (C-14), 95.4 (C-8), 95.3 (C-12), 55.2 (C-10).

MS (ESI⁻) *m/z*: Calculated for C₁₅H₁₁N₃O [M – H]⁻: 376.0. Found 376.0.

IR ν_{max} /cm⁻¹: 3672, 3254, 2988, 2901, 1625, 1562, 1521, 1453, 1408, 1384, 1358, 1260, 1242, 1197, 1163, 1141, 1109, 1076, 1066, 1057, 945, 891, 822, 808, 790.

UV/Vis (1% DMSO/water, 51 μ M): λ_{max} (ϵ) = 387 (19431), 291 (13333) nm (L.mol⁻¹.cm⁻¹).

(*E*)-3-((4-Iodophenyl)diazenyl)-1*H*-indol-6-ol: **30a**



The *general procedure D* was followed using **29a** (0.100 g, 0.26 mmol) and 1 M BBr₃ in CH₂Cl₂ (5 mL). The crude residue was purified by column chromatography on silica gel (Cyclohexane/EtOAc, 8:2) to obtain **30a** as a dark red solid (0.058 g, 0.159 mmol) in 60% yield.

R_f = 0.26 (Cyclohexane/EtOAc, 6:4)

¹H NMR (500 MHz, DMSO-*d*₆) δ : 11.82 (s, 1H, NH), 9.35 (s, 1H, OH), 8.18 (d, $J_{\text{H-2,NH}} = 3.0$ Hz, 1H, H-2), 8.14 (d, $J_{\text{H-5,H-6}} = 8.5$ Hz, 1H, H-5), 7.85 (d, $J_{\text{H-12,H-11}} = J_{\text{H-14,H-15}} = 8.5$ Hz, 2H, H-12, H-14), 7.55 (d, $J_{\text{H-11,H-12}} = J_{\text{H-15,H-14}} = 8.5$ Hz, 2H, H-11, H-15), 6.82 (d, $J_{\text{H-8,H-6}} = 2.0$ Hz, 1H, H-8), 6.72 (dd, $J_{\text{H-6,H-5}} = 8.5$ Hz, $J_{\text{H-6,H-8}} = 2.0$ Hz, 1H, H-6).

¹³C NMR (126 MHz, DMSO-*d*₆) δ : 154.9 (C-7), 152.8 (C-9), 138.2 (C-16), 137.9 (C-12, C-14), 136.0 (C-4), 133.5 (C-2), 123.2 (C-11, C-15), 123.0 (C-5), 112.4 (C-6), 111.3 (C-3), 97.4 (C-8), 94.3 (C-13).

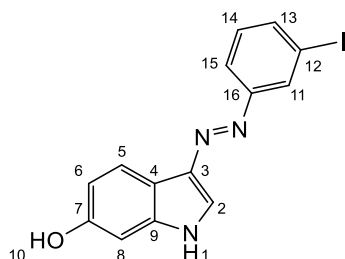
MS (ESI⁻) *m/z*: Calculated for C₁₄H₉I N₃O [M – H]⁻: 361.9. Found 362.0.

IR ν_{max} /cm⁻¹: 3421, 2972, 1626, 1532, 1453, 1380, 1343, 1328, 1235, 1159, 1099, 1053, 1002, 946, 826, 740, 719, 706.

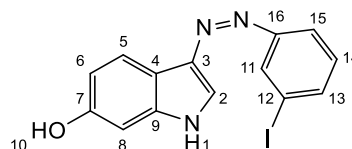
UV/Vis (1% DMSO/water, 53 μ M): λ_{\max} (ϵ) = 386 (13849), 288 (8886) nm ($L \cdot mol^{-1} \cdot cm^{-1}$).

(E)-3-((3-Iodophenyl)diazenyl)-1H-indol-6-ol: 30b

(Z)-3-((3-Iodophenyl)diazenyl)-1H-indol-6-ol



$C_{14}H_{10}IN_3O$
MW = 363.16 g/mol



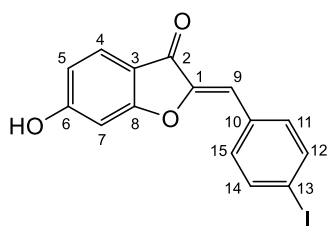
The *general procedure D* was followed using **29b** (0.100 g, 0.26 mmol) and 1 M BBr_3 in CH_2Cl_2 (5 mL). The crude residue was purified by column chromatography on silica gel (Cyclohexane/EtOAc, 8:2) to obtain **30b** as a dark red solid (0.056 g, 0.154 mmol) in 59% yield. Product obtained as *E* isomer for 23% and *Z* isomer for 77%.

Rf = 0.24 (Cyclohexane/EtOAc, 6:4)

Z isomer: 1H NMR (500 MHz, $DMSO-d_6$) δ : 9.44 (d, J = 2.5 Hz, 1H, NH), 8.83 (s, 1H, OH), 8.42 (s, 1H), 8.06 (d, J = 8.5 Hz, 1H), 7.83 (dd, J = 9.0 Hz, J = 2.0 Hz, 1H), 7.49 (dd, J = 9.0 Hz, J = 2.0 Hz, 1H), 6.49 (m, 2H), 6.28 (m, 1H), 6.20 (td, J = 8.5 Hz, J = 2.5 Hz, 1H).

MS (ESI $^+$) m/z : 364.0 $[M + H]^+$.

IR ν_{\max}/cm^{-1} : 3671, 2988, 2972, 2901, 1622, 1599, 1512, 1453, 1406, 1394, 1583, 1250, 1242, 1232, 1200, 1075, 1066, 1057, 892, 879, 837, 807.

(Z)-6-Hydroxy-2-(4-iodobenzylidene)benzofuran-3(2H)-one: 31a

$C_{15}H_9IO_3$
MW = 364.14 g/mol

The *general procedure K* was followed using a stirred solution of 6-hydroxybenzofuranone (0.200 g, 1.332 mmol) in a mixture EtOH (1.5 mL) and DMF (1.5 mL). Then 4-iodobenzaldehyde (0.309 g, 1.332 mmol) and 50% aqueous solution of KOH (0.5 mL) were added to the solution. Product **31a** was obtained as a yellow solid (0.178 g, 0.489 mmol) in 37% yield.

Rf = 0.55 (Cyclohexane/EtOAc, 6:4)

1H NMR (500 MHz, DMSO- d_6) δ : 11.25 (s, 1H, OH), 7.87 (d, $J_{H-12,H-11} = J_{H-14,H-15} = 8.0$ Hz, 2H, H-12, H-14), 7.72 (d, $J_{H-11,H-12} = J_{H-15,H-14} = 8.0$ Hz, 2H, H-11, H-15), 7.63 (d, $J_{H-4,H-5} = 8.5$ Hz, 1H, H-4), 6.79 (s, 1H, H-9), 6.76 (s, 1H, H-7), 6.73 (d, $J_{H-5,H-4} = 8.5$ Hz, H-5).

^{13}C NMR (126 MHz, DMSO- d_6) δ : 181.3 (C-2), 167.9 (C-8), 166.7 (C-6), 147.7 (C-1), 137.8 (C-12, C-14), 132.7 (C-11, C-15), 131.6 (C-10), 126.0 (C-4), 113.2 (C-5), 112.6 (C-3), 109.3 (C-7), 98.6 (C-9), 96.7 (C-13).

HRMS (ESI $^-$) m/z: Calculated for $C_{15}H_8IO_3$ [M - H] $^-$: 362.9596. Found 362.9525.

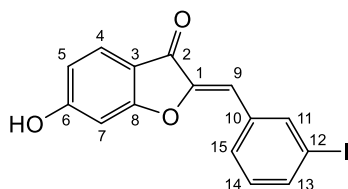
IR ν_{max}/cm^{-1} : 3064, 1678, 1615, 1574, 1480, 1452, 1398, 1385, 1334, 1309, 1286, 1253, 1195, 1133, 1117, 1110, 1059, 1005, 970, 883, 840, 810, 797, 768.

UV/Vis (DMSO, 0.055 mM): $\lambda_{max}(\epsilon) = 351$ (15200), 267 (7127) nm (L.mol $^{-1}$.cm $^{-1}$).

UV/Vis (MeOH, 0.055 mM): $\lambda_{max}(\epsilon) = 359$ (15218) nm (L.mol $^{-1}$.cm $^{-1}$).

UV/Vis (EtOAc, 0.045 mM): $\lambda_{max}(\epsilon) = 340$ (13955), 262 (4044) nm (L.mol $^{-1}$.cm $^{-1}$).

UV/Vis (0.2% DMSO/PBS 0.1 M, pH 7.2, 0.06 mM): $\lambda_{max}(\epsilon) = 378$ (13500) nm (L.mol $^{-1}$.cm $^{-1}$).

(Z)-6-Hydroxy-2-(3-iodobenzylidene)benzofuran-3(2H)-one: 31b

$C_{15}H_9IO_3$
MW = 364.14 g/mol

The *general procedure K* was followed using a stirred solution of 6-hydroxybenzofuranone (0.200 g, 1.332 mmol) in a mixture of EtOH (1.5 mL) and DMF (1.5 mL). Then 3-iodobenzaldehyde (0.309 g, 1.332 mmol) and 50% aqueous solution of KOH (0.5 mL) were added to the solution. Product **31b** was obtained as a yellow solid (0.132 g, 0.362 mmol) in 27% yield.

Rf = 0.47 (Cyclohexane/EtOAc, 6:4)

¹H NMR (500 MHz, DMSO-*d*₆) δ : 11.26 (s, 1H, OH), 8.27 (s, 1H, H-11), 8.00 (d, $J_{\text{H-13,H-14}} = 8.0$ Hz, 1H, H-13), 7.79 (d, $J_{\text{H-15,H-14}} = 8.0$ Hz, 1H, H-15), 7.64 (d, $J_{\text{H-5,H-4}} = 8.5$ Hz, 1H, H-5), 7.31 (t, $J_{\text{H-14,H-13}} = J_{\text{H-14,H-15}} = 8.0$ Hz, 1H, H-14), 6.81 (s, 1H, H-9), 6.75 (s, 1H, H-7), 6.73 (d, $J_{\text{H-4,H-5}} = 8.5$ Hz, 1H, H-4).

¹³C NMR (126 MHz, DMSO-*d*₆) δ : 181.3 (C-2), 168.0 (C-8), 166.8 (C-6), 147.8 (C-1), 139.0 (C-11), 137.9 (C-15), 134.4 (C-10), 130.9 (C-14), 130.0 (C-13), 126.1 (C-5), 113.2 (C-4), 112.5 (C-3), 108.5 (C-7), 98.7 (C-9), 95.3 (C-12).

HRMS (ESI⁻) m/z : Calculated for C₁₅H₈IO₃ [M – H]⁻: 362.9596. Found 362.9525.

IR $\nu_{\text{max}}/\text{cm}^{-1}$: 3073, 1674, 1639, 1574, 1454, 1412, 1332, 1292, 1257, 1211, 1134, 1110, 1066, 993, 970, 949, 908, 890, 833, 822, 783.

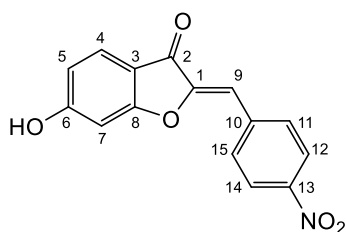
UV/Vis (DMSO, 0.055 mM): λ_{max} (ϵ) = 436 (3963), 336 (12600), 286 (10490) nm (L.mol⁻¹.cm⁻¹).

UV/Vis (MeOH, 0.055 mM): λ_{max} (ϵ) = 342 (7654), 288 (4018) nm (L.mol⁻¹.cm⁻¹).

UV/Vis (EtOAc, 0.055 mM): λ_{max} (ϵ) = 328 (11036), 280 (6490) nm (L.mol⁻¹.cm⁻¹).

UV/Vis (0.2% DMSO/PBS 0.1 M, pH 7.2, 0.055 mM): λ_{max} (ϵ) = 365 (8272) nm (L.mol⁻¹.cm⁻¹).

(Z)-6-Hydroxy-2-(4-nitrobenzylidene)benzofuran-3(2H)-one: 31c



C₁₅H₉NO₅
MW = 283.24 g/mol

The *general procedure K* was followed using a stirred solution of 6-hydroxybenzofuranone (0.200 g, 1.332 mmol) in a mixture of EtOH (1.5 mL) and DMF (1.5 mL). Then 4-nitrobenzaldehyde (0.199 g, 1.332 mmol) and 50% aqueous solution of KOH (0.5 mL) were added to the solution. Product **31c** was obtained as a yellow solid (0.145 g, 0.511 mmol) in 38% yield.

R_f = 0.40 (Cyclohexane/EtOAc, 6:4)

¹H NMR (500 MHz, DMSO-*d*₆) δ : 11.39 (s, 1H, OH), 8.32 (d, $J_{\text{H-12,H-11}} = J_{\text{H-14,H-15}} = 9.0$ Hz, 2H, H-12, H-14), 8.19 (d, $J_{\text{H-11,H-12}} = J_{\text{H-15,H-14}} = 9.0$ Hz, 2H, H-11, H-15), 7.66 (d, $J_{\text{H-4,H-5}} = 8.5$ Hz, 1H, H-4), 6.92 (s, 1H, H-9), 6.81 (d, $J_{\text{H-7,H-5}} = 2.0$ Hz, 1H, H-7), 6.74 (dd, $J_{\text{H-5,H-4}} = 8.5$ Hz, $J_{\text{H-5,H-7}} = 2.0$ Hz, 1H, H-5).

¹³C NMR (126 MHz, DMSO-*d*₆) δ : 181.2 (C-2), 168.2 (C-8), 167.2 (C-6), 149.1 (C-13), 147.0 (C-1), 138.8 (C-10), 131.7 (C-11, C-15), 126.3 (C-4), 123.9 (C-12, C-14), 113.5 (C-5), 112.2 (C-3), 107.4 (C-9), 98.8 (C-7).

HRMS (ESI⁻) m/z : Calculated for C₁₅H₈F₂NO₃ [M – H]⁻: 282.0481. Found 282.0408.

IR $\nu_{\text{max}}/\text{cm}^{-1}$: 3121, 1682, 1651, 1599, 1511, 1456, 1391, 1349, 1311, 1283, 1252, 1133, 1107, 966, 946, 884, 862, 844, 799, 767, 747.

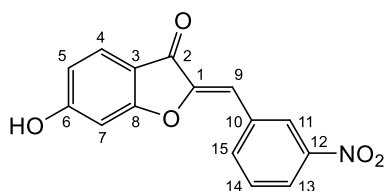
UV/Vis (DMSO, 0.068 mM): $\lambda_{\max}(\epsilon) = 480$ (3279), 363 (14191) nm ($\text{L}\cdot\text{mol}^{-1}\cdot\text{cm}^{-1}$).

UV/Vis (MeOH, 0.068 mM): $\lambda_{\max}(\epsilon) = 355$ (14573) nm ($\text{L}\cdot\text{mol}^{-1}\cdot\text{cm}^{-1}$).

UV/Vis (EtOAc, 0.068 mM): $\lambda_{\max}(\epsilon) = 348$ (10352) nm ($\text{L}\cdot\text{mol}^{-1}\cdot\text{cm}^{-1}$).

UV/Vis (0.2% DMSO/ PBS 0.1 M, pH 7.2, 0.08 mM): $\lambda_{\max}(\epsilon) = 386$ (6512), 310 (4537) nm ($\text{L}\cdot\text{mol}^{-1}\cdot\text{cm}^{-1}$).

(Z)-6-Hydroxy-2-(4-nitrobenzylidene)benzofuran-3(2H)-one: 31d



$\text{C}_{15}\text{H}_9\text{NO}_5$
MW = 283.24 g/mol

The *general procedure K* was followed using a stirred solution of 6-hydroxybenzofuranone (0.200 g, 1.332 mmol) in a mixture of EtOH (1.5 mL) and DMF (1.5 mL). Then 3-nitrobenzaldehyde (0.199 g, 1.332 mmol) and 50% aqueous solution of KOH (0.5 mL) were added to the solution. Product **31d** was obtained as a yellow solid (0.162 g, 0.571 mmol) in 51% yield.

Rf = 0.38 (Cyclohexane/EtOAc, 6:4)

^1H NMR (500 MHz, DMSO- d_6) δ : 11.33 (s, 1H, OH), 8.76 (s, 1H, H-11), 8.38 (d, $J_{\text{H-13,H-14}} = 8.0$ Hz, 1H, H-13), 8.25 (d, $J_{\text{H-15,H-14}} = 8.0$ Hz, 1H, H-15), 7.79 (t, $J_{\text{H-14,H-13}} = J_{\text{H-14,H-15}} = 8.0$ Hz, 1H, H-14), 7.66 (d, $J_{\text{H-4,H-5}} = 8.5$ Hz, 1H, H-4), 6.98 (s, 1H, H-9), 6.81 (s, 1H, H-7), 6.75 (d, $J_{\text{H-5,H-4}} = 8.5$ Hz, 1H, H-5).

^{13}C NMR (126 MHz, DMSO- d_6) δ : 181.3 (C-2), 168.1 (C-8), 167.0 (C-6), 148.5 (C-14), 148.2 (C-1), 136.8 (C-13), 133.9 (C-10), 130.5 (C-4), 126.3 (C-12), 125.0 (C-11), 123.7 (C-15), 113.4 (C-5), 112.4 (C-3), 107.7 (C-9), 98.7 (C-7).

HRMS (ESI $^-$) m/z: Calculated for $\text{C}_{15}\text{H}_8\text{NO}_5$ [$\text{M} - \text{H}$] $^-$: 282.0481. Found 282.0408.

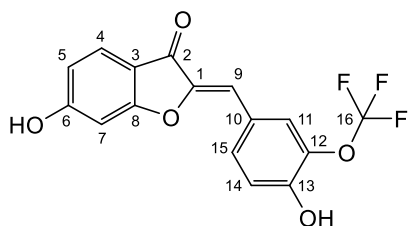
IR $\nu_{\max}/\text{cm}^{-1}$: 3165, 1683, 1659, 1589, 1533, 1496, 1348, 1315, 1299, 1274, 1244, 1201, 1156, 1133, 1100, 1001, 959, 907, 840, 735.

UV/Vis (DMSO, 0.068 mM): $\lambda_{\max}(\epsilon) = 438$ (4308), 339 (13647) nm ($\text{L}\cdot\text{mol}^{-1}\cdot\text{cm}^{-1}$).

UV/Vis (MeOH, 0.068 mM): $\lambda_{\max}(\epsilon) = 338$ (14617), 280 (8294), 260 (7514) nm ($\text{L}\cdot\text{mol}^{-1}\cdot\text{cm}^{-1}$).

UV/Vis (EtOAc, 0.068 mM): $\lambda_{\max}(\epsilon) = 329$ (10132) nm ($\text{L}\cdot\text{mol}^{-1}\cdot\text{cm}^{-1}$).

UV/Vis (0.2% DMSO/PBS 0.1 M, pH 7.2, 0.08 mM): $\lambda_{\max}(\epsilon) = 405$ (5500), 367 (5837) nm ($\text{L}\cdot\text{mol}^{-1}\cdot\text{cm}^{-1}$).

(Z)-6-hydroxy-2-(4-hydroxy-3-(trifluoromethoxy)benzylidene)benzofuran-3(2H)-one:**31e**

$C_{16}H_9F_3O_5$
MW = 338.24 g/mol

The *general procedure K* was followed using a stirred solution of 6-hydroxybenzofuranone (0.200 g, 1.332 mmol) in a mixture of EtOH (1.5 mL) and DMF (1.5 mL). Then 4-hydroxy-3-(trifluoromethyl)benzaldehyde (0.274 g, 1.332 mmol) and 50% aqueous solution of KOH (0.5 mL) were added to the solution. Product **31e** was obtained as a yellow solid (0.097 g, 0.286 mmol) in 22% yield.

Rf = 0.56 (Cyclohexane/EtOAc, 7:3)

1H NMR (500 MHz, DMSO- d_6) δ : 11.01 (s, 2H, 2 OH), 7.88 (s, 1H, H-11), 7.85 (dd, $J_{H-15,H-14}$ = 8.5 Hz, $J_{H-15,H-11}$ = 1.5 Hz, 1H, H-15), 7.61 (d, $J_{H-4,H-5}$ = 8.5 Hz, 1H, H-4), 7.13 (d, $J_{H-14,H-15}$ = 8.5 Hz, 1H, H-14), 6.78 (s, 1H, H-9), 6.77 (d, $J_{H-7,H-5}$ = 1.5 Hz, 1H, H-7), 6.72 (dd, $J_{H-5,H-4}$ = 8.5 Hz, $J_{H-5,H-7}$ = 1.5 Hz, 1H, H-5).

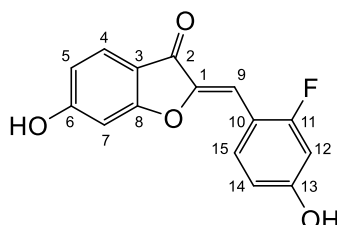
^{13}C NMR (126 MHz, DMSO- d_6) δ : 181.1 (C-2), 167.6 (C-8), 166.4 (C-6), 151.4 (C-12), 146.4 (C-13), 136.1 (C-1), 131.6 (C-15), 125.8 (C-11), 125.8 (C-4), 123.7 (C-3), 118.1 (C-14), 115.8 (q, $J_{C-16,F}$ = 255.8 Hz, C-16), 113.0 (C-10), 112.9 (C-7), 109.6 (C-9), 98.5 (C-5).

$^{19}F_{cpd}$ NMR (470 MHz, DMSO- d_6) δ : -58.3.

HRMS (ESI $^-$) m/z: Calculated for $C_{16}H_8F_3O_5$ [$M - H$] $^-$: 337.0402. Found 337.0310.

IR ν_{max}/cm^{-1} : 3225, 1672, 1639, 1611, 1582, 1519, 1456, 1438, 1381, 1342, 1296, 1282, 1247, 1213, 1169, 1134, 1110, 991, 962, 940, 902, 888, 841, 820, 768, 723.

UV/Vis (0.06% DMSO/ PBS 0.1 M, pH 7.2, 0.019 mM): $\lambda_{max}(\epsilon)$ = 439 (48000) nm (L.mol $^{-1}$.cm $^{-1}$).

(Z)-2-(2-Fluoro-4-hydroxybenzylidene)-6-hydroxybenzofuran-3(2H)-one: 31f

$C_{15}H_9FO_4$
MW = 272.23 g/mol

The *general procedure K* was followed using a stirred solution of 6-Hydroxybenzofuranone (0.200 g, 1.332 mmol) in a mixture of EtOH (1.5 mL) and DMF (1.5 mL). Then 2-fluoro-4-hydroxybenzaldehyde (0.186 g, 1.332 mmol) and 50% aqueous solution of KOH (0.5 mL) were added to the solution. Product was obtained **31f** as a yellow solid (0.128 g, 0.470 mmol) in 35% yield.

R_f = 0.24 (Cyclohexane/EtOAc, 7:3)

¹H NMR (500 MHz, DMSO-*d*₆) δ: 11.18 (s, 1H, OH), 10.61 (s, 1H, OH), 8.09 (t, *J* = 8.5 Hz, 1H), 7.62 (d, *J* = 8.5 Hz, 1H), 6.82 (dd, *J* = 8.5 Hz, *J* = 1.5 Hz, 1H), 6.78 (m, 1H), 6.73 – 6.70 (m, 2H), 6.69 (d, *J* = 1.5 Hz, 1H, H-12).

¹³C NMR (126 MHz, DMSO-*d*₆) δ: 180.9 (C-q), 167.6 (C-q), 166.4 (C-q), 161.9 (d, *J*_{C-11,F} = 251.1 Hz, C-11), 160.9 (d, *J* = 12.6 Hz, C-q), 146.5 (C-q), 132.3 (C-H), 125.9 (C-H), 113.0 (C-H), 112.9 (C-H), 112.8 (C-q), 110.5 (d, *J*_{C-10,F} = 11.3, C-10), 102.8 (d, *J*_{C-12,F} = 24.1 Hz, C-12) 101.4 (d, *J* = 7.3 Hz, C-H), 98.6 (C-H).

¹⁹F NMR (470 MHz, DMSO-*d*₆) δ: –113.9 (dd, *J* = 12.2 Hz, *J* = 9.4 Hz).

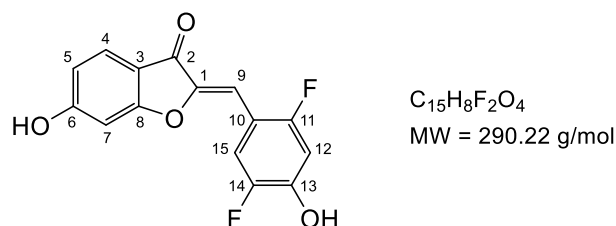
¹⁹F_{cpd} NMR (470 MHz, DMSO-*d*₆) δ: –113.9.

HRMS (ESI[–]) *m/z*: Calculated for C₁₅H₈FO₄ [M – H][–]: 271.0485. Found 271.0397.

IR ν_{max}/cm^{–1}: 3309, 3016, 2970, 2944, 1720, 1665, 1619, 1588, 1588, 1568, 1509, 1458, 1365, 1315, 1288, 1230, 1216, 1207, 1152, 1139, 1115, 1089, 966, 948, 888, 836, 805, 722.

UV/Vis (0.06% DMSO/PBS, 0.1 M, pH 7.2, 0.019 mM): λ_{max} (ε) = 416 (43260) nm (L·mol^{–1}·cm^{–1}).

(Z)-2-(2,5-Difluoro-4-hydroxybenzylidene)-6-hydroxybenzofuran-3(2H)-one: 31g



The *general procedure K* was followed using a stirred solution of 6-hydroxybenzofuranone (0.200 g, 1.332 mmol) in a mixture of EtOH (1.5 mL) and DMF (1.5 mL). Then 2,5-difluoro-4-hydroxybenzoaldehyde (0.210 g, 1.332 mmol) and 50% aqueous solution of KOH (0.5 mL) were added to the solution. Product **31g** was obtained as a yellow solid (0.223 g, 0.768 mmol) in 29% yield.

R_f = 0.24 (Cyclohexane/EtOAc, 7:3)

¹H NMR (500 MHz, DMSO-*d*₆) δ: 11.22 (s, 2H, OH-6, OH-13), 7.97 (dd, *J*_{H-12,F-11} = 12.0 Hz, *J*_{H-12,F-14} = 7.0 Hz, 1H, H-12), 7.63 (d, *J*_{H-4,H-5} = 8.5 Hz, 1H, H-4), 6.91 (dd, *J*_{H-15,F-14} = 11.5 Hz, *J*_{H-15,F-11} = 7.5 Hz, 1H, H-15), 6.86 (d, *J*_{H-7,H-5} = 2.0 Hz, 1H, H-7), 6.74 (dd, *J*_{H-5,H-4} = 8.5 Hz, *J*_{H-5,H-7} = 2.0 Hz, 1H, H-5), 6.67 (s, 1H, H-9).

¹³C NMR (126 MHz, DMSO-*d*₆) δ: 180.9 (C-2), 167.8 (C-8), 166.6 (C-6), 157.4 (d, *J*_{C-11,F-11} = 250.6 Hz, C-11), 148.5 (dd, *J*_{C-10,F-11} = 63.7 Hz, *J*_{C-10,F-14} = 13.2 Hz, C-10), 157.4 (d, *J*_{C-14,F-14} = 231 Hz, C-14), 146.9 (C-1), 125.9 (C-4), 116.9 (d, *J*_{C-12,F-11} = 21.9 Hz, C-12), 113.2 (C-5), 112.6 (C-3), 110.1 (dd, *J*_{C-13,F-14} = 13.8 Hz, *J*_{C-13,F-11} = 7.6 Hz, C-13), 104.9 (d, *J*_{C-15,F-14} = 27.8 Hz, C-15), 100.4 (C-9), 98.9 (C-7).

^{19}F NMR (470 MHz, DMSO- d_6) δ : -118.6 (d, J = 15.0 Hz), -139.2 (d, J = 14.5 Hz).

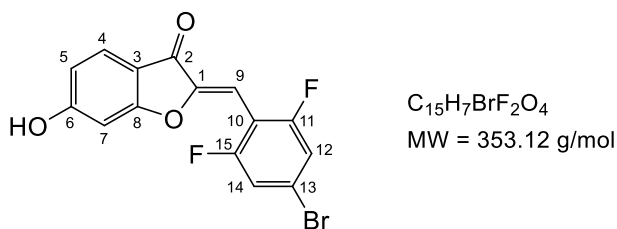
$^{19}\text{F}_{\text{cpd}}$ NMR (470 MHz, DMSO- d_6) δ : -118.6, -139.2.

MS (ESI $^-$) m/z : Calculated for $\text{C}_{15}\text{H}_7\text{F}_2\text{O}_4$ [$\text{M} - \text{H}$] $^-$: 289.0391. Found 289.0302.

IR $\nu_{\text{max}}/\text{cm}^{-1}$: 3305, 1666, 1626, 1576, 1509, 1458, 1379, 1309, 1287, 1244, 1222, 1150, 1114, 948, 891, 835, 807, 765, 734, 715.

UV/Vis (0.06% DMSO/PBS 0.1 M, pH 7.2, 0.022 mM): λ_{max} (ϵ) = 443 (33545) nm ($\text{L}\cdot\text{mol}^{-1}\cdot\text{cm}^{-1}$).

(Z)-2-(4-Bromo-3,5-difluorobenzylidene)-6-hydroxybenzofuran-3(2H)-one: 31h



The *general procedure K* was followed using a stirred solution of 6-hydroxybenzofuranone (0.200 g, 1.332 mmol) in a mixture of EtOH (1.5 mL) and DMF (1.5 mL). Then 4-bromo-2,6-difluorobenzaldehyde (0.294 g, 1.332 mmol) and 50% aqueous solution of KOH (0.5 mL) were added to the solution. Product **31h** was obtained as a yellow solid (0.223 g, 0.631 mmol) in 35% yield.

R f = 0.24 (Cyclohexane/EtOAc, 7:3)

^1H NMR (500 MHz, DMSO- d_6) δ : 11.38 (s, 1H, OH), 7.65 (d, $J_{\text{H-4,H-5}}$ = 8.5 Hz, 1H, H-4), 7.64 (d, $J_{\text{H-12,H-14}}$ = 1.5 Hz, 2H, H-12, H-14), 6.71 (dd, $J_{\text{H-5,H-4}}$ = 8.5 Hz, $J_{\text{H-5,H-7}}$ = 2.0 Hz, 1H, H-5), 6.66 (d, $J_{\text{H-7,H-5}}$ = 2.0 Hz, 1H, H-7), 6.55 (s, 1H, H-9).

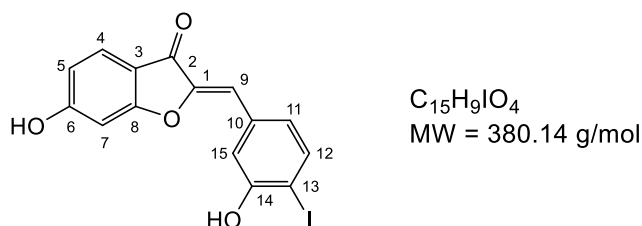
^{13}C NMR (126 MHz, DMSO- d_6) δ : 180.3 (C-2), 168.2 (C-8), 167.5 (C-6), 159.8 (dd, $J_{\text{C-11,F-11}} = J_{\text{C-15,F-15}} = 256.1$ Hz, $J_{\text{C-11,F-15}} = J_{\text{C-15,F-11}} = 7.8$ Hz, C-11, C-15), 149.6 (C-10), 126.5 (C-4), 122.8 (d, $J_{\text{C-13,F-11}} = J_{\text{C-13,F-15}} = 12.7$ Hz, C-13), 116.0 (C-12, C-14), 113.4 (C-5), 112.2 (C-3), 109.1 (C-13), 98.5 (C-7), 95.7 (C-9).

$^{19}\text{F}_{\text{cpd}}$ NMR (470 MHz, DMSO- d_6) δ : -106.1, -107.7.

HRMS (ESI $^-$) m/z : Calculated for $\text{C}_{15}\text{H}_6\text{BrF}_2\text{O}_3$ [$\text{M} - \text{H}$] $^-$: 350.9547. Found 350.9454.

IR $\nu_{\text{max}}/\text{cm}^{-1}$: 3663, 3127, 2988, 2901, 1698, 1660, 1590, 1491, 1475, 1415, 1330, 1292, 1275, 1240, 1135, 1102, 1076, 1066, 1030, 971, 872, 850, 841, 824, 817, 777, 760, 734.

UV/Vis (0.05% DMSO/PBS 0.1 M, pH 7.2, 0.014 mM): λ_{max} (ϵ) = 433 (40785), 263 (57642) nm ($\text{L}\cdot\text{mol}^{-1}\cdot\text{cm}^{-1}$).

(Z)-6-Hydroxy-2-(3-hydroxy-4-iodobenzylidene)benzofuran-3(2H)-one: 31i

The *general procedure K* was followed using a stirred solution of 6-hydroxybenzofuranone (0.200 g, 1.332 mmol) in a mixture of EtOH (1.5 mL) and DMF (1.5 mL). Then 3-hydroxy-4-iodobenzaldehyde (0.333 g, 1.332 mmol) and 50% aqueous solution of KOH (0.5 mL) were added to the solution. Product **31i** was obtained as a yellow solid (0.126 g, 0.331 mmol) in 25% yield.

R_f = 0.45 (Cyclohexane/EtOAc, 6:4)

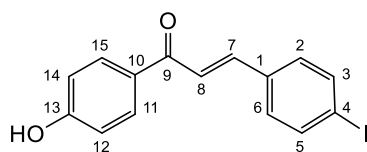
¹H NMR (500 MHz, DMSO-*d*₆) δ : 11.25 (s, 1H, OH), 10.55 (s, 1H, OH), 7.78 (d, $J_{\text{H-12,H-11}} = 8.0$ Hz, 1H, H-12), 7.63 (dd, $J_{\text{H-5,H-4}} = 8.0$ Hz, $J_{\text{H-5,H-7}} = 2.0$ Hz, 1H, H-5), 7.49 (d, $J_{\text{H-15,H-11}} = 2.0$ Hz, 1H, H-15), 7.13 (dd, $J_{\text{H-11,H-12}} = 8.0$ Hz, $J_{\text{H-11,H-15}} = 2.0$ Hz, 1H, H-11), 6.73 (s, 1H, H-4), 6.72 (d, $J_{\text{H-7,H-7}} = 2.0$ Hz, 1H, H-7), 6.66 (s, 1H, H-9).

¹³C NMR (126 MHz, DMSO-*d*₆) δ : 181.3 (C-q), 167.8 (C-q), 166.6 (C-6), 156.9 (C-14), 147.6 (C-1), 139.3 (C-12), 133.2 (C-q), 126.1 (C-5), 123.9 (C-11), 116.4 (C-15), 113.2 (C-7), 112.6 (C-q), 109.7 (C-9), 98.4 (C-4), 87.2 (C-q).

HRMS (ESI⁻) *m/z*: Calculated for C₁₅H₈IO₄ [M - H]⁻: 378.9546. Found 378.9457.

IR ν_{max} /cm⁻¹: 3491, 3134, 1668, 1626, 1582, 1495, 1417, 1335, 1302, 1289, 1247, 1218, 1190, 1156, 1127, 1109, 1020, 994, 964, 899, 837, 806, 764, 715.

UV/Vis (0.05% DMSO/PBS 0.1 M, pH 7.2, 0.013 mM): λ_{max} (ϵ) = 392 (53384) nm (L.mol⁻¹.cm⁻¹).

(E)-1-(4-hydroxyphenyl)-3-(4-iodophenyl)prop-2-en-1-one: 32C₁₅H₁₁IO₂

MW = 350.16 g/mol

A solution of 4-hydroxyacetophenone (0.200 g, 1.332 mmol) and 4-iodobenzaldehyde (0.340 g, 1.332 mmol) in ethanol (5 mL) was treated with dropwise addition of 10 M solution of KOH (0.5 mL, 4.407 mmol). The mixture was stirred at room temperature overnight. The reaction mixture was poured into 20 mL hot water with vigorous stirring and neutralized with concentrated aqueous HCl to pH 1-2. After cooling, the precipitate was filtered, washed with water, and crystallized from diethyl ether to obtain **32** as a light yellow solid (0.203 g, 0.579 mmol) in 44% yield.

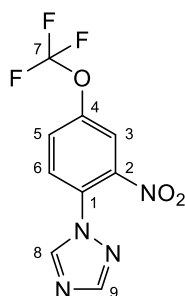
R_f = 0.30 (Cyclohexane/EtOAc, 7:3)

¹H NMR (500 MHz, DMSO-*d*₆) δ: 10.41 (s, 1H, OH), 8.07 (d, $J_{\text{H-11,H-12}} = J_{\text{H-15,H-14}} = 8.5$ Hz, 2H, H-11, H-15), 7.94 (d, $J_{\text{H-7,H-8}} = 15.5$ Hz, 1H, H-7), 7.82 (d, $J_{\text{H-3,H-2}} = J_{\text{H-5,H-6}} = 8.0$ Hz, 2H, H-3, H-5), 7.67 (d, $J_{\text{H-2,H-3}} = J_{\text{H-6,H-5}} = 8.5$ Hz, 2H, H-2, H-6), 7.61 (d, $J_{\text{H-12,H-11}} = J_{\text{H-14,H-15}} = 8.0$ Hz, 2H, H-12, H-14), 7.61 (d, $J_{\text{H-8,H-7}} = 15.5$ Hz, 1H, H-8).

HRMS (ESI⁻) m/z: Calculated for C₁₅H₁₀IO₂ [M – H]⁻: 348.9804. Found 348.9707.

IR ν_{max}/cm⁻¹: 3672, 2988, 2972, 2901, 1595, 1555, 1452, 1406, 1394, 1382, 1250, 1241, 1229, 1165, 1075, 1067, 892, 811, 781, 720.

UV/Vis (0.2% DMSO/PBS 0.1 M, pH 7.2, 0.019 mM): λ_{max} (ε) = 326 (14739), 255 (19934) nm (L.mol⁻¹.cm⁻¹).

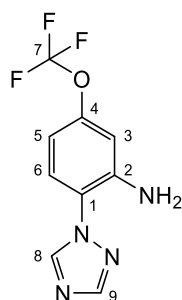
1-(2-Nitro-4-(trifluoromethoxy)phenyl)-1H-1,2,4-triazole: 33

$C_9H_5F_3N_4O_3$
MW = 274.16 g/mol

To a suspension of 1-bromo-2-nitro-4(OCF₃)benzene (3 g, 10.49 mmol), 1H-1,2,4-triazole (0.724 g, 10.49 mmol), K₃PO₄ (5.56 g, 26.22 mmol) and copper(I)iodide (0.100 g, 0.524 mmol) in DMF (104 mL) was added trans-*N,N'*-dimethylcyclohexane-1,2-diamine (0.16 mL, 1.049 mmol). The resulting suspension was degassed by vigorously bubbling argon through the mixture for 5 min. The reaction was then heated at 100 °C overnight. After cooling to room temperature, the reaction mixture was diluted with EtOAc and filtered over a celite pad. The organic phase was then washed with saturated NH₄Cl (2x20 mL), brine (2x20 mL) then dried over MgSO₄, filtered and concentrated *in vacuo*. The crude residue was purified by column chromatography on silica gel (Cyclohexane/EtOAc, 7:3) to obtain **33** as a yellow oil (1.06 g, 3.866 mmol) in 37% yield.

R_f = 0.26 (Cyclohexane/EtOAc, 6:4)

¹H NMR (500 MHz, DMSO-*d*₆) δ: 9.16 (s, 1H), 8.32 (d, *J* = 2.5 Hz, 1H), 8.29 (s, 1H), 8.09 (d, *J* = 8.5 Hz, 1H), 8.03 - 7.99 (m, 1H).

2-(1H-1,2,4-Triazol-1-yl)-5-(trifluoromethoxy)aniline: 34

$C_9H_7F_3N_4O$
MW = 244.18 g/mol

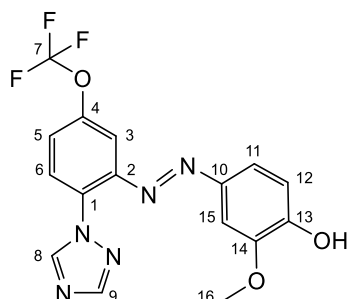
To a solution of compound **33** (1.00 g, 3.65 mmol) in EtOH/H₂O (5:1) (12 mL) was sequentially added Fe powder (2.03 g, 36.47 mmol) and NH₄Cl (1.95 g, 36.47 mmol). The resulting suspension was heated at 75 °C for 4 h. The crude reaction mixture was filtered over a celite pad and concentrated. The resulting mixture was extracted with EtOAc (3x30 mL). The organic phase was washed with saturated NaHCO₃ (2x20 mL) and brine (2x20 mL), dried over MgSO₄ and concentrated *in vacuo*. **34** was recovered as a light brown oil which was used in the next step without further purification (0.855 g, 96 % yield).

R_f = 0.50 (Cyclohexane/EtOAc, 6:4)

$^1\text{H NMR}$ (500 MHz, $\text{DMSO-}d_6$) δ : 8.86 (s, 1H), 8.25 (s, 1H), 7.35 (d, J = 8.5 Hz, 1H), 6.86 - 6.84 (m, 1H), 6.61 - 6.58 (m, 1H), 5.78 (s, 2H, NH_2).

(E)-4-((2-(1H-1,2,4-triazol-1-yl)-5-(trifluoromethoxy)phenyl)diazenyl)-2-methoxyphenol:

36



$\text{C}_{16}\text{H}_{12}\text{F}_3\text{N}_5\text{O}_3$
MW = 379.30 g/mol

The *general procedure J* was followed using **34** (0.850 g, 3.48 mmol) in 3 M HCl (3 mL), acetone (2 mL) and 1 M NaNO_2 (3.5 mL). Then the mixture was slowly added to a stirred solution of 2-methoxyphenol (0.38 mL, 3.48 mmol) in 1 M NaOH (7 mL) and acetone (2 mL). The crude residue was purified by column chromatography (Cyclohexane/EtOAc, 8:2) on silica gel to yield **36** as an orange solid (0.647 g, 1.705 mmol) in 49% yield.

Rf = 0.31 (Cyclohexane/EtOAc, 5:5)

$^1\text{H NMR}$ (500 MHz, $\text{DMSO-}d_6$) δ : 10.29 (s, 1H, OH), 8.99 (s, 1H), 8.32 (s, 1H), 8.03 (d, J = 8.5 Hz, 1H), 7.73 (s, 1H), 7.71 (s, 1H), 7.50 (d, J = 8.5 Hz, 1H), 7.33 (s, 1H), 7.00 (d, J = 8.0 Hz, 1H), 3.83 (s, 3H).

$^{13}\text{C NMR}$ (126 MHz, $\text{DMSO-}d_6$) δ : 152.4, 152.1, 148.4, 148.1, 147.2, 145.4, 144.7, 133.7, 127.6, 127.5 (q, J = 252.5 Hz, C-7), 123.3, 121.3, 115.4, 108.3, 104.3, 55.4.

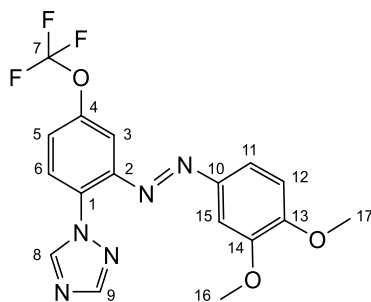
$^{19}\text{F}_{\text{cpd}}$ NMR (470 MHz, $\text{DMSO-}d_6$) δ : -58.1.

HRMS (ESI $^-$) m/z : Calculated for $\text{C}_{16}\text{H}_{11}\text{F}_3\text{N}_5\text{O}_3$ $[\text{M} - \text{H}]^-$: 378.0892. Found 378.0789.

IR $\nu_{\text{max}}/\text{cm}^{-1}$: 2959, 2929, 2859, 1725, 1592, 1504, 1467, 1411, 1381, 1270, 1217, 1173, 1131, 1119, 1103, 1074, 1020, 979, 965, 888, 849, 817, 732.

UV/Vis (DMSO/water, 1:200, 0.13 mM): λ_{max} (ϵ) = 392 (3392) nm ($\text{L}\cdot\text{mol}^{-1}\cdot\text{cm}^{-1}$).

HPLC-MS (ESI) m/z ; (λ = 235 nm): R_t = 13.16 min; 378.0804 $[\text{M} - \text{H}]^-$.

(E)-1-(2-((3,4-Dimethoxyphenyl)diazenyl)-4-(trifluoromethoxy)phenyl)-1H-1,2,4-triazole:**37**

$C_{17}H_{14}F_3N_5O_3$
 MW = 393.33 g/mol

A solution of **34** (0.200 g, 0.527 mmol) in acetone (15 mL) was stirred at room temperature, then added K_2CO_3 (0.080 g, 0.579 mmol) followed by dropwise addition of methyl iodide (0.04 mL, 0.579 mmol). The mixture was then stirred at reflux for 2 h. The resulting mixture was extracted with EtOAc (3x30 mL). The organic phase was washed with water (2x20 mL) and brine (2x20 mL), dried over $MgSO_4$ and concentrated *in vacuo*. Crystallization in pentane and recrystallization in water furnished **37** as a yellow solid (0.144 g, 0.366 mmol) in 69% yield.

R_f = 0.63 (Cyclohexane/EtOAc, 6:4)

¹H NMR (500 MHz, DMSO-*d*₆) δ: 9.01 (s, 1H), 8.33 (s, 1H), 8.05 (d, *J* = 8.5 Hz, 1H), 7.77 (s, 1H), 7.75 (s, 1H), 7.64 (dd, *J* = 8.5 Hz, *J* = 2.0 Hz, 1H), 7.32 (d, *J* = 2.0 Hz, 1H), 7.23 (d, *J* = 9.0 Hz, 1H), 3.90 (s, 3H), 3.80 (s, 3H).

¹³C NMR (126 MHz, DMSO-*d*₆) δ: 153.3, 152.2, 149.4, 148.1, 147.2, 146.2, 144.6, 133.9, 127.7, 125.5 (q, *J* = 254.7 Hz, C-7), 123.6, 121.4, 111.4, 108.4, 103.0, 55.9, 55.3.

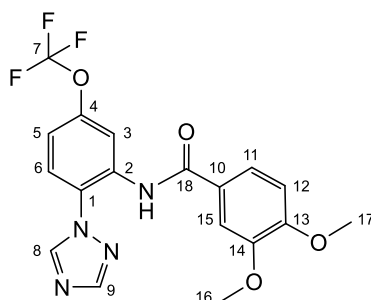
¹⁹F_{cpd} NMR (470 MHz, DMSO-*d*₆) δ: -56.8.

HRMS (ESI⁺) *m/z*: Calculated for $C_{17}H_{15}F_3N_5O_3$ [M + H]⁺: 394.1049. Found 394.1134.

IR ν_{max}/cm^{-1} : 2927, 2851, 1726, 1590, 1508, 1461, 1443, 1407, 1354, 1270, 1254, 1202, 1164, 1118, 1107, 1024, 1017, 996, 986, 972, 954, 887, 865, 858, 840, 806, 770, 733.

UV/Vis (DMSO/water, 1:200, 0.12 mM): λ_{max} (ϵ) = 412 (6208), 260 (7875) nm (L.mol⁻¹.cm⁻¹).

HPLC-MS (ESI) *m/z*; (λ = 235 nm): Rt = 14.11 min; 394.1131 [M + H]⁺.

(E)-1-(2-((3,4-Dimethoxyphenyl)diazenyl)-4-(trifluoromethoxy)phenyl)-1H-1,2,4-triazole: 35

$C_{18}H_{15}F_3N_4O_4$
 MW = 408.34 g/mol

To a solution of **34** (0,500 g, 2.047 mmol) in CH₂Cl₂ (20 mL) was sequentially added *N,N*-diisopropylethylamine (0,71 mL, 4.095 mmol), 3,4-dimethoxybenzoic acid (0.372 g, 2,047 mmol) and 1-(chloro-1-pyrrolidinylmethylene)pyrrolidinium hexafluoro-phosphate (PyCIU) (0.680 g, 2.047 mmol). The reaction was heated at 100 °C for 3 h, then left under stirring overnight at 30°C. The reaction mixture was then diluted with CH₂Cl₂ and quenched with saturated aqueous NH₄Cl. The organic layers were separated and the aqueous layer was washed with CH₂Cl₂ (3X30 mL). The crude residue was purified by column chromatography on silica gel (Cyclohexane/EtOAc, 7:3) to obtain the pure product **35** as a white solid (0.068 g, 0.166 mmol) in 8% yield.

Rf = 0.11 (Cyclohexane/EtOAc, 6:4)

¹H NMR (500 MHz, DMSO-*d*₆) δ : 10.41 (s, 1H, NH), 9.05 (s, 1H), 8.34 (s, 1H), 8.16 (s, 1H), 7.83 (d, *J* = 9.0 Hz, 1H), 7.47 (d, *J* = 9.0 Hz, 1H), 7.42 (s, 1H), 7.41 (s, 1H), 7.09 (s, 1H), 3.84 (s, 3H), 3.82 (s, 3H).

¹³C NMR (126 MHz, DMSO-*d*₆) δ : 164.7, 152.4, 152.1, 148.4, 145.1, 133.3, 128.5 (q, *J* = 254.6 Hz, C-7), 128.4, 126.5, 125.7, 122.1, 120.9, 117.7, 117.2, 111.1, 110.6, 55.7, 55.4.

¹⁹F_{cpd} NMR (470 MHz, DMSO-*d*₆) δ : -58.1.

HRMS (ESI⁻) *m/z*: Calculated for C₁₈H₁₄F₃N₄O₄ [M - H]⁻: 407.1045. Found 407.0959

IR ν_{max} /cm⁻¹: 3311, 1674, 1602, 1588, 1540, 1520, 1506, 1439, 1317, 1263, 1230, 1212, 1177, 1151, 1022, 986, 954, 883, 869, 824, 765, 748, 704.

HPLC-MS (ESI) *m/z*; (λ = 235 nm): *Rt* = 12.72 min; 407.0959 [M - H]⁻.

Molecular modelling

mGlu7R VFTD resting open model

The model we created for mGlu7R VFTD is based on 2E4Z PDB X-ray structure,⁵⁴ however a few loops were incomplete and some amino acid side-chains were missing. To start we cleaned the PDB structure of the mGlu7R dimer, by removing alternative conformations, rebuilding missing side-chains, reordering the atoms and correcting their names. For loop Q128 to K146, we used a structure of the full-length mGlu5R dimer (PDB 6N52)³⁵⁴ for which we refined the homologous loops with MODELER³⁵⁵, one on each chain, which are connected by a disulfide bridge. Then we grafted the loops to the mGlu7R dimer and refined again the loops. For loop P257 to T264, loop β 6- α 7, we built a homology model based on mGlu8R structure (PDB 6BSZ).³⁵⁶ For loop K375 to K389 and loop C430 to Y433, we grafted it from another mGlu7R structure (PDB 5C5C) and then refined it with MODELER.³⁵⁵ To finish we added the known structural ions, two calcium and three chloride ions, and used CHARMM³⁵⁷ to minimize with backbone constraint except on the repaired loops.

Docking study

Dockings were performed in Discovery Studio 2018-2019³⁵⁸ and the GOLD protocol.³⁵⁹ For the dockings toward loop β 6- α 7, side-chains of residues S226, S229, Q258, N288, E290 and D291 were set as flexible. For the docking toward alpha helix α 6, side-chains of residues S160, E185, S229, K233, E236 and S237 were set as flexible. For the docking toward the calcium site, side-chains of residues S160, I163, E185, R191, Y192, S229 and K233 were set as flexible.

Molecular Dynamics simulations

Simulations were carried out on the best selected poses with NAMD³⁶⁰ integrated in Discovery Studio 2018-2019.³⁵⁸ The systems were prepared in a water box with NaCl ion concentration of 0.15 M and boundary distance of 10 Å. Then they were minimized for 10,000 steps, heated for 100 ps and equilibrated for 900 ps. Finally, production dynamics of 5 ns were conducted for each ligands in order to assess their stability.

Bibliography

- (1) Ritthausen, K. H. L. Die Eiweisskörper Der Getreidearten, Hülsenfrüchte Und Ölsamen. Beiträge Zur Physiologie Der Samen Der Kulturgewachese, Der Nahrungs- Und Futtermittel, Bonn **1872**.
- (2) Lindemann, B. The Discovery of Umami. *Chem. Senses* **2002**, 27 (9), 843–844. <https://doi.org/10.1093/chemse/27.9.843>
- (3) Kazmi, Z.; Fatima, I.; Perveen, S.; Malik, S. S. Monosodium Glutamate: Review on Clinical Reports. *Int. J. Food Prop.* **2017**, 20 (2), 1807–1815. <https://doi.org/10.1080/10942912.2017.1295260>
- (4) Zhou, Y.; Danbolt, N. C. Glutamate as a Neurotransmitter in the Healthy Brain. *J. Neural Transm.* **2014**, 121 (8), 799–817. <https://doi.org/10.1007/s00702-014-1180-8>
- (5) Loewi, O.; Navratil, E. Über Humorale Übertragbarkeit Der Herznervenwirkung - VII. Mitteilung. *Pflugers Arch. Gesamte Physiol. Menschen Tiere* **1924**, 206 (1), 135–140. <https://doi.org/10.1007/BF01722758>
- (6) Nedergaard, M.; Takano, T.; Hansen, A. J. Beyond the Role of Glutamate as a Neurotransmitter. *Nat. Rev. Neurosci.* **2002**, 3 (9), 748–755. <https://doi.org/10.1038/nrn916>
- (7) Südhof, T. C.; Malenka, R. C. Understanding Synapses: Past, Present, and Future. *Neuron* **2008**, 60 (3), 469–476. <https://doi.org/10.1016/j.neuron.2008.10.011>
- (8) <https://www.creative-diagnostics.com/glutamatergic-synapse-pathway.htm>.
- (9) Mayer, M. L.; Armstrong, N. Structure and Function of Glutamate Receptor Ion Channels. *Annu. Rev. Physiol.* **2004**, 66 (1), 161–181. <https://doi.org/10.1146/annurev.physiol.66.050802.084104>
- (10) Twomey, E. C.; Sobolevsky, A. I. Structural Mechanisms of Gating in Ionotropic Glutamate Receptors. *Biochemistry* **2018**, 57 (3), 267–276. <https://doi.org/10.1021/acs.biochem.7b00891>
- (11) Monaghan, D. T.; Jane, D. E. Pharmacology of the NMDA Receptor. In: *Biology of the NMDA Receptor*; Ed. A. VanDongen, CRC Press, pp. 257-281 (2009).
- (12) <http://sbc.bioch.ox.ac.uk/phil/morework.html>.
- (13) Nakagawa, T.; Cheng, Y.; Ramm, E.; Sheng, M.; Walz, T. Structure and Different Conformational States of Native AMPA Receptor Complexes. *Nature* **2005**, 433 (7025), 545–549. <https://doi.org/10.1038/nature03328>
- (14) Meyerson, J. R.; Kumar, J.; Chittori, S.; Rao, P.; Pierson, J.; Bartesaghi, A.; Mayer, M. L.; Subramaniam, S. Structural Mechanism of Glutamate Receptor Activation and Desensitization. *Biophys. J.* **2015**, 108 (2), 287a. <https://doi.org/10.1016/j.bpj.2014.11.1568>
- (15) Sobolevsky, A. I.; Rosconi, M. P.; Gouaux, E. X-Ray Structure, Symmetry and Mechanism of an AMPA-Subtype Glutamate Receptor. *Nature* **2009**, 462 (7274), 745–756. <https://doi.org/10.1038/nature08624>
- (16) Sobolevsky, A. I. Structure and Gating of Tetrameric Glutamate Receptors. *J. Physiol.* **2015**,

- 593 (1), 29–38. <https://doi.org/10.1113/jphysiol.2013.264911>
- (17) Armstrong, N.; Jasti, J.; Beich-Frandsen, M.; Gouaux, E. Measurement of Conformational Changes Accompanying Desensitization in an Ionotropic Glutamate Receptor. *Cell* **2006**, *127* (1), 85–97. <https://doi.org/10.1016/j.cell.2006.08.037>
- (18) Krieger, J.; Lee, J. Y.; Greger, I. H.; Bahar, I. Activation and Desensitization of Ionotropic Glutamate Receptors by Selectively Triggering Pre-Existing Motions. *Neurosci. Lett.* **2019**, *700* (December 2017), 22–29. <https://doi.org/10.1016/j.neulet.2018.02.050>
- (19) Kleckner, N. W.; Dingledine, R. Requirement for Glycine in Activation of NMDA-Receptors Expressed in *Xenopus* Oocytes. *Science* **1988**, *241* (4867), 835–837. <https://doi.org/10.1126/science.2841759>
- (20) Mothet, J. P.; Parent, A. T.; Wolosker, H.; Brady, R. O.; Linden, D. J.; Ferris, C. D.; Rogawski, M. A.; Snyder, S. H. D-Serine Is an Endogenous Ligand for the Glycine Site of the N-Methyl-D-Aspartate Receptor. *Proc. Natl. Acad. Sci. U. S. A.* **2000**, *97* (9), 4926–4931. <https://doi.org/10.1073/pnas.97.9.4926>
- (21) Martineau M, Baux G, M. J. D-Serine Signalling in the Brain: Friend and Foe. *Trends Neurosci.* **2006**, *29* (8), 481–491. <https://doi.org/10.1016/j.tins.2006.06.008>
- (22) Yao, Y.; Mayer, M. L. Characterization of a Soluble Ligand Binding Domain of the NMDA Receptor Regulatory Subunit NR3A. *J. Neurosci.* **2006**, *26* (17), 4559–4566. <https://doi.org/10.1523/JNEUROSCI.0560-06.2006>
- (23) Mayer, M. L.; Westbrook, G. L. Permeation and Block of *N*-methyl-D-aspartic Acid Receptor Channels by Divalent Cations in Mouse Cultured Central Neurons. *J. Physiol.* **1987**, *394* (1), 501–527. <https://doi.org/10.1113/jphysiol.1987.sp016883>
- (24) Amy, B.; MacDermott, M. L.; Mayer, G. L.; Westbrook, G. L., Smith, S. J. NMDA-Receptor Activation Increases Cytoplasmic Calcium Concentration in Cultured Spinal Cord Neurons. *Nature* **1986**, *321*, 519–522. <https://doi.org/10.1038/321519a0>
- (25) Monaghan, D. T.; Jane, D. E. Pharmacology of NMDA Receptors. In *Biology of NMDA Receptors*; pp. 283 - 287, **2009**.
- (26) Bey, T.; Patel, A. Phencyclidine Intoxication and Adverse Effects: A Clinical and Pharmacological Review of an Illicit Drug. *Calif. J. Emerg. Med.* **2007**, *8* (1), 9–14.
- (27) Adachi, N.; Numakawa, T.; Kumamaru, E.; Itami, C.; Chiba, S.; Iijima, Y.; Richards, M.; Katoh-Semba, R.; Kunugi, H. Phencyclidine-Induced Decrease of Synaptic Connectivity *via* Inhibition of BDNF Secretion in Cultured Cortical Neurons. *Cereb. Cortex* **2013**, *23* (4), 847–858. <https://doi.org/10.1093/cercor/bhs074>
- (28) Yamamoto, H.; Kamegaya, E.; Sawada, W.; Hasegawa, R.; Yamamoto, T.; Hagino, Y.; Takamatsu, Y.; Imai, K.; Koga, H.; Mishina, M.; Ikeda, K. Involvement of the *N*-Methyl-D-Aspartate Receptor GluN2D Subunit in Phencyclidine-Induced Motor Impairment, Gene Expression, and Increased Fos Immunoreactivity. *Mol. Brain* **2013**, *6* (1), 1–16. <https://doi.org/10.1186/1756-6606-6-56>
- (29) Kao, H. Y.; Dvořák, D.; Park, E.; Kenney, J.; Kelemen, E.; Fenton, A. A. Phencyclidine Discoordinates Hippocampal Network Activity but Not Place Fields. *J. Neurosci.* **2017**, *37* (49), 12031–12049. <https://doi.org/10.1523/JNEUROSCI.0630-17.2017>

- (30) Brigman, J. L.; Ihne, J.; Saksida, L. M.; Bussey, T. J.; Holmes, A. Effects of Subchronic Phencyclidine (PCP) Treatment on Social Behaviors, and Operant Discrimination and Reversal Learning in C57BL/6J Mice. *Front. Behav. Neurosci.* **2009**, *3* (FEB), 1–11. <https://doi.org/10.3389/neuro.08.002.2009>
- (31) Domino, E. F. Taming the Ketamine Tiger. *Anesthesiology* **2010**, *113* (3), 678–684. <https://doi.org/10.1097/ALN.0b013e3181ed09a2>
- (32) Li, L.; Vlisides, P. E. Ketamine: 50 Years of Modulating the Mind. *Front. Hum. Neurosci.* **2016**, *10* (NOV2016), 1–15. <https://doi.org/10.3389/fnhum.2016.00612>
- (33) Lodge, D.; Mercier, M. S. Ketamine and Phencyclidine: The Good, the Bad and the Unexpected. *Br. J. Pharmacol.* **2015**, *172* (17), 4254–4276. <https://doi.org/10.1111/bph.13222>
- (34) Kraus, C.; Wasserman, D.; Henter, I. D.; Acevedo-Diaz, E.; Kadriu, B.; Zarate, C. A. The Influence of Ketamine on Drug Discovery in Depression. *Drug Discov. Today* **2019**, *24* (10), 2033–2043. <https://doi.org/10.1016/j.drudis.2019.07.007>
- (35) Wong, E. H. F.; Kemp, J. A.; Priestley, T.; Knight, A. R.; Woodruff, G. N.; Iversen, L. L. The Anticonvulsant MK-801 Is a Potent N-Methyl-D-Aspartate Antagonist. *Proc. Natl. Acad. Sci. U. S. A.* **1986**, *83* (18), 7104–7108. <https://doi.org/10.1073/pnas.83.18.7104>
- (36) Wang, X.; Ding, S.; Lu, Y.; Jiao, Z.; Zhang, L.; Zhang, Y.; Yang, Y.; Zhang, Y.; Li, W.; Lv, L. Effects of Sodium Nitroprusside in the Acute Dizocilpine (MK-801) Animal Model of Schizophrenia. *Brain Res. Bull.* **2019**, *147* (February), 140–147. <https://doi.org/10.1016/j.brainresbull.2019.02.008>
- (37) Folch, J.; Busquets, O.; Ettcheto, M.; Sánchez-López, E.; Castro-Torres, R. D.; Verdaguer, E.; Garcia, M. L.; Olloquequi, J.; Casadesús, G.; Beas-Zarate, C.; Pelegri, C.; Vilaplana, J.; Auladell, C.; Camins, A. Memantine for the Treatment of Dementia: A Review on Its Current and Future Applications. *J. Alzheimer's Dis.* **2018**, *62* (3), 1223–1240. <https://doi.org/10.3233/JAD-170672>
- (38) Herguedas, B.; Watson, J. F.; Ho, H.; Cais, O.; García-Nafria, J.; Greger, I. H. Architecture of the Heteromeric GluA1/2 AMPA Receptor in Complex with the Auxiliary Subunit TARP G8. *Science* **2019**, *364* (6438). <https://doi.org/10.1126/science.aav9011>
- (39) Wright, A.; Vissel, B. The Essential Role of AMPA Receptor GluA2 Subunit RNA Editing in the Normal and Diseased Brain. *Front. Mol. Neurosci.* **2012**, *5* (April), 1–13. <https://doi.org/10.3389/fnmol.2012.00034>
- (40) M Hollmann, M Hartley, S. H. No TitleCa²⁺ Permeability of KA-AMPA--Gated Glutamate Receptor Channels Depends on Subunit Composition. *Science* **1991**, *252* (5007), 851–853
- (41) Wenthold, R. J.; Petralia, R. S.; Blahos, J.; Niedzielski, A. S. Evidence for Multiple AMPA Receptor Complexes in Hippocampal CA1/CA2 Neurons. *J. Neurosci.* **1996**, *16* (6), 1982–1989. <https://doi.org/10.1523/jneurosci.16-06-01982.1996>
- (42) Janesh Kumar, Peter Schuck, and M. L. M. Structure and Assembly Mechanism for Heteromeric Kainate Receptors. *Neuron* **2011**, *71* (2), 319–331. <https://doi.org/10.1016/j.neuron.2011.05.038>
- (43) Lerma, J.; Marques, J. M. Kainate Receptors in Health and Disease. *Neuron* **2013**, *80* (2),

- 292–311. <https://doi.org/10.1016/j.neuron.2013.09.045>
- (44) Jane, D.E.; Lodge, D.; Collingridge, G. L. Kainate Receptors: Pharmacology, Function and Therapeutic Potential. *Neuropharmacology* **2009**, *56* (1), 90–113. <https://doi.org/10.1016/j.neuropharm.2008.08.023>
- (45) Wilding, T. J.; Huettner, J. E. Activation and Desensitization of Hippocampal Kainate Receptors. *J. Neurosci.* **1997**, *17* (8), 2713–2721. <https://doi.org/10.1523/jneurosci.17-08-02713.1997>
- (46) Contractor, A.; Mulle, C.; Swanson, G. T. Kainate Receptors Coming of Age: Milestones of Two Decades of Research. *Trends Neurosci.* **2011**, *34* (3), 154–163. <https://doi.org/10.1016/j.tins.2010.12.002>
- (47) Nicoletti, F.; Iadarola, M. J.; Wroblewski, J. T.; Costa, E. Excitatory Amino Acid Recognition Sites Coupled with Inositol Phospholipid Metabolism: Developmental Changes and Interaction with A1-Adrenoceptors. *Proc. Natl. Acad. Sci. U. S. A.* **1986**, *83* (6), 1931–1935. <https://doi.org/10.1073/pnas.83.6.1931>
- (48) Sladeczek F, Pin J. P., Récasens M, Bockaert J, W. S. Glutamate Stimulates Inositol Phosphate Formation in Striatal Neurons. *Nature* **1985**, *317* (6039), 717–719. <https://doi.org/10.1038/317717a0>
- (49) Culhane, K. J.; Liu, Y.; Cai, Y.; Yan, E. C. Y. Transmembrane Signal Transduction by Peptide Hormones via Family B G Protein-Coupled Receptors. *Front. Pharmacol.* **2015**, *6* (November), 1–23. <https://doi.org/10.3389/fphar.2015.00264>
- (50) Conn, P. J.; Pin, J. P. Pharmacology and Functions of Metabotropic Glutamate Receptors. *Annu. Rev. Pharmacol. Toxicol.* **1997**, *37*, 205–237. <https://doi.org/10.1146/annurev.pharmtox.37.1.205>
- (51) Schoepp, D. D. Unveiling the Functions of Presynaptic Metabotropic Glutamate Receptors in the Central Nervous System. *J Pharmacol Exp Ther.* **2001**, *299* (1), 12–20.
- (52) Niswender, C. M.; Conn, P. J. Metabotropic Glutamate Receptors: Physiology, Pharmacology, and Disease. *Annu. Rev. Pharmacol. Toxicol.* **2010**, *50* (1), 295–322. <https://doi.org/10.1146/annurev.pharmtox.011008.145533>
- (53) Crupi, R.; Impellizzeri, D.; Cuzzocrea, S. Role of Metabotropic Glutamate Receptors in Neurological Disorders. *Front. Mol. Neurosci.* **2019**, *12* (February), 1–11. <https://doi.org/10.3389/fnmol.2019.00020>
- (54) Muto, T.; Tsuchiya, D.; Morikawa, K.; Jingami, H. Structures of the Extracellular Regions of the Group II/III Metabotropic Glutamate Receptors. *Proc. Natl. Acad. Sci. U. S. A.* **2007**, *104* (10), 3759–3764. <https://doi.org/10.1073/pnas.0611577104>
- (55) Wu, H.; Wang, C.; Gregory, K. J.; Han, G.W.; Cho, H. P.; Xia, Y. Niswender, C.M.; Katritch, V.; Meiler, J.; Cherezov, V.; Conn, P. J.. Structure of a Class C GPCR Metabotropic Glutamate Receptor 1 Bound to an Allosteric Modulator. *Science* **2014**, *344* (6179), 58–64. <https://doi.org/10.1126/science.1249489>
- (56) Doré, A. S.; Okrasa, K.; Patel, J. C.; Serrano-Vega, M.; Bennett, K.; Cooke, R. M.; Errey, J. C.; Jazayeri, A.; Khan, S.; Tehan, B.; Weir, M.; Wiggin, G. R.; Marshall, F. H. Structure of Class C GPCR Metabotropic Glutamate Receptor 5 Transmembrane Domain. *Nature* **2014**, *511*

- (7511), 557–562. <https://doi.org/10.1038/nature13396>
- (57) Amalric, M.; Lopez, S.; Goudet, C.; Fisone, G.; Battaglia, G.; Nicoletti, F.; Pin, J. P.; Acher, F. C. Group III and Subtype 4 Metabotropic Glutamate Receptor Agonists: Discovery and Pathophysiological Applications in Parkinson's Disease. *Neuropharmacology* **2013**, *66*, 53–64. <https://doi.org/10.1016/j.neuropharm.2012.05.026>
- (58) Yin, S.; Niswender, C. Progress toward Advanced Understanding of Metabotropic Glutamate Receptors: Structure, Signaling and Therapeutic Indications. *Cell Signal* **2014**, *26* (10), 2284–2297
- (59) Pin, J. P.; Bettler, B. Organization and Functions of MGlu and GABA B Receptor Complexes. *Nature* **2016**, *540* (7631), 60–68. <https://doi.org/10.1038/nature20566>
- (60) Kunishima, N.; Shimada, Y.; Tsuji, Y.; Sato, T.; Yamamoto, M.; Kumasaka, T.; Nakanishi, S.; Jingami, H.; Morikawa, K. Structural Basis of Glutamate Recognition by a Dimeric Metabotropic Glutamate Receptor. *Nature* **2000**, *407* (6807), 971–977. <https://doi.org/10.1038/35039564>
- (61) Delgado, D. M.; Møller, T. C.; Ster, J.; Giraldo, J.; Maurel, D.; Rovira, X.; Scholler, P.; Zwier, J. M.; Perroy, J.; Durroux, T.; Trinquet, E.; Prezeau, L.; Rondard, P.; Pin, J. P. Pharmacological Evidence for a Metabotropic Glutamate Receptor Heterodimer in Neuronal Cells. *Elife* **2017**, *6* (group I), 1–33. <https://doi.org/10.7554/eLife.25233>
- (62) Rovira, X.; Malhaire, F.; Scholler, P.; Rodrigo, J.; Gonzalez-Bulnes, P.; Llebaria, A.; Pin, J. P.; Giraldo, J.; Goudet, C. Overlapping Binding Sites Drive Allosteric Agonism and Positive Cooperativity in Type 4 Metabotropic Glutamate Receptors. *FASEB J.* **2015**, *29* (1), 116–130. <https://doi.org/10.1096/fj.14-257287>
- (63) Goudet, C.; Gaven, F.; Kniazeff, J.; Vol, C.; Liu, J.; Cohen-Gonsaud, M.; Acher, F.; Prézeau, L.; Pin, J. P. Heptahelical Domain of Metabotropic Glutamate Receptor 5 Behaves like Rhodopsin-like Receptors. *Proc. Natl. Acad. Sci. U. S. A.* **2004**, *101* (1), 378–383. <https://doi.org/10.1073/pnas.0304699101>
- (64) Rondard, P.; Pin, J. P. Dynamics and Modulation of Metabotropic Glutamate Receptors. *Curr. Opin. Pharmacol.* **2015**, *20*, 95–101.
- (65) Wang, H.; Zhuo, M. Group I Metabotropic Glutamate Receptor-Mediated Gene Transcription and Implications for Synaptic Plasticity and Diseases. *Front. Pharmacol.* **2012**, *3* NOV (November), 1–8. <https://doi.org/10.3389/fphar.2012.00189>
- (66) Nicoletti, F.; Bockaert, J.; Collingridge, G. L.; Conn P. J.; Ferraguti, F.; Schoepp, D. D.; Wroblewski, J. T.; P. J. Metabotropic Glutamate Receptors: From the Workbench to the Bedside. *Neuropharmacology* **2011**, *60* (7–8), 1017–1041.
- (67) Shi-Hao, G.; Hui-Zhong, W.; Lin-Lin, S.; Yan-Dong, Z.; Huai-Zhen, R. Activation of MGluR1 Contributes to Neuronal Hyperexcitability in the Rat Anterior Cingulate Cortex *via* Inhibition of HCN Channels. *Neuropharmacology* **2016**, *105*, 361–377.
- (68) Naito, R.; Kassai, H.; Sakai, Y.; Schönherr, S.; Fukaya, M.; Schwarzer, C.; Sakagami, H.; Nakao, K.; Aiba, A.; Ferraguti, F. New Features on the Expression and Trafficking of Mglur1 Splice Variants Exposed by Two Novel Mutant Mouse Lines. *Front. Mol. Neurosci.* **2018**, *11* (December), 1–12. <https://doi.org/10.3389/fnmol.2018.00439>

- (69) Nakao, H.; Kishimoto, Y.; Hashimoto, K.; Kitamura, K.; Yamasaki, M.; Nakao, K.; Watanabe, M.; Kano, M.; Kirino, Y.; Aiba, A. MGLuR1 in Cerebellar Purkinje Cells Is Essential for the Formation but Not Expression of Associative Eyeblink Memory. *Sci. Rep.* **2019**, *9* (1), 1–10. <https://doi.org/10.1038/s41598-019-43744-z>
- (70) Yu, F.; Zhong, P.; Liu, X.; Sun, D.; Gao, H. Q.; Liu, Q. S. Metabotropic Glutamate Receptor 1 (Mglur1) Antagonism Impairs Cocaine-Induced Conditioned Place Preference *via* Inhibition of Protein Synthesis. *Neuropsychopharmacology* **2013**, *38* (7), 1308–1321. <https://doi.org/10.1038/npp.2013.29>
- (71) Lim, J.; Kim, E.; Noh, H. J.; Kang, S.; Phillips, B. U.; Kim, D. G.; Bussey, T. J.; Saksida, L.; Heath, C. J.; Kim, C. H. Assessment of MGLuR5 KO Mice under Conditions of Low Stress Using a Rodent Touchscreen Apparatus Reveals Impaired Behavioural Flexibility Driven by Perseverative Responses. *Mol. Brain* **2019**, *12* (1), 1–13. <https://doi.org/10.1186/s13041-019-0441-8>.
- (72) Li, X.; Peng, X. Q.; Jordan, C. J.; Li, J.; Bi, G. H.; He, Y.; Yang, H. J.; Zhang, H. Y.; Gardner, E. L.; Xi, Z. X. MGLuR5 Antagonism Inhibits Cocaine Reinforcement and Relapse by Elevation of Extracellular Glutamate in the Nucleus Accumbens *via* a CB1 Receptor Mechanism. *Sci. Rep.* **2018**, *8* (1), 1–14. <https://doi.org/10.1038/s41598-018-22087-1>.
- (73) Umpierre, A. D.; West, P. J.; White, J. A.; Wilcox, K. S. Conditional Knock-out of MGLuR5 from Astrocytes during Epilepsy Development Impairs High-Frequency Glutamate Uptake. *J. Neurosci.* **2019**, *39* (4), 727–742. <https://doi.org/10.1523/JNEUROSCI.1148-18.2018>.
- (74) Olive, M. F. Metabotropic Glutamate Receptor Ligands as Potential Therapeutics for Addiction. *Curr. Drug Abuse Rev.* **2009**, *2* (1), 83–98. <https://doi.org/10.2174/1874473710902010083>.
- (75) Wolfarth, S.; Konieczny, J.; Lorenc-Koci, E.; Ossowska, K.; Pilc, A. The Role of Metabotropic Glutamate Receptor (MGLuR) Ligands in Parkinsonian Muscle Rigidity. *Amino Acids* **2000**, *19* (1), 95–101. <https://doi.org/10.1007/s007260070038>.
- (76) Maksymetz, J.; Moran, S. P.; Conn, P. J. Targeting Metabotropic Glutamate Receptors for Novel Treatments of Schizophrenia Tim Bliss. *Mol. Brain* **2017**, *10* (1), 1–19. <https://doi.org/10.1186/s13041-017-0293-z>.
- (77) Muguruza, C.; Meana, J. J.; Callado, L. F. Group II Metabotropic Glutamate Receptors as Targets for Novel Antipsychotic Drugs. *Front. Pharmacol.* **2016**, *7* (MAY), 1–12. <https://doi.org/10.3389/fphar.2016.00130>.
- (78) Liu, J.; Zhang, Z.; Moreno-Delgado, D.; Dalton, J. A. R.; Rovira, X.; Trapero, A.; Goudet, C.; Llebaria, A.; Giraldo, J.; Yuan, Q.; Rondard, P.; Huang, S.; Liu, J.; Pin, J. P. Allosteric Control of an Asymmetric Transduction in a G Protein-Coupled Receptor Heterodimer. *Elife* **2017**, *6*. <https://doi.org/10.7554/eLife.26985>.
- (79) Mazzitelli, M.; Palazzo, E.; Maione, S.; Neugebauer, V. Group II Metabotropic Glutamate Receptors: Role in Pain Mechanisms and Pain Modulation. *Front. Mol. Neurosci.* **2018**, *11* (October), 1–11. <https://doi.org/10.3389/fnmol.2018.00383>.
- (80) Trepanier, C.; Lei, G.; Xie, Y. F.; MacDonald, J. F. Group II Metabotropic Glutamate Receptors Modify N-Methyl-D-Aspartate Receptors *via* Src Kinase. *Sci. Rep.* **2013**, *3*, 1–9. <https://doi.org/10.1038/srep00926>.

- (81) Kingston, A. E.; Ornstein, P. L.; Wright, R. A.; Johnson, B. G.; Mayne, N. G.; Burnett, J. P.; Belagaje, R.; Wu, S.; Schoepp, D. D. LY341495 Is a Nanomolar Potent and Selective Antagonist of Group II Metabotropic Glutamate Receptors. *Neuropharmacology* **1998**, *37* (1), 1–12. [https://doi.org/10.1016/S0028-3908\(97\)00191-3](https://doi.org/10.1016/S0028-3908(97)00191-3).
- (82) Podkowa, K.; Pochwat, B.; Brański, P.; Pilc, A.; Pałucha-Poniewiera, A. Group II MGLu Receptor Antagonist LY341495 Enhances the Antidepressant-like Effects of Ketamine in the Forced Swim Test in Rats. *Psychopharmacology (Berl)*. **2016**, *233* (15–16), 2901–2914. <https://doi.org/10.1007/s00213-016-4325-7>.
- (83) Witkin, J. M.; Monn, J. A.; Schoepp, D. D.; Li, X.; Overshiner, C.; Mitchell, S. N.; Carter, G.; Johnson, B.; Rasmussen, K.; Rorick-Kehn, L. M. The Rapidly Acting Antidepressant Ketamine and the MGLu2/3 Receptor Antagonist LY341495 Rapidly Engage Dopaminergic Mood Circuits. *J. Pharmacol. Exp. Ther.* **2016**, *358* (1), 71–82. <https://doi.org/10.1124/jpet.116.233627>.
- (84) McCulloch, T. W.; Kammermeier, P. J. Target Validation: Weak Selectivity of LY341495 for MGLuR2 over MGLuR4 Makes Glutamate a Less Selective Agonist. *Pharmacol. Res. Perspect.* **2019**, *7* (3). <https://doi.org/10.1002/prp2.471>.
- (85) Patil, S. T.; Zhang, L.; Martenyi, F.; Lowe, S. L.; Jackson, K. A.; Andreev, B. V.; Avedisova, A. S.; Bardenstein, L. M.; Gurovich, I. Y.; Morozova, M. A.; Mosolov, S. N.; Neznanov, N. G.; Reznik, A. M.; Smulevich, A. B.; Tochilov, V. A.; Johnson, B. G.; Monn, J. A.; Schoepp, D. D. Activation of MGLu2/3 Receptors as a New Approach to Treat Schizophrenia: A Randomized Phase 2 Clinical Trial. *Nat. Med.* **2007**, *13*, 1102.
- (86) Mezler, M.; Geneste, H.; Gault, L.; Marek, G. J. LY-2140023, a Prodrug of the Group II Metabotropic Glutamate Receptor Agonist LY-404039 for the Potential Treatment of Schizophrenia. *Curr. Opin. Investig. Drugs* **2010**, *11* (7), 833–845.
- (87) Lilly Stops Phase III Development of Pomaglumetad Methionil For the Treatment of Schizophrenia Based on Efficacy Results <https://investor.lilly.com/releasedetail.cfm?ReleaseID=703018>.
- (88) Hovelso, N.; Sotty, F.; P. Montezinho, L.; S. Pinheiro, P.; F. Herrik, K.; Mork, A. Therapeutic Potential of Metabotropic Glutamate Receptor Modulators. *Curr. Neuropharmacol.* **2012**, *10* (1), 12–48. <https://doi.org/10.2174/157015912799362805>.
- (89) Nakajima, Y.; Iwakabe, H.; Akazawa, C.; Nawa, H.; Shigemoto, R.; Mizuno, N.; Nakanishi, S. Molecular Characterization of a Novel Retinal Metabotropic Glutamate Receptor MGLuR6 with a High Agonist Selectivity for L-2-Amino-4- Phosphonobutyrate. *J. Biol. Chem.* **1993**, *268* (16), 11868–11873.
- (90) MS1, Mercier, L. D. Group III Metabotropic Glutamate Receptors: Pharmacology, Physiology and Therapeutic Potential. *Neurochem Res.* **2014**, *39* (10), 1876–1894.
- (91) Billups, B.; Graham, B. P.; Wong, A. Y. C.; Forsythe, I. D. Unmasking Group III Metabotropic Glutamate Autoreceptor Function at Excitatory Synapses in the Rat CNS. *J. Physiol.* **2005**, *565* (3), 885–896. <https://doi.org/10.1113/jphysiol.2005.086736>.
- (92) Dammann, F.; Kirschstein, T.; Guli, X.; Müller, S.; Porath, K.; Rohde, M.; Tokay, T.; Kohling, R. Bidirectional Shift of Group III Metabotropic Glutamate Receptor-Mediated Synaptic Depression in the Epileptic Hippocampus. *Epilepsy Res.* **2018**, *139*, 157–163.

- (93) Sun, Y.; Feng, X.; Ding, Y.; Li, M.; Yao, J.; Wang, L.; Gao, Z. Phased Treatment Strategies for Cerebral Ischemia Based on Glutamate Receptors. *Front. Cell. Neurosci.* **2019**, *13* (April), 1–9. <https://doi.org/10.3389/fncel.2019.00168>.
- (94) Pałucha, A.; Tatarczyńska, E.; Brański, P.; Szewczyk, B.; Wierońska, J. M.; Kłak, K.; Chojnacka-Wójcik, E.; Nowak, G.; Pilc, A. Group III MGLu Receptor Agonists Produce Anxiolytic- and Antidepressant-like Effects after Central Administration in Rats. *Neuropharmacology* **2004**, *46* (2), 151–159.
- (95) Wierońska, J.; Stachowicz, K.; Pałucha-Poniewiera, A.; Acher, F.; Brański, P.; Pilc, A. Metabotropic Glutamate Receptor 4 Novel Agonist LSP1-2111 with Anxiolytic, but Not Antidepressant-like Activity, Mediated by Serotonergic and GABAergic Systems. *Neuropharmacology* **2010**, *59* (7–8), 627–634.
- (96) Avdeeva, N. V.; Sidorova, S. A.; Gudyrev, O. S.; Osipova, O. A.; Golubev, I. V. Mechanism of Neuroprotective Effect of MGLuR4 Agonists. *Res. Results Pharmacol.* **2019**, *5* (2), 43–47. <https://doi.org/10.3897/rpharmacology.5.36565>.
- (97) Valerio, A.; Zoppi, N.; Ferraboli, S.; Paterlini, M.; Ferrario, M.; Barlati, S.; Spano, P. Alternative Splicing of MGLu6 Gene Generates a Truncated Glutamate Receptor in Rat Retina. *Neuroreport*. **2001**, *12* (27), 2711–2715.
- (98) Zeitz, C.; Forster, U.; Neidhardt, J.; Feil, S.; Kälin, S.; Leifert, D.; Flor, P. J.; Berger, W. Night Blindness-Associated Mutations in the Ligand-Binding, Cysteine-Rich, and Intracellular Domains of the Metabotropic Glutamate Receptor 6 Abolish Protein Trafficking. *Hum. Mutat.* **2007**, *28* (8), 771–780. <https://doi.org/10.1002/humu.20499>.
- (99) Fendt, M.; Schmid, S.; Thakker, D. R.; Jacobson, L. H.; Yamamoto, R.; Mitsukawa, K.; Maier, R.; Natt, F.; Hüsken, D.; Kelly, P. H.; McAllister, K. H.; Hoyer, D.; Van Der Putten, H.; Cryan, J. F.; Flor, P. J. MGLuR7 Facilitates Extinction of Aversive Memories and Controls Amygdala Plasticity. *Mol. Psychiatry* **2008**, *13* (10), 970–979. <https://doi.org/10.1038/sj.mp.4002073>.
- (100) Mitsukawa, K.; Mombereau, C.; Lötscher, E.; Uzunov, D. P.; Van Der Putten, H.; Flor, P. J.; Cryan, J. F. Metabotropic Glutamate Receptor Subtype 7 Ablation Causes Dysregulation of the HPA Axis and Increases Hippocampal BDNF Protein Levels: Implications for Stress-Related Psychiatric Disorders. *Neuropsychopharmacology* **2006**, *31* (6), 1112–1122. <https://doi.org/10.1038/sj.npp.1300926>.
- (101) Ren, W.; Palazzo, E.; Maione, S.; Neugebauer, V. Differential Effects of MGLuR7 and MGLuR8 Activation on Painrelated Synaptic Activity in the Amygdala. *Neuropharmacology* **2011**, *61* (8), 1334–1344.
- (102) Gyetvai, B.; Simonyi, A.; Oros, M.; Saito, M.; Smiley, J.; Vadasz, C. MGLuR7 Genetics and Alcohol: Intersection Yields Clues for Addiction. *Neurochem Res.* **2011**, *36* (6), 1087–1100.
- (103) Hajasova, Z.; Canestrelli, C.; Acher, F.; Noble, F.; Marie, N. Role of MGLu7 Receptor in Morphine Rewarding Effects Is Uncovered by a Novel Orthosteric Agonist. *Neuropharmacology* **2018**, *131*, 424–430. <https://doi.org/10.1016/j.neuropharm.2018.01.002>.
- (104) Lebourgeois, S.; Vilpoux, C.; Jeanblanc, J.; Acher, F.; Marie, N.; Noble, F.; Naassila, M. Pharmacological Activation of MGLu4 and MGLu7 Receptors, by LSP2-9166, Reduces Ethanol Consumption and Relapse in Rat. *Neuropharmacology* **2018**, *133*, 163–170.

<https://doi.org/10.1016/j.neuropharm.2018.01.031>.

- (105) Girard, B.; Tuduri, P.; Moreno, M. P.; Sakkaki, S.; Barboux, C.; Bouschet, T.; Varrault, A.; Vitre, J.; McCort-Tranchepain, I.; Dairou, J.; Acher, F.; Fagni, L.; Marchi, N.; Perroy, J.; Bertaso, F. The MGLu7 Receptor Provides Protective Effects against Epileptogenesis and Epileptic Seizures. *Neurobiol. Dis.* **2019**, *129* (0), 13–28. <https://doi.org/10.1016/j.nbd.2019.04.016>.
- (106) Konieczny, J.; Lenda, T. Contribution of the MGLu7 Receptor to Antiparkinsonian-like Effects in Rats: A Behavioral Study with the Selective Agonist AMN082. *Pharmacol. Reports* **2013**, *65* (5), 1194–1203. [https://doi.org/10.1016/S1734-1140\(13\)71477-4](https://doi.org/10.1016/S1734-1140(13)71477-4).
- (107) Gu, Z.; Cheng, J.; Zhong, P.; Qin, L.; Liu, W.; Yan, Z. A β Selectively Impairs MGLu7 Modulation of NMDA Signaling in Basal Forebrain Cholinergic Neurons: Implication in Alzheimer's Disease. *J. Neurosci.* **2014**, *34* (41), 13614–13628. <https://doi.org/10.1523/JNEUROSCI.1204-14.2014>.
- (108) Linden, A. M.; Johnson, B.G.; Peters, S.C.; Shannon, H.E.; Tian, M.; Wang, Y.; Yu, J.L.; Köster, A.; Baez, M. S. D. Increased Anxiety-Related Behavior in Mice Deficient for Metabotropic Glutamate 8 (MGLu8) Receptor. *Neuropharmacology* **2002**, *43* (2), 251–259.
- (109) Chiechio, S. Modulation of Chronic Pain by Metabotropic Glutamate Receptors. *Adv Pharmacol.* **2016**, *75*, 63–89.
- (110) Thomsen, C. The L-AP4 Receptor. *Gen. Pharmacol.* **1997**, *29* (2), 151–158.
- (111) Eriksen, L.; Thomsen, C. [3H]-L-2-amino-4-phosphonobutyrate Labels a Metabotropic Glutamate Receptor, MGLuR4a. *Br. J. Pharmacol.* **1995**, *116* (8), 3279–3287. <https://doi.org/10.1111/j.1476-5381.1995.tb15136.x>.
- (112) Selvam, C.; Oueslati, N.; Lemasson, I. A.; Brabet, I.; Rigault, D.; Courtiol, T.; Cesarini, S.; Triballeau, N.; Bertrand, H. O.; Goudet, C.; Pin, J. P.; Acher, F. C. A Virtual Screening Hit Reveals New Possibilities for Developing Group III Metabotropic Glutamate Receptor Agonists. *J. Med. Chem.* **2010**, *53* (7), 2797–2813. <https://doi.org/10.1021/jm901523t>.
- (113) Selvam, C.; Lemasson, I.; Brabet, I.; Oueslati, N.; Karaman, B.; Cabaye, A.; Tora, A.; Commare, B.; Courtiol, T.; Cesarini, S.; McCort-Tranchepain, I.; Rigault, D.; Mony, L.; Bessiron, T.; McLean, H.; Leroux, F.; Colobert, F.; Daniel, H.; Goupil-Lamy, A.; Bertrand, H.-O.; Goudet, C.; Pin, J.-P.; Acher, F. J. Increased Potency and Selectivity for Group III Metabotropic Glutamate Receptor Agonists Binding at Dual Sites. *J. Med. Chem.* **2018**, *61* (5), 169–1989.
- (114) Acher, F.; Pin, J.P.; Goudet, C.; Eschalié, A.; Busserolles, J.; Rigault, D.; Lemasson, I.; Cesarini, S.; Commare, B. WO2012156931 - Hypophosphorous acid derivatives having antihyperalgesic activity and biological applications thereof, **2012**.
- (115) Beurrier, C.; Revy, D.; Lopez, S.; Lherondel, C.; Goudet, C.; Acher, F.; Amalric, M. LSP1-2111, a New Orthosteric Group III MGLuR Agonist with Preferential Activity on MGLuR4, Modulates the Striatopallidal Synapse and Alleviates Parkinsonian Symptoms. *Neuropharmacology* **2008**, *55* (4), 587–588.
- (116) Cuomo, D.; Martella, G.; Barabino, E.; Platania, P.; Vita, D.; Madeo, G.; Selvam, C.; Goudet, C.; Oueslati, N.; Pin, J. P.; Acher, F.; Pisani, A.; Beurrier, C.; Melon, C.; Kerkerian-Le Goff, L.;

- Gubellini, P. Metabotropic Glutamate Receptor Subtype 4 Selectively Modulates Both Glutamate and GABA Transmission in the Striatum: Implications for Parkinson's Disease Treatment. *J. Neurochem.* **2009**, *109* (4), 1096–1105. <https://doi.org/10.1111/j.1471-4159.2009.06036.x>.
- (117) Goudet, C.; Vilar, B.; Courtiol, T.; Deltheil, T.; Bessiron, T.; Brabet, I.; Oueslati, N.; Rigault, D.; Bertrand, H.; McLean, H.; Daniel, H.; Amalric, M.; Acher, F.; Pin, J. A Novel Selective Metabotropic Glutamate Receptor 4 Agonist Reveals New Possibilities for Developing Subtype Selective Ligands with Therapeutic Potential. *FASEB J.* **2012**, *26* (4), 1682–1693. <https://doi.org/10.1096/fj.11-195941>.
- (118) Cajina, M.; Nattini, M.; Song, D.; Smagin, G.; Jørgensen, E. B.; Chandrasena, G.; Bundgaard, C.; Toft, D. B.; Huang, X.; Acher, F.; Doller, D. Qualification of LSP1-2111 as a Brain Penetrant Group III Metabotropic Glutamate Receptor Orthosteric Agonist. *ACS Med. Chem. Lett.* **2014**, *5* (2), 119–123. <https://doi.org/10.1021/ml400338f>.
- (119) Podkowa, K.; Rzeźniczek, S.; Marciniak, M.; Acher, F.; Pilc, A.; Pałucha-Poniewiera, A. A Novel MGLu4 Selective Agonist LSP4-2022 Increases Behavioral Despair in Mouse Models of Antidepressant Action. *Neuropharmacology* **2015**, *97*, 338–345.
- (120) Cieślak, P.; Woźniak, M.; Rook, J. M.; Tantawy, M. N.; Conn, P. J.; Acher, F.; Tokarski, K.; Kusek, M.; Pilc, A.; Wierońska, J. M. Mutual Activation of Glutamatergic MGLu4 and Muscarinic M4 Receptors Reverses Schizophrenia-Related Changes in Rodents. *Psychopharmacology (Berl.)* **2018**, *235* (10), 2897–2913. <https://doi.org/10.1007/s00213-018-4980-y>.
- (121) Acher, F. C.; Tellier, F. J.; Azerad, R.; Brabet, I. N.; Fagni, L.; Pin, J. R. Synthesis and Pharmacological Characterization of Aminocyclopentanetricarboxylic Acids: New Tools to Discriminate between Metabotropic Glutamate Receptor Subtypes. *J. Med. Chem.* **1997**, *40* (19), 3119–3129. <https://doi.org/10.1021/jm970207b>.
- (122) Lopez, S.; Turle-Lorenzo, N.; Acher, F.; De Leonibus, E.; Mele, A.; Amalric, M. Targeting Group III Metabotropic Glutamate Receptors Produces Complex Behavioral Effects in Rodent Models of Parkinson's Disease. *J. Neurosci.* **2007**, *27* (25), 6701–6711. <https://doi.org/10.1523/JNEUROSCI.0299-07.2007>.
- (123) Thomas, N.; Wright, R.; Howson, P.; Kingston, A.; Schoepp, D.; Jane, D. (S)-3,4-DCPG, a Potent and Selective MGLu8a Receptor Agonist, Activates Metabotropic Glutamate Receptors on Primary Afferent Terminals in the Neonatal Rat Spinal Cord. *Neuropharmacology* **2001**, *40* (3), 311–318.
- (124) Gasparini, F.; Bruno, V.; Battaglia, G.; Lukic, S.; Leonhardt, T.; Inderbitzin, W.; Laurie, D.; Sommer, B.; Varney, M. A.; Hess, S. D.; Johnson, E. C.; Kuhn, R.; Urwyler, S.; Sauer, D.; Portet, C.; Schmutz, M.; Nicoletti, F.; Flor, P. J. (R,S)-4-Phosphonophenylglycine, a Potent and Selective Group III Metabotropic Glutamate Receptor Agonist, Is Anticonvulsive and Neuroprotective in Vivo. *J. Pharmacol. Exp. Ther.* **1999**, *289* (3), 1678–1687.
- (125) Fazio, F.; Lionetto, L.; Molinaro, G.; Bertrand, H. O.; Acher, F.; Ngomba, R. T.; Notartomaso, S.; Curini, M.; Rosati, O.; Scarselli, P.; Di Marco, R.; Battaglia, G.; Bruno, V.; Simmaco, M.; Pin, J. P.; Nicoletti, F.; Goudet, C. Cinnabarinic Acid, an Endogenous Metabolite of the Kynurenine Pathway, Activates Type 4 Metabotropic Glutamate Receptors. *Mol. Pharmacol.* **2012**, *81* (5), 643–656. <https://doi.org/10.1124/mol.111.074765>.

- (126) Knöpfel, T.; Lukic, S.; Leonardt, T.; Flor, P. J.; Kuhn, R.; Gasparini, F. Pharmacological Characterization of MCCG and MAP4 at the MGLuR1b, MGLuR2 and MGLuR4a Human Metabotropic Glutamate Receptor Subtypes. *Neuropharmacology* **1995**, *34* (8), 1099–1102. [https://doi.org/10.1016/0028-3908\(95\)00111-1](https://doi.org/10.1016/0028-3908(95)00111-1).
- (127) https://www.tocris.com/products/mppg_0853.
- (128) Toms, N.; Jane, D.; Kemp, M.; Bedingfield, J.; Roberts, P. The Effects of (RS)-Alpha-Cyclopropyl-4-Phosphonophenylglycine ((RS)-CPPG), a Potent and Selective Metabotropic Glutamate Receptor Antagonist. *Br J Pharmacol* **1996**, *119* (5), 851–854.
- (129) Conway, S. J.; Miller, J. C.; Howson, P. A.; Clark, B. P.; Jane, D. E. Synthesis of Phenylglycine Derivatives as Potent and Selective Antagonists of Group III Metabotropic Glutamate Receptors. *Bioorganic Med. Chem. Lett.* **2001**, *11* (6), 777–780. [https://doi.org/10.1016/S0960-894X\(01\)00052-X](https://doi.org/10.1016/S0960-894X(01)00052-X).
- (130) Miller, J. C.; Howson, P. A.; Conway, S. J.; Williams, R. V.; Clark, B. P.; Jane, D. E. Phenylglycine Derivatives as Antagonists of Group III Metabotropic Glutamate Receptors Expressed on Neonatal Rat Primary Afferent Terminals. *Br. J. Pharmacol.* **2003**, *139* (8), 1523–1531. <https://doi.org/10.1038/sj.bjp.0705377>.
- (131) Stephens, B.; Handel, T. *Chemokine Receptor Oligomerization and Allostery. Progress in Molecular Biology and Translational Science*; 2013.
- (132) Jeffrey Conn, P.; Christopoulos, A.; Lindsley, C. W. Allosteric Modulators of GPCRs: A Novel Approach for the Treatment of CNS Disorders. *Nat. Rev. Drug Discov.* **2009**, *8* (1), 41–54. <https://doi.org/10.1038/nrd2760>.
- (133) Abdel-Magid, A. F. Allosteric Modulators: An Emerging Concept in Drug Discovery. *ACS Med. Chem. Lett.* **2015**, *6* (2), 104–107. <https://doi.org/10.1021/ml5005365>.
- (134) Annoura, H.; Fukunaga, A.; Uesugi, M.; Tatsuoka, T.; Horikawa, Y. A Novel Class of Antagonists for Metabotropic Glutamate Receptors, 7-(Hydroxyimino)Cyclopropa[b]Chromen-1a-Carboxylates. *Bioorganic Med. Chem. Lett.* **1996**, *6* (7), 763–766. [https://doi.org/10.1016/0960-894X\(96\)00104-7](https://doi.org/10.1016/0960-894X(96)00104-7).
- (135) Maj, M.; Bruno, V.; Dragic, Z.; Yamamoto, R.; Battaglia, G.; Inderbitzin, W.; Stoehr, N.; Stein, T.; Gasparini, F.; Vranesic, I.; Kuhn, R.; Nicoletti, F.; Flor, P. J. (-)-PHCCC, a Positive Allosteric Modulator of MGLuR4: Characterization, Mechanism of Action, and Neuroprotection. *Neuropharmacology* **2003**, *45* (7), 895–906. [https://doi.org/10.1016/S0028-3908\(03\)00271-5](https://doi.org/10.1016/S0028-3908(03)00271-5).
- (136) Williams, R.; Zhou, Y.; Niswender, C. M.; Luo, Q.; Conn, P. J.; Lindsley, C. W.; Hopkins, C. R. Re-Exploration of the PHCCC Scaffold: Discovery of Improved Positive Allosteric Modulators of MGLuR4. *ACS Chem. Neurosci.* **2010**, *1* (6), 411–419. <https://doi.org/10.1021/cn9000318>.
- (137) Niswender, C. M.; Johnson, K. A.; Weaver, C. D.; Jones, C. K.; Xiang, Z.; Luo, Q.; Rodriguez, A. L.; Marlo, J. E.; De Paulis, T.; Thompson, A. D.; Days, E. L.; Nalywajko, T.; Austin, C. A.; Williams, M. B.; Ayala, J. E.; Williams, R.; Lindsley, C. W.; Conn, P. J. Discovery, Characterization, and Antiparkinsonian Effect of Novel Positive Allosteric Modulators of Metabotropic Glutamate Receptor 4. *Mol. Pharmacol.* **2008**, *74* (5), 1345–1358. <https://doi.org/10.1124/mol.108.049551>.

- (138) Niswender, C. M.; Lebois, E. P.; Luo, Q.; Kim, K.; Muchalski, H.; Yin, H.; Conn, P. J.; Lindsley, C. W. Positive Allosteric Modulators of the Metabotropic Glutamate Receptor Subtype 4 (MGLuR4): Part I. Discovery of Pyrazolo[3,4-d]Pyrimidines as Novel MGLuR4 Positive Allosteric Modulators. *Bioorganic Med. Chem. Lett.* **2008**, *18* (20), 5626–5630. <https://doi.org/10.1016/j.bmcl.2008.08.087>.
- (139) Williams, R.; Niswender, C. M.; Luo, Q.; Le, U.; Conn, P. J.; Lindsley, C. W. Positive Allosteric Modulators of the Metabotropic Glutamate Receptor Subtype 4 (MGLuR4). Part II: Challenges in Hit-to-Lead. *Bioorganic Med. Chem. Lett.* **2009**, *19* (3), 962–966. <https://doi.org/10.1016/j.bmcl.2008.11.104>.
- (140) Niswender, C. M.; Jones, C. K.; Lin, X.; Bubser, M.; Thompson Gray, A.; Blobaum, A. L.; Engers, D. W.; Rodriguez, A. L.; Loch, M. T.; Daniels, J. S.; Lindsley, C. W.; Hopkins, C. R.; Javitch, J. A.; Conn, P. J. Development and Antiparkinsonian Activity of VU0418506, a Selective Positive Allosteric Modulator of Metabotropic Glutamate Receptor 4 Homomers without Activity at MGLu2/4 Heteromers. *ACS Chem. Neurosci.* **2016**, *7* (9), 1201–1211. <https://doi.org/10.1021/acschemneuro.6b00036>.
- (141) Bennouar, K. E.; Uberti, M. A.; Melon, C.; Bacolod, M. D.; Jimenez, H. N.; Cajina, M.; Kerkerian-Le Goff, L.; Doller, D.; Gubellini, P. Synergy between L-DOPA and a Novel Positive Allosteric Modulator of Metabotropic Glutamate Receptor 4: Implications for Parkinson's Disease Treatment and Dyskinesia. *Neuropharmacology* **2013**, *66*, 158–169. <https://doi.org/10.1016/j.neuropharm.2012.03.022>.
- (142) Sławińska, A.; Wierońska, J. M.; Stachowicz, K.; Pałucha-Poniewiera, A.; Uberti, M. A.; Bacolod, M. A.; Doller, D.; Pilc, A. Anxiolytic- but Not Antidepressant-like Activity of Lu AF21934, a Novel, Selective Positive Allosteric Modulator of the MGLu4 Receptor. *Neuropharmacology* **2013**, *66*, 225–235. <https://doi.org/10.1016/j.neuropharm.2012.05.001>.
- (143) Ossowska, K.; Wardas, J.; Berghauzen-Maciejewska, K.; Głowacka, U.; Kuter, K.; Pilc, A.; Zorn, S. H.; Doller, D. Lu AF21934, a Positive Allosteric Modulator of MGLu4 Receptors, Reduces the Harmaline-Induced Hyperactivity but Not Tremor in Rats. *Neuropharmacology* **2014**, *83*, 28–35. <https://doi.org/10.1016/j.neuropharm.2014.03.018>.
- (144) Fulton, M. G.; Loch, M. T.; Cuoco, C. A.; Rodriguez, A. L.; Days, E.; Vinson, P. N.; Kozek, K. A.; Weaver, C. D.; Blobaum, A. L.; Conn, P. J.; Niswender, C. M.; Lindsley, C. W. Challenges in the Discovery and Optimization of MGLu2/4 Heterodimer Positive Allosteric Modulators. *Lett. Drug Des. Discov.* **2018**, *16* (12), 1387–1394. <https://doi.org/10.2174/1570180815666181017131349>.
- (145) Engers, D. W.; Blobaum, A. L.; Gogliotti, R. D.; Cheung, Y. Y.; Salovich, J. M.; Garcia-Barrantes, P. M.; Daniels, J. S.; Morrison, R.; Jones, C. K.; Soars, M. G.; Zhuo, X.; Hurley, J.; Macor, J. E.; Bronson, J. J.; Conn, P. J.; Lindsley, C. W.; Niswender, C. M.; Hopkins, C. R. Discovery, Synthesis, and Preclinical Characterization of *N*-(3-Chloro-4-Fluorophenyl)-1*H*-Pyrazolo[4,3-*b*]Pyridin-3-Amine (VU0418506), a Novel Positive Allosteric Modulator of the Metabotropic Glutamate Receptor 4 (MGLu4). *ACS Chem. Neurosci.* **2016**, *7* (9), 1192–1200. <https://doi.org/10.1021/acschemneuro.6b00035>.
- (146) Panarese, J. D.; Engers, D. W.; Wu, Y. J.; Bronson, J. J.; Macor, J. E.; Chun, A.; Rodriguez, A. L.; Felts, A. S.; Engers, J. L.; Loch, M. T.; Emmitte, K. A.; Castelhana, A. L.; Kates, M. J.; Nader, M. A.; Jones, C. K.; Blobaum, A. L.; Conn, P. J.; Niswender, C. M.; Hopkins, C. R.; Lindsley, C.

- W. Discovery of VU2957 (Valiglurax): An MGLu 4 Positive Allosteric Modulator Evaluated as a Preclinical Candidate for the Treatment of Parkinson's Disease. *ACS Med. Chem. Lett.* **2019**, *10* (3), 255–260. <https://doi.org/10.1021/acsmchemlett.8b00426>.
- (147) Panarese, J. D.; Engers, D. W.; Wu, Y. J.; Guernon, J. M.; Chun, A.; Gregro, A. R.; Bender, A. M.; Capstick, R. A.; Wieting, J. M.; Bronson, J. J.; Macor, J. E.; Westphal, R.; Soars, M.; Engers, J. E.; Felts, A. S.; Rodriguez, A. L.; Emmitte, K. A.; Jones, C. K.; Blobaum, A. L.; Jeffrey Conn, P.; Niswender, C. M.; Hopkins, C. R.; Lindsley, C. W. The Discovery of VU0652957 (VU2957, Valiglurax): SAR and DMPK Challenges En Route to an MGLu4 PAM Development Candidate. *Bioorganic Med. Chem. Lett.* **2019**, *29* (2), 342–346. <https://doi.org/10.1016/j.bmcl.2018.10.050>.
- (148) Kalinichev, M.; Le Poul, E.; Boléa, C.; Girard, F.; Campo, B.; Fonsi, M.; Royer-Urios, I.; Browne, S. E.; Uslander, J. M.; Davis, M. J.; Raber, J.; Duvoisin, R.; Bate, S. T.; Reynolds, I. J.; Poli, S.; Celanire, S. Characterization of the Novel Positive Allosteric Modulator of the Metabotropic Glutamate Receptor 4 ADX88178 in Rodent Models of Neuropsychiatric Disorders. *J. Pharmacol. Exp. Ther.* **2014**, *350* (3), 495–505. <https://doi.org/10.1124/jpet.114.214437>.
- (149) Aakanksha, D.; Sumit, C.; Nripendra, S.; Chandrashekhar, U. Discovery and Characterization of TAS-4: A Potent and Selective Metabotropic Glutamate Receptor 4 Positive Allosteric Modulator Im- Proves Movement in Rodent Models of Parkinson's Disease. *IJSER*.
- (150) Charvin, D.; Pomel, V.; Ortiz, M.; Frauli, M.; Scheffler, S.; Steinberg, E.; Baron, L.; Deshons, L.; Rudigier, R.; Thiaric, D.; Morice, C.; Manteau, B.; Mayer, S.; Graham, D.; Giethlen, B.; Brugger, N.; Hédou, G.; Conquet, F.; Schann, S. Discovery, Structure-Activity Relationship, and Antiparkinsonian Effect of a Potent and Brain-Penetrant Chemical Series of Positive Allosteric Modulators of Metabotropic Glutamate Receptor 4. *J. Med. Chem.* **2017**, *60* (20), 8515–8537. <https://doi.org/10.1021/acs.jmedchem.7b00991>.
- (151) <https://parkinsonsnewstoday.com/2020/04/03/foliglurax-fails-to-minimize-long-term-use-side-effects-of-levodopa-phase-2-trial-shows/>.
- (152) Conn, P.; Hopkins, C.; Lindsley, C.; Niswender, C.; Engers, D.; Bollinger, S. US20180022744A1 Vanderbilt University, 2018.
- (153) Conn, P.; Lindsley, C.; Felts, A.; Niswender, C.; Capstick, R.; Spearing, P.; Bollinger, S. WO2019006157A1, 2019.
- (154) Utley, T.; Haddenham, D.; Salovich, J. M.; Zamorano, R.; Vinson, P. N.; Lindsley, C. W.; Hopkins, C. R.; Niswender, C. M. Synthesis and SAR of a Novel Metabotropic Glutamate Receptor 4 (MGLu 4) Antagonist: Unexpected “molecular Switch” from a Closely Related MGLu 4 Positive Allosteric Modulator. *Bioorganic Med. Chem. Lett.* **2011**, *21* (23), 6955–6959. <https://doi.org/10.1016/j.bmcl.2011.09.131>.
- (155) Rovira, X.; Trapero, A.; Pittolo, S.; Zussy, C.; Faucherre, A.; Jopling, C.; Giraldo, J.; Pin, J. P.; Gorostiza, P.; Goudet, C.; Llebaria, A. OptoGluNAM4.1, a Photoswitchable Allosteric Antagonist for Real-Time Control of MGLu4 Receptor Activity. *Cell Chem. Biol.* **2016**, *23* (8), 929–934. <https://doi.org/10.1016/j.chembiol.2016.06.013>.
- (156) Mitsukawa, K.; Yamamoto, R.; Ofner, S.; Nozulak, J.; Pescott, O.; Lukic, S.; Stoehr, N.; Mombereau, C.; Kuhn, R.; McAllister, K. H.; Van Der Putten, H.; Cryan, J. F.; Flor, P. J. A

- Selective Metabotropic Glutamate Receptor 7 Agonist: Activation of Receptor Signaling via an Allosteric Site Modulates Stress Parameters in Vivo. *Proc. Natl. Acad. Sci. U. S. A.* **2005**, *102* (51), 18712–18717. <https://doi.org/10.1073/pnas.0508063102>.
- (157) Jenda, M.; Gawel, K.; Marszalek, M.; Komsta, L.; Kotlinska, J. H. AMN082, a Metabotropic Glutamate Receptor 7 Allosteric Agonist, Attenuates Locomotor Sensitization and Cross-Sensitization Induced by Cocaine and Morphine in Mice. *Prog. Neuro-Psychopharmacology Biol. Psychiatry* **2015**, *57*, 166–175. <https://doi.org/10.1016/j.pnpbbp.2014.11.004>.
- (158) Gawel, K.; Jenda-Wojtanowska, M.; Gibula-Bruzda, E.; Kedzierska, E.; Filarowska, J.; Marszalek-Grabska, M.; Wojtanowski, K. K.; Komsta, L.; Talarek, S.; Kotlinska, J. H. The Influence of AMN082, Metabotropic Glutamate Receptor 7 (MGLu7) Allosteric Agonist on the Acute and Chronic Antinociceptive Effects of Morphine in the Tail-Immersion Test in Mice: Comparison with MGLu5 and MGLu2/3 Ligands. *Physiol. Behav.* **2018**, *185*, 112–120. <https://doi.org/10.1016/j.physbeh.2017.12.035>.
- (159) Vatankhah, M.; Karimi-Haghighi, S.; Sarihi, A.; Haghparast, A. Intra-Accumbal Administration of AMN082, a Metabotropic Glutamate Receptor Type 7 Allosteric Agonist, Inhibits the Acquisition but Not the Expression of Morphine-Induced Conditioned Place Preference in Rats. *Neurosci. Lett.* **2018**, *681*, 56–61. <https://doi.org/10.1016/j.neulet.2018.05.031>.
- (160) Bradley, S. R.; Uslaner, J. M.; Flick, R. B.; Lee, A.; Groover, K. M.; Hutson, P. H. The MGLuR7 Allosteric Agonist AMN082 Produces Antidepressant-like Effects by Modulating Glutamatergic Signaling. *Pharmacol. Biochem. Behav.* **2012**, *101* (1), 35–40. <https://doi.org/10.1016/j.pbb.2011.11.006>.
- (161) Sukoff Rizzo, S. J.; Leonard, S. K.; Gilbert, A.; Dollings, P.; Smith, D. L.; Zhang, M. Y.; Di, L.; Platt, B. J.; Neal, S.; Dwyer, J. M.; Bender, C. N.; Zhang, J.; Lock, T.; Kowal, D.; Kramer, A.; Randall, A.; Huselton, C.; Vishwanathan, K.; Tse, S. Y.; Butera, J.; Ring, R. H.; Rosenzweig-Lipson, S.; Hughes, Z. A.; Dunlop, J. The Metabotropic Glutamate Receptor 7 Allosteric Modulator AMN082: A Monoaminergic Agent in Disguise? *J. Pharmacol. Exp. Ther.* **2011**, *338* (1), 345–352. <https://doi.org/10.1124/jpet.110.177378>.
- (162) Teall, M.; White, J.; Mack, S.; Liwicki, G.; Stephenson, A.; Dickson, L. Takeda - 2018 - R7_Takeda_WO2018092921.Pdf, 2018.
- (163) Goldby, A.; Liwicki, G.; Mack, S.; Teall, M.; White, K. US20190031599A1 TAKEDA.Pdf, 2019.
- (164) Abe, M.; Seto, M.; Gogliotti, R. G.; Loch, M. T.; Bollinger, K. A.; Chang, S.; Engelberg, E. M.; Luscombe, V. B.; Harp, J. M.; Bubser, M.; Engers, D. W.; Jones, C. K.; Rodriguez, A. L.; Blobaum, A. L.; Conn, P. J.; Niswender, C. M.; Lindsley, C. W. Discovery of VU6005649, a CNS Penetrant MGLu7/8 Receptor PAM Derived from a Series of Pyrazolo[1,5-a]Pyrimidines. *ACS Med. Chem. Lett.* **2017**, *8* (10), 1110–1115. <https://doi.org/10.1021/acsmchemlett.7b00317>.
- (165) Reed, C. W.; Kalbfleisch, J. J.; Wong, M. J.; Washecheck, J. P.; Hunter, A.; Rodriguez, A. L.; Blobaum, A. L.; Conn, P. J.; Niswender, C. M.; Lindsley, C. W. Discovery of VU6027459: A First-in-Class Selective and CNS Penetrant MGLu7 PAM Tool Compound. *ACS Med. Chem. Lett.* **2020**. <https://doi.org/10.1021/acsmchemlett.0c00432>.
- (166) Suzuki, G.; Tsukamoto, N.; Fushiki, H.; Kawagishi, A.; Nakamura, M.; Kurihara, H.; Mitsuya,

- M.; Ohkubo, M.; Ohta, H. In Vitro Pharmacological Characterization of Novel Isoxazolopyridone Derivatives as Allosteric Metabotropic Glutamate Receptor 7 Antagonists. *J. Pharmacol. Exp. Ther.* **2007**, *323* (1), 147–156. <https://doi.org/10.1124/jpet.107.124701>.
- (167) Pałucha-Poniewiera, A.; Pilc, A. A Selective MGLu7 Receptor Antagonist MMPIP Reversed Antidepressant-like Effects of AMN082 in Rats. *Behav. Brain Res.* **2013**, *238* (1), 109–112. <https://doi.org/10.1016/j.bbr.2012.10.004>.
- (168) Palazzo, E.; Romano, R.; Luongo, L.; Boccella, S.; De Gregorio, D.; Giordano, M. E.; Rossi, F.; Marabese, I.; Scafuro, M. A.; De Novellis, V.; Maione, S. MMPIP, an MGLu7-Selective Negative Allosteric Modulator, Alleviates Pain and Normalizes Affective and Cognitive Behavior in Neuropathic Mice. *Pain* **2015**, *156* (6), 1060–1073. <https://doi.org/10.1097/j.pain.000000000000150>.
- (169) Kalinichev, M.; Rouillier, M.; Girard, F.; Royer-Urios, I.; Bournique, B.; Finn, T.; Charvin, D.; Campo, B.; Poul, E. Le; Mutel, V.; Poli, S.; Neale, S. A.; Salt, T. E.; Lütjens, R. ADX71743, a Potent and Selective Negative Allosteric Modulator of Metabotropic Glutamate Receptor 7: In Vitro and in Vivo Characterization. *J. Pharmacol. Exp. Ther.* **2013**, *344* (3), 624–636. <https://doi.org/10.1124/jpet.112.200915>.
- (170) Moloney, R. D.; Golubeva, A. V.; O'Connor, R. M.; Kalinichev, M.; Dinan, T. G.; Cryan, J. F. Negative Allosteric Modulation of the MGLu7 Receptor Reduces Visceral Hypersensitivity in a Stress-Sensitive Rat Strain. *Neurobiol. Stress* **2015**, *2*, 28–33. <https://doi.org/10.1016/j.ynstr.2015.04.001>.
- (171) No Title <https://www.addextherapeutics.com/en/news-and-events/press-releases/addex-led-consortium-receives-485-million-eurostars-grant-develop-novel-allosteric-modulator-treat-post-traumatic-stress-disorde/>.
- (172) Duvey, G.; Celanire, S. WO2019063596A1 Pragma Therapeutics. 2019, p 163.
- (173) Reed, C. W.; McGowan, K. M.; Spearing, P. K.; Stansley, B. J.; Roenfanz, H. F.; Engers, D. W.; Rodriguez, A. L.; Engelberg, E. M.; Luscombe, V. B.; Loch, M. T.; Remke, D. H.; Rook, J. M.; Blobaum, A. L.; Conn, P. J.; Niswender, C. M.; Lindsley, C. W. VU6010608, a Novel MGLu7 NAM from a Series of N-(2-(1H-1,2,4-Triazol-1-Yl)-5-(Trifluoromethoxy)Phenyl)Benzamides. *ACS Med. Chem. Lett.* **2017**, *8* (12), 1326–1330. <https://doi.org/10.1021/acsmchemlett.7b00429>.
- (174) Reed, C. W.; Yohn, S. E.; Washecheck, J. P.; Roenfanz, H. F.; Quitalig, M. C.; Luscombe, V. B.; Jenkins, M. T.; Rodriguez, A. L.; Engers, D. W.; Blobaum, A. L.; Conn, P. J.; Niswender, C. M.; Lindsley, C. W. Discovery of an Orally Bioavailable and Central Nervous System (CNS) Penetrant MGLu 7 Negative Allosteric Modulator (NAM) in Vivo Tool Compound: N-(2-(1 H-1,2,4-Triazol-1-Yl)-5-(Trifluoromethoxy)Phenyl)-4-(Cyclopropylmethoxy)-3-Methoxybenzamide (VU6012962). *J. Med. Chem.* **2019**, *62* (3). <https://doi.org/10.1021/acs.jmedchem.8b01810>.
- (175) Gee, C. E.; Peterlik, D.; Neuhäuser, C.; Bouhelal, R.; Kaupmann, K.; Laue, G.; Uschold-Schmidt, N.; Feuerbach, D.; Zimmermann, K.; Ofner, S.; Cryan, J. F.; Van Der Putten, H.; Fendt, M.; Vranesic, I.; Glatthar, R.; Flor, P. J. Blocking Metabotropic Glutamate Receptor Subtype 7 (MGLu7) via the Venus Flytrap Domain (VFTD) Inhibits Amygdala Plasticity, Stress, and Anxiety-Related Behavior. *J. Biol. Chem.* **2014**, *289* (16), 10975–10987.

- <https://doi.org/10.1074/jbc.M113.542654>.
- (176) Duvoisin, R. M.; Pfankuch, T.; Wilson, J. M.; Grabell, J.; Chhajlani, V.; Brown, D. G.; Johnson, E.; Raber, J. Acute Pharmacological Modulation of MGluR8 Reduces Measures of Anxiety. *Behav. Brain Res.* **2010**, *212* (2), 168–173. <https://doi.org/10.1016/j.bbr.2010.04.006>.
- (177) Duvoisin, R. M.; Villasana, L.; Davis, M. J.; Winder, D. G.; Raber, J. Opposing Roles of MGluR8 in Measures of Anxiety Involving Non-Social and Social Challenges. *Behav. Brain Res.* **2011**, *221* (1), 50–54. <https://doi.org/10.1016/j.bbr.2011.02.049>.
- (178) Doumazane, E.; Scholler, P.; Zwier, J. M.; Trinquet, E.; Rondard, P.; Pin, J. A New Approach to Analyze Cell Surface Protein Complexes Reveals Specific Heterodimeric Metabotropic Glutamate Receptors. *FASEB J.* **2011**, *25* (1), 66–77. <https://doi.org/10.1096/fj.10-163147>.
- (179) Habrian, C. H.; Levitz, J.; Vyklicky, V.; Fu, Z.; Hoagland, A.; McCort-Tranchepain, I.; Acher, F.; Isacoff, E. Y. Conformational Pathway Provides Unique Sensitivity to a Synaptic MGluR. *Nat. Commun.* **2019**, *10* (1). <https://doi.org/10.1038/s41467-019-13407-8>.
- (180) Lee, J.; Gutzeit, V.; Levitz, J. T. Probing the Homo- and Hetero-Dimerization Propensities of Metabotropic Glutamate Receptors. *Biophys. J.* **2020**, *118* (3), 96a. <https://doi.org/10.1016/j.bpj.2019.11.687>.
- (181) Hassanzadeh-Ghassabeh, G.; Devoogdt, N.; De Pauw, P.; Vincke, C.; Muyldermans, S. Nanobodies and Their Potential Applications. *Nanomedicine* **2013**, *8* (6), 1013–1026. <https://doi.org/10.2217/nnm.13.86>.
- (182) Scholler, P.; Nevoltris, D.; De Bundel, D.; Bossi, S.; Moreno-Delgado, D.; Rovira, X.; Møller, T. C.; El Moustaine, D.; Mathieu, M.; Blanc, E.; McLean, H.; Dupuis, E.; Mathis, G.; Trinquet, E.; Daniel, H.; Valjent, E.; Baty, D.; Chames, P.; Rondard, P.; Pin, J. P. Allosteric Nanobodies Uncover a Role of Hippocampal MGlu2 Receptor Homodimers in Contextual Fear Consolidation. *Nat. Commun.* **2017**, *8* (1). <https://doi.org/10.1038/s41467-017-01489-1>.
- (183) Patel, K. R.; Cherian, J.; Gohil, K.; Atkinson, D. Schizophrenia: Overview and Treatment Options. *P T* **2014**, *39* (9), 638–645.
- (184) Insel, T. Rethinking Schizophrenia. *Nature* **2010**, *468*, 187–193.
- (185) Woo, T. U. W. Neurobiology of Schizophrenia Onset. *Curr. Top. Behav. Neurosci.* **2014**, *16*, 267–295. https://doi.org/10.1007/7854_2013_243.
- (186) Brish, R., Saniotis, A.; Wolf, R., Bernstein, H., H.-G., Steiner, B.; J., Bogerts, B., Braun, A.K., Jankowski, Z., Kumaratilake, J., Henneberg, M.; Gos, T. The Role of Dopamine in Schizophrenia from a Neurobiological and Evolutionary Perspective: Old Fashioned, but Still in Vogue. *Front. Psychiatry* **2014**, *5* (MAY).
- (187) Iqbal, N.; Van Praag, H. The Role of Serotonin in Schizophrenia. *Eur Neuropsychopharmacol* **1995**, *5*, 11–23.
- (188) Meltzer, H. Y. The Role of Serotonin in Schizophrenia and the Place of Serotonin-Dopamine Antagonist Antipsychotics. *J. Clin. Psychopharmacol.* **1995**, *15* (1), 2S-3S. <https://doi.org/10.1097/00004714-199502001-00001>.
- (189) King, R.; Faull, K. F.; Stahl, S. M.; Mefford, I. N.; Thiemann, S.; Barchas, J. D.; Berger, P. A. Serotonin and Schizophrenia: Correlations between Serotonergic Activity and Schizophrenic

- Motor Behavior. *Psychiatry Res.* **1985**, *14* (3), 235–240. [https://doi.org/10.1016/0165-1781\(85\)90018-6](https://doi.org/10.1016/0165-1781(85)90018-6).
- (190) Steeds, H.; Carhart-Harris, R. L.; Stone, J. M. Drug Models of Schizophrenia. *Ther. Adv. Psychopharmacol.* **2015**, *5* (1), 43–58. <https://doi.org/10.1177/2045125314557797>.
- (191) Frohlich, J.; Van Horn, J. D. Reviewing the Ketamine Model for Schizophrenia. *J. Psychopharmacol.* **2014**, *28* (4), 287–302. <https://doi.org/10.1177/0269881113512909>.
- (192) Lahti, A. C.; Weiler, M. A.; Michaelidis, T.; Parwani, A.; Tamminga, C. A. Effects of Ketamine in Normal and Schizophrenic Volunteers. *Neuropsychopharmacology* **2001**, *25* (4), 455–467. [https://doi.org/10.1016/S0893-133X\(01\)00243-3](https://doi.org/10.1016/S0893-133X(01)00243-3).
- (193) Coyle, J. T. Glutamate and Schizophrenia: Beyond the Dopamine Hypothesis. *Cell. Mol. Neurobiol.* **2006**, *26* (4–6), 365–384. <https://doi.org/10.1007/s10571-006-9062-8>.
- (194) Stone, J. M. Glutamatergic Antipsychotic Drugs: A New Dawn in the Treatment of Schizophrenia? *Ther. Adv. Psychopharmacol.* **2011**, *1* (1), 5–18. <https://doi.org/10.1177/2045125311400779>.
- (195) Rorick-Kehn, L. M.; Johnson, B. G.; Burkey, J. L.; Wright, R. A.; Calligaro, D. O.; Marek, G. J.; Nisenbaum, E. S.; Catlow, J. T.; Kingston, A. E.; Giera, D. D.; Herin, M. F.; Monn, J. A.; McKinzie, D. L.; Schoepp, D. D. Pharmacological and Pharmacokinetic Properties of a Structurally Novel, Potent, and Selective Metabotropic Glutamate 2/3 Receptor Agonist: In Vitro Characterization of Agonist (-)-(1R,4S,5S,6S)-4-Amino-2-Sulfonylbicyclo[3.1.0]-Hexane-4,6-Dicarboxylic Acid. *J. Pharmacol. Exp. Ther.* **2007**, *321* (1), 308–317. <https://doi.org/10.1124/jpet.106.110809>.
- (196) Kanter, J. W.; Busch, A. M.; Weeks, C. E.; Landes, S. J. The Nature of Clinical Depression: Symptoms, Syndromes, and Behavior Analysis. *Behav. Anal.* **2008**, *31* (1), 1–21. <https://doi.org/10.1007/BF03392158>.
- (197) Beck, A. T.; Ward, C. H.; Mendelson, M.; Mock, J.; Erbaugh, J. An Inventory for Measuring Depression. *Arch. Gen. Psychiatry* **1961**, *4* (6), 561–571. <https://doi.org/10.1001/archpsyc.1961.01710120031004>.
- (198) <https://www.psychiatry.org/patients-families/depression/what-is-depression>.
- (199) Duval, F.; Lebowitz, B. D.; Macher, J. P. Treatments in Depression. *Dialogues Clin. Neurosci.* **2006**, *8* (2), 191–206.
- (200) Depression: {How} Effective Are Antidepressants? *PubMed Heal.* **2017**, 1–10. <https://doi.org/10.1016/j.cpr.2011.07.004>.
- (201) Donoghue, J. Antidepressants in the Treatment of Major Depression: A Changing Landscape for Clinical Decision Making. *Clin. Pharm.* **2019**, *11* (4). <https://doi.org/10.1211/CP.2019.20206214>.
- (202) Ballenger, J. C. Targeting the Glutamatergic System to Treat Major Depressive Disorder: Rationale and Progress to Date. *Yearb. Psychiatry Appl. Ment. Heal.* **2013**, *2013*, 334–335. <https://doi.org/10.1016/j.ypsy.2012.08.041>.
- (203) Sanacora, G.; Treccani, G.; Popoli, M. Towards a Glutamate Hypothesis of Depression: An Emerging Frontier of Neuropsychopharmacology for Mood Disorders. *Neuropharmacology*

- 2012**, 62 (1), 63–77. <https://doi.org/10.1016/j.neuropharm.2011.07.036>.
- (204) K., W.; V.L., E. Do Glutamatergic Drugs Have a Role in Treating Depression? *Curr. Psychiatr.* **2015**, 14 (2), 14–16 and 27.
- (205) Duman, R. S.; Sanacora, G.; Krystal, J. H. Altered Connectivity in Depression: GABA and Glutamate Neurotransmitter Deficits and Reversal by Novel Treatments. *Neuron* **2019**, 102 (1), 75–90. <https://doi.org/10.1016/j.neuron.2019.03.013>.
- (206) Gerhard, D. M.; Wohleb, E. S.; Duman, R. S. Emerging Treatment Mechanisms for Depression: Focus on Glutamate and Synaptic Plasticity. *Drug Discov. Today* **2016**, 21 (3), 454–464. <https://doi.org/10.1016/j.drudis.2016.01.016>.
- (207) Barnes, S. A.; Sheffler, D. J.; Semenova, S.; Cosford, N. D. P.; Beshpalov, A. Metabotropic Glutamate Receptor 5 as a Target for the Treatment of Depression and Smoking: Robust Preclinical Data but Inconclusive Clinical Efficacy. *Biol. Psychiatry* **2018**, 83 (11), 955–962. <https://doi.org/10.1016/j.biopsych.2018.03.001>.
- (208) Gladding, C. M.; Fitzjohn, S. M.; Molnár, E. Metabotropic Glutamate Receptor-Mediated Long-Term Depression: Molecular Mechanisms. *Pharmacol. Rev.* **2009**, 61 (4), 395–412. <https://doi.org/10.1124/pr.109.001735>.
- (209) Cortese, B. M.; Phan, K. L. The Role of Glutamate in Anxiety and Related Disorders. *CNS Spectr.* **2005**, 10 (10), 820–830. <https://doi.org/10.1017/S1092852900010427>.
- (210) Amiel, J. M.; Mathew, S. J. Glutamate and Anxiety Disorders. *Curr. Psychiatry Rep.* **2007**, 9 (4), 278–283. <https://doi.org/10.1007/s11920-007-0033-7>.
- (211) Simon, A. B.; Gorman, J. M. Advances in the Treatment of Anxiety: Targeting Glutamate. *NeuroRx* **2006**, 3 (1), 57–68. <https://doi.org/10.1016/j.nurx.2005.12.005>.
- (212) Ferraguti, F. Metabotropic Glutamate Receptors as Targets for Novel Anxiolytics. *Curr. Opin. Pharmacol.* **2018**, 38, 37–42. <https://doi.org/10.1016/j.coph.2018.02.004>.
- (213) No Title <https://www.addtherapeutics.com/en/pipeline/researches/mglur4-pam/>.
- (214) Zhan, Y.; Xia, J.; Wang, X. Effects of Glutamate-Related Drugs on Anxiety and Compulsive Behavior in Rats with Obsessive-Compulsive Disorder. *Int. J. Neurosci.* **2019**. <https://doi.org/10.1080/00207454.2019.1684276>.
- (215) Tzschentke, T. M.; Schmidt, W. J. Glutamatergic Mechanisms in Addiction. *Mol. Psychiatry* **2003**, 8 (4), 373–382. <https://doi.org/10.1038/sj.mp.4001269>.
- (216) D’Souza, M. S. Glutamatergic Transmission in Drug Reward: Implications for Drug Addiction. *Front. Neurosci.* **2015**, 9 (NOV). <https://doi.org/10.3389/fnins.2015.00404>.
- (217) Spencer, S.; Scofield, M.; Kalivas, P. W. The Good and Bad News about Glutamate in Drug Addiction. *J. Psychopharmacol.* **2016**, 30 (11), 1095–1098. <https://doi.org/10.1177/0269881116655248>.
- (218) S.E., T.; A.L., L.; N.E., N.; Olive, M. F. NMDA Receptor Modulators in the Treatment of Drug Addiction. *Pharmaceuticals* **2013**, 6 (2), 251–268.
- (219) D’Ascenzo, M.; Podda, M. V.; Grassi, C. The Role of D-Serine as Co-Agonist of NMDA Receptors in the Nucleus Accumbens: Relevance to Cocaine Addiction. *Front. Synaptic*

- Neurosci.* **2014**, *6* (JUL). <https://doi.org/10.3389/fnsyn.2014.00016>.
- (220) Mao, L.; Guo, M.; Jin, D.; Xue, B.; Wang, J. Q. Group III Metabotropic Glutamate Receptors and Drug Addiction. *Front. Med. China* **2013**, *7* (4), 445–451. <https://doi.org/10.1007/s11684-013-0291-1>.
- (221) Hippus, H.; Neundörfer, G. The Discovery of Alzheimer's Disease. *Dialogues Clin. Neurosci.* **2003**, *5* (1), 101–108.
- (222) Jia, Q.; Deng, Y.; Qing, H. Potential Therapeutic Strategies for Alzheimer's Disease Targeting or beyond β -Amyloid: Insights from Clinical Trials. *Biomed Res. Int.* **2014**, *2014*. <https://doi.org/10.1155/2014/837157>.
- (223) Waring, S. C.; Rosenberg, R. N. Genome-Wide Association Studies in Alzheimer Disease. *Arch. Neurol.* **2008**, *65* (3), 329–334. <https://doi.org/10.1001/archneur.65.3.329>.
- (224) Strittmatter, W. J.; Saunders, A. M.; Schmechel, D.; Pericak-Vance, M.; Enghild, J.; Salvesen, G. S.; Roses, A. D. Apolipoprotein E: High-Avidity Binding to β -Amyloid and Increased Frequency of Type 4 Allele in Late-Onset Familial Alzheimer Disease. *Proc. Natl. Acad. Sci. U. S. A.* **1993**, *90* (5), 1977–1981. <https://doi.org/10.1073/pnas.90.5.1977>.
- (225) Pimplikar, S. W. Reassessing the Amyloid Cascade Hypothesis of Alzheimer's Disease. *Int. J. Biochem. Cell Biol.* **2009**, *41* (6), 1261–1268. <https://doi.org/10.1016/j.biocel.2008.12.015>.
- (226) Nunomura, A.; Moreira, P.; Lee, H.; Zhu, X.; Castellani, R.; Smith, M.; Perry, G. Neuronal Death and Survival Under Oxidative Stress in Alzheimer and Parkinson Diseases. *CNS Neurol. Disord. - Drug Targets* **2008**, *6* (6), 411–423. <https://doi.org/10.2174/187152707783399201>.
- (227) Goedert, M. Tau Protein and the Neurofibrillary Pathology of Alzheimer's Disease. *Apolipoprotein E Alzheimer's Dis.* **1996**, 103–125. https://doi.org/10.1007/978-3-642-80109-9_9.
- (228) Hamley, I. W. The Amyloid Beta Peptide: A Chemist's Perspective. Role in Alzheimer's and Fibrillization. *Chem. Rev.* **2012**, *112* (10), 5147–5192. <https://doi.org/10.1021/cr3000994>.
- (229) Gharreb, D.; Mohamed, S.; El-Sayed, M. The Inter-Relationship between Insulin Resistance and Alzheimer Development. *J Biomed. Sci. Eng.* **2013**, *6*, 754.
- (230) Ye, J.; Zhai, H. Z. Oxidative Stress and Alzheimer Disease. *Chinese J. Clin. Rehabil.* **2005**, *9* (33), 117–119.
- (231) Zhao, Y.; Zhao, B. Oxidative Stress and the Pathogenesis of Alzheimer's Disease. *Oxid. Med. Cell. Longev.* **2013**. <https://doi.org/10.1155/2013/316523>.
- (232) Sinclair, L. I.; Kumar, A.; Taher, D.-S.; Love, S. Alzheimer's Research and Therapy. **2019**, *11* (1). <https://doi.org/10.1186/s13195>.
- (233) Davies, P. Challenging the Cholinergic Hypothesis in Alzheimer Disease. *J. Am. Med. Assoc.* **1999**, *281* (15), 1433–1434. <https://doi.org/10.1001/jama.281.15.1433>.
- (234) Cacabelos, R.; Takeda, M.; Winblad, B. The Glutamatergic System and Neurodegeneration in Dementia: Preventive Strategies in Alzheimer's Disease. *Int. J. Geriatr. Psychiatry* **1999**, *14* (1), 3–47..

- (235) Reisberg, B.; Doody, R.; Stoffler, A.; Schmitt, F.; Ferris, S.; Mobius, H. Memantine in Moderater-to-Severe Alzheimer's Disease. *N Engl J Med* **2003**, *348* (14), 1333–1341.
- (236) DeMaagd, G.; Philip, A. Parkinson's Disease and Its Management Part 1: Disease Entity, Risk Factors, Pathophysiology, Clinical Presentation, and Diagnosis. *P T* **2015**, *40* (8), 504–532.
- (237) Hayes, M. T. Parkinson's Disease and Parkinsonism. *Am. J. Med.* **2019**, *132* (7), 802–807. <https://doi.org/10.1016/j.amjmed.2019.03.001>.
- (238) Savitt, J. M.; Dawson, V. L.; Dawson, T. M. Diagnosis and Treatment of Parkinson Disease: Molecules to Medicine. *J. Clin. Invest.* **2006**, *116* (7), 1744–1754. <https://doi.org/10.1172/JCI29178>.
- (239) Johnson, K.; Conn, P.; Niswender, C. Glutamate Receptors as Therapeutic Targets for Parkinsons Disease. *CNS Neurol. Disord. - Drug Targets* **2012**, *8* (6), 475–491. <https://doi.org/10.2174/187152709789824606>.
- (240) Carrillo-Mora, P.; Silva-Adaya, D.; Villaseñor-Aguayo, K. Glutamate in Parkinson's Disease: Role of Antiglutamatergic Drugs. *Basal Ganglia* **2013**, *3* (3), 147–157. <https://doi.org/10.1016/j.baga.2013.09.001>.
- (241) Zhang, Z.; Zhang, S.; Fu, P.; Zhang, Z.; Lin, K.; Ko, J. K. S.; Yung, K. K. L. Roles of Glutamate Receptors in Parkinson's Disease. *Int. J. Mol. Sci.* **2019**, *20* (18). <https://doi.org/10.3390/ijms20184391>.
- (242) Battaglia, G.; Busceti, C. L.; Molinaro, G.; Biagioni, F.; Traficante, A.; Nicoletti, F.; Bruno, V. Pharmacological Activation of MGlu4 Metabotropic Glutamate Receptors Reduces Nigrostriatal Degeneration in Mice Treated with 1-Methyl-4-Phenyl-1,2,3,6-Tetrahydropyridine. *J. Neurosci.* **2006**, *26* (27), 7222–7229. <https://doi.org/10.1523/JNEUROSCI.1595-06.2006>.
- (243) Betts, M.; O'Neill, M.; Duty, S. Allosteric Modulation of the Group III MGlu4 Receptor Provides Functional Neuroprotection in the 6-Hydroxydopamine Rat Model of Parkinson's Disease. *Br J Pharmacol* **2012**, *166* (8), 2317–2330.
- (244) <https://www.addextherapeutics.com/en/pipeline/clinical-pipeline/>.
- (245) Stafstrom, C. E.; Carmant, L. Seizures and Epilepsy: An Overview for Neuroscientists. *Cold Spring Harb. Perspect. Biol.* **2015**, *7* (5), 1–19. <https://doi.org/10.1101/cshperspect.a022426>.
- (246) Manford, M. Recent Advances in Epilepsy. *J Neurol* **2017**, *264* (8), 1811–1824.
- (247) Hanada, T. Ionotropic Glutamate Receptors in Epilepsy: A Review Focusing on AMPA and NMDA Receptors. *Biomolecules* **2020**, *10* (3). <https://doi.org/10.3390/biom10030464>.
- (248) Besag, F. M. C.; Patsalos, P. N. Clinical Efficacy of Perampnel for Partial-Onset and Primary Generalized Tonic–Clonic Seizures. *Neuropsychiatr. Dis. Treat.* **2016**, *12*, 1215–1220. <https://doi.org/10.2147/NDT.S83842>.
- (249) Taylor, G. W.; Merlin, L. R.; Wong, R. K. S. Synchronized Oscillations in Hippocampal CA3 Neurons Induced by Metabotropic Glutamate Receptor Activation. *J. Neurosci.* **1995**, *15* (12), 8039–8052. <https://doi.org/10.1523/jneurosci.15-12-08039.1995>.
- (250) Suzuki, K.; Mori, N.; Kittaka, H.; Iwata, Y.; Yamada, Y.; Osonoe, K.; Niwa, S. I. Anticonvulsant

- Action of Metabotropic Glutamate Receptor Agonists in Kindled Amygdala of Rats. *Neurosci. Lett.* **1996**, *204* (1–2), 41–44. [https://doi.org/10.1016/0304-3940\(96\)12311-9](https://doi.org/10.1016/0304-3940(96)12311-9).
- (251) Ghauri, M.; Chapman, A. G.; Meldrum, B. S. Convulsant and Anticonvulsant Actions of Agonists and Antagonists of Group III mGluRs. *Neuroreport* **1996**, *7* (9), 1469–1474. <https://doi.org/10.1097/00001756-199606170-00005>.
- (252) Wang, X.; Ai, J.; Hampson, D. R.; Snead, O. C. Altered Glutamate and GABA Release within Thalamocortical Circuitry in Metabotropic Glutamate Receptor 4 Knockout Mice. *Neuroscience* **2005**, *134* (4), 1195–1203. <https://doi.org/10.1016/j.neuroscience.2005.05.033>.
- (253) Snead, O. C.; Banerjee, P. K.; Burnham, M.; Hampson, D. Modulation of Absence Seizures by the GABA(A) Receptor: A Critical Role for Metabotropic Glutamate Receptor 4 (mGluR4). *J. Neurosci.* **2000**, *20* (16), 6218–6224. <https://doi.org/10.1523/JNEUROSCI.20-16-06218.2000>.
- (254) Celli, R.; Santolini, I.; Van Luijckelaar, G.; Ngomba, R. T.; Bruno, V.; Nicoletti, F. Targeting Metabotropic Glutamate Receptors in the Treatment of Epilepsy: Rationale and Current Status. *Expert Opin. Ther. Targets* **2019**. <https://doi.org/10.1080/14728222.2019.1586885>.
- (255) Lerch, M. M.; Hansen, M. J.; van Dam, G. M.; Szymanski, W.; Feringa, B. L. Emerging Targets in Photopharmacology. *Angew. Chemie - Int. Ed.* **2016**, *55* (37), 10978–10999. <https://doi.org/10.1002/anie.201601931>.
- (256) Goudet, C.; Rovira, X.; Llebaria, A. Shedding Light on Metabotropic Glutamate Receptors Using Optogenetics and Photopharmacology. *Curr. Opin. Pharmacol.* **2018**, *38*, 8–15. <https://doi.org/10.1016/j.coph.2018.01.007>.
- (257) Piant, S.; Bolze, F.; Specht, A. Two-Photon Uncaging, from Neuroscience to Materials. *Opt. Mater. Express* **2016**, *6* (5), 1679. <https://doi.org/10.1364/ome.6.001679>.
- (258) Engels, J.; Schlaeger, E. J. Synthesis, Structure, and Reactivity of Adenosine Cyclic 3',5'-Phosphate-Benzyl Triesters. *J. Med. Chem.* **1977**, *20* (7), 907–911. <https://doi.org/10.1021/jm00217a008>.
- (259) Kaplan, J. H.; Forbush, B.; Hoffman, J. F. Rapid Photolytic Release of Adenosine 5'-Triphosphate from a Protected Analogue: Utilization by the Na:K Pump of Human Red Blood Cell Ghosts. *Biochemistry* **1978**, *17* (10), 1929–1935. <https://doi.org/10.1021/bi00603a020>.
- (260) Ellis-Davies, G. C. R. Caged Compounds: Photorelease Technology for Control of Cellular Chemistry and Physiology. *Nat. Methods* **2007**, *4* (8), 619–628. <https://doi.org/10.1038/nmeth1072>.
- (261) Abe, M.; Chitose, Y.; Jakkampudi, S.; Thuy, P. T. T.; Lin, Q.; Van, B. T.; Yamada, A.; Oyama, R.; Sasaki, M.; Katan, C. Design and Synthesis of Two-Photon Responsive Chromophores for Near-Infrared Light-Induced Uncaging Reactions. *Synth.* **2017**, *49* (15), 3337–3346. <https://doi.org/10.1055/s-0036-1590813>.
- (262) Ellis-Davies, G. C. R. Chemist and Biologist Talk to Each Other about Caged Neurotransmitters. *Beilstein J. Org. Chem.* **2013**, *9* (1), 64–73. <https://doi.org/10.3762/bjoc.9.8>.
- (263) Ellis-Davies, G. C. R. Two-Photon Uncaging of Glutamate. *Front. Synaptic Neurosci.* **2019**, *10*

- (January), 1–13. <https://doi.org/10.3389/fnsyn.2018.00048>.
- (264) Pianowski, Z. L. Recent Implementations of Molecular Photoswitches into Smart Materials and Biological Systems. *Chem. - A Eur. J.* **2019**, *25* (20), 5128–5144. <https://doi.org/10.1002/chem.201805814>.
- (265) Irie, M. Photochromism: Memories and Switches Introduction. *Chem. Rev.* **2000**, *100* (5), 1683–1684. <https://doi.org/10.1021/cr980068l>.
- (266) Helmy, S.; Leibfarth, F. A.; Oh, S.; Poelma, J. E.; Hawker, C. J.; De Alaniz, J. R. Photoswitching Using Visible Light: A New Class of Organic Photochromic Molecules. *J. Am. Chem. Soc.* **2014**, *136* (23), 8169–8172. <https://doi.org/10.1021/ja503016b>.
- (267) Lewis, K. G.; Mulquiney, C. E. Aspects of the formation and use of stenhouse salts and related compounds. *Tetrahedron* **1977**, *33* (26).
- (268) Hemmer, J. R.; Poelma, S. O.; Treat, N.; Page, Z. A.; Dolinski, N. D.; Diaz, Y. J.; Tomlinson, W.; Clark, K. D.; Hooper, J. P.; Hawker, C.; Read De Alaniz, J. Tunable Visible and Near Infrared Photoswitches. *J. Am. Chem. Soc.* **2016**, *138* (42), 13960–13966. <https://doi.org/10.1021/jacs.6b07434>.
- (269) Laurent, A. D.; Medved', M.; Jacquemin, D. Using Time-Dependent Density Functional Theory to Probe the Nature of Donor–Acceptor Stenhouse Adduct Photochromes. *ChemPhysChem* **2016**, 1846–1851. <https://doi.org/10.1002/cphc.201600041>.
- (270) Saha, R.; Devaraj, A.; Bhattacharyya, S.; Das, S.; Zangrando, E.; Mukherjee, P. S. Unusual Behavior of Donor-Acceptor Stenhouse Adducts in Confined Space of a Water-Soluble PdII Molecular Vessel. *J. Am. Chem. Soc.* **2019**, *141* (21), 8638–8645. <https://doi.org/10.1021/jacs.9b03924>.
- (271) Lui, B. F.; Tierce, N. T.; Tong, F.; Sroda, M. M.; Lu, H.; Read De Alaniz, J.; Bardeen, C. J. Unusual Concentration Dependence of the Photoisomerization Reaction in Donor-Acceptor Stenhouse Adducts. *Photochem. Photobiol. Sci.* **2019**, *18* (6), 1587–1595. <https://doi.org/10.1039/c9pp00130a>.
- (272) Irie, M. *Diarylethenes for Memories and Switches*; 2000; Vol. 100. <https://doi.org/10.1021/cr980069d>.
- (273) Kellogg, R. M.; Groen, M. B.; Wynberg, H. Photochemically Induced Cyclization of Some Furyl- and Thienylethenes. *J. Org. Chem.* **1967**, *32* (10), 3093–3100. <https://doi.org/10.1021/jo01285a035>.
- (274) Tang, S.; Song, F.; Lu, M.; Han, K.; Peng, X. Rational Design of a Visible-Light Photochromic Diarylethene: A Simple Strategy by Extending Conjugation with Electron Donating Groups. *Sci. China Chem.* **2019**, *62* (4), 451–459. <https://doi.org/10.1007/s11426-018-9381-1>.
- (275) Transitions, I.; Multiple, R.; Transitions, I.; Temperatures, L. Ifztevnal Transitions a n Some Spiropyran,. *Order A J. Theory Ordered Sets Its Appl.* **1951**, No. Iv, 297–303.
- (276) Marturano, V.; Cerruti, P.; Giamberini, M.; Tylkowski, B.; Ambrogi, V. Light-Responsive Polymer Micro- and Nano-Capsules. *Polymers (Basel)*. **2017**, *9* (1). <https://doi.org/10.3390/polym9010008>.
- (277) Dzintra, A.; Khabdual, A. Study on tribological and mechanical properties of PTFE

- composites copolymer brushes with spiropyran and methyl methacrylate segments. *J. Am. Chem. Soc.* **2005**, *41* (3), 1–31.
- (278) Kortekaas, L.; Browne, W. R. The Evolution of Spiropyran: Fundamentals and Progress of an Extraordinarily Versatile Photochrome. *Chem. Soc. Rev.* **2019**, *48* (12), 3406–3424. <https://doi.org/10.1039/c9cs00203k>.
- (279) Bletz, M.; Pfeifer-Fukumura, U.; Kolb, U.; Baumann, W. Ground- and First-Excited-Singlet-State Electric Dipole Moments of Some Photochromic Spirobenzopyrans in Their Spiropyran and Merocyanine Form. *J. Phys. Chem. A* **2002**, *106* (10), 2232–2236. <https://doi.org/10.1021/jp012562q>.
- (280) Brode, W. R.; Gould, J. H.; Wyman, G. M. The Relation between the Absorption Spectra and the Chemical Constitution of Dyes. XXV. Phototropism and Cis-Trans Isomerism in Aromatic Azo Compounds. *J. Am. Chem. Soc.* **1952**, *74* (18), 4641–4646. <https://doi.org/10.1021/ja01138a059>.
- (281) Bandara, H. M. D.; Burdette, S. C. Photoisomerization in Different Classes of Azobenzene. *Chem. Soc. Rev.* **2012**, *41* (5), 1809–1825. <https://doi.org/10.1039/c1cs15179g>.
- (282) Crecca, C. R.; Roitberg, A. E. Theoretical Study of the Isomerization Mechanism of Azobenzene and Disubstituted Azobenzene Derivatives. *J. Phys. Chem. A* **2006**, *110* (26), 8188–8203. <https://doi.org/10.1021/jp057413c>.
- (283) Bahrenburg, J.; Röttger, K.; Siewertsen, R.; Renth, F.; Temps, F. Sequential Photoisomerisation Dynamics of the Push-Pull Azobenzene Disperse Red 1. *Photochem. Photobiol. Sci.* **2012**, *11* (7), 1210–1219. <https://doi.org/10.1039/c2pp05400k>.
- (284) Dong, M.; Babalhavaeji, A.; Samanta, S.; Beharry, A. A.; Woolley, G. A. Red-Shifting Azobenzene Photoswitches for in Vivo Use. *Acc. Chem. Res.* **2015**, *48* (10), 2662–2670. <https://doi.org/10.1021/acs.accounts.5b00270>.
- (285) Knie, C.; Utecht, M.; Zhao, F.; Kulla, H.; Kovalenko, S.; Brouwer, A. M.; Saalfrank, P.; Hecht, S.; Bléger, D. Ortho-Fluoroazobenzenes: Visible Light Switches with Very Long-Lived Z Isomers. *Chem. - A Eur. J.* **2014**, *20* (50), 16492–16501. <https://doi.org/10.1002/chem.201404649>.
- (286) Ahmed, Z.; Siiskonen, A.; Virkki, M.; Priimagi, A. Controlling Azobenzene Photoswitching through Combined: Ortho -Fluorination and -Amination. *Chem. Commun.* **2017**, *53* (93), 12520–12523. <https://doi.org/10.1039/c7cc07308a>.
- (287) Kaiser, M.; Leitner, S. P.; Hirtenlehner, C.; List, M.; Gerisch, A.; Monkowius, U. Azobenzene-Functionalized N-Heterocyclic Carbenes as Photochromic Ligands in Silver(i) and Gold(i) Complexes. *Dalt. Trans.* **2013**, *42* (41), 14749–14756. <https://doi.org/10.1039/c3dt51565f>.
- (288) Leippe, P.; Frank, J. A. Designing Azobenzene-Based Tools for Controlling Neurotransmission. *Curr. Opin. Struct. Biol.* **2019**, *57*, 23–30. <https://doi.org/10.1016/j.sbi.2019.01.022>.
- (289) Cabré, G.; Garrido-Charles, A.; Moreno, M.; Bosch, M.; Porta-de-la-Riva, M.; Krieg, M.; Gascón-Moya, M.; Camarero, N.; Gelabert, R.; Lluch, J. M.; Busqué, F.; Hernando, J.; Gorostiza, P.; Alibés, R. Rationally Designed Azobenzene Photoswitches for Efficient Two-Photon Neuronal Excitation. *Nat. Commun.* **2019**, *10* (1). <https://doi.org/10.1038/s41467->

- 019-08796-9.
- (290) Sun, S.; Liang, S.; Xu, W.-C.; Xu, G.; Wu, S. Photoresponsive Polymers with Multi-Azobenzene Groups. *Polym. Chem.* **2019**, *10* (32), 4389–4401. <https://doi.org/10.1039/c9py00793h>.
- (291) Wang, Z.-Z.; Zhang, H.-Q. Synthesis of an Azobenzene-Containing Main-Chain Crystalline Polymer and Photodeformation Behaviors of Its Supramolecular Hydrogen-Bonded Fibers. *Chinese J. Polym. Sci.* **2019**, 9–10. <https://doi.org/10.1007/s10118-019-2302-4>.
- (292) Morstein, J.; Awale, M.; Reymond, J. L.; Trauner, D. Mapping the Azolog Space Enables the Optical Control of New Biological Targets. *ACS Cent. Sci.* **2019**, *5* (4), 607–618. <https://doi.org/10.1021/acscentsci.8b00881>.
- (293) Rustler, K.; Maleeva, G.; Bregestovski, P.; König, B. Azologization of Serotonin 5-HT 3 Receptor Antagonists. *Beilstein J. Org. Chem.* **2019**, *15*, 780–788. <https://doi.org/10.3762/bjoc.15.74>.
- (294) Cheng, B.; Morstein, J.; Ladefoged, L. K.; Maesen, J. B.; Schiøtt, B.; Sinning, S.; Trauner, D. A Photoswitchable Inhibitor of the Human Serotonin Transporter. *ACS Chem. Neurosci.* **2020**. <https://doi.org/10.1021/acchemneuro.9b00521>.
- (295) Duran Corbera, A.; Catena, J.; Otero Viñas, M.; Llebaria, A.; Rovira, xavier. Photoswitchable Antagonists for a Precise Spatiotemporal Control of β 2 -Adrenoceptors . *J. Med. Chem.* **2020**. <https://doi.org/10.1021/acs.jmedchem.0c00831>.
- (296) Petermayer, C.; Dube, H. Indigoid Photoswitches: Visible Light Responsive Molecular Tools. *Acc. Chem. Res.* **2018**, *51* (5), 1153–1163. <https://doi.org/10.1021/acs.accounts.7b00638>.
- (297) Schmidt, H. Indigo - 100 Jahre Industrielle Synthese. *Chemie Unserer Zeit* **1997**, *31* (3), 121–128. <https://doi.org/10.1002/ciuz.19970310304>.
- (298) Zollinger, H. Carbonyl Dyes and Pigments. In *Color Chemistry*; 2003; pp 261–262.
- (299) Petermayer, C.; Thumser, S.; Kink, F.; Mayer, P.; Dube, H. Hemiindigo: Highly Bistable Photoswitching at the Biooptical Window. *J. Am. Chem. Soc.* **2017**, *139* (42), 15060–15067. <https://doi.org/10.1021/jacs.7b07531>.
- (300) Berdnikova, D. V. Visible-Range Hemi-Indigo Photoswitch: ON–OFF Fluorescent Binder for HIV-1 RNA. *Chem. Commun.* **2019**, *55* (58), 8402–8405. <https://doi.org/10.1039/c9cc04270a>.
- (301) Wiedbrauk, S.; Dube, H. Hemithioindigo-An Emerging Photoswitch. *Tetrahedron Lett.* **2015**, *56* (29), 4266–4274. <https://doi.org/10.1016/j.tetlet.2015.05.022>.
- (302) Zweig, J. E.; Newhouse, T. R. Isomer-Specific Hydrogen Bonding as a Design Principle for Bidirectionally Quantitative and Redshifted Hemithioindigo Photoswitches. *J. Am. Chem. Soc.* **2017**, *139* (32), 10956–10959. <https://doi.org/10.1021/jacs.7b04448>.
- (303) Zweig, J. E.; Ko, T. A.; Huang, J.; Newhouse, T. R. Effects of π -Extension on Pyrrole Hemithioindigo Photoswitches. *Tetrahedron* **2019**, *75* (34), 130466. <https://doi.org/10.1016/j.tet.2019.130466>.
- (304) Kitzig, S.; Thilemann, M.; Cordes, T.; Rück-Braun, K. Light-Switchable Peptides with a Hemithioindigo Unit: Peptide Design, Photochromism, and Optical Spectroscopy. *ChemPhysChem* **2016**, *17* (9), 1252–1263. <https://doi.org/10.1002/cphc.201501050>.

- (305) Sailer, A.; Ermer, F.; Kraus, Y.; Bingham, R.; Lutter, F. H.; Ahlfeld, J.; Thorn-seshold, O. Potent Hemithioindigo-Based Antimitotics Photocontrol the Microtubule Cytoskeleton in Cellulo
Potent Hemithioindigo-Based Antimitotics Photocontrol the Microtubule Cytoskeleton in Cellulo
Keywords. **2019**, No. 2, 1–14. <https://doi.org/10.26434/chemrxiv.9176747.v1>.
- (306) Hoorens, M. W. H.; Medved', M.; Laurent, A. D.; Di Donato, M.; Fanetti, S.; Slappendel, L.; Hilbers, M.; Feringa, B. L.; Jan Buma, W.; Szymanski, W. Iminothioindoxyl as a Molecular Photoswitch with 100 Nm Band Separation in the Visible Range. *Nat. Commun.* **2019**, *10* (1), 1–11. <https://doi.org/10.1038/s41467-019-10251-8>.
- (307) Püntener, Alois G. Schlesinger, U. 9 - Natural Dyes. In *Colorants for Non-Textile Applications*; 2000; pp 382–455.
- (308) Haudecoeur, R.; Boumendjel, A. Recent Advances in the Medicinal Chemistry of Aurones. *Curr. Med. Chem.* **2012**, *16*, 2861–2875.
- (309) Ayabe, S.; Uchiyama, H.; Aoki, T.; Akashi, T. 1.24-Plant Phenolics: Phenylpropanoids. In *Comprehensive Natural Products II*; 2010; pp 929–976.
- (310) Zwergel, C.; Gaascht, F.; Valente, S.; Diederich, M.; Bagrel, D.; Kirsch, G. Aurones: Interesting Natural and Synthetic Compounds with Emerging Biological Potential. *Nat. Prod. Commun.* **2012**, *7* (3), 389–394. <https://doi.org/10.1177/1934578x1200700322>.
- (311) Schmitt, J.; Handy, S. T. A Golden Opportunity: Benzofuranone Modifications of Aurones and Their Influence on Optical Properties, Toxicity, and Potential as Dyes. *Beilstein J. Org. Chem.* **2019**, *15*, 1781–1785. <https://doi.org/10.3762/bjoc.15.171>.
- (312) Espinosa-Bustos, C.; Cortés-Arriagada, D.; Soto-Arriaza, M. A.; Robinson-Duggon, J.; Pizarro, N.; Cabrera, A. R.; Fuentealba, D.; Salas, C. O. Fluorescence Properties of Aurone Derivatives: An Experimental and Theoretical Study with Some Preliminary Biological Applications. *Photochem. Photobiol. Sci.* **2017**, *16* (8), 1268–1276. <https://doi.org/10.1039/c7pp00078b>.
- (313) Xue, Y.; Dou, Y.; An, L.; Zheng, Y.; Zhang, L.; Liu, Y. Electronic Structure and Spectral Properties of Aurones as Visible Range Fluorescent Probes: A DFT/TDDFT Study. *RSC Adv.* **2016**, *6* (9), 7002–7010. <https://doi.org/10.1039/c5ra25733f>.
- (314) Li, M.; Yang, S.; Liang, W.; Zhang, X.; Qu, D. A Novel Multiphotochromic System with Orthogonal Light Excitations. *Dye. Pigment.* **2019**, *166* (March), 239–244. <https://doi.org/10.1016/j.dyepig.2019.03.043>.
- (315) Kim, P. M.; Duan, X.; Huang, A. S.; Liu, C. Y.; Ming, G. L.; Song, H.; Snyder, S. H. Aspartate Racemase, Generating Neuronal D-Aspartate, Regulates Adult Neurogenesis. *Proc. Natl. Acad. Sci. U. S. A.* **2010**, *107* (7), 3175–3179. <https://doi.org/10.1073/pnas.0914706107>.
- (316) Wolosker, H.; Blackshaw, S.; Snyder, S. H. Serine Racemase: A Glial Enzyme Synthesizing D-Serine to Regulate Glutamate-N-Methyl-D-Aspartate Neurotransmission. *Proc. Natl. Acad. Sci.* **1999**, *96* (23), 13409–13414. <https://doi.org/10.1073/pnas.96.23.13409>.
- (317) Sason, H.; Billard, J. M.; Smith, G. P.; Safory, H.; Neame, S.; Kaplan, E.; Rosenberg, D.; Zubedat, S.; Foltyn, V. N.; Christoffersen, C. T.; Bundgaard, C.; Thomsen, C.; Avital, A.; Christensen, K. V.; Wolosker, H. Asc-1 Transporter Regulation of Synaptic Activity *via* the Tonic Release of d-Serine in the Forebrain. *Cereb. Cortex* **2016**, *27* (2), bhv350.

<https://doi.org/10.1093/cercor/bhv350>.

- (318) Mikou, A.; Cabayé, A.; Goupil, A.; Bertrand, H.-O.; Mothet, J.-P.; Acher, F. C. Asc-1 Transporter (SLC7A10): Homology Models and Molecular Dynamics Insights into the First Steps of the Transport Mechanism. *Sci. Rep.* **2020**, *10* (1), 3731. <https://doi.org/10.1038/s41598-020-60617-y>.
- (319) Kantevari, S.; Matsuzaki, M.; Kanemoto, Y.; Kasai, H.; Ellis-Davies, G. C. R. Two-Color, Two-Photon Uncaging of Glutamate and GABA. *Nat. Methods* **2010**, *7* (2), 123–125. <https://doi.org/10.1038/nmeth.1413>.
- (320) Olson, J. P.; Kwon, H. B.; Takasaki, K. T.; Chiu, C. Q.; Higley, M. J.; Sabatini, B. L.; Ellis-Davies, G. C. R. Optically Selective Two-Photon Uncaging of Glutamate at 900 Nm. *J. Am. Chem. Soc.* **2013**, *135* (16), 5954–5957. <https://doi.org/10.1021/ja4019379>.
- (321) Amatrudo, J. M.; Olson, J. P.; Lur, G.; Chiu, C. Q.; Higley, M. J.; Ellis-davies, G. C. R. Wavelength-Selective One- and Two-Photon Uncaging of GABA. **2013**.
- (322) Amatrudo, J. M.; Olson, J. P.; Lur, G.; Chiu, C. Q.; Higley, M. J.; Ellis-Davies, G. C. R. Wavelength-Selective One- and Two-Photon Uncaging of Gaba. *ACS Chem. Neurosci.* **2014**, *5* (1), 64–70. <https://doi.org/10.1021/cn400185r>.
- (323) Taniguchi, A.; Skwarczynski, M.; Sohma, Y.; Okada, T.; Ikeda, K.; Prakash, H.; Mukai, H.; Hayashi, Y.; Kimura, T.; Hirota, S.; Matsuzaki, K.; Kiso, Y. Controlled Production of Amyloid Beta Peptide from a Photo-Triggered, Water-Soluble Precursor “Click Peptide”. *Chembiochem* **2008**, *9* (18), 3055–3065. <https://doi.org/10.1002/cbic.200800503>.
- (324) Noguchi, M.; Skwarczynski, M.; Prakash, H.; Hirota, S.; Kimura, T.; Hayashi, Y.; Kiso, Y. Development of Novel Water-Soluble Photocleavable Protective Group and Its Application for Design of Photoresponsive Paclitaxel Prodrugs. *Bioorganic Med. Chem.* **2008**, *16* (10), 5389–5397. <https://doi.org/10.1016/j.bmc.2008.04.022>.
- (325) Tyndall, S.; Wong, K. F.; Vanalstine-Parris, M. A. Insight into the Mechanism of the Pechmann Condensation Reaction Using NMR. *J. Org. Chem.* **2015**, *80* (18), 8951–8953. <https://doi.org/10.1021/acs.joc.5b01802>.
- (326) Potdar, M. K.; Mohile, S. S.; Salunkhe, M. M. Coumarin Syntheses via Pechmann Condensation in Lewis Acidic Chloroaluminate Ionic Liquid. *Tetrahedron Lett.* **2001**, *42* (52), 9285–9287. [https://doi.org/10.1016/S0040-4039\(01\)02041-X](https://doi.org/10.1016/S0040-4039(01)02041-X).
- (327) Ito, K.; Nakajima, K. Selenium Dioxide Oxidation of Alkylcoumarins and Related Methyl-substituted Heteroaromatics. *J. Heterocycl. Chem.* **1988**, *25* (2), 511–515. <https://doi.org/10.1002/jhet.5570250229>.
- (328) Ghosh, A. K.; Brindisi, M. Organic Carbamates in Drug Design and Medicinal Chemistry. *J. Med. Chem.* **2015**, *58* (7), 2895–2940. <https://doi.org/10.1021/jm501371s>.
- (329) Cürten, B.; Kullmann, H. M. P.; Bier, M. E.; Kandler, K.; Schmidt, B. F. Synthesis, Photophysical, Photochemical and Biological Properties of Caged GABA, 4-[[[(2H-1-Benzopyran-2-one-7-Amino-4-Methoxy) Carbonyl] Amino] Butanoic Acid. *Photochem. Photobiol.* **2004**. <https://doi.org/10.1562/2004-07-08-ra-226>.
- (330) Cappa, A.; Marcantoni, E.; Torregiani, E.; Bartoli, G.; Bellucci, M. C.; Bosco, M.; Sambri, L. A Simple Method for the Selective Deprotection of *p*-Methoxybenzyl Ethers by Cerium(III)

- Chloride Heptahydrate and Sodium Iodide. *J. Org. Chem.* **2000**, *65* (15), 4782–4782. <https://doi.org/10.1021/jo0040238>.
- (331) Marcantoni, E.; Massaccesi, M.; Torregiani, E.; Bartoli, G.; Bosco, M.; Sambri, L. Selective Deprotection of N-Boc-Protected Tert-Butyl Ester Amino Acids by the CeCl₃·7H₂O-NaI System in Acetonitrile. *J. Org. Chem.* **2001**, *66* (12), 4430–4432. <https://doi.org/10.1021/jo010010y>.
- (332) Miller, C. P.; Collini, M. D.; Harris, H. A. Constrained Phytoestrogens and Analogues as ER β Selective Ligands. *Bioorganic Med. Chem. Lett.* **2003**, *13* (14), 2399–2403. [https://doi.org/10.1016/S0960-894X\(03\)00394-9](https://doi.org/10.1016/S0960-894X(03)00394-9).
- (333) Horie, T.; Tominaga, H.; Kawamura, Y.; Yamada, T. Studies of the Selective O-Alkylation and Dealkylation of Flavonoids. 13 An Improved Method for Synthesizing 5,6,7-Trihydroxyflavones from 6-Hydroxy-5,7-Dimethoxy Flavones. *J. Org. Chem.* **1992**, *57* (12), 3343–3347. <https://doi.org/10.1021/jo00038a023>.
- (334) Uchikawa, Y.; Tazoe, K.; Tanaka, S.; Feng, X.; Matsumoto, T.; Tanaka, J.; Yamato, T. Synthesis and Demethylation of 4,22-Dimethoxy[2.10]Metacyclophan-1-yne with BBr₃ to Afford a Novel [10](2,9)-5a,11a-Benzofuro-5a-Bora-11-Bromochromenophane. *Can. J. Chem.* **2012**, *90* (5), 441–449. <https://doi.org/10.1139/v2012-014>.
- (335) Kosak, T. M.; Conrad, H. A.; Korich, A. L.; Lord, R. L. Ether Cleavage Re-Investigated: Elucidating the Mechanism of BBr₃-Facilitated Demethylation of Aryl Methyl Ethers. *European J. Org. Chem.* **2015**, *2015* (34), 7460–7467. <https://doi.org/10.1002/ejoc.201501042>.
- (336) Jeong, K.-W.; Lee, J.-H.; Park, S.-M.; Choi, J.-H.; Jeong, D.-Y.; Choi, D.-H.; Nam, Y.; Park, J.-H.; Lee, K.-N.; Kim, S.-M.; Ku, J.-M. Synthesis and In-Vitro Evaluation of 2-Amino-4-Arylthiazole as Inhibitor of 3D Polymerase against Foot-and-Mouth Disease (FMD). *Eur. J. Med. Chem.* **2015**, *102*, 387–397. <https://doi.org/10.1016/j.ejmech.2015.08.020>.
- (337) Anderson, D. R.; Volkmann, R. A.; Menniti, F. S. Selective Octahydrocyclopenta[c]Pyrroles as Negative Modulators of NR2B and Their Preparation, 2015.
- (338) Hudkins, R. L.; Josef, K. A.; Tao, M. Preparation of Pyridizinones as Histamine H₃ Inhibitors., 2008.
- (339) Wang, M.; Funabiki, K.; Matsui, M. Synthesis and Properties of Bis(Hetaryl)Azo Dyes. *Dye. Pigment.* **2003**, *57* (1), 77–86. [https://doi.org/10.1016/S0143-7208\(03\)00011-1](https://doi.org/10.1016/S0143-7208(03)00011-1).
- (340) Merino, E. Synthesis of Azobenzenes: The Coloured Pieces of Molecular Materials. *Chem. Soc. Rev.* **2011**, *40* (7), 3835–3853. <https://doi.org/10.1039/c0cs00183j>.
- (341) Favre-Besse, F.-C. Modulateurs Du Transport Vésiculaire Du Glutamate : Développement d'outils Pharmacologiques et de Diagnostic Pour La Maladie d'Alzheimer, 2012.
- (342) Gaspar, A.; Matos, M. J.; Garrido, J.; Uriarte, E.; Borges, F. Chromone: A Valid Scaffold in Medicinal Chemistry. *Chem. Rev.* **2014**, *114* (9), 4960–4992. <https://doi.org/10.1021/cr400265z>.
- (343) Keri, R. S.; Budagumpi, S.; Pai, R. K.; Balakrishna, R. G. Chromones as a Privileged Scaffold in Drug Discovery: A Review. *Eur. J. Med. Chem.* **2014**, *78*, 340–374. <https://doi.org/10.1016/j.ejmech.2014.03.047>.

- (344) Seifert, T.; Malo, M.; Kokkola, T.; Stéen, E. J. L.; Meinander, K.; Wallén, E. A. A.; Jarho, E. M.; Luthman, K. A Scaffold Replacement Approach towards New Sirtuin 2 Inhibitors. *Bioorganic Med. Chem.* **2020**, *28* (2). <https://doi.org/10.1016/j.bmc.2019.115231>.
- (345) Simeth, N. A.; Crespi, S.; Fagnoni, M.; König, B. Tuning the Thermal Isomerization of Phenylazaindole Photoswitches from Days to Nanoseconds. *J. Am. Chem. Soc.* **2018**, *140* (8), 2940–2946. <https://doi.org/10.1021/jacs.7b12871>.
- (346) Crespi, S.; Simeth, N. A.; Bellisario, A.; Fagnoni, M.; König, B. Unraveling the Thermal Isomerization Mechanisms of Heteroaryl Azoswitches: Phenylazaindoles as Case Study. *J. Phys. Chem. A* **2019**, *123* (9), 1814–1823. <https://doi.org/10.1021/acs.jpca.8b11734>.
- (347) Nielsen, A. T.; Houlihan, W. J. The Aldol Condensation. *Org. React.* **2011**, 1–438. <https://doi.org/10.1002/0471264180.or016.01>.
- (348) Perrin, C. L.; Chang, K. L. The Complete Mechanism of an Aldol Condensation. *J. Org. Chem.* **2016**, *81* (13), 5631–5635. <https://doi.org/10.1021/acs.joc.6b00959>.
- (349) Shanker, N.; Dilek, O.; Mukherjee, K.; McGee, D. W.; Bane, S. L. Aurones: Small Molecule Visible Range Fluorescent Probes Suitable for Biomacromolecules. *J. Fluoresc.* **2011**, *21* (6), 2173–2184. <https://doi.org/10.1007/s10895-011-0919-y>.
- (350) Dong, J.; Abulwerdi, F.; Baldrige, A.; Kowalik, J.; Solntsev, K. M.; Tolbert, L. M. Isomerization in Fluorescent Protein Chromophores Involves Addition/Elimination. *J. Am. Chem. Soc.* **2008**, *130* (43), 14096–14098. <https://doi.org/10.1021/ja803416h>.
- (351) Zhuang, C.; Zhang, W.; Sheng, C.; Zhang, W.; Xing, C.; Miao, Z. Chalcone: A Privileged Structure in Medicinal Chemistry. *Chem. Rev.* **2017**, *117* (12), 7762–7810. <https://doi.org/10.1021/acs.chemrev.7b00020>.
- (352) Ha, S. T.; Low, Y. W. Synthesis and Phase Transition Behaviours of New Chalcone Derivatives. *J. Chem.* **2013**. <https://doi.org/10.1155/2013/943723>.
- (353) Cavallo, G.; Metrangolo, P.; Milani, R.; Pilati, T.; Priimagi, A.; Resnati, G.; Terraneo, G. The Halogen Bond. *Chem. Rev.* **2016**, *116* (4), 2478–2601. <https://doi.org/10.1021/acs.chemrev.5b00484>.
- (354) Koehl, A.; Hu, H.; Feng, D.; Sun, B.; Zhang, Y.; Robertson, M. J.; Chu, M.; Kobilka, T. S.; Laermans, T.; Steyaert, J.; Tarrasch, J.; Dutta, S.; Fonseca, R.; Weis, W. I.; Mathiesen, J. M.; Skiniotis, G.; Kobilka, B. K. Structural Insights into the Activation of Metabotropic Glutamate Receptors. *Nature* **2019**, *566* (7742), 79–84. <https://doi.org/10.1038/s41586-019-0881-4>.
- (355) Šali, A.; Blundell, T. L. Comparative Protein Modelling by Satisfaction of Spatial Restraints. *J. Mol. Biol.* **1993**, *234* (3), 779–815. <https://doi.org/10.1006/jmbi.1993.1626>.
- (356) Schkeryantz, J. M.; Chen, Q.; Ho, J. D.; Atwell, S.; Zhang, A.; Vargas, M. C.; Wang, J.; Monn, J. A.; Hao, J. Determination of L-AP4-Bound Human MGlur8 Receptor Amino Terminal Domain Structure and the Molecular Basis for L-AP4's Group III MGlur Receptor Functional Potency and Selectivity. *Bioorganic Med. Chem. Lett.* **2018**, *28* (4), 612–617. <https://doi.org/10.1016/j.bmcl.2018.01.037>.
- (357) Brooks, B. R.; Brooks, C. L.; Mackerell, A. D.; Nilsson, L.; Petrella, R. J.; Roux, B.; Won, Y.; Archontis, G.; Bartels, C.; Boresch, S.; Caflisch, A.; Caves, L.; Cui, Q.; Dinner, A. R.; Feig, M.; Fischer, S.; Gao, J.; Hodoscek, M.; Im, W.; Kuczera, K.; Lazaridis, T.; Ma, J.; Ovchinnikov, V.;

Paci, E.; Pastor, R. W.; Post, C. B.; Pu, J. Z.; Schaefer, M.; Tidor, B.; Venable, R. M.; Woodcock, H. L.; Wu, X.; Yang, W.; York, D. M.; Karplus, M. CHARMM: The Biomolecular Simulation Program. *J. Comput. Chem.* **2009**, *30* (10), 1545–1614. <https://doi.org/10.1002/jcc.21287>.

- (358) Dassault Systèmes BIOVIA. Discovery Studio Modeling Environment. San Diego: Dassault Systèmes 2020.
- (359) Jones, G.; Willett, P.; Glen, R. C.; Leach, A. R.; Taylor, R. Development and Validation of a Genetic Algorithm for Flexible Docking. *J. Mol. Biol.* **1997**, *267* (3), 727–748. <https://doi.org/10.1006/jmbi.1996.0897>.
- (360) Phillips, J. C.; Braun, R.; Wang, W.; Gumbart, J.; Tajkhorshid, E.; Villa, E.; Chipot, C.; Skeel, R. D.; Kalé, L.; Schulten, K. Scalable Molecular Dynamics with NAMD. *J. Comput. Chem.* **2005**, *26* (16), 1781–1802. <https://doi.org/10.1002/jcc.20289>.

Synthesis of classical and light activated ligands for the glutamatergic transmission

Glutamate is the major excitatory neurotransmitter of the mammalian central nervous system (CNS) and is able to bind two different families of receptors: ionotropic (iGluRs) and metabotropic glutamate receptors. NMDA receptors are iGluRs involved in the rapid transmission of the signal. Their activation is physiologically due to the binding of the agonist glutamate and the co-agonists glycine or D-serine. mGluRs are class C G-protein coupled receptors (GPCRs) dimers responsible for slower neuromodulatory actions of glutamate. Depending on sequence homology, signal transduction and pharmacology, mGluRs are subdivided into three groups: group-I mGluRs (mGlu1,5), group-II (mGlu2,3) and group-III (mGlu4,6,7,8). Among the 8 subtypes of mGlu receptors, mGlu7 has been shown to be related to autism, drug abuse, anxiety, depression, pain and epilepsy. Photopharmacology is an emerging field related to the biological application of light on molecules allowing the modulation of the pharmacological activity. In this thesis, novel photoactivable ligands, also called caged compounds, of NMDA receptors as well as classical and photoswitchable tools of mGlu7 receptors have been designed and synthesized. The first part of this work is based on the synthesis of the two cages *N*-DCAC-D-serine and *N*-DCAC-glycine in order to be able to independently release the biological active co-agonists of NMDA receptors after irradiation and perform electrophysiological studies. The second part is related to the investigation of XAP044, a negative allosteric modulator (NAM) of mGlu7R disclosed by Novartis scientists. They found XAP044 was not binding in a classical manner but they could not carry out further investigations. Various derivatives and photoswitch analogs of XAP044 have been synthesized allowing to find a more potent analog and to elucidate its binding mode. In the final part, the approach of the azologization was investigated for the NAM VU6010608. The central amide linker of VU6010608 was replaced with a diazene bond to obtain the corresponding photoswitch azolog.

Synthèse de ligands classiques et activés par la lumière pour la transmission glutamatergique

Le glutamate est le principal neurotransmetteur exciteur du système nerveux central des mammifères (SNC) et est capable de lier deux familles différentes de récepteurs : les récepteurs ionotropiques (iGluR) et métabotropiques (mGluR) du glutamate. Les récepteurs NMDA sont des iGluR impliqués dans la transmission rapide du signal. Leur activation est due physiologiquement à la liaison de l'agoniste glutamate et du co-agoniste glycine ou D-serine. Les mGluR appartiennent à la classe C des récepteurs couplés aux protéines G (GPCR), ils fonctionnent en dimère et sont responsables d'actions neuromodulatrices plus lentes du glutamate. Selon l'homologie de séquence, la transduction du signal et la pharmacologie, les mGluR sont subdivisés en trois groupes : les mGluR de groupe (mGlu1,5), le groupe-II (mGlu2,3) et le groupe-III (mGlu4,6,7,8). Parmi les 8 sous-types de récepteurs mGlu, mGlu7 a été montré comme étant lié à l'autisme, l'addiction, l'anxiété, la dépression, la douleur et l'épilepsie. La photopharmacologie est un domaine émergent lié à l'application biologique de la lumière sur les molécules permettant la modulation de l'activité pharmacologique. Dans cette thèse, de nouveaux ligands photoactivables, également appelés composés cagés, des récepteurs NMDA ainsi que des outils classiques et photoswitchables des récepteurs mGlu7 ont été conçus et synthétisés. La première partie de ce travail est basée sur la synthèse des deux cages *N*-DCAC-D-sérine et *N*-DCAC-glycine afin de pouvoir libérer indépendamment les co-agonistes biologiquement actifs des récepteurs NMDA après irradiation et effectuer des études d'électrophysiologie. La deuxième partie a concerné l'étude du XAP044, un modulateur allostérique négatif (NAM) de mGlu7R révélé par les scientifiques de Novartis. Ils ont constaté que le XAP044 ne se lie pas dans le domaine classique des NAM, mais n'ont pas pu apporter d'autres précisions. Différents analogues classiques et des photoswitch du XAP044 ont été synthétisés permettant de trouver un analogue plus puissant et d'élucider son mode de liaison. Dans la dernière partie, l'approche d'azologisation a été étudiée pour le NAM VU6010608. Le linker central amide du VU6010608 a été remplacé par un liaison diazène pour obtenir le photoswitch azolog correspondant.